

**Architecture of fluvio-deltaic sandbodies: the  
Namurian of Co. Clare, Ireland, as an analogue  
for the Plio-Pleistocene of the Nile Delta**

By

Eleanor Jane Stirling

Submitted in accordance with the requirements  
for the degree of Doctor of Philosophy

University of Leeds  
School of Earth Sciences

December 2003

The candidate confirms that the work submitted is her own and that appropriate credit  
has been given where reference has been made to the work of others.

This copy has been supplied on the understanding that it is copyright material and that  
no quotation from the thesis may be published without proper acknowledgement.

## **Acknowledgements**

I would like to thank NERC and BG for providing the funding for this research, and my supervisors Professor Jim Best, Dr. Paul Wignall and, at BG, Mick Oates for setting up the project. Guidance and advice from Jim and Paul throughout my PhD has been much appreciated. I am grateful to those at BG who have contributed thoughts and ideas to my research, including Ross Garden, Mark Simmons, Helen Jackson and Rob Cook. For the time I was able to spend in Egypt my warm thanks go to Niall Hoey, Andy Samuel and Maher Ayyad at BG; Greig Cowan and Mohamed Nashaat at Rashpetco; and Drs. Mohammed Darwish and Ahmed Niazy from the geology department of Cairo University. My time in the desert was a great experience thanks to you all.

For helpful discussions and geological advice whilst on various relevant fieldtrips I would like to thank my supervisors Jim and Paul, Jeff Peakall, Sarah Davies, Andy Pulham, Trevor Elliot, Janok Bhattacharya, Brian Willis, and Doug Boyd. Thanks also to Jane Francis for aiding me with the identification of various Carboniferous plant fossils.

A big thank you goes to the incredibly helpful team at Roxar, who provided me with the IRAP RMS software at no cost to the university, and who also provided excellent training and technical support throughout the time I was working with RMS. Thanks go to James Cheeseman, Mark Whelan, Aonghus O'Carroll, and Dave Hardy.

Many thanks are due to those intrepid individuals who gave their time and geology skills for free to help me with my fieldwork; Laura Faulkenberry, Liz Harris and Claire Davies, your able assistance and your company has been much appreciated.

I'd like to thank my long-term office mates in the Railway Carriage - Rufus, Richard, Tim, and Siska - for useful advice, computer support, textbook loans, interesting conversations, and general laughs. Best wishes also to the other PhD-ers who passed through the department during my time at Leeds and who made me feel at home when I first arrived - Laura, Claire, Claire, Jo, Dave, Loz.... and many others.

Thanks to those at BP who believed in me enough to offer me not only a summer placement but also a job. The three months I spent with the UTG team in Aberdeen taught me a lot, helped me to gain confidence in my own abilities and was also a timely break from PhD stress. Thank you Laura Banfield, Doug Boyd, Simon Payne, Steve Cawley, and anyone else who remembers me! A mention must also be made of my four housemates from that time, Nick, Nadine, Helen and Pàraic, who were the perfect pals for investigating Aberdeen's many delights. Cheers, roomies!

I really appreciate the friendship and prayerful support of my friends at Calvary Chapel. Who knew I'd arrive in Leeds to do a PhD and end up living in Harrogate and meeting such a totally sound group of people. Mike, Theresa, Doug, Lisa, Vikki, Rodrigo, Nicolette, Jason, Sandra, Jim, Linda, Veronica, Dennis, Henry, Pauline, Linda, Sam, Ed, Daniel, Cheryl, Kevin, Eric, April, Melissa, Amy, Ann and everyone else..... you guys are the best!

My family has been a tremendous support to me throughout my PhD. Without their love and encouragement I really couldn't have made it. Mum, thank you for your prayers, for listening to me moan and for giving me so much good advice and lots of hugs; Dad, thanks for always being there for me and for bringing me up to believe that I can do whatever I put my mind to; Chloe, thanks for being a breath of fresh air, especially during my last few months of being buried in the books, and for reminding me that there's more to life than a thesis. I love you all loads!

Finally, and most importantly, thank you God. For giving me this PhD with all the amazing opportunities it has afforded, for helping me find the strength to keep going when I wanted to quit, for working things out when circumstances made it seem impossible, and for keeping me on track through all the various ups and downs of what has, at times, been a pretty bumpy road. I couldn't have done it without you, and you deserve all the credit. Thank you.

## **Abstract**

Understanding and predicting the size, shape and internal architecture of sandbodies is of fundamental importance in hydrocarbon exploration. High quality hydrocarbon reservoirs are often formed in deltaic environments where there is a complex interplay between changes in relative sea level, sediment input and climate. When combined with the intrinsic sedimentary variability of deltas, this makes prediction of the internal facies distributions and architectures of deltaic sandbodies a challenging task. The aim of this thesis is to conduct a detailed qualitative and quantitative field study of fluvial and deltaic sandbody architecture and facies distribution, and to assess the usefulness of the data thus obtained in predicting the architecture and sedimentary characteristics of reservoir sandstones in the subsurface.

The El Wastani Formation of the Nile Delta, Egypt, has previously been identified as an interval of reservoir quality sandstones within the Plio-Pleistocene deltaic succession. Limited core data, and poor seismic imaging due to gas seepage effects, hindered past attempts to assess the internal architecture and facies of the sandbodies. Therefore it was considered appropriate to use an outcrop analogue to aid understanding of the El Wastani Formation reservoir characteristics. From a review of literature, the Upper Carboniferous fluvial and deltaic sandstones of the Central Clare Group, County Clare, western Ireland, were found to be suitable analogues for the El Wastani Formation sandstones. Controls on the two sedimentary systems were similar; both were fluvial-dominated and wave-influenced, and both show evidence for fluctuating relative sea-level. Comparisons of facies observed in outcrop (Co. Clare) and interpreted from image logs (Nile Delta) show similar facies and sedimentary successions in the two systems, improving confidence in the choice of analogue.

Fieldwork carried out on the Upper Carboniferous (Namurian) coastal outcrops of Co. Clare produced detailed measurements of facies distributions and bed geometries, which, together with sedimentary logs, palaeocurrent studies and outcrop-scale photomontages, enabled interpretation and quantification of channel dimensions, internal architectures and stacking patterns. Based on these data, the Tullig Sandstone, a major sandbody within the Central Clare Group, is interpreted to be a low-sinuosity, braided fluvial system that flowed to the north-northeast. This sandbody shows decreasing amounts of erosion and conglomeratic facies in both downstream and vertical directions, interpreted to reflect the combined effects of delta subsidence and sea-level rise over time, influencing the downstream reaches of the system first. The mean sand to non-sand ratio for the Tullig Sandstone is 97% by area, and connectivity of sandstone facies within this sandbody is 93%. In contrast, mouthbar sandbodies that were studied have a mean sand to non-sand ratio of 90%, and greatly reduced sandstone connectivity, at 65%. The data that characterise the field outcrops can be taken as indicative of the probable characteristics of the El Wastani sandbodies.

The data generated from the quantitative field studies were used to construct computer models of the outcrops, in order to see how well the modelling software was able to reproduce the outcrop architectures and facies distributions, and also to test the sensitivity of the models to different scales of data. One large-scale model was built to include all the Tullig Sandstone outcrops along the coastline, with a vertical resolution (cell height) of 1m. A second smaller model was constructed to cover just the Trusklieve outcrop, and was built using a vertical cell height of 0.1m. Each model was designed to fit the sedimentary log data, and was conditioned to reflect the facies percentages and channel dimensions measured and calculated respectively from the outcrops. The results showed that although the larger modelling grid, with lower vertical and horizontal data resolution, showed significant differences in fine-grained facies distribution from the outcrops, it was reasonably successful at reproducing the channel shapes and stacking patterns seen in outcrop. In addition, the high sand to non-sand ratio meant that sandstone connectivity was not reduced compared with either the outcrops or the small, high-resolution model. The small model was better at reproducing the geometries of beds of fine-grained facies, but lacked the ability to accurately simulate the channel architectures and stacking patterns.

# Contents

Acknowledgements.....	II
Abstract.....	IV
Contents.....	V
List of figures.....	XI
List of tables.....	XIV
List of Appendices.....	XV
List of Enclosures.....	XVI
List of equations and abbreviations.....	XVI

## Chapter 1. Introduction and background to the study

1.1 Introduction.....	1
1.2 The importance of the description and quantification of sedimentary architecture...1	1
1.3 The use of outcrop analogues.....	2
1.4 Research objectives.....	3
1.5 Analytical approach.....	3
1.6 Thesis structure.....	4

## Chapter 2. The Co. Clare field analogue and the Nile Delta hydrocarbon play

2.1 Introduction.....	6
2.2 Geology of the field area, County Clare, Ireland.....	6
2.2.1 Introduction.....	6
2.2.2 Tectonic setting.....	6
2.2.3 Stratigraphy and sedimentology.....	11
2.2.3.1 <i>Clare Shale Formation</i> .....	11
2.2.3.2 <i>Ross Sandstone Formation</i> .....	12
2.2.3.3 <i>Gull Island Formation</i> .....	13
2.2.3.4 <i>Central Clare Group deltaic deposits</i> .....	14
2.2.4 Deformation.....	17
2.2.5 The Tullig, Kilkee and Doonlicky Sandstone Members.....	18
2.2.5.1 <i>The Tullig Sandstone Member</i> .....	18
2.2.5.2 <i>Kilkee and Doonlicky Sandstone Members</i> .....	19
2.2.6 Summary.....	20
2.3 The Nile Delta: initiation and evolution.....	22

2.3.1	Introduction.....	22
2.3.2	Present-day delta morphology.....	22
2.3.3	Tectonic setting.....	23
2.3.4	Delta initiation.....	26
2.3.5	Delta evolution.....	27
2.3.6	Hydrocarbon exploration.....	30
2.3.7	Summary.....	31
<b>2.4</b>	<b>The El Wastani play in the Rosetta concession.....</b>	<b>31</b>
2.4.1	Introduction.....	31
2.4.2	Exploration history.....	32
2.4.3	El Wastani Formation: controls on deposition and facies.....	33
2.4.4	El Wastani Formation: sedimentology and reservoir characteristics.....	37
2.4.5	Hydrocarbon potential.....	38
2.4.6	Summary.....	39
<b>2.5</b>	<b>Comparison of potential analogues.....</b>	<b>40</b>

### **Chapter 3. Fluvial and deltaic facies descriptions, interpretations, and associations from County Clare fieldwork**

<b>3.1</b>	<b>Introduction.....</b>	<b>43</b>
<b>3.2</b>	<b>Methodology.....</b>	<b>43</b>
3.2.1	Logs and facies definition.....	43
3.2.2	Palaeocurrent data.....	45
<b>3.3</b>	<b>Facies descriptions and interpretations.....</b>	<b>49</b>
3.3.1	Massive to faintly bedded sandstone (Sm).....	49
3.3.1.1	<i>Description.....</i>	49
3.3.1.2	<i>Interpretation.....</i>	49
3.3.2	Massive to faintly bedded sandstone with conglomeratic lag (Smc).....	51
3.3.2.1	<i>Description.....</i>	51
3.3.2.2	<i>Interpretation.....</i>	52
3.3.3	Horizontally laminated sandstone (Sh).....	52
3.3.3.1	<i>Description.....</i>	52
3.3.3.2	<i>Interpretation.....</i>	53
3.3.4	Horizontally bedded sandstone with conglomeratic lag (Shc).....	53
3.3.4.1	<i>Description.....</i>	53
3.3.4.2	<i>Interpretation.....</i>	53
3.3.5	Low-angle cross-bedded sandstone (Sl and Sl <sub>2</sub> ).....	55

3.3.5.1	<i>Description</i> .....	55
3.3.5.2	<i>Interpretation</i> .....	56
3.3.6	Planar cross-bedded sandstone (Sp and Sp <sub>2</sub> ).....	56
3.3.6.1	<i>Description</i> .....	56
3.3.6.2	<i>Interpretation</i> .....	57
3.3.7	Trough cross-bedded sandstone (St).....	59
3.3.7.1	<i>Description</i> .....	59
3.3.7.2	<i>Interpretation</i> .....	59
3.3.8	Low-angle, planar or trough cross-bedded sandstone with clastic lag (Sc).....	59
3.3.8.1	<i>Description</i> .....	59
3.3.8.2	<i>Interpretation</i> .....	61
3.3.9	Clast-supported sandstone conglomerate (Ccm).....	61
3.3.9.1	<i>Description</i> .....	61
3.3.9.2	<i>Interpretation</i> .....	61
3.3.10	Deformed sandstone (Sd).....	63
3.3.10.1	<i>Description</i> .....	63
3.3.10.2	<i>Interpretation</i> .....	63
3.3.11	Ripple cross-laminated sandstone (Sr).....	64
3.3.11.1	<i>Description</i> .....	64
3.3.11.2	<i>Interpretation</i> .....	66
3.3.12	Climbing ripple cross-laminated sandstone (Sr <sub>c</sub> ).....	66
3.3.12.1	<i>Description</i> .....	66
3.3.12.2	<i>Interpretation</i> .....	68
3.3.13	Wave ripple cross-laminated sandstone (Sr <sub>w</sub> ).....	68
3.3.13.1	<i>Description</i> .....	68
3.3.13.2	<i>Interpretation</i> .....	69
3.3.14	Hummocky cross-stratified sandstone (Shcs).....	70
3.3.14.1	<i>Description</i> .....	70
3.3.14.2	<i>Interpretation</i> .....	70
3.3.15	Horizontally laminated sandstone type 2 (Sh <sub>2</sub> ).....	70
3.3.15.1	<i>Description</i> .....	70
3.3.15.2	<i>Interpretation</i> .....	72
3.3.16	Interlaminated sandstone, siltstone and mudstone (Flh).....	74
3.3.16.1	<i>Description</i> .....	74
3.3.16.2	<i>Interpretation</i> .....	76
3.3.17	Laminated siltstone (Fls).....	77
3.3.17.1	<i>Description</i> .....	77

3.3.17.2	<i>Interpretation</i> .....	77
3.3.18	Laminated mudstone (Flm).....	77
3.3.18.1	<i>Description</i> .....	77
3.3.18.2	<i>Interpretation</i> .....	77
3.3.19	Ichnofacies.....	79
3.3.19.1	<i>Description</i> .....	79
3.3.19.2	<i>Summary and interpretation</i> .....	80
3.3.20	Plant material.....	83
3.3.20.1	<i>Description</i> .....	83
3.3.20.2	<i>Interpretation</i> .....	83
<b>3.4</b>	<b>Facies associations and interpretations</b> .....	<b>86</b>
3.4.1	Mouthbar facies association.....	86
3.4.2	Interdistributary bay association.....	90
3.4.3	Fluvial and alluvial association.....	92
<b>3.5</b>	<b>Summary</b> .....	<b>95</b>
<b>3.6</b>	<b>Comparison of facies between Ireland and Egypt</b> .....	<b>95</b>
3.6.1	FMI tool description.....	95
3.6.2	FMI log descriptions and interpretations.....	96
3.6.2.1	<i>B sand description and interpretation</i> .....	96
3.6.2.2	<i>C sand description and interpretation</i> .....	97
3.6.2.3	<i>D sand description and interpretation</i> .....	98
3.6.3	Summary.....	99
<b>Chapter 4.</b>	<b>Fluvial and deltaic facies architecture: description and interpretation</b>	
<b>4.1</b>	<b>Introduction</b> .....	<b>101</b>
<b>4.2</b>	<b>Methodology</b> .....	<b>101</b>
<b>4.3</b>	<b>Outcrop descriptions and interpretations</b> .....	<b>102</b>
4.3.1	The Tullig Sandstone at Trusklieve.....	102
4.3.1.1	<i>Storey one: description and interpretation</i> .....	107
4.3.1.2	<i>Storey two: description and interpretation</i> .....	112
4.3.1.3	<i>Storey three: description and interpretation</i> .....	116
4.3.1.4	<i>Storey four: description and interpretation</i> .....	120
4.3.1.5	<i>Storey five: description and interpretation</i> .....	123
4.3.1.6	<i>Summary and discussion of the Trusklieve outcrop</i> .....	124
4.3.2	The Tullig Sandstone at Pulleen.....	130
4.3.2.1	<i>Storey one: description and interpretation</i> .....	130

4.3.2.2	<i>Storey two: description and interpretation</i> .....	132
4.3.2.3	<i>Storey three: description and interpretation</i> .....	133
4.3.2.4	<i>Summary and discussion of the Pulleen outcrop</i> .....	137
4.3.3	The Tullig Sandstone at Killard.....	139
4.3.3.1	<i>Storey one: description and interpretation</i> .....	139
4.3.3.2	<i>Storey two: description and interpretation</i> .....	145
4.3.3.3	<i>Summary and discussion of the Killard outcrop</i> .....	147
4.3.4	The Tullig Sandstone at Carrowmore Point.....	150
4.3.4.1	<i>Storey one: description and interpretation</i> .....	153
4.3.4.2	<i>Storey two: description and interpretation</i> .....	154
4.3.4.3	<i>Summary and discussion of the Carrowmore Point outcrop</i> .....	160
4.3.5	The Tullig Sandstone at Furreera, Liscannor Bay.....	162
4.3.5.1	<i>Storey one: description and interpretation</i> .....	162
4.3.5.2	<i>Summary and discussion of the Furreera outcrop, Liscannor Bay</i> .....	165
4.3.6	Tullig Cyclothem mouthbar sandbody at Tullig Point.....	166
4.3.6.1	<i>Lowermost 2-3m of the sandbody: description and interpretation</i> .....	168
4.3.6.2	<i>Upper 6-7m of the sandbody: description and interpretation</i> .....	168
4.3.6.3	<i>Summary and discussion of the Tullig Point outcrop</i> .....	170
4.3.7	Tullig Cyclothem mouthbar sandbody at Killard.....	172
4.3.7.1	<i>Lower part of sequence: description and interpretation</i> .....	172
4.3.7.2	<i>Upper sandy part of sequence: description and interpretation</i> .....	176
4.3.7.3	<i>Summary and discussion of the Killard mouthbar outcrop</i> .....	178
4.4	<b>Summary and palaeoenvironmental interpretation</b> .....	181
4.4.1	The Tullig Sandstone.....	181
4.4.2	Tullig Cyclothem mouthbar sandbodies.....	186
4.4.3	The Tullig Cyclothem palaeoenvironment.....	187

## **Chapter 5. Quantification of fluvial and deltaic facies distribution and sedimentary architecture**

5.1	<b>Introduction</b> .....	189
5.2	<b>Methodology</b> .....	189
5.2.1	Quantification of sedimentary architecture.....	189
5.2.2	Quantification of facies distribution.....	191
5.3	<b>Architecture and facies distribution quantification: results</b> .....	191
5.3.1	The Tullig Sandstone.....	191
5.3.1.1	<i>Trusklieve</i> .....	191
5.3.1.2	<i>Pulleen</i> .....	198

5.3.1.3	<i>Killard</i> .....	200
5.3.1.4	<i>Carrowmore Point</i> .....	202
5.3.1.5	<i>Furreera, Liscannor Bay</i> .....	208
5.3.2	Tullig Cyclothem mouthbar sandbodies.....	209
5.3.2.1	<i>Tullig Point mouthbar</i> .....	209
5.3.2.2	<i>Killard mouthbar</i> .....	212
<b>5.4</b>	<b>Summary and discussion</b> .....	<b>215</b>
5.4.1	Internal architecture statistics.....	216
5.4.2	Facies distribution statistics.....	219
5.4.3	Other potential uses of the data.....	222
<b>Chapter 6. Outcrop-based reservoir modelling of fluvial facies architecture</b>		
<b>6.1</b>	<b>Introduction</b> .....	<b>223</b>
<b>6.2</b>	<b>Background to reservoir modelling</b> .....	<b>223</b>
6.2.1	The definition and importance of geological reservoir models.....	223
6.2.2	Use of outcrop data.....	224
6.2.3	Different modelling methods.....	225
6.2.4	Summary.....	227
<b>6.3</b>	<b>Methodology</b> .....	<b>228</b>
<b>6.4</b>	<b>Modelling specifications</b> .....	<b>234</b>
6.4.1	Large modelling grid: Truskievee to Carrowmore Point.....	234
6.4.2	Small modelling grid: Truskievee.....	240
<b>6.5</b>	<b>Modelling results</b> .....	<b>244</b>
6.5.1	Results from the large modelling grid.....	244
6.5.2	Results from the small modelling grid.....	246
<b>6.6</b>	<b>Discussion</b> .....	<b>247</b>
6.6.1	Similarity of models to field observations.....	247
6.6.2	Limitations of models.....	251
<b>Chapter 7. Conclusions and recommendations for further work</b> ..... <b>253</b>		
<b>7.1</b>	<b>Conclusions</b> .....	<b>253</b>
<b>7.2</b>	<b>Recommendations for further work</b> .....	<b>256</b>
<b>References</b> .....		<b>259</b>
<b>Appendices A to D</b> .....		<b>276</b>

## List of Figures

### Chapter 2

2.1 Map of County Clare, showing outcrop localities and Namurian stratigraphy.....	7
2.2a) and b) Maps showing plate tectonic movements affecting WINB development..	8
2.3 Schematic diagram of WINB model accepted by Collinson <i>et al.</i> (1991).....	10
2.4 Schematic diagram of WINB model proposed by Wignall & Best (2000).....	10
2.5 Namurian lithostratigraphy of County Clare .....	12
2.6. Principal geographical features of the Nile Delta and Cone region.....	24
2.7 Structural and tectonic regions of NE Egypt and the SE Mediterranean.....	24
2.8 Schematic N-S section showing Nile Delta stratigraphy.....	25
2.9 Nile Delta stratigraphy with lithologies and main seismic markers.....	25
2.10 Location map showing Rosetta block outlines, wells and prospects.....	32
2.11 Nile Delta cross-section based on seismic and well logs.....	34
2.12 Schematic profile of shelf and slope stratigraphy, showing main play type.....	34
2.13 Schematic section through the El Wastani reservoir sands.....	34
2.14 Sequence stratigraphic system for the west Nile Delta area.....	36

### Chapter 3

3.1 Map of County Clare, showing field localities and Namurian stratigraphy.....	40
3.2 Facies Sm, example from Storey 4 at Trusklieve.....	50
3.3 Facies S <sub>mc</sub> , example from Storey 4 at Trusklieve.....	51
3.4 Facies Sh, example from Storey 3 at Trusklieve.....	54
3.5 Facies Sh and Sp, example from Storey 3 at Trusklieve.....	54
3.6 Facies Sl, example from Storey 1 at Killard.....	55
3.7 Facies Sp, example from Storey 3 at Trusklieve.....	58
3.8 Facies Sp, example from Storey 2 at Killard.....	58
3.9 Facies St, example from Storey 2 at Killard.....	60
3.10 Facies St, example from Storey 2 at Killard.....	60
3.11 Facies C <sub>cm</sub> , example from Storey 1 at Trusklieve.....	62
3.12 Facies S <sub>d</sub> , example from Storey 2 at Killard.....	62
3.13 Facies S <sub>r</sub> , example from mouthbar below the Tullig Sandstone at Trusklieve..	65
3.14 Facies S <sub>r</sub> , example from Storey 3 at Trusklieve.....	65
3.15 Facies S <sub>r<sub>c</sub></sub> , example from Liscannor.....	67
3.16 Facies S <sub>r<sub>c</sub></sub> , example from Killard mouthbar.....	67
3.17 Facies S <sub>r<sub>w</sub></sub> , example from mouthbar below the Tullig Sandstone at Trusklieve..	69
3.18 Facies Sh <sub>cs</sub> , example from Killard mouthbar.....	71
3.19 Facies Sh <sub>cs</sub> , example from Killard mouthbar.....	71
3.20 Facies Sh <sub>2</sub> , example from Killard mouthbar.....	73
3.21 Facies Sh <sub>2</sub> , example from Killard mouthbar.....	73
3.22 Facies Fl <sub>h</sub> , example from Killard mouthbar.....	75
3.23 Facies Fl <sub>h</sub> , example from mouthbar below the Tullig Sandstone at Trusklieve..	75
3.24 Facies Fl <sub>m</sub> , example from Storey 3 at Trusklieve.....	78
3.25 Facies Fl <sub>m</sub> , example from Storey 3 at Trusklieve.....	78
3.26 Trace fossils within facies Fl <sub>h</sub> , example from Killard.....	81
3.27 Trace fossils within facies Sh <sub>2</sub> , example from Killard.....	82
3.28 Plant fossils, example from Storey 3 at Trusklieve.....	84
3.29 Plant fossils, example from Storey 3 at Trusklieve.....	84
3.30 Plant fossils, example from Storey 3 at Trusklieve.....	84
3.31 Plant fossils, example from Killard mouthbar.....	85

3.32 Plant fossil, example from Storey 2 at Trusklieve.....	85
3.33 Plant fossil, example from Killard.....	85
3.34 Mouthbar facies association: example from Killard.....	87
3.35 Interdistributary bay facies: example from Furreera.....	91
3.36 Fluvial and alluvial facies association: example from Killard.....	93
3.37 FMI logs, interpretations and palaeoenvironmental setting.....	100

## Chapter 4

4.1a) and b) Photomosaic of the Trusklieve outcrop.....	103
4.2 Log correlation panel, Trusklieve.....	104
4.3a) Photomosaic of the southern part of the Trusklieve outcrop.....	105
4.3b) Southern part of the Trusklieve outcrop, showing facies interpretations.....	106
4.4a) and b) Photomosaics and interpretations of Storeys 1 and 2, Trusklieve.....	110
4.4c) to e) Photomosaics and interpretations of Storeys 3 to 5, Trusklieve.....	111
4.5 Schematic diagram to show formation of Storey 1, Trusklieve.....	112
4.6a) and b) Schematic diagram to show formation of Storey 2, Trusklieve.....	115
4.7a) and b) Schematic diagram to show formation of Storey 3, Trusklieve.....	119
4.8 Storey 4, Trusklieve, showing well-developed low-angle cross bedding.....	121
4.9 Log from the Tullig Sandstone at Pulleen.....	131
4.10 a) and b) Photomosaic of cliff section at Pulleen.....	134
4.11 Photomosaic of sea stack cliff section at Pulleen.....	135
4.12 Log correlation panel, Killard.....	141
4.13 a) and b) Photomosaic of cliff section, north limb, Killard.....	142
4.14 Base of the Tullig Sandstone, north limb, Killard.....	143
4.15 Log correlation panel, Carrowmore Point.....	151
4.16 Photomosaic of the Carrowmore Point outcrop, northern limb.....	152
4.17 Photomosaic of the Carrowmore Point outcrop, southern limb.....	156
4.18 View of Storey 2, northern limb, Carrowmore, showing well-bedded facies...157	
4.19 View of Storey 2, southern limb, Carrowmore, showing fine-grained facies...157	
4.20 Sketches showing internal structures in unit Z, southern limb, Carrowmore...160	
4.21 Log from the Tullig Sandstone and underlying sequence, Furreera.....	163
4.22 Trough cross bedding in the Tullig Sandstone, Furreera.....	163
4.23a) and b) Photomosaic of a section of the Furreera outcrop.....	164
4.24a) and b) Photo of cliff section at Tullig Point, showing mouthbar sandbody...167	
4.25 Log from the Tullig Point sandbody.....	167
4.26 Log from the Killard mouthbar succession, southern limb of syncline.....	173
4.27a) Photo of the sandy upper part of the Killard mouthbar succession.....	174
4.27b) Upper part of Killard mouthbar succession, showing facies interpretation...175	
4.28 Cross bedding in the Killard mouthbar, southern limb.....	178
4.29a) and b) Photomosaic of the Killard mouthbar, northern limb.....	180
4.30 Palaeocurrent data from the Tullig Sandstone.....	181
4.31a) to d) Schematic block diagrams showing evolution of the depositional environment of the Tullig Sandstone .....	188

## Chapter 5

5.1 Photomosaic close-up of Storey 1, Trusklieve, showing bed measurements.....	193
5.2 Vertical proportion curve, Tullig Sandstone, Trusklieve.....	196
5.3 Horizontal proportion curve, Tullig Sandstone, Trusklieve.....	197
5.4 Vertical proportion curve, Tullig Sandstone, Pulleen.....	200
5.5 Vertical proportion curve, Tullig Sandstone, Killard.....	203

5.6 Vertical proportion curve, Tullig Sandstone, Carrowmore Point.....	203
5.7 Horizontal proportion curve, Tullig Sandstone, Carrowmore Point.....	207
5.8 Vertical proportion curve, mouthbar sandbody, Tullig Point.....	211
5.9 Horizontal proportion curve, mouthbar sandbody, Tullig Point.....	211
5.10 Vertical proportion curve, mouthbar sandbody, Killard.....	214
5.11 Graph of sandstone connectivity for Tullig Sandstone along the coastline.....	218
5.12 Graph of mean bed thicknesses for the Tullig Sandstone along the coastline...	218
5.13 Graph of mean bed lengths for the Tullig Sandstone along the coastline.....	218
5.14 Graph of continuity indices for the Tullig Sandstone along the coastline.....	218
5.15 Graph of percentages of the two main sandy facies along coastline .....	220
5.16 Graph of percentages of coarse- and fine-grained facies along coastline.....	220

## Chapter 6

6.1 Map of position of modelling grids relative to logged localities in Co. Clare....	230
6.2 Conversion of sedimentary log into facies log for input to modelling grids.....	232
6.3 Blocked wells from Trusklieve, created for large modelling grid.....	235
6.4 Blocked wells from other localities created for large modelling grid.....	235
6.5 Histogram of facies thickness distribution, from blocked wells of large grid....	237
6.6 Blocked wells from Trusklieve, created for the small modelling grid.....	241
6.7 Histogram of facies thickness distribution, from blocked wells of small grid....	241
6.8 Image of facies model created for the large modelling grid.....	244
6.9 Close-up cross-section through northernmost wells in large grid.....	245
6.10 Drainable volume for large grid model.....	248
6.11 Cross-section through large grid, showing drainable volume.....	248
6.12 Image of facies model created for the small modelling grid.....	249
6.13 Drainable volume for the small grid model.....	249

## List of Tables

### Chapter 2

- 2.1 Comparison of the two main models of sandbody formation for Co. Clare.....16
- 2.2 Reservoir characteristics for El Wastani sandstones.....38
- 2.3 Division of gas pay between reservoir sands in the P1 structure.....39

### Chapter 3

- 3.1 Facies codes, descriptions and interpretations.....46-48

### Chapter 4

- Table 4.1. Summary of statistics from the Tullig Sandstone at each locality.....182

### Chapter 5

- 5.1 Sandstone bed data for Trusklieve, Storey1.....192
- 5.2 Sandstone bed data for the Tullig Sandstone, Trusklieve, Storey 3.....194
- 5.3 Tullig Sandstone vertical facies proportions, Trusklieve.....195
- 5.4 Tullig Sandstone vertical facies proportions, Pulleen.....199
- 5.5 Tullig Sandstone vertical facies proportions, north limb, Killard.....201
- 5.6 Sandstone bed data for north limb, Carrowmore Point.....204
- 5.7 Tullig Sandstone vertical facies proportions, north limb, Carrowmore Point....206
- 5.8 Sandstone bed data for mouthbar sandbody, Tullig Point.....209
- 5.9 Tullig Point mouthbar sandbody vertical facies proportions.....210
- 5.10 Sandstone bed data for mouthbar sandbody, south limb, Killard.....213
- 5.11 Sandstone bed data for mouthbar sandbody, north limb, Killard.....214
- 5.12 Sandstone bed data for all Tullig Sandstone and mouthbar outcrops.....215
- 5.13 Summary of facies distribution statistics from all Tullig Sandstone outcrops...212
- 5.14 Summary of facies distributions statistics from mouthbar sandbodies.....214

### Chapter 6

- 6.1 Horizon names and dimensions used in modelling.....229
- 6.2 Corner-point locations, grid and cell dimensions of the two modelling grids...231
- 6.3 Composite facies created for modelling.....233
- 6.4 List of names of logs input to the two geological modelling grids.....234
- 6.5 Percentages of each facies in each blocked well, large grid.....236
- 6.6 Specifications used for facies modelling in the large grid.....239
- 6.7 Percentages of each facies in each blocked well, small grid.....242
- 6.8 Specifications used for facies modelling in the small grid.....243

<b>Appendices.....</b>	<b>276</b>
A1 Key to log symbols, ornaments and labels.....	277
A2 Tullig Sandstone log from Trusklieve, #1.....	278
A3 Tullig Sandstone log from Trusklieve, #2.....	280
A4 Tullig Sandstone log from Trusklieve, #3.....	282
A5 Tullig Sandstone log from Trusklieve, #4.....	284
A6 Tullig Sandstone log from Pulleen.....	287
A7 Tullig Sandstone log from Killard, south limb of syncline.....	291
A8 Tullig Sandstone log from Killard, north limb of syncline.....	296
A9 Tullig Sandstone log from Carrowmore, southeast.....	302
A10 Tullig Sandstone log from Carrowmore, southwest.....	307
A11 Tullig Sandstone log from Carrowmore, northwest.....	309
A12 Tullig Sandstone log from Carrowmore, north-central.....	313
A13 Tullig Sandstone log from Carrowmore, northeast.....	314
A14 Tullig Sandstone log from Furreera, Liscannor Bay.....	316
A15 Tullig Cycle mouthbar log from Tullig Point.....	317
A16 Tullig Cycle mouthbar log from Killard (south limb).....	319
A17 Cross bed set thicknesses (graph and table).....	323
A18 Cross bed foreset dip angle measurements (graph and table).....	325
A19 Ripple index measurements (graph and table).....	327
B1 Bed thickness data from Trusklieve, Storeys 1 to 5.....	328
B2 Cross bed thickness data from Trusklieve, Storeys 1 to 5.....	329
B3 Bed thickness data from all outcrops.....	329
C1 Outcrop line-drawing with bed labels, Tullig Sandstone, Trusklieve.....	330
C2 Horizontal facies distribution data, Tullig Sandstone, Trusklieve.....	331
C3 Horizontal facies distribution data, Tullig Sandstone, Carrowmore Point.....	332
C4 Horizontal facies distribution data, mouthbar sandbody, Tullig Point.....	334
D1 Log Trusklieve 1, formatted for importing into large modelling grid in RMS...	335
D2 Log Trusklieve 2, formatted for importing into large modelling grid in RMS...	335
D3 Log Trusklieve 3, formatted for importing into large modelling grid in RMS...	336
D4 Log Trusklieve 4, formatted for importing into large modelling grid in RMS...	336
D5 Pulleen log, formatted for importing into large modelling grid in RMS.....	337
D6 Killard N log, formatted for importing into large modelling grid in RMS.....	337
D7 Killard S log, formatted for importing into large modelling grid in RMS.....	338
D8 Carrowmore SE log, formatted for importing into large grid in RMS.....	338
D9 Carrowmore NW log, formatted for importing into large grid in RMS.....	339
D10 Log Trusklieve 1, formatted for importing into small modelling grid.....	339
D11 Log Trusklieve 2, formatted for importing into small modelling grid.....	341
D12 Log Trusklieve 3, formatted for importing into small modelling grid.....	343
D13 Log Trusklieve 4, formatted for importing into small modelling grid.....	346
D14 "General" preferences tab for Facies Channels simulation, large grid.....	349
D15 "Volume fraction" tab for Facies Channels simulation, large grid.....	349
D16 "Geometry" tab for Facies Channels simulation, large grid.....	350
D17 "Form/repulsion" tab for Facies Channels simulation, large grid.....	350
D18 "Form/repulsion" tab for Facies Channels simulation, large grid.....	350
D19 "Correlation" tab for Facies Channels simulation, large grid.....	351
D20 "Correlation display" tab for Facies Channels simulation, large grid.....	351

D21 Histogram of Sm/Sh bed thicknesses, large grid.....	352
D22 Histogram of Sp/St/S1 bed thicknesses, large grid.....	352
D23 Histogram of Ccm bed thicknesses, large grid .....	352
D24 Histogram of Sh <sub>2</sub> /Sp <sub>2</sub> /Sl <sub>2</sub> bed thicknesses, large grid .....	353
D25 Histogram of Flh bed thicknesses, large grid .....	353
D26 Histogram of Fls/Flm bed thicknesses, large grid.....	353
D27 Histogram of Sm/Sh bed thicknesses, small grid.....	354
D28 Histogram of Sp/St/S1 bed thicknesses, small grid.....	354
D29 Histogram of Ccm bed thicknesses, small grid .....	355
D30 Histogram of Fls/Flm bed thicknesses, large grid .....	355
D31-D35 Graphs showing variable monitored during the modelling process...	356-357

**Enclosures 1-3.....pockets 358-360**

### **List of equations and abbreviations**

Eq. 4.1:  $Y \sim 6h$  where Y is flow depth and h is the height of a wholly preserved dune form.

Eq. 4.2:  $h = 2.9 (\pm 0.7) \times d$  where h is the mean height of a wholly preserved dune and d is the mean cross set thickness

FMI – Fullbore Formation MicroImager

RMS – reservoir modelling system

WINB – Western Irish Namurian Basin

# Chapter 1

## Introduction and background to the study

### ***1.1 Introduction***

The hydrocarbon exploration and production industry is very interested in reducing the risks associated with exploration, and the costs associated with production; a good understanding of the characteristics and variability of fluvial and deltaic reservoir sandbodies helps the industry to achieve these goals. This PhD was therefore initiated as a CASE project with BG as the industrial partner, with the objective of improving understanding of fluvio-deltaic sandbody architecture by using field outcrops as analogues for subsurface hydrocarbon reservoir sandbodies. The subsurface reservoir sandbodies under investigation are located in the Plio-Pleistocene deposits of the Nile Delta, offshore Egypt. The proposed field analogue comprises the fluvio-deltaic coastal outcrops of the Upper Carboniferous, County Clare, Ireland.

### ***1.2 The importance of the description and quantification of sedimentary architecture***

Sedimentary “architecture” refers to the three-dimensional geometry, proportion, and spatial distribution of various pre-defined elements within a particular sedimentary succession. The scale of the succession being studied can vary widely, and many architecture studies are large-scale, concerning for example the arrangement of channel-belts and floodplain deposits in a sedimentary basin. This PhD focuses on a slightly smaller scale, concentrating on the internal architecture of an individual fluvial channel-belt and discrete deltaic sandbodies. The elements that comprise sandbodies are packets of genetically related strata, bounded by bedding contacts that are hierarchically ordered (Allen, 1983a). Fluvial architectural elements include channel-fill elements, various types of bar-form, sheet flood deposits and sediment gravity flow lobes (Miall, 1996). Examining these elements on an individual basis reveals that they, too, have distinctive internal architectures.

Accurately describing sandbody architecture is fundamental to the understanding of sedimentological processes, facies distributions and associations, and to the

interpretation of depositional environments. Sandbody architecture description is also a very important aspect of hydrocarbon reservoir characterisation. The architecture of fluvial and deltaic systems has therefore been the subject of much research during the past few decades, both in ancient deposits (e.g. Campbell, 1976; Marzo *et al.*, 1988; Lowry and Raheim, 1991; Halfar *et al.*, 1998; Jo and Chough, 2001; Corbeanu *et al.*, 2001) and in modern rivers and deltas (e.g. Cant and Walker, 1978; Miall, 1985; Bristow, 1987; Gawthorpe *et al.*, 1993).

### **1.3 The use of outcrop analogues**

Although the rapid evolution of technology in the oil and gas industry allows continual improvements in the imaging and sampling of subsurface reservoir sandbodies, there is still a real need for detailed sandbody information that can only be provided by accessible field outcrops. Field outcrops provide two- and often three-dimensional exposures of sedimentary successions, allowing detailed study of geometries, stacking patterns, vertical profiles, bedding architectures, facies distributions, and variations in grainsize, porosity, and permeability. Reservoir geologists, who use limited 1-D data (cores, geophysical logs) and comparatively low-resolution 2- and 3-D data (seismic surveys) to try to predict the geometries and internal variability of sandbodies, often use detailed outcrop data to inform and constrain the models they produce.

While qualitative descriptions and models based on field outcrops are very useful to the geologist working with complex subsurface successions, quantitative outcrop data is even more helpful. Dreyer *et al.* (1993) do not overstate the case when they say that “quantified information on the geometries of sandbodies and their internal heterogeneities is a necessary prerequisite for the realistic modelling of reservoirs and their behaviour during production”. The establishment in 1988 of the “Sedimentary Architectures of Field Analogues for Reservoir Information” (SAFARI) project by a number of Norwegian oil companies illustrates the importance to the hydrocarbon industry of just such quantified outcrop information. However, as pointed out by Bridge and Tye (2000) and Bridge (2003), there are problems with using outcrop analogues; the most obvious being that an outcrop which does not represent an analogous depositional environment will result in seriously flawed predictions and models for the subsurface strata. Care must therefore be taken to establish the similarity of the potential outcrop analogue to the studied subsurface system.

## **1.4 Research objectives**

The objectives of this research are:

- 1) To describe, interpret and quantify the external geometry, internal sedimentary architecture and facies distribution of the fluvial Tullig Sandstone and associated deltaic sandbodies from coastal outcrops of the Upper Carboniferous of County Clare, Ireland.
- 2) To establish or refute, by reviewing literature and comparing available data, the credibility of the analogy between the Co. Clare outcrops and the Plio-Pleistocene fluvio-deltaic sandbody reservoirs of the Nile Delta, Egypt.
- 3) To construct a 3-D model of the Tullig Sandstone in IRAP RMS using data from the main outcrop localities, and to compare the model with the outcrop data to see how effective the modelling process is at incorporating outcrop data and reproducing outcrop architectures and facies distributions.
- 4) To evaluate current models for the depositional environment of the Western Irish Namurian Basin in the light of the architectural and facies distribution data from the Tullig Sandstone, Co. Clare.

## **1.5 Analytical approach**

To achieve the aims given above, the following methodology was employed:

- 1) The most extensive outcrops of the Tullig Sandstone and associated Tullig cyclothem sandbodies that occur along the coastline of Co. Clare were chosen as sites of study. These outcrop localities are spread along the coastline, with a total of 45km between the southernmost and northernmost outcrops. At the majority of localities, both the top and base of the Tullig Sandstone are visible, allowing the sedimentary successions above and below the sandbody to be studied. The chosen outcrops have been worked on by previous researchers (e.g. Pulham, 1987; Davies and Elliott, 1996) and are recognised as useful exposures for study of the Tullig Cyclothem sediments.
- 2) Photomontages were created for each field outcrop, imaging as much of the outcrop as possible (at cliff-style exposures such as Truskleeve it was possible to image the entire outcrop). Detailed sedimentary logs were made, in more than one location for outcrops that were laterally extensive. Sketches and bed measurements were also made, and used together with the logs to interpret the photomontages in terms of bedding architecture and facies distribution. Using these interpreted

photomontages, the facies distributions and bedding architectures were quantified for all outcrops.

- 3) FMI (formation micro-imaging) logs from wells in the Nile Delta were interpreted in terms of facies and architectures; these logs were compared with those from Co. Clare, and with the field outcrops in general. A literature study was conducted on both the Tullig Sandstone system in Co. Clare and the geologic history and Plio-Pleistocene depositional record of the Nile Delta, Egypt; the similarities and differences of the two fluvio-deltaic systems were assessed.
- 4) The data from the Co. Clare Tullig Sandstone outcrops were used to construct a 3-D reservoir model of the Tullig Sandstone, using IRAP RMS (reservoir modelling system). The modelling results were visually compared with the field outcrops to assess their similarity. The modelling method was assessed in terms of its capability of producing realistic, outcrop-simulating models from field data.

### **1.6 Thesis structure**

The chapters of this thesis are arranged as follows. Chapter 2 gives the regional geological setting for the Upper Carboniferous sediments of Co. Clare, and discusses the stratigraphic sequence seen in the cliff sections of the outcrops studied. The main controls on the depositional system are discussed, and the Tullig Sandstone itself is described and set in its stratigraphic context. Points of continuing debate regarding the succession and basin history are also reviewed. The chapter then describes the regional geology of the Nile Delta sedimentary system, including the evolution of the River Nile and the stratigraphy of the delta. The main controls on the Plio-Pleistocene depositional environment are discussed, and the exploration and production history of the plays in the Plio-Pleistocene is outlined, as are the main factors affecting the quality of the hydrocarbon reservoir intervals (excluding any detailed petrophysics). Comparisons are then made between the two fluvio-deltaic systems, and an assessment is made of the suitability of the Co. Clare field outcrops as an analogue for the Plio-Pleistocene Nile Delta.

Chapter 3 describes the Upper Carboniferous sedimentary facies encountered, logged and mapped during fieldwork in Co. Clare. Photographs, detailed descriptions and interpretations are given, and explanations of facies associations in terms of depositional environments are presented. The final section in Chapter 3 presents the

facies interpretation of three imaging logs from the reservoir sandbodies in the Plio-Pleistocene Nile Delta sequence. This section makes a comparison between the two data sets based on facies, to aid in assessment of the similarity between the two fluvio-deltaic systems.

Chapter 4 describes and interprets the architecture of the sedimentary facies seen in the Co. Clare field outcrops. Photomontages are presented and interpreted, and diagrams to explain the formation of the architectures are also given. Palaeocurrent data and summary logs are given in this chapter, while the original detailed sedimentological logs are presented in the appendices. The overall depositional setting and changes in palaeoenvironment are presented as a series of three-dimensional palaeoenvironmental diagrams. The discussion compares the fieldwork interpretations with previous models for the formation of the Tullig Cyclothem.

Chapter 5 presents the quantitative data collected from the Co. Clare fieldwork. A series of graphs shows the facies distributions and bed dimension statistics, which are summarised and used to strengthen the palaeoenvironmental interpretation given in Chapter 4.

Chapter 6 describes the reservoir modelling process, and presents the results of the models created using data collected from the Co. Clare sandbodies. The models are compared with outcrop data to highlight the advantages and limitations of modelling detailed facies distributions using reservoir modelling programs.

Chapter 7 summarises the research findings and presents the conclusions. The benefits and limitations of this analogue study are reviewed and summarised, together with recommendations for future work.

## **Chapter 2**

# **The County Clare field analogue and the Nile Delta hydrocarbon play**

### **2.1 Introduction**

This chapter presents the geologic background and context to the field area, County Clare in Ireland, and to the Nile Delta, the area for which the field outcrops are a proposed analogue. The aim is to review the current literature available about both areas, and to point out the similarities and differences between the two locations, in terms of both the sedimentary successions and the factors that influenced those successions.

### **2.2 Geology of the field area, County Clare, Ireland**

#### **2.2.1 Introduction**

A great deal of work has been conducted on the Upper Carboniferous succession of the Western Ireland Namurian Basin (WINB), the sediments of which crop out along the west coast of Ireland in County Clare (Fig. 2.1). With a stratigraphic succession that records the passage of the region from a deep marine basin to a prograding deltaic shoreline, the coastal outcrops have lent themselves to studies of turbidites, goniatite fauna, slope instability and deltaic cyclicity. The geological history of the basin is summarised in this section, and the various differing views and models of the basin development are discussed, focussing on the fluvio-deltaic sediments of the Central Clare Group that form the outcrops studied in this thesis.

#### **2.2.2 Tectonic setting**

Prior to the establishment of the WINB, the area was affected by significant tectonism. The Iapetus Ocean, formerly covering the region, closed during the Silurian, with collision of the Eurasian and North American continental plates in end-Silurian times to create the Caledonian orogenic belt (Maynard, 1997; Shannon, 1991; see Fig. 2.2a). The WINB lies either to the north (Crocker, 1995) or directly above (Collinson *et al.*, 1991) the Iapetus suture zone, and, along with the other sedimentary basins developed across Western Europe during the Carboniferous, is influenced by the structural grain of



Figure 2.1. Map of western Ireland showing the coastal succession, principal outcrop locations, main towns and other sites of interest (modified from Wignall and Best, 2000). Inset map, top left: outline map of Ireland, showing the Variscan Front (Shannon, 1991); the location, according to Morris and Max (1995), of the Iapetus Suture (IS) and Aran-Waterford Line (AWL); and, in contrast, the interpreted location of the suture (IS\*) and the coincident Silvermines-Navan Fault (SNF) according to Collinson and Elliott (1991).

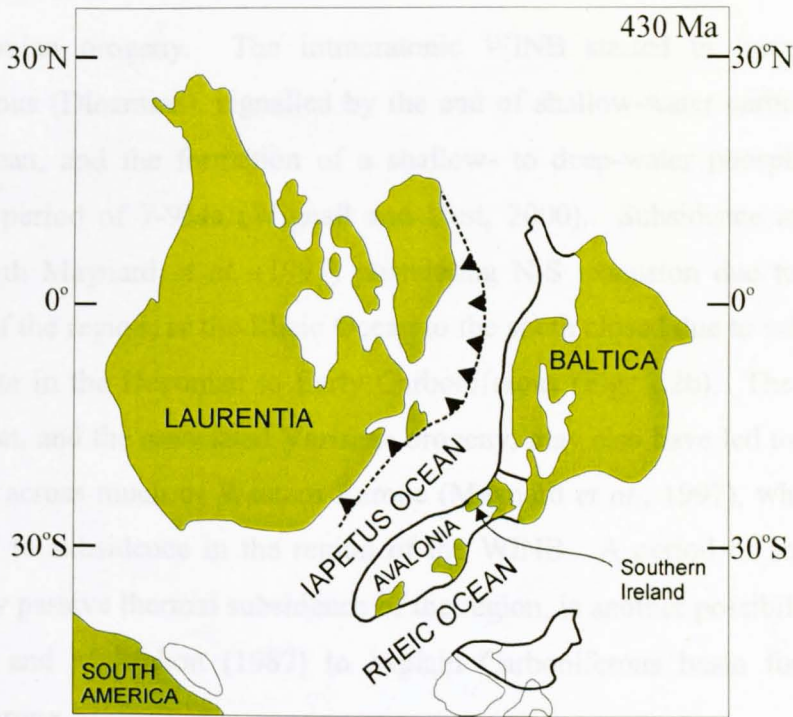


Figure 2.2a. The position of southern Ireland (part of Avalonia) with respect to Laurentia and the Iapetus and Rheic Oceans during the Early Silurian. At 430Ma the Iapetus Ocean was still significantly open. Modified from Windley, 1995.

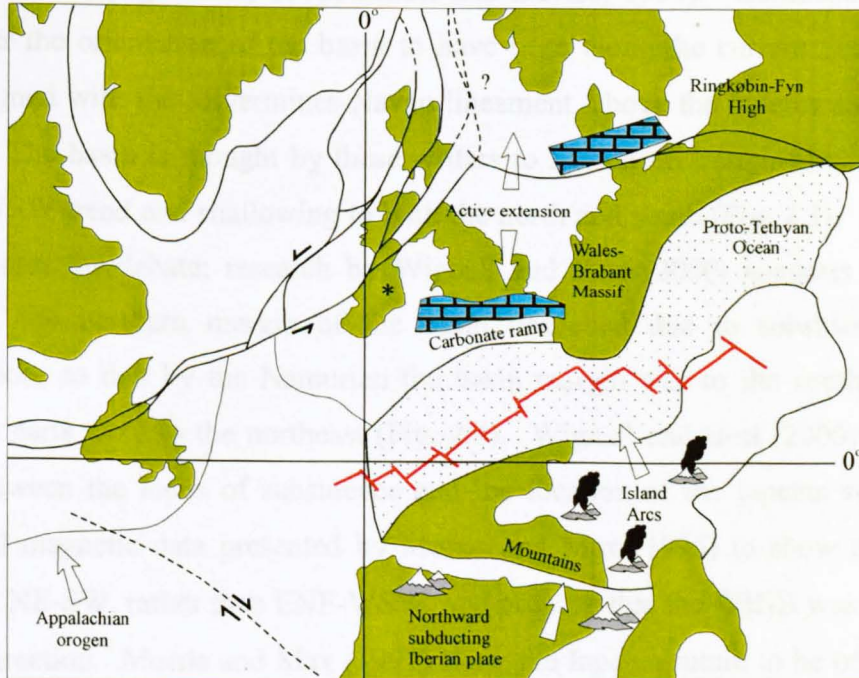


Figure 2.2b. The position of southern Ireland (marked \*) with respect to the rest of northwestern Europe and the opening Proto-Tethys during the Early Carboniferous (Tournaisian, 354Ma). Thick black lines show plate boundaries, red lines show rift margins, large arrows show plate movements and small paired arrows show relative movements at plate boundaries. Green areas represent present-day landmasses as they existed in the Tournaisian. Carbonate ramps in blue. Modified from Maynard *et al.*, 1997.

the Caledonian orogeny. The intracratonic WINB started to form in the Early Carboniferous (Dinantian), signalled by the end of shallow-water carbonate formation in the Visean, and the formation of a shallow- to deep-water phosphatic layer that spanned a period of 7-9Ma (Wignall and Best, 2000). Subsidence mechanisms are unclear, with Maynard *et al.* (1997) postulating N-S extension due to the westward extrusion of the region, as the Rheic Ocean to the south closed due to subduction of the Iberian Plate in the Devonian to Early Carboniferous (Fig. 2.2b). The closure of the Rheic Ocean, and the associated Variscan orogeny, may also have led to foreland basin subsidence across much of Western Europe (Maynard *et al.*, 1997), which could have contributed to subsidence in the region of the WINB. A period of active extension, followed by passive thermal subsidence of the region, is another possibility put forward by Leeder and McMahon (1987) to explain Carboniferous basin formation across Western Europe.

Whatever the mechanism, the location and orientation of basin subsidence are considered by most researchers to be influenced by a structural trend coincident with the Iapetus suture (e.g. Rider, 1978; Elliott and Davies, 1994). Collinson *et al.* (1989) consider the orientation of the basin to have been along the current Shannon Estuary and aligned with the Silvermines-Navan lineament, above the Iapetus suture (Fig. 2.1, inset). The basin is thought by these writers to have been trough-like, elongate in an ENE-WSW trend and shallowing to both the north and south (Fig. 2.3). However, this is a matter for debate; research by Wignall and Best (2000) suggests that after the Visean, the northern margin of the basin deepened due to subsidence and non-deposition, so that by the Namurian the basin margin was to the southwest, and the deepest parts were to the northeast (Fig. 2.4). Wignall and Best (2000) also favour a link between the locus of subsidence and the location of the Iapetus suture, but cite regional magnetic data presented by Morris and Max (1995) to show that the suture trended NE-SW, rather than ENE-WSW, and propose that the WINB was aligned in the same direction. Morris and Max (1995) show the Iapetus suture to be offset by strike-slip movement on the Aran-Waterford line (Fig. 2.1, inset), the location of which coincides with the northernmost extent of the Ross Sandstone (one of the depositional units within the basin-fill; see Section 2.2.3.2), suggesting that the Aran-Waterford line may also have played a role in defining the extent of the basin.

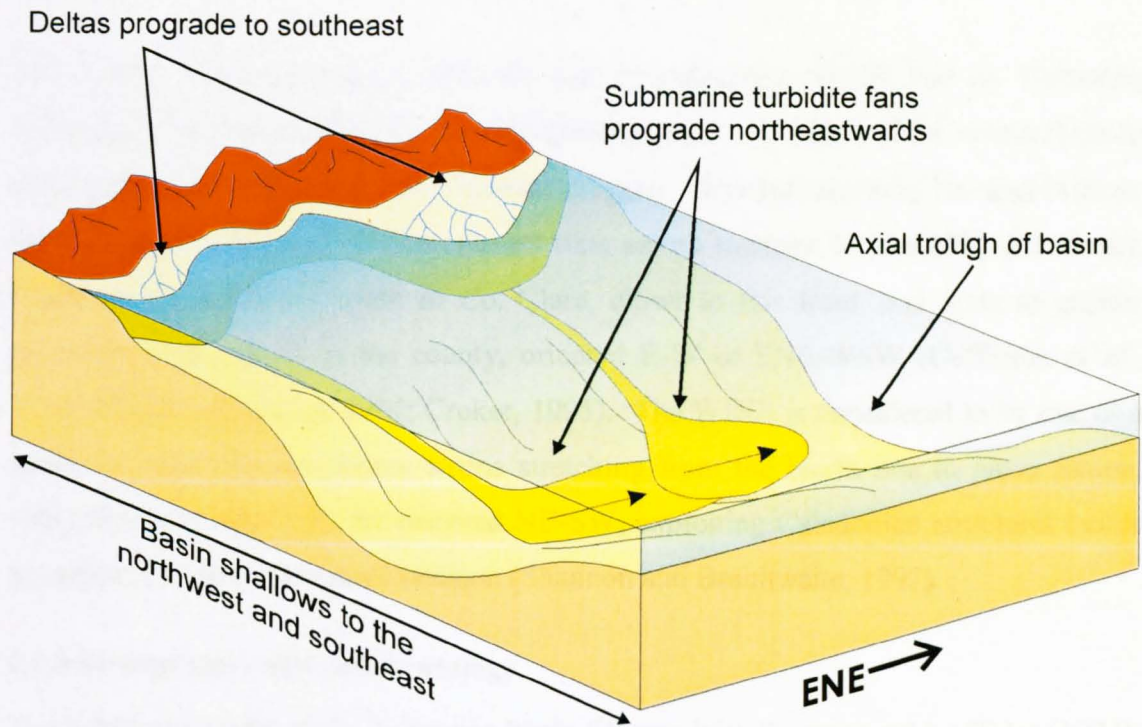


Figure 2.3. Schematic block diagram of the WINB model accepted by Collinson *et al.* (1991), showing the orientation of the coastline with respect to the trough-like basin depocentre, the east-northeasterly axial progradation direction of the submarine fan system, and the predominantly southeasterly direction of slope and delta progradation. Collinson *et al.* consider this basin geometry to have prevailed throughout the Namurian.

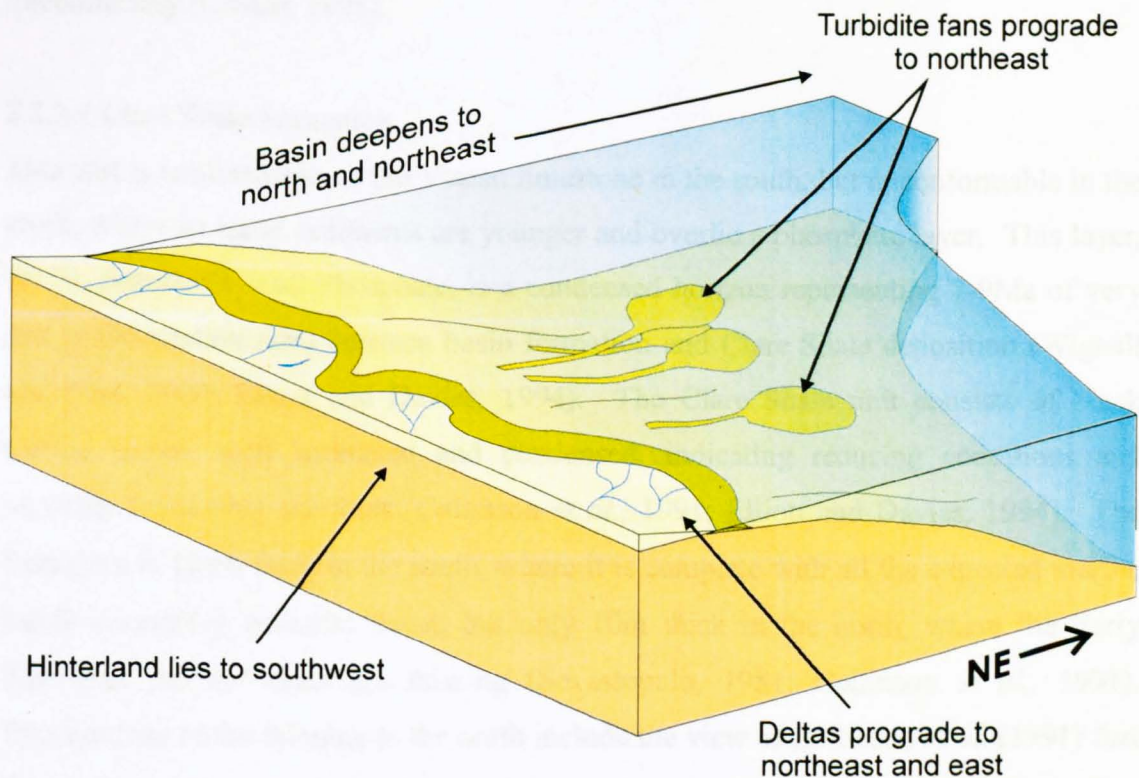


Figure 2.4. Schematic block diagram depicting the WINB model proposed by Wignall and Best (2000), showing NW-SE orientation of coastline with respect to the basinal depocentre and progradation direction of the submarine fan/slope/delta system. Note the differing basin geometry compared with the Collinson *et al.* model in Fig. 2.3.

The southern part of what is now Ireland, including the WINB and its Namurian sedimentary fill, was folded in the Westphalian as it was affected by compressional deformation associated with the Variscan orogeny. The line marking the approximate northerly limit of major Variscan thrusts runs across southern Ireland (Fig. 2.1, inset). Folds are tighter in the south of Co. Clare, closer to this front, and open to gentler structures in the north of the county, oriented E-W or ENE-WSW (Collinson *et al.*, 1989; Elliott and Davies, 1994; Croker, 1995). The WINB is considered to be one of a series of linked Carboniferous basins stretching from the North Sea to Nova Scotia. Other basins in the chain are oriented NE-SW, exploiting Caledonian structural trends in response to post-Variscan extension (Shannon and Braithwaite, 1997).

### 2.2.3 Stratigraphy and sedimentology

The lithostratigraphy of the Namurian basin fill was initially proposed by Rider (1974); it comprises the Shannon Group, subdivided into the Clare Shale, Ross and Gull Island Formations, and the Central Clare Group, represented by five deltaic sequences or cyclothems (Fig. 2.5). The substrate upon which these sediments were deposited is Visean shallow-water limestone, which was partially eroded to give a minor unconformity (Croker, 1995).

#### 2.2.3.1 Clare Shale Formation

This unit is conformable on the Visean limestone in the south, but unconformable in the north, where its basal sediments are younger and overlie a phosphate layer. This layer, the St. Brendan's Well Phosphate, is a condensed horizon representing 7-9Ma of very low sedimentation rates between basin formation and Clare Shale deposition (Wignall and Best, 2000; Elliott and Davies, 1994). The Clare Shale unit consists of black marine shales, well laminated and condensed, indicating reducing conditions and probable fluctuating salinities (Collinson *et al.*, 1991; Elliott and Davies, 1994). The formation is 180m thick in the south, where it is complete with all the expected marine bands containing goniatite fauna, but only 10m thick in the north, where the Early Namurian marine bands are missing (Sevastopulo, 1981; Collinson *et al.*, 1991). Explanations of the thinning to the north include the view of Collinson *et al.* (1991) that the northern region was part of the shallow northern margin of the ENE-WSW trending WINB trough, the shallow depth giving a thinner succession and the elevation leading to sand starvation. The alternative view (Wignall and Best, 2000) is that the northern

area was in fact the deeper part of the basin, leading to coarse sediment starvation due to increased distance from source to the south or southeast (compare Figs 2.3 and 2.4).

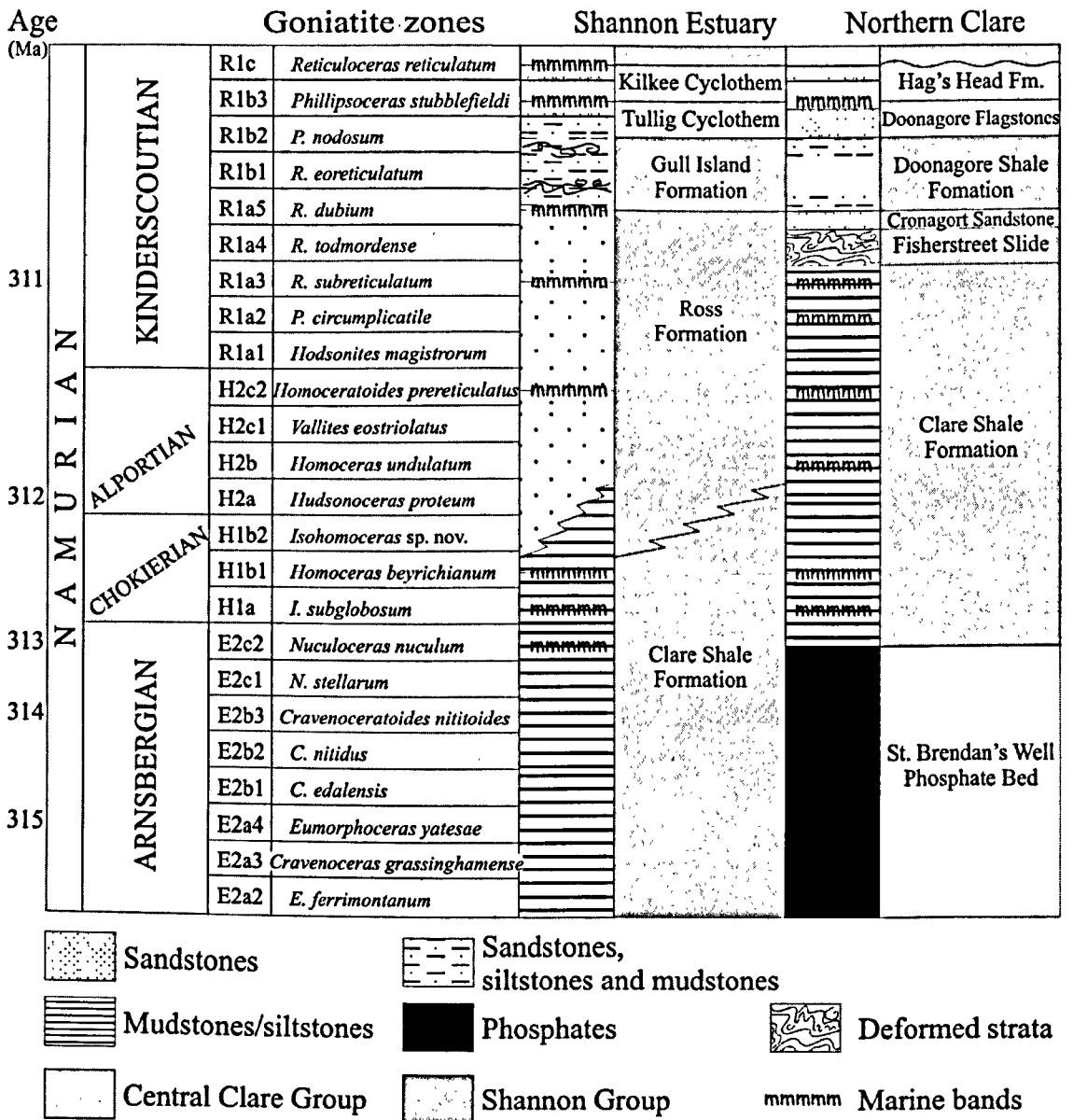


Fig. 2.5. Comparison of Namurian lithostratigraphy and goniatite biostratigraphy of north and south County Clare (after Hodson and Lewarne, 1961).

### 2.2.3.2 Ross Sandstone Formation

This formation comprises deep marine turbidites deposited by flows from multiple shifting point sources (Rider, 1969; Collinson *et al.*, 1991; Chapin *et al.*, 1994; e.g. Figs 2.3 and 2.4). The formation is thickest (380-400m) in the southwest of County Clare, and extends as far as Fisherstreet Bay to the northeast (Fig. 2.1), where the Cronagort

Sandstones and Fisherstreet Slide (Fig. 2.5) show similar characteristics to, and are thus interpreted as equivalent to, the top of the Ross Formation (Wignall and Best, 2000). The Ross Sandstone comprises sheet-like turbidite sands (centimetres to metres thick), incised channelised sandbodies up to 10m thick and interbedded thin silty mudstones and shales that progressively onlap the Clare Shale (Wignall and Best, 2000). The lowest 50m of the formation see an increase in frequency and thickness of sand sheets while the upper section exhibits more channels and slumps (Elliott and Davies, 1994). Palaeocurrents show that flow was directed mainly to the northeast (Elliott and Davies, 1994; Chapin *et al.*, 1994; Wignall and Best, 2000) although it appears to swing round towards the northwest and southeast at the base and top of the formation respectively (Collinson *et al.*, 1991). The overall palaeocurrent trend is believed by some to indicate deposition along the axial zone of the proposed ENE-WSW trending WINB (Elliott and Davies, 1994), although this implies some element of up-slope movement for the NE- and NW-directed turbidites. The formation is entirely absent to the north of the basin, beyond Fisherstreet Bay, which Wignall and Best (2000) take to indicate that flow was towards the NE but that the turbidites did not reach the further limits of the basin envisaged in their model (Fig. 2.3).

#### 2.2.3.3 Gull Island Formation

This formation marks the passage from deep marine turbidites to the finer-grained deposits of an unstable slope prograding into the basin. There is no apparent evidence for any long-lived feeder channel or canyon; instead the slope appears to have been crossed by many small turbidite channels, supporting the idea of Collinson *et al.* (1991) of multiple point sources for the preceding Ross Formation. The Gull Island Formation is 550m thick in the south, and comprises laterally persistent sand sheets less than 1m thick in packages up to 15m thick. This sheeted, sandy, facies accounts for 25-50% of the formation thickness (Wignall and Best, 2000). In the north of the basin, however, the formation is only 130m thick, less than a quarter of its thickness in the south (Elliott and Davies, 1994). Collinson *et al.* (1991) and others invoke a greater subsidence rate in the south of the basin to explain this difference. The basin geometry of the Wignall and Best model (2000) provides an alternative explanation, since only thin distal deposits would be found in the north.

The Gull Island Formation is exceptional for its extensive soft sediment deformation, with estimates of 70% (Elliott and Davies, 1994) and 75% (Wignall and Best, 2000) of the formation being deformed. The lower two-thirds exhibit mostly slumps and slides, whereas in the upper third deformation is more commonly expressed as growth faults. The palaeoslope is held to be to the ESE or SE by Collinson *et al.* (1991) and Elliott and Davies (1994). Both groups, however, agree that palaeocurrents are directed towards the northeast in lower parts, only swinging round to the southeast in the upper parts of the formation. Wignall and Best (2000) show evidence of similar northeasterly current directions throughout the formation; they also suggest that the location of the cited southeasterly palaeocurrents, immediately above major slumps, reduces their validity as representative of the entire formation.

#### 2.2.3.4 Central Clare Group deltaic deposits

These cyclic sedimentary sequences record a succession of prograding deltas (e.g. Pulham, 1987). Each coarsening-up succession comprises prodelta fines and mouthbar or interdistributary bay deposits, and each culminates in an erosively based fluvial sandstone body up to 40m thick and 30+km wide (Collinson *et al.*, 1991; Elliott and Davies, 1994; Shannon and Braithwaite, 1997; Wignall and Best, 2000). Each cycle is considered to span a time-period in the order of 100ka, controlled by glacio-eustatic sea-level changes linked to Milankovitch eccentricity cycles (Collier *et al.*, 1990; Hampson *et al.*, 1997). The cyclothem durations may even have been as short as 65ka (Riley *et al.*, 1994). The total thickness of the Central Clare Group is a maximum of 900m, 70-80% of which is fine-grained mud to silt, the rest being fine to medium sand (Elliott and Davies, 1994) showing strong compaction and cementation. The erosion surfaces at the base of the sandbodies are of a composite nature, depths of individual channels being up to 8m (Wignall and Best, 2000).

Early work on the Central Clare Group (e.g. Hodson, 1954; Hodson and Lewarne, 1961; Rider 1974, 1978) referred to division of the sediments into cyclothem; these repeating sedimentary cycles were delimited using goniatite-bearing marine bands, which represent sea-level highstands when the basin was fully marine. There are five such cyclothem, from oldest to youngest: The Tullig, the Kilkee, the Doonlicky and two thinner un-named Late Namurian cyclothem. Subsequent work (e.g. Hampson *et al.*, 1997; Elliott and Davies, 1994; Davies and Elliott, 1996) has reinterpreted the

succession within a sequence stratigraphic framework, defining the cycles by sequence boundaries – erosional and correlative non-erosional surfaces that divide one set of genetically linked strata from another. The sequence stratigraphic approach reinterprets the Central Clare Group sandbodies, previously thought to be distributary-type sandbodies linked to the sediments beneath them, as genetically unrelated to the sediments they erode. According to the sequence stratigraphic model, the sandbodies, deposited over erosional surfaces interpreted as sequence boundaries, represent the fill of incised valleys created during a marked basinward shift of the fluvial system in response to falling relative sea-level. However, the original cyclothem-based model still has its proponents, including Wignall and Best (2000) who interpret the sandbodies as deposits of the deltaic distributary system and therefore an integral part of the delta top sedimentary succession. The main points of the two models are presented, together with a summary of the supporting evidence, in Table 2.1.

The palaeocurrent data from the Central Clare Group is varied. Each deltaic sequence exhibits a different pattern of flow directions, leading to differing opinions on the overall progradation direction of the delta. Elliott and Davies (1994) cite southeast- or easterly-directed currents, seen for example in the fluvial deposits of the Kilkee Cyclothem, to support progradation in this direction (i.e. from the shallow, northwestern margin of their envisaged basin to the deeper ENE-WSW trending central trough - Fig. 2.3). In contrast, Wignall and Best (2000) find that the majority of palaeocurrent data shows flow from the south or southwest (for example in the Tullig Cyclothem), indicating northeastward progradation towards what, in their model, would be the deeper parts of the basin to the northeast (Fig. 2.4). The earlier work of Pulham (1987, 1989) shows that the Tullig fluvial sandbody, at the top of the first deltaic cyclothem, exhibits palaeocurrents almost entirely directed to the northeast.

The mouthbars of the Tullig Cyclothem, which are fluvial-dominated and wave-influenced with no evidence of tidal processes, show an ENE current direction with a subordinate NE trend (Pulham, 1987). The Kilkee Cyclothem fluvial sandbody, however, shows a prevailing southeasterly flow direction, while the Kilkee mouthbars indicate flow to the east and southeast (Pulham, 1987). For the Doonlicky Cyclothem, palaeocurrents from mouthbars range from northeast to southeast, the latter being the preferential direction, but associated syn-sedimentary faults are downthrown to the

northeast. From this available palaeocurrent and structural data it appears that the delta was prograding to the northeast, east *and* southeast, although not necessarily in all three directions at once. This may be a reasonable conclusion, since individual channels within a delta system may enter the basin at a variety of angles to the general shoreline trend, and different deltaic lobes can build in different directions - a process seen in many present-day deltas such as the Mississippi.

Table 2.1. Field evidence from the County Clare fluvio-deltaic sediments, and implications for the two main models of sandbody formation.

Field evidence	Hampson <i>et al.</i> (1997)	Wignall and Best (2000)
Sediments incised by erosively based sandbodies are mouthbar and interdistributary bay sediments, the usual precursors to delta top fluvial environments (Pulham, 1989).	Evidence queries claim that sandbodies incise unrelated sediments.	Evidence supports claim that sandbodies are genetically linked to underlying deposits.
Laterally equivalent facies to sandbodies (not including Tullig Sandstone) include interdistributary bay deposits (Pulham, 1989).	Queries claim that fluvial channels were formed by marked basinward facies shift.	Supports claim that fluvial channels were part of delta top distributary network.
Channels are multistorey and multilateral to south, but single storey and smaller to north.	Explained by higher subsidence rates to the south, agreeing with Pulham's idea that slow subsidence leads to stable, single channels but rapid subsidence creates multistorey sandbodies.	Supports theory of N/NEward progradation, since single and multistorey channels usually belong to lower and upper delta plain respectively (Horne <i>et al.</i> , 1978).
Depth of individual erosion surfaces averages 6-10 m; overall depth >30 m in parts (Pulham, 1989).	Explained as transgressive systems tract channelised infill of incised river valleys created at sea-level lowstand.	Explained as autocyclic delta top erosion by fluvial channels (cf. Best and Ashworth, 1997).
Carboniferous known to be period of glacio-eustasy (e.g. Caputo and Crowell, 1985; Windley, 1995).	Sea-level change incorporated as important part of cyclical sedimentation, and cause of incision.	Sea-level change not considered to be an important factor in fluvio-deltaic incision.
Local palaeosol development (e.g. Doonlicky sequence, Spanish Point; Davies and Elliott, 1996).	Occurrence of these palaeosols at levels apparently equivalent to sandbodies cited as confirmation of allocyclic incision.	Localised nature of palaeosols, plus their immaturity in Tullig and Kilkee sequences, cited as evidence against allocyclic incision.

Wave ripples, common in the more proximal mouthbar deposits of the deltaics, show a NE-SW crest-line orientation; waves could have approached from either the northwest or southeast (e.g. Pulham, 1989). While this would give an unremarkable high angle between the wave approach direction and the coastline as envisaged by Elliott and Davies (1994), it would mean a wave approach almost parallel to the coastline in Wignall and Best's model, which is more unusual. However, refraction of waves in the shallow water of a delta front commonly causes a wide range of wave approach directions, particularly as the delta projects from the coastline and changes the local profile of the coast, so this observation does not provide conclusive evidence of the main coastline orientation.

#### **2.2.4 Deformation**

The lowermost formation exhibiting deformation is the Ross Sandstone. Major slide sheets are seen in the turbidite intervals, for example the Ross Slide (more correctly identified as a slump – Strachan, 2002) and the Fisherstreet Slide. Both are 2-8.5m thick, dominated by muds but including sandstones, and are extensively deformed. Both slides show structures indicative of NE- to ENE-directed movement (Gill 1979; Collinson *et al.*, 1989, Strachan, 2002), which does not support the assertion made by Elliott and Davies (1994) and others that the slope direction is towards the southeast. However, neither does it rule it out entirely, since a delta is a three-dimensional feature that will have slopes facing in more than one direction, although evidence of other movement directions has not been found.

The deformation present in the Gull Island Formation is most commonly in the form of mud slumps and slides. The slumps can be up to 15m thick, either tabular or lenticular, and with considerable internal deformation including folding, faults and shear zones (Collinson *et al.*, 1991). There is no consensus of opinion on the predominant direction of downslope movement, with Gill (1979) and Collinson *et al.* (1991) suggesting a predominance of ESE to SE indicators, but growth faults in upper levels are commonly downthrown to the north or northwest (Rider, 1978).

Deformation of the deltaic cycles is mainly by growth faulting, according to Rider (1978), with some post-depositional soft sediment faulting, sliding and diapirism (Pulham, 1989; Collinson *et al.*, 1991). Rider (1978) states that faulting was most

active during sand deposition (i.e. in the upper parts of each cyclothem), and that most faults are downthrown to the northeast, with some to the WNW. More recent work by Wignall and Best (in press) highlights a series of large-scale northeast-directed growth faults affecting the Kilkee Cyclothem to the north of Liscannor Bay (Fig. 2.1). These growth faults formed in a retrogressive pattern, stepping progressively to the southwest (interpreted as landward by the authors) over time. Similar fault patterns are documented in deltas today (e.g. Hampton *et al.*, 1996), where the direction of throw is coincident with the slope and progradation direction: This evidence supports Wignall and Best's interpretation, and agrees with their basin model (Wignall and Best, 2000), with the system prograding from the southwest towards the distal parts of the basin in the northeast (Fig. 2.4).

### **2.2.5 The Tullig, Kilkee and Doonlicky Sandstone Members**

These sandbodies occur at the tops of the first, second and third progradational deltaic cyclothem, or at the bases of the second, third and fourth sequences, if the incised valley sequence stratigraphic model is adopted. This section summarises the individual sedimentological and architectural characteristics of these major sandbodies.

#### **2.2.5.1 The Tullig Sandstone Member**

This sandbody is seen in a number of coastal exposures in Co. Clare, for example at Tullig Point, Killard and Truskieve (Fig. 2.1), and was considered sufficiently extensive and thick to be granted Member status (Rider, 1969). The sandbody was studied by Williams and Soek (1993), who define it as a low sinuosity multistorey and multilateral channel complex, which, according to palaeocurrent data from unidirectional sedimentary structures such as cross bed foresets, flowed to the NNE. The Tullig Sandstone comprises several individual channels which rest on a composite basal erosion surface, and which are stacked to give an overall average thickness of 35m (Pulham, 1987; Elliott and Davies, 1994). However, in the northernmost outcrops at Liscannor, the sandbody is only one storey, and less than 15m thick. The lateral extent of the sandbody is also fairly limited in the Liscannor area, unlike in the south where widths are around 30km (Pulham, 1989). However, the measurement of sandbody width depends on the orientation of the section with respect to the flow direction – a coastal section 30km in extent will be seen as a “width” in Pulham's model, which

interprets channel orientation close to perpendicular to the coastline, but as a downstream distance in models interpreting flow to be to the northeast.

The Tullig Sandstone is erosively based, incising underlying interdistributary bay deposits and mouthbars (Pulham, 1987; Hampson *et al.*, 1997). Conglomeratic lag deposits are found at the bases of individual channels. Such channels are recorded to be 6-10m thick and sometimes up to 15m in thickness, and there is evidence that their basal surfaces are composite, comprising lots of closely spaced crosscutting erosion surfaces separated by thin intraformational conglomerates and sandstones (Pulham, 1987). The implication is that rate of increase of accommodation was slow during this phase of deposition (Hampson *et al.*, 1997). Hampson *et al.* (1997) also note that the spacing of erosion surfaces increases upwards within the sandbody, suggesting an increase in the rate of creation of accommodation space with time. This observation, if correct, may be explained by a rising eustatic sea-level or an increase in subsidence rate.

Pulham (1989) draws the distinction between closely and widely spaced erosion surfaces across different areas rather than different times. Pulham proposes that the north of Co. Clare was the more tectonically stable, with thinner Tullig Sandstone deposits and a dominance of emergent abandonment facies indicating a slow subsidence rate. The south of the county, in contrast, shows the Tullig Sandstone to be a laterally and vertically composite sandbody with only rare signs of emergence (e.g. rootlets) and more frequent signs of submergence (bioturbation, wave ripples). Pulham (1989) therefore concludes that the subsidence rate in the southern area was high. Apart from occasional rootlets and ripples, the channels also exhibit trough cross bedding, and are almost entirely sand filled, with any overbank or floodplain shales or muds having a very low preservation potential. The Tullig Sandstone as a whole is capped by a bioturbated transgressive surface and some finer mouthbar-type deposits before a marine band bearing the goniatite *Phillipsoceras stubblefieldi* marks the maximum flooding surface and onset of the next coarsening-up cyclothem (Fig. 2.5).

#### 2.2.5.2 Kilkee and Doonlicky Sandstone Members

These sandbodies are slightly less extensive than the Tullig Sandstone but exhibit many similar characteristics. The Kilkee channel complex is 20km wide (Collinson and Elliott, 1991) and an average of 30m thick. Palaeocurrent data shows that flow was

from NW to SE, normal to the present coastline (Pulham, 1987). The channel complex fill comprises several individual channels of similar dimensions to those within the Tullig Sandstone, each exhibiting unidirectional trough cross bedding. Again, abandonment facies are seen at the top of the channel facies, prior to the occurrence of two progradational shoreline sequences topped by another marine band representing maximum flooding (Collinson and Elliott, 1991).

The Doonlicky sandbody is significantly smaller in size than the Kilkee and Tullig sandbodies, and as a result is not granted member status. The sandstone is erosively based and shows a lag of mudstone and siltstone intraclasts. The sandbody erodes into the underlying coarsening-up mouthbar facies and is itself around 10-15m thick (Pulham, 1987); it shows wave- and current-generated cross lamination, and, above a second erosion surface, clear easterly palaeocurrents from unidirectional trough cross bedding. Pulham (1987) interprets the sandbody as a distributary channel incising the delta front due to continued progradation of the river mouths. Shallow, delta top conditions did not prevail for long, and are superseded by a transgressive surface and a shallow water progradational sequence representing the delta front. This is then topped by the next marine band, after which two other coarsening-up cycles conclude the Central Clare Group succession.

#### **2.2.6 Summary**

- The WINB was created in the Dinantian (Early Carboniferous) by tectonic movements and north-south extension possibly related to Variscan tectonics, and influenced by pre-existing Caledonian structural trends such as the Iapetus suture.
- The basin-fill is Namurian in age; the stratigraphy includes the Shannon Group, comprising the Clare Shale Formation, Ross Sandstone Formation, and Gull Island Formation, and the Central Clare Group, comprising the Tullig, Kilkee and Doonlicky Cyclothems and two other un-named cycles. The stratigraphy as a whole represents a prograding shelf, with the succession changing from deep basinal shales through turbidites and deformed slope sediments to deltaic and finally fluvial deposits.
- There are two main models for the geometry and fill of the basin. One, originally suggested by Hodson and Lewarne (1961), sees an ENE-WSW elongate trough being filled with sediments sourced in the northwest. Transport is thought to have

been dominantly to the southeast, with subordinate axial trends. The thicker section in the south of County Clare is attributed to faster subsidence rates along the trough axis, while the thinner deposits in the north are seen as those of a starved shelf. The alternative model, advocated by Wignall and Best (2000), sees the basin as deepening to the northeast and filling with sediments from the southwest. The thin northern sediments become distal deposits of a deep marine basin, while the thicker southern section corresponds to the subsiding margin of a landmass to the southwest.

- The sandbodies seen in the deltaic sequences (or cyclothems) are fluvial in origin, but there is a difference of opinion as to their process of formation. While the majority of researchers (e.g. Rider, 1974; Pulham, 1989; Wignall and Best, 2000) believe them to be an integral part of a delta top system, representing incision and fill of distributary channels, others see them in a sequence stratigraphic context as incised valley fills, the incision being due to falling relative sea-level (e.g. Hampson *et al.*, 1997).

## **2.3 The Nile Delta: initiation and evolution**

### **2.3.1 Introduction**

The Nile Delta is a major morphological feature in the southeastern Mediterranean, on the continental shelf of the African Plate. While local and regional tectonics have played an important role in the evolution of the delta, the main controlling factors have been sea-level and climate. Fluctuations in these factors have combined to alter the hydrological regime of the Nile River and its precursors and hence affect deltaic depositional patterns.

The delta region exhibits a stratigraphic succession which has been sampled by coring to depths of Middle Miocene age and which consists of three major sedimentary cycles; Miocene, Plio-Pleistocene and Holocene. The first fluvio-deltaic sediments were deposited in the Late Miocene, as the Nile Valley (Fig. 2.6) was cut by the Eonile (Said, 1981). The main phase of delta progradation was during the Late Pliocene and Pleistocene, while the Holocene saw aggradation and establishment of the present-day hydrological regime of the Nile.

The delta area has become the focus of exploration for hydrocarbon reserves, and gas in particular, sourced from several possible intervals in the Cretaceous, Jurassic, Oligocene, Miocene and Pliocene (Kamel *et al.*, 1998; Cowan *et al.*, 1998). Much of the stratigraphic information on the area comes from wells drilled for exploration purposes, and sands of Pliocene and Pleistocene age have proved to be excellent reservoirs for large gas accumulations.

### **2.3.2 Present-day delta morphology**

The Nile River is 6,690km long, drains 2,880,000km<sup>2</sup>, and, before damming in 1964, had an average annual discharge of 84 billion m<sup>3</sup> (Hurst, 1931-1966), carrying 160 million tonnes of sediment per year (Quelennec and Kruk, 1976). This huge sediment load has formed the Nile Delta (Fig. 2.6), which is situated at the mouth of the river, forming an arcuate length of coastline that stretches for about 285km from west of Alexandria to east of Port Said in North Sinai (Wells and Coleman, 1984). The delta tapers classically to a point about 200km inland, and covers over 22,000km<sup>2</sup> (Bellaiche and Mart, 1995). The delta is divided into three regions by its two currently active

distributaries, the Rosetta branch in the west and the Damietta branch in the east. The delta top and front can be regarded in terms of the following provinces (Sestini, 1989):

- 1) upper (abandoned) delta plain, with channel-interchannel fluvial deposition;
- 2) lower (active) delta plain, including lagoon belt and transitional elements;
- 3) delta front and beach dune complex shaped by coastal currents.

Within the upper delta area, the two active distributaries have created well-developed meander belts 3-4km wide, reflecting the very low slope of the delta (the land is only 18m above sea-level at Cairo, 150km south of the coast (Sestini, 1989)). In contrast, the lower delta plain is dominated by coastal lakes, shallow lagoons and salt pans. The morphology of the delta front is controlled by river and wave influence; tides in the area are insignificant, the tidal range being only 0.45m (Wells and Coleman, 1984). Fluvial and wave processes, combined with the action of longshore coastal currents from west to east, have created a 400km long coastal barrier complex comprising the beach zone, backshore plains and dunes, and the sub-deltas of Rosetta and Damietta. Offshore, the delta extends across the narrow (15 to 50km) continental shelf and slope, with Nile-derived clastic sediments being found as far as 270km away on the southern flanks of the Mediterranean Ridge to the north, and on the continental shelf of Israel to the east (Gvirtzman *et al.*, 1997). These distal sediments are part of the Nile Cone, a deep sea fan complex that covers more than 140,000km<sup>2</sup> (Fig. 2.6). The development of the Nile Cone, and evolution of the delta itself, has been controlled by tectonics and the hydrological/climatic regime of the region.

### 2.3.3 Tectonic setting

The Nile Delta lies on the northern margin of the African Plate, in a zone characterised by long-term tectonic stability (Bellaiche and Mart, 1995). The delta is situated on continental crust that thins progressively basinward – from 27km thick on the continental rise (Lort, 1973) to 24km in the Herodotus abyssal plain (Malovitskiy *et al.* 1975; see Fig 2.6 for location). According to Garfunkel and Derin (1984), the area has been a transition zone between land and sea since the Permian, and part of the Tethyan divergent margin since the Cretaceous (Bellaiche and Mart, 1995). However, post-Palaeogene tectonics have had an effect on regional structure. Two sets of faults, active since the Miocene, cut the Levantine Basin and its margins, trending WNW-ESE and

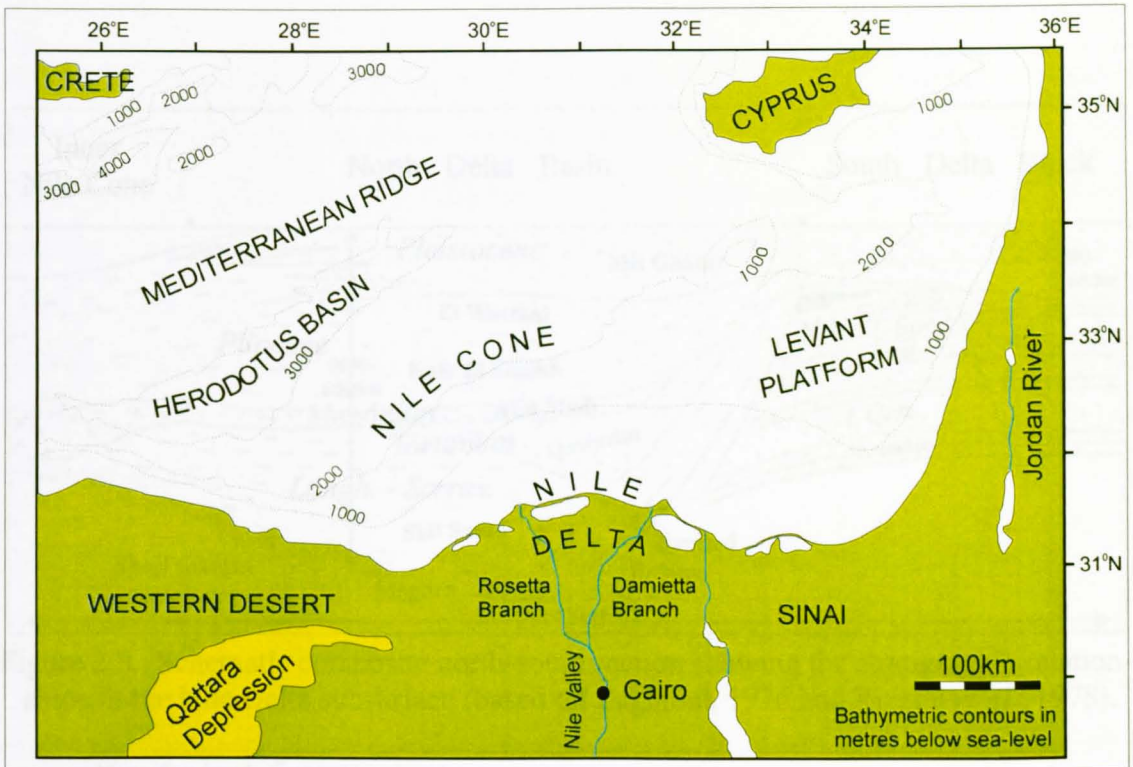


Figure 2.6. Principal geographic and bathymetric features of the Nile Delta and Cone region (after Sestini, 1989).

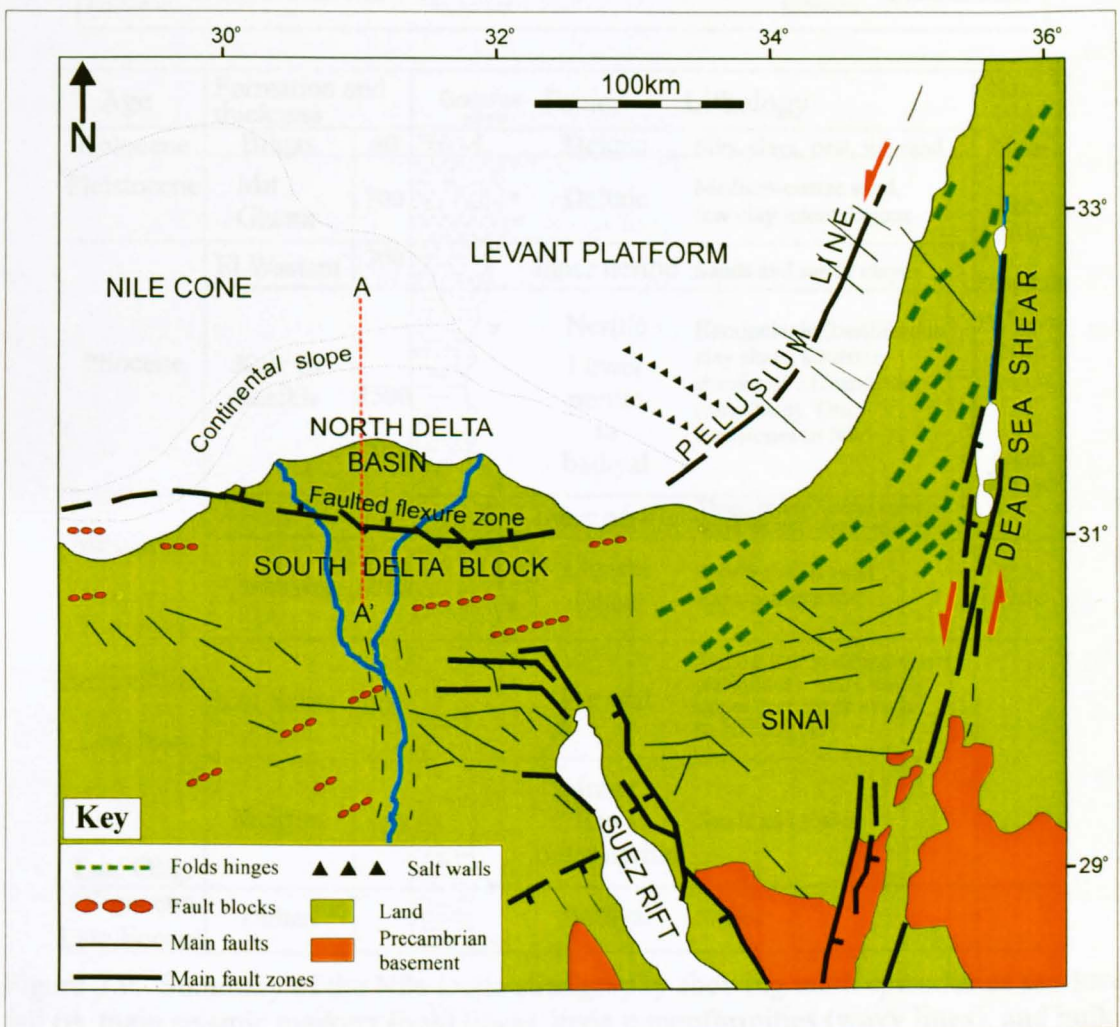


Figure 2.7. Principal structures and tectonic regions of NE Egypt and the SE Mediterranean (after Sestini, 1989). A to A' indicates approximate cross-section line of Fig. 2.8.

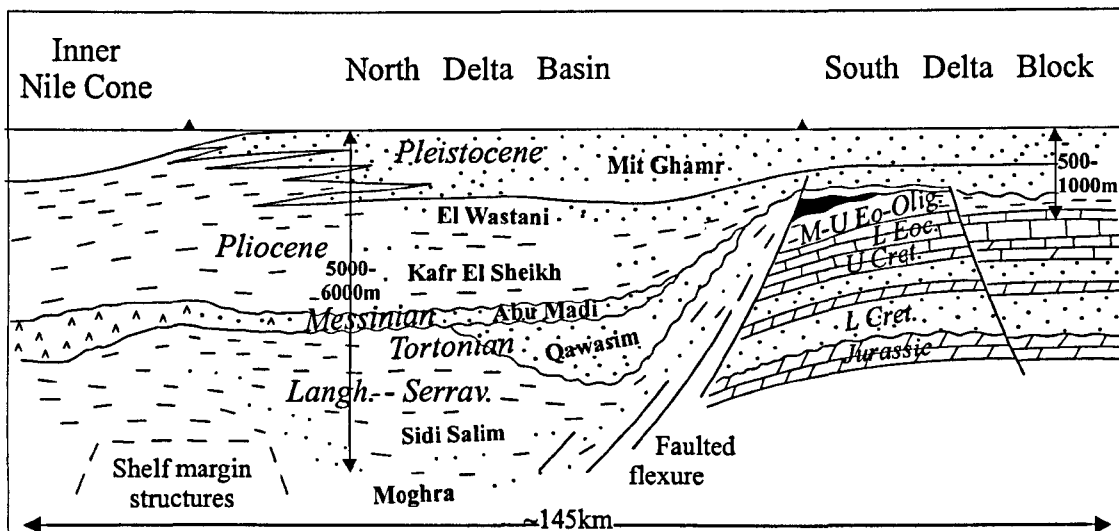
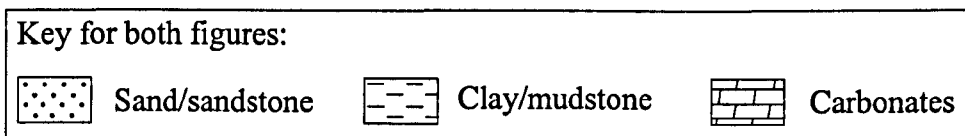


Figure 2.8. Schematic composite north-south section showing the stratigraphic relationships in the Nile Delta subsurface (based on Zaghloul, 1976 and Rizzini *et al.*, 1978).



Age	Formation and thickness	Grainsize abcd	Facies - Lithology	Said, 1981
Holocene	Bilqas	40	Deltaic Silts, clays, peat, v.f. sand	Neo-
Pleistocene	Mit Ghamr	700	Deltaic Medium-coarse sand, few clay intercalations	Pre-Nile
Pliocene	El Wastani	300	Inner neritic Sands and sandy clays	Proto-Nile
	Kafr El Sheikh	1500	Neritic Lower neritic to bathyal Hemipelagic fossiliferous clay shale, siltstone, streaks of v.f. sandstone (turbidites). Thin limestones in NW	Palaeo-Nile
Messinian	Abu Madi	300	Inner neritic Thick sands, some conglomerates and shale interbeds	Gulf Phase
	Qawasim	>700	Littoral deltaic Poorly sorted sand and conglomerate	
Tortonian				
Serravallian	Sidi Salim	700	Bathyal Shales, few sand interbeds, (turbidites), more sandy upper part, more sandy to NE and NW	
Langhian				
Late Olig.	Moghra	500	Inner to outer neritic Sands and shales	
Oligocene				
Late Eocene	Dabaa		Bathyal Shales	

Figure 2.9. Summary of the Nile Delta stratigraphy showing main episodes of sea-level fall (▼), main seismic markers (bold lines), main unconformities (wavy lines), and bulk grain sizes (a, clay; b, silt; c, fine-medium sand; d, coarse sand). The various stages of the Nile River evolution as named by Said (1981) are also shown (after Sestini, 1989).

NNE-SSW (Sestini, 1984; see Fig. 2.7). A major east-west zone of faulting and flexure occurs at around 31°N and divides the delta into the South Delta Block and the North Delta Basin (Figs 2.7 and 2.8). The downthrow on these normal faults is to the north, resulting in a sediment thickness change within the Tertiary from 500-1000m in the south to 5000-6000m in the north (Sestini, 1989). The faulting here and in the vicinity relates to the tensional regime set up by the Gulf of Suez rifting; uplift inland around Cairo and Sinai was balanced by extensional tectonics further north and across the continental shelf.

#### 2.3.4 Delta initiation

The coastal sequence of Egypt exhibits a thick Cenozoic sedimentary pile of Eocene to Recent ages (Figs 2.8 and 2.9). The Early Miocene was the first Tertiary epoch to see deltaic sedimentation relating to drainage from Egypt by an ancestral Nile. The Moghra Formation, comprising deltaic sands and clays, formed to the west and southwest of the present delta (Salem, 1976) and its clastic sediments are exposed at the northern margin of the Qattara Depression (Sestini, 1984). Deposition of the Moghra Formation was related to the Late Oligocene to Early Miocene Qattara-Moghra regression. Subsequent transgression due to global sea-level rise led to the deposition of deeper water facies during the Early to Middle Miocene - the 700m thick Sidi Salim Formation, comprising clays, infrequent marls and rare sandstones and siltstones (Rizzini *et al.*, 1978). The Flexure Zone separating the North Basin from the South Delta Block was active by this time.

The upper limit of the Sidi Salim Formation is marked by an unconformity and a switch to thick, sandy conglomerates of the overlying Late Miocene Qawasim Formation (Zaghloul *et al.*, 1977). These coarse deltaic clastic sediments are over 900m thick in the eastern part of the North Basin. Their sudden appearance is thought to reflect a base-level fall combined with a short (Serravallian to Tortonian) phase of tectonism that resulted in uplift of the Gulf of Suez margin, the Western Desert and the area to the south-east of Cairo, and a regional eastward tilt (Ross and Uchupi, 1977). This tectonic movement led to a change in the course of the ancestral Nile, which migrated eastwards to take up a route very similar to that seen today, between the uplifted areas (Salem, 1976). This first phase of the Nile's history (6.0 – 5.4Ma BP) is referred to as the Eonile period (Said, 1981; see Fig. 2.9).

The Qawasim Formation, comprising thick sands, sandstones, and conglomerates, with occasional interbedded clays, exhibits large and rather steep deltaic foresets, which are badly disturbed by gravity tectonics (Rizzini *et al.*, 1978). The steep angle and deformation suggest rapid deposition. Rizzini *et al.* (1978) believe that the switching of the Nile's course would not solely account for such a large sediment volume and such swift deposition, and they invoke a significant sea-level fall to explain the Qawasim sediments. This theory of sea-level fall agrees well with the generally accepted model of desiccation of the Mediterranean basin during the Messinian (late Miocene). The basin was almost as deep as it is today and, due to its separation from the Atlantic, became evaporitic in all but its deepest parts, signifying a fall in sea-level of around 3500m (Said, 1981). Such a pronounced fall led to drastic downcutting of the Eonile through the elevated Tertiary rocks of the Eastern Desert and Egyptian Plateau, eroding down to the crystalline basement (Sestini, 1984). This erosion produced a deeply incised canyon, comparable in scale to the Grand Canyon of Arizona and even deeper in its seaward stretches (seismic data show depths to the canyon floor of 2500m below present sea-level just north of Cairo, and of more than 4000m in the northernmost parts of the South Delta Block (Said, 1993b)). This incised canyon determined the course of the Nile River today, and its erosion provided the coarse clastic sediments of the first phase of the Nile Delta. It is estimated that the Eonile deposited 7000km<sup>3</sup> of sediment in less than 2 million years (Said, 1993a).

### **2.3.5 Delta evolution**

Reconnection of the Mediterranean to the Atlantic heralded the end of the Messinian Salinity Crisis. Rising sea-levels caused the flooding of the newly eroded Nile Valley as far inland as Aswan, 800km south of the present coastline (Chumakov, 1967). This period of the river's history, labelled the Gulf Phase by Said (1981), and lasting from 5.4 – 3.3Ma, is recorded in the delta area by the fining-up Abu Madi Formation. This formation commences with thick fluvial quartzose sands and rare conglomerates, later becoming dominated by increasingly frequent and thick clay interbeds. These clays contain marine fauna of Early Pliocene age. As a whole the Abu Madi Formation records a change from continued deltaic deposition to marine coastal sedimentation (Rizzini *et al.*, 1978). By the start of the overlying Kafr El Sheikh Formation in the Middle Pliocene, the prevailing environment was outer shelf or slope, and saw uniform

deposition of muds and silts with occasional thin interbedded sands (Deibis *et al.*, 1986).

Sea-level began to fall again during the Upper Pliocene (Abu-Ollo and El Kholy, 1992), and fluvial conditions were re-established in the upper reaches of the Nile Valley as the Palaeonile phase commenced (3.3 – 1.8Ma; Said, 1981). The valley was progressively filled with sediments from this river, until the gradient of its long profile was almost as it is today, and the surface of the delta area was level with the top of the South Delta Block (Fig. 2.8). Despite the fact that the Palaeonile was probably sourced locally, from drainage basins within Egypt, (Said, 1993a), the sediments of this river are entirely fine grained, suggesting that the climate must have been very wet and humid to cause such chemical disintegration of the sub-soil. In the delta region, the Upper Pliocene is recorded by the Kafr El Sheikh Formation (Zaghloul *et al.*, 1977), which comprises fluvio-deltaic sands and sandstones with occasional shale interbeds (El Heiny and Morsi, 1992). This formation represents the northward advancement of the delta front and exhibits a coarsening/shallowing-up trend due to the high sedimentation rate (Mosconi *et al.*, 1996; Gezeiry and Shandawily, 1994) – during the Upper Pliocene sediment supply rates exceeded rates of accommodation creation, leading to progradation.

Said (1993a) records that the hot, wet climatic phase of the Upper Pliocene was followed by a hot, dry phase as Egypt entered an arid episode around the Late Pliocene-Early Pleistocene. Between 1.8 – 0.8Ma the Palaeonile dried up and Egypt became a desert. This hyper-arid phase was punctuated by two short wetter episodes, the first of which was sufficiently wet to feed an ephemeral river, which Said (1981) calls the Protonile, and which deposited coarse sands, gravels and cobbles along the river course.

The real breakthrough in delta development came with the establishment of the Prenile, which was the first of the Nile's precursors to have a drainage connection to the central African continent. Sourced in the Ethiopian highlands, fed by the Atbara and the Blue Nile tributaries, the Prenile was able to cross the Nubian massif and meet the Nile Valley course. This breakthrough was related to tectonic movements along the Main Ethiopian Rift (part of the East African Rift), which tilted the region and directed drainage towards the Nile rather than the Red Sea. The result of this massive increase

in discharge was the fluviially dominated Prenile delta, which was deposited across the same area as the present delta, with a shoreline extending over 50km further into the Mediterranean. The total area of the Prenile delta was at least three times that of the modern Nile delta (Said, 1993a).

The initial deposits of the Prenile delta were the thick sands (the sediments are still unconsolidated at the present day) and thin clays of the El Wastani Formation, which exhibit large foresets indicative of deltaic progradation (Rizzini *et al.*, 1978). The main volume of the Prenile delta, however, comprises the Mit Ghamr Formation, which spans the Pleistocene and Early Holocene (El Heiny and Morsi, 1992; Sarhan *et al.*, 1996), and which, though now much reduced in size by erosion, forms the core of the present-day delta. The Mit Ghamr Formation consists of thick layers of sand (quartzose, medium to coarse) and pebbles (quartzite, chert and dolomite) with thin clay interbeds in its lower parts (Rizzini *et al.*, 1978; Deibis *et al.*, 1986; Wigger *et al.*, 1996). These sediments are thought to reflect fluctuation between beach-type and deltaic depositional settings (Zaghloul *et al.*, 1977). The thickness of the Mit Ghamr Formation changes gradually from zero near Cairo to a maximum of 975m at about 60km southwest of Damietta Mouth (Zaghloul *et al.*, 1977). The Mit Ghamr Formation represents the deposition of an estimated 100 million m<sup>3</sup> of sediment per year of the Prenile's life (0.8 - 0.4Ma), which is more than double the depositional rate for the modern Nile (Said, 1993b). The increased load and erosive power of the Prenile river has been attributed to the combination of increased rainfall in the newly-connected source regions of Ethiopia, and several sea-level lowstands related to glacial periods (Sestini, 1989), superimposed on a general fall in sea-level (Haq *et al.*, 1987). The delta was fluviially dominated during the Prenile phase, with subordinate wave influence (Helmy and Fouad, 1994).

Climatic conditions and further tectonic activity in the source region led to the severing of the Ethiopian connection at around 0.4Ma (Said, 1993b). The Prenile period came to an end and the river became less competent and far more dependent on climatic fluctuations. This Neonile period saw three main pluvial episodes, correlating with glacial periods throughout Europe, but the overall effect on the delta was one of degradation. The sediment supply was insufficient to maintain the extensive Prenile delta, and a combination of erosion, subsidence and mass wasting reduced it to smaller than its present volume, although the arcuate shape was retained.

The present incarnation of the Nile as a perennial river deposited the Bilqas Formation as a drape across the delta, signifying an end to the destructive Ne Nile phase but adding only around 35 million tons of sediment annually for about 7 or 8ka (Said, 1993b). The Bilqas Formation covers the entire subaerial delta and its fringes further offshore, having been deposited in a variety of environments on the delta from continental and fluvial to lagoonal and beach (Zaghloul *et al.*, 1977). At its base, the Bilqas Formation comprises thin clays with sand interbeds, abundant peat, and coastal or lagoonal fauna (Rizzini *et al.*, 1978). The rest of the formation comprises fine to medium sands with clay interbeds; the overall maximum thickness is 77m, and the age is Holocene (Zaghloul *et al.*, 1977). The Bilqas Formation forms the present-day surface of the delta, and the upper, exposed parts of this formation are currently being reworked by the existing network of active distributary channels and by beach processes.

### 2.3.6 Hydrocarbon exploration

The Holocene and Recent history of the Nile Delta and Cone have been discussed by numerous researchers (Maldonado and Stanley, 1976; Ross and Uchupi, 1977; Summerhayes *et al.*, 1978; Coleman *et al.*, 1981; Sneh *et al.*, 1986; Coutellier and Stanley, 1987; Said, 1993; Stanley and Warne, 1994; Bellaiche and Mart, 1995; Omran and Fathy, 1997). While Recent delta development is relatively unimportant in terms of delta geology and hydrocarbon potential, the Nile Cone is crucial to the economic importance of the area. The Nile Cone is usually considered to comprise two morphological zones: the eastern fan, dissected by salt ridges (Fig. 2.7) and deformed by halokinesis; and the smooth, uninterrupted, western fan. Seismic stratigraphy has revealed significant marker horizons such as the top and base of the Messinian evaporites, and regional unconformities (Omran and Fathy, 1997). Together with bio- and sequence stratigraphy (Harwood *et al.*, 1998), seismic exploration has led to the discovery of significant volumes of gas in Plio-Pleistocene deltaic and shelf/slope sands (Cowan *et al.*, 1998). The sands are shallow, undercompacted and unconsolidated, making them ideal for observing direct hydrocarbon indicators but challenging for exploration and production (Maddox *et al.*, 1998). Nonetheless, the Nile Delta region and its offshore sedimentological provinces have proved highly valuable hydrocarbon targets.

### **2.3.7 Summary**

- The initiation of the Nile Delta occurred during the Late Miocene due to a combination of tectonic tilting, which caused the Nile River to migrate east, and the lowering of sea-level in the Mediterranean. The Nile Valley was formed, funnelling sediments towards a single coastal outlet and causing the delta to be established.
- The main phase of delta growth was during the Late Pliocene and Pleistocene when the Prenile river delivered sediment from as far away as Ethiopia into the basin. Subsequent Late Pleistocene and Holocene sea-level fluctuations saw the partial destruction of the delta, but the last 7-8ka have marked a change to aggradation.
- The stratigraphy of the delta comprises the sands and conglomerates of the Early Pliocene Abu Madi Formation, the fine-grained transgressive record of the thick Kafr El Sheikh Formation, the thick sandstones of the El Wastani and Mit Ghamr Formations marking the main period of delta construction throughout the Pleistocene, and the thin clays and sands of the Holocene Bilqas Formation.
- Hydrocarbon exploration has focussed mainly on the offshore deposits of the Nile Cone, which incorporates much of the remaining Pleistocene deltaics. Delta-front and slope/fan channel sands have proved excellent reservoirs for gas and the area is one of exciting new developments for the petroleum industry.

## **2.4 The El Wastani play in the Rosetta concession**

### **2.4.1 Introduction**

The Rosetta concession in the offshore Nile Delta (Fig. 2.10) has, in recent years, proved highly productive in exploration terms. Large accumulations of gas have been discovered, and several wells drilled, some of which are currently in production. The play that is being exploited by the newest wells is of Pliocene age, gas being trapped in the stacked reservoir sandstones of the Upper Pliocene El Wastani Formation (Cowan *et al.*, 1998; Fig. 2.11). The trap is both structural and stratigraphic, the seal being provided by interbedded layers of marine mudstones (BG internal report, 1997; Fig. 2.12). This section of the chapter puts the play in its structural and stratigraphic context, and considers the controls on the facies and deposition of the El Wastani reservoir sands.

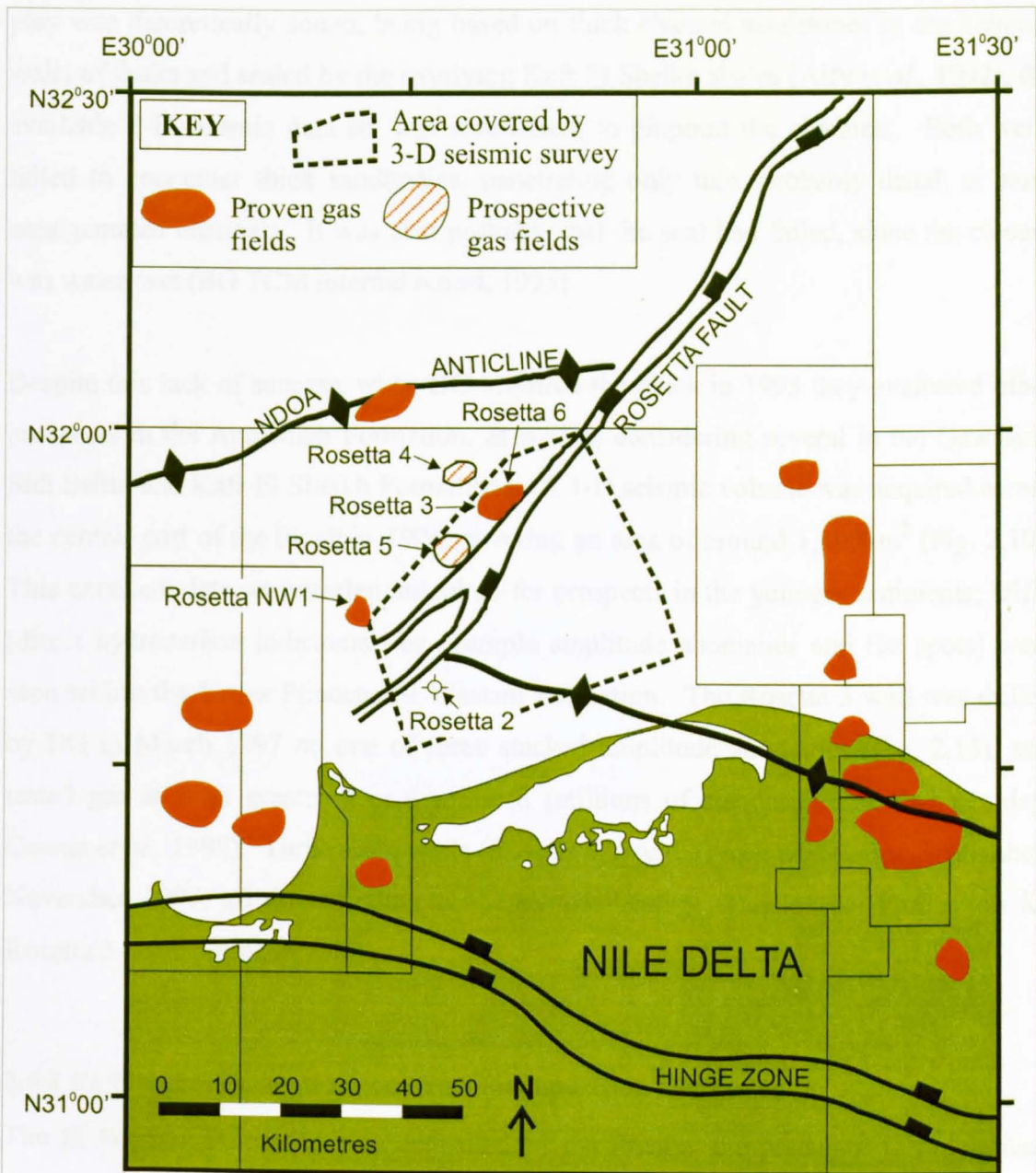


Figure 2.10. Location map showing the position of Rosetta wells and prospects, significant proven gas fields, block outlines, location of the 3D data set and important structural features (as labelled). Modified from BG internal report, 1997.

#### 2.4.2 Exploration history

The first two wells drilled in the Rosetta concession were Rosetta NW1 (IEOC, 1985) and Rosetta 2 (IEOC, 1968; Fig. 2.10), which were drilled to investigate Miocene targets; both reached the Sidi Salim Formation at depths of over 3.1km (Fig. 2.11). The prospective reservoir sands of the fluvial-dominated Late Miocene Abu Madi and Qawasim Formations were found to be water-wet and hence unproductive. While the

play was theoretically sound, being based on thick channel sandstones in the hanging walls of faults and sealed by the overlying Kafr El Sheikh shales (Alfy *et al.*, 1992), the available 2-D seismic data set was insufficient to pinpoint the channels. Both wells failed to encounter thick sandbodies, penetrating only thin, probably distal, or non-amalgamated channels. It was also probable that the seal had failed, since the closure was water-wet (BG TCM internal report, 1995).

Despite this lack of success, when BG acquired the block in 1995 they evaluated other prospects in the Abu Madi Formation, as well as considering several in the Qawasim, Sidi Salim and Kafr El Sheikh Formations. A 3-D seismic volume was acquired across the central part of the block in 1996, covering an area of around 1,400km<sup>2</sup> (Fig. 2.10). This excellent data set revealed unlooked-for prospects in the younger sediments; DHIs (direct hydrocarbon indicators, for example amplitude anomalies and flat spots) were seen within the Upper Pliocene El Wastani Formation. The Rosetta 3 well was drilled by BG in March 1997 on one of three stacked amplitude anomalies (Fig. 2.13), and tested gas at rates greater than 60mmscfd (millions of standard cubic feet per day; Cowan *et al.*, 1998). Three more wells (Rosetta 4, 5 and 6) followed during September-November 1997, all three finding economic gas-bearing sandstones. Production for Rosetta 3 came online in 1999.

#### **2.4.3 El Wastani Formation: controls on deposition and facies**

The El Wastani Formation was deposited by the Prenile, the precursor to the modern River Nile (Said, 1993). The climate throughout the drainage basin during its deposition was controlled by global glacial/interglacial cycles (Helmy and Fouad, 1994). Interglacial periods resulted in arid to hyper-arid conditions while glacial periods were pluvial periods in Egypt. This climatic cyclicity affected the sedimentation rate, and, coupled with the effects of glacio-eustatic sea-level changes, led to a clear cyclical pattern of facies change within the El Wastani Formation. The greater erosive power of the river during glacial lowstands reinforced the effect of the wet climate, leading to a significant increase in the sedimentation rate throughout the delta system during such times. Bellaiche and Mart (1995) note that a wet climate and corresponding low sea-level were responsible for the period of highest sedimentation rates on the Nile Fan (Holocene, 0.28-0.17Ma BP). The results of similar conditions in

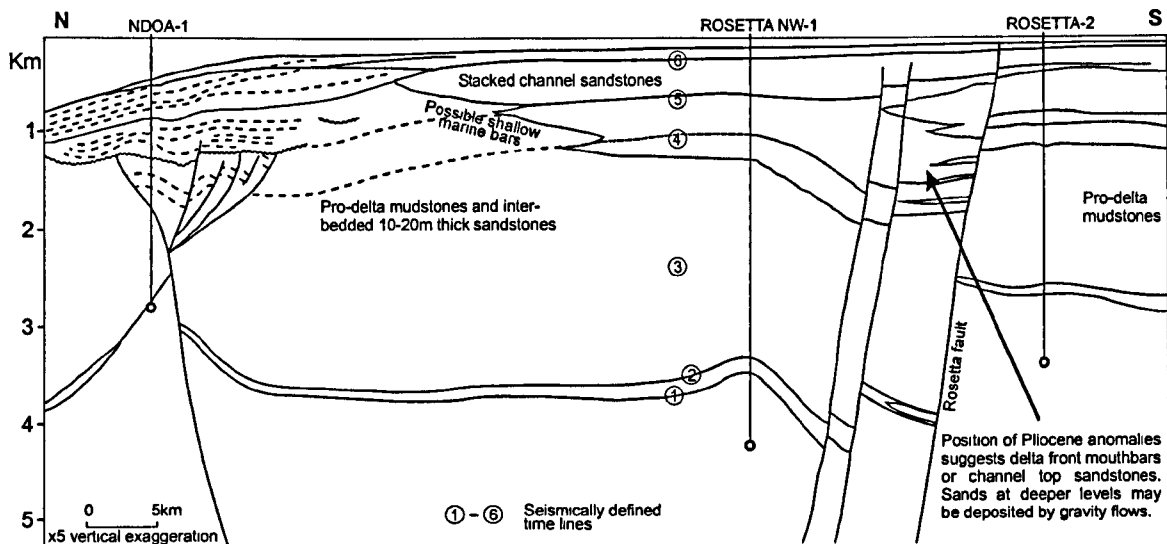


Fig. 2.11 - Cross-section of the Nile Delta based on a seismic section through three wells with interpreted wireline logs (positions only shown; log and seismic data confidential). Dashed lines show less certain interpretations. Modified from Cowan *et al.*, 1998.

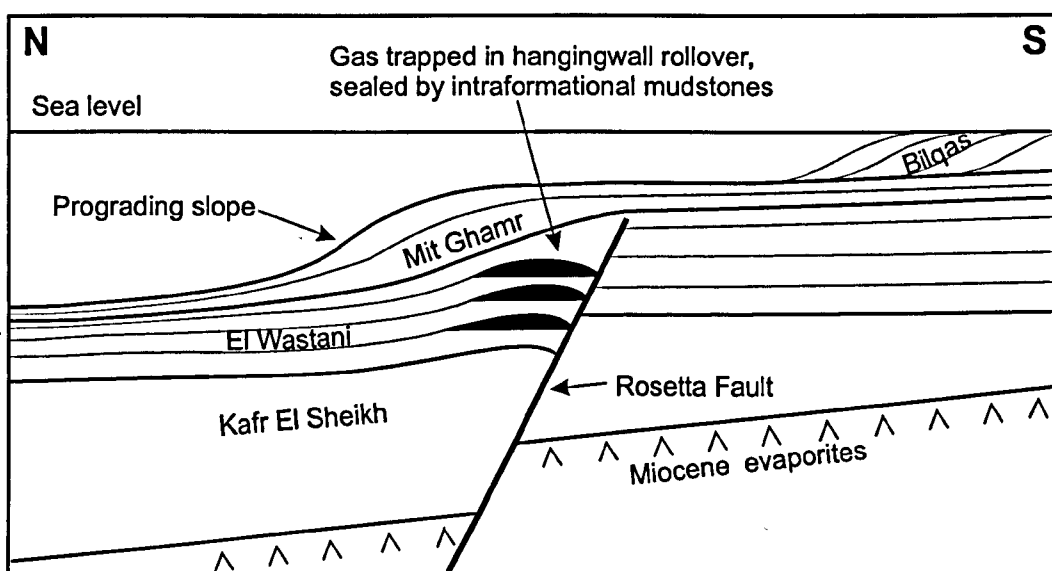


Figure 2.12. Schematic north-south cross-section of the Nile Delta, shelf and slope, showing the stratigraphic formations and the main play type (gas trapped in Plio-Pleistocene deltaic sandstones, folded in hanging wall rollover anticlines).

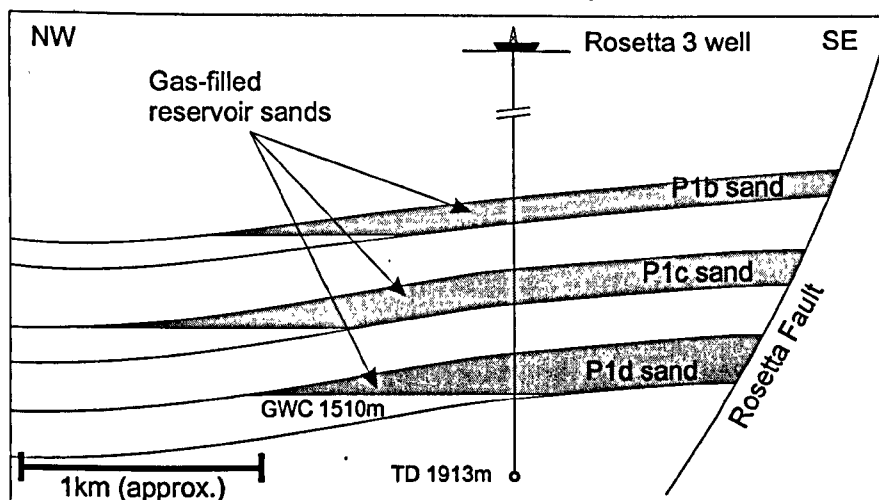


Figure 2.13. Schematic cross-section through the reservoir sands targeted by well Rosetta 3. Each reservoir interval comprises 4-6 sub-layers. After Cowan *et al.*, 1998.

the Upper Pliocene were the thick sand units of the El Wastani Formation, representing delta front mouth bars (Cowan *et al.*, 1998), and delta top channel sandstones (Doherty *et al.*, 1988; BG TCM internal report, 1996). Further seaward, clinoforms seen on seismic sections represent related deltaic foresets (Rizzini *et al.*, 1978). Each coarsening-up sedimentary cycle within the formation has been interpreted as a candidate sequence (Fig. 2.14), correlating to global glacio-eustatic cycles (Harwood *et al.*, 1998). These cycles almost certainly correspond to fifth order sea-level changes controlled by Milankovitch eccentricity cycles, with periodicities of around 100ka; such cycles also have been documented from other parts of the world (e.g. Carter *et al.*, 1991). The main control on sandbody deposition therefore appears to be eustatic sea-level fluctuation.

The facies changes within each cycle, as expected, have a significant effect on the reservoir potential of the formation. Halim *et al.* (1996) noted this for the sandstones of the Kafr El Sheikh, Abu Madi and Sidi Salim Formations as well. The sands most suitable for hydrocarbon reservoirs are the coarsest ones, which occur at the top of the coarsening-up, shallowing-up cycles. These cyclical packages are more sand prone in the southern, proximal part of the delta (sand/shale ratio 3:1) and there is an overall fining seaward to sandy shale (sand/shale ratio 5:7) in the north (Zaghloul *et al.*, 1977).

Transgressions following the high- to lowstand delta progradation have created marine flooding surfaces, draping the extensive sandbodies with muds and shales, providing excellent intraformational seals (Cowan *et al.*, 1998). The activity of gravity-driven synsedimentary faults within the delta area has led not only to the accumulation of thicker pockets of sand in the hanging walls (Barsoum *et al.*, 1998), but also to the creation of structural traps (Figs 2.12 and 2.13). The slight rollover of the hanging walls creates 3-way dip closures, with the remaining fourth sides sealed by the faults themselves. It is exactly this form of trap that prevails in the hanging wall of the Rosetta Fault, which is a normal fault downthrown to the northwest that stretches in a NE-SW orientation across the western half of the Rosetta concession (Cowan *et al.*, 1998; see Figs 2.10 and 2.11).

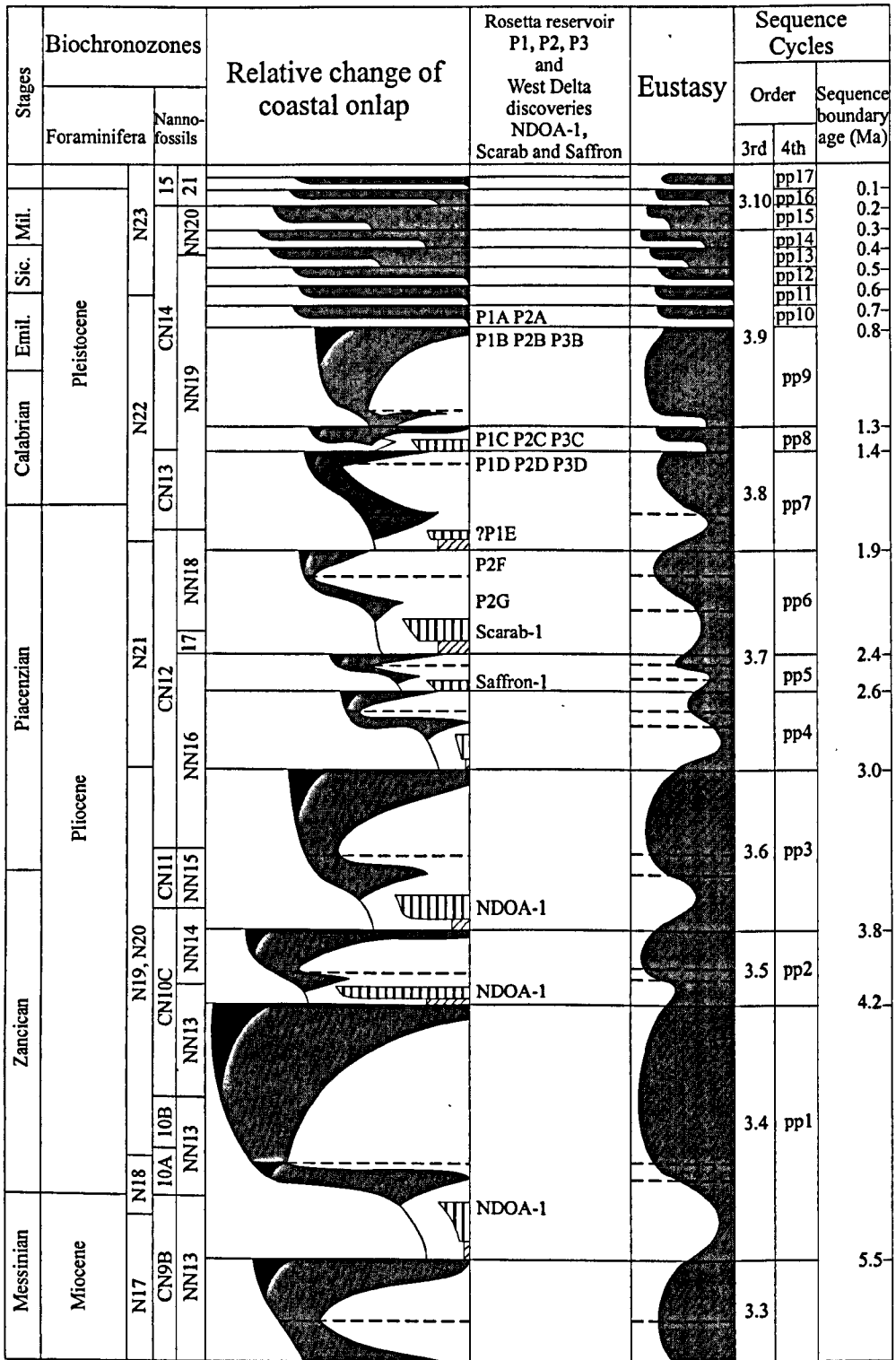


Figure 2.14. Sequence stratigraphic system for the west Nile Delta area, showing ages, biozones, onlap curves, global eustatic sea-level changes, and assigned cycles and sequence boundaries. After Harwood *et al.* (1998) and Wornhart and Vail (1991).

 lowstand fan   
  lowstand wedge   
  slope and shelf   
  fluvio-deltaics

#### **2.4.4 El Wastani Formation: sedimentology and reservoir characteristics**

The detailed sedimentology of the reservoir sandstones is based on small sections of core and sidewall samples, as well as on the interpretation of seismic lines and geophysical well logs. Although amplitude mapping was attempted to define reservoir properties, the effect of the gas in the sands masked any subtle variations and rendered the method ineffectual. The information given in this section is derived from unpublished in-house BG reports and from the prospect summary of Cowan *et al.* (1998).

The stacked sandstones of the El Wastani Formation are part of progradational wedges, bounded by marine flooding surfaces represented on logs by gamma ray peaks. The sands have been labelled from young to old as sequences A to F, which range in thickness from 10m to 60m, and which are subdivided into individual units (numbered consecutively from youngest to oldest). FMI (Fullbore Formation MicroImager) interpretation from well Rosetta 3 shows that the sands correspond to a variety of depositional environments from delta front to delta plain. For example, the basal 35m of the lowermost productive sandstone (D1) are part of a major distributary channel complex, and are overlain by 23m of crevasse splay sands and minor mouth bar sands (Enclosure 3). FMI interpretation in Rosetta 6 reveals that the C sand is a shallowing-up sequence of delta front sediments (mouthbar sands and interdistributary bay deposits) that have been extensively bioturbated and slumped into a prodelta setting (Enclosure 2 shows a similar sequence from Rosetta 3). Although FMI data from Rosetta 3 reveal a 7m-thick interval of storm-influenced sands at the top of the B sandbody (Enclosure 1), the dominant facies types throughout the El Wastani sandbodies in wells Rosetta 3, 5 and 6 are mouthbar, interdistributary bay and fluvial channel facies, rather than wave or storm-influenced facies.

A 9m length of core was recovered from Rosetta 5, revealing sedimentary details of the C2 sand. Petrography work done by BG reveals the sandstones in the sample to be olive-green to grey in colour, well sorted and generally fine-grained, with coarser intervals and very coarse to granular lag deposits. Petrographic analysis shows them to be subfeldspathic arenites (13-25% feldspar, 70+% quartz, up to 16% glauconite, rare lithics and mica). Porosity and permeability are excellent (Table 2.2). Average porosity

is 37.7% and average permeability is 2.384 Darcies. This, however, is only for the cored interval; any heterogeneity that may be present has not been reflected in this sample. The poorly cemented nature of the sands makes retrieving intact core challenging, and to date little other core data are available. Table 2.2 shows the poroperm characteristics for the cored interval and for the gross sandstone thicknesses in wells Rosetta 3 and Rosetta 6.

Table 2.2. Reservoir characteristics for El Wastani sandstones (Cowan *et al.*, 1998).

	C2 sand, Rosetta 5	Rosetta 3	Rosetta 6
Core length / gross pay (metres)	9	333	204
Average net/gross (percent)	100	81-94	54-100
Average porosity (percent)	37.7	32-37	19-29
Av. permeability (Darcies)	2.384	Not available	Not available
Max. permeability (Darcies)	7.309	5.8	Not available

#### 2.4.5 Hydrocarbon potential

There are three structural traps in the area, P1 P2 and P3. The Rosetta 3 well was drilled to drain P1 (Fig. 2.13), and Rosetta 6 penetrates the northeastern extension of this structure (Fig. 2.10). Wells 4 and 5 discovered gas in prospects P2 and P3 respectively. The total gas initially in place (GIIP) for P1 (calculated deterministically as the "P50", or most likely, case) is 1.3TCF (trillion cubic feet). Table 2.3 indicates the distribution of gas between the three main reservoir sands. The gas is very high quality, with less than 1.5% impurity, and there are an average of 1-2 barrels of condensate per million cubic feet of gas (DeGolyer and McNaughton, BG commissioned unpublished report, 1997). Rosetta 3 tested 21,160tcf (thousand cubic feet) per day from sand d, and 15,200tcf per day from sands b and c.

Geochemical analysis of gas accumulations elsewhere in the Nile Delta area determined a number of potential source rocks (Kamel *et al.*, 1998). Oligocene and Early, Middle and Late Miocene sources are all gas prone with TOC (total organic carbon) values of 0.7% - 5.0%. Burial history and maturity modelling suggest that the low geothermal

Table 2.3. Division of gas pay between reservoir sands in the P1 (prospect 1) structure (Cowan *et al.*, 1998). See Fig. 2.13.

Reservoir unit	% Gas initially in place (GIIP)
P1 – B sand	10.1
P1 – C sand	48.9
P1 – D sand	41.0

gradient of the passive margin has led to a deep window for gas generation, the top of this window being at around 6km (BG internal report, 1998). The proposed source rocks for the Pliocene gas plays are Oligocene/Lower Miocene gas prone shales, believed to have been deposited in a deltaic/delta top environment (BG internal report, 1997). Maturation is thought to have been as recent as the Plio-Pleistocene, with migration ensuing rapidly, occurring along Miocene normal faults and linked Pliocene growth faults. The gas fraction found in the Upper Pliocene reservoirs is very dry and isotopically light (due to a high percentage of methane), suggesting fractionation during migration (Kamel *et al.*, 1998). Fractionation is confirmed by the occurrence of residual wetter gas, condensate and even oil in the deeper reservoirs, for example in the Abu Madi and Kafr El Sheikh Formations (Kamel *et al.*, 1998).

#### 2.4.6 Summary

- The Upper Pliocene plays in the Rosetta concession involve stacked reservoir sandstones within the El Wastani Formation, with gas trapped in hanging wall rollovers of the Rosetta Fault and sealed by intraformational muds. Source rocks are probably Oligo-Miocene gas-prone shales which matured relatively recently during the Plio-Pleistocene. Gas migration was along Miocene and Pliocene faults.
- The depositional model for the sandstones is strongly linked to Pliocene glacio-eustatic sea-level changes and corresponding climatic fluctuations. A series of coarsening-up sequences, separated by marine flooding surface mud drapes, is seen in the Upper Pliocene. The reservoir sands occur at the tops of these progradational packages and represent delta top distributary channel sands, interdistributary bays, crevasse splays and mouth bar sands.
- The issue of lateral variation in reservoir quality is important to address as it affects reservoir models and management strategy. Attempts have been made to map facies changes using seismic amplitude variations, but have proved impractical due to the

masking effect of the gas in the reservoirs. Generalised models have been produced using well log, seismic, and limited core data, but detailed information is lacking. Finding a suitable analogue for the reservoir in which such variations could be qualified would be very useful, enabling predictions of reservoir quality to be made.

## **2.5 Comparison of potential analogues**

The main similarities and contrasts between the two deltaic systems described in Sections 2.1 through 2.4 above are summarised below. The significance of the similarities and differences is also highlighted.

Both depositional systems experienced similar extrinsic controls. This makes the systems suitable for at least coarse comparison, since the facies distributions, associations and geometries attributable to the extrinsic controls would be expected to be similar, assuming (perhaps over-simplistically) that the intrinsic controls were not dissimilar in the two systems. The resemblance between the extrinsic controls in the two systems is outlined below:

- 1) Both the Nile Delta system of the Plio-Pleistocene and the Namurian delta system of County Clare were influenced by cyclical sea-level changes. The Namurian and the Plio-Pleistocene were both times of glacio-eustasy, and sediments of both epochs show cyclical patterns related to glacial-interglacial stages, with durations in the order of 100ka, related to Milankovitch eccentricity cycles (Collier *et al.*, 1990; Holdsworth and Collinson, 1988; Hampson *et al.*, 1997; Carter *et al.*, 1991). The effects of sea-level changes are recorded in the sedimentary successions. The El Wastani Formation of the Nile Delta shows repeated units of sand divided by intraformational marine mudstone seals, representing late highstand/early lowstand and transgression/early highstand respectively. The Co. Clare succession displays a similar cyclical pattern of sandy deltaic deposits and fine-grained basinal sediments containing marine fauna, also reflecting change from falling sea-level to transgression.
- 2) Both delta systems appear to have been fluvially dominated. The Co. Clare deposits record strong fluvial influence, and show no positive signs of tidal processes (e.g. Pulham, 1989); similarly, the Nile Delta of the Plio-Pleistocene was fed by a highly

competent river with a vast discharge (the Prenile – Said, 1993a) but, since the river debouched into the micro-tidal Mediterranean, was not influenced greatly by tides.

- 3) Both delta systems show some wave influence; numerous wave-rippled bedding surfaces are seen in the Co. Clare deltaic sediments, and the Plio-Pleistocene Nile Delta formed under similar conditions to the modern Delta, which is known to be significantly influenced by wave action. It is worth noting that while the modern Nile Delta is wave dominated, the greater discharge of the Prenile relative to the modern Nile meant that the Prenile Delta was, in contrast, fluviially dominated.

The El Wastani reservoir sands in the Nile Delta represent depositional environments akin to those of sandstones in the Namurian of Co. Clare. Cowan *et al.* (1998) and Doherty *et al.* (1988) interpret delta top channel sandstones and sandy mouthbars in the El Wastani Formation, both of which are also encountered in the Co. Clare deltaics. Although such an obvious correspondence would be expected between any two fluviially dominated deltas, the strong sedimentological similarity of the two successions is also supported by the favourable comparison of sedimentary facies between the sandbodies of the two systems (see the facies descriptions in Chapter 3). Finding similar facies in the two deltaic successions is crucial if they are to be considered good analogues.

The grainsize in both the El Wastani sands and the Co. Clare sandstones is predominantly fine sandstone. For the El Wastani sands, it is probable that this fine grainsize reflects warm and wet climatic conditions (known to have existed at that time; Said, 1993a; see also Fig. 2.14, P1B to P1D sands), which favoured rapid chemical weathering and thus reduced the dominant grainsize available for transportation. The same reasoning could be applied to the Co. Clare deltaic sandstones, since the Upper Carboniferous was also a warm, wet phase for the region. Alternatively the fine grainsizes in each system could be due to similarly long transport histories. A third possible explanation for the fine grainsize of the Co. Clare sandstones is that the rivers were not able to transport coarser material; however, this is unlikely because, had a range of grain sizes been available, one would expect to see coarser grains during higher flow periods, for example, associated with conglomeratic lags, and this is not the case. Therefore a tentative case can be made for similarity in the climatic controls or transport lengths that prevailed in the catchments of both the Prenile and the Co. Clare fluviio-deltaic systems, which is significant in that it may contribute to a similarity in the

textural quality of the reservoir sands. (The Clare Sandstones, being diagenetically altered and cemented, are not reservoir quality at the present day, but from cross-section work done on the Tullig Sandstone in the course of this project, the original texture appears to have had significant porosity.)

Overall, the similarity of the extrinsic controls, facies associations and sedimentological characteristics across the two delta systems makes Co. Clare a suitable analogue for the Plio-Pleistocene Nile Delta, at least on initial assessment. Whether the similarities translate into a solid correspondence in the more detailed sedimentary architecture and sedimentology of the systems will be discussed later in this thesis.

## Chapter 3

# Fluvial and deltaic facies descriptions, interpretations, and associations from County Clare fieldwork

### **3.1 Introduction**

The deltaic cycles of County Clare provide an excellent example of deltaic sandbody architecture for field study. This fieldwork had the dual aims of interpreting the facies and depositional environments, and quantifying the internal architecture and facies relationships of the sandbodies. The localities studied were, in order from south to north: Tullig Point, Trusklieve, Killard, Carrowmore Point and Furreera (at Liscannor Bay; see map in Fig. 3.1). The fluvio-deltaic sandbodies of the Tullig cyclothem are exposed at each locality, allowing comparative study. The thickest, most extensive of these sandbodies caps the cyclothem and is known as the Tullig Sandstone.

The work focussed on the sandbodies, producing results that include detailed sedimentological logs, photomontages, outcrop facies maps, and measurements of architectural element thickness, length, lenticularity, contact and distribution. These data were collected to condition computer-generated reservoir models at a later date. The facies descriptions and interpretations are presented in this chapter, while the architectural and quantitative data are presented in Chapters 4 and 5 respectively.

### **3.2 Methodology**

#### **3.2.1 Logs and facies definition**

Initial work was in the form of sedimentological logs (for key, see App. A1). At Trusklieve, four logs were made at intervals across the outcrop (App. A, 2 to 5). At Pulleen a single log was made (App. A6). The Killard outcrop is folded in a gentle ENE-WSW trending syncline; one log was taken on each side of the syncline (App. A7 and A8) and a third was made through the mouthbar sediments (App. A16). The Carrowmore Point outcrop extends across an open anticlinal fold also trending ENE WSW; three logs were made on the northern limb and two on the southern limb (App. A9 to 13). One log was also taken at Furreera, Liscannor Bay (App. A14). At Tullig Point, the outcrop is in an inaccessible cliff section, and so only one log was taken where the dipping beds intersect the cliff edge (App. A15).

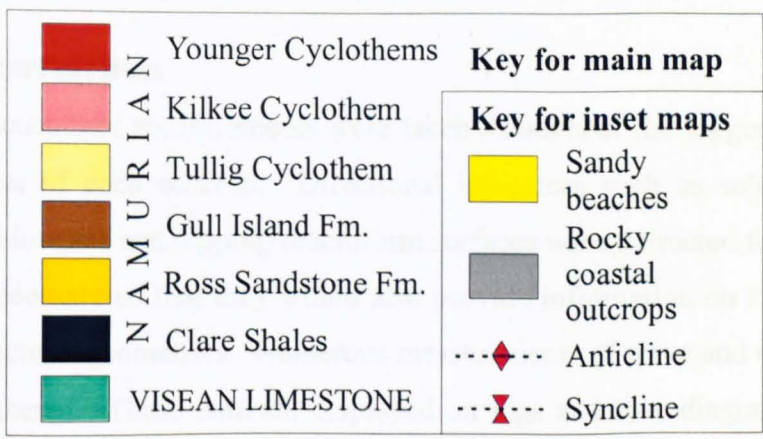
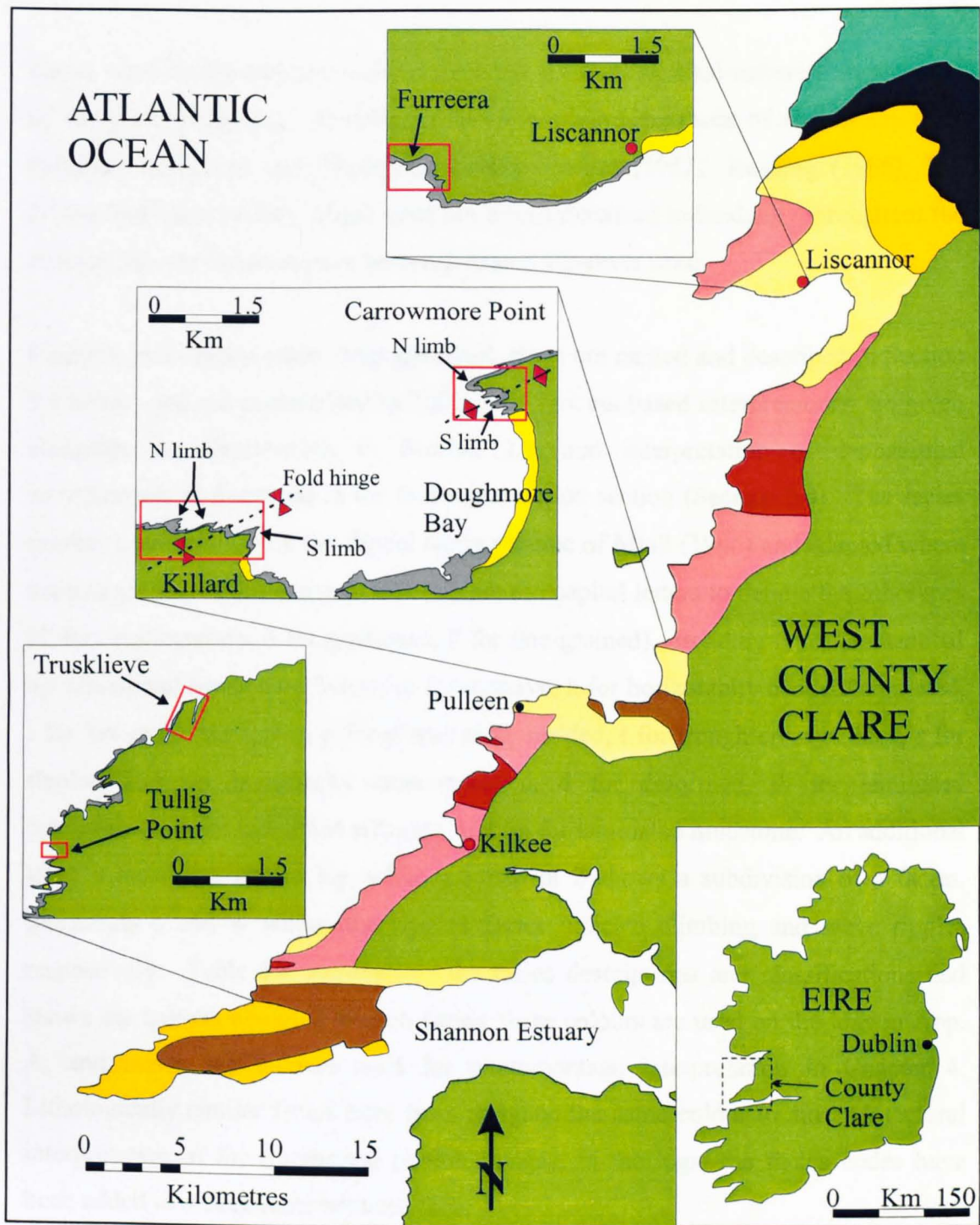


Figure 3.1. Map of County Clare showing Namurian coastal geology and detailed inset maps with fieldwork localities boxed in red (after Wignall and Best, 2000).

Facies were interpreted and defined from the sedimentological information provided by the detailed logging. In defining facies, use has been made of several key texts including Collinson and Thompson (1982), Leeder (1982), Reading (1986), Pye (1994) and Miall (1996), which have not been referenced individually throughout the chapter; all other sources have been referenced wherever used.

Eighteen main facies types were identified; these are named and described in Section 3.3 below, and are summarised in Table 3.1. Process-based interpretations are given alongside the descriptions in Section 3.3, and interpretation of depositional environments is discussed in the facies association section (Section 3.4). The facies scheme used is based on the fluvial facies scheme of Miall (1996) and adapted where necessary. The facies codes in this scheme use capital letters to denote the lithotypes (C for conglomerate, S for sandstone, F for fine-grained). Bedding types are denoted by subsequent lower case letters: m for massive, h for horizontally bedded/laminated, l for low-angle laminated, p for planar cross-bedded, t for trough cross-bedded, r for rippled, hcs for hummocky cross-stratified, d for deformed, lh for laminated heterolithics, ls for laminated siltstone, and lm for laminated mudstone. An additional letter c denotes a coarse lag, while a subscript 2 shows a subdivision of a facies. Subscripts c and w within the rippled facies indicate climbing and wave ripples respectively. Table 3.1 summarises the facies descriptions and classifications and shows the colours assigned to each facies; these colours are used on the logs in App. A, and match the colours used for photomontage interpretation in Chapter 4. Lithologically similar facies have been assigned the same colour to aid architectural interpretation of the interpreted photomontages; in the logs, the facies codes have been added to differentiate between them.

### **3.2.2 Palaeocurrent data**

Detailed palaeocurrent measurements were taken throughout the logged sections and across the rest of each outcrop. Directional indicators such as sole marks were recorded, and foresets and dipping macroform surfaces were corrected for the regional dips where necessary so that they would also provide information on flow directions and/or architectural geometries. Numerous measurements of wave and current ripples were also gathered. These data are displayed on logs and rose diagrams in Section 4.3, and on logs in App. A.

Table 3.1. Facies scheme used to classify sedimentary rocks observed in the field area. Facies codes are from Miall (1996) where interpretations agree with his fluvial facies scheme; other codes, not representing existing facies schemes, have been chosen specifically for facies seen in the outcrops studied.

Code	Lithofacies type	Description	Depositional process/interpretation	Facies association
Sm	Massive to faintly bedded sandstone	Well sorted, clean, yellow massive sand with occasional faint, patchy lamination.	Deposited by sediment gravity flows, for example in small channels due to bank collapse. Alternatively due to very rapid deposition and subsequent homogeneous dewatering.	Smc, Sh, Shc, Sl, Sp, St, Sc, Ccm, Sd, Sr (channel-fill facies)
Smc	Sm with conglomeratic lag and/or floating clasts	Well sorted, clean, yellow massive sand with occasional faint, patchy lamination Clastic lag at base and rare floating clasts.	Deposited as for facies Sm, but with additional coarse material deposited at the base of the bed (as flow wanes) or higher in the bed (due to gravitational overpassing).	Sm, Sh, Shc, Sl, Sp, St, Sc, Ccm, Sd, Sr (channel-fill facies)
Sh	Horizontally laminated sandstone	Well sorted, clean, yellow sand, parallel laminated, with primary current lineation.	Bedforms swept out by high velocity unidirectional flow, forming upper stage plane beds.	Sm, Smc, Shc, Sl, Sp, St, Sc, Ccm, Sr (channel-fill facies)
Shc	Sh with conglomeratic lag and/or floating clasts	Well sorted, clean, yellow sand, parallel laminated, with primary current lineation. Clastic lag at base and rare floating clasts. Shows crude imbrication.	Upper stage plane beds (as above) with deposition of coarse bedload fraction at base of bed.	Sm, Smc, Sh, Sl, Sp, St, Sc, Ccm, Sr (channel-fill facies)
Sl/Sl <sub>2</sub>	Low angle cross-bedded sandstone	Low angle (<10°) cross beds in well-sorted yellow sandstone. Sl <sub>2</sub> contains fine-grained silty laminae.	Sl develops at the transition from dunes to upper stage plane beds as bedforms are swept out by unidirectional flow. Sl <sub>2</sub> formed by deposition from suspension on gently dipping surfaces.	Sm, Sh, Shc, Sp, St, Sc, Ccm (channel fill facies) (plus Flh, Fls, Flm for Sl <sub>2</sub> )
Sp/Sp <sub>2</sub>	Planar cross-bedded sandstone	Varying scale of planar cross-bedding in well sorted, clean yellow sandstone. Foresets are typically asymptotic towards the flat lower set surfaces, and in Sp <sub>2</sub> show mud drapes.	Migration of straight crested (2-D) dune bedforms within unidirectional flow.	Sm, Sh, Shc, St, Sc, Sl, Ccm (channel-fill facies) (plus Sh <sub>2</sub> , Sl <sub>2</sub> )

Table 3.1 continued.

Code	Lithofacies type	Description	Depositional process/interpretation	Facies association
St	Trough cross-bedded sandstone	Scoop-shaped erosional bases to sets of trough cross beds averaging 0.5 to 1.5m thick. Foresets are asymptotic at base. Well sorted, clean, yellow sands.	Migration of sinuous crested (3-D) dunes within unidirectional flow.	Sm, Smc, Sh, Shc, Sp, Sc, Sl, Ccm (channel-fill facies)
Sc	Sp, St or Sl with clast lag	As for Sl, Sp and St, with a lag of coarse material (gravel to pebble sized) at the base, and rare "floating" clasts. Clasts predominantly mud/silt, angular, and frequently deformed.	Erosion of fine channel fill or overbank material during channel reoccupation or splay channel breakout. Deposition of gravel/cobble fraction at base of new channel scour as peak flows wane.	Sm, Smc, Sh, Shc, Sp, St, Sl, Ccm (channel-fill facies)
Ccm	Clast-supported massive to crudely bedded conglomerate	Gravel to cobble-sized clasts, predominantly mud/silt. Poorly sorted, angular to rounded, including deformed clasts. Organic debris often present. Patchy crude imbrication and horizontal stratification. Matrix of fine sand to muddy silt showing compaction related deformation.	Eroded overbank or channel abandonment material incorporated in coarse bedload. Gravel and cobble fraction deposited of at base of newly formed channel scour as strongly erosive peak flows wane.	Sm, Smc, Sh, Shc, Sp, St, Sc, Sl (channel fill facies)
Sd	Deformed sandstone	Clean, well-sorted yellow sandstone with convolute lamination, loading and other deformational features. Sometimes without any remaining sign of bedding.	Formed by soft-sediment deformation due to liquefaction and fluidization, possibly caused by a seismic shock or by sudden burial and overpressure.	Sm, Smc, Sh, Shc, Sp, St, Sc (channel facies)
Sr	Ripple cross-laminated sandstone	Cross lamination (5-40 mm high) in well-sorted but slightly silty sand. Occurs in sandstone beds or as discrete thin (5-30cm) beds within finer sediments..	Develop at low to moderate flow velocities in a unidirectional current.	Sp, Flh, Fls, Flm (channel fill, mouthbar or bay fill facies)
Sr <sub>c</sub>	Climbing ripple cross-laminated sandstone	Climbing cross lamination in well-sorted but slightly silty sand. Stoss and lee sides of ripples preserved	Develop during rapid deposition within a waning unidirectional current.	Sp, Flh, Fls, Flm (bay fill facies)

Table 3.1 continued.

Code	Lithofacies type	Description	Depositional process/interpretation	Facies association
<b>Sr<sub>w</sub></b>	Wave ripple cross-laminated sandstone	Symmetric ripples with continuous crests and bi-directional cross-lamination in well-sorted, slightly silty sand.	Develop during wave reworking of previously deposited sands.	Sp, Flh, Fls, Flm (mouthbar and bay fill facies)
<b>Shcs</b>	Hummocky cross-stratified sandstone	3-D cross beds in dome-shaped features in well-sorted clean yellow sandstone. Dome surfaces often preserved, with wave-reworked tops.	Formed by storm wave reworking of sediment, usually in shelfal conditions but also nearer shore.	Sp, St, Sr, Flh, Fls, Flm (mouthbar facies)
<b>Sh<sub>2</sub></b>	Horizontally laminated sandstone (type 2)	Well sorted, pale yellow parallel laminated sandstone with thin (<10mm) silty lamiantions.	Formed by rapid deposition from suspension immediately in front of distributary mouth, producing laminated sands with silt layers at times of lower flow.	Sp, St, Sl <sub>2</sub> , Sr, Flh, Fls, Flm (mouthbar facies)
<b>Flh</b>	Interlaminated sand, silt and mud	Parallel to occasionally wavy bedded inter-laminated fine sands, silts and muds. Dark grey where muddier, through mid-grey silts to pale cream sands. Sand layers commonly show lenticular bedding (uni- and bi-directional).	Deposited from suspension with weak tractional currents and/or wave reworking producing ripple trains in sand and sandy silt. Interdistributary bay to general lower delta plain overbank environment.	Fls, Flm, Sh <sub>2</sub> , Sr, Srw, Src, Shcs (mouthbar or bay-fill facies)
<b>Fls</b>	Laminated silt	Parallel laminated pale grey silt. Occasional bioturbation in some beds.	Fine material deposited from suspension in quiet water (marine, below wave base, or (where no bioturbation) overbank or abandoned channel environment.	Flh, Flm, Sh <sub>2</sub> , Sr, Srw, Src, Shcs (mouthbar or bay-fill facies)
<b>Flm</b>	Laminated mud	Parallel laminated dark grey mud. Occasional bioturbation.	As above, but further from the sediment source.	As above (mouthbar or bay-fill facies)

### **3.3 Facies descriptions and interpretations**

#### **3.3.1 Massive to faintly bedded sandstone (Sm)**

##### **3.3.1.1 Description**

This facies comprises lower-fine to lower-medium grained (125-350 $\mu$ m), very well sorted, moderately well rounded sandstone. Thin-section work shows the sandstone is relatively clean and quartz rich with a lithic component of less than 5%. The basal surface of the facies is commonly erosional, internal bedding is poorly developed, and identifiable bed boundaries are uneven and widely spaced, being 1m apart or more. Facies Sm usually lacks any sedimentary structures discernable with the naked eye, although occasionally faint horizontal or sub-horizontal lamination is visible, which is restricted to discrete patches (<0.5m<sup>2</sup>) within beds. Figure 3.2 shows the featureless appearance of facies Sm compared with well-bedded facies; App. A shows logged examples (e.g. at 11.5m in A2; 4.7 - 9.7m in A10; and 13.6 - 14.6m in A7).

##### **3.3.1.2 Interpretation**

Massive beds can be formed by depositional (Collinson, 1970; McCabe 1977; Jones and Rust, 1983; Lowe, 1988) or post-depositional processes (Allen and Banks, 1972; Allen, 1986). There is no evidence of bioturbation in the Sm facies, nor are there any apparent structures that could be associated with fluidisation. These two post-depositional processes are not therefore considered responsible for the massive appearance of this facies. Crystallization contributes to the massive appearance, but since crystallization has also occurred in the other sandstone facies, another process must be responsible for the distinct massive nature of facies Sm. Post-depositional homogeneous dewatering or liquefaction are possible explanations, since these processes often leave no particular indicative features. Alternatively, the massive structure could be the result of rapid deposition from suspension. In this process, grains are deposited so rapidly that there is no time for significant bedload movement before they are buried and immobilised. Such rapid deposition is usually caused by the deceleration of a heavily sediment-laden current, for example a sediment gravity flow or short-lived mass-flow (Hjellbakk, 1997). Flows intermediate between debris-flows and normal stream-flows have been termed 'hyperconcentrated flood-flows' by Smith (1986), and can deposit their load very rapidly when small changes in velocity cause turbulence to fall below a critical value (Lowe, 1982).



Figure 3.2. Photomosaic showing the contact (marked in yellow) between the third and fourth storeys within the Tullig Sandstone at Trusklieve (the log in App. A4 was measured 2m to the right of this photo, and the section from 4.25 to 7.25m in that figure is similar to the succession seen here). The difference in appearance between the planar cross-bedded facies (Sp) and the massive sandstone, Sm, is clear. Facies Sm shows faint signs of large-scale bedding but no lamination is seen in outcrop. In contrast facies Sp is very well bedded (an enlargement of the boxed area is seen in Figure 3.7). The tape (arrowed) is 2m long.

### 3.3.2 Massive to faintly bedded sandstone with a conglomeratic lag (Smc)

#### 3.3.2.1 Description

Beds of this facies are similar in appearance to those of facies Sm, but exhibit clasts of other lithologies within them, usually as a basal lag. The clasts are poorly sorted, ranging in size from 10 to 300mm, and can be either rounded or angular. Some clasts were clearly not lithified when incorporated in the sandstone; these clasts are deformed, and some can be seen to have been in the process of breaking apart in an almost fluid manner when deposited and buried (see Fig. 3.3). These deformed clasts are, without exception, laminated siltstones and mudstones that look identical to silty and muddy facies described later in this section (facies Flh, Fls and Flm). Occasional large (>0.2m) shale clasts seen in facies Smc contain fossil estheriids (freshwater crustacea). The undeformed clasts are smooth and rounded and have more diverse lithologies, ranging from organic-rich mudstone to silts and rare quartzites.



Figure 3.3. Photo showing the erosional base of a bed of facies Smc (marked in yellow). The massive, structureless appearance of the sandstone (marked A) is clear. B marks a clast of deformed siltstone close to the base of the bed, and other clasts can also be seen, two of which are marked with asterisks. The tape is 0.8m long.

The clasts are generally clustered at the base of a bed, forming a conglomeratic lag. In all cases, the lag is recognised as part of the bed rather than a separate bed because it fines up into the featureless massive sandstone. The character of the lag varies, sometimes being clast supported and less frequently being matrix supported, although it may change from the former to the latter with height through the bed. Sorting of the clasts may be absent, although crude imbrication, in which the long axes of the clasts are aligned parallel to the bed base, is seen in some cases. Occasional “floating” clasts occur within the bed above the lag, but are few in number, widely spaced, and frequently associated with faint or patchy lamination. Examples of this facies are shown in the logs in App. A (for example, between 10.3 and 10.8m in A5; and between 2.45 and 4.7m in A11).

### 3.3.2.2 Interpretation

The depositional process suggested for facies Smc is the same as that described in Section 3.3.1.2 above for facies Sm. The massive sand and larger clasts are deposited very rapidly from mass-flows, possibly derived from the collapse of bank material (see Section 3.4.3), including sands and laminated, unlithified overbank muds and silts. A similar process has been documented from fluvial sediments in Norway by Hjellbakk (1997). Some clasts were probably also ripped up from underlying fine-grained beds, with the larger clasts being deposited first and subsequently covered by the fallout of the finer sand suspended load. In some cases deposition was not swift enough to prevent some current imbrication of the clastic lag. The collapsed overbank muds and silts give rise to the deformed fine-grained clasts. The rounder, smoother clasts represent existing bedload entrained within the mass-flow. The “floating” clasts are deposited by overpassing, a process caused by increased current influence in the upper parts of the Smc beds, leading to the entrainment and of occasional large clasts, which pass over the surface of the bed, accompanied by faint lamination (Allen, 1983b).

### 3.3.3 Horizontally laminated sandstone (Sh)

#### 3.3.3.1 Description

This facies (Figs 3.4 and 3.5) is lithologically similar to facies Sm, comprising lower-fine to lower-medium grained well-sorted and moderately well-rounded sandstone. The facies is recognisable by its laminated appearance; both in the field and under the

microscope the rock shows parallel planar laminae on a sub-millimetre scale (between 5-20 grains). Thin-sections show a unidirectional grain fabric. The laminae are not revealed by weathering and therefore are only visible under close inspection in the field. Bedding surfaces show primary current lineation. The appearance of this facies in the field is similar to the Sm facies, as it also looks blocky, but it shows better horizontal bedding. The Sh facies sometimes changes gradationally into the Sp or Sl facies within a single bed. Examples of this facies can be seen in the logs in App. A (e.g. between 10.9 and 11.4m in A2; and between 3.5 and 4.25m in A4).

### 3.3.3.2 Interpretation

Facies Sh is formed by deposition under conditions of high (but still subcritical) mean unidirectional flow velocity (e.g. Best and Bridge, 1992), resulting in upper stage plane beds. The existence of low-relief bedwaves in such flows is responsible for the formation of the planar laminae (Best and Bridge, 1992). The associated primary current lineation is flow-parallel, and is caused by fast unidirectional flow over the nearly flat bed (Allen, 1964).

### 3.3.4 Horizontally bedded sandstone with conglomeratic lag (Shc)

#### 3.3.4.1 Description

This facies is similar to facies Sh, but has a clastic lag at the base of a bed. Beds of facies Shc show erosion and scour at their bases, and contain clasts ripped up from finer facies beneath. The clasts are of similar sizes, lithologies and roughness to those described for facies Smc (Section 3.3.2.1). Floating clasts are sometimes present, and these show the same size variation as the clasts found in facies Smc. Examples of the Shc facies can be seen in the logs in App. A (for example, between 9.3 and 10.5m in A8).

#### 3.3.4.2 Interpretation

Facies Shc is deposited under strong flow conditions, within the upper stage plane bed field, as for the Sh facies. The erosional bed bases and large clasts are further evidence of high velocity flow; to move particles greater than 10mm in diameter, flow velocity (at 1m above the bed) has to be greater than around  $1.5\text{ms}^{-1}$ , and to move clasts of 100mm in diameter requires velocities of  $3\text{ms}^{-1}$  or greater (Miller *et al.*, 1977).

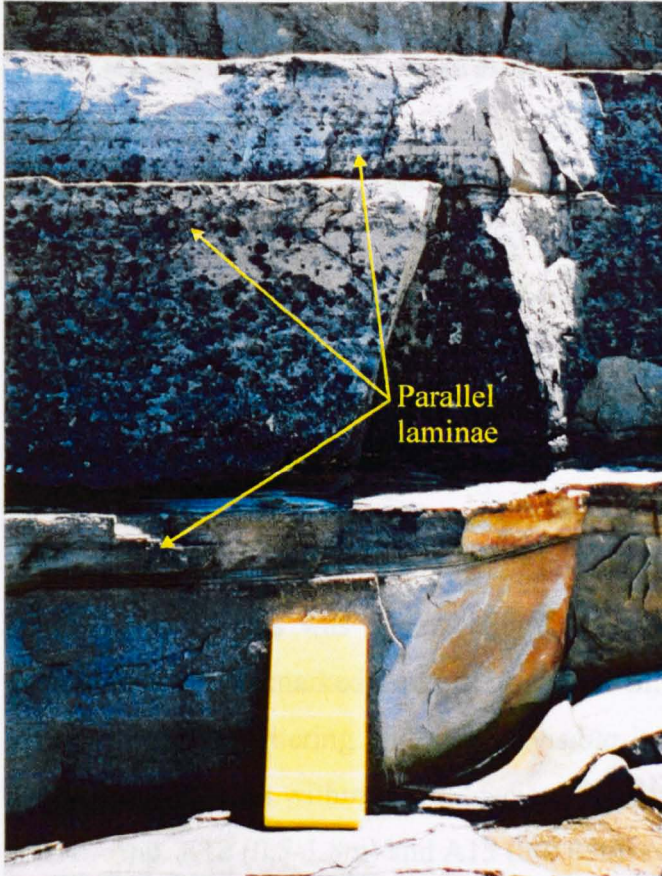


Figure 3.4. Photograph from the third story of the Tullig Sandstone at Trusklieve (at 3.55-4.25m in App. A4), showing the parallel lamination typical of facies Sh. The visible laminae here are just under a centimetre apart, but between these are many less obvious laminae, visible with a hand lens or in thin-section. The notebook is 0.2m tall.

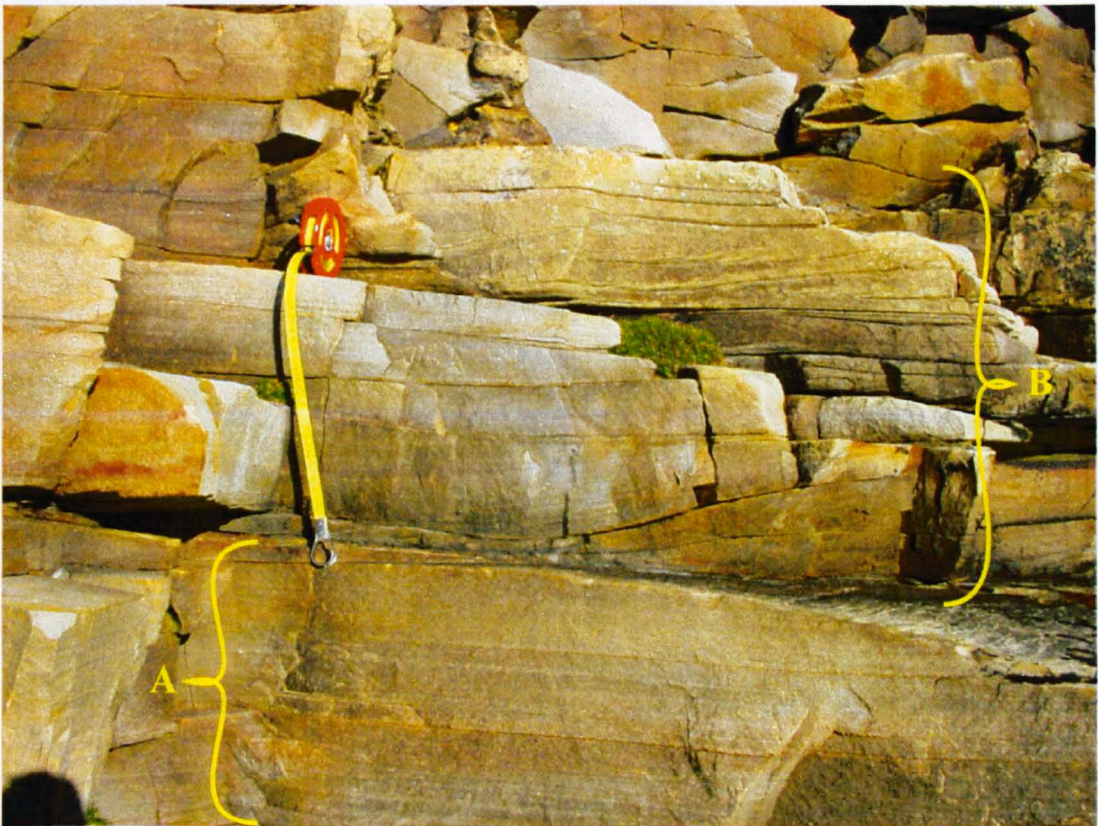


Figure 3.5. Photograph from the third storey at Trusklieve (section labelled R' in Fig. 4.3b) showing very well-developed parallel lamination of the Sh facies (labelled A). Here the laminae are clear and only millimetres thick. Vertically, facies Sh changes to facies Sl/Sp as cross beds appear (labelled B). The tape is 0.4m long.

### 3.3.5 Low-angle cross-bedded sandstone (S1 and S1<sub>2</sub>)

#### 3.3.5.1 Description

These facies, lithologically similar to those previously described, can be mistaken for facies Sh at a close view. However, a wider view reveals large-scale, low-angle planar cross beds. Photographs of the Killard outcrop (Fig. 3.6) show this clearly for facies S1. The sets are laterally continuous over distances of tens of metres, and first order bedding surfaces are sub-horizontal, not exceeding 10° and more usually only around 2-5°. Within individual sets (up to 1m thick), lamination is nearly parallel to the bed base, and again dips do not exceed 10° with respect to the lower bounding surfaces. Foreset surfaces in subfacies S1 occasionally show traces of primary current lineation; in S1<sub>2</sub> this was absent. Subfacies S1<sub>2</sub> shows similar low-angle bedding geometries, but in marked contrast to facies S1, silty laminae are present and are picked out by weathering and clearly visible in the field. Some apparent normal grading is also seen within the S1<sub>2</sub> facies. Examples of subfacies S1 and S1<sub>2</sub> can be seen in App. A12 (0.5-1.8m) and A15 (0-0.45m) respectively.

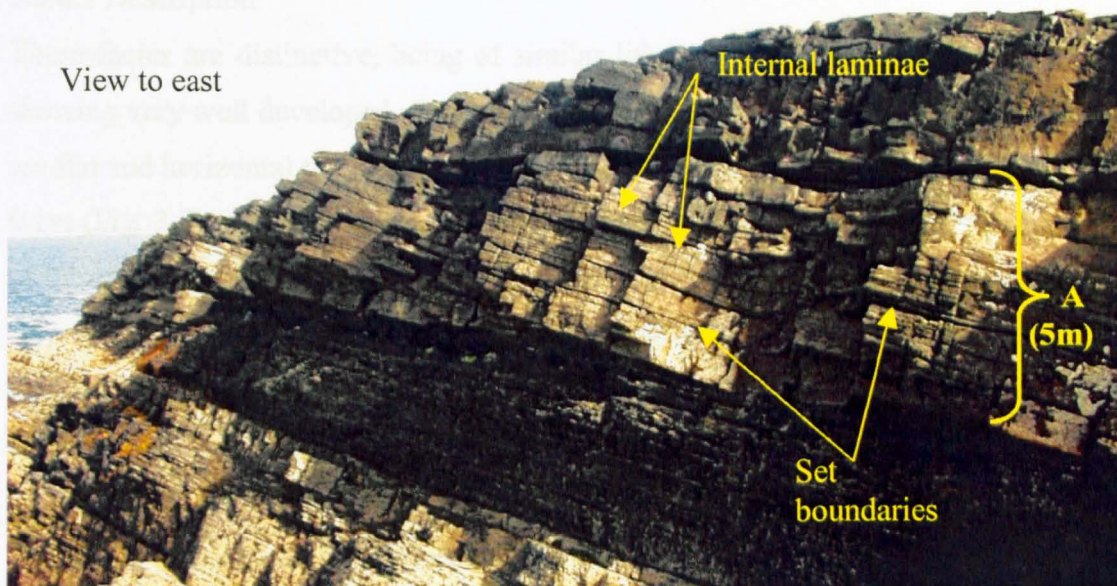


Figure 3.6. Low-angle cross-bedded sandstone, facies S1. The first storey of the Tullig Sandstone at Killard (A) is dominated by well-developed low-angle cross beds.

### 3.3.5.2 Interpretation

The low angles and rare primary current lineation of subfacies S1 cross beds suggest a transition between upper stage plane beds and planar cross bedding. The low angle is due to the “washing-out” of dune-type bedforms under unidirectional flow conditions, transitional between the dune stability field and the upper stage plane bed field (Bridge and Best, 1988; Miall, 1996). This would suggest bed shear stresses of between 2 and 5 Nm<sup>-2</sup> and velocities of between 0.8 and 1.1ms<sup>-1</sup> for flow depths between 0.25 and 0.4m (Ashley 1990), although in deeper flows similar bed shear stresses could be expected at lower velocities.

In contrast to subfacies S1, S1<sub>2</sub> shows no current-related structures, and contains more silty laminae in its laterally extensive sets than S1. This indicates that S1<sub>2</sub> is deposited from suspension in relatively quiet water, and that the low-angle beds represent deposition on a dipping surface. The silty laminae represent periods of reduced flow strength when the sediment size reaching the locus of deposition is reduced.

### 3.3.6 Planar cross-bedded sandstone (Sp and Sp<sub>2</sub>)

#### 3.3.6.1 Description

These facies are distinctive, being of similar lithology to facies Sm, Sh and S1, but showing very well developed planar cross bed sets. First order set-bounding surfaces are flat and horizontal to gently dipping. Bed set heights vary, from as little as around 0.1m (Fig. 3.7) up to 0.9m, but the larger examples are exceptional, and the majority of the sets across the localities studied were 0.15-0.33m thick (see graph and table in App. A17). The mean cross bed thickness from the Tullig Sandstone localities is 0.25m. Foreset laminae become asymptotic with bed bases in most cases, although angular contacts are present. The maximum foreset dip recorded is 36°, and the minimum 3°, but dips between 15° and 17° are most common (App. A18). Slight changes in grain size cause the foreset laminae to be picked out by weathering so they are clearly visible in the field. Stoss sides are rarely seen preserved in the field. Figures 3.7 and 3.8 show examples of facies Sp from Truskleeve and Killard.

At two of the localities, Tullig Point and the stratigraphically lower part of the Killard outcrop, the foresets show silty to muddy laminations at intervals, and are therefore given the facies name Sp<sub>2</sub> to distinguish them from the cleaner Sp cross sets. The

finer laminae seen in the Sp<sub>2</sub> facies are not in bundles and do not show any cyclical pattern. The silty laminae often coalesce at the base of each set to form a fine-grained lower bed boundary, and they do not cover the entire foreset, being confined to the lower third to two-thirds. These particular Sp<sub>2</sub> planar cross beds are not found in any of the other outcrops. Examples of these two types of planar cross-bedded facies can be seen in the logs in App. A (for example, between 18 and 20m in A8; and between 4.0 and 4.8m in A15).

### 3.3.6.2 Interpretation

Planar cross bedding is the result of straight-crested (2-D) dune migration, caused by unidirectional currents greater than a certain strength passing over a sandy bed. The foreset laminae are created by repeated avalanching of sand grains down the slip face of the dune. The slight asymptotic shape of the foresets is due to the generation of scour troughs in the dune lee by separation zone eddies, and may signify a higher flow speed than that associated with the grainflow-dominated angular-based foresets (Miall, 1996). The fact that stoss sides are not often preserved means that the set heights do not reflect the total height of the dune bedforms that created them.

In facies Sp<sub>2</sub>, where fine, silty laminations are seen at intervals on the foresets, this implies a slowing of currents sufficient to allow deposition of sub-sand sized particles from suspension. This suggests that deposition of the siltier cross bed sets occurred under slightly different conditions from the clean, planar cross-bedded units; while unidirectional flows were active, and strong enough to form dunes, there were also periods of reduced current flow not seen in the Sp facies. This could equate to flood events and inter-flood quiescent periods, which suggests a possible seasonality to the drapes. The fact that the drapes are not in bundles (i.e. concentrated in some places and more widely spaced in others), and do not possess any related oscillatory flow structures, shows that they are not related to the diurnal changes in flow velocity related to tidal processes.

The interpretations of other facies, which are found in association with each type of planar cross beds (Sp and Sp<sub>2</sub>), are important in confirming the interpretations given here. These facies associations will be discussed more fully in the facies association section (Section 3.4).

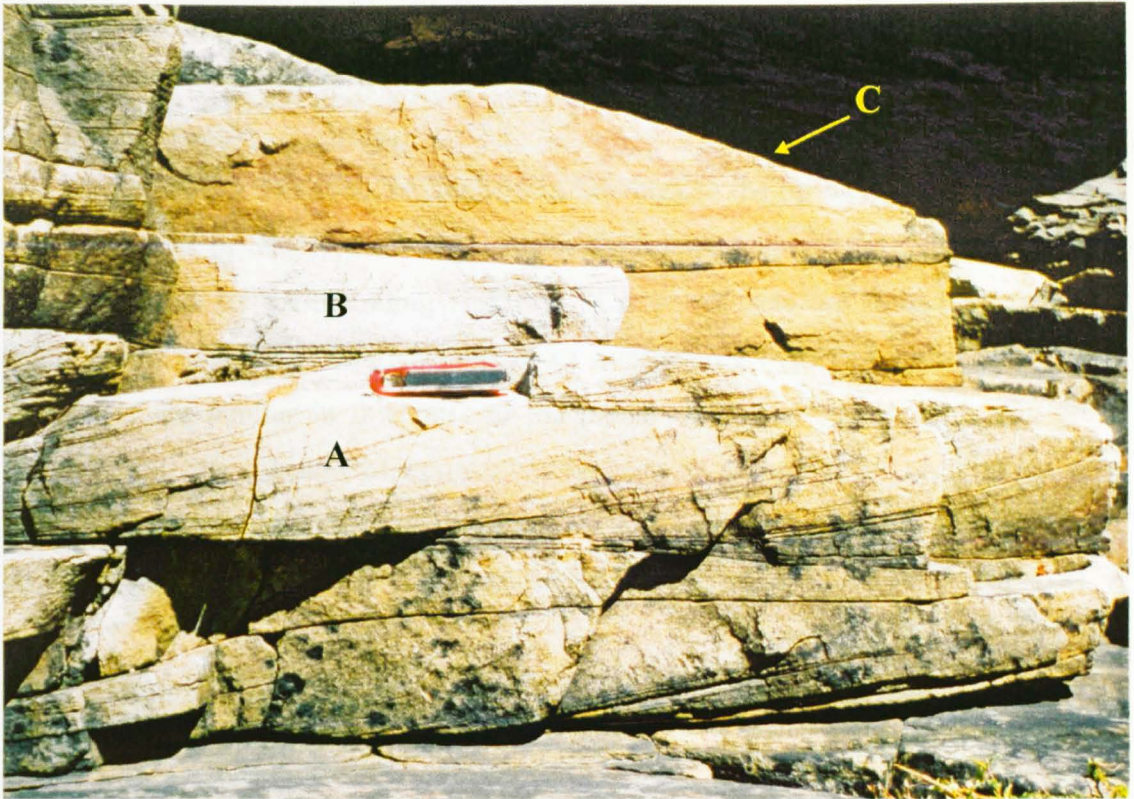


Figure 3.7. Planar cross-bedding (facies Sp) in fine to medium sandstone within the Tullig Sandstone at Trusklieve (see Figure 3.2 for location). Note the difference in foreset dip between beds A and B, and the truncation of the beds by a steep erosional surface dipping to the right (C). The compass is 0.1m long.

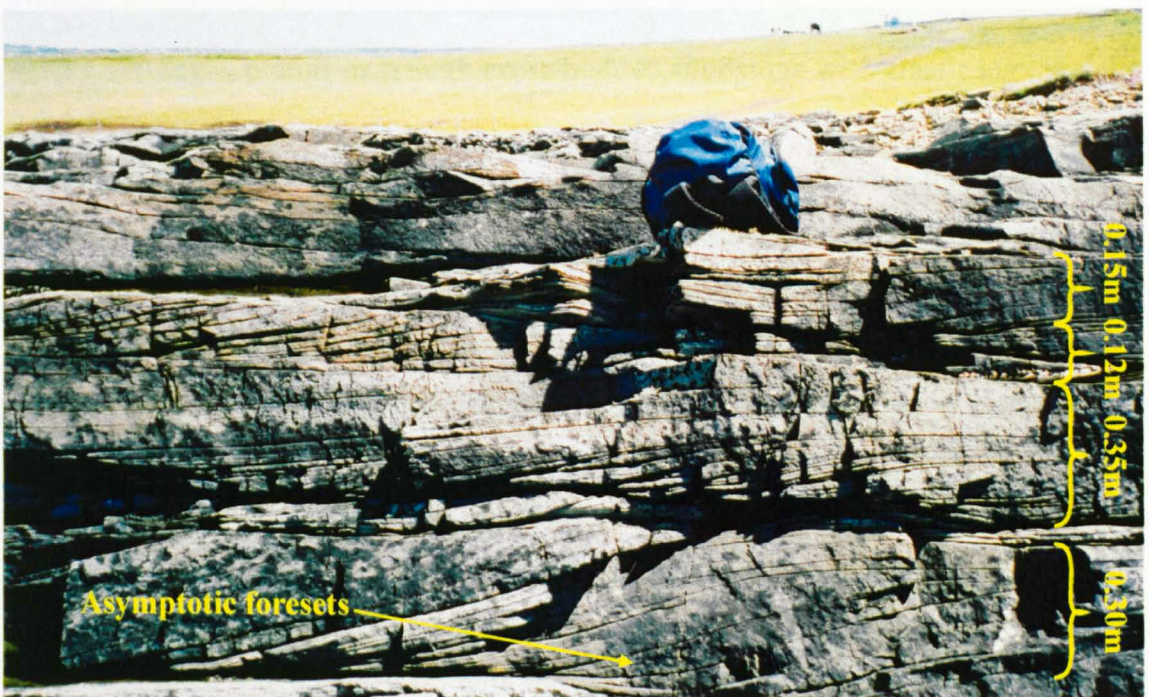


Figure 3.8. Planar cross-bedded fine to medium sandstone (facies Sp) within the Tullig Sandstone at Killard (between 19.5 and 20.5m in Appendix A8). Note the consistency in dip direction, foreset surfaces dipping to the left. Set heights at this locality vary from 0.12m to 0.40m, and the thicknesses of a single set often varies along strike; note the asymptotic foresets in the lowest set, and the flattening-out of foresets in the 0.35m-thick bed to give horizontal bedding.

### **3.3.7 Trough cross-bedded sandstone (St)**

#### **3.3.7.1 Description**

This facies, referred to as St, is identical in lithology to the Sp facies described above, but is distinct in that it exhibits concave-upwards asymptotic foresets and trough-shaped first order set-bounding surfaces. Cross bed sets are mutually erosional, cutting into each other and stacking in an overlapping manner. Individual trough cross sets are similar in thickness to the planar cross bed sets, heights clustering around 0.2-0.3m. Widths of troughs can be seen on second order bedding surfaces and vary between 0.7 and 1.2m (see Figs 3.9 and 3.10). Examples of this facies can be seen in the logs in App. A (for example, at 22 and 24m in A8; and at 2m in A12).

#### **3.3.7.2 Interpretation**

Trough cross beds are formed by the migration of three-dimensional (sinuous crested) dunes under the influence of unidirectional currents. They may form at higher flow speeds (for a given grain size and flow depth) than planar cross beds, and/or are associated with flows of longer duration than the flows that form planar cross beds (Baas, 1994).

### **3.3.8 Low-angle, planar or trough cross-bedded sandstone with clastic lag (Sc)**

#### **3.3.8.1 Description**

This facies is a variant on facies Sl, Sp and St. The only difference is the inclusion of a clastic lag deposit above the erosional bases of cross bed sets or co-sets. The clasts that comprise the lag are similar in size, shape and lithology to those seen in other lag deposit facies (e.g. Shc, Smc), ranging from 1cm to 25cm in length and including deformed rip-up clasts of laminated muddy siltstone. In some cases, clasts show crude imbrication and at times smaller clasts (<50mm) are seen aligned with the foresets within a bed. The lag is generally clast-supported at the base but becomes matrix supported as it grades into the cross beds above. Clasts are not seen “floating” at higher levels within bed sets, but are confined to the bases of sets (and to the lower third of foresets where associated with them). Examples of this facies can be seen in the logs in App. A (for example, between 8.95 and 9.3m in A8, and between 10.8 and 11.4m in A5).



Figure 3.9. A bedding surface within facies St in the Tullig Sandstone at Killard (see App. A8 at 22m). The intersections of the trough cross-bed laminae with the bedding plane are clearly shown. Note the clear curved shapes produced (some lines marked in yellow), and the way in which adjacent sets intersect each other. The hammer shaft is 0.3m long.

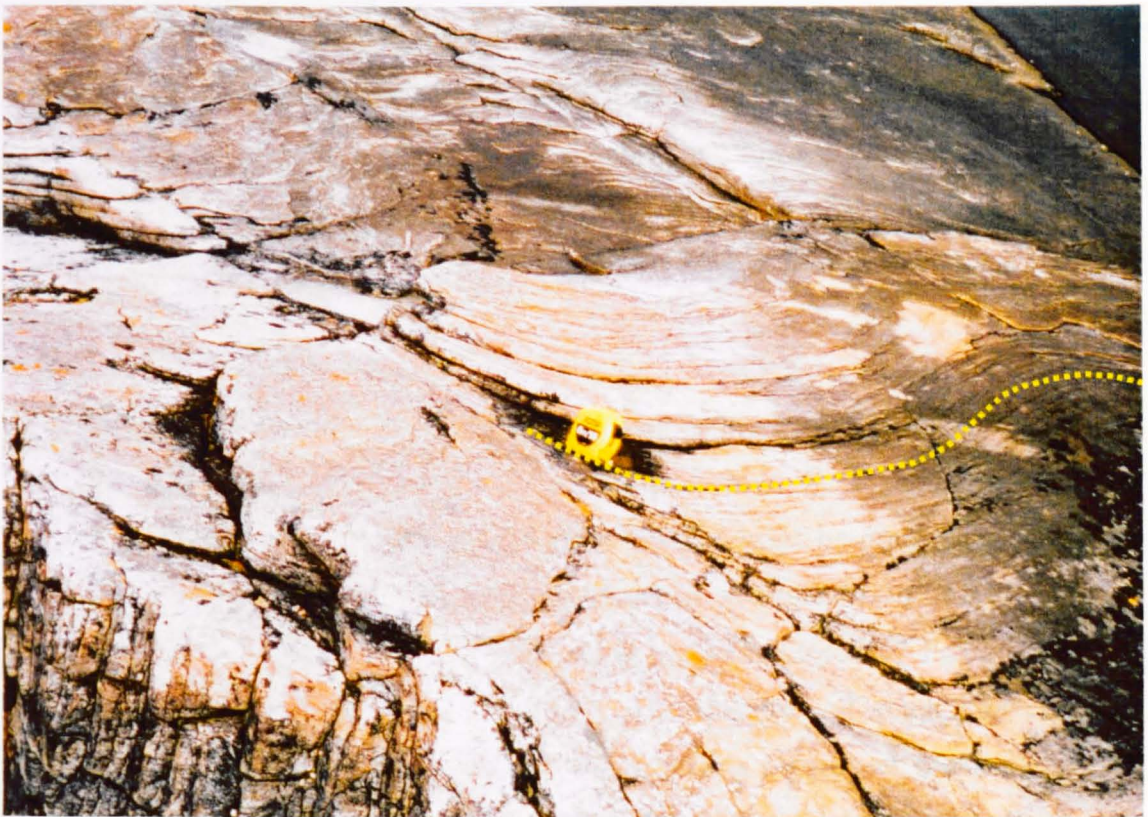


Figure 3.10. Trough cross- bedding (St) within the same bed as in Figure 3.9 above. The sinuous shapes of the foreset laminae (marked in yellow) give an idea of the shape of the original dune crest. The tape is 75 by 75mm.

### 3.3.8.2 Interpretation

The interpretation of this facies is that an initially strong erosive unidirectional current, carrying a coarse clastic bedload, wanes to deposit first the coarse bedload and then the finer sandy bedload, which forms dunes in continuum with the conglomeratic lag. The flow strength is sufficient to erode and carry large clasts before it wanes, and it remains strong enough to cause dune migration.

### 3.3.9 Clast-supported sandstone conglomerate (Ccm)

#### 3.3.9.1 Description

The conglomeratic facies, Ccm (Fig. 3.11), is erosively based, massive, and clast supported, with a fine to medium grained sandy matrix. It does not show any fining up and does not grade into sandy facies, instead showing a sharp contact with overlying beds. Clasts vary in size from very coarse sand (1-2mm) through pebbles (4mm-64mm) to cobbles (up to 300mm), with very little sorting. Some flow alignment and imbrication is sometimes present but it is not pervasive. Clasts show a range of lithologies, including laminated mudstone and siltstone, fine-grained sandstone, and occasional quartz and feldspar grains. The roundness and sphericity of the clasts varies considerably, with the majority of clasts being rounded to well rounded, but in places the facies is dominated by sub-angular clasts showing signs of deformation and folding. These deformed clasts are always siltstone or mudstone, and are usually elongate parallel to their internal lamination. Examples of facies Ccm are seen in the logs in App. A (e.g. in A2 between 5.0 and 5.5m, and in A8 at 10.7m).

#### 3.3.9.2 Interpretation

The size and rounding of the clasts incorporated in the Ccm facies shows that they have been moved by a strong unidirectional aqueous flow. Experimental work shows that flow velocities at a height of 1m above the bed must be greater than  $3\text{ms}^{-1}$  in order to move grains larger than 0.1m in diameter in water of  $20^{\circ}\text{C}$  (Miller *et al.*, 1977). The erosional bases of Ccm beds are also evidence of flows with high velocities and high erosional capabilities. The rounding of some rare clasts of extraformational lithologies (e.g. quartzite) suggests a significant transport history, although the deformed and angular clastic component tells a different story. The deformed clasts were ripped up shortly before they were deposited; their silty/muddy lithologies show that the flow was eroding through fine-grained facies. The clasts



Figure 3.11. Photo showing conglomeratic facies Ccm (marked A) in the section between 3.5 and 6.0m in Appendix A2. The chaotic, massive appearance of the bed reflects its poorly sorted internal structure. Note its erosional base cutting out the sandy bed below (marked B) and the sharp upper contact with the sandy facies above (marked C). The tape is 75 x 75mm.



Figure 3.12. Sandstone deformed by liquefaction and fluidisation (facies Sd) seen in the Tullig Sandstone at Killard (see Appendix A7, 20.35-22.5m). In the centre of the photo, the original bedding has been preserved (A), while the beds above and below are folded and contorted. Some obvious folds are marked (B), as is a ball and flame structure (C - relative movements are shown by red arrows). The rucksack is 0.35m tall.

were deformed as they were ripped up and while they were being transported, because the substrate they were derived from was not lithified when it underwent erosion.

The clasts were deposited rapidly, along with the sandy matrix, when the strong flows decelerated and were unable to support such a coarse bedload (a process documented by Bridge, 2003). The scour created by the strong flow was then filled with clasts and sand, and the waning currents were sometimes strong enough to cause flow alignment of the smaller clasts.

### **3.3.10 Deformed sandstone (Sd)**

#### **3.3.10.1 Description**

Lithologically, facies Sd is the same as sandstone facies Sm, Sh, Sl, Sp and St, but while originally either horizontally or cross-bedded, it now exhibits folded and deformed bedding (Fig. 3.12, and in logs in App.A7 (20.35-24.0m) and A8 (27.2-28.45m)). Internal load structures are seen, with intervening narrow, vertical “pipe” features with massive to faintly vertically laminated internal structure. Load casts and flame structures are common features of the lower boundary of this facies. In some places the original bedding is no longer visible and the sandstone appears massive and featureless.

#### **3.3.10.2 Interpretation**

Facies Sd is only encountered in the Tullig Sandstone at three localities – the north and south outcrops at Killard, and the southern outcrop at nearby Carrowmore Point. In each case the deformed beds are found at roughly the same height above the base of the sandbody (14.5m, 18.5m and 16.7m respectively), suggesting that the process causing the deformation was widespread laterally (there is a distance of 4km between the outcrops; see Fig. 3.1) but confined to within 1-2m at a particular level within the succession. The internal structure of the beds shows that they have behaved in a fluid fashion, flowing and deforming under gravity. The process that allows the sediment to behave in this liquid manner is liquefaction, which is caused by a reduction in the shear strength of the sediment. This can occur due to a shock, for example an earthquake, often associated with synsedimentary fault movement, or a sudden increase in loading caused by rapid deposition (Tucker, 1996). The vertical “pipes” visible at some points within the facies show that water has flowed upward through

the sandstone, entraining sand grains and creating fluid escape structures (the process of fluidisation), between which load casts (or “pillows”) are formed as sand sinks into the space left by the escaping water.

The fact that the liquefaction affects only a discrete layer within the Tullig Sandstone, and that this horizon is close to the top of the sandbody, gives a clear picture of the possible cause. It suggests that the beds beneath the deformed horizon were sufficiently compacted and lithified to retain their cohesiveness when subjected to an externally generated shock (perhaps movement on a nearby fault plane) so that only the most recently deposited, least compacted, beds were affected. It is unlikely that a sudden loading event could have affected the entire area from Killard to Carrowmore Point (see Fig. 3.1) equally and simultaneously to induce deformation.

### **3.3.11 Ripple cross-laminated sandstone (Sr)**

#### **3.3.11.1 Description**

This facies occurs in fine to medium-grained, well-sorted sandstone, and also in silty sandstone, and is distinguished by well-developed cross-lamination. Cross sets are less than 40mm in height, and are more typically 10-20mm. The foreset cross laminae all dip in the same direction within any one ripple or ripple set, although successive sets may have slightly different foreset dip directions (the variation is usually less than 90°). In some cases, facies Sr occurs as single sets within a finer grained facies (Fig. 3.13, and App. A2 at 4.3m); here each set shows an undulating upper, and occasionally lower, surface. The ripples thus outlined are asymmetric in cross-sectional profile, with steeper foresets and gentler stoss slopes. The wavelength of these ripples is between 50 and 150mm; heights, measured from peak to trough, vary from 3-20mm. This gives ripple indices that cluster around 12, where ripple index = wavelength/crest-to-trough height (see App. A19).

Facies Sr also occurs within other sandy facies (Fig. 3.14, and App. A8 at 10.4m) where there is a gradational change from a different sedimentary structure (e.g. planar cross bedding or horizontal bedding) to the rippled Sr facies.

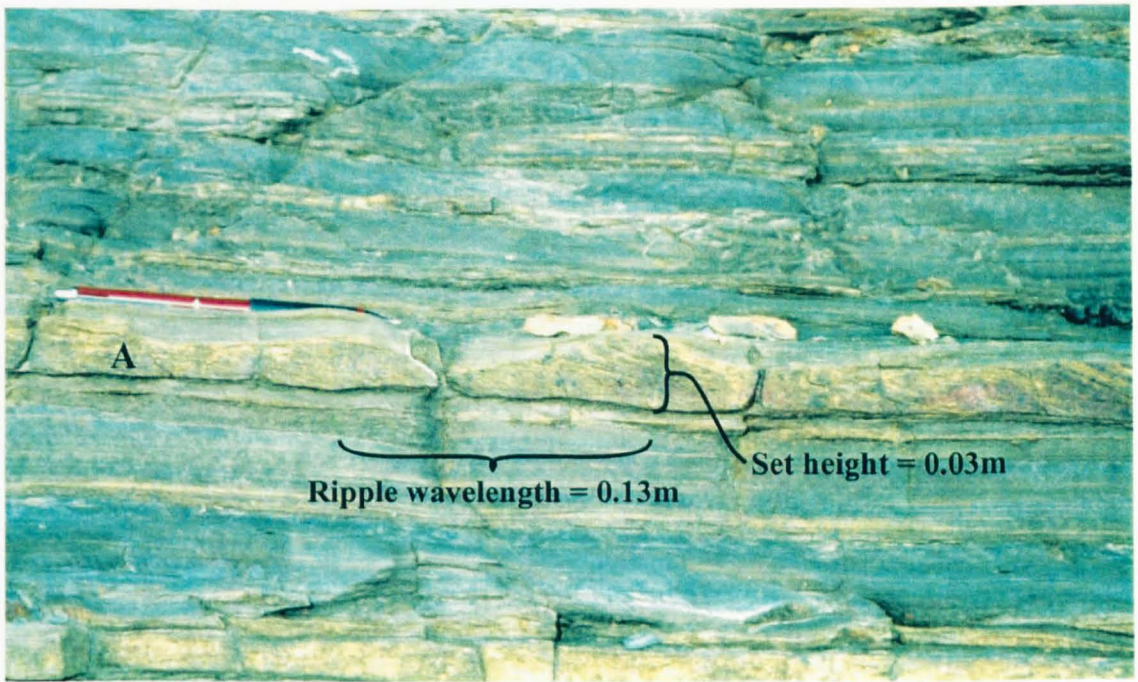


Figure 3.13. Sandstone (A) appears as a thin ripple cross-laminated bed (facies Sr) within laminated siltstone (see log in App. A2, at 4.3m). The foresets dip to the right, indicating that this is the direction of flow. Other thin (1-5mm) sandy layers interrupt the silt and mud, making up the fine-grained heterolithic facies (Flh). The pencil is 0.14m long. The view is looking east at the cliff face at Trusklieve.

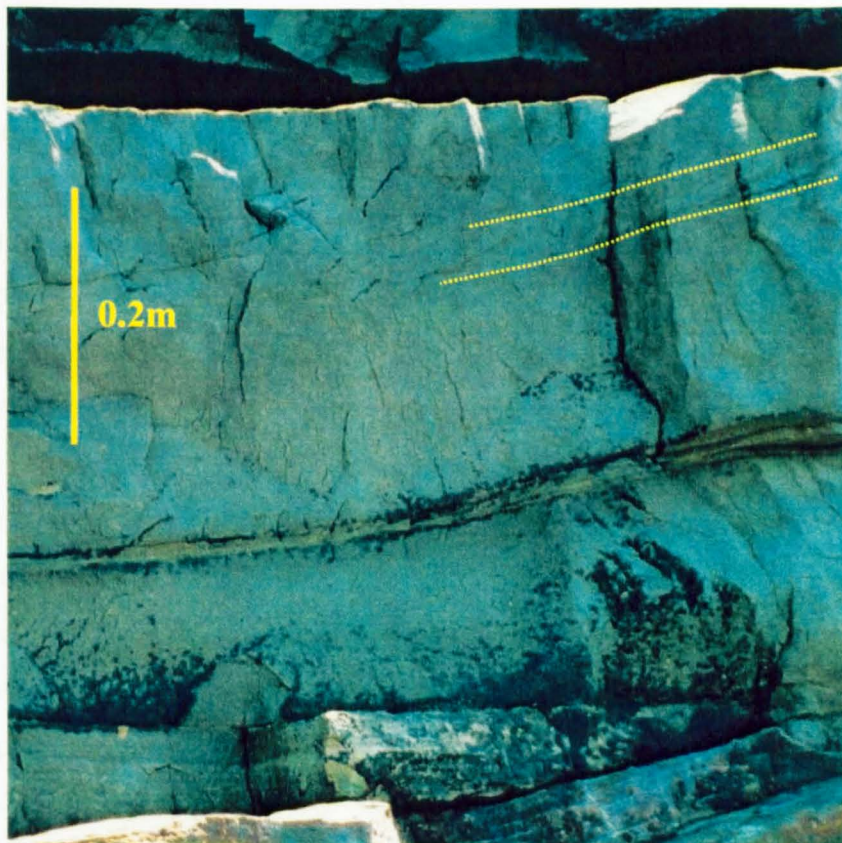


Figure 3.14. This photo (taken at a height of 4.2m in the log in App. A4) shows a single set of ripple cross-laminae (Sr, outlined in yellow) within a bed of horizontally laminated sandstone (facies Sh). The set is 0.03m thick. The ripples appear near the top of the bed, suggesting a waning flow over time. The foresets dip to the left, indicating that this is the flow direction. The view is to the east-southeast, at the Trusklieve outcrop.

### 3.3.11.2 Interpretation

The ripples that characterise facies Sr are generated by unidirectional fluid flow over a sandy surface, at flow velocities lower than those required to form dunes (for the same calibre sediment). For fine-grained sandstone, this would be below  $0.8\text{ms}^{-1}$  (Ashley, 1990) and probably lower than  $0.6\text{ms}^{-1}$  (Harms *et al.*, 1975) for mean flow depths of 0.25-0.40m. The ripple indices are dominantly between 9 and 19 (App. A19), which agrees with the classification of current ripples given by Tucker (1996), who states that ripple indices for water-formed unidirectional current ripples are greater than five and should mainly fall in the range of 8-15. This agreement confirms that the ripples are formed by unidirectional water currents.

Where facies Sr appears as isolated sets within finer grained facies, the amount of sand available for transportation and deposition is limited, leading to the “stranding” and subsequent burial of the ripple train. These ripple sets represent pulses of tractional flow, allowing deposition of fine sand-sized particles in areas normally experiencing deposition of finer material (silt and mud) from suspension. Where facies Sr occurs in gradational association with facies Sp or Sh, it represents a reduction of flow velocity sufficient to subdue or halt dune migration and to allow the development of ripples on top of the dune or planar bed.

### 3.3.12 Climbing ripple cross-laminated sandstone (Sr<sub>c</sub>)

#### 3.3.12.1 Description

This facies also occurs in silty sandstone and fine-grained sandstone, but differs significantly from facies Sr in terms of its sedimentary structure. The ripple cross-laminated sets in facies Sr<sub>c</sub> stack upon each other (Fig. 3.15) so that the base of each set is at an angle to the horizontal. Internally, the foreset laminae in each set dip in a single, constant direction, opposite to the dip of the set boundaries. Within each set, the lee and the stoss sides of the ripples are preserved. The crest of each successive ripple is offset by a few millimetres from the one beneath, in the same direction as the foreset dip. The angle of climb in successive sets of these climbing ripples can vary (Fig. 3.15), being between  $10^\circ$  and  $15^\circ$  in most cases. Ripple indices (wavelength/height) vary between 15 and 35. Ripple heights vary between 4 and 10mm, and wavelengths are 70-120mm. Examples of facies Sr<sub>c</sub> are seen in App. A2 (at 0.5m) and A14, (at 1.7m). Purely aggradational ripples, which show no forward



Figure 3.15. Asymmetric climbing ripples produced by rapid deposition of fine sand from a unidirectional flow (towards the right). This facies ( $Sr_c$ ) occurs at the top of a coarsening-up heterolithic package (Flh) below the Tullig Sandstone at Liscannor (see Appendix A13, at 2m). Ripple wavelengths are 70-120mm, heights are 4-10mm. The sunglasses are 140mm wide; the red and yellow scale is 40mm tall.



Figure 3.16. Facies  $Sr_c$  (photo from Killard, at 8.2m, App. A15). Purely aggradational climbing ripples are marked A. The lowermost visible ripple set (B) is asymmetric; in the field, unidirectional cross laminae are visible, indicating action of unidirectional currents. Wavelength of ripples is 70mm (on average). The compass is 100mm long.

migration of ripple crests, are also seen in one locality (at 7.75m and 8.15m in App. A16, and in Fig. 3.16).

### 3.3.12.2 Interpretation

The climbing ripples that comprise facies  $Sr_c$  have high ripple indices ( $>15$ ), which show that the ripples are current-generated and are formed when a unidirectional flow deposits sediment at an aggradation rate relatively high compared with their rate of migration. The angle of climb is greater than the angle of the stoss sides of the ripples, meaning that the stoss faces are preserved. The ripple height and angle of climb can be used to calculate either the rate of sediment deposition normal to the bed or the bedload transport rate, where one of the latter two values is known (Allen, 1970a). In this case, there is insufficient information to calculate these values, but the graphs provided by Allen (1970a) allow deposition rate to be estimated, assuming a critical flow velocity of  $0.36\text{ms}^{-1}$ . For an angle of climb of  $15^\circ$  and a ripple height of 6mm (the average height recorded in the field), the rate of deposition is estimated to be  $0.0056\text{gcm}^{-2}\text{s}^{-1}$  (which for a bulk density of  $1.9\text{gcm}^{-3}$  works out to 10.65cm of vertical aggradation per hour).

### 3.3.13 Wave ripple cross-laminated sandstone ( $Sr_w$ )

#### 3.3.13.1 Description

Facies  $Sr_w$  is lithologically similar to facies  $Sr$  and  $Sr_c$ , but is distinct in that the ripples are symmetric in cross-section, and exhibit changing foreset dips, both between sets, within sets, and within individual ripples (chevron interlaminae). The ripple crests are continuous and sometimes sinuous (Fig. 3.17), with ripple wavelengths ranging from 55mm to 200mm, and ripple heights ranging from 4mm to 30mm. Ripple indices for these ripples are less than 15 (see graph and table in App. A19). In some cases, ripple crests are modified and less continuous (Fig. 3.17). Logged examples are seen in App. A16 at 11-12m, and A9 at 28.0-28.3m.

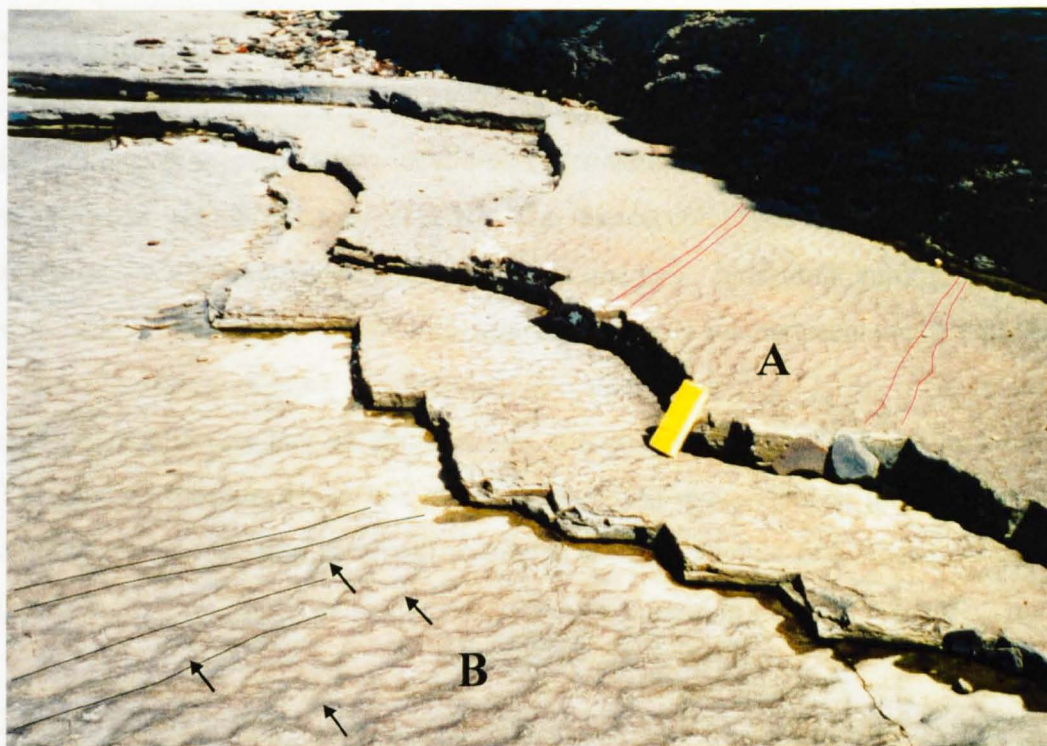


Figure 3.17. Photo taken 0.5m below the base of log A3, showing facies  $Sr_w$ . Symmetrical ripples with continuous crests (marked A; some crests highlighted in red) have been produced by wave reworking of fine sand layers at the top of a coarsening-up heterolithic package (facies  $Fl_h$ ). Bed B shows additional reworking by currents to give slightly less continuous crests. Black lines show ripple crests, arrows show flow direction and point of ripple modification. The average ripple wavelength is 70mm. The notebook is 0.2m tall.

### 3.3.13.2 Interpretation

These symmetric ripples are interpreted as wave-generated ripples; continuous crest lines, symmetrical cross-sectional profiles and internal chevron interlaminae are all typical features of wave ripples, being formed by the short period oscillating currents produced by waves. The low values for ripple indices (<13 – see App. A19) agree with the assertion of Tucker (1996) that wave ripples have indices between 4 and 13 and confirm that these ripples are formed by wave action. Ripples with slightly less continuous crests are likely to have been modified by unidirectional currents during, or after, formation.

### **3.3.14 Hummocky cross-stratified sandstone (Shcs)**

#### **3.3.14.1 Description**

Facies Shcs is present at two localities, Carrowmore and Killard, and occurs only in single beds, not in successive beds. The facies comprises fine to lower medium sandstone, with large-scale hummocky cross bedding. Individual hummocks range in size from 2-4m across, often with intervals of 10-15m between them, and exhibit internal surfaces dipping in different directions (see Fig. 3.18). These internal surfaces can be both convex and concave, and generally dip at angles of less than 15°. The tops of the hummocks are often capped with wave ripples; the ripples on one dipping surface of the hummock may be at a distinct angle from those on the other (see Fig. 3.19). Logged examples occur in App. A16 at 20.6m and A9 at 27.25m.

#### **3.3.14.2 Interpretation**

Hummocky cross stratification is recognised as a bedform produced by storm wave action and the action of complex, multidirectional flows (for example Dott and Borgeois, 1982). Dott and Borgeois (1982) recognise that the internal laminae of the hummocks are produced by individual wave oscillations or pulsations of wave trains, which can happen in a few seconds to several minutes. Dott and Borgeois (1982) also recognise a second order of internal surface, which bounds bundles of hummocky bedforms, and they explain these bundles as representing pulses within a single storm event that could last for hours, days, or even weeks. In the outcrops studied, however, no bundles of Shcs were seen, probably an indication that the storms creating the Shcs were short-lived events and produced only single beds of hummocky cross stratification. The wave ripples seen on the upper surfaces of the hummocks are evidence for decreasing wave power, allowing smaller waves to rework the top surfaces of the hummocks. In the example at Killard, the Shcs bed is found at the top of a coarsening-up sequence, and shows another sign of abandonment (besides ripples) in that it is intensely bioturbated in its upper 30-50mm (App. A16, 20.75m).

### **3.3.15 Horizontally laminated sandstone type 2 (Sh<sub>2</sub>)**

#### **3.3.15.1 Description**

Facies Sh<sub>2</sub> initially resembles facies Sh, in that it is parallel-laminated sandstone. However, there are four important differences. Firstly, there is no evidence of primary current lineation in facies Sh<sub>2</sub>. Bed surfaces are featureless, and bed bases

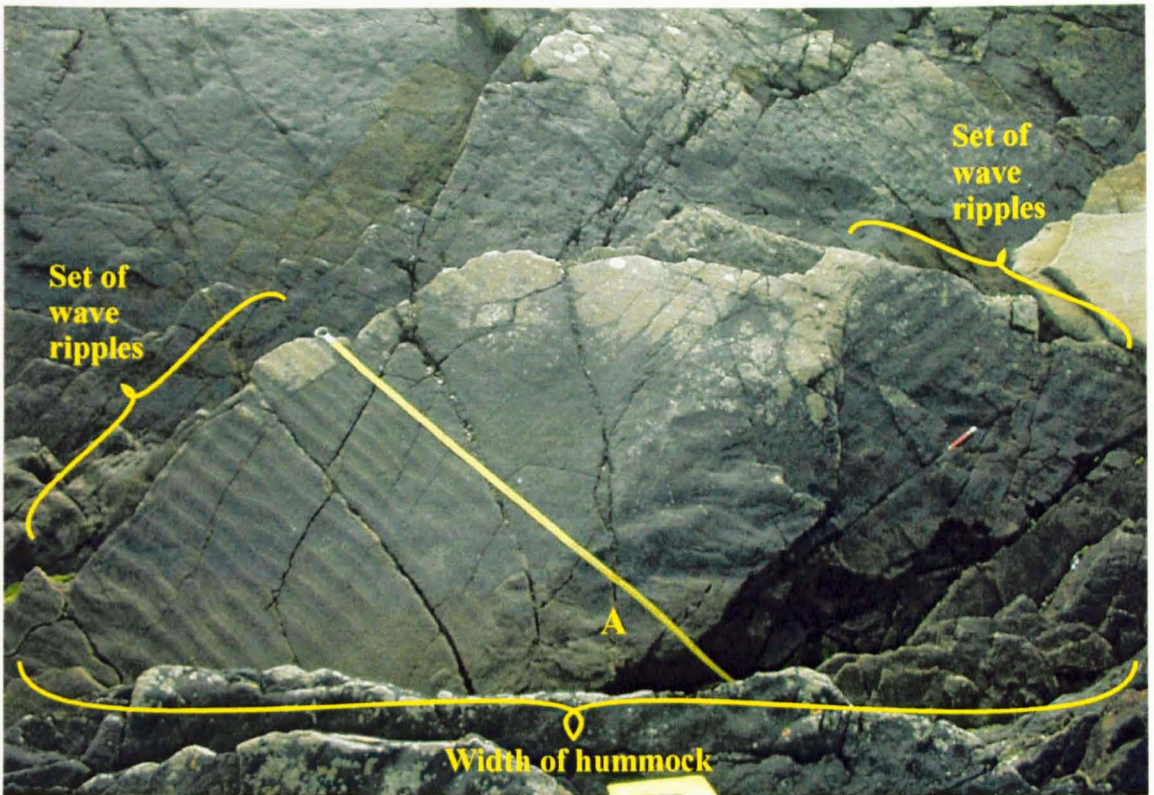


Figure 3.18. Facies Shcs, showing a plan view of a hummock at Killard (see App. A16, at 18.25m). It is dome-shaped, dipping radially from its centre (marked A). These dipping surfaces have been wave reworked, with the crests of the wave ripples oriented differently from each other. The tape, 1.10m long, is aligned parallel to one ripple set. The red pencil (70mm long) is aligned parallel to the other set.



Figure 3.19. Facies Shcs, showing a cross-section through a hummock in the same bed as in Fig. 3.18. The hummock crest is marked A. Internal surfaces dip in three directions (marked by yellow arrows), and note their convexity at B. The dashed yellow line marks the top of the logged sequence (App. 16 and Fig. 4.26). The tape is 0.4m long.

are sharp but non-erosional. Secondly, there is an increase in the fine-grained component in Sh<sub>2</sub> compared with Sh; silt and mud-sized grains are apparent both between the sand grains, and also occasionally in discrete laminae, when the rock is viewed in thin section. The discrete silty sand laminae are also just visible in the field, as the different grain size leads to slight differences in weathering which allow such laminae to be seen. The laminae are no more than 1-2mm thick, and are spaced at intervals of 10-50mm (Fig. 3.20). Thirdly, some beds show faint fining-up grading, and in one location (see 7.7-9.0m in App. A16) this is associated with climbing ripples. The fourth difference between facies Sh and Sh<sub>2</sub> is that the latter sometimes shows moderate bioturbation, whereas the former shows none. In facies Sh<sub>2</sub>, trace fossils such as *Monocraterion* and *Skolithos* occur, and frequently bivalve escape traces (fugichnia) 0.1-0.2m in vertical length are seen (see Figs 3.20 and 3.21). For logged examples of facies Sh<sub>2</sub>, see App. A15 (1.0-3.0m) and A16 (3.0-3.5m).

#### 3.3.15.2 Interpretation

Facies Sh<sub>2</sub> is interpreted as having been deposited rapidly from suspension, giving rise to the graded parallel laminations, with periods of reduced velocity allowing deposition of the finer-grained laminae. Any tractional influence leaves no evidence of its existence within the Sh<sub>2</sub> facies; although the close association of climbing ripples (Sr<sub>c</sub>) in some places shows that the prevailing process is one of very rapid deposition from a decelerating unidirectional current. Support for the rapidity of sedimentation is also found in the occurrence of bivalve escape shafts (fugichnia), which form as bivalves move upward through the sediment to prevent themselves being buried. Escape shafts between 0.1 and 0.2m long signify the instantaneous deposition of 0.1-0.2m of sediment. The presence of bivalves, together with rarer (in the Sh<sub>2</sub> facies) *Monocraterion* and *Skolithos*, is indicative of a brackish water or shallow marine environment; the restricted faunal assemblage indicates the former. Baines (1977) records a similar trace fossil assemblage within the delta top and upper delta slope of the Pendelian (Namurian) Sequence around Skipton, in the Central Pennine Basin. The similarity of the trace fossil assemblage described from facies Sh<sub>2</sub> to that described from the Pendelian of the Central Pennine Basin by Eager *et al.* (1985) also supports the idea that the environment of deposition is a shallow water delta front. This interpretation is further discussed in the facies association section, Section 3.4.

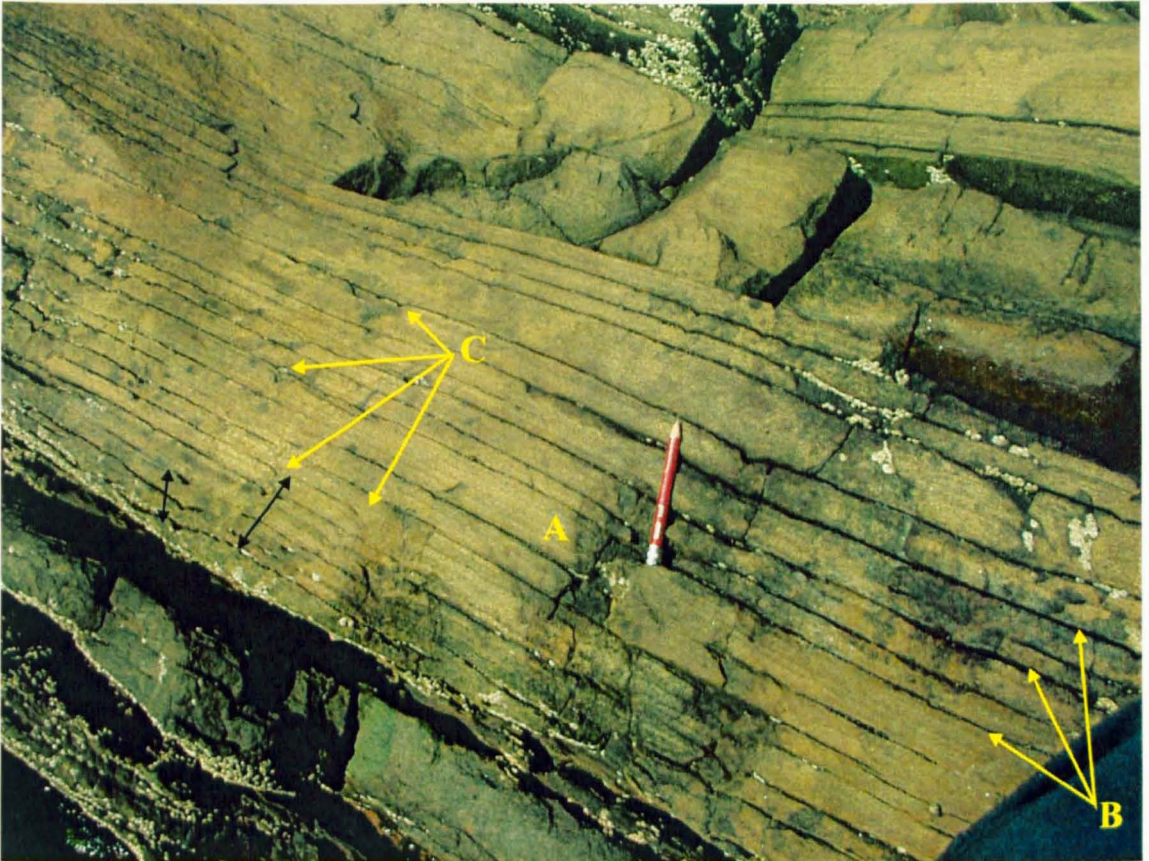


Figure 3.20. Facies  $Sh_2$ , at Killard (at 11.9m in App. A15). Note the excellent parallel lamination (e.g. at A), with finer grained laminae (marked B) picked out by weathering. Bioturbation is evident; bivalve escape burrows (fugichnia - marked C), are present, implying instantaneous deposition of 100-200mm of sediment. Individual traces disrupt bedding and may be up to 100mm long (black arrows). The pencil is 100mm long.



Figure 3.21. Top surface of the bed shown in Figure 3.20 above. The bivalve resting traces (*Lockeia* - marked A) are seen at the tops and bases of the escape shafts, which comprise a series of *Lockeia* marks. The pencil is 100mm long.

### 3.3.16 Interlaminated sandstone, siltstone and mudstone (Flh)

#### 3.3.16.1 Description

Facies Flh (Figs 3.22 and 3.23) is laminated and heterolithic in appearance. The facies comprises laminated mudstone, siltstone, and fine sandstone, interbedded on a scale of 2-100mm. In some cases there is a discernible trend within the facies, in that the thickness and frequency of sandstone beds often increases upwards (App. A8 between 5.0 and 7.8m). At Killard, the laminae within facies Flh are undulating, although still parallel, in one part of the section (App. A8, 0-3.4m); this type of undulating interbedding, with roughly equal proportions of sand and silt/mud, is termed wavy bedding.

The sandstone layers within facies Flh are frequently ripple cross-laminated. These rippled beds, where laterally connected, and thicker than a few centimetres, can be classified as part of facies Sr (as described in Section 3.3.11 and Fig. 3.13). However, in many cases the rippled sandstones are only one set thick, and individual ripples are not laterally connected. The term lenticular bedding is used for isolated ripples within a fine-grained succession like this (Fig. 3.22). Because of its thin-bedded nature and occurrence only within facies Flh, lenticular bedding is considered part of facies Flh rather than facies Sr (see App. A3 at 4.3m, and A9 at 3.25m). While the majority of lenticular beds show unidirectional ripples, bi-directional ripples are rarely present (for example between 4.5 and 5.7m in A10).

Other features of facies Flh include asymmetric ripples in the sandy silt (different from the Sr facies, which is in clean sand), bioturbation, siderite nodules and plant material (App. A9, 0-11m, and App. A7, 0-2.7m). The trace fossils include *Arenicolites*, *Asterichnus*, *Curvolithus*, *Monocraterion*, *Lockeia* and *Skolithos* (see Section 3.3.19 below). The latter three trace fossils are more common in the sandy beds while the rest occur within, or originate in, the thinly bedded siltstones. Figures 3.21, 3.26 and 3.27 show examples of these trace fossils and Section 3.3.19 explains their origin and environmental significance. The siderite nodules commonly occur in particular layers (muds or silty muds) within facies Flh, and are sometimes laterally continuous beds rather than discrete nodules. Individual nodules are ovoid in shape and between 0.1 and 0.5m in lateral extent. The nodules may be as thick as 0.3m, although this is unusual; thicknesses are normally in the 0.5-0.15m range.



Figure 3.22. Overall appearance of the interbedded mudstone, siltstone and fine sandstone that comprise the heterolithic facies (Flh; covering the section between 1 and 4.2m in App. A6). Individual beds are horizontally laminated and are not usually thicker than 100mm, often being as thin as 3-5mm. Beds are very laterally extensive, continuing across entire outcrops (160m+). The tape is 75mm by 75mm.



Figure 3.23. Close-up view of interbedded mudstone, siltstone and very fine sandstone (facies Flh) from 4.3m in App. A3. The sandstone occurs as trains of isolated ripples within the silt (lenticular bedding, marked A) or just as very thin laminae (up to 3mm thick). The compass is 60mm by 100mm.

Laminae in the sediments surrounding the nodules are deformed around them, while the laminae within the nodules remain parallel and undeformed. No evidence of *in situ* plant material or rootlets is found within the Flh facies, although thin layers (<0.05m) of silt or sand containing numerous broken plant fragments are common.

### 3.3.16.2 Interpretation

The parallel-laminated and mud/silt dominated character of facies Flh is attributed to deposition from suspension in a body of quiet water that is not continually influenced by waves and currents. The rippled silts and lenticular sands represent periods of higher energy that bring coarser sediment to the site of deposition. Such higher velocity flow conditions could be related to periods of flood discharge, and/or storm events. The asymmetric ripples in the sand and sandy-silt intercalations indicate the action of unidirectional currents, suggesting that unidirectional flows, rather than currents related to storm or wave processes, are the more likely cause. However, the bi-directional symmetric ripples occasionally seen in lenticular beds within facies Flh do result from oscillatory wave action, indicating deposition in shallow water above fair weather wave base.

The siderite ( $\text{Fe}_2\text{CO}_3$ ) nodules are formed soon after deposition, which is why the surrounding laminae that are not siderite-cemented are compacted and deformed around them. Siderite forms by the reaction:



due to the iron reduction and bacterial methanogenesis of organic carbon compounds (Curtis, 1986). The iron is derived from the reduction of detrital iron oxides in a strongly reducing, organic-rich sedimentary environment. Siderite formation is inhibited in marine environments because  $\text{Ca}^{2+}$  ions react preferentially with the bicarbonate ( $\text{CaCO}_3$ ) present in seawater (Bennington, 1999). In a reducing marine environment,  $\text{Fe}^{2+}$  ions react preferentially with sulphides to form pyrite, and are thus prevented from building up to concentrations that would allow siderite formation. Therefore, only in a "nonsulphidic environment" can  $\text{Fe}^{2+}$  be precipitated as siderite (Berner, 1981). Sulphide-poor pore waters are achieved in organic-rich, non-marine sedimentary environments, which therefore provide optimal conditions for siderite formation (Berner, 1981). The presence of siderite within the Flh facies indicates that the facies is formed in a non-marine, organic-rich depositional environment.

### **3.3.17 Laminated siltstone (Fls)**

#### **3.3.17.1 Description**

Facies Fls comprises mid-grey siltstone laminated on a sub-mm scale. In most cases there is limited bioturbation (*Skolithos*, *Asterichnus*, *Monocraterion*) within the siltstone (for example, in App. A9 between 4.8 and 5.5m), but in some beds bioturbation is completely absent (for example at 10.5m in A2). Siderite nodules sometimes occur within this facies.

#### **3.3.17.2 Interpretation**

Facies Fls represents deposition from suspension in low energy, quiet water conditions. Where bioturbation is present, the ichnofacies suggest a brackish environment, since no characteristic Upper Carboniferous marine taxa (e.g. echinoderms, cephalopods and brachiopods) are found. The lack of sandstone laminae or any kind of current structure indicates that the silt was deposited below storm wave base and beyond the reach of flood discharge-related current deposition. In laminated silts that show no bioturbation, the environment is more likely to be fresh water.

### **3.3.18 Laminated mudstone (Flm)**

#### **3.3.18.1 Description**

Facies Flm is finer-grained than facies Fls, comprising mid to dark grey mudstone laminated on a sub-mm scale (Fig. 3.24). In most cases limited bioturbation is present within the mudstone (for example, in App. A9 between 3.5 and 4.5m), and in these cases siderite nodules are often present (App. A10 between 0 and 7m). In some mudstone beds bioturbation is completely absent, for example between 9.3 and 10.4m in A5. Facies Flm is also sometimes associated with plant rootlets (e.g. App. A4), and in places is affected by soft-sediment deformation, in the form of convolute laminae and load and flame structures at the top of some beds (Fig. 3.25). Facies Flm can also exhibit internal slumping and sliding (Fig. 3.24), and in some cases any traces of original lamination have been obliterated.

#### **3.3.18.2 Interpretation**

Laminated mudstone forms by pulses of deposition from suspension in low energy, quiet water conditions. The convolute laminae seen in places suggest that the facies

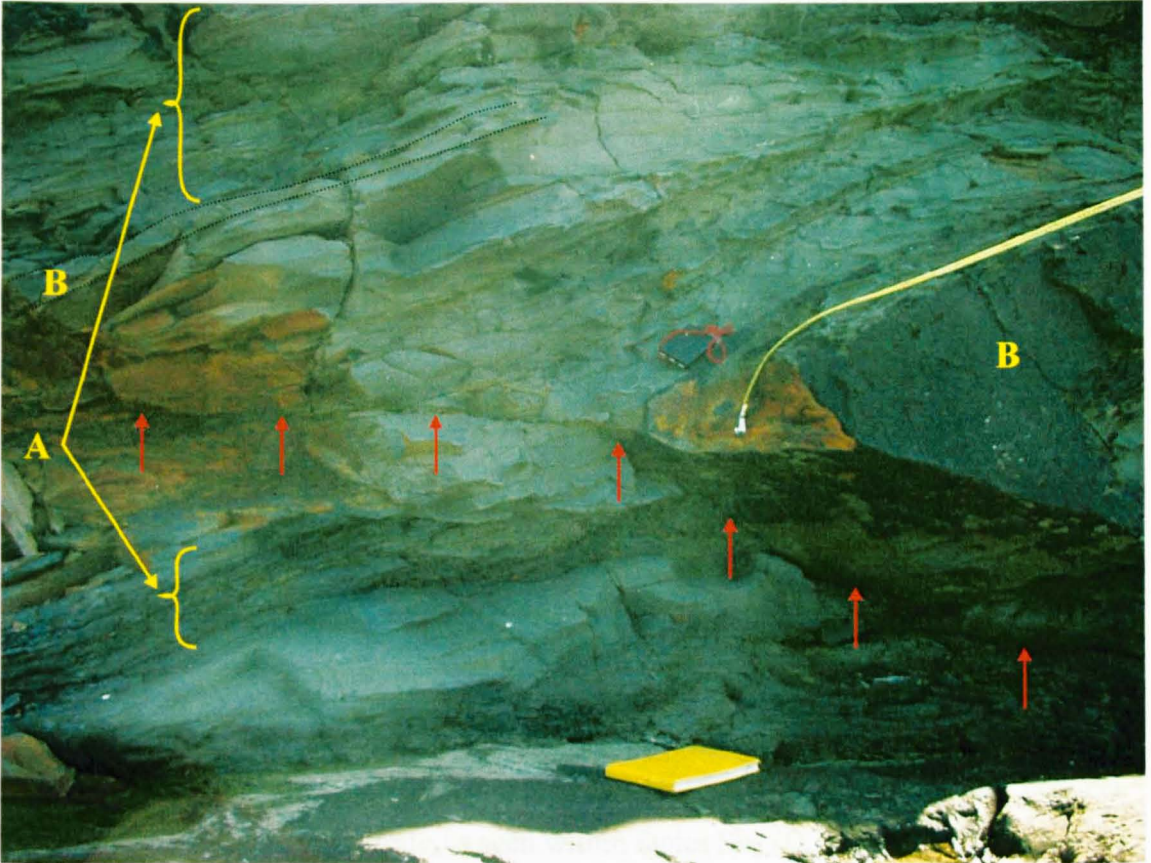


Figure 3.24. Facies Flm, in the Tullig Sandstone at Trusklieve (5.0-5.8m, App. A4). Parallel lamination is apparent (clearest intervals marked A), and an internal slide plane is arrowed. Note weathering differences, related to small changes in grainsize and cementation. Two silty-sand lenses, marked B, occur in the mudstone. The tape is 0.75m long.

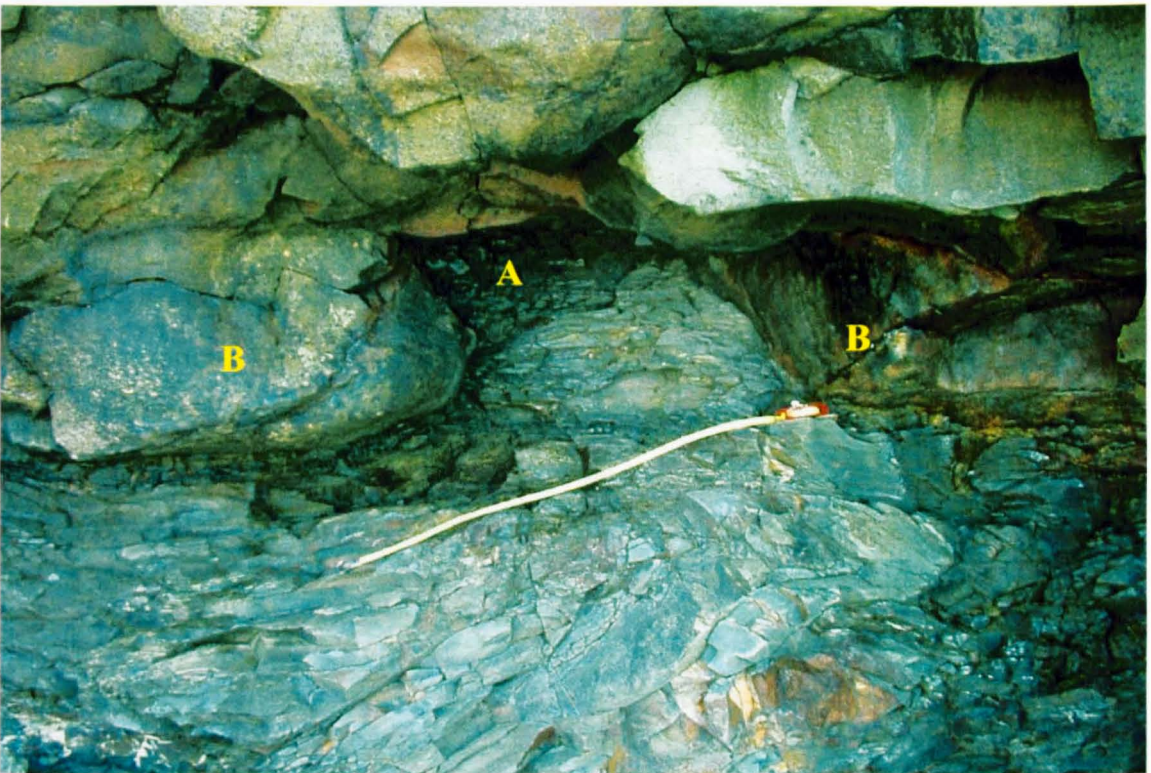


Figure 3.25. Facies Flm, laminated mudstone, from the same bed as Fig. 3.24. Parallel lamination (marked A) is apparent in part of a large flame structure. Elsewhere lamination is not evident, the bed having been comprehensively deformed. Load casts in the sandstone bed above (labelled B) accompany the flame structure. The tape is 1m long.

responds to loading and instability by dewatering and deforming internally. Where siderite is present, the pore water chemistry can be assumed to have been fresh to brackish, but definitely not marine, at the time of deposition. The limited trace fossil assemblage seen in some sections indicates brackish, shallow water conditions. The environment of deposition is discussed further in Section 3.4.

### 3.3.19 Ichnofacies

#### 3.3.19.1 Description

Several types of trace fossil are seen within the sediments at the studied outcrops, which bear close comparison with trace fossils found in the deltaic sediments of the Central Pennine Basin (Eager *et al.*, 1985).

#### *Arenicolites* sp.

This U-shaped burrow, about 1-3mm in diameter, with 15-30mm spacing between linked shafts and lacking spreite, is seen within facies Sh<sub>2</sub> (D, Fig. 3.26). The burrows extend downwards (up to 20mm) from thin muddy partings into the laminated sandstone (see App. A8, between 3.7 and 4.9m). *Arenicolites* burrows are interpreted as the dwelling structures of either suspension or deposit feeding invertebrates.

#### *Asterichnus*

This trace fossil occurs on the surface of fine sand beds, and is infilled with organic-rich muddy or silty sediment, which gives it a dark appearance. The trace is an irregular star shape, with shallow grooves no more than 1-2mm deep radiating from a round infilled hole, about 3mm in diameter, in the centre (Fig. 3.26). The radiating grooves are straight to slightly sinuous, and up to 30mm in length. *Asterichnus* occurs in the sandstone layers within facies Sh<sub>2</sub> and Flh (for example, between 3.7 and 4.9m in App. A8). It is not fully understood what organism is responsible for producing *Asterichnus* traces (Bandel, 1967) although the traces are thought to record a combination of domichnia/pascichnia activity (typical of modern tellinid bivalves).

#### *Curvolithus*

*Curvolithus* occurs on the surface of fine sand beds, which are often wave rippled. It appears as straight to slightly curved, often intersecting, trails with positive relief of up to 3mm. The trails are commonly 5-10mm wide, and may be up to 300mm long,

occasionally changing direction through angles of up to 25° (Fig. 3.27). *Curvolithus* appears to be a form of locomotive or feeding trace (Eager *et al.*, 1985).

#### *Monocraterion* and *Skolithos*

Both these names are applied to the same type of trace fossil, which is a single straight vertical burrow, passing upwards into a funnel-shaped, slightly wider burrow. The name *Monocraterion* is used when the funnel part is apparent. The vertical tubes are 2-4mm in diameter, with the funnels opening out up to 8mm (Fig. 3.26). *Monocraterion* is interpreted as the dwelling structure of a small worm-like invertebrate (Eager *et al.*, 1985).

#### *Lockeia*

This trace fossil combines an impression on a bedding plane and a vertical shaft cutting through bedding. The surface impressions (negative epichnia) are ovoid or almond-shaped, and are seen in great numbers on particular bedding planes (see Fig. 3.21). They are often aligned parallel or sub-parallel with each other, and frequently occur in ripple troughs, in which case their long axes are parallel to the ripple crests. Extending downwards from these epichnia are vertical shafts, which disrupt lamination and are the same width as the epichnia, approximately 8-20mm. The shafts are interpreted as escape paths (fugichnia) formed by bivalves, while the epichnia represent the bivalve resting traces.

#### 3.3.19.2 Summary and interpretation

The different trace fossils occur within different lithologies, but similar environments, and all those described above are commonly associated with Carboniferous deltaic facies (Eager *et al.* 1985). *Curvolithus* is found within the thinly bedded, striped siltstones of the Flh facies, while *Monocraterion* and *Lockeia* are found in sandier intervals (Sh<sub>2</sub>, Sr, Sr<sub>w</sub> and thin sands within the Flh facies). *Asterichnus* occurs on sandstone bedding surfaces within facies Flh, Sr and Sr<sub>w</sub>, while *Arenicolites* extends down from muddy laminae within Sh<sub>2</sub> or Flh sandy intervals. *Monocraterion* and *Lockeia* characterise the marine to brackish shallow water *Cruziana* and *Skolithos* ichnofacies of Frey and Seilacher (1980), and are typical of upper delta slope and delta front environments. The other trace fossils, although known to have slightly wider ranges of occurrence, are nonetheless very frequently associated with these

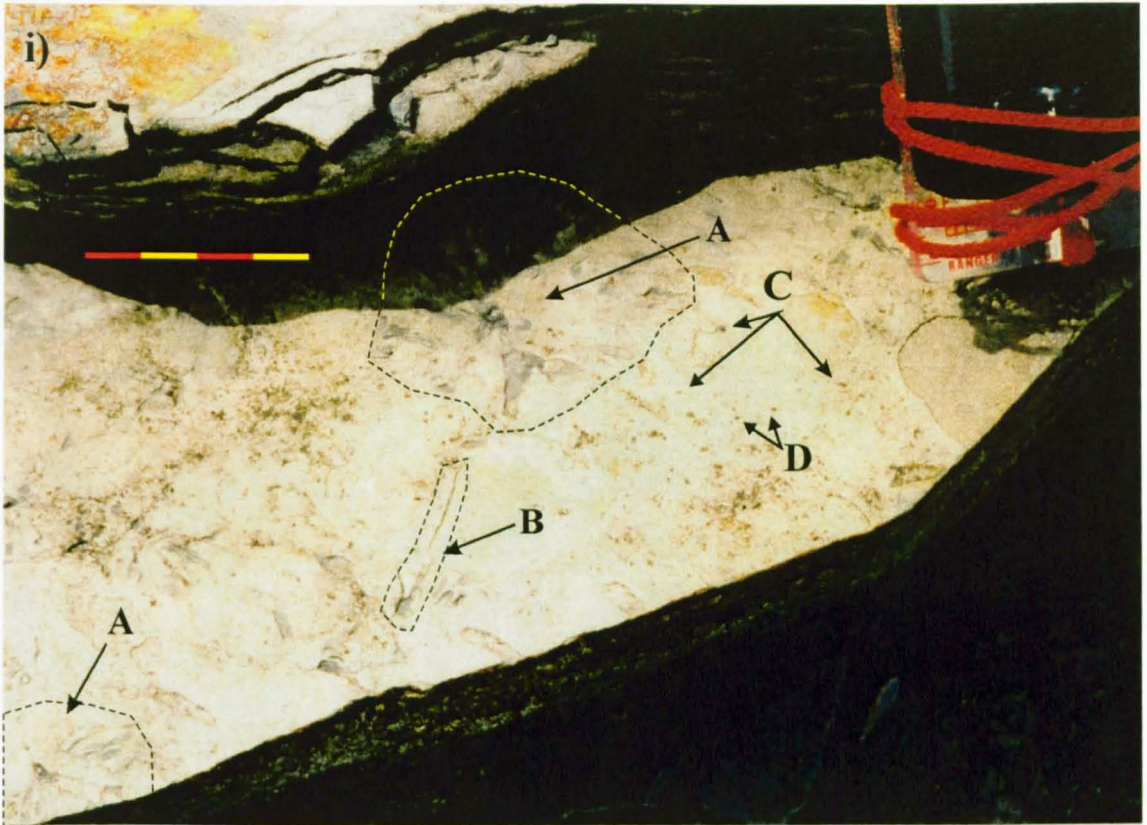
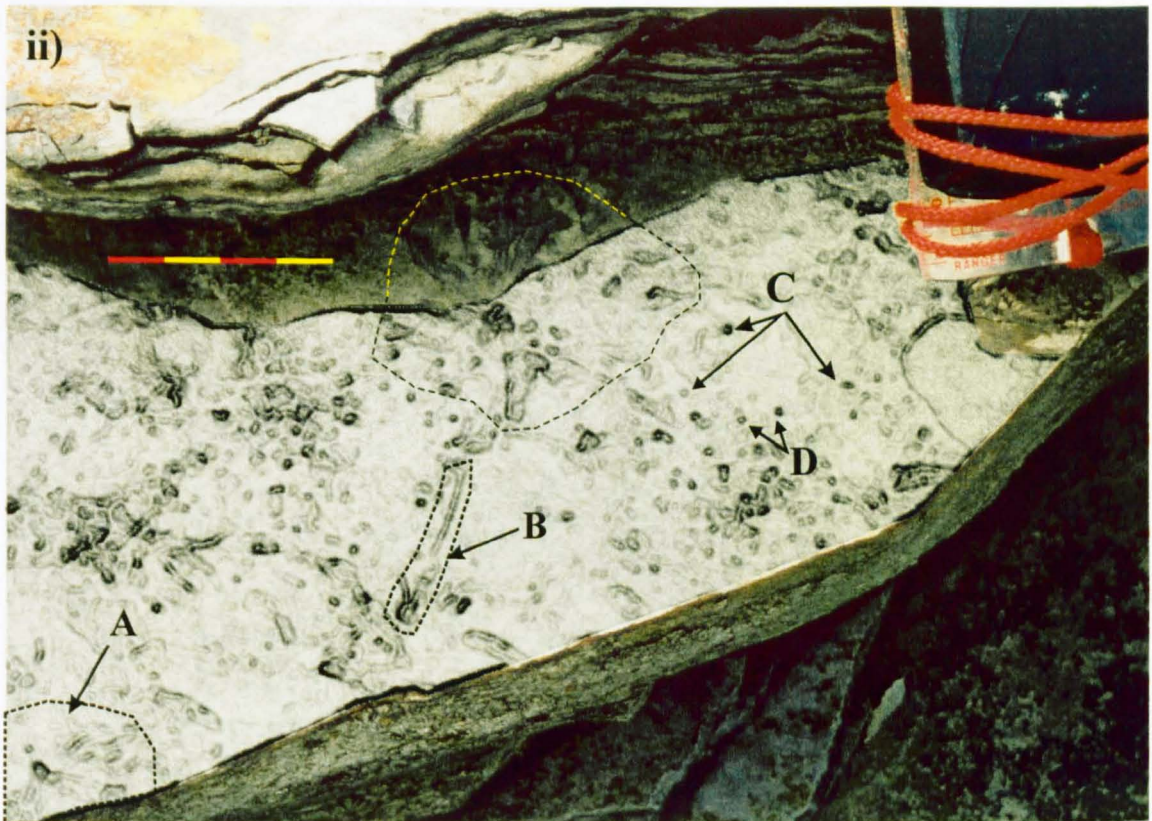


Figure 3.26 i) and ii). Photograph i) (taken at Killard - at 1.1m in Appendix A7) shows trace fossils occurring on the surface of a sandy silt bed within the heterolithic facies (Flh). The charcoal rendering shown in ii) picks out the traces more clearly. A = *Asterichnus*, B = *Curvolithus* or *Muensteria*, C = *Monocraterion* and/or *Skolithos*, and D = *Arenicolites*. The red and yellow scale bar is 40mm long.



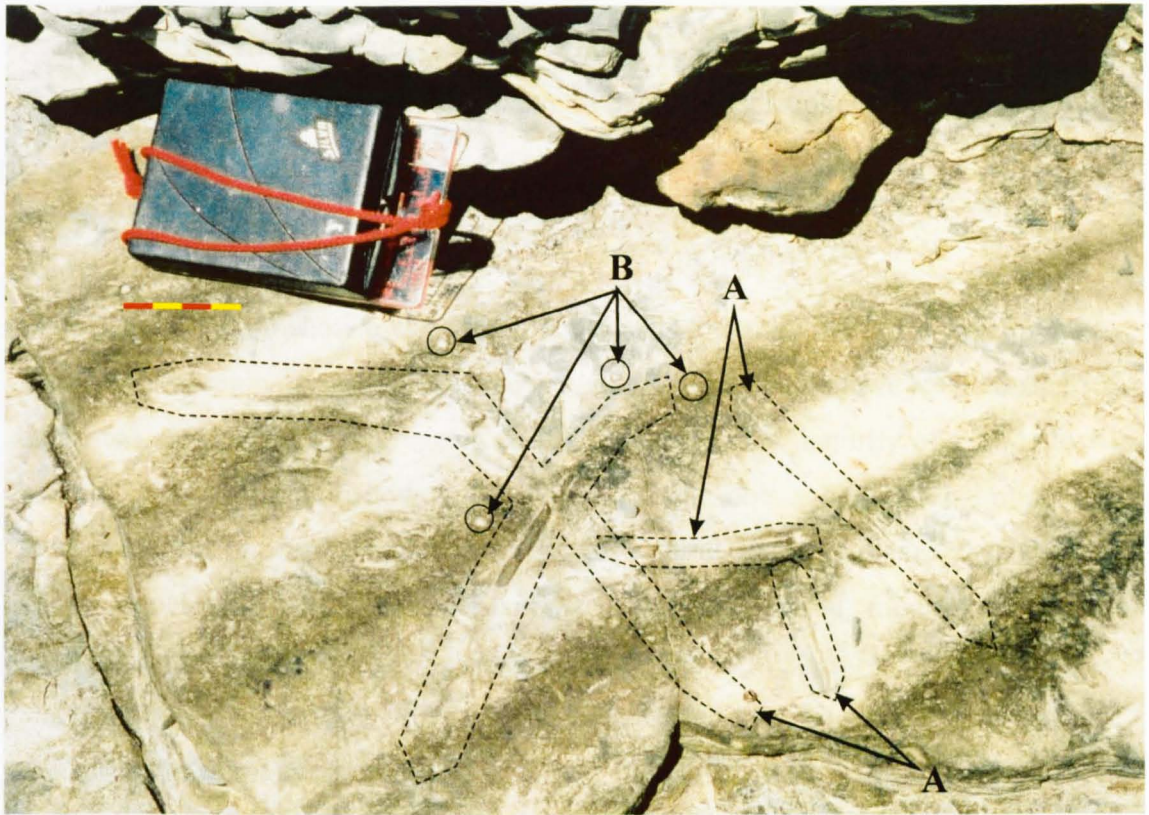
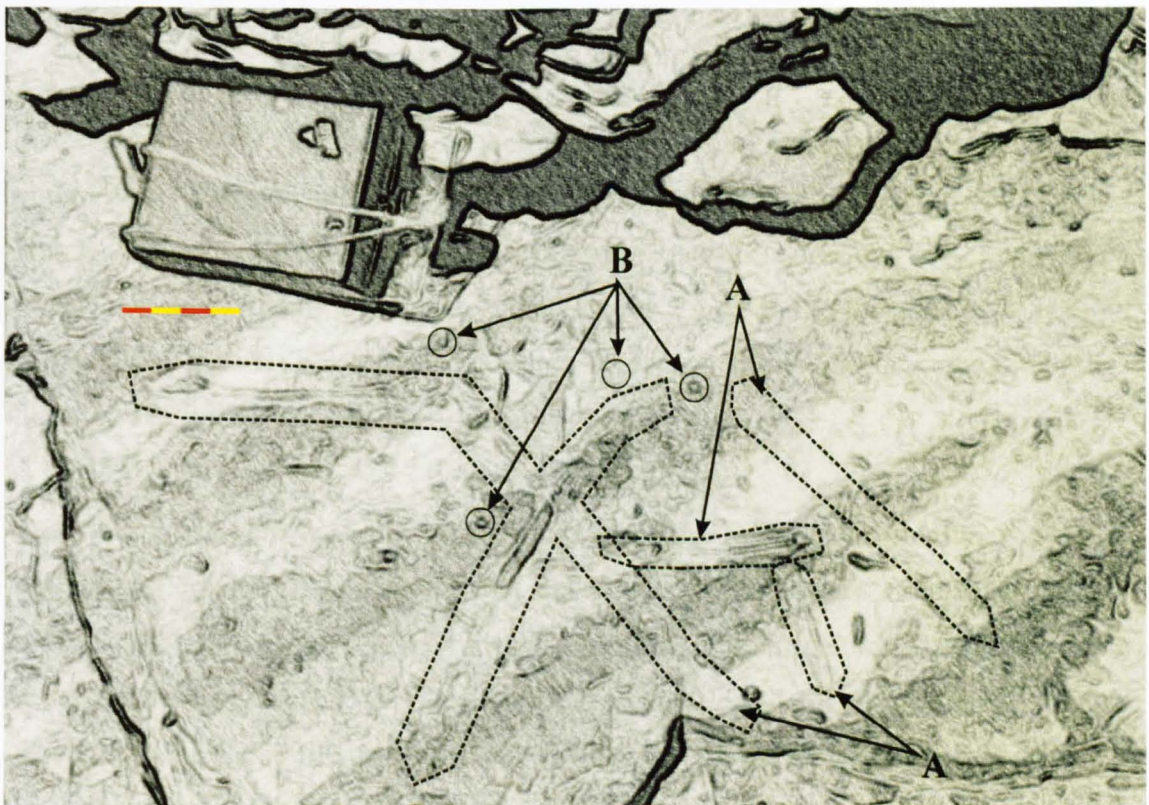


Figure 3.27 i) and ii). Photograph i) (taken at Killard, at 4.6m in Appendix A7) shows trace fossils occurring on the surface of a wave-reworked fine sand bed within facies Sh<sub>2</sub>. The charcoal rendering shown in ii) (below) picks out the traces more clearly. A = *Curvolithus*, B = *Skolithos* or *Monocraterion*. The red and yellow scale is 40mm long.



shallow deltaic environments (Eager *et al.*, 1985). Their occurrence in sediments within the field area is therefore indicative of deltaic deposition in a brackish basin.

### 3.3.20 Plant material

#### 3.3.20.1 Description

Figures 3.28 to 3.33 show a variety of plant fossils found within the studied outcrops. There are two main categories: i) those *in situ* and ii) those that have been transported, deposited, and partly disaggregated in the process. The majority of *in situ* fossils belong to *Stigmaria*, and show well-developed trunk roots and occasional minor side roots radiating outward from the “trunk” in a spiral fashion (Figs 3.28 and 3.30). These are found within parallel-laminated non-bioturbated mudstones, and in sandstones immediately underlying these mudstones.

The plant fossils that are clearly not *in situ* include *Lepidodendron* (a type of club moss, Fig. 3.33), and possible examples of *Tempskya* and horsetails. *Tempskya*, a large tree fern, has a trunk composed of a complex mass of narrow roots and wider stems (Fig. 3.32). A possible example of a horsetail fragment is shown in Fig. 3.31. All these plant fossils occur as broken fragments up to a few metres long (but more usually less than one metre in length).

#### 3.3.20.2 Interpretation

The roots found *in situ*, *Stigmaria*, belong to a group of Carboniferous plants called clubmosses. These plants were found throughout the Carboniferous in warm climates and freshwater swampy environments (Thomas, 1981). *Stigmaria* can therefore be interpreted as indicating a pause in sedimentation long enough for plant colonisation. If found rooting into brackish-water facies, *Stigmaria* show that the environment has changed and become freshwater instead.

The incomplete and flat-lying nature of some of the fossils confirms that they have been transported and are not in life position. These plant fragments provide information about the vegetation and prevailing conditions of the surrounding terrestrial environment. *Lepidodendron* was common in warm and wet environments throughout the Carboniferous, as were *Tempskya* and horsetails, which were the other major plant group that thrived in the Carboniferous besides clubmosses.

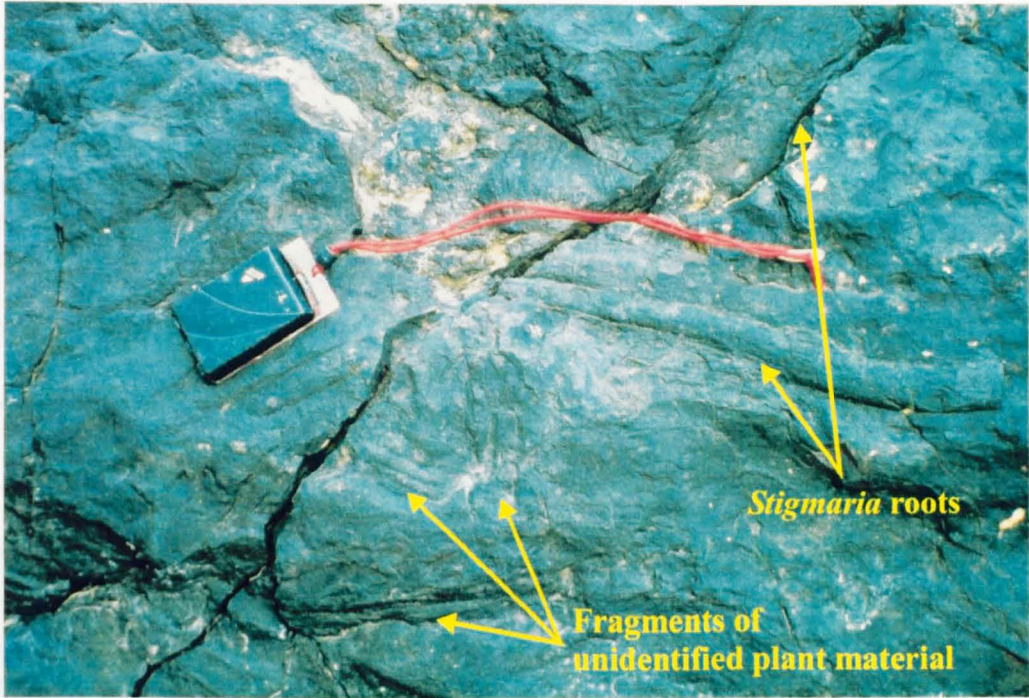


Figure 3.28. Two pieces of *Stigmaria* root, fossilised in muddy sandstone at Trusklive (at 9.3m in Appendix A5). The compass is 60 by 100mm.

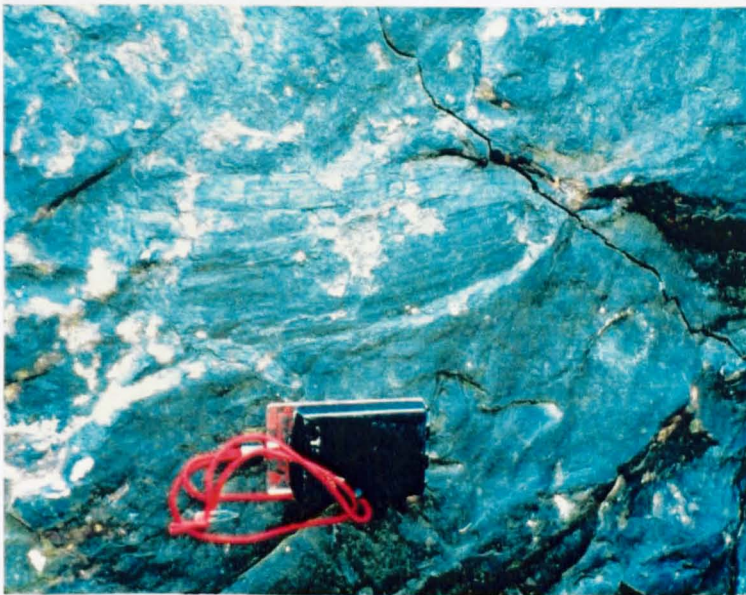


Figure 3.29 (left). Plant fossil of a horsetail-type species, possibly *Calamites*. It is preserved in the bed just beneath that in Fig. 3.28, with numerous fragments of unidentified plant material.

Figure 3.30 (below). A *Stigmaria* root with smaller side rootlets still attached. Preserved *in situ* within the same bed as that in Fig. 3.28.

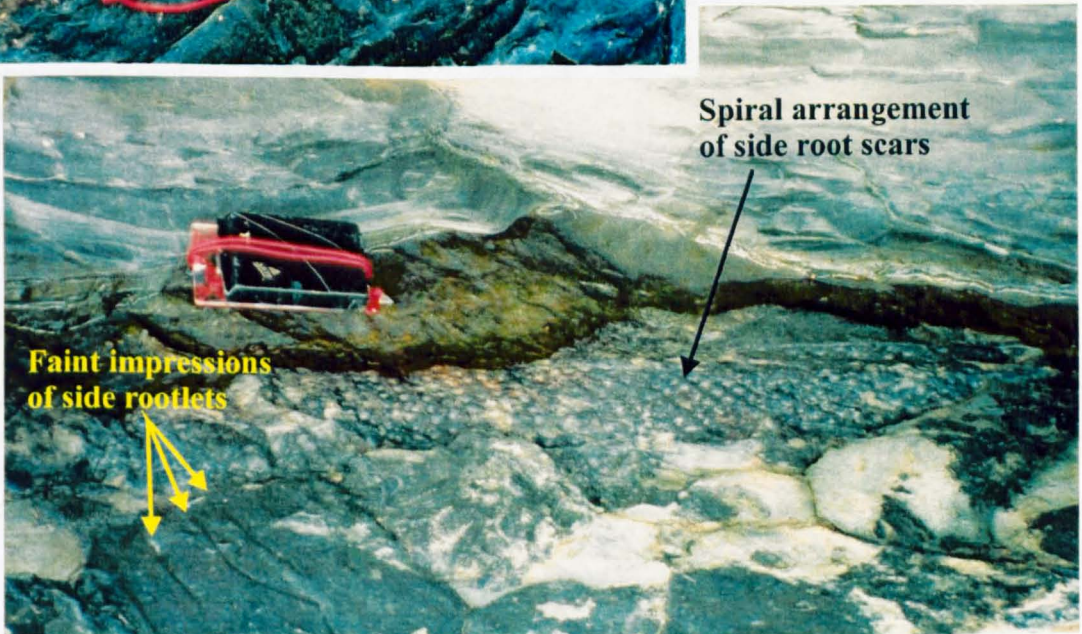


Figure 3.31. A bedding surface showing many macerated pieces of unidentified plants, including stem material, not *in situ*. From Killard, at 11m in App. A15. The compass is 60 by 100mm



**Elongate ridges and grooves covered with dark carbonaceous material**

Figure 3.32 (left). A large section of carbonaceous plant material, not *in situ*, possibly part of the trunk of a giant fern such as *Tempskya*. This is preserved on the underside of a sandstone bed (facies Sh) at Trusklieve (8.25m in App. A5). The tape is 0.54m long.

Figure 3.33. A very well-preserved section of a *Lepidodendron* plant, in a bed of fine sandstone at Killard (30.4m in App. A7). Note the oval-shaped leaf scars arranged spirally around the branch. The arrow shows the direction of the leaf scar tracks. The hammer shaft is 0.32m long.



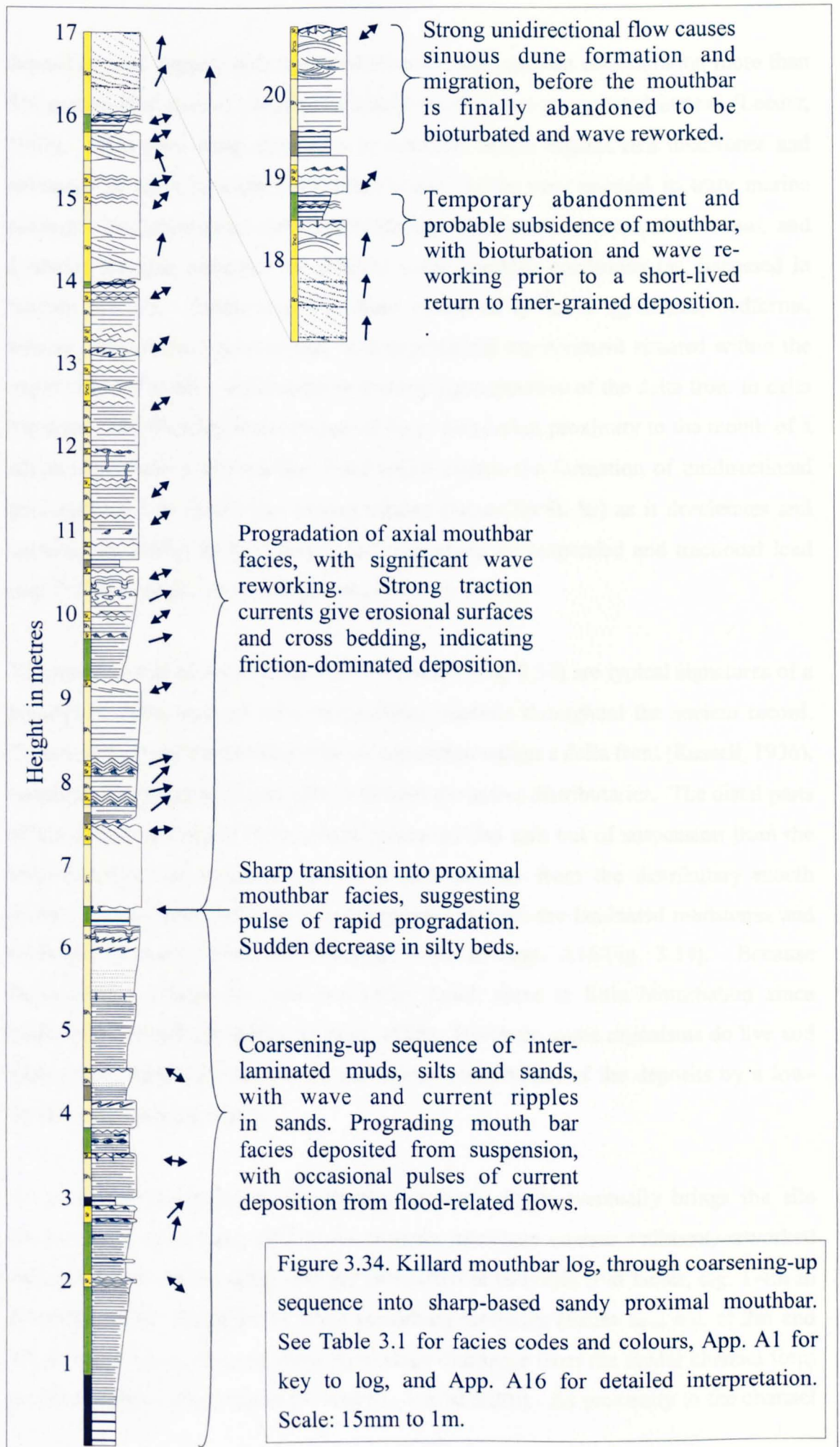
### **3.4 Facies associations and interpretations**

The sections below describe the three facies associations observed in the field and discuss the depositional environments interpreted from them. The vertical relationship of these associations is that the mouthbar association occurs lower in the stratigraphy, and is succeeded by either the interdistributary bay facies association or the fluvial association or both, the fluvial association always being the uppermost in all sections. Palaeoenvironmental interpretations based on the facies associations and their mutual relationships are compared with other studies of the Tullig Cyclothem deposits.

#### **3.4.1 Mouthbar facies association**

A common facies association present at several of the field localities is the grouping of facies Sp, Sp<sub>2</sub>, St, Shcs, Sr, Sr<sub>w</sub>, Sr<sub>c</sub>, Sh<sub>2</sub>, Flh (bioturbated), Fls (bioturbated) and Flm (bioturbated). The sequence seen in the field, from base to top, is as follows: parallel-laminated mud/siltstone (Flm, Fls), changing to intercalated mudstone, siltstone and sandstone (Flh), and progressing upward into thicker, more laterally continuous sandstone beds with sedimentary structures reflecting high sedimentation rates, the action of tractional currents, and wave reworking (Sh<sub>2</sub>, Sp, Sp<sub>2</sub>, St, Sr, Sr<sub>c</sub>, Shcs and Sr<sub>w</sub>). An example of this succession is the part of the Killard section below the Tullig Sandstone (App. A16; also shown in summarised form in Fig. 3.34). The Killard example will be examined and used to explain the mouthbar facies association. This coarsening-up type of facies sequence typifies mouthbar progradation (e.g. Trowbridge, 1930; Fisk *et al.*, 1954; Coleman and Wright, 1975; Wright and Coleman, 1973, 1974; Coleman, 1981; Wright, 1985), and the accompanying ichnofacies are typical of Carboniferous deltaic facies (Eager *et al.*, 1985; see Section 3.3.19.2).

The coarsening-up signature (Fig. 3.34) is clear, and shows the increasing influence of unidirectional currents by the change from suspension-dominated deposition (Flm, Fls, Flh, Sh<sub>2</sub>) to traction-dominated deposition (Sr, Sp). This change is accompanied by an increase in wave influence, as seen in the more frequent occurrence of facies Sr<sub>w</sub> and Shcs higher in the succession. These changes indicate that over time, the site of deposition was becoming shallower, and increasingly close to the point of sediment supply. The presence of siderite nodules indicates that the ambient pore water post-



deposition was organic-rich and sulphate-poor, with an iron concentration more than 5% greater than that of calcium, or calcite would have precipitated instead (Leeder, 1982). Such pore water chemistry is common within organic-rich mudstones and siltstones in fresh to slightly brackish water, but is very unusual in truly marine settings. The ichnofacies seen within the deposits (*Monocraterion*, *Asterichnus*, and *Lockeia*) are also indicative of shallow water brackish conditions (as discussed in Section 3.3.19). Taken together, these pieces of evidence (grainsize, bedforms, siderite, ichnofacies) point clearly to a depositional environment situated within the upper slope of a delta, shallowing to become representative of the delta front to delta top area. The shoaling is accompanied by an increasing proximity to the mouth of a deltaic distributary, the outflow from which causes the formation of unidirectional bedforms such as dunes and current ripples (facies Sp/St, Sr) as it decelerates and spreads out, losing its competence and depositing its suspended and tractional load (e.g. Coleman *et al.*, 1964; Wright and Coleman, 1971).

The shoaling and coarsening-up of the sequence (Fig. 3.34) are typical signatures of a prograding delta, and are seen in mouthbar deposits throughout the ancient record. Deltaic mouthbars are the main sites of deposition within a delta front (Russell, 1936), receiving the majority of sediment load from the active distributaries. The distal parts of the mouthbar receive fine-grained sediments that rain out of suspension from the buoyant plume of sediment-rich water that extends from the distributary mouth (Bates, 1953). Silts and muds are deposited and form the laminated mudstones and siltstones of facies Flm and Fls (e.g. 0-1m in App. A16/Fig. 3.34). Because deposition is continuous, and reasonably rapid, there is little bioturbation since habitats are buried too quickly (Elliott, 1986). However, some organisms do live and feed in this distal mouthbar area, and sparse bioturbation of the deposits by a low-diversity fauna is the result.

As progradation continues, the decreasing water depth eventually brings the site above storm wave base, and storm currents introduce coarser sediment, reworked from elsewhere in the delta, into the succession at intervals (Flh facies, e.g. 1-4m in A16/Fig. 3.34). Evidence of wave reworking increases (facies Sr<sub>w</sub>, e.g. at 2m and 4.5m) and traction currents from flood-stage discharge from the feeder channel form unidirectional current ripples (Sr and Sr<sub>c</sub>, e.g. at 8.2m). As proximity to the channel

mouth increases, coarser sediment is rapidly deposited from suspension and produces  $Sh_2$  and  $Sr_c$  facies (for example 7.7-9.0m). Storm wave reworking leads to the formation of hummocky cross-stratification ( $Shcs$ , at 12.7m). These facies are typical of the mouthbar front and crest (Elliott, 1986). As the distributary channel mouth progrades further, the site experiences stronger tractional currents from the sediment-laden channelised flow, and dune-scale current bedforms ( $Sp$ ,  $Sp_2$ ,  $St$  - e.g. App. A16, 14-18m, 20.3m) are produced as the back and crest of the mouthbar are reworked by these unidirectional flows (Wright and Coleman, 1974). Macerated plant debris (e.g. at 11m) is also present, brought in by flood flows. At this stage, if the distributary channel avulses, the mouthbar is abandoned and undergoes wave and storm reworking, and colonisation by a variety of organisms leading to intense bioturbation (as seen in Fig. 3.34 at 20.5-20.75m). The succession of  $Shcs$ ,  $Sr_w$  and bioturbation is common in wave and storm influenced deltas (Elliott, 1986).

The interpretation above shows that the section illustrated is a good example of a prograding mouthbar in a delta front. While the entire succession discussed above is not always present in other logs, parts of the succession are seen in other localities. The lowermost five to seven metres in three of the logs from Trusklieve (A2, A3 and A5) show depositional sequences that can be interpreted as distal mouthbar environments, based on the association of facies  $F_{lm}/F_{ls}$ ,  $F_{lh}$ ,  $Sr$  and  $Sr_c$ . These lowermost few metres show a slight shallowing up; wave ripples appear in the form of bi-directional lenticular beds near the top of the succession (see A3 and A5, at 4.3 and 6.6m respectively), showing that the environment of deposition was above storm weather wave base at that point. The log from the northern limb of the Killard outcrop (App. A8) shows a similar association ( $F_{lm}$ ,  $F_{ls}$ ,  $F_{lh}$ ), coarsening upwards over its lowermost 4.8m to include facies  $Sh_2$  at the top of this interval. All five of the logs from Carrowmore (App. A9 to A13) show the  $F_{lh}$ ,  $F_{lm}$ ,  $F_{ls}$  association, with the ichnofacies confirming the brackish, distal mouthbar environmental interpretation.

Finally, the log from Tullig Point (App. A15) shows a predominantly sandy succession that displays the sandy facies of the mouthbar facies association –  $Sp$ ,  $St$ ,  $Sp_2$ , and  $Sh_2$  – as well as intercalations of finer-grained facies ( $F_{lh}$  and  $F_{ls}$ ). The succession may initially appear fluvial, but the low number of erosional contacts (4) compared with depositional contacts (21) and the presence of facies  $Sh_2$  are both

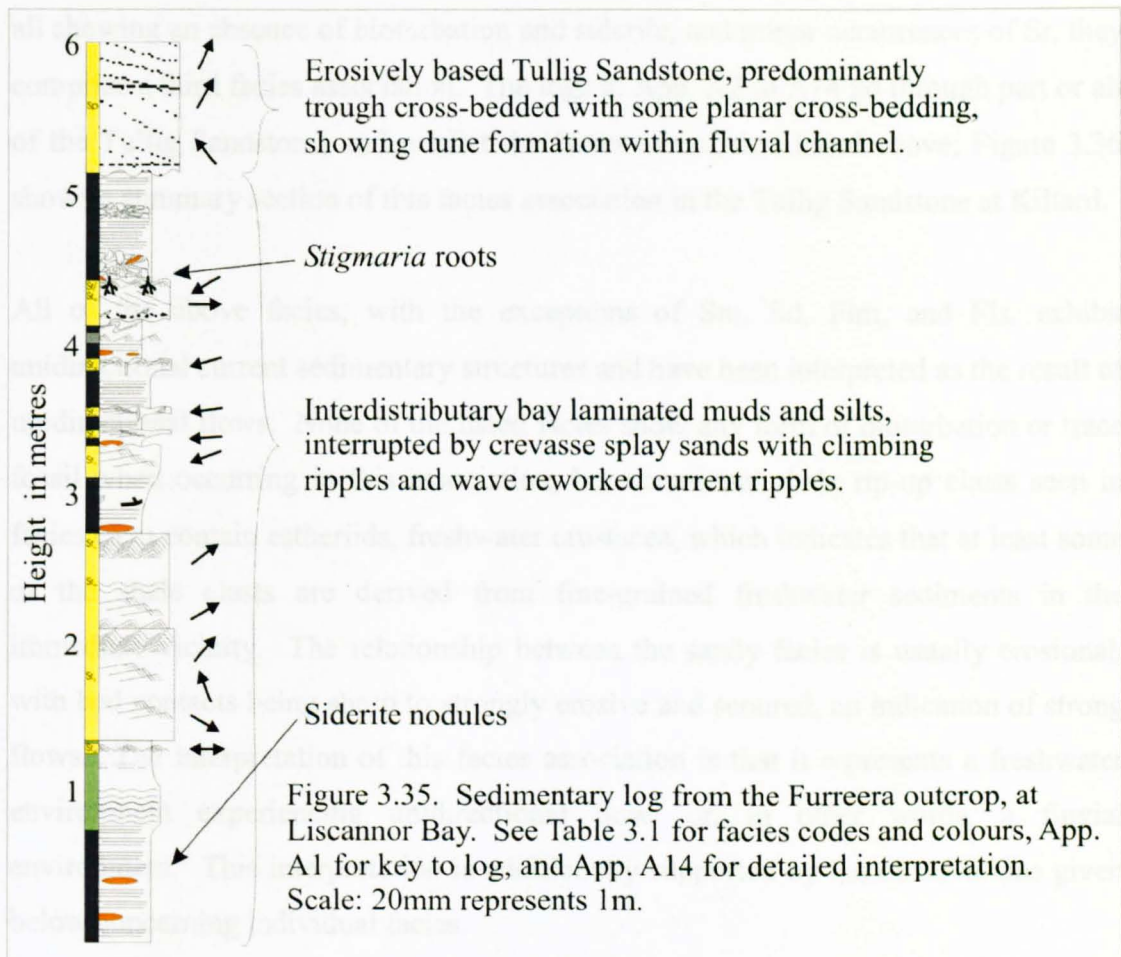
strong evidence for a mouthbar depositional environment. In addition, the silty laminae of the Sh<sub>2</sub>, Sl<sub>2</sub> and Sp<sub>2</sub> facies are evidence of periods of reduced current influence, which are common in a delta front setting where channel discharge varies and fine-grained laminae are deposited from suspension during periods of low flow. Seen together, rapid deposition from suspension, periods of reduced current influence and silt/mud deposition, and predominantly depositional bed contacts demonstrate that the environment is not fluvial but fluvial-influenced deltaic. The facies association is thus interpreted as that of a fluvially influenced mouthbar environment.

### 3.4.2 Interdistributary bay facies association

A second facies association commonly present is Flm, Fls, Flh, Sr<sub>w</sub>, Sr<sub>c</sub>, and Sr. This is similar to the mouthbar facies association described above, but differs crucially in that it shows no sandstone facies with sedimentary structures at scales larger than ripples (i.e. no Sh<sub>2</sub>, Sp, Sp<sub>2</sub>, St, Sl<sub>2</sub> or Shcs). The frequency and thickness of wave-rippled beds is greater than in the mouthbar association, and the occurrence of climbing ripples is also more frequent. A good example of this association is seen at Furreera, Liscannor Bay, below the base of the Tullig Sandstone (App. A14, summarised in Fig. 3.35). The abundance of Sr<sub>c</sub> is evident, and a number of thin (0.1-0.6m) coarsening-up packages are seen, many of which include beds of the Sr<sub>c</sub> facies. Another subtle difference between the interdistributary facies association and the mouthbar association is that the former shows a higher frequency of facies Flm interbedded with Sr, Sr<sub>w</sub>, and Sr<sub>c</sub> (compare Figs 3.34 and 3.35). The close and repeated intercalation of these facies is not present in the mouthbar association.

The process causing climbing ripples (i.e. rapid deposition from a unidirectional current) occurs in decelerating flows, for example during the falling stage of a flood in a fluvial environment (Bristow, 1993), in a decelerating turbidity current (Allen, 1972), or during levee breach and crevasse splay formation (e.g. the Stage I splays of Smith *et al.*, 1989). The latter explanation fits with the associated facies best, since the presence of facies Sr<sub>c</sub> interbedded with mudstone (Flm) shows that, in this depositional setting, rapid deposition from decelerating unidirectional currents alternated with much quieter conditions during which muds were deposited from suspension. This repetition is typical of interdistributary bay environments on a delta front; the pulses of very rapid deposition (Sr<sub>c</sub>) represent flood periods when levees are

breached and overbank flows, such as crevasse splays, bring sandy sediment into the quiet water bays (Elliott, 1974). Once the levee breach is healed, only fine-grained sedimentation occurs within the bay as clay-sized particles fall out of suspension and form the laminated mudstones that represent background sedimentation. The presence of wave ripples ( $Sr_w$ ) at the top of the  $Sr_c$  beds indicates wave reworking of the crevasse splay deposits. This shows that the depositional setting is above fair weather wave-base and exposed to the basin (Pulham, 1989), confirming the shallow water interdistributary bay interpretation.



The ichnofacies (App. A14) are another confirmation of the interdistributary bay interpretation of the Flm, Fls, Flh,  $Sr_w$ ,  $Sr_c$ , and Sr association. *Skolithos* and possibly *Curvolithus* are present, *Skolithos* typifying the shallow water *Cruziana* ichnofacies. The presence of *in situ* rootlets at the top of the succession (4.4m in App. A14) shows that the bay area was nearly filled, allowing vegetation growth. The *Stigmaria* rootlets belong to plants of the clubmoss variety, which thrive in swampy environments, and

the appearance of these roots at Furreera shows the transition to freshwater delta top swamp from brackish interdistributary bay, as the bay filled with sediment. The presence of siderite nodules in this facies association (Fig. 3.35) indicates organic-rich fresh to brackish pore waters (see Section 3.4.1) and fits with an interdistributary bay environment, where the vegetation would provide abundant organic debris.

### **3.4.3 Fluvial and alluvial facies association**

The facies Sm, Smc, Sh, Shc, Sl, Sp, St, Sc, Sd, and Ccm are found in close association throughout the Tullig Sandstone. Together with facies Flm, Fls and Flh, all showing an absence of bioturbation and siderite, and minor occurrences of Sr, they comprise a third facies association. The logs in App. A2 to A14 go through part or all of the Tullig Sandstone, and exhibit the facies association listed above; Figure 3.36 shows a summary section of this facies association in the Tullig Sandstone at Killard.

All of the above facies, with the exceptions of Sm, Sd, Flm, and Fls, exhibit unidirectional current sedimentary structures and have been interpreted as the result of unidirectional flows. None of the listed facies show any form of bioturbation or trace fossil when occurring in this association, but occasional shale rip-up clasts seen in facies Ccm contain estheriids, freshwater crustacea, which indicates that at least some of the shale clasts are derived from fine-grained freshwater sediments in the immediate vicinity. The relationship between the sandy facies is usually erosional, with bed contacts being sharp to strongly erosive and scoured, an indication of strong flows. The interpretation of this facies association is that it represents a freshwater environment experiencing unidirectional flow, or, in other words, a fluvial environment. This interpretation is additionally supported by the observations given below concerning individual facies.

The occurrence of facies Sm and Smc, interpreted as deposits of hyperconcentrated flows (Lowe, 1982; Smith, 1986), is common in alluvial settings, where such flows are caused by the collapse of a channel bank. Bank collapse leads to the formation of a minor channel, often at a high angle to the main channel (Miall, 1996). These minor channels can be narrow and steep-banked, filled with facies Sm/Smc, or broader, with irregular scoured bases containing sheets of the Sm facies (Miall, 1996). Examples of such channels are seen within the Tullig Sandstone at Trusklieve.

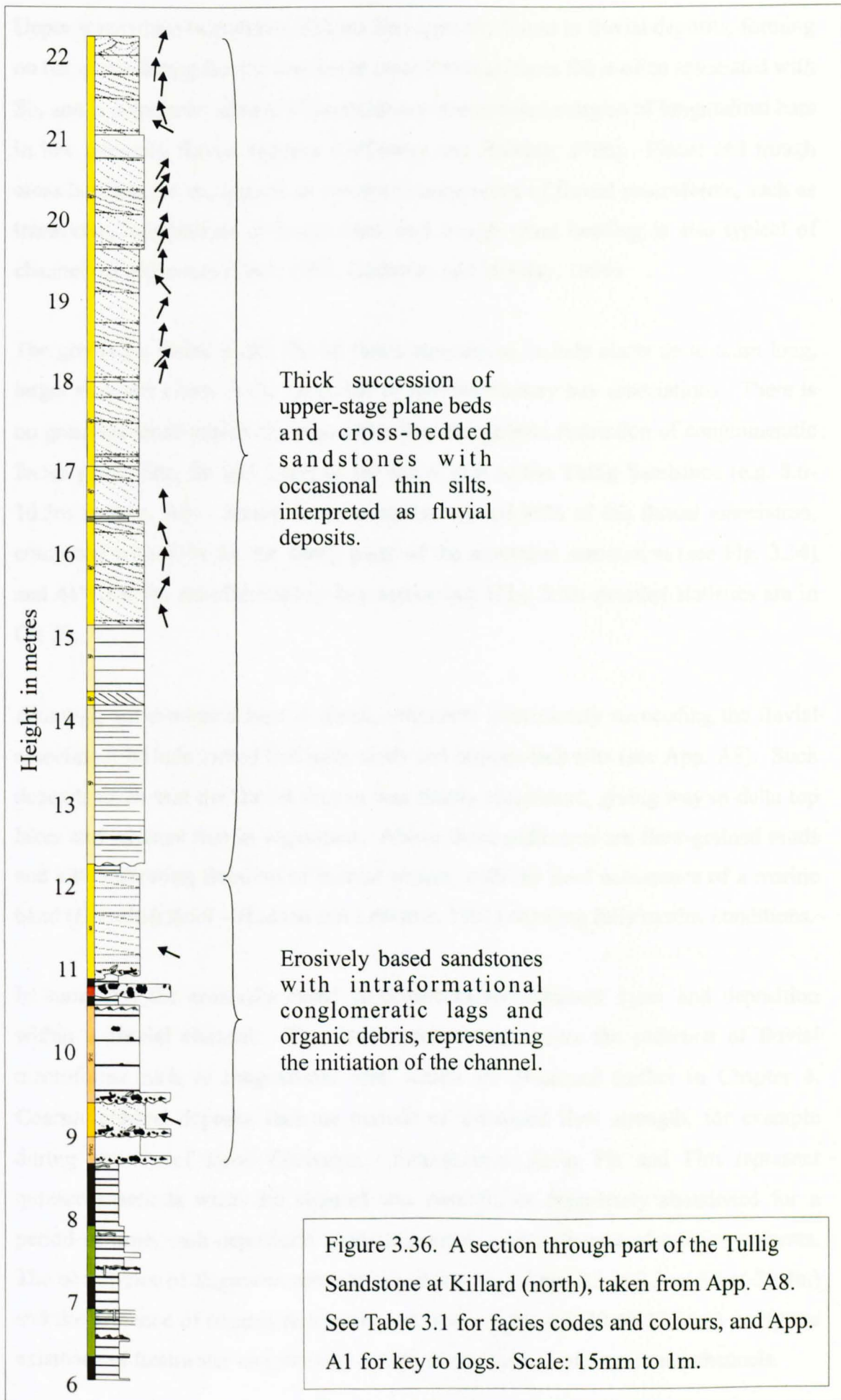


Figure 3.36. A section through part of the Tullig Sandstone at Killard (north), taken from App. A8. See Table 3.1 for facies codes and colours, and App. A1 for key to logs. Scale: 15mm to 1m.

Upper stage plane beds (faces Sh) are also typically found in fluvial deposits, forming on bar crests during floods; low-angle cross bedding (faces Sl) is often associated with Sh, and is a common feature of accretionary downstream margins of longitudinal bars in low sinuosity fluvial systems (Galloway and Hobday, 1996). Planar and trough cross bedding are recognised as common components of fluvial macroforms, such as transverse, longitudinal or lateral bars, and trough cross bedding is also typical of channel fill sequences (Cant, 1982; Galloway and Hobday, 1996).

The grainsizes found in the fluvial facies association include clasts up to 0.3m long, larger than any clasts in the mouthbar or interdistributary bay associations. There is no grainsize trend within the logs, other than the general restriction of conglomeratic facies (Smc, Shc, Sc and Ccm) to the lower part of the Tullig Sandstone (e.g. 8.6-10.5m in App. A8). Sandy facies comprise around 95% of the fluvial association, compared with 83% for the sandy parts of the mouthbar association (see Fig. 3.34) and 41% for the interdistributary bay association (Fig. 3.35; detailed statistics are in Ch. 5).

Although not discussed here in detail, sediments immediately succeeding the fluvial association include rooted horizons, coals and organic-rich silts (see App. A8). Such deposits show that the fluvial system was finally abandoned, giving way to delta top lakes and swamps rich in vegetation. Above these sediments are finer-grained muds and silts indicating flooding of basinal waters, with the final occurrence of a marine band (*P. stubblefieldi* – Hodson and Lewarne, 1961) showing fully marine conditions.

In summary, the erosively based sandstone facies represent scour and deposition within a fluvial channel. The facies architecture shows the presence of fluvial macroforms such as longitudinal bars, which are discussed further in Chapter 4. Coarser grained deposits indicate periods of increased flow strength, for example during periods of flood discharge. Fine-grained facies Fls and Flm represent quiescent periods when the channel was partially or completely abandoned for a period of time, with deposition from suspension in the absence of traction currents. The occurrence of *Stigmara* rootlets in beds of Flm (App. A5 at 9.3m, A8 at 30.4m) and the presence of organic-rich coaly sediments (App. A8, 30.40-33.15m) verify the existence of freshwater and swampy environments typical of abandoned channels.

### **3.5 Summary**

The facies and facies associations described and interpreted above have also been recognised in the Tullig cyclothem by other researchers (e.g. Hodson and Lewarne, 1961; Rider, 1969, 1974; Pulham, 1987, 1989; Davies and Elliott, 1996; Hampson *et al.*, 1997). The interpretations of depositional environment presented in this chapter are similar to those of Pulham (1987).

A number of conclusions can be drawn from this facies study concerning the depositional environments prevailing before and during the deposition of the Tullig Sandstone:

- 1) The depositional environment prevailing before deposition of the Tullig Sandstone was a prograding fluvial-dominated and wave-influenced delta.
- 2) The sub-environments recognised within this fluvio-deltaic setting include distal and proximal mouthbars, and interdistributary bays.
- 3) The Tullig Sandstone represents a subsequent facies shift to a fluvial depositional environment.

### **3.6 Comparison of facies between Ireland and Egypt**

In order to build a strong case for using the Co. Clare outcrops as an analogue for the Plio-Pleistocene fluvio-deltaics of the Nile Delta, the facies descriptions given above are now compared with those obtained from analysis of Nile Delta well-log data from the El Wastani Formation. The Rosetta 3 well (Fig. 2.9) was logged using a Schlumberger Formation MicroImager (FMI) tool, which takes detailed resistivity measurements to give a photo-like image of the inside of the hole. This log covers the three main reservoir sands, B (1142-1179m measured depth), C (1322-1369m md) and D (1491-1553m md).

#### **3.6.1 FMI tool description**

Schlumberger's Fullbore Formation MicroImager provides 80% coverage in an 8.5" hole and is capable of resolving beds down to 20 to 30mm, making the images comparable with sedimentological logs based on field outcrop or core. The FMI tool achieves these results by using four pads with hinged flaps, each pad and flap with two rows of 12 insulated button electrodes. When in use, 192 samples are recorded

around the borehole at every depth point. Each pad is held at an equipotential relative to the return electrode higher in the tool. The pad effectively sends a current into the formation and the current density across the pad is measured by the electrodes. Changes across the pad thus reflect local changes in formation resistivity (Rider, 1996).

The raw data, a series of microresistivity curves, is processed so that intervals with similar electrical properties will appear similar throughout the log. Dark colours are used for high resistivities, so brine-filled sands look pale (usually yellowish colours) and shales or hydrocarbon-bearing sands appear dark (reds to browns). Figure 3.37 shows sections from the FMI logs from Rosetta 3, and the whole logs are seen in Enclosures 1-3 (BG internal report, 1997).

### **3.6.2 FMI log descriptions and interpretations**

#### **3.6.2.1 B Sand description and interpretation**

The B Sand is recognised as a gas-bearing sequence of mixed sands and muds between 1142m and 1179m md (see Enclosure 1 and Fig. 3.37a), and the logged section is described below, from base to top.

1179-1170m md: The sequence starts with laminated mudstones and occasional fine sands and silts, and coarsens up to sandier beds with cross sets and laminae, and occasional carbonate nodules.

1170-1161.2m md: A second coarsening-up sequence follows, going from laminated silty mudstone through ripple cross-bedded sandstone to thicker cross-bedded and laminated sandstones with nodule horizons.

1161.2-1142m md: A thin mud starts this interval, followed by a thin slumped sandstone. Above this a silty mud forms the base of a third shoaling succession that coarsens up from thin heterolithic beds to thick sandstone beds (~1-2m thick) showing dunes, hummocky cross-stratification and occasional ripples. The top surface of this sequence shows vertical burrows.

The B Sand is interpreted as a prograding mouthbar facies association, showing a typical repeated coarsening-up signature and both suspension- and traction-related sedimentary structures. The succession is very similar to the mouthbar facies association seen at Killard (compare Figs 3.37a and 3.34), and the upper few metres show the same facies (cross beds, hummocky cross-stratification, ripples and bioturbation). The setting is envisaged as a wave-influenced deltaic mouthbar.

### 3.6.2.2 C Sand description and interpretation

This unit is another gas-bearing sequence of mixed sands and muds, occurring between 1322 m and 1369 m. The succession is described from base to top; a section is shown in Fig. 3.37b, with the whole log in Enclosure 2.

1369-1351m md: The succession starts with 8m of mudstone interrupted by thick (1-2m) beds of massive to laminated sands, internally deformed with sharp or faulted bases. A faulted contact then brings in a 6m unit of slumped sand, capped by 4m of mudstone containing discrete slumped sand beds and a bed of cross-stratified sand.

1351-1342m md: The slumped unit is succeeded by a thick sandstone sequence that is initially massive but exhibits some faint cross bedding and lamination upwards. Individual sandstone beds (0.5-1.5m thick) are capped by thin (~0.1m) fining-up silty sands, which occasionally show bioturbation.

1342-1322m md: This is a fining-up sequence of massive to faintly laminated sands 0.4-1.3m thick, interbedded with heterolithic and laminated muds and silts. The heterolithics show some bioturbation and occasional carbonate nodules occur in the sands. The sequence is capped by laminated mudstones.

The lower half of this succession is interpreted as background fine-grained pro-delta mudstones, with slumped sands derived from a delta front setting. The undeformed sandstones show bedding characteristic of a delta front setting, with ripples and planar bedding possibly corresponding to mouthbar deposits. These have subsequently been translated downslope to the pro-delta. The succession above 1351m is probably *in situ*; its sandy nature and cross-bedded to planar bedded appearance suggest mouthbar-type deposition. The gradual fining-up of the following 20m, with

decreasing sandstone bed thicknesses and thicker muds, suggests a progressive deepening as the mouthbar is slowly drowned. The mudstone at 1322m shows a return to a quieter, pro-delta environment. The facies association through the C Sand is similar in parts to the mouthbar associations seen in Co. Clare, with bioturbated heterolithics (facies Flh) and cross-bedded sandstones (Sp) reminiscent of those seen at Killard (Fig. 3.34). Slumped facies are also seen within the Tullig cyclothem, although not within the sandier upper parts studied here; deformation also characterises the underlying Gull Island Formation (Section 2.2.3.3).

### 3.6.2.3 D Sand description and interpretation

This gas-saturated sandstone succession, from 1491-1553m md, is described from base to top below; a section is shown in Fig. 3.37c, and the whole log in Enclosure 3.

1553-1545m md: This is a succession of erosively based sandstones, massive to parallel-laminated, with internal erosion surfaces and lags of pebbles and mud clasts. Some internal deformation occurs within the top 3m

1545-1524m md: Above the deformed sandstone is a 20m sequence of rippled, cross-bedded and planar-laminated sandstones. Cross sets vary in set height from 50 to 150mm, representing ripples and dunes. Above 1533m, thin (<0.5m) beds of heterolithics and laminated muds and silts occur at intervals of 1-4m, and the succession is capped by 1.5m of heterolithics and laminated silts and muds.

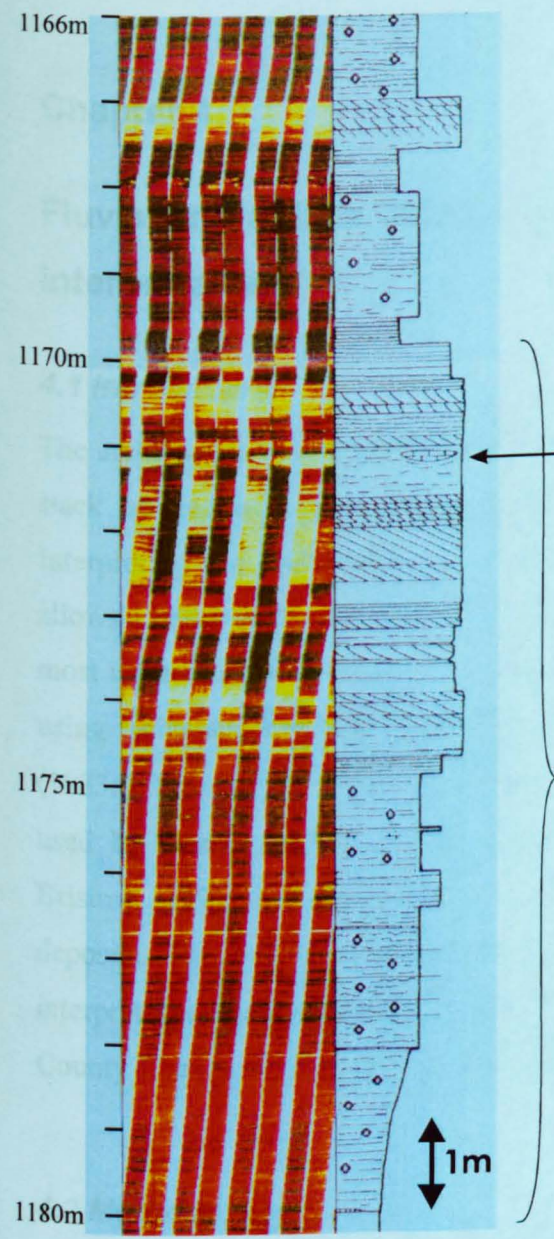
1524-1491m md: A sharp-based sandstone introduces the next sandy sequence, which exhibits parallel-bedded, rippled and massive sands, with several faults and recurring beds of mudstone and heterolithics. Sand bed thicknesses are between 0.5 and 2.5m. The top 8m starts with a thin, coarsening-up set of parallel-laminated sandstones with silty interbeds. These are succeeded by three massive sandstone beds, with some signs of bioturbation. These massive sands are capped by a rapidly fining-up silt and a thick mudstone package.

The erosively based lowermost sandy succession, with internal erosion surfaces, coarse-grained lags, dune and ripple scale cross bedding and a lack of bioturbation, is interpreted as a fluvial distributary channel, with a similar facies association to that

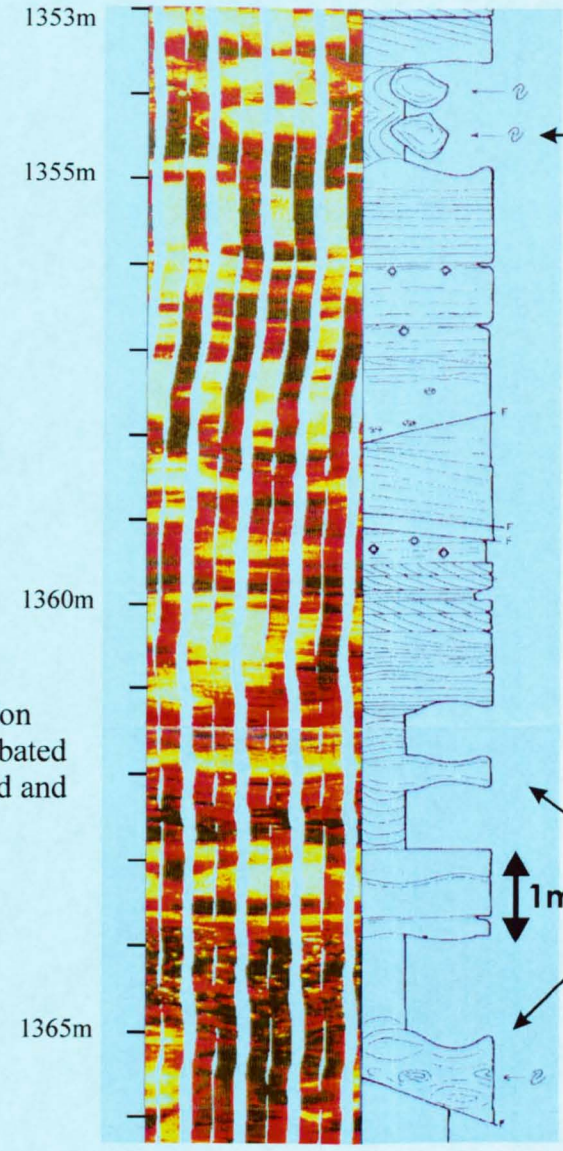
seen in the Tullig Sandstone (Fig. 3.36). The overlying sequence contains beds of fine-grained sediments and far fewer cross-bedded sandstones, suggesting that while probably still in the delta plain area, the environment experienced periods of quiet-water deposition. The parallel-bedded and rippled sands may be due to rapid deposition from crevasse splays, for example in an interdistributary region. The massive sands at the top could be reworked deposits, and the return to mudstone deposition at the top could signify a relative sea-level rise.

### **3.6.3 Summary**

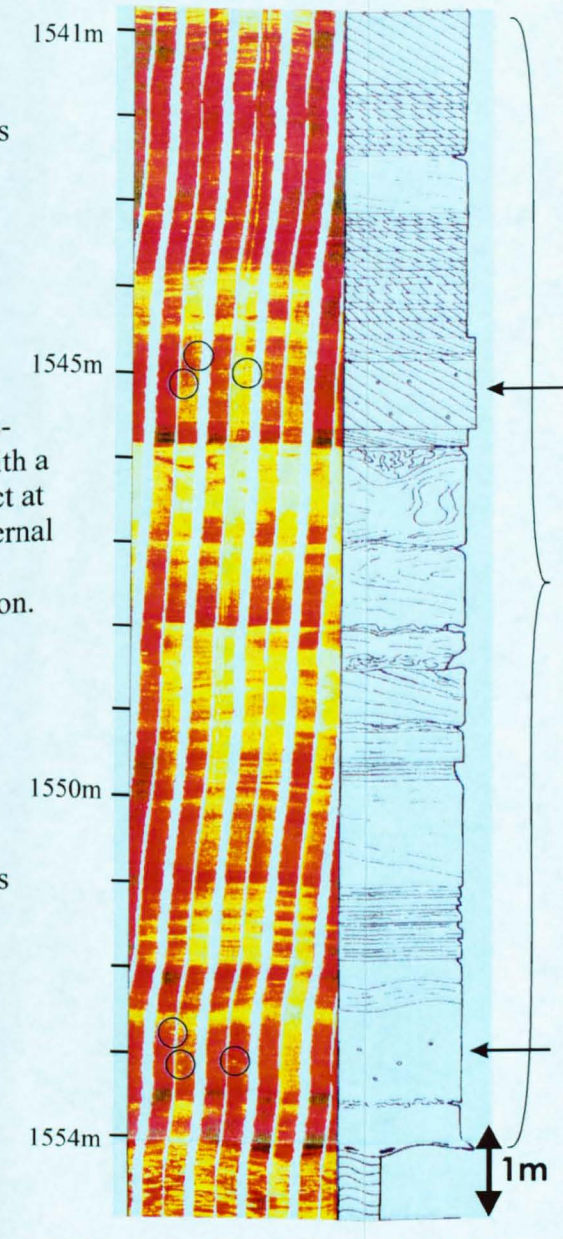
The images produced by the FMI tool are sufficiently high quality to enable comparison of facies between the Tullig cyclothem outcrops and the B, C and D sands of the El Wastani Formation of the Nile Delta. The similarities are discussed above and show that the two successions exhibit equivalent facies associations and were in all probability deposited in similar fluvial-dominated, wave-influenced deltaic environments. Beyond this, it is impossible to be more precise about the comparison; in fact, if more were known about the El Wastani sands, there would be no need for an analogue in the first place.



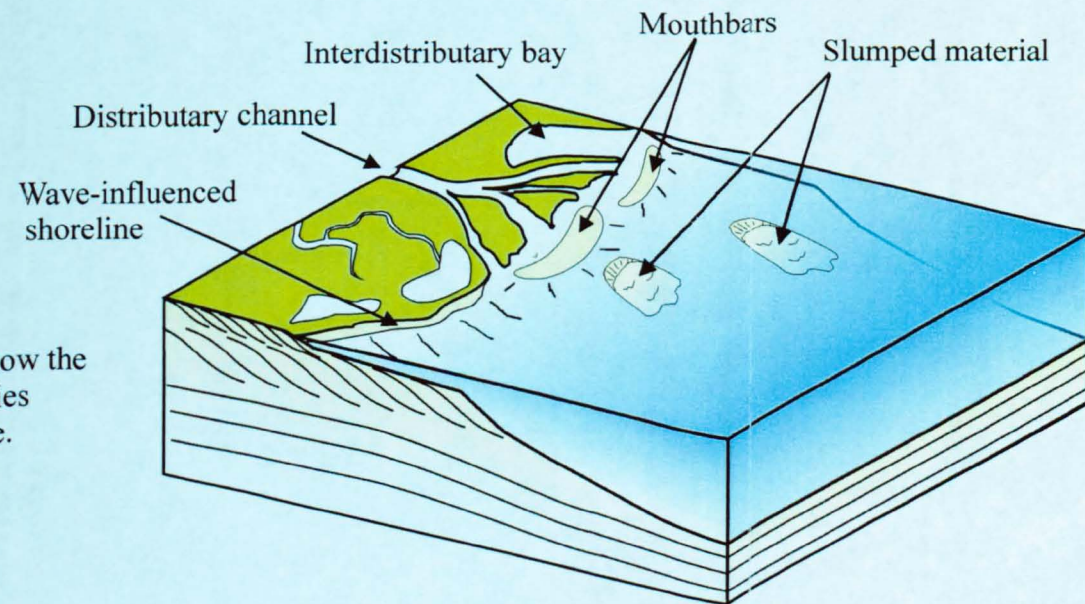
a) Section of the B Sand - 1166-1180.0 m  
Interpreted as a deltaic mouthbar succession.



b) Section of the C Sand - 1353-1366m.  
Interpreted as slumped mouthbar  
sands in a prodelta setting.



c) Section of the D Sand - 1541-1554m.  
Interpreted as a fluvial channel association.



D) Schematic block diagram to show the  
palaeoenvironment of the facies  
associations described above.

Figure 3.37. a), b) and c) are FMI log sections taken from the three main sands comprising the reservoir interval in the Rosetta 3 well, with sedimentary interpretations (from a BG internal report by Z&S Geology Ltd., 1997). d) shows an interpretation of the palaeoenvironment during deposition of these facies.

## Chapter 4

### Fluvial and deltaic facies architecture: description and interpretation

#### **4.1 Introduction**

The architecture of any sandbody is defined by the way in which the beds and facies stack up and how they relate geometrically to each other in three dimensions. Interpreting the architecture of a sandbody in terms of process and environment allows a better understanding of how the sandbody was formed and what factors were most influential in its deposition. Architectural element analysis of this kind, largely using facies and bedform classification based on the work of Jackson (1975), Allen (1983a), Friend (1983), Bridge (1984) and Miall (1977, 1978, 1985, 1996), has been used by many researchers (e.g. Marzo *et al.*, 1988; Singh and Bhardwaj, 1991; Bristow, 1993; Bentham, 1993) to define fluvial styles of modern and ancient deposits. This chapter utilises the facies interpretations from Chapter 3 to analyse and interpret the architecture of the sandbodies in the Tullig Cyclothem outcrops in County Clare, and suggests a model for their formation.

#### **4.2 Methodology**

In addition to the logs presented in Chapter 3, several series of outcrop photographs were taken at each locality and were stitched together, using EnRoute's PowerStitch™ software, to produce detailed photomontages of each outcrop. In most cases it was impossible to ensure similarity of scale from photo to photo because it was not possible to remain at a constant distance from the outcrop while moving parallel to it. Therefore, scale bars, each 0.5m long, were chalked onto the outcrops at regular intervals; these scale bars were visible in the photos and allowed accurate scales to be added to the photomontages, enabling accurate measurements to be taken from them.

To aid interpretation of the photomontages, detailed field sketches were made of the outcrops, with special attention being paid to accurate measurement of the

thicknesses, dips, geometries, and lateral extents of beds, and the vertical and lateral stacking relationships of facies. Individual elements within each outcrop were identified based on bounding surfaces and facies changes. Boundaries and erosional surfaces between beds were marked onto the rocks in chalk so that they would be clearer on the photos and enable accurate matching of the sketches to the montages. Using the logs and sketches, the facies, internal geometries and bedding planes were mapped onto the photomontages. The resulting scaled maps of the outcrops then allowed detailed study of the facies distribution and architectures (N.B. all facies codes and colours are given, with summary descriptions and interpretations, in Table 3.1). Bedding dip data, and palaeocurrent data from foresets, were corrected for the regional dip and are quoted in the format: dip angle/dip azimuth.

### ***4.3 Outcrop descriptions and interpretations***

#### **4.3.1 The Tullig Sandstone at Trusklieve**

The section at Trusklieve (Fig. 4.1a) is exposed in a NNE-SSW trending amphitheatre about 15m high, with an additional 7m of stepped exposure set back from the cliff top. The maximum sandbody thickness here is thus 22m. However, the entire thickness of the sandbody is not exposed at this locality, although the top surface does crop out a few hundred metres to the south. The entire thickness was given as 31.2m by Pulham (1987). At Trusklieve the Tullig Sandstone exhibits the fluvial/alluvial facies association described in Section 3.4.3. This is apparent from Fig. 4.1b, which shows the facies interpretation of the outcrop, and from the log correlation panel in Fig. 4.2 (shown in detail in App. A2-A5). The facies encountered within the Tullig Sandstone at Trusklieve include Sm, Smc, Sh, Shc, Sp, St, Sl, Sc, Sr, Ccm, and the non-bioturbated Flh, Fls and Flm facies. The log correlation panel shown in Fig. 4.2 shows that the base of the Tullig Sandstone is erosional, cutting down into sediments belonging to the mouthbar facies association (described in Section 3.4.1). This erosive basal surface is accessible across the whole exposure; the upper part of the Tullig Sandstone, however, is only within reach for study in the southern half of the outcrop (see Figs 4.1a and b and 4.3a and b). The appearance of the sandbody is that of a channelised unit with conglomerates common near the base, and facies heterogeneity and mud to sand ratio decreasing upwards. The log correlation panel (Fig. 4.2) shows these trends; for example, log 2 exhibits facies Smc, Sh, and Fls in the lowest 3m of the Tullig Sandstone, before changing upwards to comprise only facies Sp.

NNE

SSW

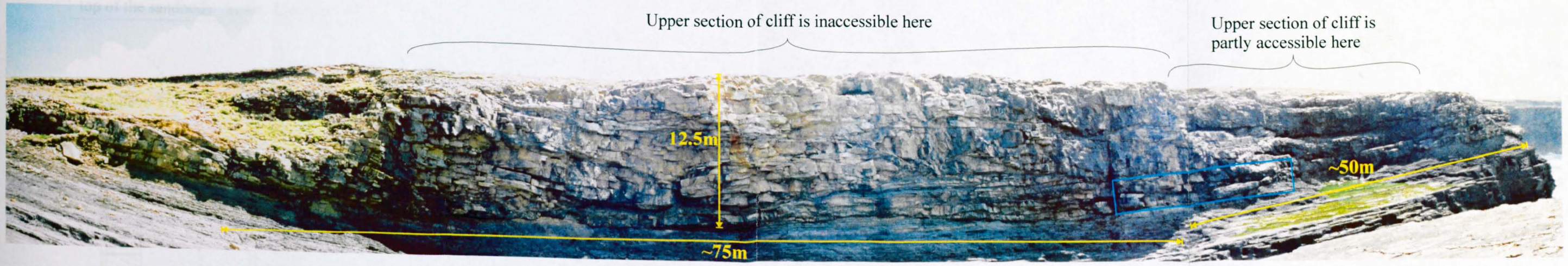


Fig. 4.1a: Five-photo panorama of the Trusklieve outcrop of the Tullig Sandstone, looking ESE. The blue rectangle shows the location of Figure 4.5.

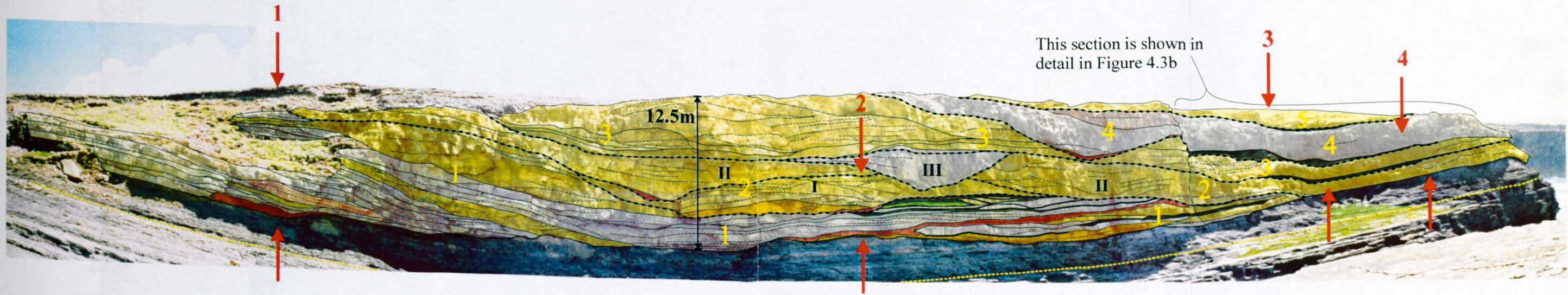
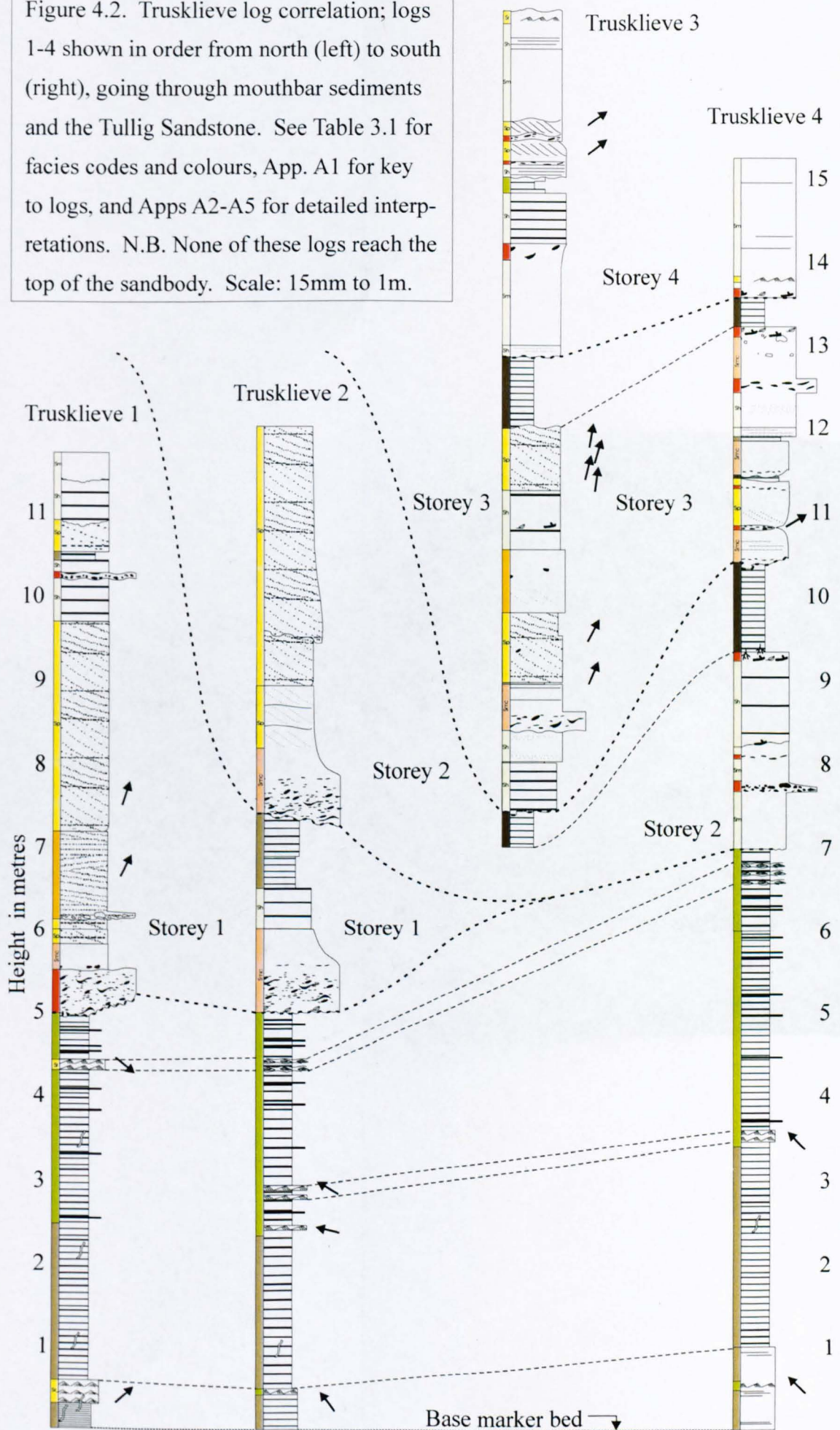


Fig. 4.1b: As above, showing facies interpretation, major erosional surfaces and beds. The red arrows indicate logged localities (Fig. 4.2, and App. A2-5). The yellow numbers correspond to the storeys described in Section 4.3.1, and the numerals I, II and III correspond to the three sub-stores in Storey 2.

Key					
	Sm, Sh		Smc, Shc		Flh
	Sp, St, Sl, Sr		Sc		Fls
			Ccm		Flm
					Major erosional channel bases
					Facies boundaries (frequently coincident with minor erosional channel or bedform bases)
					Marker horizon in mouthbar succession
					Cross-bed and reactivation surfaces
					Numbers of storeys in Tullig Sandstone

Figure 4.2. Trusklieve log correlation; logs 1-4 shown in order from north (left) to south (right), going through mouthbar sediments and the Tullig Sandstone. See Table 3.1 for facies codes and colours, App. A1 for key to logs, and Apps A2-A5 for detailed interpretations. N.B. None of these logs reach the top of the sandbody. Scale: 15mm to 1m.



These three fine-grained beds (the uppermost of which is only just visible due to the angle of the photo) continue laterally for between 16.55 and 40m. All three are eroded out in the northern part of the outcrop (see Figures 4.1b and 4.4a-e)

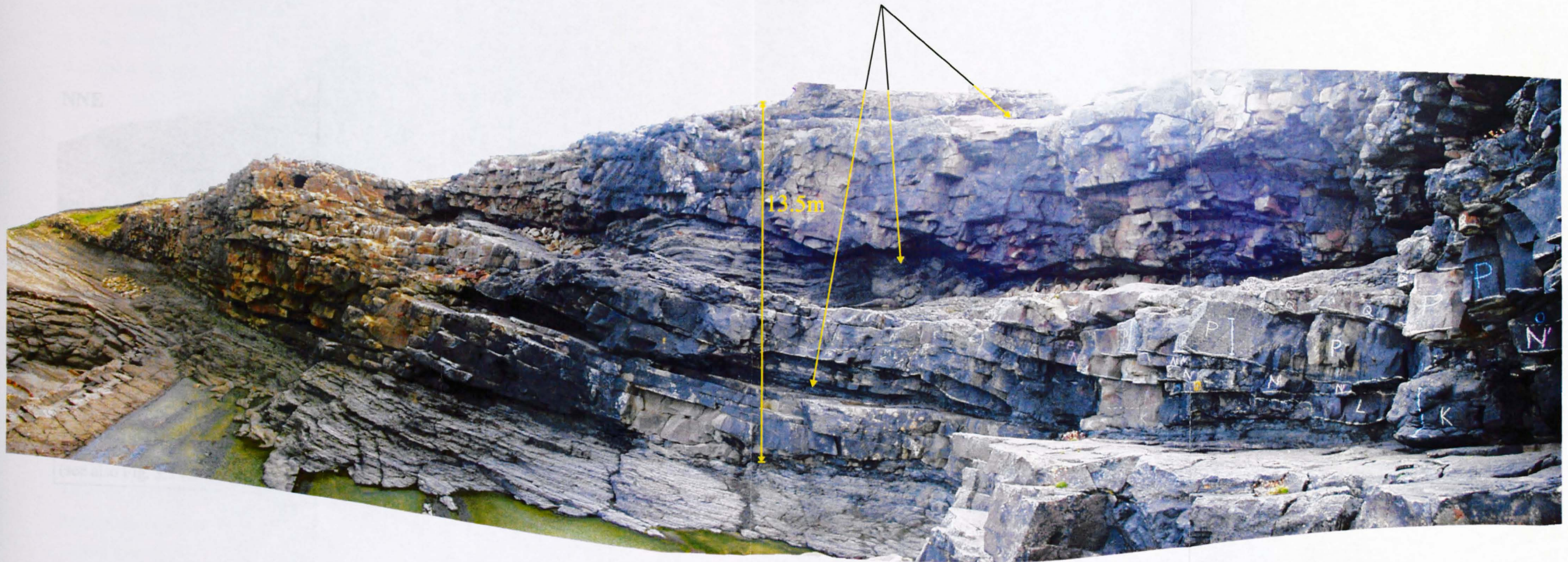


Figure 4.3a. Five-photo panel showing the southern end of the Tullig Sandstone outcrop at Truskleeve, viewed looking northeast.

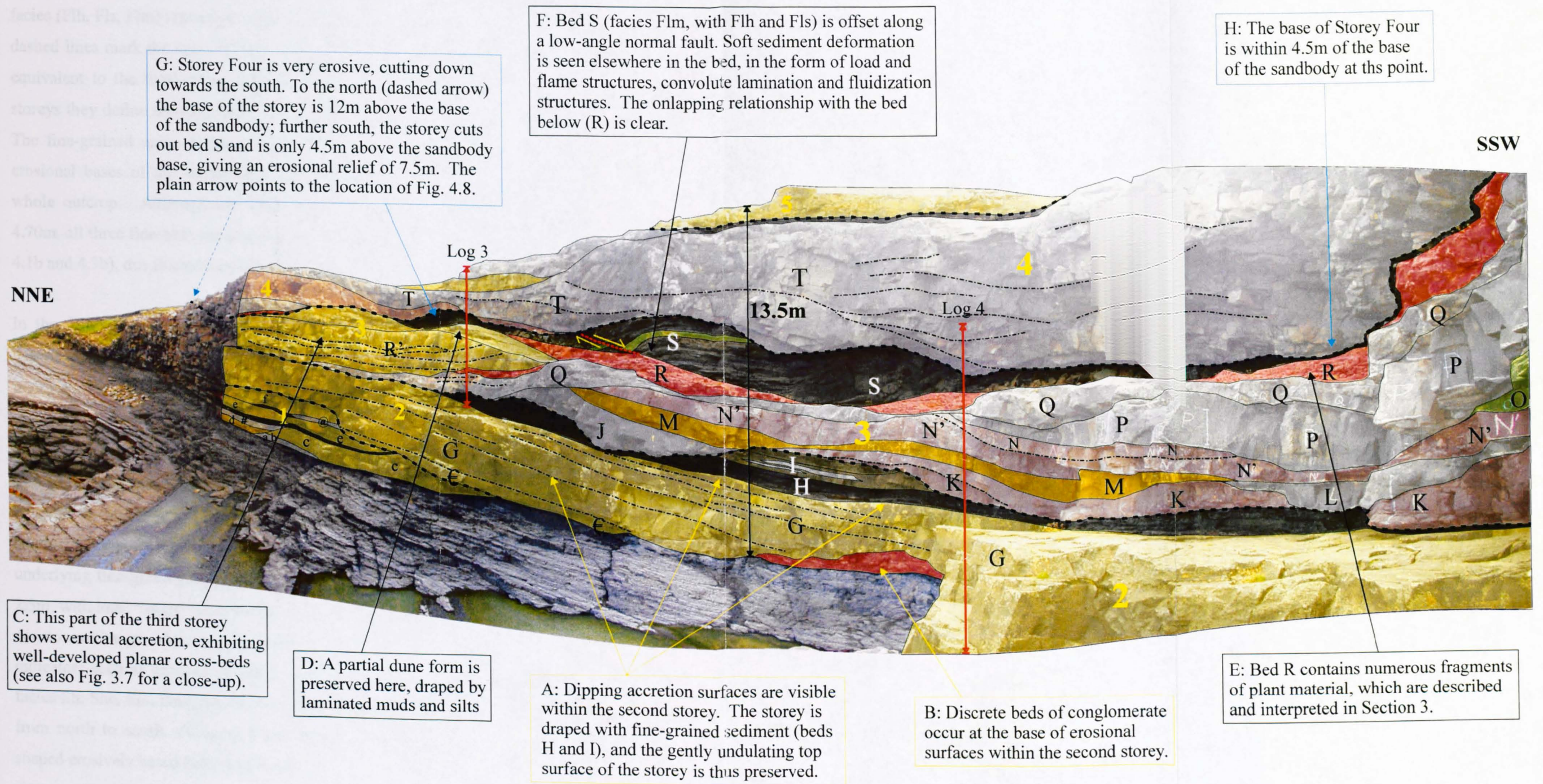


Figure 4.3b. Five-photo panel showing the southern end of the Tullig Sandstone outcrop at Trusklieve, viewed looking north-east. This figure shows facies interpretations, bed labels (used in Chapter 5) and storeys. Note the heterogeneity of Storeys One and Three compared with the homogeneity of Storeys Two, Four and Five. Captions referring to Storey Two are outlined in yellow, those for Storey Three in black, and those for Storey Four are in blue.

Key					
	Sm, Sh		Smc, Shc		Flh
	Sp, St, Sl, Sr		Sc		Fls
			Ccm		Flm
					Major erosional channel bases
					Facies boundaries (frequently coincident with minor erosional channel or bedform bases)
					Numbers of storeys in Tullig Sandstone
					Cross-bed and reactivation surfaces

There are five main storeys in the sandbody, which are identified on the basis of erosional relationships and intervening beds of fine-grained overbank or channel-fill facies (Flh, Fls, Flm) representing periods of abandonment (see Section 3.4.3). Thick dashed lines mark the bases of the storeys on Figs 4.1b and 4.3b; these surfaces are equivalent to the third-order surfaces of Allen (1983a) and Miall (1985), and the storeys they define are equivalent to the “element groups” of Jo and Chough (2001). The fine-grained units, found at the tops of three storeys (immediately below the erosional bases of the succeeding storeys), are not laterally continuous across the whole outcrop. Although one such fine bed reaches a stratigraphic thickness of 4.70m, all three fine beds are absent in the northern half of the outcrop (compare Figs 4.1b and 4.3b), due to erosion of the fines by succeeding channels.

In the following sections, the Tullig Sandstone fluvial sandbody at Trusklieve is described and interpreted one storey at a time. A summary description and interpretation of the sandbody outcrop as a whole is given in Section 4.3.1.6.

#### *4.3.1.1 Storey one: description and interpretation*

The lowermost storey is seen in the northern half of the outcrop, where it reaches 8.5m in thickness (Figs 4.1b and 4.4a), but is eroded by the downcutting second storey in the southern half (Fig. 4.4a). The basal surface is erosive, cutting into underlying fine-grained mouthbar deposits (see logs in Fig. 4.2) with a total relief of 2.5m, with local “steps” of up to 1m. The vertical nature of the cliff means that there are no overhangs where it is possible to study the basal contact for palaeocurrent indicators such as grooves or flutes. Facies are very varied in the first storey, with facies Sh, Shc, Sm, Smc, Sp, St, Sc, Ccm, Fls and Flm present. Bed geometries alter from north to south, changing from parallel, but dipping, beds to horizontal lens-shaped erosively based beds (Fig. 4.4a).

The northern end of the amphitheatre shows a succession of beds, on average 0.42m thick (App. B1), which, when corrected for regional tilt, dip gently to the northwest and southwest (see rose diagram in Fig. 4.4a). This succession of dipping beds exhibits a progressive fining-up (App. A2) from basal conglomeratic facies (Ccm) through horizontally bedded sandstone with clastic lag (Shc) to clean horizontally bedded and planar cross-bedded sandstone (Sh and Sp). The dips of the first order set

bounding surfaces (bounding surfaces are classified according to Allen's scheme, 1983a), and those of the second order coset bounding surfaces (McKee and Weir, 1953), average  $10^\circ$  to the WSW. The three steepest dips, which are easiest to measure accurately, are oriented due south. This stacked, dipping geometry, combined with the fining-up signature, indicates that these beds are part of a macroform or bar within the channel (other examples of such bars geometries are noted by Miall, 1996). Only two beds with measurable foresets were encountered; when corrected for regional tilt, these foresets show dips to the NNE ( $018^\circ$  and  $026^\circ$ ). These data suggest lateral accretion, because the angle between this NNE flow direction and the previously described WNW bar accretion direction is greater than  $60^\circ$ , meeting Miall's criterion for lateral accretion (Miall, 1996). An interpretation of this architectural element is shown in Figure 4.5.

Towards the centre of the outcrop, the first storey changes character and becomes more heterogeneous (Figs 4.1b, 4.4a and App. A3). The beds are no longer arranged in a dipping, accretionary pattern but have more concave-up bases and show increased basal erosional relief. Facies occurring here include Ccm, Sh, Sc, Sp, Flm and Fls. The higher percentage areal occurrence of conglomeratic facies (Ccm) and lag deposits (Sc) in this central part of the section (32% compared with 6% for the north section – see Chapter 5) may indicate frequent deposition from high-magnitude flood flows (a process described by Miall, 1977). The types of clasts seen are mainly angular rip-up clasts of parallel-laminated mud and silt, and the majority of these clasts are deformed. This deformation shows that the deposits ripped up by the flow were not lithified when eroded. The appearance of upper-stage plane beds (Sh) and dune-scale cross bedding (Sp) through this central part of the first storey also signifies a strong flow regime.

The deposition of Ccm, Sh and Sp facies, associated with strong flows, is interrupted by the deposition of fine-grained sediment from suspension. Fine-grained material occurs as thin (maximum thickness 0.5m) beds of laminated silt and mud (Fls and Flm) that are not laterally continuous, extending for between 4 and 28m (see Fig. 4.4b). The intercalation of high and low energy facies shows that fluctuation in flow strength in the central part of the first storey was considerable. The occurrence of lenses of sandstone within laminated muddy sediments (see Fig. 4.4a) is also an

indication of fluctuating flow strength. The relationship of the coarser facies to the finer ones, and to each other, is erosional, with each bed or bedset cutting into the preceding one. The geometries produced were measured (discussed in Chapter 5) and show a typical lens shape (Fig. 4.4a), with erosional slightly concave up bases (some showing sole marks). The original thicknesses and geometries of individual elements are impossible to determine because of the erosional relationships. Existing cross beds average 0.35m thick (App. B2). It is understood that dunes scale to flow depth (Allen, 1968; Jackson, 1976a); using the relationship between flow depth and dune height observed by Yalin (1972)

$$Y \sim 6h \quad \text{Eq. 4.1}$$

(where Y is the flow depth and h is the height of a wholly preserved dune form or foreset), and assuming that

$$h = 2.9 (\pm 0.7) \times d \quad \text{Eq. 4.2}$$

(where h is the mean height of a wholly preserved dune and d is the mean cross set thickness - LeClair and Bridge, 2001), this mean thickness of 0.35m gives a dune height of 1.02m and a mean flow depth of 6.1m. The range of possible flow depths given from these equations is 4.62–7.56m.

Flow direction in the central part of the first storey is given by cross beds and flutes, and is to the NE and ENE (see rose diagram in Fig. 4.4a). The angle between these flow directions and the bar accretion direction (WSW) described from the northern part of this first storey is greater than 60°, again meeting the criterion for lateral accretion (Miall, 1996). This confirms the interpretation of the macroform within this first storey as a laterally accreting bar. However, it should be remembered that many bars (such as mid-channel braid bars) accrete in more than one direction; downstream and lateral accretion can occur on different faces of the same bar. The outcrop of the first storey at Trusklieve is limited in extent, making identification of other faces of the first storey bar impossible. Nonetheless, lateral accretion surfaces have been identified, and their thickness can be used to estimate a channel depth. Since the lateral accretion package has a maximum thickness of 5m (see Fig. 4.4a), the guidelines proposed by Bristow (1987) that the height of a macroform is between 50 and 100% of the bankfull channel depth yield an estimate of channel depth of 5-10m. The bankfull depth calculated from the height of the dune cross beds (6.09m) is also within this depth range.

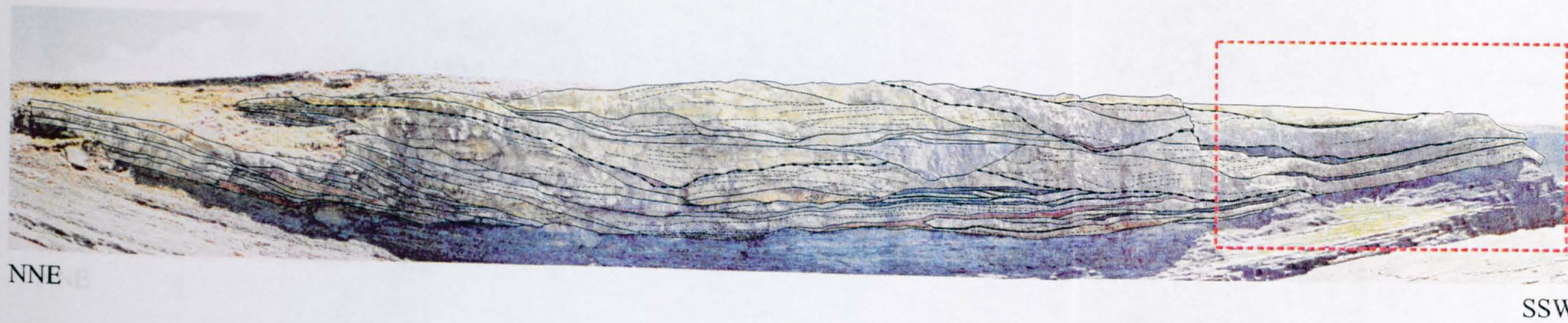
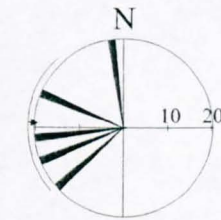


Figure 4.4. The storeys of the Tullig Sandstone at Truskelvie have been separated and enlarged to enable detailed features to be picked out. Photographic distortion was corrected for by drawing scale bars on the outcrop to ensure accurate measurements from photos. For a detailed interpretation of the southern half of the outcrop (outlined in red on the summary figure to the left) see Figure 4.3.

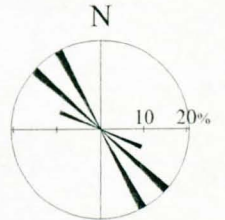
NNE

SSW

**Bedding**  
 Vector mean = 273°  
 Sample number = 5  
 Average dip = 7.0°

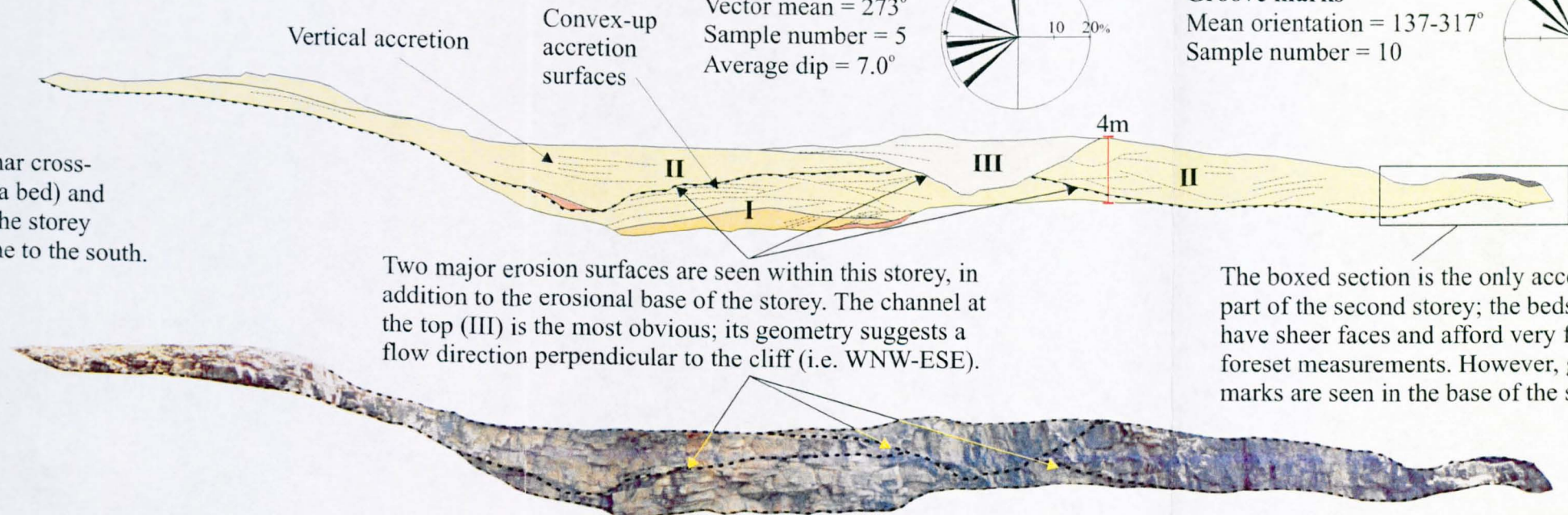


**Groove marks**  
 Mean orientation = 137-317°  
 Sample number = 10



**b) Storey Two**

This storey comprises poorly-developed planar cross-beds (sometimes changing to Sh up through a bed) and laterally impersistent conglomeratic beds. The storey is draped by laminated mudstone and siltstone to the south.



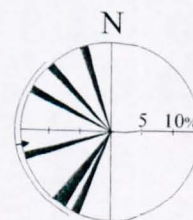
Two major erosion surfaces are seen within this storey, in addition to the erosional base of the storey. The channel at the top (III) is the most obvious; its geometry suggests a flow direction perpendicular to the cliff (i.e. WNW-ESE).

The boxed section is the only accessible part of the second storey; the beds here have sheer faces and afford very few foreset measurements. However, groove marks are seen in the base of the storey.

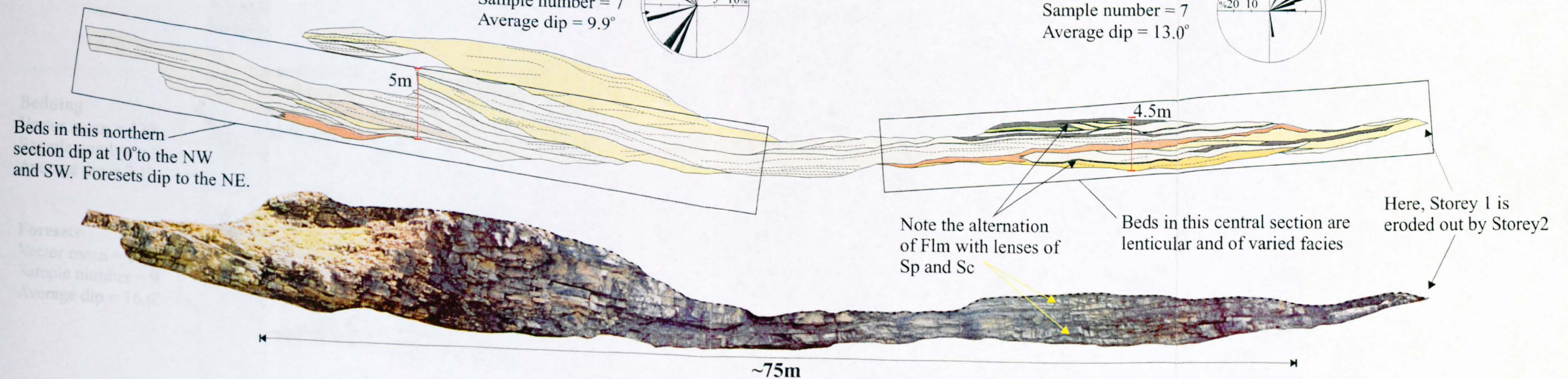
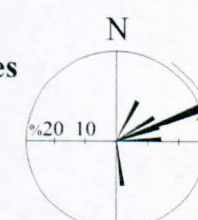
**a) Storey One**

This storey shows well-developed dipping accretion surfaces in its northern half, before becoming more heterogeneous towards the centre of the outcrop.

**Bedding**  
 Vector mean = 268°  
 Sample number = 7  
 Average dip = 9.9°



**Cross-beds and flutes**  
 Vector mean = 074°  
 Sample number = 7  
 Average dip = 13.0°



Beds in this northern section dip at 10° to the NW and SW. Foresets dip to the NE.

Note the alternation of Flm with lenses of Sp and Sc

Beds in this central section are lenticular and of varied facies

Here, Storey 1 is eroded out by Storey 2

~75m

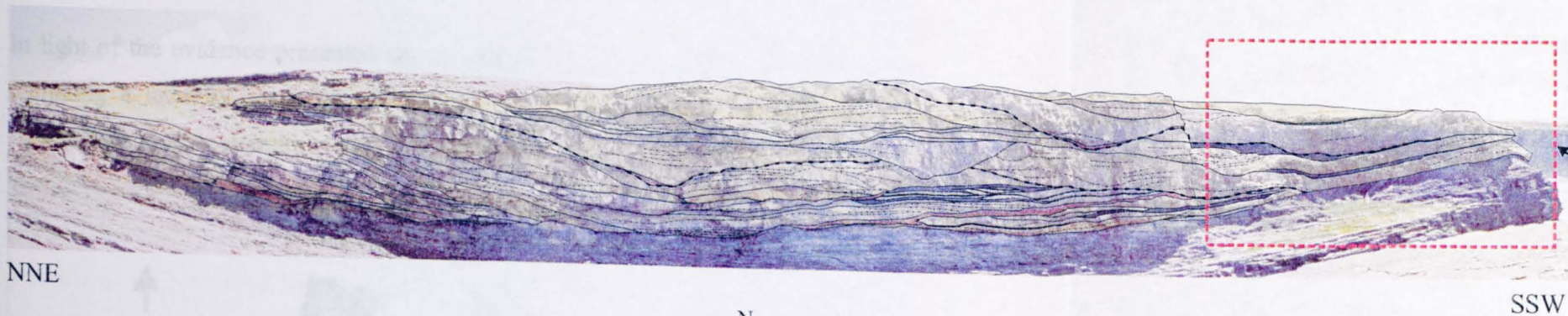
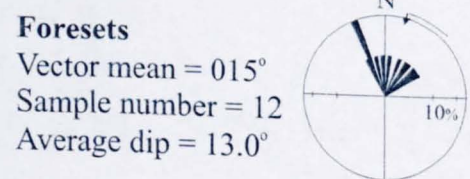
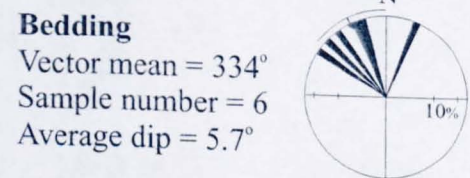
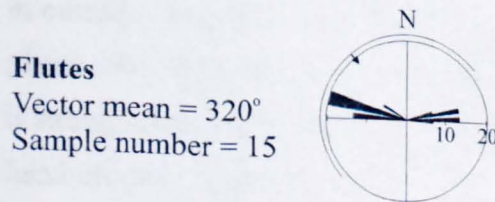
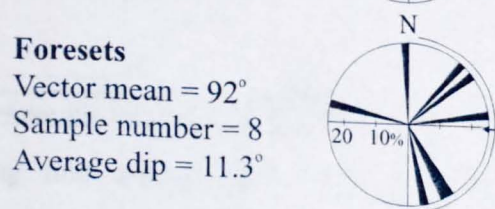
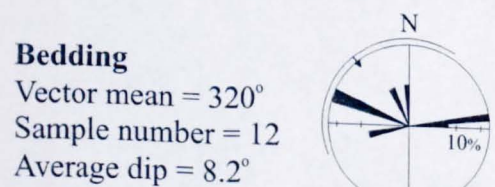
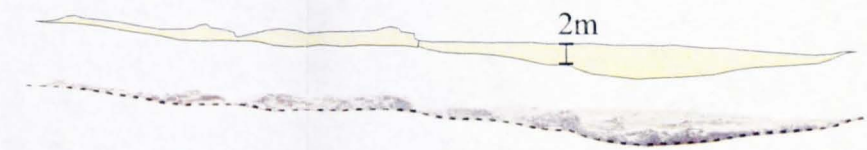


Figure 4.4 continued. The storeys of the Tullig Sandstone at Truskelvie have been separated and enlarged to enable detailed features to be picked out. Black and red scale bars are divided into 0.5m increments. For a detailed interpretation of the southern half of the outcrop, outlined in red on the summary figure (left), see Figure 4.5.



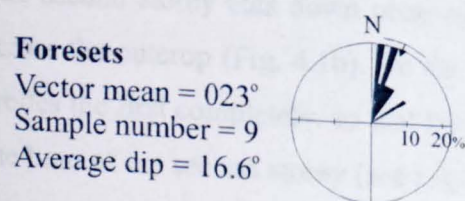
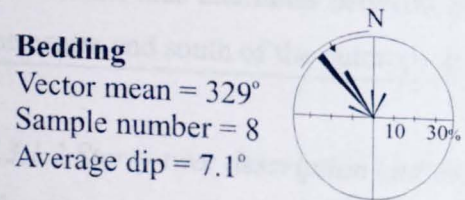
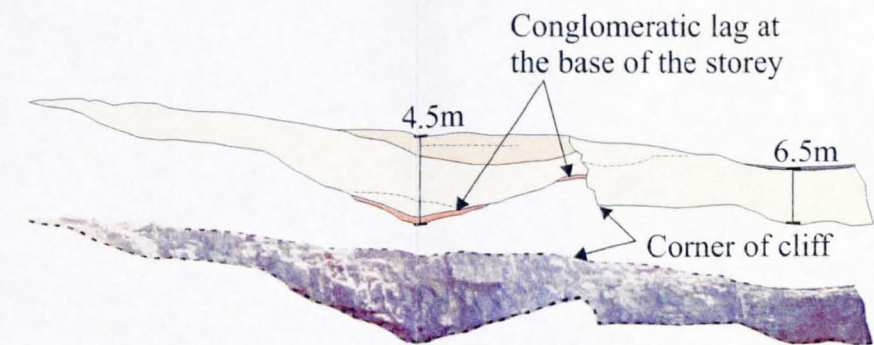
**e) Storey Five**

This storey exhibits a simple homogeneous succession of planar and trough cross-beds with set surfaces close to parallel to regional dip. The total thickness is not visible in this photograph.



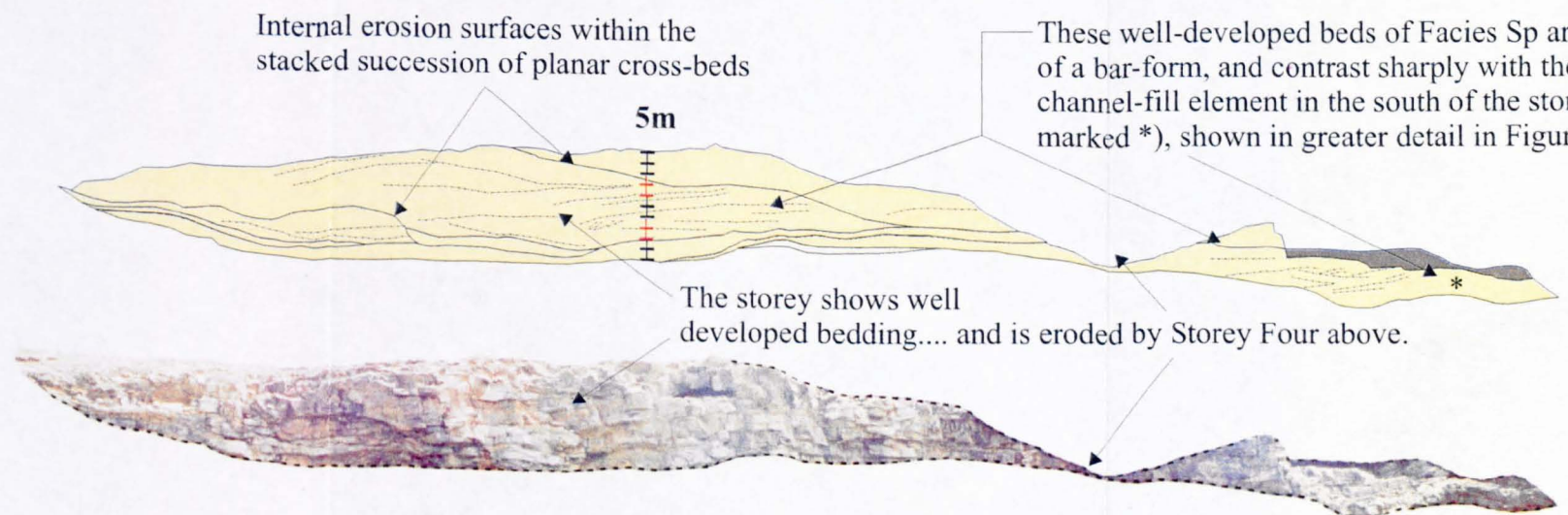
**d) Storey Four**

This storey is composed of facies Sm, Smc and Sh, with some low-angle cross-bedding (S1) and a strongly erosional base. Several thin, laterally impersistent conglomerate beds also occur. The storey is capped by a thin (<0.45m) bed of laminated silty mud. The low angle of the foresets encountered makes dip measurements less accurate than for steeper foresets, giving rise to a wide range of dip directions.



**c) Storey Three**

This storey is more heterogeneous than the others in its southern part (see Fig. 4.3b), but the northern section shown here comprises mainly planar cross bedded sandstone.



In light of the evidence presented above, the first storey is interpreted as a channel including a laterally accreting bar and a 5-10m deep channel experiencing large fluctuations in flow strength. Section 5.3.1.1 describes the first storey quantitatively.

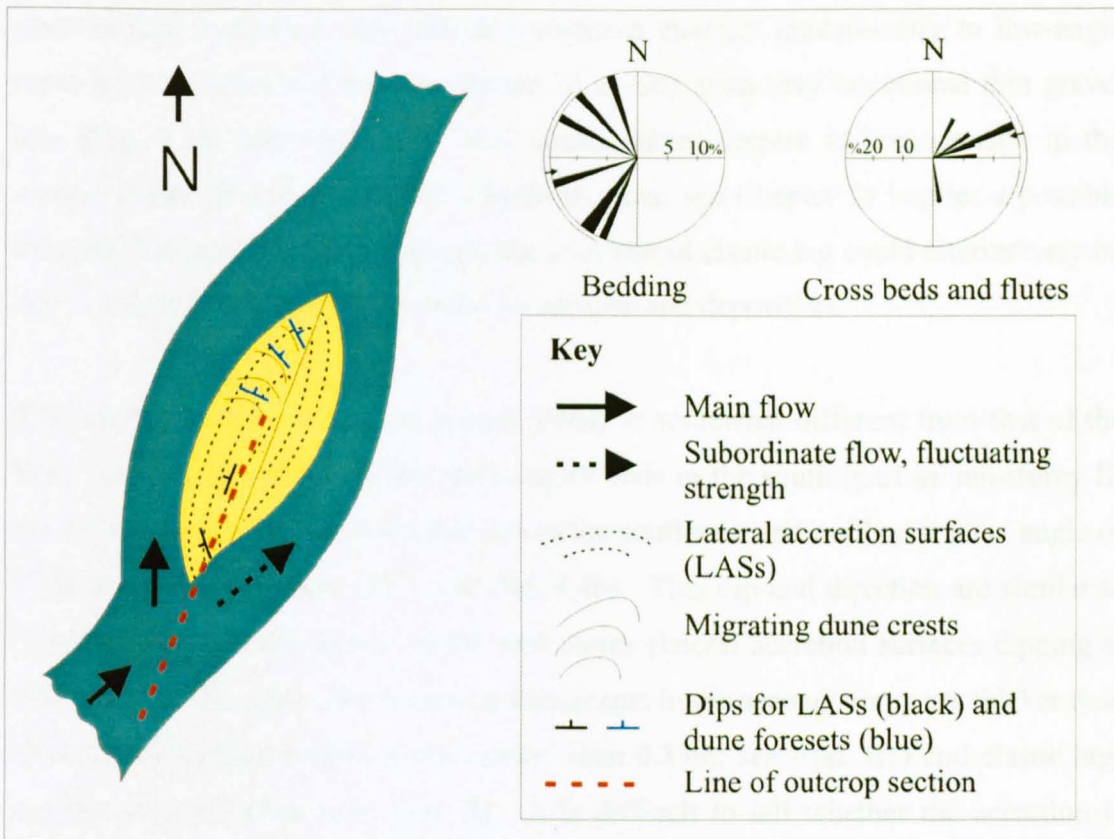


Figure 4.5. A plan view schematic diagram showing an environmental interpretation for the first storey, taking into account palaeocurrents and the geometries of architectural elements seen in outcrop. Lateral accretion surfaces form on both sides of a mid-channel bar, and planar cross beds form as dunes migrate across the bar. When flow to the northeast is strong, sands and gravels are deposited. During periods of lower flow in the right-hand channel, finer grained sediment is deposited. The channel-fill thus alternates between mud and sand with conglomeratic lag, as seen in the centre and south of the outcrop. For more palaeocurrent information, see Fig. 4.4.

#### 4.3.1.2 Storey two: description and interpretation

The second storey cuts down progressively into the first storey from north to south across the outcrop (Fig. 4.1b). In the southern half of the outcrop, the second storey erodes the first completely, so that the base of the Tullig Sandstone complex becomes the base of the second storey (see Figs 4.3b and 4.4b). The total erosional relief from

one end of the outcrop to the other is the same as the thickness of the first storey, i.e. 8.5m. Storey Two is 2m thick above the least erosive section of its basal contact (in the north of the outcrop), giving a total stratigraphic thickness of 10.5m. In contrast to Storey 1, the second storey is relatively homogeneous, comprising mainly planar cross-bedded sandstone (Sp), which sometimes changes gradationally to low-angle cross beds or horizontal bedding (facies S1 or Sh), with very occasional thin gravel lags (Fig. 4.3b, and App. A5). This considerable increase in homogeneity in the second storey (it comprises 89.3% Sp/S1 by area; see Chapter 5) implies a possible reduced fluctuation in flow strength; the decrease in clastic lag could alternatively be due to a lack of fine-grained material for erosion and deposition.

The internal architecture of the second storey is somewhat different from that of the first. The second storey shows accretionary beds in the south (part of sub-storey II; see Figs. 4.3b box A, and 4.4b) that dip to the southwest and northwest at an angle of  $7^\circ$  (average dip direction  $273^\circ$  - see Fig. 4.4b). This dip and direction are similar to those for the northern section of the first storey (lateral accretion surfaces dipping at  $9.9^\circ$  to  $267^\circ$ ). However, the accretion increments in the second storey are thicker than those in the first (averaging 0.50m rather than 0.35m; see App. B1) and clastic lags are less frequent (Fig. 4.3b, box B). It is difficult to tell whether the accretion is lateral or downstream, because the cross bedding is poorly developed in the accessible (southern) part of the storey, often changing upward within a set to low angle and then horizontal bedding, and does not provide many foresets from which to measure current direction. Three foreset dips taken from the base of the southern part of the storey give corrected dips of  $6^\circ$  towards  $279^\circ$ , which agrees with the bedding dip and therefore suggests flow-parallel rather than lateral accretion; however, the sample number of palaeocurrents is too small to allow a definite conclusion.

The northern half of the second storey, seen in the main cliff face (see Fig. 4.4b), shows marked erosion surfaces that delimit three sub-storeys, labelled I, II and III in Fig. 4.4b. The uppermost of the three erosional surfaces is concave-up and the sub-storey approximately 20m wide by 3.2m thick. The geometry of this top sub-storey is typical of a cross section through a small channel. This channel element shows a low width/depth ratio of 6.25 and appears narrow, scoop-shaped and symmetrical, suggesting that the cliff section provides a cross section close to normal to the channel

axis. An oblique section would give a wider appearance to the channel, and a higher width/depth ratio. Since the cliff trends NNE-SSW, the channel axis is likely to be oriented WNW-ESE. Flow direction in the channel cannot be determined, because the channel is within an inaccessible part of the outcrop, but through binoculars, the channel fill appears massive (facies Sm – see Fig. 4.1b).

Sub-storeys II and I show discrete areas of conglomeratic lag deposits at their bases, but mainly comprise facies Sp and Sl (Figs 4.1b and 4.4b). These sub-storeys do not have pronounced concave-up channel-shape cross sections, suggesting that unlike sub-storey III, their channel axes have oblique orientations with respect to the cliff face. In contrast to sub-storey III, sub-storeys I and II show horizontal bedding (facies Sh) and cross bedding (Sp and Sl) internally; sub-storey II also shows well-developed dipping accretion surfaces in the south of the outcrop (Fig. 4.3b, box A). The few cross beds in the accessible section of sub-storey II are 0.44m thick on average, which, using the method invoked in Section 4.3.1.1 (Yalin, 1972; LeClair and Bridge, 2001), gives a flow depth of 7.7 (range 5.8–9.5m). The dipping accretion surfaces of sub-storey II and the convex-upward accretion surfaces of sub-storey I (labelled in Fig. 4.4b) are geometries commonly seen in mid-channel bar forms/braid bars (*sensu* Bristow and Best, 1993 and Bridge, 1993 respectively; see also Jo and Chough, 2001).

The upper surface of the second storey is a preserved depositional surface, exposed in the southern part of the outcrop (Fig. 4.3b, box A). The surface is flat to gently undulating and shows no features typical of erosional truncation. The storey is draped by parallel-laminated silt and mud (Fls and Flm), with two thin sandier lenses interbedded with these facies (Fig. 4.3b). This fine-grained interval is not laterally continuous and extends for only 32m; it thins and pinches out to the south and is truncated by the third storey to the north. The preservation and draping of the upper surface of Storey 2 indicates that this part of the channel system was abandoned, and experienced only fine-grained deposition for a time.

From the evidence presented above it can be concluded that the second storey is a fluvial channel with sub-elements including a probable mid-channel bar (sub-storey I) that experienced another growth phase represented by sub-storey II, and a discrete

small channel with sandy fill (sub-storey III – possibly a third-order cross-bar channel, *sensu* Bridge 1993, or a channel resulting from a mass-flow related to channel bank collapse, as described from the Fell Sandstone Group by Turner and Monro, 1987). Subsequent abandonment of this part of the channel system allowed the bar and sandy channel-fill deposits to be draped with fine-grained abandonment sediments, with occasional pulses of sandy sediment, possibly representing high-water stage wash-over from adjacent occupied channel(s). Figure 4.6, below, shows a schematic representation of this interpretation.

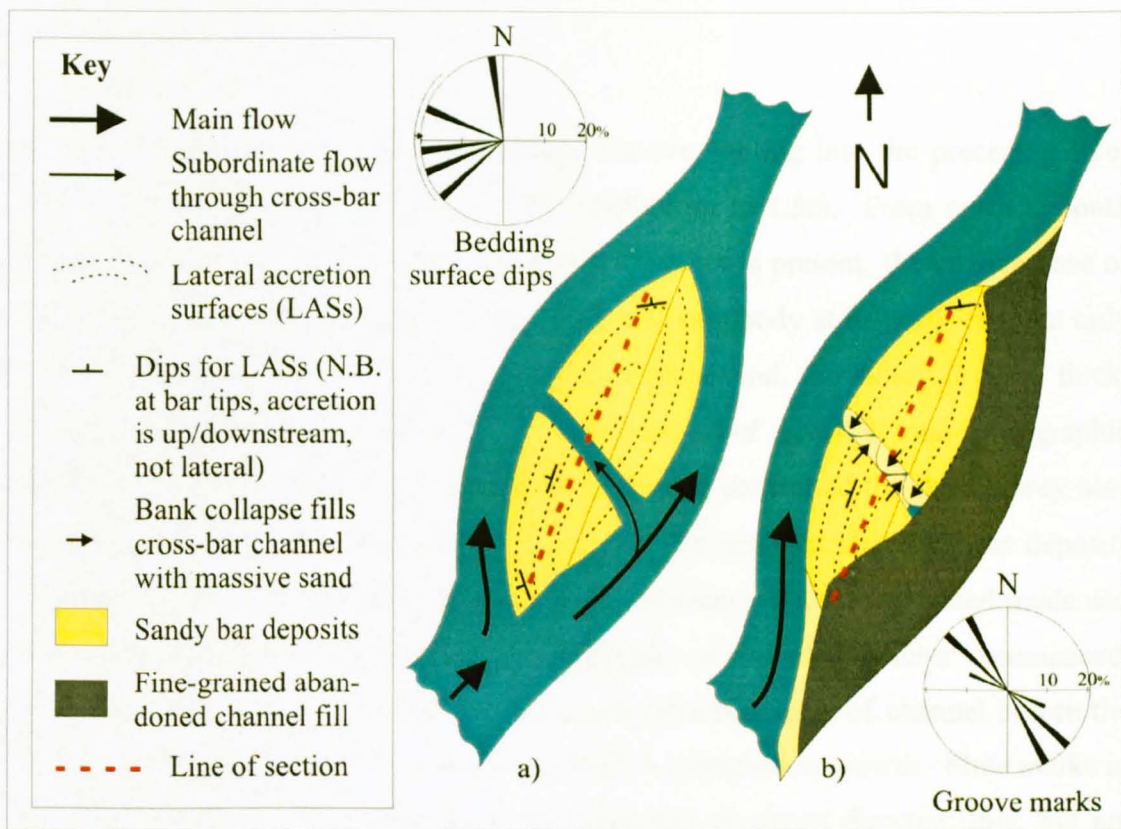


Figure 4.6. A plan view schematic diagram showing an environmental interpretation for Storey 2, taking into account palaeocurrents and the geometries of architectural elements seen in outcrop. a) Lateral accretion surfaces form on both sides of a mid-channel bar, with downstream accretion occurring at the downstream bar tip. The bar (representing sub-storeys I and II) is dissected by a shallow cross-bar channel (sub-storey III). b) The southern part of the outcrop is draped by fine-grained deposits, due to abandonment of the right-hand channel in the diagram. The cross-bar channel is filled by massive sands (facies Sm), probably from bank-collapse (a process described by Hjellbakk for braided river deposits in Norway, 1997). For more detailed palaeocurrent information, see Fig. 4.4b.

#### *4.3.1.3 Storey three: description and interpretation*

The third storey is accessible only in the south of the outcrop, and is different from the first two storeys. The dune-scale planar cross bedding is better developed in the third storey than in preceding storeys, with steeper foresets that do not shallow out to horizontal bedding as in Storey 2 (e.g. in Fig. 4.3b, box C, and Fig. 3.7). In its southern half, Storey 3 exhibits greater facies variety than Storey 2, comprising facies types Ccm, Sh, Sm, Shc, Sl, Sp, and Sc. The inaccessible northern part of the third storey, viewed through binoculars, appears more homogeneous than the southern part, comprising only facies Sp/Sl and Sh. No conglomeratic lags are seen within the northern part of the storey.

The basal surface of the storey is strongly erosive, cutting into the preceding fine-grained abandonment facies with a local relief of up to 1.5m. From north to south across the entire outcrop, a total downcutting of 5.5m is present; the erosive base of Storey 3 is 8.5m from the base of the entire Tullig sandbody at its north end, but only 3m from the base at its south end. At the northern end, the storey is 5.2m thick; adding this thickness to the 5.5m of erosional relief gives a total stratigraphic thickness of at least 10.7m for Storey 3. The basal contact of the third storey also exhibits load structures where it erodes into the fine-grained abandonment deposits capping Storey 2 (beds H and I; see Fig. 4.3b), showing that the laminated muds and silts beneath were not lithified when deposition of the sandy facies commenced. These features indicate reoccupation of the abandoned stretch of channel before the fine-grained fill could be stabilised, for example by vegetation growth. Flute marks in one place on this basal surface show northeast and southeast directed flow, but are localised and limited in number ( $n = 3$ ), and so cannot be taken as statistically representative of the channel orientation. Flute and tool marks represent localised flow directions in areas of net erosion, typically within channel thalwegs where cohesive mud is present (Bridge, 1993). It is thus possible that the southern section of the third storey, where the flutes were found, represents a channel thalweg and its fill.

The southern part of the third storey is quite varied in its internal architecture. Beds J through P accrete vertically, but pinch and swell as successive beds erode into each other (see Fig. 4.3b). Contacts between beds are typically gently concave upwards (e.g. beds L and P in Fig. 4.3b), a common characteristic in channel-fill architectural

elements (Miall, 1985). Beds of facies Sh (e.g. J, L, P) alternate with facies showing clastic lags (Shc and Sc – e.g. beds K, M, N' and N). The clasts in these beds are flow-aligned, with alpha and beta (i.e. long and medium) axes parallel to bedding planes, and several “floating” clasts are also present that were deposited by overpassing (see Section 3.3.2). Because of the lack of current direction indicators within facies Shc it is not possible to tell whether the clasts are oriented with their long (a) axes transverse or parallel to flow. Clast size varies, with laminated silt rip-up clasts reaching up to 250mm long. Occasional smaller (5-20mm) rounded pebbles of other lithologies also occur, as do pieces of plant material up to 0.7m long (see Fig. 3.32, and App. A5). The lag is therefore a mixture of freshly eroded fines, less angular particles with a longer transport history, and organic material. Overall, the upper stage plane beds (Sh) and the large clast sizes in facies Shc and Sc indicate high flow velocities; this, together with the strongly erosional internal contacts and the lack of identifiable bar accretionary surfaces, is evidence to support the idea that beds J to P in the third storey represent a channel-fill succession.

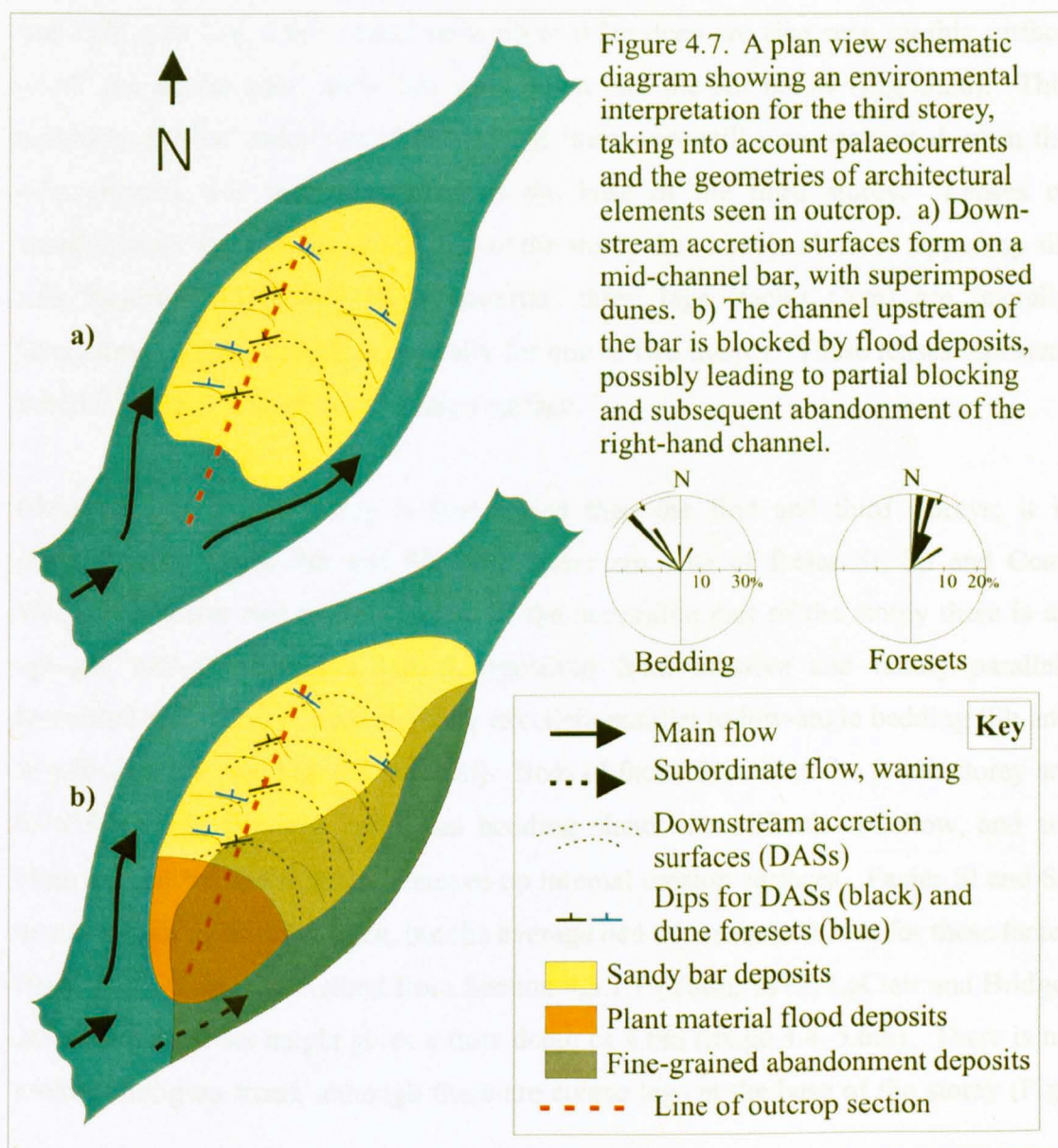
Figure 4.3b shows that above bed P there is an erosional surface at the base of bed Q, which cuts down to the north and truncates beds J, M, N', N and P. Bed Q shows horizontal bedding to rare low-angle planar cross bedding (Sh/SI) and is succeeded by a conglomeratic bed (R) and, further to the north, a series of laterally and vertically accreting planar cross beds (labelled R' in Fig. 4.3b). The change from Sh and Shc (beds J-N) to Sp (beds labelled R') suggests a slight decrease in flow velocity, allowing dunes to form and migrate within the channel. The cross sets of these dunes are particularly well developed and average ~0.20m thick (App. B2), with foresets dipping at 16.6° towards the north-northeast (008°-035° - see Fig. 4.4c). The bed boundaries dip towards the northwest (averaging 07° towards 329°), indicating probable downstream migration (the difference in dip direction between the foresets and beds is 55°, five degrees below the 60° suggested by Miall (1996) for positive identification of laterally accreting macroforms). The dip directions are very similar to those recorded by Williams and Soek (1993) for this storey. Using the method invoked in Section 4.3.1.1 (Yalin, 1972; LeClair and Bridge, 2001) the flow depth calculated from the cross bed thicknesses in Unit R' is 3.5m (range 2.64–4.32m). From observing the continuation of the cross beds northward into the inaccessible part of the cliff face (Figs 4.1a and b, and 4.4c), the accessible cross beds are seen to be

part of a thicker succession of vertically and laterally accreting beds. This succession forms the main part of the third storey; it extends laterally for over 72m, reaches 5m in thickness, and exhibits numerous internal accretion surfaces and a few obvious internal erosion surfaces (arrowed in Fig. 4.4c). Walker and Cant (1984) and Miall (1985) state that planar cross bedding is commonly formed in shallow channels and on submerged bar tops or sand flats by straight-crested dunes, transverse bars or sand waves. It is probable that the deep erosion of the Storey 3 channel thalweg in the south of the outcrop (discussed above) led to the deposition of coarser channel-fill deposits in the south (including beds of facies Ccm, Shc and Sc), while decreased erosion in the northern half (Fig. 4.1b) encouraged the formation and migration of straight-crested bedforms (facies Sp) in the shallower water depths.

In the accessible southern part of the third storey, the depositional upper surface of one partial dune form is preserved at the top of R', the planar cross-bedded succession (box D in Fig. 4.3b). This dune form, 0.5m thick, forms the top surface of the storey, but it is not laterally continuous, and further to the south pinches out against bed R, which then forms the top surface of the storey. The upper surface of bed R is also preserved, but in contrast to the smoothly convex surface of the dune, it is uneven and shows considerable topography. This topography is due to the nature of bed R, which comprises a matrix of fine to lower medium sandstone and large (up to 0.6m) fragments of organic debris, mainly woody plant material (logs 3 and 4 in Fig. 4.2; box E in Fig. 4.3b). Burial compaction has transformed the plant material to coaly seams, but the original clumping of debris and associated build-up of sand is still apparent and gives the bed its uneven nature. Bed R is interpreted to represent a large flood deposit of broken-up plant material swept downstream by high stage flow conditions. The sudden abandonment of this part of the channel after deposition of bed R allowed the depositional topography to be draped by fines (bed S in Fig. 4.3b; see comment in box F in this figure). The topography was thus preserved intact.

The fine-grained material of bed S, which drapes and onlaps the third storey, is parallel-laminated silty mud with a stratigraphic thickness of up to 4.70m. Due to both the uneven top and basal surfaces and the internal deformation of the bed, the total thickness of bed S is not wholly preserved in any one place; the bed is no thicker than 2.90m at any given point. Bed S contains a 0.3m thick parallel-laminated silty

sand layer 2.55m from its base (the lower “B” bed in Fig. 3.24). There are also occasional thin (<15mm) sands between 1.75m and 2.55m within bed S, showing poorly developed ripple cross lamination. The bed returns to muddy silt above 2.55m. Bed S also shows load structures and deformation (ball and flame structures, convolute lamination), low-angle faults with small offsets (<0.2m) and slight rollover folding related to these faults (see Figs 3.24, 3.25 and 4.3b, box F). The faults are confined to bed S and are part of the limited soft sediment deformation seen within it. Bed S continues laterally for 35m before being cut out in both directions by the erosively based fourth storey above. Bed S is interpreted as an abandonment-stage channel-fill (Fig. 4.7), with silty and sandy intercalations deposited from turbulent eddies overspilling from the main channel (a process described by Miall, 1996).



In summary, the third storey comprises a strongly erosively based channel-fill element (beds J-P in the south of the outcrop), conglomeratic flood deposits (bed R, again in the south), and straight-crested bedforms migrating downstream and accreting vertically in shallower water depths of around 3.5m (in the centre and north of the outcrop). The channel was abandoned and subsequently infilled with fine-grained channel-fill and overbank deposits (Fig. 4.7), and colonised by plants (Fig. 3.30, and Fig. 4.2 at 9.3m in log 4).

#### *4.3.1.4 Storey four: description and interpretation*

The base of the fourth storey is strongly erosional, with up to 7.5m of relief (see Fig. 4.3b boxes G and H, and Fig. 4.4d). This surface shows numerous clusters of sole marks, predominantly flute casts, which show current directions towards the WNW and ENE (see Fig. 4.4d). Load casts up to 0.2m deep are also seen on this surface where the denser sand above has sunk down into the silt below (Fig. 3.26). This indicates that the underlying abandonment fines were still water-saturated when the next channel was incised, similar to the base of the third storey. Lenses of conglomeratic lag are seen at the base of the storey that contain clasts of ripped-up silt and fragments of woody plant material; these lags (facies Ccm) are laterally discontinuous, only extending laterally for one or two metres. These lenses represent initial fill of the scoured basal erosion surface.

Internally, the fourth storey is less varied than the first and third storeys; it is dominated by facies Sm and Sh, with lesser amounts of facies Sl, Sp and Ccm. Within the lower two to four metres of the accessible part of the storey there is an upward, and sometimes a lateral, transition from massive and faintly parallel-laminated beds (Sm) to beds showing excellent parallel to low-angle bedding (Sh and Sl with rare Sp - see Fig. 4.8 overleaf). Beds of facies Sh within the fourth storey are 0.7-0.9m thick, although individual bedding planes are difficult to follow, and are often cut out by minor gently concave-up internal erosion surfaces. Facies Sl and Sp occur in beds up to 0.5m thick, but the average bed thickness is 0.26m for these facies (App. B2). Using the method from Section 4.3.1.1 (Yalin, 1972; LeClair and Bridge, 2001) this cross set height gives a flow depth of 4.6m (range 3.4–5.6m). There is no overall fining-up trend, although there are coarse lags at the base of the storey (Figs

4.1b and 4.3b), a feature also noted by Cant and Walker (1978) in their descriptions of channel-fill deposits in the modern braided South Saskatchewan River.

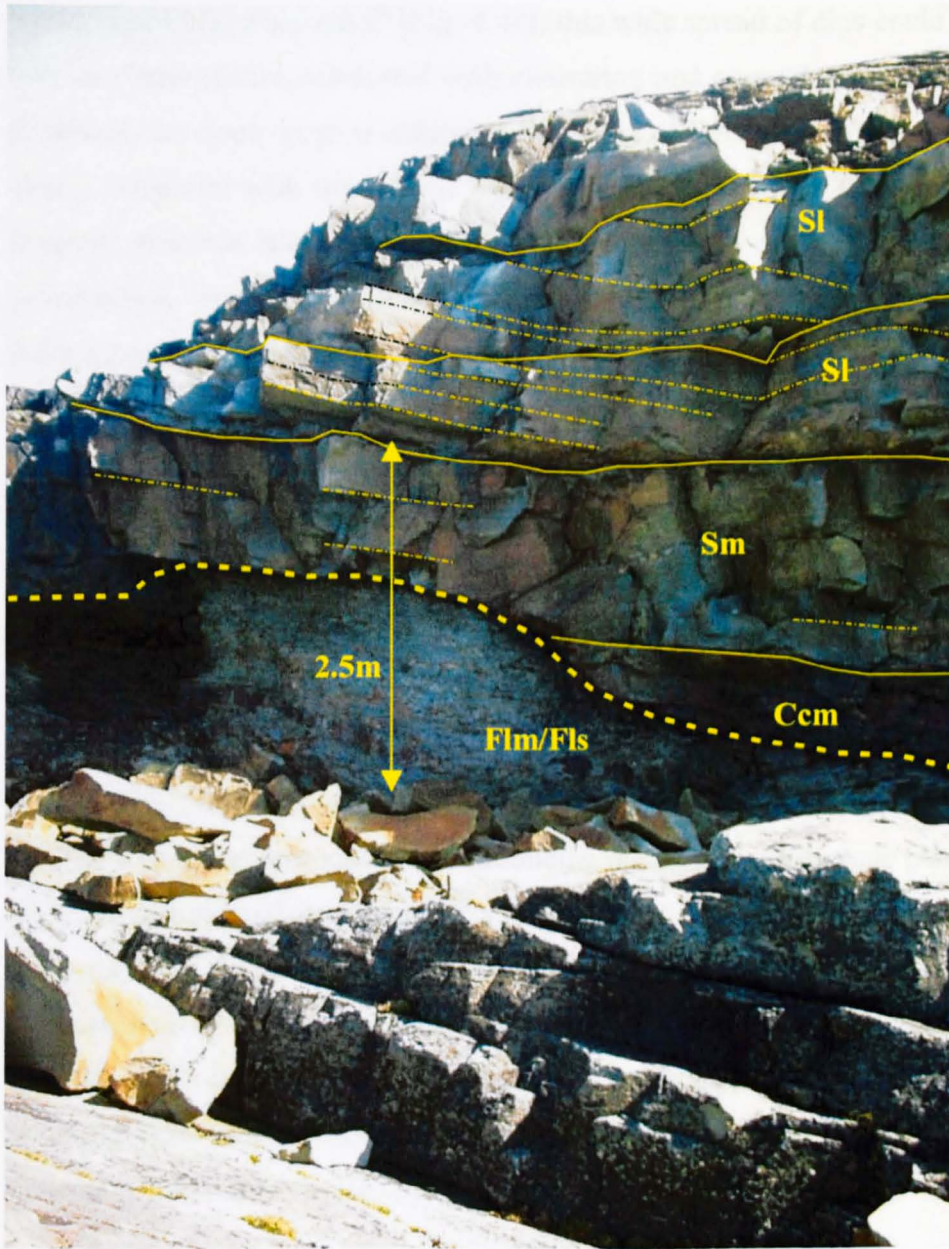


Figure 4.8. A view of the fine-grained channel plug at the top of Storey 3, and the lower few metres of Storey 4. Notice the erosional relief on the base of Storey 4 (thick dashed line), and the upward change in facies within this storey, from conglomerate (Ccm) through massive sandstone (Sm) to low-angle cross-bedded sandstone (SI). Thin solid lines mark main bed boundaries; thin dashed lines mark laminae and cross laminae.

Low-angle cross bedding is well developed in beds close to the northern cut-off of the underlying abandonment facies (see Figs 4.3b and 4.8), and foresets dip towards the north-northeast (Fig. 4.4d). Bed set boundaries are more variable, dipping to the WNW and ENE at around  $8^\circ$  (Fig. 4.4d); this wide spread of dips could be due to the inherent inaccuracies associated with measuring and correcting such low angle dips. However, the wide range is similar to the range of flute directions mentioned above. When compared with the foreset dips to the NNE, bedding surface dip directions suggests possible lateral accretion, but with such low dip angles, and no obvious architectural evidence such as large-scale dipping surfaces, it is impossible to determine this conclusively.

The fourth storey succession is more likely to be a channel-fill, with conglomeratic lag facies Ccm and bank-collapse facies Sm followed by vertical accretion of dunes and planar bedforms (facies Sp and Sh) migrating downstream across broad, near flat bedding surfaces (a succession described by Jo and Chough, 2001, from channel-fill sequences in southeast Korea). The lateral and vertical transitions between facies Sh and Sl/Sp seen in Storey 4 match the description of the "CHS" (cross-stratified and horizontally stratified sets) architectural element of Jo and Chough (2001), and suggest a range of flow conditions producing dunes and upper-stage plane beds under highly aggradational conditions (Saunderson and Lockett, 1983; Chakraborty and Bose, 1992). The concave-up minor internal erosion surfaces are also characteristic of shallow scours within a channel-fill succession (Miall, 1985), and although they are not filled with any lag, the sandy fill shows bedding parallel to the scour surface (a feature described from other fluvial systems by Allen, 1963, Miall, 1977, Singh and Bhardwaj, 1991 and others).

Overall, the fourth storey has a stratigraphic thickness of 8.5m, an estimated flow depth of 4.6m in parts, comprises mainly sandy facies, and can be interpreted as a fluvial channel with a strong flow regime that led to the dominance of facies Sh and Sl. The outcrop of the storey is smaller than previous storeys, and does not provide sufficient area for positive identification of bar or channel geometries. However, the presence of hyperconcentrated flow deposits from bank collapse (facies Sm/Smc; see Sections 3.3.1 and 3.3.2) and the well-developed Sl facies in scour fills suggest that the storey represents a channel-fill architectural element.

#### 4.3.1.5 Storey five: description and interpretation

A thin (<0.45m) laminated silt layer (Fls) separates the fourth and fifth storeys (Fig. 4.3b). This silt layer extends laterally for 16.5m and includes a small sand lens, 0.1m thick and ~1.5m long. The silt bed onlaps the upper surface of the fourth storey, and is eroded out in both directions by the downcutting base of the fifth storey. Storey 5, the uppermost present in this outcrop, is more homogeneous than those preceding it. The sandstones in this storey are clean, uniformly fine, and show no grading. Facies St dominates the storey, accounting for approximately 70% of the outcrop by area (see Chapter 5); facies Sp is the only other facies present, occurring immediately above the erosional surface at the base of the storey for a thickness of approximately 1.3m. The total exposed thickness of this storey reaches a maximum of 6.55m, but the limited extent of outcrop means that the total relief on the basal erosion surface is not necessarily visible. Visible relief on this surface is less than 2m, the lowest seen on the basal surface of any storey at this locality.

Bedding planes and coset boundaries, corrected for regional tilt, are close to horizontal, but show small dips (average  $5.7^\circ$ ) towards the NNW (Fig. 4.4e). Corrected foresets show a migration direction towards the north and NNE (Fig. 4.4e). The angle between these directions is low and suggests downstream accretion, but the fact that the bedding dips are so low means that the measured dip directions could be inaccurate. To the careful observer there is no evidence of obvious dipping accretion surfaces, either lateral or downstream; however, as with the fourth storey, the outcrop (a stepped area set back from the cliff top) does not lend itself to observations of large-scale bedding architecture. Nevertheless, the apparent lack of lateral accretion surfaces and major convex-up bedding surfaces suggests that the succession represents fields or trains of individual bedforms (an architectural style described by Miall, 1985). Cross bed thicknesses range from 0.13 to 0.51m, with an average value of 0.27m (App. B2); employing equations 4.1 and 4.2 (Yalin, 1972; LeClair and Bridge, 2001) gives an average flow depth of 4.8m (range 3.6–5.6m).

The vertical profile is also instructive, showing a change from planar to trough cross bedding as previously described. These facies (Sp and St) are typical of the fill of channel scours by migrating straight- and sinuous-crested dunes (Miall, 1977; Collinson and Thompson, 1982; Singh and Bhardwaj, 1991; Jo and Chough, 2001).

Miall (1985) states that trough cross beds “characteristically occupy the deeper portions of active channels wherever the bedload is predominantly sand”, indicating that this fifth storey represents deposition in a deep part of an active channel.

The fifth storey can therefore be interpreted as a deep part of a channel with a strong but stable flow regime, with a field of straight- to sinuous-crested dunes migrating along it. The development of trough cross bedding is indicative of continuous sediment transport under sustained flow conditions, with curved-crested dunes developing from straight crested dunes over time (Leeder, 1999) or at times of increased flow speed (Miall, 1996). The homogeneity of this fifth storey in terms of facies exceeds that of all previous storeys, being dominated by faces St. The storey concludes a progression from mixed fine and coarse facies and complex architectures in the lower storeys (see Fig. 4.4a and b) to predominantly sandy facies and simpler architectures in the higher storeys (see Fig. 4.4c, d and e).

#### *4.3.1.6 Summary and discussion of the Trusklieve outcrop*

A storey-by-storey summary is given below.

- 1) Storey 1 exhibits laterally accreting bar deposits up to 5m thick, and a laterally equivalent channel-fill succession comprising conglomerates, sands and silts. The storey shows 2.5m of erosion on its basal surface, and is 8.5m thick (probably thicker before erosion by Storey 2). Flow depths of 6.1m are calculated from cross bed heights, and palaeocurrents show flow to the northeast.
- 2) Storey 2 comprises three sub-storeys representing a downstream accreting mid-channel bar form and a minor cross-bar channel. The storey shows 8.5m of erosion on its basal surface, reaches a thickness of 10.5m, and gives flow depths of 7.7m from Eq. 4.1.
- 3) Storey 3 is composed of a channel-fill succession and, towards the north, planar cross beds comprising probable downstream accretion increments. Storey 3 shows 5.5m of erosion on its basal surface and is 10.7m thick in outcrop. Calculations of flow depth give a value of 3.5m for the less deeply eroded northern part of the storey. Palaeoflow was to the north-northeast.
- 4) Storey 4 represents a sandy channel-fill, with bank collapse facies (Sm), migrating straight-crested dunes and planar bedforms, internal scour surfaces, and conglomeratic lags of limited extent at the base. The storey has a measurable

stratigraphic thickness of 8.5m and its basal surface erodes 7.5m into the underlying storey. Calculations of flow depth give a depth of 4.6m.

- 5) Storey 5 is interpreted as a dune field migrating through an active channel, forming beds of facies Sp and St. Flow depths of 4.8m are calculated from these cross beds, which also show palaeoflow to the NNE. The exposed thickness of the storey is 6.55m, with 2m of erosion on the limited exposure of the basal surface.

Based on the observations and interpretations in Sections 4.3.1.1 to 4.3.1.5, the outcrop of the Tullig Sandstone at Trusklieve is interpreted as a nearly flow-parallel section through a braided fluvial system flowing to the northeast. The occurrence of lateral and downstream accretion surfaces is evidence of the migration of mid-channel bars. Combined with the occurrence of a discrete, small, cross-bar channel (typical of braided systems; e.g. Williams and Rust, 1969, Bristow, 1987, Bridge, 1993), this evidence indicates a degree of braiding within the fluvial system (e.g. Miall 1977). The high proportion of channel-fill deposits (seen in all five storeys) relative to lateral accretion deposits (only positively identified in Storey 1) is also indicative of braiding, since the proportion of channel-fill deposits relative to lateral accretion deposits is known to increase with increasing braiding parameter (Bridge, 1985).

The low percentage of fine-grained deposits in vertical profiles (see Fig. 4.2) and by area (5.29% - see Chapter 5) also points towards a braided character, because braided systems are usually found to contain much less mud and silt than meandering systems (e.g. Walker and Cant, 1984). However, a low percentage of fines is not by itself a sufficient criterion for identifying braiding (Friend, 1983), since some braided systems contain over 40% by volume of fines (Bentham *et al.*, 1993). Nonetheless, the typical fining-up meandering profile (Allen, 1970b) is not seen anywhere within the outcrop; the grainsize is uniformly fine to medium sand, and apart from a general concentration of clasts at the base of individual storeys, there is no indication of changing grainsize within each storey. The observation that the mean grainsize of the channel-fills (e.g. Storey 4) is the same as the mean grainsize of the lateral accretion deposits (Storey 1) conforms to Bridge's assertion (1985) that channel and lateral accretion elements should exhibit similar grain sizes in low-sinuosity channels, and thus increases confidence in the interpretation of the fluvial system as a low-sinuosity braided system.

From bedform measurements and dune heights, the flow depths of each channel storey are calculated to be between 3.5 and 7.7m. This agrees reasonably well with the measured range of channel storey stratigraphic thicknesses, from 6.55m for Storey 5 to 10.7m for Storey 3, although original thicknesses would have been greater before compaction. Etheridge and Schumm (1978) and Lorenz *et al.* (1985) use an arbitrary decompaction of 10% for channel bars, which in the case of Trusklieve gives original channel thicknesses of between 7.28 and 11.89m. These thicknesses are greater than the flow depths, but it is quite reasonable for channel-fill and braid bar deposits to be thicker than the flows forming them, due to vertical accretion over time. It is also important to remember that channel depth will vary across a channel, and that flow depths generating dunes in one part of the channel may be less than flow depths elsewhere; this observation is made in Storey 3 (Section 4.3.1.3).

The bar forms observed at Trusklieve are on a scale that allows their changing geometries to be seen in the outcrop, which is over 100m in length from north to south; this suggests that the bars are of a similar scale to the outcrop. The lateral accretion element in Storey 1 has a measured thickness of 5m. Channel widths are much harder to assess, since the channel edges are not visible in the outcrop, with the exception of the probable cross-bar channel (sub-storey III in Storey 2). The pitfalls of empirical methods of calculating channel widths from channel depths are discussed by Bridge and Mackey (1993) and Bridge (2003). Many empirical methods require some understanding of the sinuosity and meander wavelength of the channels (e.g. Leeder, 1973; Williams, 1986) and are therefore not suitable for application to the Trusklieve outcrop, where measurements of these characteristics are not possible. However, Bridge and Mackey (1993) use channel-belt width and bankfull depth data from modern rivers to construct a regression plot expressing the relationship between width and depth; on the resulting graph, the flow depths calculated from Trusklieve give channel-belt widths in the (very wide) range 250-15000m at 95% confidence, and (more realistically) between 650m and 2500m using Bridge and Mackey's combined equation (1993). It should be noted that the flow depths calculated for Trusklieve might not represent true bankfull depths. An alternative method of channel-belt width calculation would be to use the bar form height from Storey 1 (5m) to give a bankfull depth of 5-10m (assuming macroform height is between one-half and the total bankfull channel depth; Bristow, 1987). This bankfull depth range gives

a channel-belt width of between 1000m and 3000m from the regression plot of Bridge and Mackey (1993), similar to the width range generated by using the flow depths.

The scale of the channel storeys is similar to that of channel bodies described by Marzo *et al.* (1988) from the lower sandstone complex in the Eocene Castissent Formation, Spain. These Eocene channel storeys are interpreted by Marzo *et al.* (1988) as part of a braided system, and are 0.5 to 5m thick; the sandbody they coalesce to form is 25m thick (similar to the 22m+ thickness measured for the Tullig Sandstone at Trusklieve). The channel dimensions seen in the Tullig Sandstone at Trusklieve are also very similar to those recorded by Jo and Chough (2001) in Cretaceous braided fluvial sequences in the Kyongsang Basin, southeast Korea, where individual channels are a few to 10m deep and 9m to several tens of metres wide; widths of the channel-belt are not given.

The most obvious trends observed at Trusklieve are the increasing facies homogeneity and progressively simpler architecture with height (noted in Section 4.3.1.5). The increasing facies homogeneity is logical, since the sediment being eroded changes from delta front silts and muds to the channel sands over time (i.e. with height), reducing the frequency of occurrence of conglomeratic facies. However, the upward progression to storeys increasingly dominated by trough cross bedding and simple channel-fill architectures cannot be explained by this. Instead, this trend may be due to the filling-up and shallowing of the channel system; Miall (1996) recognises that while shallow braided rivers are dominated by fields of dunes that produce facies St (or Sp), with simple sheet-like architectures, deeper braided rivers are more complex and varied in facies and architecture. This model would suggest that the more complex lower storeys at Trusklieve represent a deeper river than the simpler, more homogeneous storeys nearer the top of the Tullig Sandstone at Trusklieve.

Comparisons between the Tullig Sandstone at Trusklieve and other Namurian fluvial systems of western Europe highlight some interesting differences. For example, Okolo's observations (1983) of postulated fluvial distributary channels in the Namurian Fletcher Bank Grit, Lancashire, England, are similar in some aspects to the observations discussed here, but differ markedly in terms of sandbody geometries and architecture. The channel storeys Okolo describes show similar thicknesses (3.6m to

29.0m) to those at Trusklieve, but in general exhibit less than 4m of scour on their basal surfaces, and show architecturally simple fills that fine upwards; neither of these observations is true at Trusklieve. Nor is there an upward decrease in bedform size at Trusklieve, like that described by Okolo, 1983 (see graph of cross-bed thicknesses for each storey in App. B2). More detailed quantitative observations regarding facies percentages and vertical distributions will be presented and discussed in Chapter Five.

Another example of Namurian fluvio-deltaic sediments is seen in the Pennine Basin in northern England, a basin that was created at the same time as the WINB and that was filled by a similar series of cyclothems defined by goniatite-bearing marine bands. The topmost Namurian cycle comprises the Rough Rock Group, which as a whole is interpreted as a sheet delta (Elliot, 1978); the uppermost unit in the Group is the Rough Rock. Bristow and Myers (1989) describe the Rough Rock as being mainly composed of trough and planar cross-bedded sandstone facies, with internal scours and occasional coarse intraformational conglomeratic lags; the authors interpret the succession to be a major braided fluvial distributary channel. They cite the cross-stratification style, the unidirectional palaeocurrents and the lack of change in grainsize and sedimentary structures in either vertical or downstream directions as evidence for few macroforms and a braided channel pattern. This description agrees particularly well with Storey 5 at Trusklieve, and also resonates with sections of Storeys 3 and 4, overall supporting the interpretation of the Tullig Sandstone as a braided fluvial system. In addition, the individual channels in the Rough Rock are thought to be at least 6.5m deep, and the width of the channel-belt is estimated at around 1km (Bristow, 1987). Both dimensions are very similar to those calculated for the Tullig Sandstone channels from the Trusklieve outcrop (depths of 3.5-7.7m calculated from cross-beds, and 6.55m-10.7m measured from outcrop; channel-belt widths of between 650m and 2.5km).

However, there are some important differences between the Tullig Sandstone and the Rough Rock: the latter is known to be a maximum of 50-60m thick (Maynard, 1992), around twice the thickness of the Tullig Sandstone, and is present over an area of approximately 10,000km<sup>2</sup> in northern and central England (Bristow and Myers, 1989), which is a far greater area than that covered by the Tullig Sandstone. Additionally, the grainsize of the facies is coarse to very coarse, and the cross sets are

larger scale, being up to 2m thick (a thickness about ten times greater than the majority of cross sets seen at Trusklieve).

Work done on the Trusklieve outcrop by Pulham (1987) is less detailed than the research presented here, but he does mention some of the features noted in this chapter. For example, Pulham also observed five storeys within the outcrop (although he defined them slightly differently), and concluded that the overall palaeocurrent direction was to the NNE. Pulham also noted the presence of conglomeratic lags immediately above some of the storey bases, and observed the predominance of trough cross bedding in Storey 5. However, Pulham recorded a southeasterly palaeoflow direction for Storey 5, which is not apparent from the data presented here (see Fig. 4.4e); he also considered the storeys to increase in thickness upwards through the succession, which is not demonstrated by this research. Pulham's interpretation of the outcrop, based on the overall thickness and sedimentary context, is that it represents a section through a distributary channel complex, and as such is genetically linked with the underlying delta front deposits (Pulham, 1987 and 1989). The validity of this conclusion will be discussed in Section 4.4.1

Overall, the architectural style, facies associations and channel dimensions seen within the Tullig Sandstone at Trusklieve favour the interpretation of the fluvial system as a low-sinuosity braided system, probably filling up and becoming shallower over time. The channel dimensions calculated or measured from the outcrop compare favourably with other documented braided systems (Marzo *et al.*, 1988; Jo and Chough 2001), and the facies and channel dimensions are similar to those described by Bristow and Myers (1989) from the Namurian Rough Rock braided fluvial channels, although those at Trusklieve show a finer grain size and smaller sedimentary structures. The Namurian channels of the Fletcher Bank Grit studied by Okolo (1983) also show some similarities to the Trusklieve channels in terms of facies, but the channel dimensions and erosional relief Okolo describes, although of a similar order, are nonetheless smaller than those measured and calculated from Trusklieve.

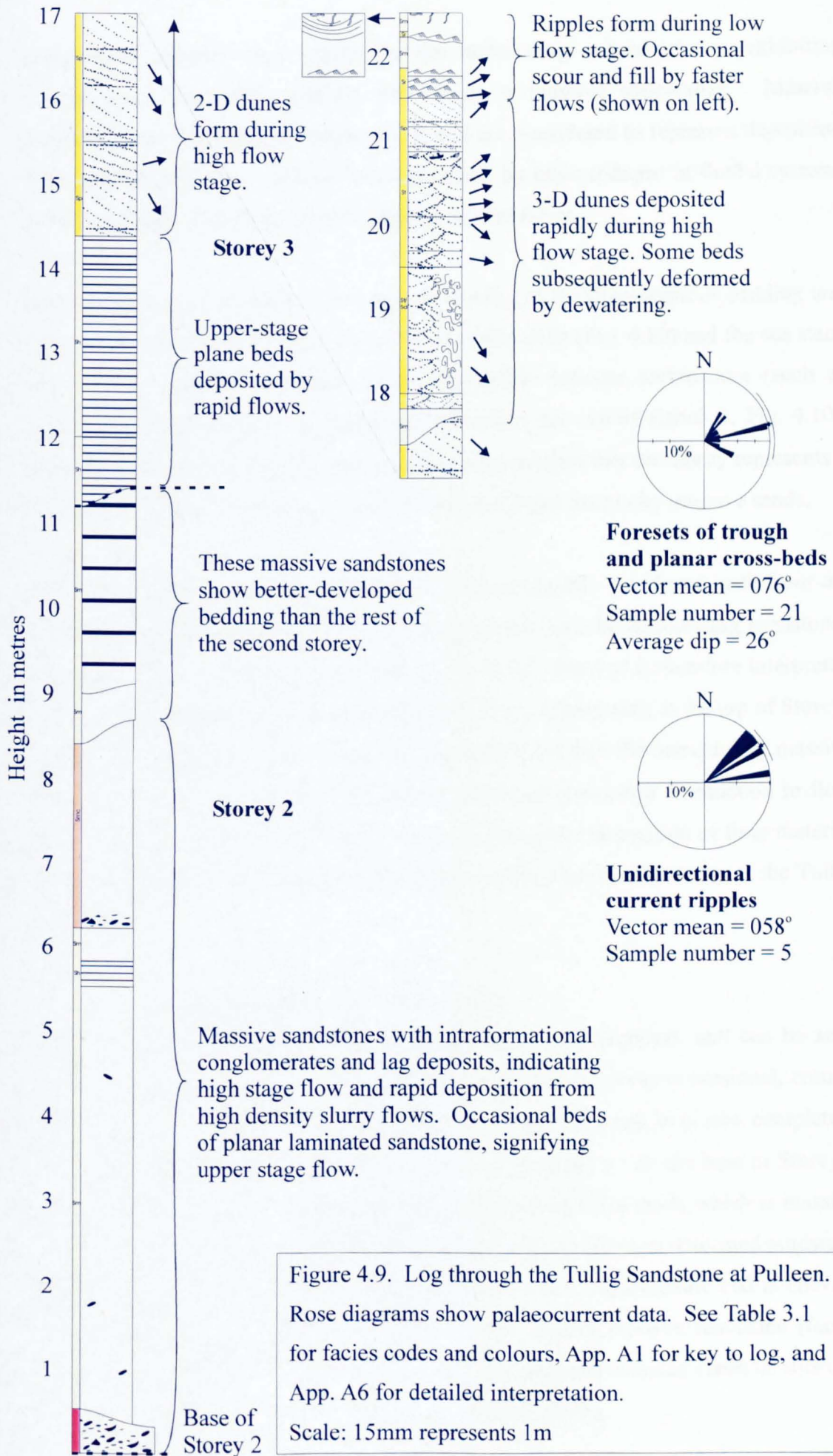
### 4.3.2 The Tullig Sandstone at Pulleen

The exposure of the Tullig Sandstone at Pulleen is located 19km along the coast to the northeast of Truskleeve. The outcrop comprises a headland with an exposed stepped area of about 40m by 20m, showing the whole thickness of the Tullig Sandstone in a succession of dipping beds, and an inaccessible cliff face and sea stack, which were both photographed for additional architectural detail. The total thickness of the Tullig Sandstone from base to top is 22.5m, and comprises three storeys; a logged section through this entire thickness is shown in detail in App. A6, and in a summarised form in Fig. 4.9. As at Truskleeve, the facies association in the Tullig Sandstone at Pulleen matches the fluvial/alluvial association described in Section 3.4.3; the sandbody is therefore interpreted to be fluvial in origin. The Tullig Sandstone at Pulleen is erosively based, cutting down into mouthbar-type fine-grained sediments. To the south of the cliff top exposure is a long inaccessible cliff section where the immediately underlying fine-grained sediments of the Tullig Cyclothem are exposed (Pulham, 1987). The beds below the Tullig Sandstone, and those within it, dip to the south (azimuth 186°) at an average angle of 24° (see Fig. 4.9). Palaeocurrent measurements from the Tullig Sandstone were corrected to remove this regional dip.

#### 4.3.2.1 Storey one: description and interpretation

Immediately below the base of the first storey is an underlying sequence comprising around 5m of low-angle bedded and ripple-laminated sandstones with interbedded siltstones (also recorded by Pulham, 1987). Although this underlying sandy sequence was inaccessible, its appearance in the cliff face (labelled M in Fig. 4.10) is very similar both in terms of bedding architecture and facies proportions to the appearance of the sandbody seen at Tullig Point, which is discussed in Section 4.3.6 and is interpreted as a fluvially dominated sandy mouthbar. For this reason the sequence underlying the Tullig Sandstone at Pulleen is interpreted here as a mouthbar sequence.

The first storey of the Tullig Sandstone erodes into the mouthbar sequence with up to 0.4m of visible relief (label A in Fig. 4.10b). The thickness of Storey 1 is variable; in the log location it was completely eroded by the downcutting base of the second storey, while in the photographs of the cliff face it is clearly visible and reaches a thickness of about 1.6m (the storey is labelled "1" in Fig. 4.10). Because it was not logged, the detailed sedimentology of Storey 1 was not determined, but from the cliff



exposure it appears very similar to the succeeding second storey, exhibiting discontinuous horizontal bedding and having a massive appearance. Massive sandstones are discussed in Section 3.3.1, and are considered to represent deposition from high-density flows such as those generated by bank collapse in fluvial systems or by very rapid deposition from flood-stage fluvial flows.

The architecture of Storey 1 is not easy to see due to the discontinuous bedding and the lack of accessible outcrops. From views of the cliffs (Fig. 4.10) and the sea stack (Fig. 4.11) it appears that there is no discernible bar-type architecture (such as successive dipping beds). Instead erosional scours are visible (label B, Fig. 4.10), which, combined with the discontinuous bedding, suggest that the storey represents a channel-fill element formed by repeated scour and filled mainly by massive sands.

At the top of Storey 1 is a bed that has been preferentially weathered back from the cliff face; although not accessible, this bed is darker than the surrounding sandstones and appears to be parallel bedded (label C, Fig. 4.10). The bed is therefore interpreted as a bed of laminated siltstone or mudstone, similar to those seen at the top of Storeys 3 and 4 at Trusklieve, which is more easily weathered than the surrounding massive sandstones. The occurrence of this fine-grained bed shows that a reduction in flow velocity led to the end of sand deposition and allowed the deposition of finer material from suspension. This indicates abandonment of the first channel storey of the Tullig Sandstone.

#### *4.3.2.2 Storey two: description and interpretation*

The second storey was logged in its entirety across the headland, and can be seen between 0 and 11.2m in Fig. 4.9. The base of the second storey is erosional, cutting into Storey 1 with up to 1.6m of relief (label D in Fig. 4.10) and, in places, completely cutting out the siltstone/mudstone bed at the top of Storey 1. At the base of Storey 2 is an intraformational conglomerate (facies Ccm), up to 0.5m thick, which is massive in appearance and contains both angular and sub-angular clasts of deformed mudstone and siltstone (0-0.5m, Fig.4.9). The top surface of the conglomeratic bed is uneven, and the topography is infilled by the succeeding bed of massive sandstone (facies Sm). This massive sandstone exhibits occasional scattered rounded clasts of siltstone up to 50mm in diameter, and has poorly developed bedding.

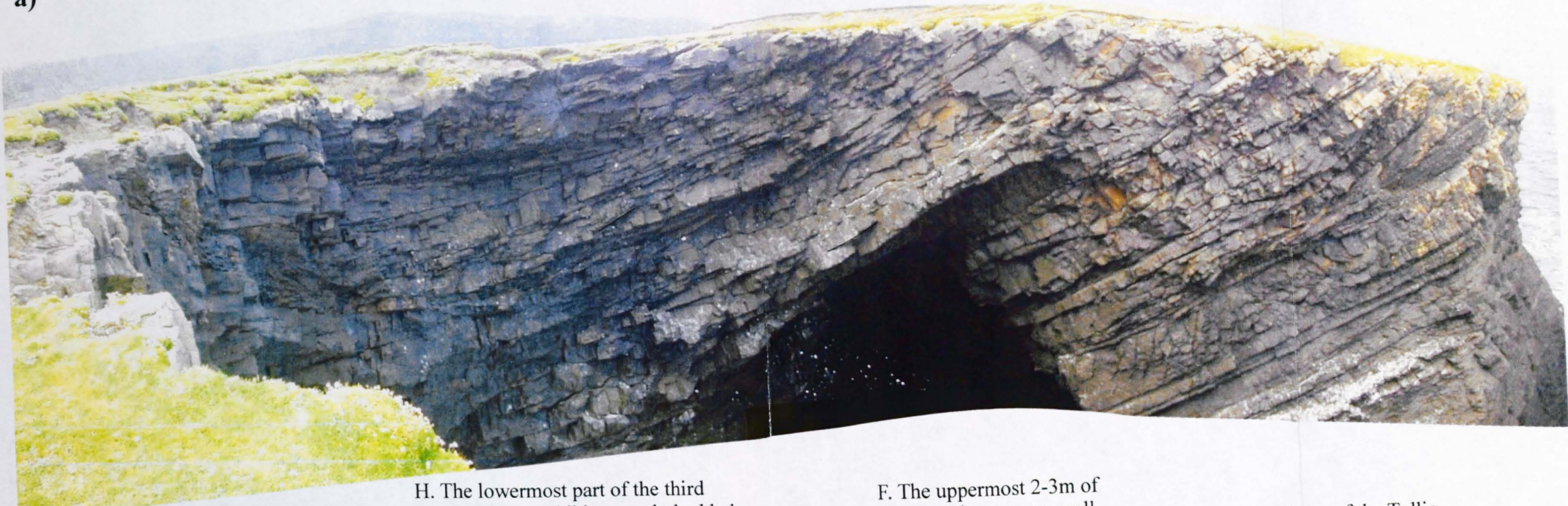
At a height of 5.5m from the base of Storey 2 (Fig. 4.9) a 0.3m thick bed of parallel-laminated sandstone (facies Sh) occurs, indicating the increased influence of traction currents, forming upper stage plane beds under conditions of high flow velocity. Massive sandstone (facies Sm) reoccurs above the parallel-laminated bed and, as in the Sm section below, shows laterally discontinuous bedding planes, internal scour surfaces and, in one place, a localised lag of siltstone clasts. With the exception of the planar laminated bed at 5.5m, the entire lower 9m of Storey 2 display poorly developed bedding (label E, Fig. 4.10b). Above 9.1m, however, the massive sandstone becomes better bedded, showing laterally continuous bedding planes with a spacing of around 0.3m (label F, Fig. 4.10b). The transition between poorly and well-developed bedding within Storey 2 is clearly evident in the offshore stack (Fig. 4.11).

#### *4.3.2.3 Storey three: description and interpretation*

Another transition that is very obvious in the sea stack cliff section is the change from the second to the third storey (label A, Fig. 4.11). The erosional base of Storey 3 exhibits downcutting relief of up to 3m, visible in the stack cliff section (1.5m of relief was measured at the log location – label G, Fig. 4.10b). Above this basal surface are 3.2m of planar laminated sandstone beds (facies Sh), that onlap and infill the erosional topography (see label B, Fig. 4.11). The bedding surfaces within this planar laminated succession are horizontal when corrected for regional dip, indicating purely vertical rather than lateral or downstream accretion.

At the top of the planar laminated succession is a sharp, flat contact with overlying well-developed planar cross bed sets. Two sets, 0.7 and 0.4m thick, are followed by two significantly thicker tabular cross sets whose bedding surfaces are laterally continuous over tens of metres. These large tabular-planar cross sets reach up to 0.85m in thickness and can be seen within the sea stack (label C in Fig. 4.11); using Eq. 4.2 the height of the bedforms they represent is calculated to be 2.47m. The large cross sets are likely to result from the migration of large dune bedforms termed cross-channel bars by Allen (1983a) and Cant and Walker (1978), and transverse bars by Levey (1978) and Miall (1977). Such bars are described from the South Saskatchewan River by Cant and Walker (1978), who record a height range of 0.3-2.5m, which agrees with the original bedform heights calculated from the large cross sets at Pulleen.

a)



b)

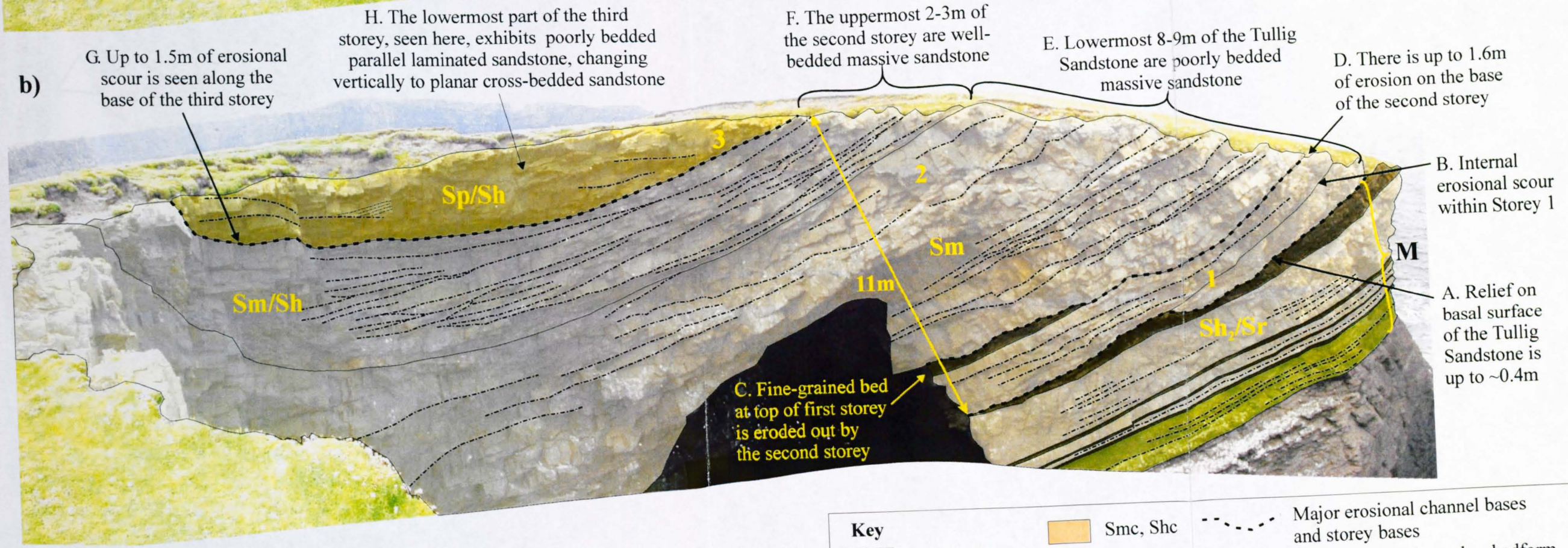


Figure 4.10. A: three-photo panel showing an inaccessible cliff exposure of the Tullig Sandstone at Puleen, viewed looking south. The location of the log is out of sight a few metres beyond the crest of the grassy cliff top. B: facies interpretations and storey labels. Note the underlying succession of interbedded sands and muds (M), interpreted as mouthbar sediments; within M the dashed lines represent thin (<50mm) siltstone or mudstone beds.

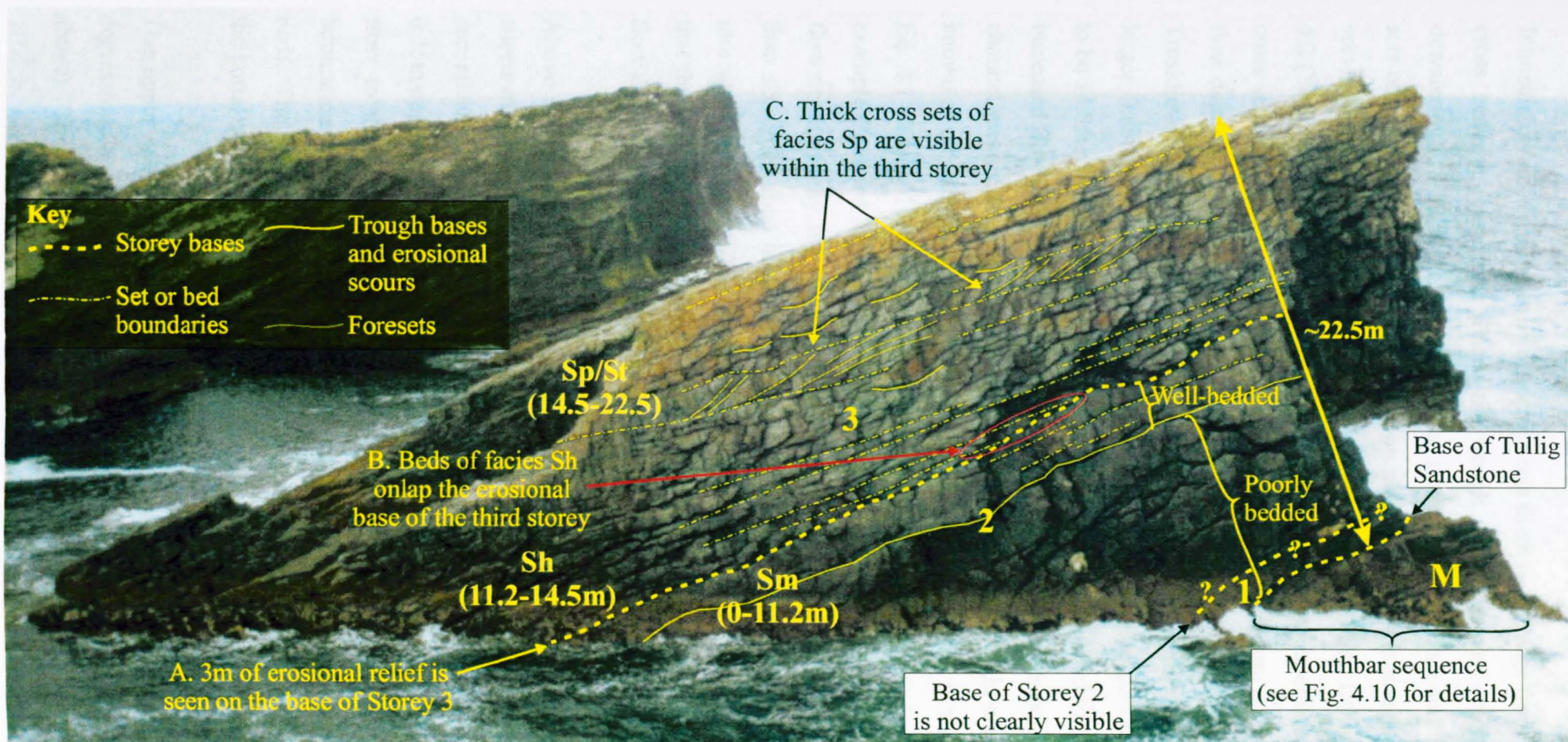


Figure 4.11. This sea stack, immediately to the west of the Pulleen outcrop, shows the changing facies and bedding geometries within the Tullig Sandstone. The base of the Tullig Sandstone is visible at the bottom right of the stack, and the total thickness up to the top surface is displayed in the cliff face. Note the flat bedding (horizontal when corrected for regional tilt) and the change from a poorly bedded blocky appearance near the base to trough and planar cross-bedding nearer the top. The change comes approximately half way through the sandbody thickness, and corresponds to the base of the third storey (at 11.2m in Fig. 4.9). There is also a transition from poorly to well-bedded sandstone within the second storey (at 9.1m in Fig. 4.9).

Immediately above these two large cross sets there is a change from planar to trough cross bedding. In some places the trough cross sets are deformed by intense dewatering (18-19.5m in Fig. 4.9). The trough cross sets are succeeded by several sets of planar cross bedding; the variation in thickness of the trough and planar cross sets is from 0.2 to 0.75m, with the average value being 0.36m. Using Eq. 4.1 and Eq. 4.2 (Yalin, 1972; LeClair and Bridge, 2001) the flow depth associated with this mean cross set thickness is calculated to be 6.3m (with a range from 4.8m to 7.8m). This flow depth of 6.3m is very similar to the flow depths calculated for the five storeys at Trusklieve (which range from 3.5m to 7.7m). The flow depth necessary to form the larger, 0.85m thick tabular cross sets discussed in the previous paragraph is calculated to be 14.8m, considerably greater than the flow depths calculated for Trusklieve. This increased flow depth shows that for at least a period of its existence, the second storey channel was sufficiently deep to allow formation of large straight-crested dune forms, known as cross-channel bars or transverse bars. It is important to note, however, that Eq. 4.1 (Yalin, 1972) does not always give an accurate result for flow depth; for example Cant and Walker (1978) record dune heights of 1.5m in a flood stage mean flow depth of only 3m, meaning flow depth in that case was twice dune height, rather than six times dune height as in Eq. 4.1. Therefore, although the large cross sets indicate an increased flow depth compared with the smaller cross sets, it is possible that the very high flow depth of 14.8m is an inappropriate figure and that the actual flow depth in which the large cross sets formed was somewhat smaller.

Above the cross-bedded succession, which continues up to 21.5m in Fig. 4.9, two sheets of ripple-laminated sandstone occur. The first sheet is 0.25m thick; within the second sheet, only the lowermost 0.1m shows ripple lamination, while the upper 0.35m appears massive. The ripples are unidirectional, with cross lamination showing flow to the northeast (see rose diagram in Fig. 4.9). The occurrence of ripple lamination indicates a decrease in flow velocity compared with the underlying cross beds. The massive upper part of the second rippled sheet could have been formed by the burial of the rippled laminae by a slurry flow from a collapsing sandy bank.

The upper half of the second rippled sheet is scoured in places, with trough-like depressions up to 0.3m deep occurring in its top surface (see Fig. 4.9, at 22m and above). These troughs are infilled by sandstone displaying either laminae parallel to

the trough sides or ripple lamination. The top of the third storey, which is also the top of the Tullig Sandstone at Pulleen, is the surface comprising the tops of the trough fills and the top of the second ripple laminated sandstone sheet. This top surface of the sandbody exhibits both vertical and horizontal trace fossils. The vertical structures are either holes left by rootlets, or more probably some form of unidentified burrow; none of the structures were visible in cross section and from the top view alone it was not possible to determine the origin of the features unequivocally. The horizontal structures, which are rare, are identified as *Thalassinoides* traces.

#### 4.3.2.4 Summary and discussion of the Pulleen outcrop

A storey-by-storey summary is given below.

- 1) Storey 1, though not accessible, is interpreted as a channel-fill succession, and exhibits internal scour surfaces and massive sandstones. It reaches a maximum thickness of 1.6m in this outcrop.
- 2) Storey 2 is 11.2 m thick and shows over 1.6m of erosional relief on its basal surface. The dominant facies is Sm, becoming better bedded upwards; no cross beds are present so calculations of flow depth cannot be made.
- 3) Storey 3 is 11.3m thick and erodes up to 3m into Storey 2 below. Storey 3 comprises planar and trough cross beds, the latter becoming more dominant upwards, and is capped by rippled sandstones showing bioturbation on the top surface. The flow depth is calculated as 6.3m. Palaeocurrents are directed to the east-northeast. The bioturbated top surface indicates abandonment and flooding.

The first obvious difference between the Tullig Sandstone at Pulleen and Trusklieve, separated by a distance of 19km, is the lower number of storeys at Pulleen, which has three rather than five. The thicknesses of Storeys 2 and 3 are comparable between the outcrops, though - 11.2m and 11.3m at Pulleen, and 10.5m and 10.7m at Trusklieve. The other marked difference between the two localities is in the facies distributions; at Trusklieve each storey typically shows a variety of facies (with the exception of Storey 5, which is entirely cross-bedded), whereas at Pulleen Storeys 2 and 3 are characterized almost entirely by massive sandstones and cross-bedded sandstones respectively. This apparent homogeneity of facies within each storey at Pulleen suggests that the outcrop exhibits only single architectural elements within each

storey, rather than several elements (as occurs at Trusklieve, for example, the channel-fill, cross-bar channel and bar form elements seen within Storey 3).

It is apparent from the flat-lying accretion surfaces within the Pulleen outcrop that no downstream or laterally accreting bar forms are present. No dipping bed surfaces (other than scour surfaces) are measured in the logged section, and the surfaces seen in the sea stack conform to the regional dip and would therefore be horizontal after structural restoration. The interpretation of Storeys 2 and 3 is that they each represent vertically accreting channel-fill elements; the facies in both stories are common channel-fill facies (Miall, 1977, 1996; Collinson and Thompson, 1982; Singh and Bhardwaj, 1991; Jo and Chough, 2001), as discussed in Sections 4.3.3.3 and 4.3.3.5. The very low amount of fine-grained facies preserved in the Pulleen outcrop indicates either that this section of the channel system was continually active, and not abandoned at any point, or that the erosion at the bases of the storeys was sufficient to remove any fine-grained abandonment facies that may have been deposited between storeys. However, the absence of fine-grained rip-up clasts within the third storey suggests that no fine-grained facies were present (draping Storey 2) that could have provided material for reworking into lag conglomerates.

The flow depth calculated for Storey 3 is, at 6.26m, just over half the thickness of the storey. This apparent discrepancy between channel size and flow depth can be explained by continuing aggradation of the channel, without avulsion; if the channel remained in the same position while continually aggrading, the thickness of the deposits of a single storey could exceed the flow depth. There are a number of factors that could cause a channel to remain in a fixed position: Structurally controlled subsidence can “pin” a channel in a particular place, as can confining topography, for example if the channel is flowing through a previously-incised valley (e.g. Bridge, 2003). Further implications of the relative thicknesses and depths of the storeys and flow depths will be discussed in Section 4.4.

Without evidence of lateral or downstream accretion it is not possible to draw conclusions about the geometry of the channel system represented by the Pulleen outcrop, although the absence of any fining-upward grainsize trends and general lack of fine-grained material favours a low-sinuosity, braided system (as discussed in

Section 4.3.1.6). The only place that waning flows are indicated is the upper metre of Storey 2, where rippled sandstones indicate a reduction in flow velocity compared with the cross beds beneath. The bioturbated upper surface of the Tullig Sandstone indicates the final abandonment of the channel system.

### **4.3.3 The Tullig Sandstone at Killard**

At Killard, the Tullig Sandstone crops out on both limbs of an ENE-WSW trending syncline (Fig. 3.1). The total thickness of the sandbody is exposed at this locality, and measures 18.65m on the southern limb and 21.38m on the northern limb, with the top of the sandbody being marked by a rootlet horizon and coaly organic-rich mudstone. Logs in App. A7 and A8 show the north and south limbs respectively, and Fig. 4.12 shows a summary log correlation panel, hung from the top of the sandbody. At Killard, as at Trusklieve, the sandbody has an erosional base, cutting into fine-grained delta front muds and silts similar to those underlying it at Trusklieve (compare Fig. 4.1a and b with 4.13a and b). The internal architecture of the sandbody at Killard is significantly different from Trusklieve; instead of several storeys eroding into each other, there are only two, and the second storey does not cut down more than a metre into the first. However, the facies seen at Killard are the same fluvial facies as those seen at Trusklieve, although coarse lag material is less prevalent, fewer fine-grained deposits are preserved, and planar, low-angle and trough cross bedding dominate.

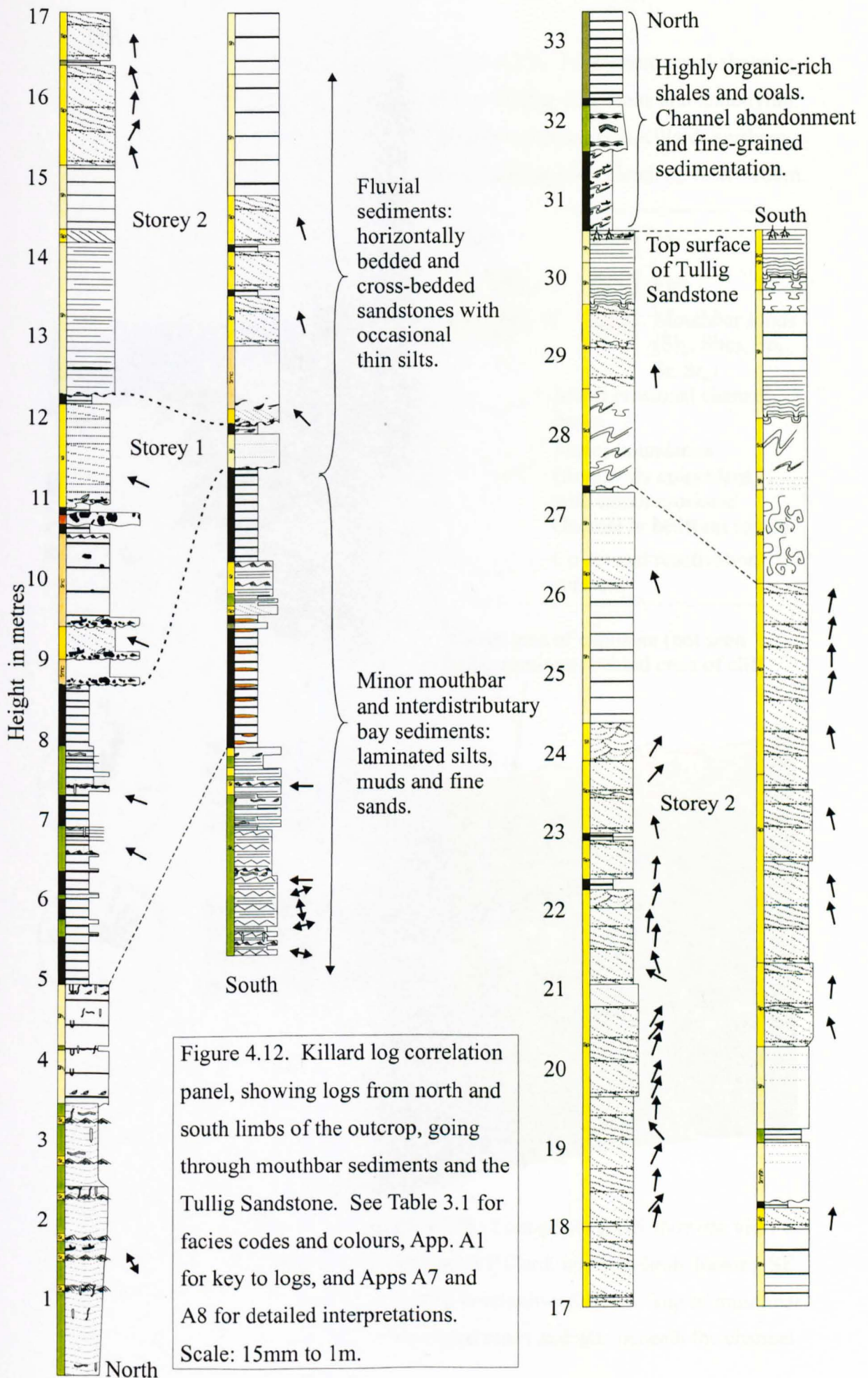
#### *4.3.3.1 Storey one: description and interpretation*

The first storey, as seen on the northern limb (see Fig. 3.1), averages 4.5m thick, and maintains a near-constant thickness ( $\pm 0.6\text{m}$ ) in the eastern half of the section (Fig. 4.13a and b). The western half of the storey is thinner, decreasing to 3.5m thick at the logged locality (see Fig. 4.12). Storey 1 is also thinner on the southern limb ( $\sim 0.5\text{m}$ ), where it is partly eroded by the downcutting second storey (Fig. 4.12). The base of Storey 1 (i.e. the sandbody base) is erosional but does not cut down strongly where it is exposed; it erodes parallel to bedding in the laminated silty mudstones beneath, with rare discrete erosional cuts with a maximum relief of only 0.1m. Relief on the base of the north limb totals less than 0.25m over a horizontal distance of more than 150m. The base of the first storey on the southern limb of the fold exhibits similarly low erosional relief. From the marker bed in the mud and siltstones below the channel (see log correlation in Fig. 4.12) it can be seen that there is no more than

0.25m difference in downcutting across the two limbs, which are about 500m apart. This low relief basal surface contrasts markedly with the Trusklieve outcrop, where obvious erosional "steps" cut down up to 1m over distances of less than 5m, and the total relief on the base of the sandbody is 2.5m. No erosional sole marks were found on the southern limb at Killard, and only two were seen on the north limb, directed towards the northeast.

The first storey on the north limb is dominated by facies Sh and Sl; the western half of the limb also shows facies Ccm, Sc, Shc and Flm. Several thin (~50mm) lag deposits and conglomeratic beds (facies Ccm, Smc, Shc and Sc) occur within the lowermost metre on both limbs, immediately above internal erosional surfaces (see logs in Fig. 4.13). Clasts are characteristically 30-100mm in length and vary between angular, but distorted, laminated mudstone rip-ups and rounded mud clasts. Organic material is prevalent, including woody coalified clasts up to 0.6m in length (Fig. 4.14). On the southern limb, clasts appear both at the base of beds (Shc and Sc facies) and occasionally as "floating" clasts in massive to faintly horizontally laminated sandstone beds (facies Smc, as discussed in Sections 3.3.2.1 and 3.3.2.2; see 6.6-7.0m in App. A7). Neither occurrence is laterally continuous; "floating" clasts are usually isolated, and conglomeratic lags grade into the fine clean sands of Sh, Sl or Sp facies over horizontal distances of 3-4m. These sandy facies form laterally continuous sets 0.1 to 0.6m thick with rare thin (<20mm) silty/muddy layers between sets.

The finer facies present within the sandbody occur mainly near the base of the first fluvial channel storey (between 10m and 13m in Fig. 4.12). In the outcrop on the northern limb, a thin (~0.3m) layer of laminated mudstone occurs at a height of 2m from the base of Storey 1. This bed is laterally continuous over a distance of over 20m, after which it thins and pinches out to drape a set of low-angle cross beds. For part of its length, the mudstone encloses a thin (0.1m), contorted, matrix-supported mudclast conglomerate (see App. A8 at 10.9m). The laminated mudstone bed represents a period of lower flow stage, allowing fine-grained deposition, prior to the resumption of sandstone deposition by higher-stage flow. The small thickness and limited lateral extent of the mudstone indicate that it is unlikely to represent a prolonged, widespread period of abandonment. The enclosed conglomerate is related genetically to the muds; its sandy, deformed matrix appears to have been injected into

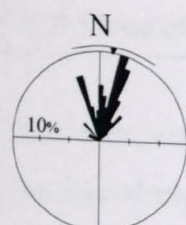
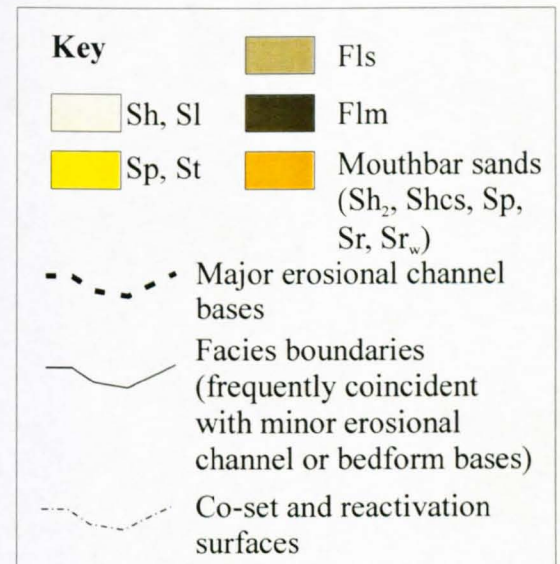


NE

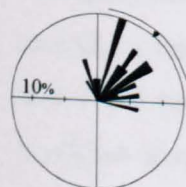
SW



Figure 4.13a. Four-photo panel showing view of Tullig Sandstone and underlying mouthbar sediments at Killard, northern limb, looking SSE. Depth of view ~100m.



**North limb foresets**  
 Vector mean = 009°  
 Sample number = 56  
 Average dip = 13°



**South limb foresets**  
 Vector mean = 041°  
 Sample number = 31  
 Average dip = 13°

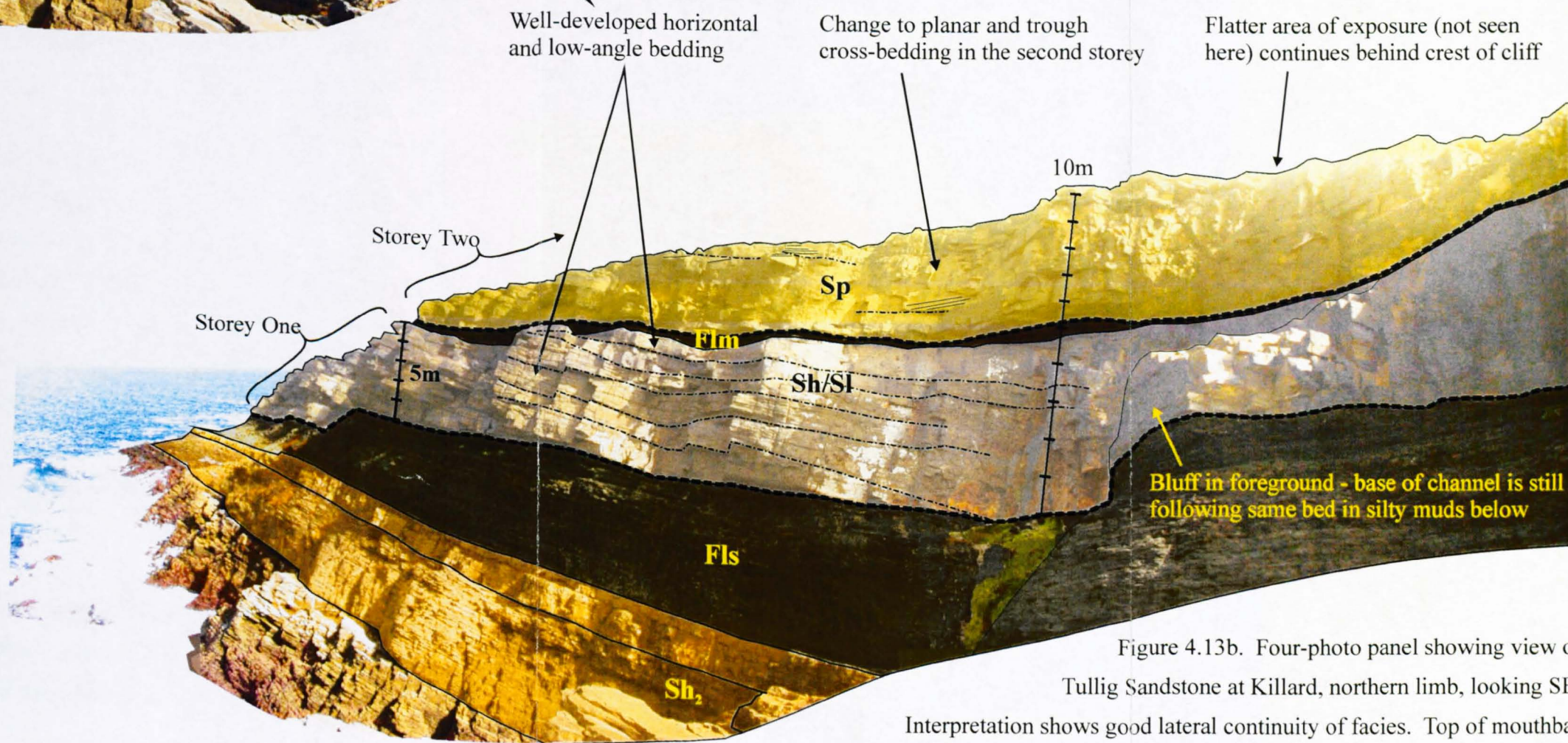


Figure 4.13b. Four-photo panel showing view of Tullig Sandstone at Killard, northern limb, looking SE. Interpretation shows good lateral continuity of facies. Top of mouthbar sands is seen in pale brown below the laminated muds and silts beneath the channel.

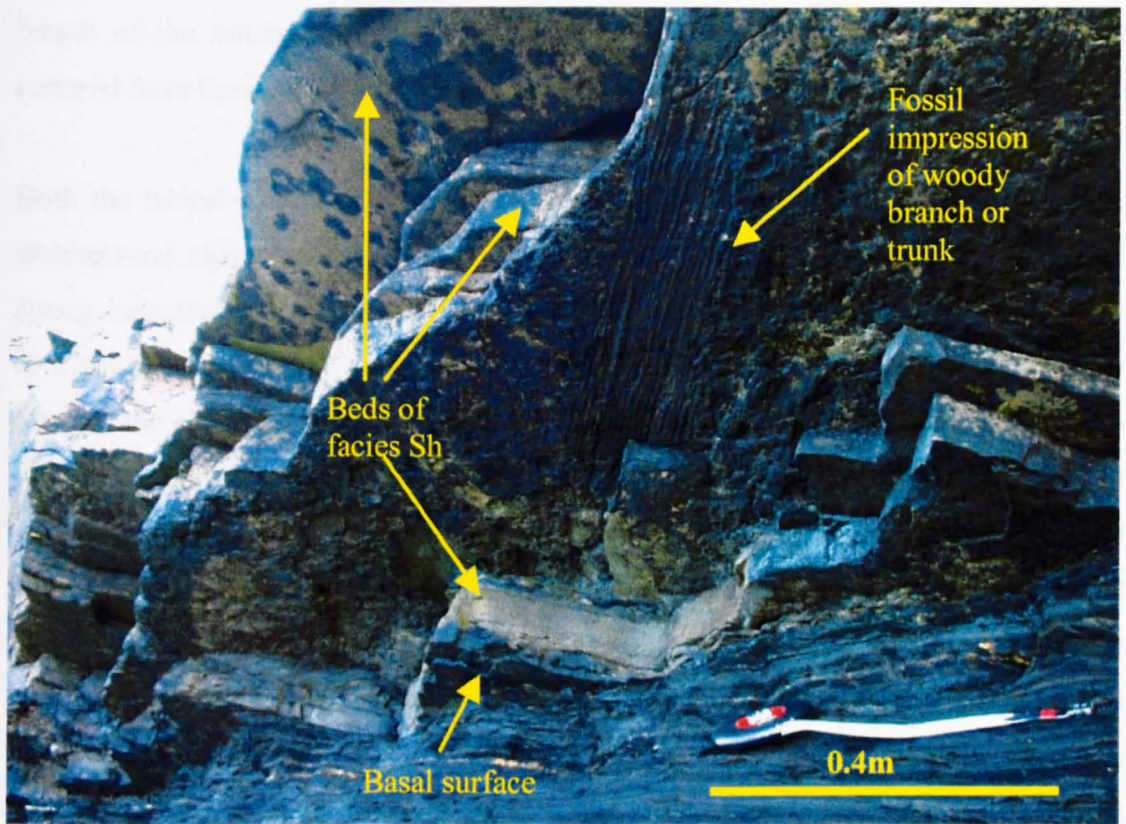


Figure 4.14. Base of the Tullig Sandstone on the north limb of the syncline at Killard. Note the flat base of the storey, parallel to the mudstone laminae, and the plant fossil in the base of the overhanging bed.

the muds, contorting and ripping them up in the process to produce a sand-supported jumble of angular, deformed mud clasts. The base of the sandstone bed immediately overlying the mudstone is loaded and erosive, suggesting that the conglomerate is actually a result of sand injection into the mudstone bed below. The sandstone bed above the mudstone incorporates a large amount of organic matter in the form of coalified plant material (at 10.9m on the north log in Fig. 4.12). This organic signature is seen at the base of several other erosively based beds close to the base of Storey 1 (at 8.8m, 9.0m and 9.4m in Fig. 4.12). The large size of some of the plant fragments (Fig. 4.14) suggests that these organic debris-rich beds are the result of high-stage flood flows.

Above the conglomeratic lags, clean well-bedded sandstones of facies S1 and Sh dominate Storey 1. Each co-set of low-angle cross bedding is traceable laterally for more than 50m, and in most cases coset-bounding surfaces can be followed for the

length of the outcrops on each limb (160m+). Set and coset boundaries, when restored from the regional dip, are around horizontal.

Both the lateral continuity and the horizontal bedding differ substantially from the architectural characteristics of the Trusklieve outcrop; at Killard there is no sign of strong erosional downcutting or lateral/downstream macroform accretion, as there is at Trusklieve. Restored foresets from low-angle cross sets show dips consistently towards the north and northeast on both limbs of the fold (see palaeocurrent arrows on Fig. 4.12, and rose diagrams in Fig. 4.13), and illustrate a north-northeasterly flow (a vector mean of  $020^{\circ}$ ). The orientation of the outcrop (WSW-ENE) is such that one would expect lateral and downstream accretionary macroforms to be visible in oblique and cross section respectively if present. The lack of any obvious dipping set or coset boundaries or lateral/downstream accretionary geometries indicates that the bedforms here comprise vertically accreting channel-fill deposits dominated by dunes, rather than larger bars or macroforms. The low-angle and planar bedding indicates current velocities close to, and at times within, the upper flow regime. Beds and cross bed sets of S1 and Sh average 0.58m thick. Because the cross beds dip at such a low angle (often  $3-5^{\circ}$ ) and are formed in a different way from steeper dune cross beds, it is not appropriate to use the set heights given above to calculate dune height or flow depth.

A silty mudstone bed appears close to the top of Storey 1 on the southern limb of the outcrop, directly below the transition to Storey 2 (6.5m in App. A7). The bed contains abundant plant debris, and may therefore correlate with the similarly plant-rich mudstones seen near the base of Storey 1 on the north limb (e.g. at 10.55m in App. A8), although potential correlations cannot be walked out in the field.

In the eastern, seaward, part of the northern limb (Fig. 4.13a and b), the upper surface of Storey 1 is a bedding surface draped by a thick, laterally continuous laminated silty mudstone (facies Flm/Fls – see Fig. 4.12, and at 12.25m in App. A8). This mudstone bed varies between 0.3 and 0.8m thick for most of its length, reaching a maximum of 0.92m thick, and extends for over 150m before being cut out by Storey 2 towards the west. Internally, the silty mudstone shows occasional soft sediment deformation in the form of distorted, but not comprehensively convoluted, bedding, and also exhibits infrequent lenticular bedding and silty sand lenses up to 0.15m thick and 2-3m in

lateral extent (facies Flh). The laterally extensive silty mudstone bed can be interpreted as representing a sudden abandonment of the channel, which silted up before being reoccupied by the channel represented by Storey 2.

The difference in thickness of Storey 1 across the fold hinge (~4.5m thick on the northern limb, ~0.5m on the southern limb) implies that Storey 2 cuts down at least three metres more into the first storey on the south limb than on the north limb (see Fig. 4.12). This increased erosion on the south limb accounts for the non-occurrence of the silty mudstone that drapes Storey 1 on the north limb. Overall, Storey 1 is interpreted as a channel-fill succession, due to the occurrence of numerous scours and conglomeratic lags, and the absence of lateral and downstream accretion surfaces.

#### *4.3.3.2 Storey two: description and interpretation*

The base of the second storey is marked by a strongly erosive contact that, on the southern limb, is immediately succeeded by a clastic lag with deformed mudstone rip-up clasts derived from the underlying fine-grained abandonment deposits, and organic debris (see Fig. 4.12, or App. A7 at 6.6m). Above this basal surface, on both limbs of the fold, the second storey comprises clean, well-bedded sandstones of facies Sh, Sp and St (Fig. 4.13a and b), with very occasional thin (maximum 50mm) laterally discontinuous laminated silts (facies Fls). The thin silts appear at the base of some cross bed sets (see Storey 2, Fig. 4.12) and extend for less than 30m (in most cases less than 10m) before pinching out. There are no floating clasts, conglomeratic lenses or lags, other than the basal lag, although transitions from Sp and St to Sh, and vice versa, indicate that flow strength does fluctuate slightly (cf. Jo and Chough (2001) in other fluvial sequences). The Sp to Sh transition can happen laterally and vertically within sets (see the 0.35m-thick bed in Fig. 3.8), as seen at Trusklieve (Section 4.3.1.4) and observed by Jo and Chough (2001) in the Kyongsang fluvial system.

The overall trend in Storey 2 is an upward transition from planar cross bedding (Sp) to trough cross bedding (St). Bed sets are of a similar thickness throughout, with set heights varying from 0.07m to 0.8m but mostly ranging from 0.25m to 0.4m (e.g. Fig. 3.8). Using Eq. 4.1 (Yalin, 1972) and Eq. 4.2 (LeClair and Bridge, 2001), the average cross bed height of 0.32m gives a mean dune height of 0.93m and a flow depth of 5.6m (range 4.2–6.9m). As in Storey 1, set and coset bounding surfaces do not show

downstream or lateral accretion geometries, but are laterally continuous over tens of metres to over 100m. This lateral continuity of beds and sets decreases slightly towards the top of Storey 2 as trough cross bedding starts to dominate, and individual cross sets scour into each other (Fig. 3.9). The restored palaeocurrents throughout Storey 2 show horizontal set boundaries and foresets that dip to the NNW to NE, very similar to the first storey (see Fig. 4.14).

Within the uppermost 3.5m of Storey 2 on both limbs, a bed of intensely deformed sandstone occurs, 1-2m thick (see Figs 3.12 and 4.12, and App. A7 and A8 for more detail). The base of this bed (seen at 27.2m in A8) is erosive in nature and also displays load structures in places, with pillows and balls sinking into the bed below. The highly deformed bed exhibits internal load structures, convolute bedding, patches appearing structureless and massive, and also discrete areas or layers that still retain traces of original undeformed bedding (Fig. 3.12). The internal structure becomes more coherent within the upper 0.2-0.5m of the bed on the northern limb, where planar cross bedding is seen (at 28.45-28.95m in A8). The top surface is loaded by the less-deformed bed above, which shows slightly distorted horizontal lamination (Sh) on the south limb of the outcrop and planar cross bedding (Sp) on the north limb (see Apps A7 and A8 respectively). The remaining 2-3m from the top of the intensely deformed horizon to the top of the sandbody show beds with loaded bases, which exhibit occasional internal loaded layers with up to 0.4m of relief (in the form of load and flame structures) but no comprehensive obliteration of bedding. Both the intensely deformed bed and those above it with loaded bases are laterally extensive, continuing across both limbs for the whole extent of the outcrop (150m along strike and ~450m from one limb to the other).

The interpretation of the deformed beds is that they were originally sets of facies Sh, Sp and/or St that were liquefied shortly after deposition, whilst still uncompacted and water-saturated. The thickness of the less-deformed beds is very similar to the thicknesses of undeformed beds. It is probable that the intensely deformed bed was more water-saturated than those above it, or was subjected to a greater load, and was therefore more susceptible to liquefaction and deformation. The deformation of the upper three or four beds of Storey 2 is evidence of a process other than simple fluvial deposition. While it is possible that the liquefaction and deformation were caused by

a depositional process (for example, by very rapid sedimentation leading to loading and instability, or by the hydraulic head developed between bar top and channel floor), the very wide area over which the deformation occurs (the entire outcrop, ~160m by 450m) makes an alternative explanation more likely. Post-depositional liquefaction, caused by localised seismic activity (Allen and Banks, 1972) probably related to faulting in the underlying unstable deltaic sequence (Pulham, 1987, see also Section 2.2.4) is the preferred explanation.

The upper surface of Storey 2 forms the top of the Tullig Sandstone on both limbs of the fold. The surface is gently undulating due to the presence of numerous *in situ* fossilised roots (*Stigmaria*) more than a metre long and other pieces of fossilised plant debris up to 0.5m in length (e.g. Fig. 3.33). In places, poorly defined impressions have been left from much larger plants; on the top of the south limb, an elongate concavity around 0.8m wide stretches for 5m. This depression shows traces of carbonaceous material on its inner surface, and appears to be the imprint left by a (now removed) fallen tree. Above this rooted surface the succession changes dramatically. The top 2.8m of the log in App. A8 (the south log in Fig. 4.12) starts with a metre of highly organic-rich carbonaceous laminated mudstones containing rootlets. This bed shows internal deformation in the form of small-scale folding and faulting, and also exhibits numerous thin (<50mm) layers and lenses of coal. The carbonaceous mudstone is followed by an erosively based silty fine sand that fines up to muddy siltstone. This silty sand erodes into the mudstone with a maximum relief of less than 30mm; it includes discrete patches of convolute lamination and, near the top, where the background sediment has fined to muddy siltstone, rare sandy silt lenses with ripple cross lamination. A 50mm thick mudstone layer separates the fining-up silty sand from a 0.9m thick bed of laminated siltstone. The end of fluvial sandstone deposition, the growth of vegetation on the abandonment surface, and the formation of humic organic-rich carbonaceous and coaly deposits testify to the abandonment of the second channel storey and the change of the environment from fluvial channel to swamp-like floodplain.

#### 4.3.3.3 Summary and discussion of the Killard outcrop

- 1) Storey 1 exhibits well-developed horizontal and low-angle cross bedding with horizontal set and co-set surfaces indicating channel-fill by vertical accretion

rather than bar migration. Palaeocurrents are to the north-northeast. Lateral variation within the storey shows the well-bedded facies to be occasionally interrupted by internal erosion surfaces and conglomeratic lags, rich in plant material and deformed mudstone rip-up clasts; these scours and coarser facies (Ccm, Sc) indicate flood-related erosion and deposition, and may signify individual channel bases within the storey. Storey 1 shows less than 0.25m of erosion on its basal surface, and reaches a maximum thickness of 5.1m before being abandoned and draped by a laterally persistent laminated silty mudstone averaging 0.45m thick.

- 2) Storey 2 erodes into the first storey with relief of up to 4m. Internally Storey 2 is similar to the first, with vertical accretion of facies Sp, Sh and St. The main differences are the lack of conglomeratic facies (Ccm, Sc), and the reduced amount of fine-grained facies (Flm, Fls) in Storey 2 compared with the first storey. Flow depth is calculated to be around 5.6m. Palaeocurrents are again to the north-northeast, and Storey 2 is thicker than the first, reaching a maximum of 18.2m on the north limb. The top surface of Storey 2 is an abandonment surface, with *in situ* roots and rootlets, and organic rich coaly muds above.

Based on the observations and interpretations in Sections 4.3.3.1 and 4.3.3.2 above, the outcrop of the Tullig Sandstone at Killard is interpreted as a section through a fluvial depositional system flowing to the northeast. The differences between Killard, Pulleen and Trusklieve include the decrease in number of storeys (two rather than three or five), and the reduced erosional relief at the base of the first storey (0.25m compared with 2.5m at Trusklieve). It is difficult to make any convincing correlation between the storeys at the three localities, although the heterogeneity of the first storey at Trusklieve and Killard indicates that these outcrops could show different sections of the same storey. The second storey at Killard resembles the fifth storey at Trusklieve, in that both are dominated by planar and trough cross bedding, although there is no way of physically confirming them as the same storey in the field. Storey 2 at Killard is also very similar in appearance and facies to Storey 3 at Pulleen, showing the same dominance of cross bedding and a similar upward transition from planar to trough cross bedding. Flow depths at each locality are of the same order of magnitude, 5.6m for Killard, 6.3m for Pulleen, and 3.5-7.7m for Trusklieve, suggesting that the scale of the channels did not vary significantly along palaeoflow

from one locality to the next (an overall distance of 20km). As at Pulleen, the flow depths calculated for Killard are significantly less than the storey thickness, which again could be related to continuing aggradation of the channel in the same position.

Another way in which Killard and Trusklieve differ is that the architecture of the Killard storeys is much simpler than that at Trusklieve, and more like that at Pulleen. The lack of dipping accretion surfaces in the Killard outcrop (which covers an area of around 160m by 450m) is evidence that neither downstream nor laterally accreting bar forms are represented in the outcrop, unlike at Trusklieve, where both of these types of macroform occur (Section 4.3.1). At Killard, only vertical accretion of facies Sp, Sl, Sh and St is seen, suggesting channel fill by a combination of migrating straight-crested dunes (facies Sp), and sinuous-crested dunes (facies St), with upper-stage plane beds (facies Sh) forming as bed shear stress and sediment transport rate increased in fast but still sub-critical flows (Bridge, 2003). There is no upward fining of grainsize or other indication of waning flow, which suggests that the channels were not cut, abandoned, and then filled, but that channel deposits accumulated during the active life of the channel. The high proportion of channel-fill deposits (seen in both storeys) relative to lateral accretion deposits (not seen in either storey) is indicative of braiding, since the ratio is known to increase with increasing braiding parameter (Bridge, 1985). There is no palaeocurrent evidence to support a meandering channel style in this outcrop, with all the current indicators pointing towards the north-northeast, in agreement with those from Trusklieve and similar to the ENE-directed palaeoflow recorded for Pulleen. More detailed quantitative observations regarding architectures will be presented and discussed in Chapter 5.

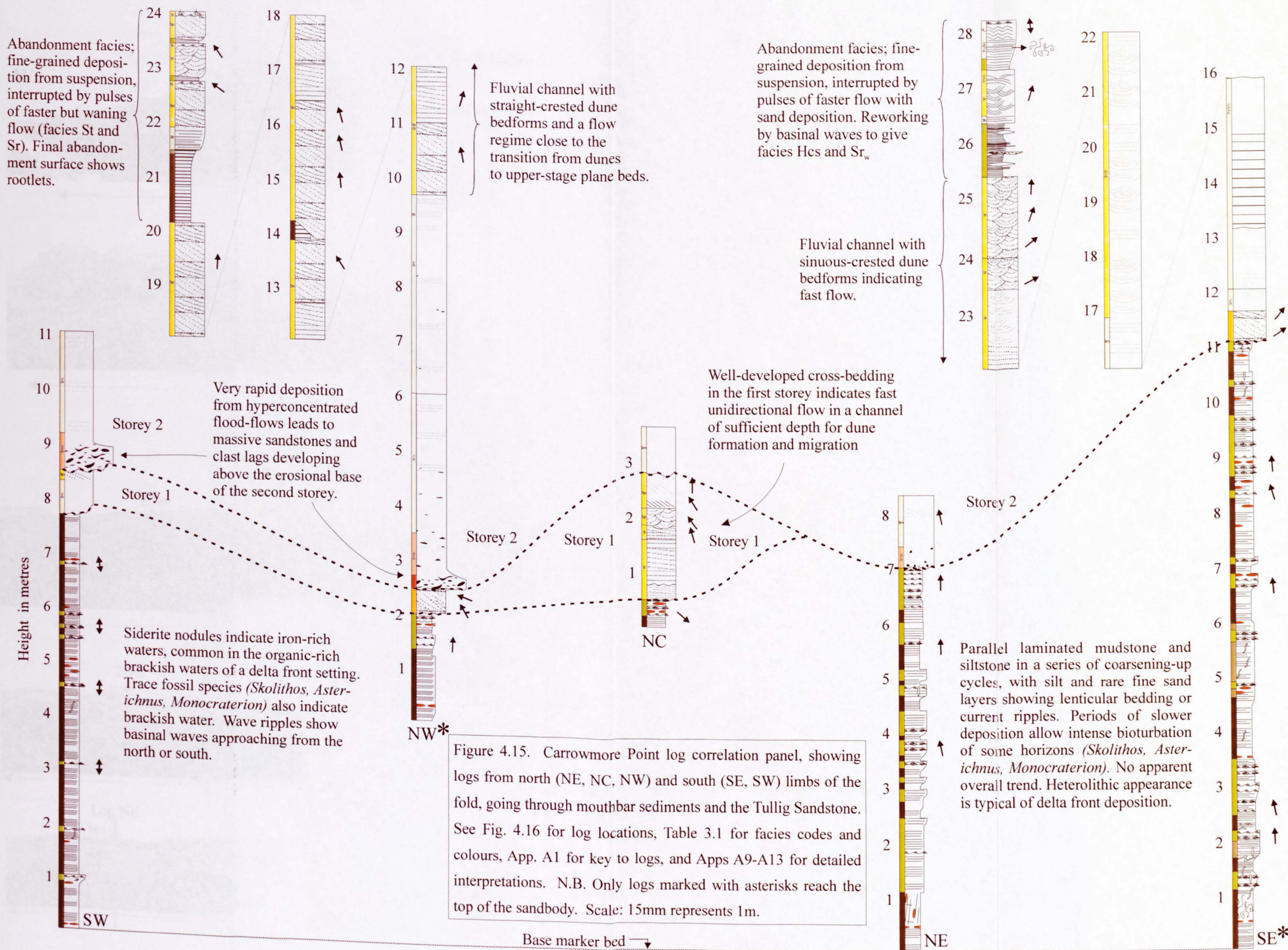
Another difference between Killard and Trusklieve is the difference in facies. While both localities exhibit the fluvial facies association described in Section 3.4.3, the Tullig Sandstone at Killard is less heterolithic than at Trusklieve, being dominated by well-bedded sandstone facies and having a lower percentage of fine-grained deposits (see Chapter 5 for quantification). At Killard, as at Trusklieve and Pulleen, the typical fining-up meandering profile (Allen, 1970b) is absent. Coarse-grained facies (Ccm, Shc, Smc, Sc) are also less prevalent at Killard than at Trusklieve, with 5.12% calculated from the log, compared with 10.73% at Trusklieve (see Chapter 5).

Vertical trends seen within the Tullig Sandstone at Killard are limited to increasing facies homogeneity with height, as at Trusklieve (quantified in Chapter 5).

From the abundance of plant material and the *in situ* roots seen in the uppermost bed of Storey 2, it is apparent that the top surface of this storey records the abandonment and subsequent colonisation by plants of this part of the fluvial system. On this occasion the abandonment was permanent; no re-occupation of the channel system occurred, and after the interval of coaly and organic-rich mudstones indicative of swamp-type freshwater conditions, a succession of shallow to deeper water mouthbar sediments are succeeded by a goniatite bearing marine band that heralds the start of the next cyclothem (e.g. Pulham, 1987; see also Section 2.2.5.1).

#### 4.3.4 The Tullig Sandstone at Carrowmore Point

The exposure of the Tullig Sandstone at Carrowmore Point is across Doughmore Bay from Killard, to the northeast, and crops out on the limbs of an open ENE-WSW trending anticline (Fig. 3.1). The total thickness of the sandbody was measured on both the northern and southern limbs of the anticline, being 22m thick on the northern limb and 21.64m on the southern limb. The sandbody is erosively based, cutting down into sediments interpreted as delta front facies based on the numerous coarsening-up cycles and the lack of any *in situ* plant fossils (see the log correlation panel in Fig. 4.15). The lowermost few metres of the sandbody thickness are exposed in a 1-4m high cliff section that exceeds 150m in lateral extent on the northern limb. A photomontage was constructed for this cliff (Fig. 4.16), and a second montage was made for the top of the Tullig Sandstone on the south limb. Other parts of the outcrop (the south limb, and the western (seaward) end of the north limb) are flatter exposures in which the dipping beds cannot be seen from the distances required to take photos. These unevenly eroded flatter parts of the outcrop are difficult to take architectural measurements from, but it is nonetheless clear that the internal architecture of the sandbody at Carrowmore is similar to the Killard outcrop. The Tullig Sandstone at Carrowmore can be subdivided into two storeys separated by a strongly erosive contact. The facies association displayed conforms to the fluvial/alluvial facies association detailed in Section 3.4.3, although within the topmost three to four metres, the association changes to include wave-reworked deposits.





#### *4.3.4.1 Storey one: description and interpretation*

The thickness of the first storey is greatest at the western (seaward) end of the northern limb of the outcrop, where the storey reaches 2.5m before being cut out by Storey 2. To the east, within 50m of the eastern limit of the outcrop, the first storey is completely cut out by the second. The basal surface of the first storey is strongly erosive, showing a total relief of 4m between the north and south limbs of the anticline. A bed in the silts below the sandbody, chosen because of its recognisable proud-weathering appearance, was traced across the outcrop to act as a marker bed. The base of the sandbody is 4m closer to this marker bed at the southeast end of the outcrop than at the northeast end (Fig. 4.15). In terms of discrete areas of erosion, downcuts or steps of between 0.08 and 0.25m are seen over short horizontal distances (e.g. 0.1-2.0m) on the north limb. The orientation of the “hinges” of these steps varies between 108°-288° and 143°-323°. On the south limb a deeper discrete scour occurs, which cuts down 1.41m and back up 1.19m over a total horizontal distance of only 3.5m. The orientation of the scour is not possible to determine because it is only exposed in 2-D. A similar problem prevents useful data being obtained from flutes or grooves; only a few were found in 2-D profile, and the poor exposure of the basal surface made orientations difficult to measure with any certainty. One measured groove was oriented 008°-188°, suggesting flow to the north (or south).

Storey 1 consists mainly of facies Sp and Sl, with low and variable amounts by area of Sh, Ccm, Sm, and Fls (see Fig. 4.16). The internal sandbody architecture is variable through the first storey; the majority of beds have sharp to erosive contacts that cut into preceding beds and give lens-shape geometries and low lateral continuity (this low continuity is quantified in Chapter 5). When corrected for the regional dip, most beds are flat, but some bedding surfaces (labelled in Fig. 4.16) dip down gently towards the northeast (e.g. 06°/084°, 08°/042°), tapering off against the basal erosion surface. These dipping surfaces could be downstream accretion surfaces, because they dip in the same direction as the northeast-dipping cross bed foresets (see rose diagram in Fig. 4.16). However, the wide spacing and low angle of the surfaces, together with the limited vertical exposure due to the low thickness of the first storey, makes it difficult to state unequivocally that the dipping surfaces define a macroform. The limited thickness also makes it impossible to see any vertical trends in either facies or geometries within the first storey. The only change with height is the loss of

conglomeratic facies Ccm, two beds of which are found above the basal erosion surface; none are found higher in the first storey.

The thicknesses of cross bed sets in the first storey provide the only indication of channel depth. Sets of cross bedding vary in thickness from 0.15m to 0.5m, with an average thickness of 0.29m. Using Equations 4.1 and 4.2 (Yalin, 1972; LeClair and Bridge, 2001) this thickness gives a dune height of 0.84m and a mean flow depth of 5.0m (range 3.8–6.3m). This flow depth is within the same range as flow depths for the channels at Trusklieve, Pulleen and Killard.

#### *4.3.4.2 Storey two: description and interpretation*

The base of the second storey is strongly erosional and irregular, cutting down into the first storey with relief of up to 3m. Immediately above the erosion surface is a thick (1-7m) unit of massive sandstone (facies Sm), frequently exhibiting randomly distributed rounded and angular clasts of mudstone and siltstone (facies Smc), and occasional lenses of intraformational mudclast conglomerate (facies Ccm) at its base. The massive sandstone shows very poorly developed bedding that frequently disappears along strike and is impossible to follow for lateral distances over 10-15m. Dividing the unit into beds has therefore not been attempted for most parts of the photomontage in Fig. 4.16, although in individual logs some bedding surfaces have been recorded (see 11.5-13m in App. A9, and 2.5-9.0m in App. A11). Occasionally, intervals of parallel lamination appear within the massive sandstone, dying out over a few metres laterally (e.g. 11.55-13.10m in App. A9). These laminated intervals are occasionally associated with thin (<50mm) layers of angular to sub-rounded rip-up clasts; the clasts are less than 60mm in length and lie with their alpha and beta axes parallel to bedding. It is not possible to tell the flow direction in these faintly laminated sandstones in order to work out the clast orientation relative to flow.

The conglomeratic lenses immediately above the basal erosion surface, like those seen within the Tullig Sandstone at other localities, comprise deformed rip-up clasts of laminated siltstone and mudstone. At Carrowmore the clasts have been stretched and elongated parallel to flow to such an extent that the conglomerates frequently take on a “fluid” appearance, looking more like mud and silt “flowing” through a sandy

matrix than discrete flow aligned clasts in a sand matrix. This suggests that the clasts were ripped up and deformed when still very soft.

Trends within the second storey include an upward increase in bedding definition, and a decrease in clast numbers, within the massive sandstone facies on both sides of the fold. Another important change is seen in the second storey, at a height above the base of the sandbody of between 6.73m and 7.65m on the northern limb, and of 14.49m on the southern limb. At this point there is a sharp transition from massive or faintly laminated poorly bedded sandstone (Sm) to very well-bedded cross-bedded sandstone. On the northern limb, planar and low-angle cross bedding (Sl, Sp) occur above the transition, while on the southern limb planar and trough cross bedding dominate (see logs SE and NW in Fig. 4.15). The transition from massive to cross-bedded sandstone is not accompanied by a marked erosion surface or any coarse lag or fine-grained deposition, and this level is not therefore considered to be the start of a third storey but rather simply a facies change within Storey 2. However it is possible that a third storey, showing very little erosional relief and no conglomeratic lag, begins at this level.

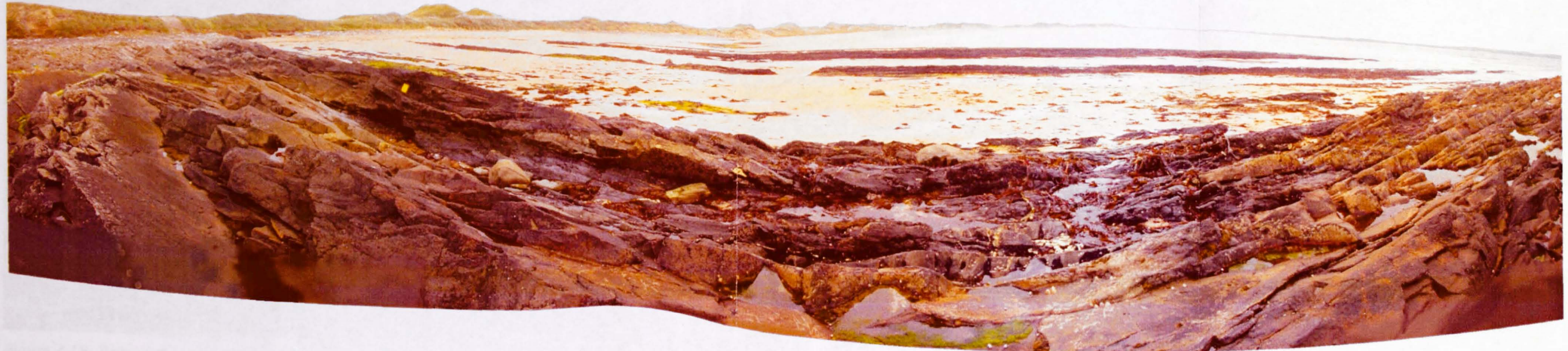
The cross beds within the middle part of Storey 2 are well-developed and laterally continuous, with set bounding surfaces easily traceable for up to 80m on the north limb; the scoop-shaped trough cross strata on the southern limb makes individual beds more lenticular and therefore harder to follow, but set boundaries are still traceable for tens of metres laterally (see Fig. 4.17 for a montage of the top of the southern limb, and Fig. 4.18 for detail of the northern limb cross beds). There is limited evidence of downcutting internal erosion surfaces within this homogeneous middle section of the second storey on the northern limb, with a rare example being an erosively based lenticular sandstone bed (Fig. 4.18). Set-bounding surfaces throughout this cross-bedded interval, when restored, are horizontal. No evidence of dipping accretion surfaces or bar forms is seen, suggesting that the beds are part of a vertical channel-fill succession rather than part of a macroform such as a mid-channel or bank-attached bar. Trough cross bedding, commonly the main component of channel-fill sequences rather than bars (e.g. Cant and Walker, 1978; Collinson, 1986; Galloway and Hobday, 1996), dominates the southern part of the second storey and helps to confirm the storey as an aggradational channel-fill succession.

Figure 4.17. a) Photomontage of the upper part of the south limb exposure at Carrowmore Point.  
 b) As above, with facies interpretations, faults and bedding added.

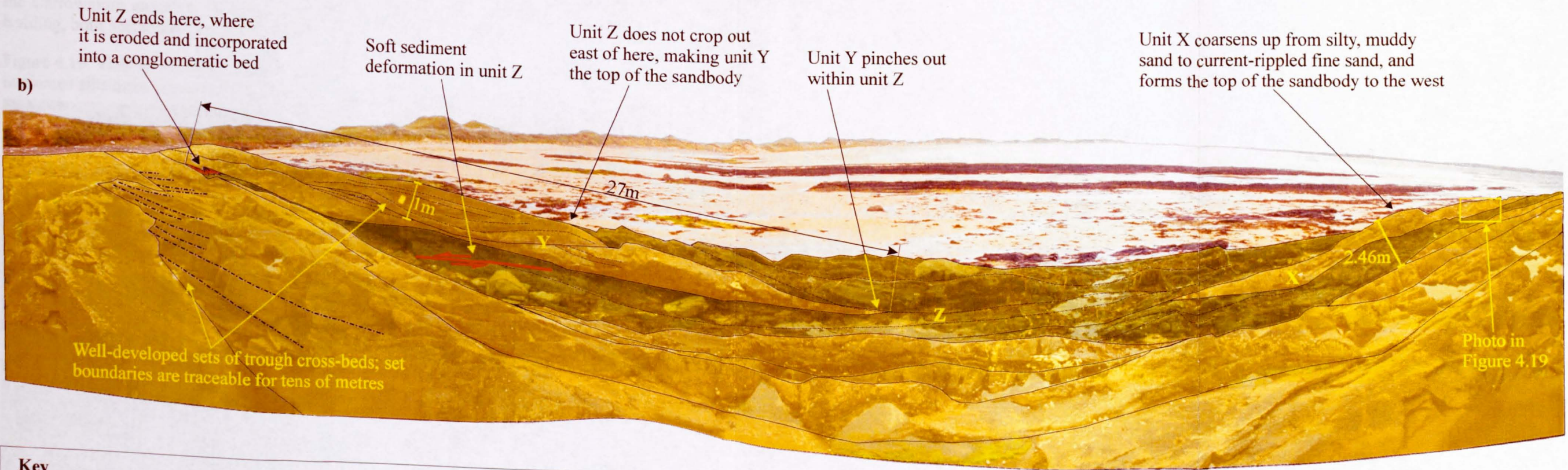
E

W

a)



b)



Key			
<span style="display:inline-block; width:15px; height:15px; background-color:yellow; border:1px solid black;"></span>	Sp, St		Major erosional channel bases
<span style="display:inline-block; width:15px; height:15px; background-color:olive; border:1px solid black;"></span>	Flh		Bedding planes and erosional contacts, frequently coincident with facies boundaries
			Syn-sedimentary fault
			Cross-bed and reactivation surfaces

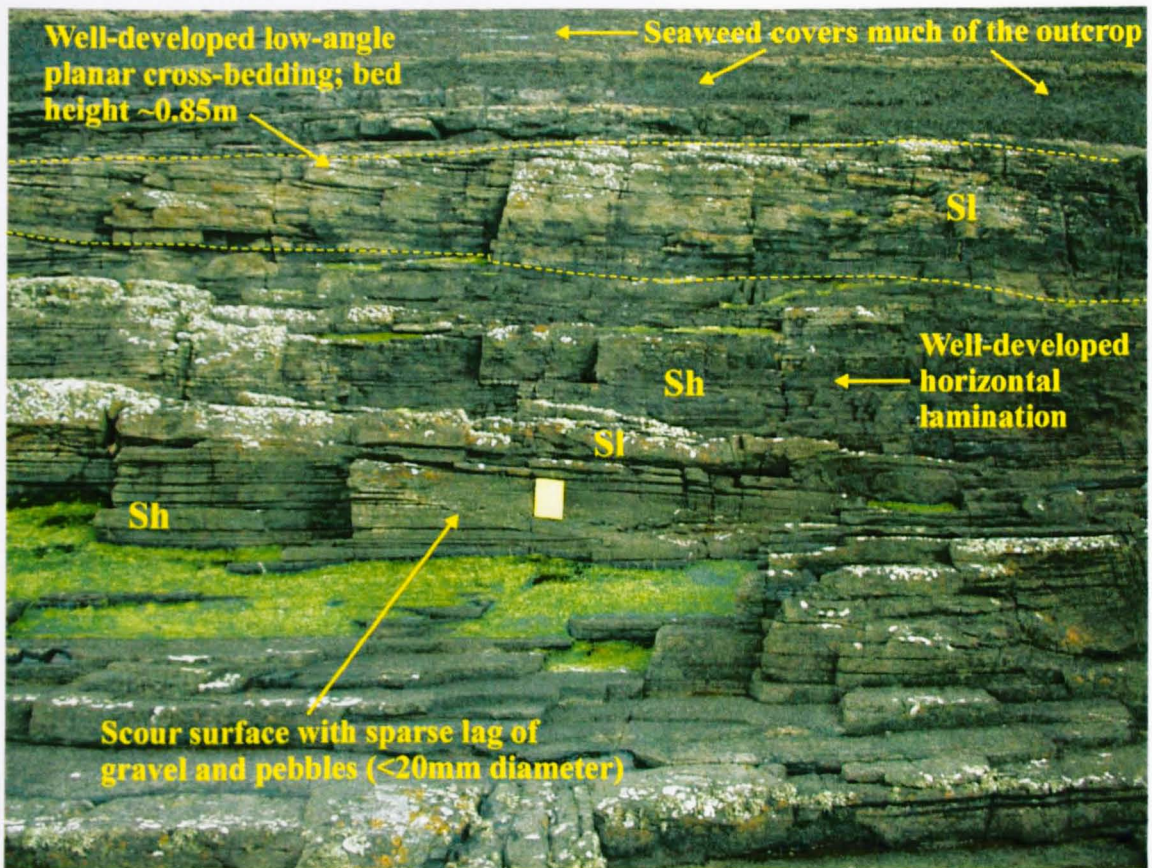
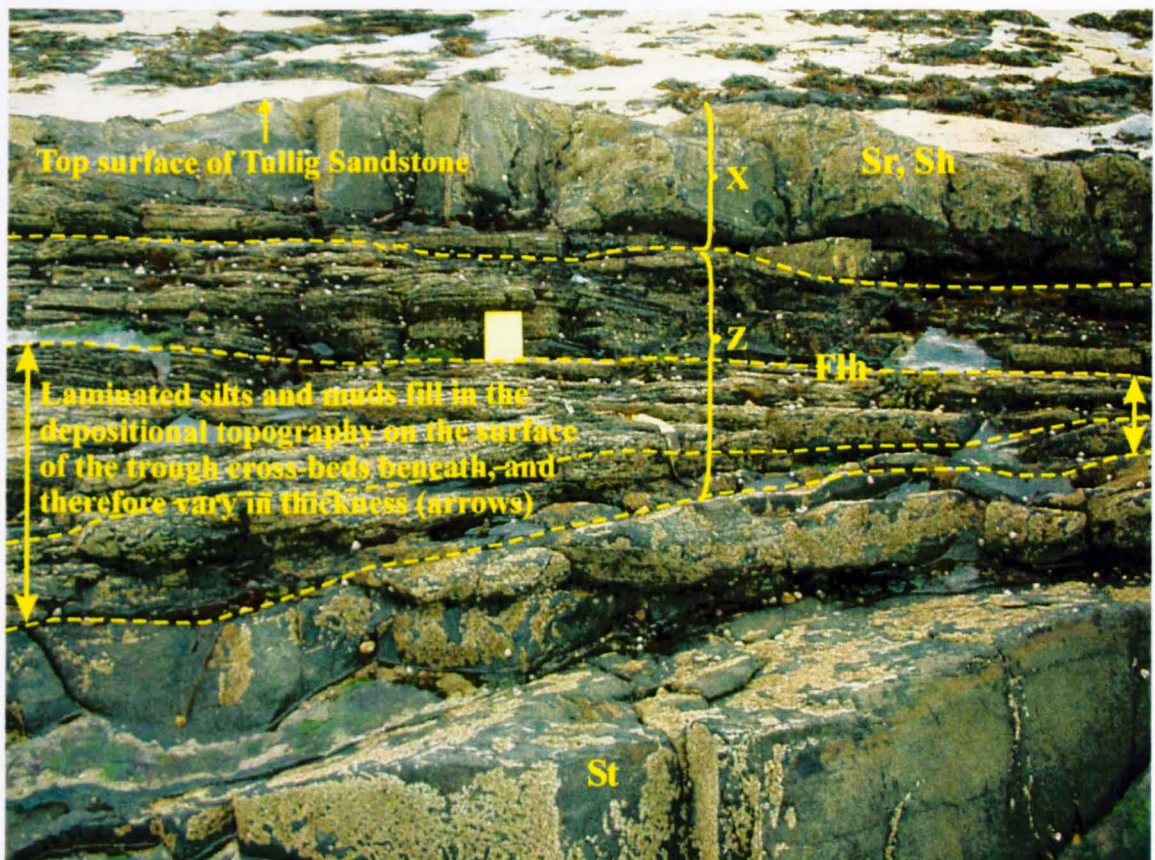


Figure 4.18. Part of the second storey of the Tullig Sandstone, on the northern limb of the Carrowmore anticline. Note the lateral continuity of the beds and well-developed bedding, both horizontal (Sh) and cross-bedding (SI and Sp). The notebook is 0.2m tall.

Figure 4.19. View of Storey 2 on the southern limb of the Carrowmore anticline, showing laminated siltstones between sandstone beds within 3m of the top surface of the sandbody.



Cross bed heights in the second storey are between 0.15 and 0.60m. Although there are no recognisable macroforms or lateral accretion surfaces to aid calculation of channel depth, Equations 4.1 and 4.2 (Yalin, 1972; LeClair and Bridge, 2001) can be used to reconstruct channel depth from cross bed heights. The result, taking an average bed thickness of 0.40m, is a flow depth of 7.0m (range 5.3–8.6m). This figure is similar to the 5.0m calculated for Storey 1, and is also close to the values calculated for Trusklieve, Pulleen and Killard. As at the latter two localities, the flow depth for Storey 2 at Carrowmore is considerably less than the storey thickness, which could be achieved if the channel was aggrading in a fixed position during subsidence (see Section 4.4.1).

The upper part of Storey 2 is different from the lower and middle sections described above. For the first time within the sandbody at Carrowmore, significant amounts of finer material are present. On the northern limb, the succession is interrupted by two lenses of laminated muddy siltstone (Fls), neither of which is laterally continuous. The western lens continues laterally for 4m, reaching a maximum thickness of 0.85m (see App. A11 at 13.8 to 14.2m); the lens to the east is traceable for 7m and has a maximum thickness of 0.67m. These two fine-grained beds are not at the same level within the sandbody. Each lens represents a brief period of low flow, in at least part of the channel system, during which suspended load was deposited within the channel, being partially eroded at a later time.

Within the top 4m of the sandbody on the northern limb there is a return to fine-grained facies, with the occurrence of a silty mud bed between 1.3 and 1.55m thick, which is laterally continuous for the extent of the outcrop (~80m). This bed coarsens up from silty mud to fine sandstone, and is succeeded by fine-to-medium planar cross-bedded sandstone, which has a thickness of between 1.3 and 2.57m (see App. A11, between 20.1 and 23.9m). This final sandy interval is interrupted by thin beds of silty sand (<20mm thick), and is characterized by thin layers of current ripples within the sandy intervals, showing current directions to the north and northeast.

The second storey on the southern limb shows no fine-grained facies until the top 4m, where a bed of thinly laminated muddy silt with silty sand intervals occurs (labelled Z in Figs 4.17 and 4.19; see 25.5-26.45m in App. A9). The bed is between 0 and 2.86m

thick and is probably equivalent to the laterally continuous silty mud bed near the top of the northern limb, although it is not possible to trace the bed across the fold hinge because the outcrop is eroded out in the hinge region. However, while the lithology and thickness of Unit Z remain similar across the two limbs, its internal geometry is different between the southern and northern outcrops. Within Unit Z on the south limb, the laminae are often convoluted, and small faults and associated minor folds occur (Fig. 4.20a, b). This soft-sediment deformation suggests some water escape, slumping or sliding within the bed, probably resulting from loading or bank collapse.

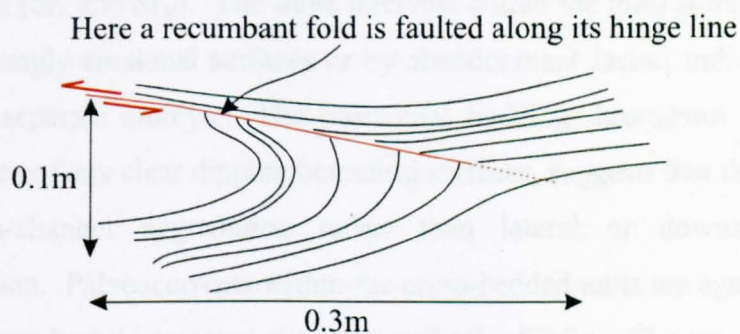
Unit Z is eroded out to the east and replaced by a lens of intraformational conglomerate (Fig. 4.17) but continues for the whole length of the outcrop to the west. A westward-thickening lens, 1.5 to 3m thick, of coarsening-up interbedded mud, silt, and sand occurs within Unit Z (labelled X in Figs 4.17 and 4.19), and marks the top of the Tullig Sandstone in the western half of the southern outcrop. To the east, where Unit X pinches out, a second sandy lens occurs at a slightly higher stratigraphic level within Unit Z (see unit labelled Y in Fig. 4.17). This sandy lens Y shows well-developed trough cross beds and, at its eastern end, some liquefaction and loading features within its top two metres, similar to those seen at the top of the Tullig Sandstone at Killard (Fig. 3.12). Moving west, Unit Y develops a coarsening-up bed within its upper metre, showing climbing ripples and well-developed wave ripples at the top before thinning towards the centre of the outcrop and pinching out. The top surface of Unit Y marks the top of the sandbody in the eastern half of the southern outcrop. Above Units X and Y, Unit Z continues in the form of a thick laminated muddy silt that marks the final abandonment of the channel system (Fig. 4.17).

The interfingering geometries of Units X, Y and Z suggest contemporaneous deposition of sandy and silty/muddy facies within a small area (the outcrop area of the south limb is no more than 50m by 150m). The climbing ripples (facies Sr<sub>c</sub>) within the upper bed of Unit Y (28.0-28.3m, App. A9) indicate very rapid deposition from decelerating, sediment-laden unidirectional currents. The interpretation of the uppermost 3-4m of the Tullig Sandstone is that it represents the abandonment of the fluvial channel system, the development of fine-grained channel-fill and overbank deposits, and the deposition of the last sandy beds from overbank flows of limited areal extent (facies Sr<sub>c</sub>). The bi-directional ripple lamination at the top of the

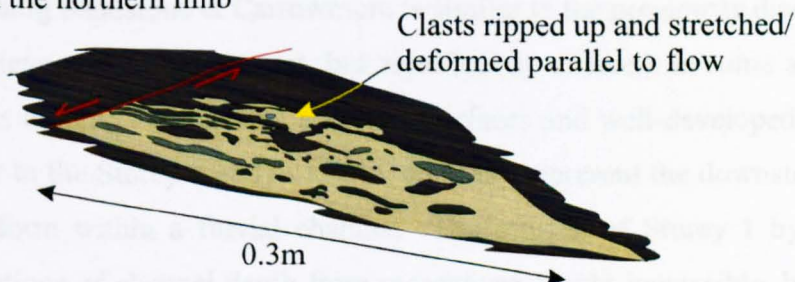
sandbody (28.0-m, App. A9) indicates wave reworking of the last fluvial and alluvial deposits. This wave reworking shows either that the abandoned channel was a quiet body of standing water affected by waves, or that it was exposed to basinal waves, due to subsidence of the area or a rise in relative sea-level.

Figure 4.20. Sketches showing details of internal structure of unit Z, top of southern limb, Carrowmore Point.

a) Significant internal deformation within fine layer, e.g. recumbent folding of mud/siltstone laminae, and small-displacement faults.



b) Sandy patch within laminated fine-grained bed, exhibiting mud/silt clasts and layers. This is similar to the intraformational conglomeratic facies seen above the base of the second storey on the northern limb



#### 4.3.4.3 Summary and discussion of the Carrowmore Point outcrop

A storey-by-storey summary is given below.

- 1) Storey 1 exhibits well-developed low-angle and planar cross bedding with northeast-dipping internal erosion surfaces and co-set surfaces, indicating probable macroform migration to the northeast. Palaeocurrents from cross beds are also directed northeast, suggesting downstream rather than lateral accretion. Rare conglomeratic lags of deformed mudstone rip-up clasts are seen. Basal erosional relief totals 1.41m, with up to 4m of erosion implied by correlation

between the two limbs of the outcrop. The storey reaches a maximum thickness of 2.5m before being eroded out by the downcutting base of the second storey. Flow depths of around 5.0m are calculated from the cross bed thicknesses.

- 2) Storey 2 reaches a maximum thickness of 21.65m, and erodes into Storey 1 with relief of up to 3m, cutting it out completely to the east. Storey 2 has three main intervals showing different facies: i) massive sandstone with intraformational conglomerates; ii) well-bedded sandstone (Sh, Sl, Sp and St) with horizontal bedding surfaces; iii) finer-grained facies (Fls, Flh) interbedded with trough and planar cross-bedded sandstones (St, Sp), climbing unidirectional ripples and wave ripples (Sr<sub>c</sub> and Sr<sub>w</sub>). The three intervals within the third storey are not separated by strongly erosional surfaces or by abandonment facies, indicating that it is not three separate storeys. The horizontal bedding throughout Storey 2, and the absence of any clear dipping bounding surfaces, suggests that the storey represents within-channel aggradation rather than lateral or downstream macroform accretion. Palaeocurrents within the cross-bedded units are again to the northeast, and cross bed thicknesses give a flow depth of 7.0m. The top surface of Storey 2 on the northern limb is an abandonment surface, with *in situ* rootlets.

The Tullig Sandstone at Carrowmore is similar to the previously discussed outcrops at Truskieve and Killard in part, but significantly different in some aspects. Storey 1, with its dipping downstream accretion surfaces and well-developed cross bedding, is similar to the Storey 2 at Truskieve, and may represent the downstream migration of a bar form within a fluvial channel. The erosion of Storey 1 by Storey 2 makes calculations of channel depth from macroform height impossible, but the flow depth of 5.0m obtained from cross set heights is similar to flow depths calculated for other Tullig Sandstone outcrops.

The second storey is initially very similar to the fourth storey at Truskieve, with a strongly erosive base and an upward transition from massive to planar and trough cross-bedded sandstone. The two storeys can be interpreted in a similar way, as channel-fills formed under flow conditions conducive to dune formation, but with no evidence for macroforms such as mid-channel bars. The palaeocurrents from Carrowmore show palaeoflow was to the northeast (Fig. 4.16), similar to Pulleen, Killard and Truskieve. Channel depth is calculated from cross bed heights as 7.0m.

The main differences between the Carrowmore outcrop of the Tullig Sandstone and the Trusklieve and Killard outcrops are at the base and top of the sandbody. The base is more erosive in places at Carrowmore (4m of scour relief) than at Killard (0.25m) and Trusklieve (2.5m). However, the generally flat basal surface, similar to that seen at these other localities, is a typical feature of sand-rich low-sinuosity channel systems (Galloway and Hobday, 1996). The top of the Tullig Sandstone at Carrowmore shows a more gradual transition to abandonment than at Killard, with interbedded muds, silts and fine sands (facies Flh) interrupting sand deposition. These finer-grained facies are evidence of prolonged periods of abandonment during the later stages of channel evolution, prior to its permanent abandonment. The wave reworking seen within the sandy and silty facies near the top of the sandbody (Unit Y) is further evidence of abandonment, and could indicate the influence of basinal waves.

#### **4.3.5 The Tullig Sandstone at Furreera, Liscannor Bay**

The outcrop at Furreera, a further twenty kilometres northeast along the coast from Carrowmore, consists of a south-facing cliff face up to 6m high, showing the basal contact of the Tullig Sandstone. Although similar in appearance to the Carrowmore outcrop, the sandbody at Furreera cuts into interdistributary bay facies (Fig. 4.21 and App. A14) rather than mouthbar facies as at other localities. At Furreera the sandbody is also much thinner than at the other localities, reaching a maximum thickness of only 4.80m before it is capped by finer material. The range of facies is also much reduced, comprising only cross-bedded (Fig. 4.22) and horizontally laminated beds (St, Sp and Sh), and the architecture is simple, with only one storey.

##### *4.3.5.1 Storey one: description and interpretation*

The basal contact of the Tullig Sandstone at Furreera is very flat, following the bedding in the fine-grained facies below (Fig. 4.23), and has no apparent sole marks. Instead of commencing with conglomerates, massive sands and low-angle cross bedding, as at other localities, the Furreera outcrop shows well-developed trough cross bedding from the base and throughout the storey (Figs 4.22 and 4.23), with occasional beds of facies Sp, Sl and (rarely) Sh. Foresets dip towards the northwest and northeast (Fig. 4.21). Set boundaries can be continuous laterally, but are more often lens-shaped over horizontal distances greater than about 10m, due to the dominance of trough cross bedding (Fig. 4.23). Set heights range from 0.15 to 0.7m,

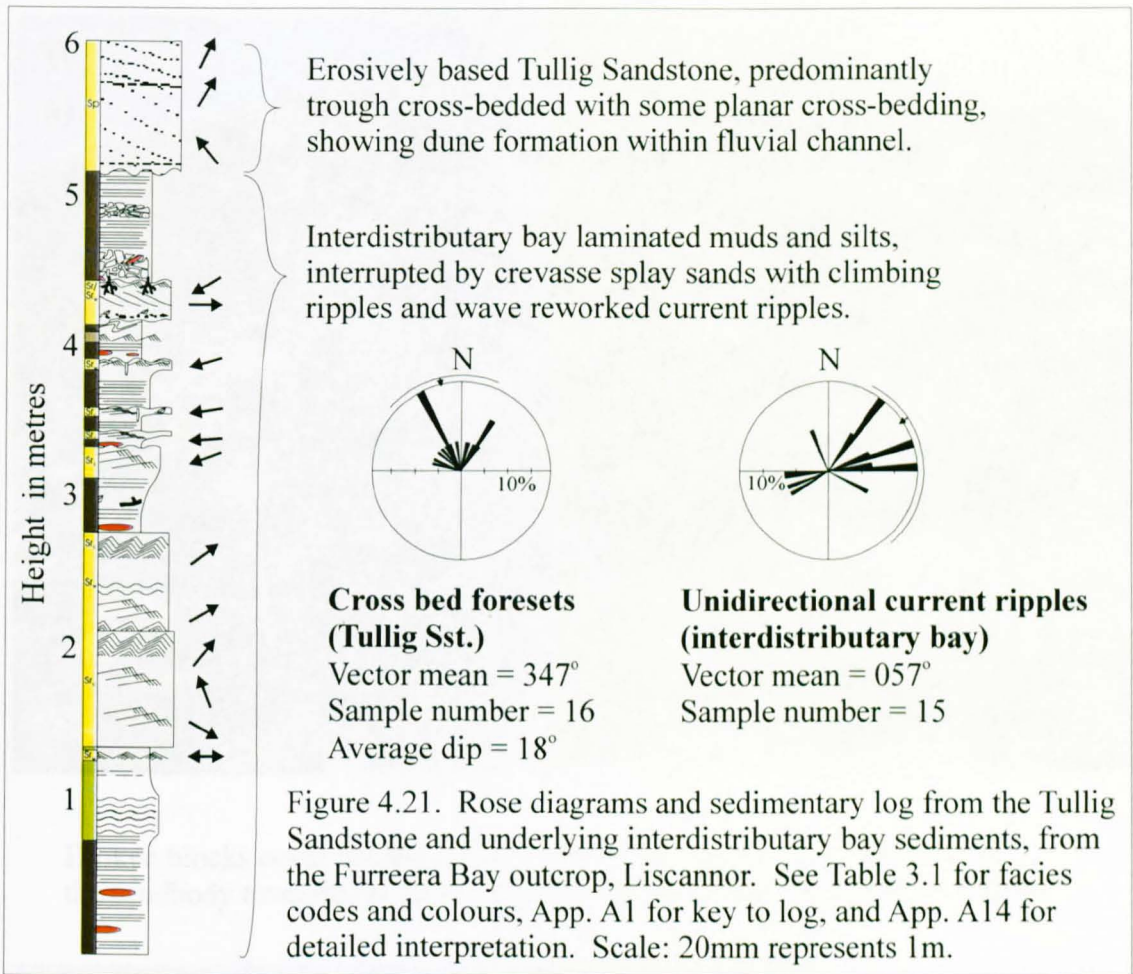


Figure 4.22. Photo of the Tullig Sandstone at Furreera, showing well-developed trough cross-bedding, with foresets picked out in colour to show detailed geometries. Notebook is 0.2m tall.





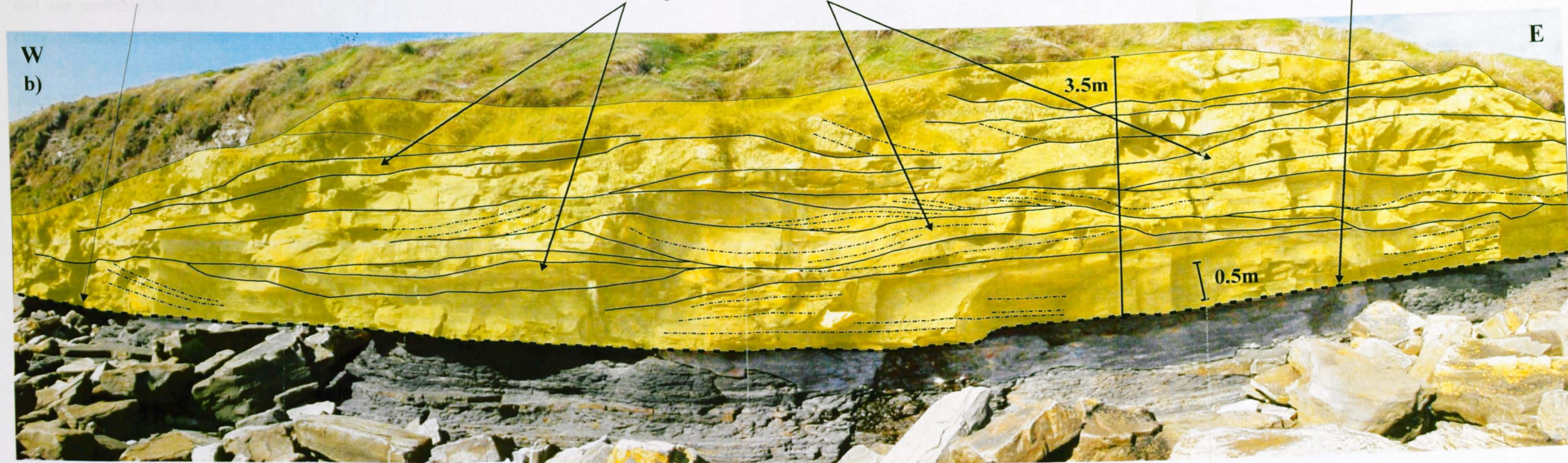
W  
a)

E

Broken blocks cover the base of the sandbody towards the west.

Beds are often lenticular in shape as they are eroded by the downcutting bases of the trough cross sets above.

The basal surface is very flat, following the bedding in the laminated muds and silts below.



W  
b)

E

3.5m

0.5m

**Key**

	Sp, St, Sl		Major erosional channel bases
			Bedding planes, erosional contacts and reactivation surfaces
			Fosets and laminations

Figure 4.23. Four-photo panorama of a section of the Tullig Sandstone outcrop at Furreera, Liscannor Bay. The shadowed areas of the photos have been artificially lightened to allow the bedding details to be seen. Note the dominance of trough cross bedding and the lack of any conglomeratic or mud/silt facies.

clustering around 0.30m. The calculated average cross bed thickness for the outcrop is 0.29m, which gives a figure for flow depth of 5.0m (range 3.8–6.3m) using Equations 4.1 and 4.2 (Yalin, 1972; LeClair and Bridge, 2001). This is consistent with the maximum measured thickness of the sandbody at Furreera, which is 4.8m, and is within the range calculated for the other Tullig Sandstone outcrops (3.5-7.7m).

The amount of fine-grained material in this outcrop is very small, with silts and muds restricted to occasional thin layers at the base of cross bed sets, often partially draping the foresets and coalescing at the bed base. These layers are usually 5-30mm thick and are laterally discontinuous even within a single cross bed set. The thickest example (50mm thick) extends for only 3.62 metres before grading into the sandy cross beds immediately above. The uppermost parts of the sandbody are completely vegetated, so if there is any finer material above the sandbody, it cannot be seen. Coarse material is not prevalent at this locality either. A very few large, rounded clasts of siltstone are seen in isolated occurrences at the bases of trough cross beds and are probably the result of particle overpassing (Allen, 1983b). No lags or conglomeratic beds are present.

#### *4.3.5.2 Summary and discussion of the Furreera outcrop, Liscannor Bay*

The single storey at Furreera is dominated by trough cross beds and lenticular bed geometries, with very small amounts of fine-grained and coarse-grained sediment. Channel depth is calculated to be 5.0m, and foresets show flow directions towards the northwest, north and northeast. The measured thickness of the sandbody is 4.80m.

The interpretation of this outcrop is that it is part of the same fluvial system as the other localities, but that it is in a different position relative to the delta front. The decreased thickness, coupled with low volume of fines, show that it represents a single storey fluvial channel. It is therefore likely that this channel represents a location either close to the margins of the fluvial system, or a locality close to the river delta, where the trunk river has diverged into numerous smaller channels (an interpretation advocated by Rider, 1969 and 1974). There is considerable support in the literature for thicker, multistorey fluvial complexes to represent upstream parts of fluvial systems, while thinner, single storey channels have been shown to represent sections of fluvial systems in downstream, deltaic, locations (Dreyer, 1990; Dreyer *et*

*al.*, 1990; Flores *et al.*, 1991; Olsen, 1993; Reynolds, 1999). It is even possible to distinguish upper and lower delta plain facies by the architecture of the channel sandbodies, with those in the lower delta plain commonly being thin, single storey channels while those in the upper delta plain are thick, multistorey channel sandstones (Horne *et al.*, 1978). According to the observations of the above authors, Liscannor would be expected to represent a downstream location within the Tullig Sandstone fluvial system, and probably a location within the lower delta plain. Observations made in this chapter support this interpretation because the palaeocurrents from all outcrops show north to northeast directed flow, meaning that Liscannor is downstream of the other locations, and could represent a part of the fluvial system close to the river mouth in a lower delta plain environment.

The marked differences between Liscannor and the other localities show that the Tullig Sandstone fluvial system changed in style downstream. If the Liscannor outcrop represented a channel on the margins of a fluvial system, rather than in a deltaic setting, it would be expected to show a higher percentage of fines than axial locations such as Killard and Trusklieve, since the margins of channel-belts show finer-grained channel-fills and low-permeability strata (Pryor, 1973). In fact the Liscannor outcrop of the Tullig Sandstone exhibits a higher percentage of sand by area than any of the other localities (99.9%), making a marginal setting very unlikely. The interpretation of the Liscannor outcrop as a stretch of channel closer to the mouth of the fluvial system is therefore a better one.

#### **4.3.6 Tullig Cyclothem mouthbar sandbody at Tullig Point**

Tullig Point is located on the coastline of County Clare, 2.5km to the southwest of the Trusklieve outcrop (Fig. 3.1). At Tullig Point, just over ten metres below the base of the Tullig Sandstone, a second sandbody is exposed within the Tullig Cyclothem in an inaccessible cliff section. This sandbody was photographed from an adjacent cliff top, and a section through it was logged at the only place it is accessible, where it intersects with the cliff edge (Fig. 4.24). The geometries, thicknesses and detailed sedimentology were interpreted by extending the logged interpretation to the rest of the sandbody using the photographic evidence. The cliff was also viewed with binoculars and detailed sketches were made to help tie the logged details to the visible sedimentary structures through the rest of the outcrop.



Figure 4.24. a) Photomontage of the Tullig Point outcrop, showing a mouthbar sandbody (centre of cliff) and the Tullig Sandstone (cropping out at the top left of cliff). b) As above, showing facies interpretation, bed labels (capital letters for sandstones, lower case letters for fine-grained beds), and marker bed in silts beneath to demonstrate very slight erosion on the base of the sandbody. See text for further explanation.

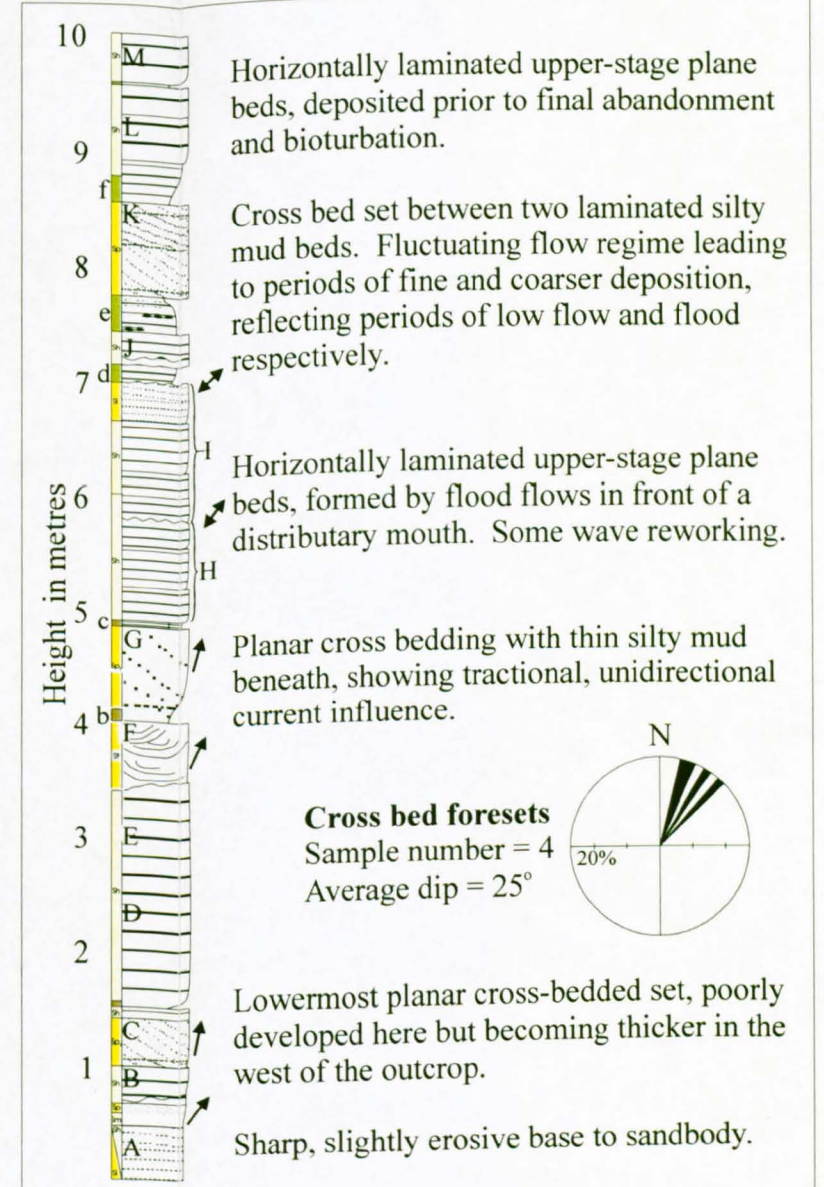
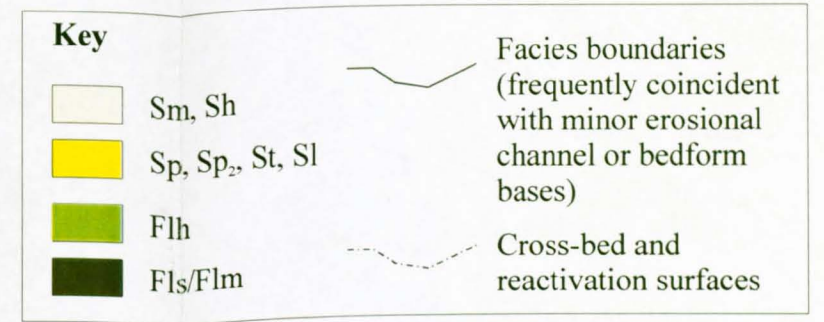
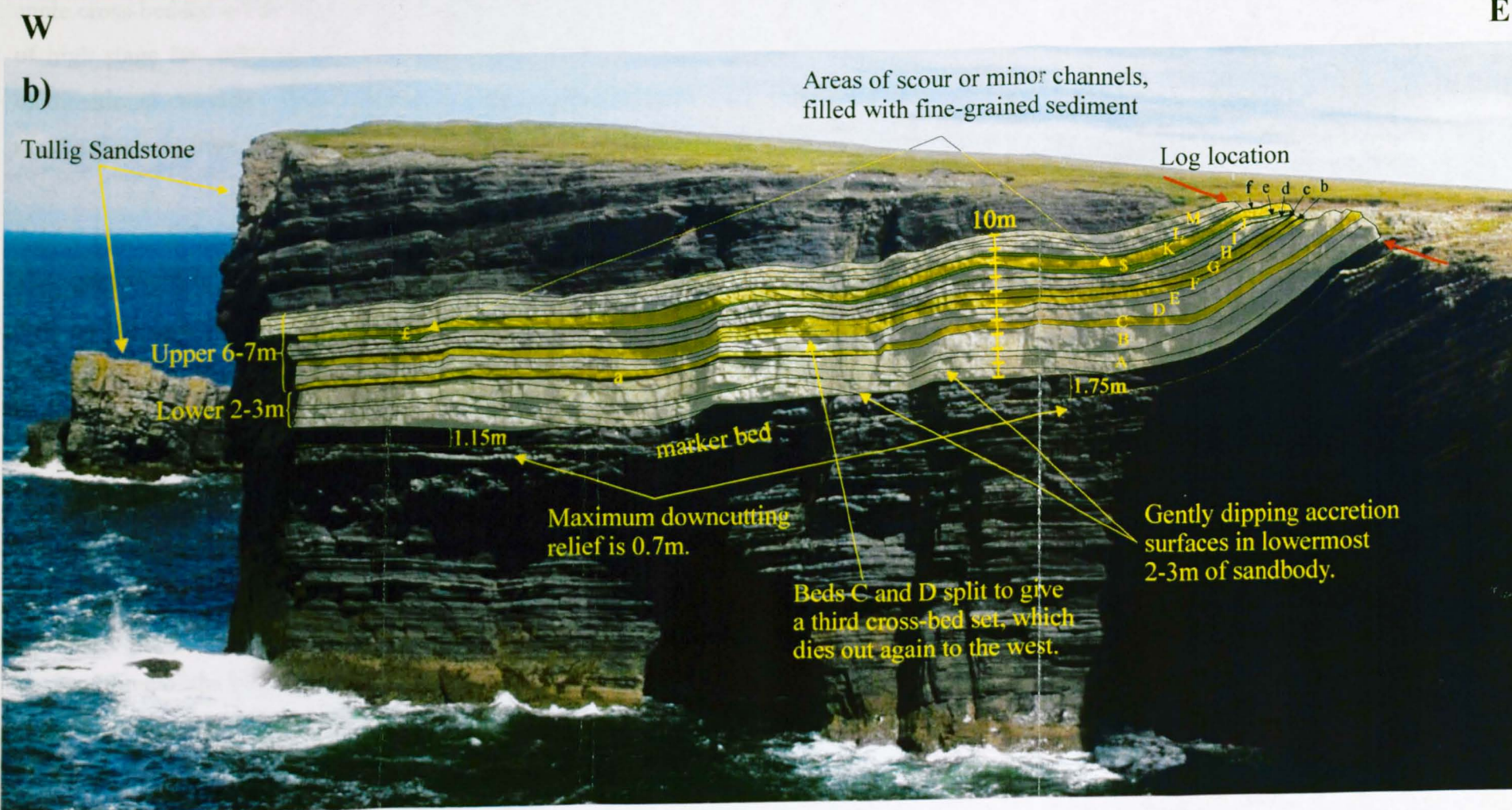


Figure 4.25. Sedimentary log from the sharp base to the top of the mouthbar sandbody at Tullig Point. Capital and lower case letters relate to labels in Fig. 4.24b. Scale: 15mm represents 1m.

#### *4.3.6.1 Lowermost 2-3m of the sandbody: description and interpretation*

The base of the sandbody is sharp and slightly erosional, cutting down less than 0.7m into the fine-grained distal mouthbar facies beneath (see Fig. 4.24a and b, and Fig. 4.25). No sole marks or directional indicators were found on the base at the logging point. The architecture of the first two to three metres of the sandbody is simple, with beds dipping gently towards the basal surface (Fig. 4.24a and b, and App. A15). Because the cliff only provides a two-dimensional exposure of the sandbody, it is difficult to measure precisely the depositional dip direction of the lowermost beds. They appear to dip gently, between 5° and 8°, to the east (Fig. 4.24), but could also dip more steeply to the northeast, which would produce the same gentle easterly dip seen in the east-west section exposed in the cliff. The palaeocurrent measurements obtained from the cross bed foresets within the first 2m of the sandbody show currents directed to the NNE (Fig. 4.25), suggesting that the gently dipping surfaces are downstream accretion surfaces, showing progradation of a bar form.

The dominant facies over the first 2-3m are Sh and Sl, horizontally bedded and low-angle cross-bedded sandstones. The presence of these facies attests to the occurrence of high stage but sub-critical flow, and therefore signifies the influence of strong unidirectional currents. The occurrence of facies Sm (massive sandstone) indicates rapid deposition from waning currents.

#### *4.3.6.2 Upper 6-7m of the sandbody: description and interpretation*

The upper six to seven metres of the sandbody are also dominated by facies Sh. Three more facies, Sp<sub>2</sub>, Flh and Fls, also become important components of the succession (Fig. 4.25). The first two beds within the upper part of the sandbody, labelled a and C in Fig. 4.24b, are facies Fls and Sp<sub>2</sub> respectively. The cross bed set (C) extends across the outcrop, while the fine-grained bed (a) pinches out half way across (reaching a visible lateral extent of 40m). Neither bed dips towards the basal surface of the sandbody. In fact the entire upper two-thirds of the sandbody shows a vertical (rather than lateral or downstream) aggradational bedding architecture. Throughout the upper 6-7m no dipping surfaces are present, and there is only limited internal erosion. The bases of three of the beds (B, F and J) are erosional but not strongly downcutting (Fig. 4.25), and in addition the outcrop photos show that the penultimate bed of facies Flh (Bed e) is erosively based. From Fig. 4.24a and b it is clear that there are two areas

(labelled £ and \$) where the fine-grained facies of Bed e fill erosional scours in the top of Bed J beneath. These discrete areas of erosion are the only significant interruptions of the aggradational sequence.

While the architecture is simple, the facies patterns of the upper part of the sandbody are slightly more complex. Upper stage, subcritical flow dominates, producing beds of facies Sh, but there are also three intervals of cross bedding that can be traced across the whole cliff outcrop (Bed C, Beds F and G, and Bed K – see Fig. 4.24b). All three cross-bedded intervals are capped or underlain (or both) by thin fine-grained beds of facies Flh or Fls, which are no thicker than 0.37m, and usually less than 0.15m (see log, Fig. 4.25). Bed K is sandwiched between two beds of Flh (Beds e and f) while the middle cross-bedded interval is divided into two cross sets, Beds F and G, by a thin siltstone (b), and is also draped with a laterally extensive bed of Flh (c). The lowermost cross bed set (Bed B) is immediately underlain by a bed of laminated siltstone (a). The three cross-bedded intervals are roughly evenly spaced vertically throughout the section, being 1-2m apart. The pattern produced by the repetition of paired Sp/St and Flh/Fls beds indicates a recurring fluctuation between fine-grained deposition in the absence of tractional currents, and unidirectional flows with tractional currents creating dune bedforms. The cross beds themselves show a shorter time-scale high flow-low flow fluctuation, with the foresets draped by thin (<3mm) layers of silt and mud, which represent periods of reduced current activity and deposition from suspension (sub-facies Sp<sub>2</sub>, discussed in Section 3.3.6).

The scours or channels seen in the top of Bed J (Fig. 4.24a and b) are further evidence of tractional current influence on the sandbody. These scours both occur in the same bed and were therefore formed at around the same time, suggesting a period of increased flow velocity that caused erosion. These discrete areas of erosion were subsequently filled by parallel-laminated fine-grained sediments, indicating a switch to deposition from suspension in the absence of tractional currents. The cutting and filling of the scours is further evidence for fluctuating flows.

A final feature of the upper part of the Tullig Point sandbody is the occurrence of wave ripples at the top of two of the beds, with crests oriented NW-SE. Although not widespread throughout the sandbody, wave ripples indicate that basinal waves are

influencing the environment of deposition, and are approaching from either the northeast or southwest. Wave approach from the northeast implies that the basin is to the northeast, which is consistent with the northeasterly progradation direction implied by the cross bed foreset dip directions.

#### *4.3.6.3 Summary and discussion of the Tullig Point outcrop*

- 1) The basal surface of the sandbody is sharp but only slightly erosive, showing less than 0.7m of relief. The lower 2-3m are dominated by horizontally laminated sandstone (facies Sh) and display dipping accretion surfaces indicating progradation to the northeast.
- 2) The upper 6-7m of the sandbody are again dominated by facies Sh and also exhibit repeated high flow-low flow bed couplets - beds of dune-scale cross bedding (facies Sp/Sp<sub>2</sub>/St) immediately succeeded by parallel-laminated fine-grained sediment (facies Fls/Flh). Facies architecture represents vertical, rather than lateral or downstream aggradation, with some evidence of limited erosion, apparently concentrated on the level of Bed E. Wave ripples indicate occasional reworking by basinal waves.

The facies association seen in the Tullig Point sandbody initially appears similar to the fluvial facies association discussed in Section 3.4.3. The dominance of facies formed in the subcritical upper flow regime (Sh and Sl) indicates action of strong unidirectional tractional currents. However, the significant amount of fine-grained material, the very good lateral continuity of the beds, and the lack of pronounced scour and downcutting testify to an environment where erosion is limited and deposition from suspension, with little or no tractional current influence, is important. The fluctuation between tractional unidirectional processes and non-tractional settling processes can occur in a purely fluvial environment, but usually fine-grained deposits in such an environment are restricted to abandoned channel reaches and floodplains. The thin, laterally extensive fine-grained beds seen in this outcrop are not channel fills, show none of the features associated with floodplains (rootlets, bioturbation), and are dissimilar to the fluvial abandonment facies seen in the Tullig Sandstone at Trusklieve.

In light of these observations, the Tullig Point sandbody is interpreted as a fluvially dominated mouthbar deposited in a delta front environment. The crest of a mouthbar, for example, experiences very strong sediment-laden traction currents during flood stage flow (Wright and Coleman, 1974). Deposition and subsequent reworking by waning fluvial currents causes the mouthbar to prograde (Coleman *et al.*, 1974) and produces beds of facies Sh, Sl and Sp (Wright and Coleman, 1974). The prograding accretionary geometries of the lowermost beds fits with this understanding of mouthbar progradation (e.g. see Wright, 1977). During low river stage a mouthbar crest is subject to fine-grained deposition from the plumes of suspended sediment extending from the mouth of its feeder distributary channel (e.g. Wright, 1985). The repeated fluctuation between high and low flow is responsible for the repeated facies pattern seen in the outcrop. The lateral continuity of the beds is explained by the spreading out of the plume of sediment from the distributary mouth into the receiving basin, which allowed fine-grained deposition over a wide area and also led to a reduction in average bed thickness compared with the Tullig Sandstone (see App. B3).

The sharp but low-relief base of the sandbody probably reflects the avulsion of a feeder channel into the area, causing erosion and an increase in depositional grain size. The discrete scours higher in the sequence represent a period of erosion, probably during a particularly high flood stage. The limited occurrence and depth of erosion elsewhere is explained by the deceleration of the river waters as they enter the receiving basin, leading to deposition rather than erosion. The occurrence of wave ripples in the succession can be explained by the action of basinal waves, reworking the sediment during low flow stage. The apparent absence of trace fossils, which are seen in other mouthbar sequences (see Section 3.4.1), could be due to a rapid rate of sedimentation and reworking, which is what would be expected in an active mouthbar crest environment.

The sandbody at Tullig Point is therefore interpreted to represent the crest of a sandy mouthbar prograding towards the northeast. The facies represent mouthbar crest deposition and reworking, and are principally the result of flood flow from the distributary channel supplying the mouthbar. For this reason, facies formed by tractional fluvial processes dominate the succession, while fine-grained sediments

deposited from the effluent plume make up a lesser proportion of the sequence. The sandbody architecture indicates progradation to the northeast followed by aggradation. This interpretation agrees with detailed logging work by Pulham (1987), who considered the sandbody to represent an axial river mouthbar.

#### 4.3.7 Tullig Cyclothem mouthbar sandbody at Killard

Below the base of the Tullig Sandstone at Killard is a coarsening-up succession of interbedded muds, silts and sands. This succession was logged (Fig. 4.26) on the southern limb of the outcrop (Fig. 3.1), starting from an arbitrary point where the succession started to change from laminated mudstone to interbedded laminated mudstone, siltstone and fine sand. The log was continued up to the sharp upper surface of the coarsening-up succession, marked by a strongly bioturbated abandonment surface. Above this surface is an interval of laminated mudstone and siltstone 9-10m thick, which is terminated by the erosional base of the Tullig Sandstone. The upper part of the coarsening-up succession is dominantly sandy, and has a sharp, erosive base (Fig. 4.27a and b). The discussion below focuses first on the lower part of the sequence, and then on the sharp-based sandy upper part.

##### 4.3.7.1 Lower part of sequence: description and interpretation

The lower part of the succession (0-6.5m in Fig. 4.26 and App. 16) comprises a series of coarsening-up beds of interlaminated mud, silt and fine sand (facies Fl<sub>h</sub>), interspersed with ungraded beds of parallel-laminated fine sandstone (facies Sh<sub>2</sub>), siltstone (Fl<sub>s</sub>) and mudstone (Fl<sub>m</sub>). The sandier beds frequently contain asymmetric current ripples, showing flow to the northeast (Fig. 4.26), and/or wave ripples (facies Sr and Sr<sub>w</sub>), mainly approaching from either the northeast or southwest (Fig. 4.26). The thickness and frequency of sandy laminae and beds increases upwards. Bioturbation occurs within the tops of three of the sandy beds, suggesting a brief pause in or slowing of sedimentation, enabling colonisation of the newly deposited sediment. The trace fossils include *Asterichnus*, *Lockeia* and *Monocraterion*; all three are typical of Carboniferous upper delta slope and delta front environments (Eager *et al.*, 1985), and *Monocraterion* is characteristic of the marine to brackish shallow water *Skolithos* ichnofacies of Frey and Seilacher, 1980 (see Section 3.3.19 and Figs 3.20, 3.21, 3.26 and 3.27).

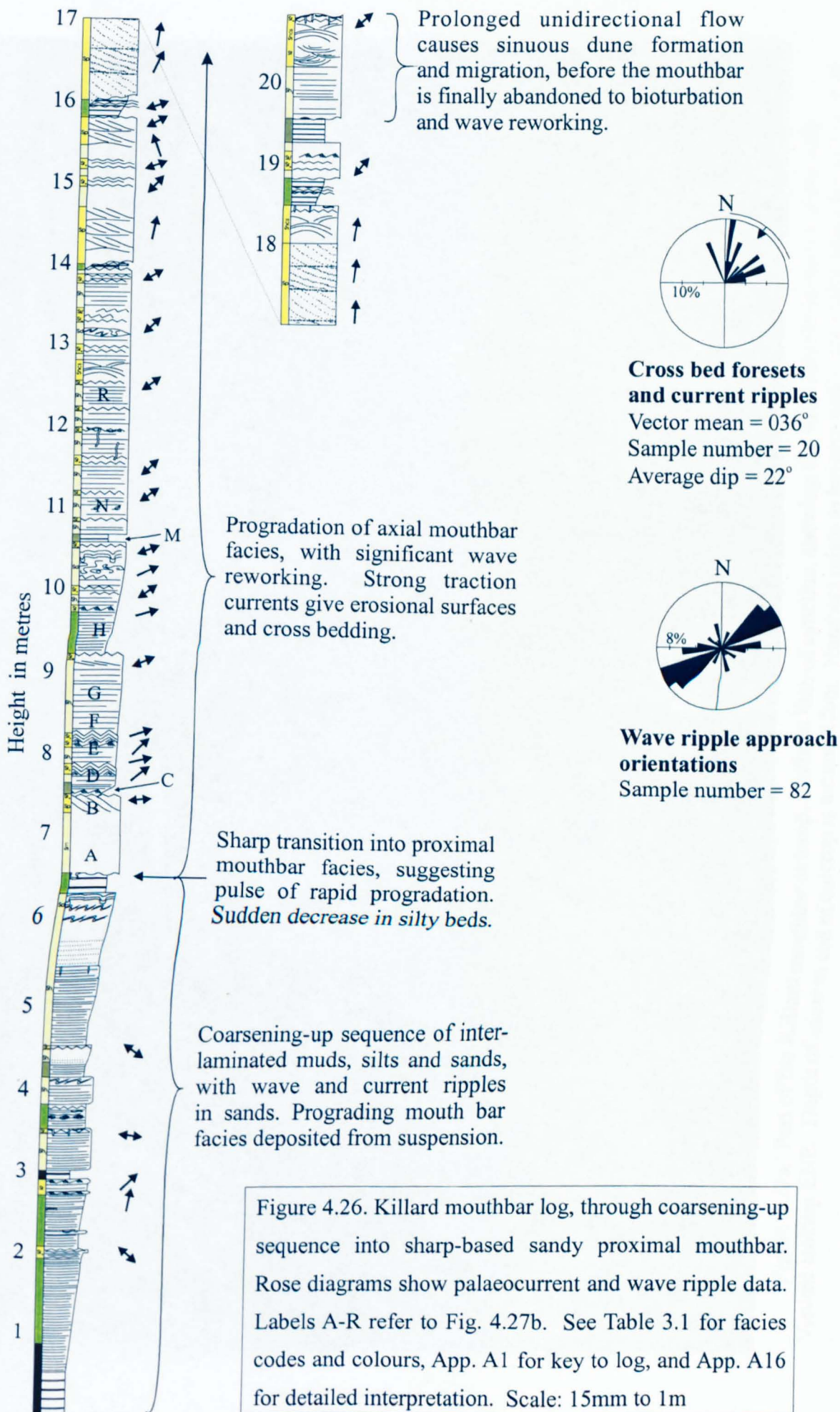


Figure 4.26. Killard mouthbar log, through coarsening-up sequence into sharp-based sandy proximal mouthbar. Rose diagrams show palaeocurrent and wave ripple data. Labels A-R refer to Fig. 4.27b. See Table 3.1 for facies codes and colours, App. A1 for key to log, and App. A16 for detailed interpretation. Scale: 15mm to 1m

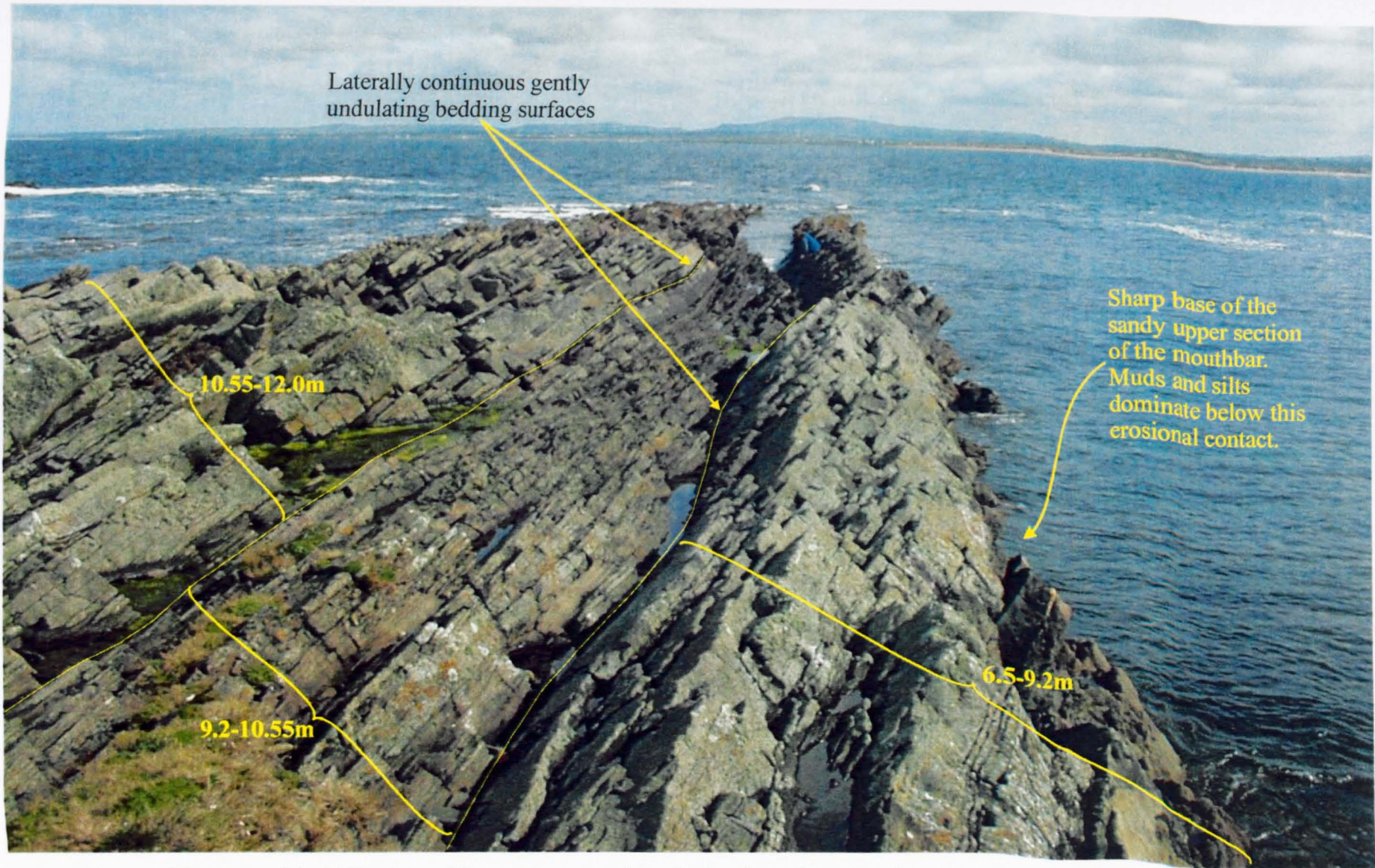


Figure 4.27a. Part of the Killard mouthbar outcrop, southern limb of syncline, showing the good lateral continuity of the beds. Viewed looking ENE. Depth of view to end of outcrop is around 120m. Numbers relate to heights within the sedimentary log in Fig. 4.26.

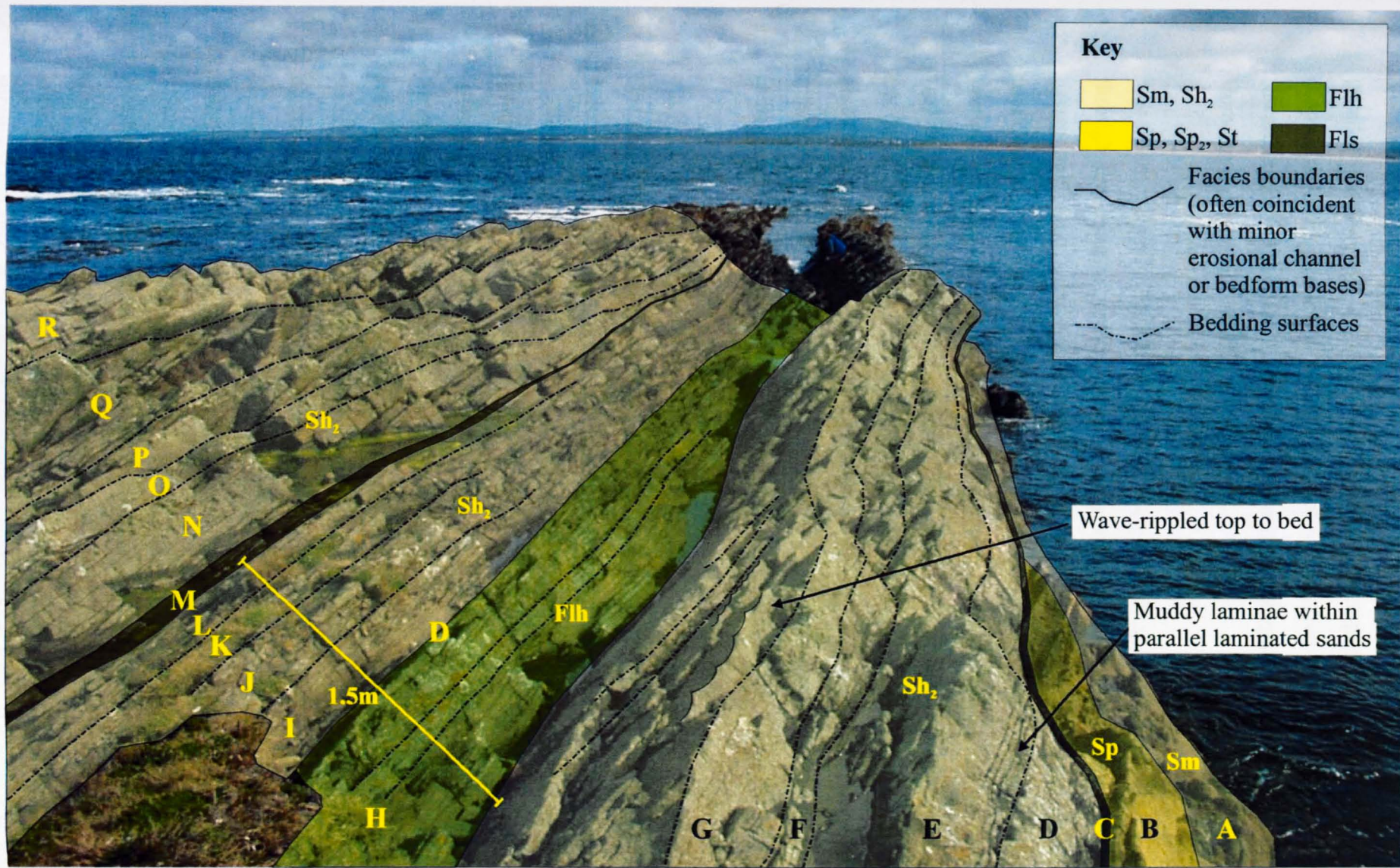


Figure 4.27b. As for Fig. 4.27a, with added facies interpretation and bedding surfaces. Bed labels (A-R) are related to Table 5.10 in Chapter 5, and some are included on the sedimentary log in Fig. 4.26.

The facies architecture of this lower part of the sequence is dominated by simple parallel bedding with frequent wave- and current-rippled intervals, and shows no dipping accretion or erosion surfaces. Palaeocurrents from current ripples are directed towards the northeast ( $010^{\circ}$ ,  $045^{\circ}$ ), and wave ripples show a dominant wave approach from the northwest or southeast (Fig. 4.26).

The interpretation of this lower part of the sequence is that it represents a section through the distal to intermediate deposits of a prograding mouthbar. The facies assemblage and coarsening-up signature are both typical of a progradational mouthbar-type delta front environment, as discussed in Section 3.4.1. The purely vertical stacking architecture, with only rare current-generated bedforms (current ripples, facies Sr), confirms deposition from suspension in the almost total absence of tractional currents, indicating that the environment is that of a distal bar (*sensu* Wright and Coleman, 1974). The ichnofacies and wave ripples support the environmental interpretation, since they are indicative of shallow, brackish, basinal waters (Frey and Seilacher, 1980) and shallow-water basinal waves respectively.

#### *4.3.7.2 Upper sandy part of sequence: description and interpretation*

The sandy upper interval of the coarsening-up sequence at Killard (6.5-20.75m in Fig. 4.26 and App. 16) is 14.25m thick, and shows very laterally continuous bedding (Fig. 4.27a and b). The base is erosive, with numerous sole marks but no distinct flutes, so a definite flow direction is not possible to measure. The flow trends shown by the sole marks vary considerably, from  $004^{\circ}$ - $184^{\circ}$  through  $097^{\circ}$ - $277^{\circ}$  to  $146^{\circ}$ - $326^{\circ}$ , and so provide no conclusive evidence for flow direction. The architecture of the sandbody is typified by a lack of dipping accretion surfaces and a purely vertical stacking pattern of laterally continuous beds (Fig. 4.27). Sandy facies are laterally continuous for the entire extent of the outcrop (100m+), while fine-grained facies tend to die out laterally (see Chapter 5 for details). Bed boundaries are flat to slightly undulating, and when corrected for regional dip, are horizontal.

The facies present include horizontally laminated sandstone (Sh<sub>2</sub>), trough and planar cross bedding (St, Sp, Sp<sub>2</sub>), current, wave and climbing ripples (Sr, Sr<sub>w</sub>, Sr<sub>c</sub>), laminated interbedded sands, silts and muds (Flh), and laminated siltstone (Fls). A summary log (Fig. 4.26) shows a series of coarsening-up packages of fine to medium

sandstone with numerous wave-rippled beds and some unidirectional current ripples. The wave ripples in this sandbody show wave approach from the northeast or southwest, unlike those in the finer-grained lower part of the succession (which show southeast-northwest wave approach - see Section 4.3.7.1). The current ripples give a flow direction towards the northeast (see rose diagram, Fig. 4.26). The dominant facies throughout the first 7.5m of the sandbody is Sh<sub>2</sub>, with Flh and Fls also comprising a significant proportion of beds (6.5-14.0m, Fig. 4.26). Dune cross beds do not appear until the upper 6-7m of the sandbody. The cross-bedded units have erosional bases, in some cases cutting out the finer-grained Flh/Fls beds beneath them (Fig. 4.26 and Fig. 4.28). The dune foreset dip data, when corrected for regional dip, show the same palaeoflow direction as the current ripples – towards the northeast (see rose diagram, Fig. 4.26).

The top 3m of the sandbody, while still dominated by sandy facies, exhibit evidence of changing processes. The facies change from sandy cross beds to wave reworked beds and finer-grained deposits (Fig. 4.26; see also Fig. 3.19, which shows the logged section from 18m to the top). Two laterally continuous fine-grained beds occur (at 18.6 and 19.4m in Fig. 4.26), indicating pauses in tractional current influence. The presence of hummocky cross stratification and wave ripples within the upper 2m of the sandbody (Figs 3.18, 3.19 and 4.26) shows that the top of the sandbody was reworked by waves during periods of reduced fluvial influence. Bioturbation is also seen in these beds, although it is not prevalent elsewhere in the sandbody. Trace fossils are concentrated on the upper surface of the sandbody, which is intensely bioturbated, indicating abandonment of the sandbody and non-deposition. The trace fossil assemblage (*Monocraterion*, *Asterichnus* and *Lockeia*) shows that the abandoned surface was colonised by brackish shallow water fauna. Between the top of the mouthbar sandbody and the base of the Tullig Sandstone is a succession around 9-10m thick comprising facies Sr, Flh, Fls and Flm, and exhibiting numerous layers of siderite concretions - evidence of organic-rich, sulphate-rich and iron-poor waters (Fig. 4.12, App. A7). This dominantly fine-grained succession capping the mouthbar is interpreted to represent a delta front interdistributary bay environment that developed after mouthbar abandonment.

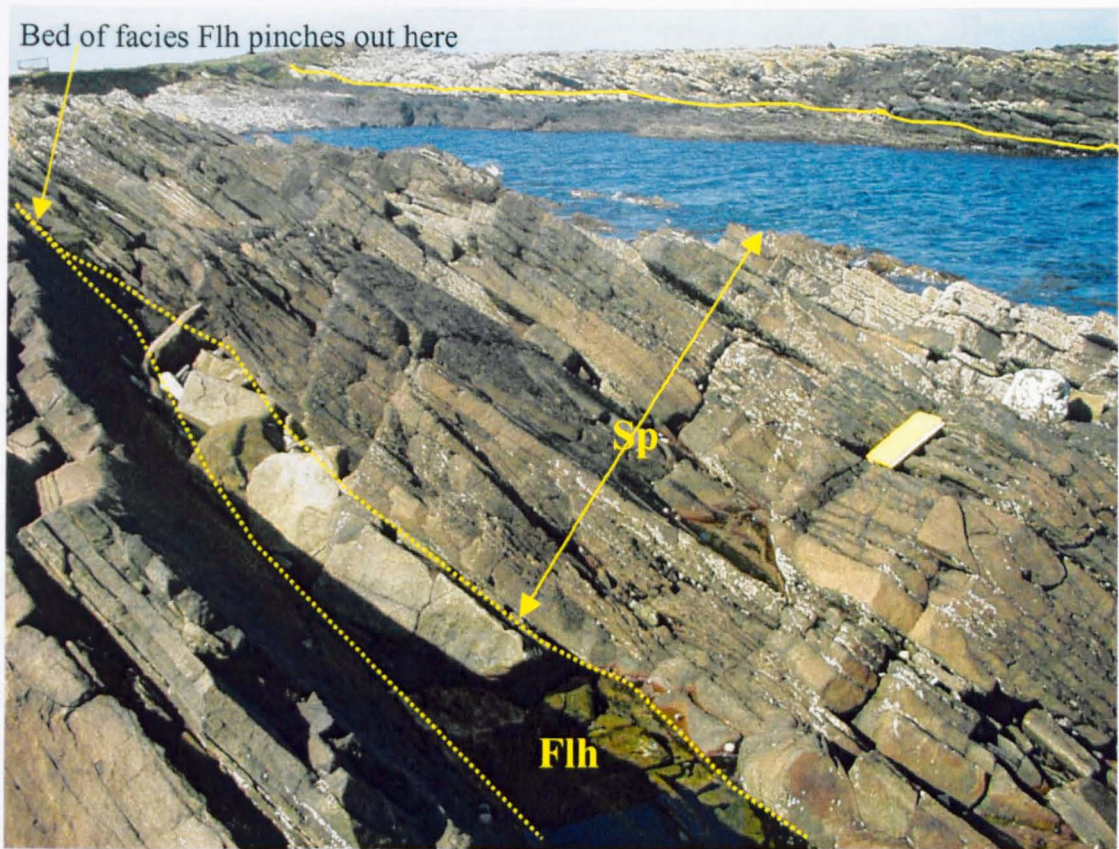


Figure 4.28. Top of the Killard mouthbar (15-17.5m in Fig. 4.26), looking west, with the Tullig Sandstone in the distance (solid yellow line marks base). Note the well-developed cross bedding (facies Sp) and the eroded fine-grained bed (yellow dotted outline) that pinches out to the left as it is eroded out by the base of the cross bed above. The notebook is 0.2m tall.

#### 4.3.7.3 Summary and discussion of the Killard mouthbar outcrop

A summary of the sandbody is given below.

- 1) The lower finer grained part of the coarsening-up mouthbar succession is dominated by facies Flh, Fls and Sh<sub>2</sub>. Wave ripples show northwest or southeast wave approach, and current ripples show flow to the northeast. Bedding architecture is purely vertical stacking, with little erosion and no large-scale dipping accretion surfaces.
- 2) The upper sandy part of the coarsening-up mouthbar sequence is dominated by facies Sh<sub>2</sub> and Sp, with numerous wave-rippled beds showing wave approach from the northeast or southwest. The basal surface of the sandbody is sharp and erosive. Palaeocurrent data from dune foresets shows flow to the north-northeast. Bedding architecture is again purely vertical stacking, with well-developed lateral continuity, particularly of sandy beds. The top surface shows abandonment, wave

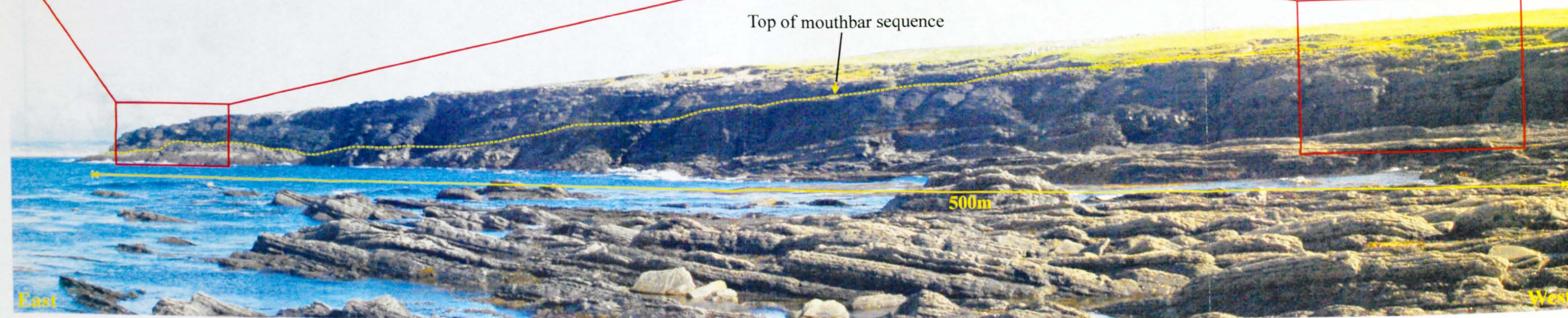
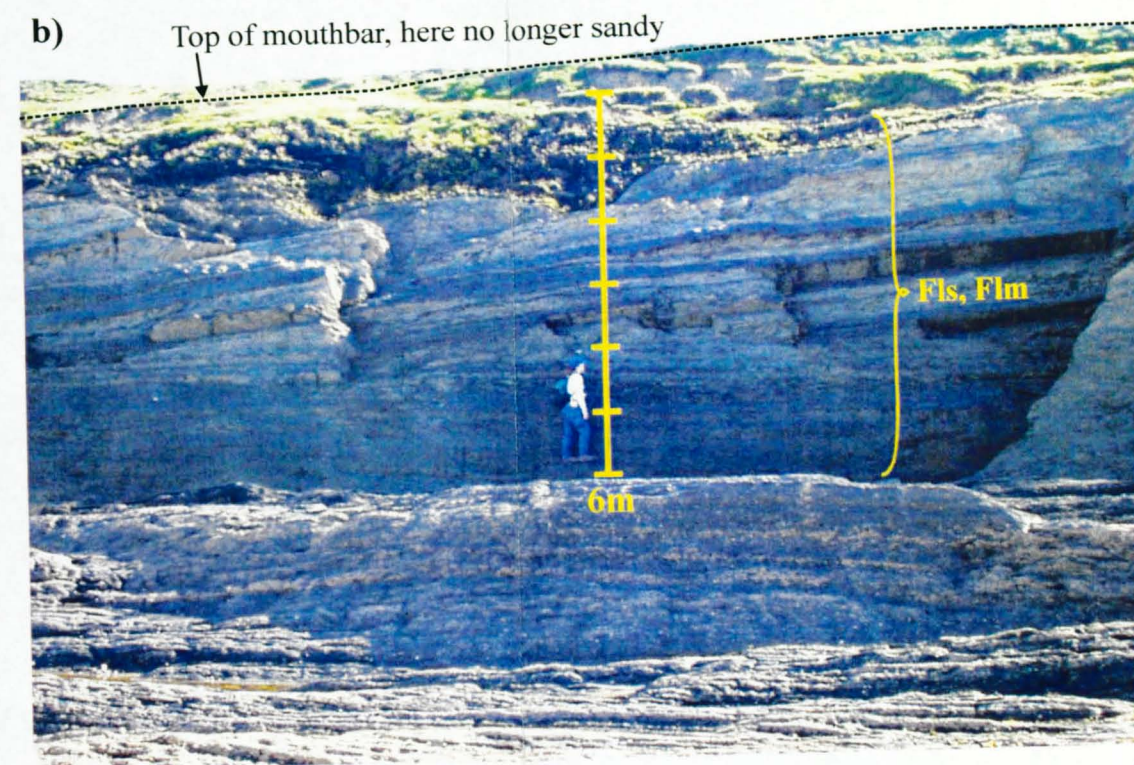
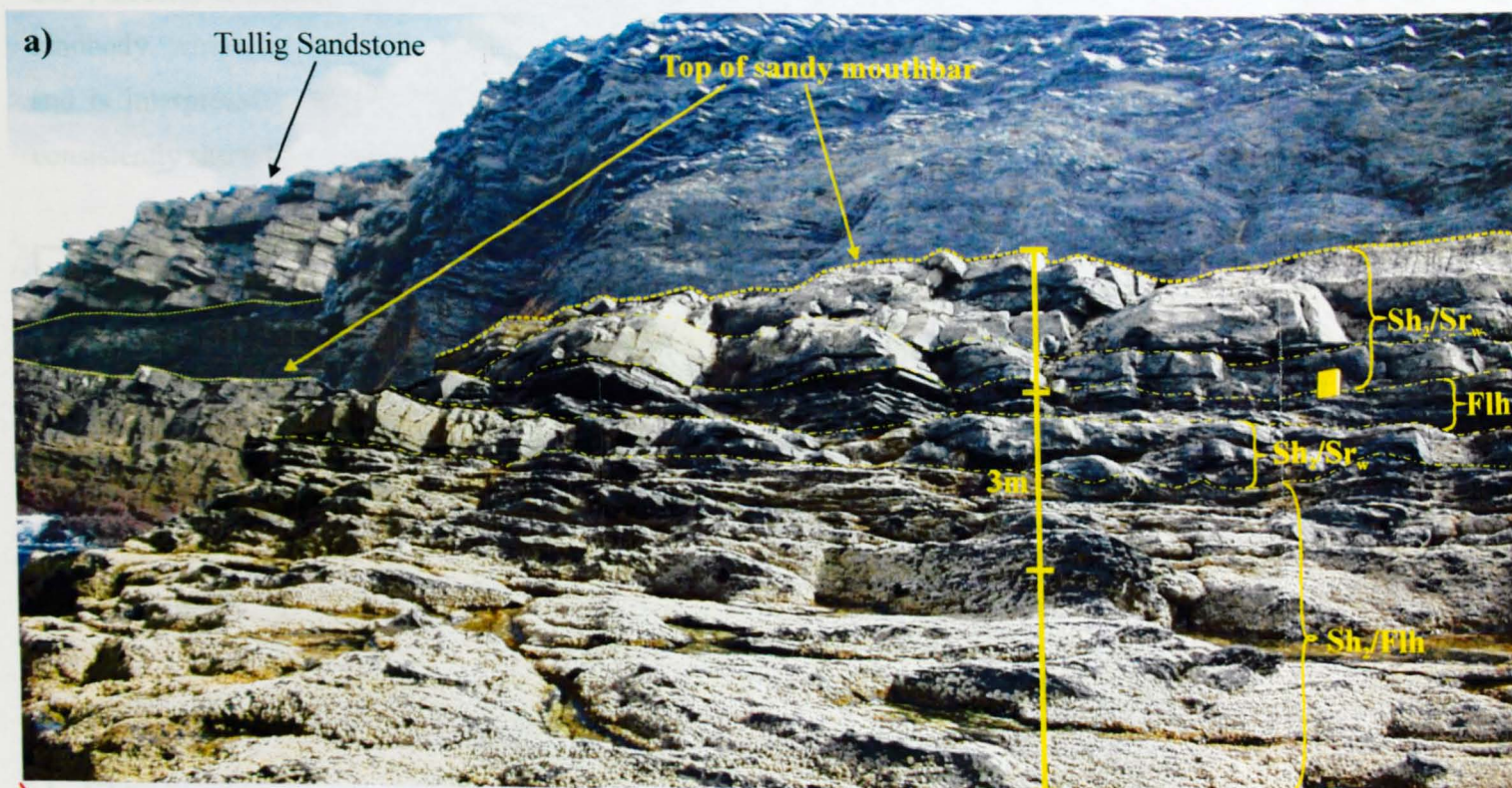
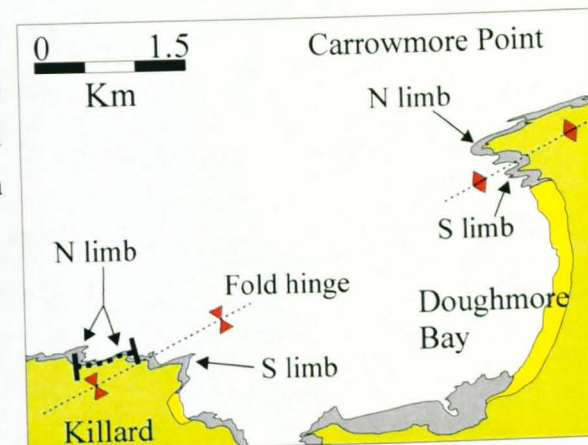
reworking, and bioturbation by a brackish shallow water fauna. The overall thickness of the sandbody is 14.25m.

The architecture and facies described above are interpreted in Section 3.4.1 as exemplifying the coarsening-up succession seen in prograding mouthbars. Fine-grained laminated facies and parallel-laminated sandstones are formed by sediment settling out of suspension from an effluent plume in front of a distributary mouth (see Sections 3.3.15 to 3.3.18, and 3.4.1). The cross beds at the top of the succession indicate the action of tractional currents, evidence of unidirectional current influence in the bar crest and bar back regions of the mouthbar. The wave ripples seen throughout indicate significant wave influence, and the action of storm waves is evidenced by the hummocky cross stratification at the top of the sequence. The mouthbar is finally abandoned and reworked by wave action and bioturbation.

The mouthbar is also exposed on the northern limb of the Killard outcrop. The main difference between the two limbs is that the northern outcrop of the mouthbar shows a marked decrease in sandy facies compared with the southern outcrop (Fig. 4.29). At the eastern end of the northern outcrop, only the top 3-4m of the mouthbar comprise sand-rich beds, while below this the succession is finer grained, comprising mainly facies Flh, Fls and Flm. This thin sandy interval contrasts markedly with the southern limb described above, where sandy facies dominate the upper 14m of the succession, and where thick cross-bedded facies indicate the influence of tractional unidirectional currents. There is comparatively less cross bedding on the north side (compare Fig. 4.28 with Enlargement a) in Fig. 4.29), showing a decreased influence of tractional unidirectional currents. A further decrease in sand facies occurs from east to west along the northern limb; the sandy upper part of the mouthbar succession, 3-4m thick at the eastern end, thins and becomes increasingly fine-grained to the west (Fig. 4.29a and b), changing gradationally to silty and muddy parallel-laminated beds. The east-to-west decrease in sand content indicates that the environment to the west is a more distal part of the mouthbar, further away from the influence of the distributary feeder channel. The change from thick sandy mouthbar crest facies on the southern limb to fine-grained distal mouthbar facies at the western end of the northern limb occurs over a distance of about 1km, which suggests that the mouthbar is about 2km wide normal to palaeoflow, assuming a similar change from crest to distal facies to the east.

Figure 4.29. Photomontage of the northern limb of the Killard syncline, with two areas of the outcrop enlarged to show details of the facies. Enlargement a) shows the east end of the outcrop, showing beds of facies  $Sh_2$  and  $Sr_w$  at the top of a coarsening-up mouthbar succession, with interbedded silts and sands (facies  $Flh$  and  $Sh_2$ ) immediately below. Enlargement b) shows the western end of the outcrop, where sandy facies are absent, and where the upper few metres of the mouthbar comprise laminated silts and muds (facies  $Fls$  and  $Flm$ ). The change from bar front to distal bar facies from a) to b) occurs over a distance of just five hundred metres. The rapid reduction in sandy facies towards the east indicates that the mouthbar is limited in its lateral extent; see text for more detail.

This map, taken from Fig. 3.1, shows the location of the Killard outcrop and, highlighted by a thick black dashed line, the part of the coastline shown in the photo-panorama below.

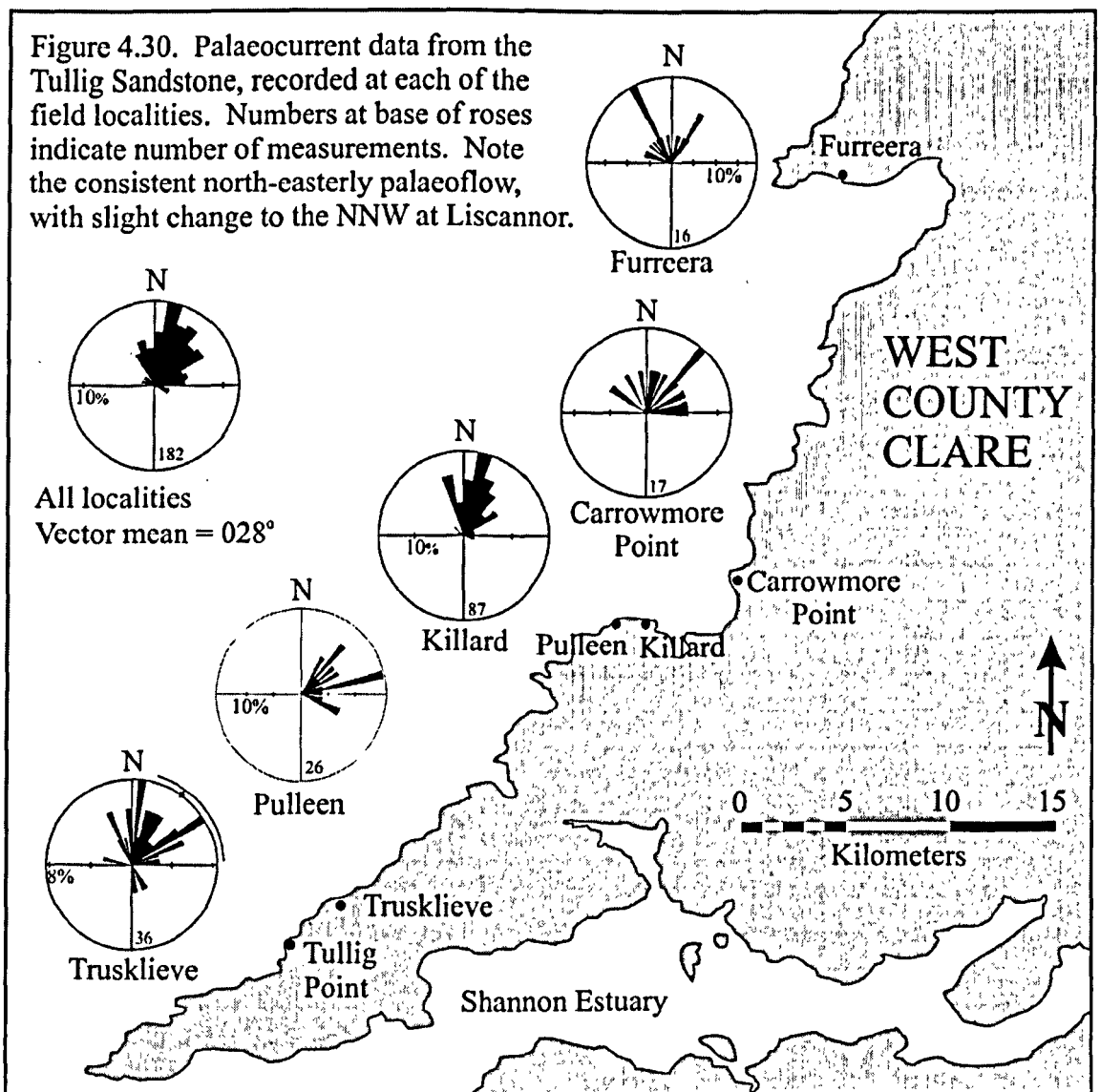


#### 4.4 Summary and palaeoenvironmental interpretation

This section draws together the observations and interpretations made in this chapter and compares them with literature to arrive at a comprehensive interpretation of the palaeoenvironment in which the Tullig Sandstone and associated mouthbar sandbodies were deposited.

##### 4.4.1 The Tullig Sandstone

From the outcrops of this sandbody seen at Trusklieve, Pulleen, Killard, Carrowmore and Furreera, it is apparent that the Tullig Sandstone is a thick, multistorey fluvial sandbody, which is oriented northeast-southwest along the coastline of County Clare and is interpreted to have a low sinuosity braided pattern. The palaeocurrent data consistently show flow to the north and northeast, as seen in Fig. 4.30 below, and give



a vector mean of  $0.28^\circ$ . The downstream distance over which the Tullig Sandstone extends exceeds 50km from Tullig Point to Liscannor; over this distance the sandbody changes character, which can be seen by comparing features between outcrops.

At Trusklieve, the bases of the individual storeys are strongly erosive, showing up to 8.5m of downcutting. The storeys themselves reach thicknesses of up to 10.7m (see Table 4.1 below). Moving downstream, to the northeast, the outcrop at Pulleen exhibits fewer storeys (3 in total), which show decreased erosional relief on their basal surfaces; the maximum downcut positively identified is 1.6m. Storey thickness at Pulleen is slightly greater than at Trusklieve, reaching a maximum of 11.3m. Moving further downstream, to Killard, the number of storeys decreases to two, and the storey thickness increases, reaching 18.2m for the second storey. Erosional relief on the storey bases is up to 4m. Further to the northeast, at Carrowmore, the number of storeys remains unchanged at two, while thicknesses are similar (up to 21.65m for the second storey). Downcutting measured in the field does not exceed 4m. Finally at Furreera, Liscannor Bay, there is a dramatic reduction in thickness of the Tullig Sandstone, with the single storey reaching a thickness of only 4.8m in outcrop. Relief on the basal surface is also reduced, to less than a metre.

**Table 4.1. Summary of statistics from the Tullig Sandstone at each locality.**

Locality	Erosional relief (m)	Maximum thickness (m)	Flow depth (m)	Total sandbody thickness (m)
Trusklieve: Storey 1	2.5	8.5	6.1	
Storey 2	8.5	10.5	7.7	
Storey 3	5.5	10.7	> 3.5	
Storey 4	7.5	8.5	4.6	
Storey 5	2.0	>6.55	4.8	
<b>Averages for locality</b>	<b>5.2</b>	<b>8.95</b>	<b>5.3</b>	<b>31.2</b>
Pulleen: Storey 1	> 1.0	> 1.6	/	
Storey 2	1.6	11.2	/	
Storey 3	3.0	11.3	6.3	
<b>Averages for locality</b>	<b>2.3</b>	<b>11.25</b>	<b>6.3</b>	<b>22.5</b>
Killard: Storey 1	0.25	5.1	/	
Storey 2	4.0	18.2	5.6	
<b>Averages for locality</b>	<b>2.125</b>	<b>11.65</b>	<b>5.6</b>	<b>21.4</b>
Carrowmore: Storey 1	4.0	2.5	5.0	
Storey 2	> 3.0	21.65	7.0	
<b>Averages for locality</b>	<b>3.5</b>	<b>12.075</b>	<b>6.0</b>	<b>22.0</b>
Furreera: Storey 1	<1	4.8	5.0	<b>4.8</b>

From these data, a general trend is apparent, of decreasing number of storeys, decreasing erosional relief and increasing storey thickness in a downstream (northeasterly) direction. There is also an accompanying decrease in the total thickness of the Tullig Sandstone, which changes from around 31m thick at Trusklieve (Pulham, 1987) to only 4.80m thick at Liscannor. The flow depths remain similar from southwest to northeast. The interpretation of these trends is that the fluvial system is changing from a vertically stacked braided fluvial channel succession, in an upper coastal plain alluvial environment, to a diverging network of single storey distributary channels in a delta-top environment. This interpretation agrees with the observation made by many researchers (e.g. Horne *et al.*, 1978 Dreyer, 1990; Dreyer *et al.*, 1990; Flores *et al.*, 1991; Olsen, 1993; Reynolds, 1999) that multistorey sandbodies and single storey sandbodies represent upstream environments and downstream, lower deltaic plain environments respectively, as discussed in Section 4.3.5.2. The reduction in erosional relief on channel bases downstream complies with this theory, being consistent with the dominance of depositional processes over erosional processes in the lower delta plain.

The fact that in most cases storey thickness is greater than flow depth can be attributed to the continued aggradation of individual channels in the same location, without avulsing. A low rate of avulsion is favoured by low relative sea-level, as observed from the Quaternary history of the Mississippi fluvial system (e.g. Autin *et al.*, 1991; Saucier, 1994). The increased erosional potential of rivers rejuvenated by base level fall encourages downcutting rather than avulsion, and causes channels to tend to remain in the same places (e.g. Bridge, 2003). At low to slightly rising relative sea-level, deposition will occur, but the channels may still remain relatively fixed in their courses, allowing individual channels (represented by storeys in outcrop) to aggrade and create thick vertical sedimentary successions.

An alternative explanation of the storey thickness has been offered by Pulham (1989), who considers that the southern part of the basin was subsiding rapidly during the deposition of the Tullig Sandstone, leading to the formation of thick, stacked channel sandstones (e.g. at Trusklieve). However, Pulham (1989) also states that the channels were relatively fixed, which is unusual, since avulsion frequency is known to increase with the increasing accommodation space that would result from subsidence, and avulsion would favour lateral, rather than vertical stacking of the channels. Pulham also

proposes that during a later stage of delta evolution, high subsidence rates did indeed lead to high avulsion rates, which he invokes to explain the extensive coastline-parallel “width” of the Tullig Sandstone. However, Pulham considers the system to be oriented close to normal to the NE-SW trending coastline, and so considers the coastal outcrops to represent an across-channel-belt, rather than downstream, section. There is no need to explain the extensive coastline-parallel sandstone deposition by avulsion and lateral migration if the coastal section is an along-channel section, as it is inferred to be here.

The characteristics of the Tullig Sandstone show some marked similarities to the characteristics of the Mississippi during the Pleistocene, which were documented by Autin *et al.* (1991) and Saucier (1994), and are summarised by Bridge (2003). The Pleistocene history of the Mississippi includes a period of low sea-level during the last glacial maximum, and a subsequent deglaciation and sea-level rise. The coastal plain section of the Mississippi river system during the glacial maximum was characterized by a low avulsion frequency, a braided channel pattern, a high channel-belt depth and a high proportion of channel deposits (as opposed to floodplain deposits). All these attributes have been either observed directly (e.g. the high proportion of channel-fill) or interpreted (e.g. braided pattern, low avulsion frequency) in the Tullig Sandstone fluvial system, and would be consistent with a low to rising relative sea-level. Since the Upper Carboniferous was a time of glacio-eustasy (Caputo and Crowell, 1985) it is reasonable to conclude that the deposition of the Tullig Sandstone, like the similar Pleistocene Mississippi system, coincided with a glacial period when relative sea-level was low.

Similarities can also be drawn between the Tullig Sandstone and the Namurian Rough Rock Sandstone Formation of the Pennine Basin, northern England, which is considered by some (e.g. Maynard, 1992a, 1992b; Maynard and Leeder, 1992) to represent a progradational fluvio-deltaic wedge that formed during sea-level lowstand to transgression. Like the Tullig Sandstone, the Rough Rock is underlain by an erosional surface deemed a sequence boundary by the above authors, and is overlain by early transgression coals and then by a marine band indicating maximum flooding by marine waters. As noted in Section 4.3.1.6, the Rough Rock contains planar and trough cross-bedded sandstone facies, scours and coarse lags, which are interpreted by Bristow (1988) to comprise a stack of multistorey braided fluvio-deltaic channels, agreeing with the interpretation of the Tullig Sandstone given in this Chapter. A marine band under-lying the Rough Rock

is calculated to represent a sea-level rise of 40m (Maynard and Leeder, 1992), and the erosional base of the Rough Rock is linked to a sea-level fall, because the sediments comprising the unit are from a renewed source area (Collinson *et al.*, 1992).

Incision of the Tullig fluvial system has effected a local seaward facies shift from delta front to fluvial, which can be observed in the outcrops. This facies shift is not very dramatic, since the incised sediments (mouthbar and interdistributary bay sequences) are related to the incising fluvial system, which has been inferred in this Section to represent a multistorey trunk channel to the southwest and a distributary channel network to the northeast. Some writers (e.g. Hampson *et al.*, 1997; see Section 2.2.3.4) contend that the Tullig Sandstone represents a fluvial incised valley-fill complex, and that the facies shift and basal erosion surface mark a period of incision related to sea-level fall, a theory that would fit well with the Mississippi and Rough Rock analogies discussed above. The 35m thickness of the Tullig Sandstone could then be seen to signify the fill of an incised valley 35m deep. Incision on this scale would suggest sea-level fluctuations of tens of metres, which is consistent with sea-level changes calculated from other Namurian basins in the UK (e.g. Maynard and Leeder, 1992). However, in any delta system a shift from delta front to fluvial facies can be generated solely by autocyclic processes such as progradation and avulsion, and channel incision can be related simply to erosional scour (Best and Ashworth, 1997). In the Ganges delta, for example, scour at the Jamuna-Ganges River confluence, located nearly 200km inland of the delta front, is sufficiently deep (up to 30m) to incise delta front sediments buried beneath what is now the upper delta plain (Best and Ashworth, 1997). The flow depths calculated for the multistorey Tullig Sandstone outcrops, which are between 3.5 and 7.7m, are similar to the mean channel depth upstream of the Jamuna-Ganges confluence (6m; Best and Ashworth, 1997), and indicate that scour depths of up to 30m are not impossible, or even improbable, in the Tullig system. Such depths of scour, if present, could account for the superposition of thick, stacked multistorey sandstones on delta front sediments, removing the need for incision caused by sea-level fall.

Overall, it is probable that both scour-related, autocyclic incision and allocyclic incision related to falling sea-level were influential in the incision and deposition of the Tullig Sandstone. The field data, though abundant, is inconclusive, so neither alternative can be ruled out entirely.

#### 4.4.2 Tullig Cyclothem mouthbar sandbodies

The mouthbar successions of the Tullig cyclothem are coarsening-up packages of muddy to sandy sediments, which in the case of Tullig Point and Killard, are capped by sandbodies that are interpreted to represent the mouthbar crests. The thicknesses of the Tullig Point and Killard mouthbar sandbodies are 10m and 14m respectively. The palaeocurrents measured at both localities show flow and progradation to the northeast. The facies and architecture of these sandbodies are evidence of the discharge of distributary channels into a basin experiencing wave, and occasional storm, influence. Dimensions measured from the Killard mouthbar show a sandbody on the order of 2km wide normal to palaeoflow, suggesting that the width of the channel forming it was in the order of 0.5 to 1km. This is a similar channel width to that calculated in Section 4.3.1.6 from the flow depths at Truskleeve, using Bridge and Mackey's combined equation (1993), i.e. between 650m and 2500m wide. The fact that the interpreted channel widths correspond to the mouthbar dimensions supports the argument that the channels are genetically related to the mouthbars, rather than representing an unrelated incised valley-fill succession. Pulham (1989) did not consider the channels to be as narrow as is interpreted here, because he interpreted the system to be prograding from northwest to southeast, meaning that channel-belt width in his model had to encompass the entire coastal section from Truskleeve to Carrowmore, a distance of over 22km.

Reynolds (1999), in his paper collecting and classifying paralic sandbody data, found that "mouthbars commonly characterize strongly prograding conditions and are often developed in late highstand and early lowstand", an observation that is supported by a number of writers (Weise, 1979; Ryer, 1981; Bhattacharya and Walker, 1991; Shanley and McCabe, 1993; Fitzsimmons, 1994). If the Tullig mouthbars were formed during this part of the sea-level cycle, it would compliment the interpretation that the succeeding Tullig Sandstone was deposited during a subsequent lowstand of sea-level. It is possible that the Tullig fluvial sandbody was deposited in continuing late highstand conditions, but this is less likely, considering that the sediments succeeding the Tullig Sandstone indicate a drowning of the fluvial system and an accompanying retrogradation of parasequences during transgression (e.g. Wignall and Best, 2000). For a period of sea-level highstand to be followed by a further sea-level rise would be unusual; therefore the interpretation of mouthbar formation during highstand, channel erosion and deposition during a succeeding lowstand to early transgression, and

retrograding parasequence deposition during further transgression is the preferred interpretation. While not undermining the role of channel scour in the incision of the Tullig Sandstone fluvial system, the above argument supports the influence of sea-level changes on the sedimentary succession.

#### 4.4.3 The Tullig Cyclothem palaeoenvironment

A summary of the palaeoenvironment of the Tullig Cyclothem mouthbars and the Tullig Sandstone is shown in Figure 3.31 a to d. The main points are as follows:

- 1) The depositional environment interpreted for the mouthbars is a fluvial-dominated, wave-influenced delta front, which prograded to the northeast, with wave approach from the northeast.
- 2) The Tullig Sandstone is interpreted as a braided, low-sinuosity fluvial channel system that flowed to the northeast and incised the previous delta front by a combination of autocyclic scour and allocyclic incision related to sea-level fall.
- 3) The drowning of the Tullig Sandstone system, and subsequent retrogradation, prior to the onset of marine conditions and the deposition of the *Reticuloceras stubblefieldi* marine band, relate to a subsequent rise in relative sea-level.

This interpretation is based on the observations discussed in Chapters 3 and 4, and on the large body of literature that concerns the Tullig Cyclothem. The different viewpoints expressed in previous work show that despite the good outcrop evidence, there is more than one possible interpretation of the data. From the extensive architectural study presented here it is the conclusion of this study that Fig. 30 represents the model that most closely corresponds to the available evidence. The bar form and channel geometries presented, in particular, as well as the many palaeocurrent measurements and coastline-parallel facies progressions strongly suggest that the sedimentary system was braided and was flowing and prograding towards the north-northeast.

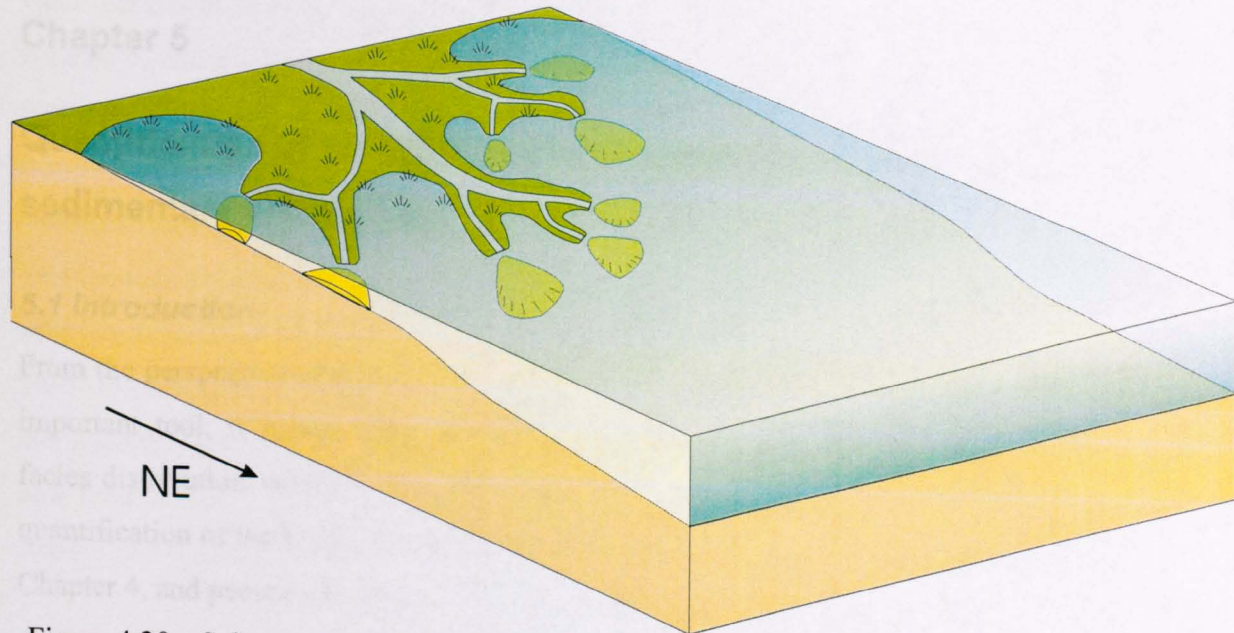


Figure 4.30a. Schematic block diagram showing the environment prevailing at the time of mouthbar formation and progradation in the Tullig Point and Killard areas. A fluvially dominated delta front with discrete, small-scale mouthbars progrades to the northeast.

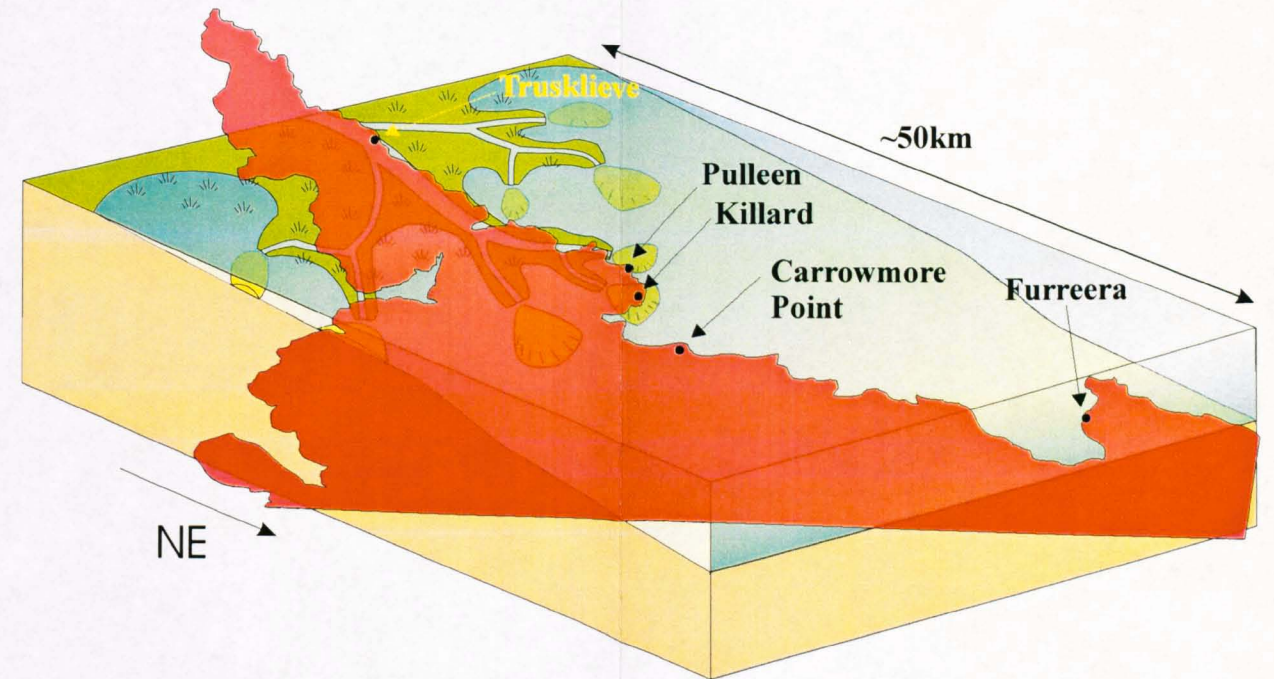


Figure 4.30b. Schematic block diagram showing the environment prevailing at the time of mouthbar formation and progradation in the Tullig Point and Killard areas, with the present-day coastline of County Clare superimposed to show the proposed position of the delta relative to the field localities.

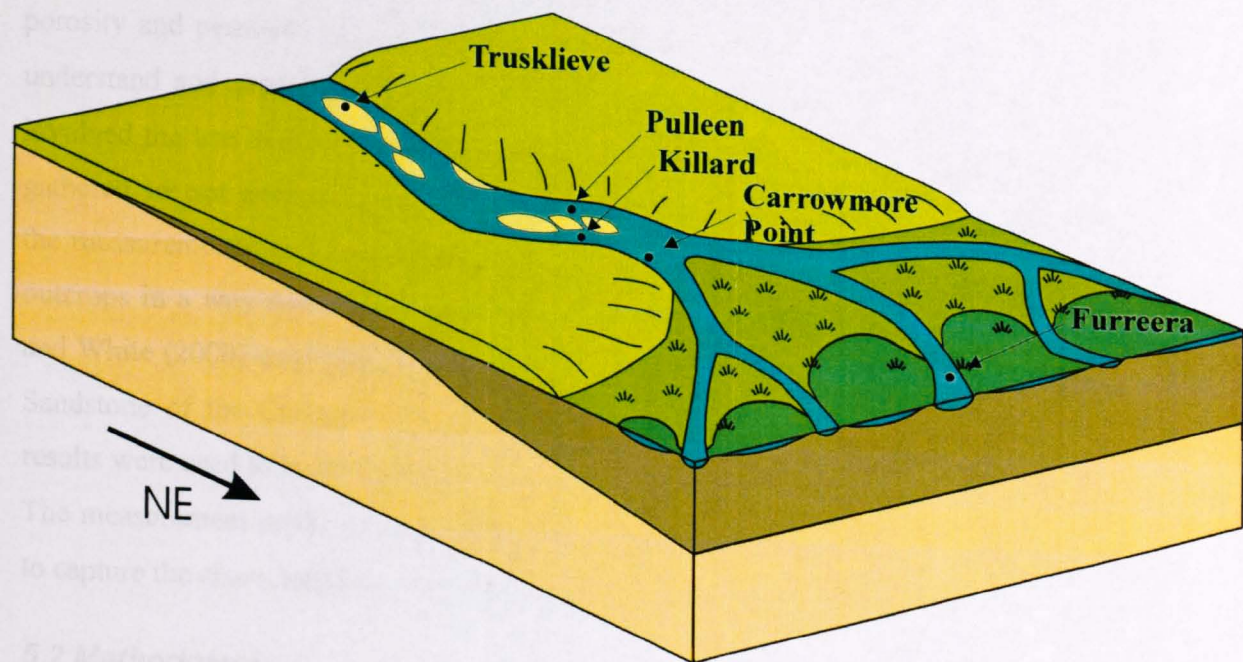


Figure 4.30c. Schematic block diagram showing the environment prevailing at the time of the Tullig Sandstone formation. A braided, low sinuosity fluvial system incises the pre-existing delta front deposits, and the locus of delta plain/delta front deposition has shifted over 50km to the northeast. Truskilieve now represents a location in the upper delta plain, while Furreera is in the lower delta plain.

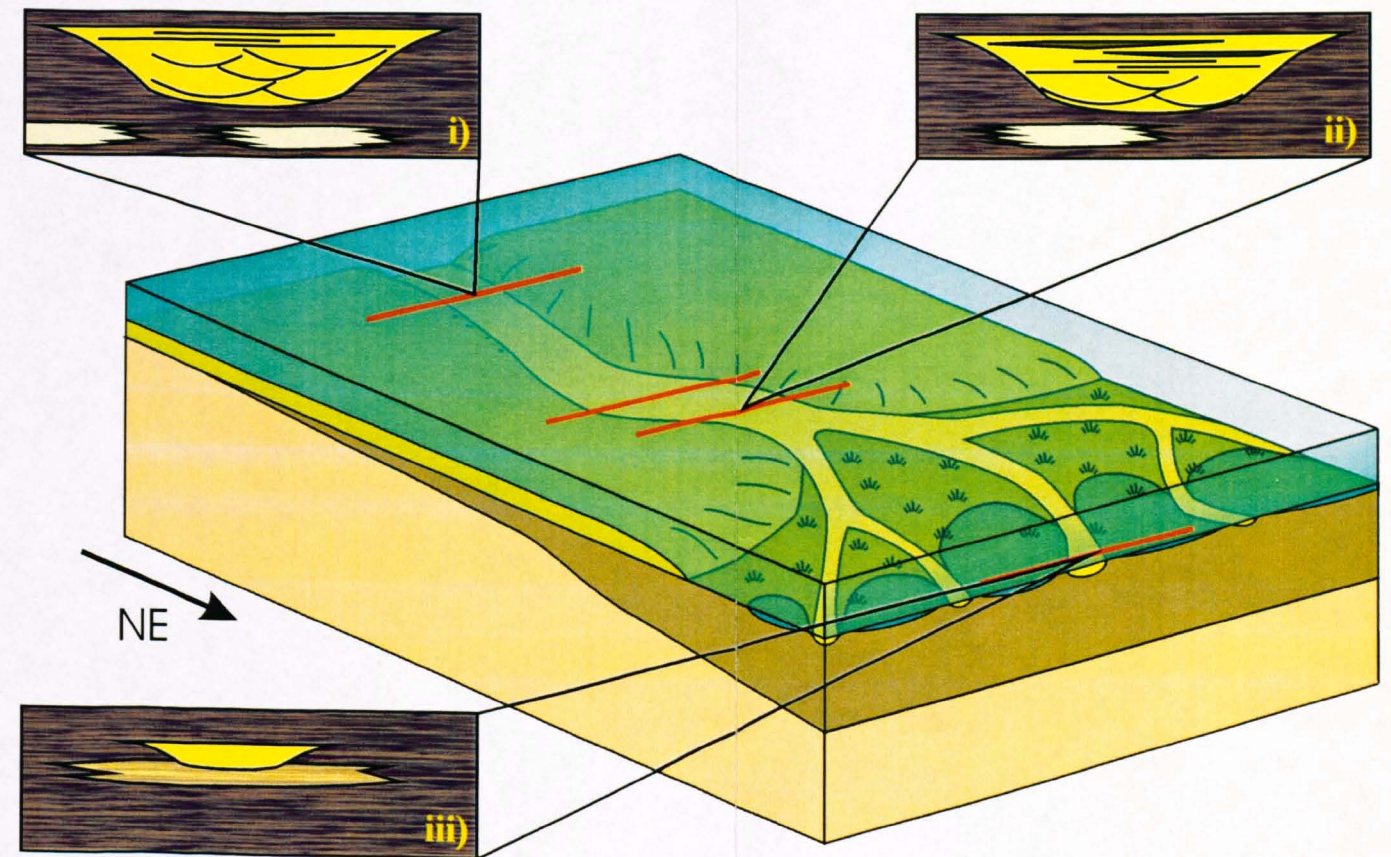


Figure 4.30d. Schematic block diagram showing the environment prevailing after the abandonment of the Tullig Sandstone and the flooding of the area by brackish to marine basinal waters. The three cartoon cross-sections (i, ii and iii) show the stratigraphic relationships between the Tullig Sandstone and the underlying deltaic sediments at Truskilieve, Carrowmore and Furreera respectively.

## Chapter 5

# Quantification of fluvial and deltaic facies distribution and sedimentary architecture

### 5.1 Introduction

From the perspective of a reservoir geologist, although facies interpretation is a very important tool, it means little without an additional, quantified, understanding of facies distribution within a potential reservoir sandbody. This chapter concerns the quantification of the facies distributions and architectures described and interpreted in Chapter 4, and presents a statistical analysis of the data collected in the field.

Existing literature gives many examples where detailed measurements of architecture, bed lengths, facies distributions and permeability have been used to inform geological model-building (e.g. Haldorsen and Chang, 1983; Hearn *et al.*, 1986; Jackson *et al.*, 1991). In many cases these data came from onshore hydrocarbon fields, where closely spaced wells provided a dense picture of subsurface facies distributions and porosity and permeability characteristics, which were used to create models to help understand and predict fluid flow within the reservoir. More recent attempts have involved the use of outcrop analogues (e.g. Willis and White, 2000), where the data gathered are not primarily from well logs or cores but from cliff faces. In such cases the measurements made are designed to capture the geological characteristics of the outcrops in a way that is easy to transfer to computer models. For example, Willis and White (2000) used photomosaics to digitally map beds and facies in the Frewens Sandstone of the Cretaceous Frontier Formation of central Wyoming, USA. The results were used to build flow simulation models that recreated the outcrop specifics. The measurement methods used for this thesis, described below, were also designed to capture the characteristics of the studied outcrops for reproduction in models.

### 5.2 Methodology

#### 5.2.1 Quantification of sedimentary architecture

Individual architectural elements within the accessible parts of each sandbody outcrop were identified based on an examination of bounding surfaces and facies changes, and

were marked in chalk on the outcrops (see Chapter 4). The length of each bed was measured, and thickness measurements were made at intervals (typically every 2m) along each bed, with maximum, minimum and mean thickness being recorded. These data were used to calculate a continuity index (length/maximum thickness), which is useful for comparing lateral continuity between facies types and between outcrops. The lengths of basal contacts for each sandstone bed that were sand-on-sand versus sand-on-mud/shale were also measured, and tabulated as percentages, which were used to calculate a mean value for each sandbody outcrop, representing the connectivity within the sandbodies. These data revealed the extents of facies types and their stacking patterns and connectivity relationships. Thicknesses of whole sandbodies were measured if possible, at several places laterally along each outcrop.

The reasoning behind the connectivity and continuity calculations is that these two characteristics are of prime importance in understanding fluid flow in hydrocarbon reservoirs. Although modelling can provide answers to questions about fluid behaviour, it is additionally useful to have an indication of how interconnected the sandy facies of a reservoir body are, prior to more detailed modelling; hence the connectivity calculations. Measuring bed lengths is also useful, especially in the case of fine-grained beds, which hinder flow and make flow pathways tortuous. Much work has been done to quantify shale length distribution (Haldorsen and Chang, 1986; Haldorsen *et al.*, 1987; Geehan and Underwood, 1993), and generating a database of shale lengths is not the objective of this thesis. However, the continuity index is a simple way of quantifying bed length and thickness and is a useful statistic for comparing outcrops. The disadvantage of measuring lengths from outcrop is that the length of any bed is simply a cross-section through it in one place; as pointed out by Geehan and Underwood (1993), this depends on outcrop orientation and facies geometries and orientations, and is very unlikely to be the longest or shortest possible cross-section, meaning that measurements of individual beds cannot be fairly compared. Additionally, not all bed lengths can be measured completely, since many beds are limited by the edges of the outcrop and cannot be seen in full. Geehan and Underwood (1993) suggest methods to combat such problems, but for this chapter the intention is not to derive a statistically “correct” shale length distribution, but simply to record lengths seen in outcrop for comparison with the results of the modelling process described in Chapter 6.

### **5.2.2 Quantification of facies distribution**

The scaled maps of the outcrops produced from photomontages allowed vertical sampling lines to be constructed at regular intervals (every 2m) along each exposure. Facies type was recorded every 0.5m along these lines, from the base to the top of each sandbody. These data were used to create vertical proportion graphs, showing how the percentages of each facies type vary with height in the sandbody. Horizontal proportion curves were also created for Trusklieve and Carrowmore Point. The percentage area of each outcrop by facies was calculated from these data, allowing net to gross values to be calculated. The facies percentages thus calculated were put into the RMS models described in Chapter 6. In this way the relative proportions of each facies occurring in the model matched the proportions observed in outcrop.

### **5.3 Architecture and facies distribution quantification: results**

The following tables and graphs present the quantitative results of each outcrop study. The related photomontages were presented in Chapter 4; the facies colour key used there is applied here to make the results easy to compare. Where bed labels are referred to, the labels and beds are shown in App. C, and some also appear in Ch. 4.

#### **5.3.1 The Tullig Sandstone**

##### *5.3.1.1 Trusklieve*

Data from accessible parts of the outcrop in Storeys 1 and 2 are shown in Table 5.1. The data show that the likelihood of a sandstone bed being in contact with another sandstone bed is 70.7%, reflecting the high percentage of sandy beds in the first storey. Data in Table 5.2 shows that the third storey has an almost identical connectivity, of 70.6%. For the other three storeys, detailed bed measurements were not made in the field due to lack of accessibility; estimates from the photomontages indicate a sand-on-sand connectivity of 80-100%, making the overall estimated value for the entire sandbody outcrop close to 80%. The mean and maximum bed thicknesses average 0.38m and 0.58m respectively across Storeys 1 and 3 (see Tables 5.1 and 5.2 for individual storey data). Mean lateral bed extent is 13.55m across the two measured storeys, and the continuity index is low, averaging 27.5 across the two storeys, showing that the beds are not very laterally continuous, but more lens-shaped. These data confirm the erosive nature of the contacts within Storeys 1 and 3. The

range of continuity is large for both these storeys (Table 5.1), confirming their architectural heterogeneity, since they both comprise channel-fill and bar elements.

Table 5.1. Sandstone bed data for the accessible part of the cliff section, first storey. Bed labels are in alphabetical order from the base of the sandbody upwards and from south to north. Some labelled beds are shown in Fig. 5.1, others in Fig. 4.3b and App. C1. The sand-on-sand and sand-on-mud percentages of mean bed contacts exclude beds along the base (marked /), since these contacts are not internal to the sandbody. Where beds contacts change from basal to internal, only the internal part of the contact is considered in the percentages.

Bed	Contact type		Thickness (m)		Bed length (m)	Continuity (length/thick)
	%s/s	%s/m	Mean	Max.		
ζ	100	0	0.54	0.87	>37	>42.5
ε	100	0	0.28	0.33	7.2	21.8
δ	100	0	0.30	0.36	12.4	34.4
?	100	0	0.48	0.62	>17	>27.4
β	100	0	0.34	0.44	>14	>31.8
a	100	0	0.25	0.31	9.6	31.0
z	100	0	0.50	0.71	>23	>32.4
y	100	0	0.26	0.36	>12.3	>34.2
x	100	0	0.17	0.26	10.7	41.2
w	/	/	0.55	0.57	>8	>14.0
v	/	/	0.48	0.58	10.4	17.9
u	/	/	0.30	0.45	8.9	19.8
t	100	0	0.55	0.91	10.1	11.1
s	100	0	0.47	0.56	23.6	42.1
r	0	100	0.20	0.35	7.7	22.0
q	0	100	0.12	0.15	2.5	16.7
p	0	100	0.15	0.35	4.9	14.0
o	60	40	0.25	0.42	2.9	6.9
n	0	100	0.17	0.74	18.1	24.5
m	0	100	0.43	0.51	10.9	21.4
l	0	100	0.21	0.39	4.0	10.3
k	100	0	0.20	0.50	18.4	36.8
j	100	0	0.45	0.65	34.0	52.3
i	51	49	0.36	0.48	9.9	20.6
h	76	24	0.25	0.40	10.5	26.3
g	100	0	1.80	2.66	?	?
f	60	40	0.70	0.90	13	14.4
@	80	20	0.25	0.53	4.0	7.5
e	0	100	0.40	0.67	15.0	22.4
€	100	0	0.24	0.50	13.7	27.4
#	65	35	0.40	0.47	22.0	46.8
d	100	0	0.30	0.55	30.0	54.5
c	100	0	0.65	0.97	13.0	13.4
b	100	0	0.15	0.34	1.0	2.9
a	/	/	0.25	0.45	6.0	13.3
<b>Range</b>	0-100	0-100	0.12-1.80	15-2.66	1-36+	2.9-54.5
<b>Mean</b>	70.7%	29.3%	0.38	0.58	12.73	24.5

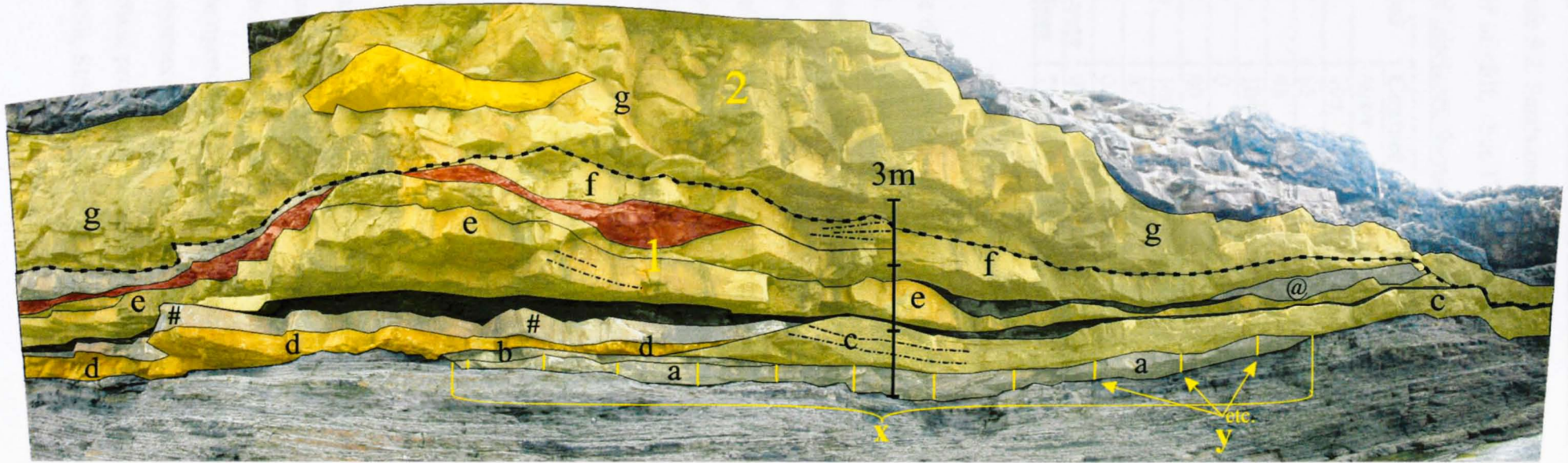


Figure 5.1. Four-photo panel showing a close-up of the central section of the Trusklieve outcrop of the Tullig Sandstone, showing facies interpretation, bed labels and measurements described in Section 5.2. X = bed length. Y = evenly-spaced bed thickness measurements. See Table 3.1 for facies definitions.

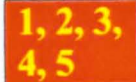
Key					
	Sm, Sh		Smc, Shc		Flh
	Sp, St, Sl, Sr		Sc		Fls
			Ccm		Flm
					Major erosional channel storey bases
					Bed boundaries (frequently coincident with facies boundaries)
					Foresets and reactivation surfaces
					Storey numbers in the Tullig Sandstone

Table 5.2. Sandstone bed data for the Tullig Sandstone, Trusklieve: Storey 3, southern half of cliff. See Fig. 4.3 for the photomontage and interpretation of this outcrop. Bed labels are shown in Fig. 4.3b.

Bed	Contact type		Thickness (m)		Bed length (m)	Continuity (length/thick)
	%s/s	%s/m	Mean	Max.		
R	100	0	0.50	0.75	~29	38.7
Q	85	15	0.27	0.50	37?	74.0
P	95	5	0.55	0.82	10.4	12.7
O	100	0	0.30	0.55	~3	5.5
N	0	100	0.28	0.42	>23	>54.8
N'	90	10	0.42	0.81	7	8.6
M	100	0	0.26	0.52	20.5	39.4
L	65	35	0.19	0.38	>4	>10.5
K	0	100	0.45	0.72	>17	>23.6
<b>Range</b>	0-100	0-100	0.19-0.55	0.38-0.82	3-37	5.5-54.8
<b>Mean</b>	70.6%	29.4%	0.36	0.61	16.8	30.5

The data on which the vertical proportion curve (Fig. 5.2) is based are shown in Table 5.3. The percentages at each 0.5m height interval were calculated from the observations made at these heights every 2m across the whole width of the outcrop. The data show that the dominant facies in the Tullig Sandstone at Trusklieve are Sm/Sh and Sl/Sp/St, comprising 34.1% and 49.9% respectively of the outcrop area. The distribution of facies Sm/Sh shows relative increases near the top and base of the outcrop, while facies Sl/Sp/St dominate the middle section; thus, there is a crude inversely proportional relationship between the abundance of these two facies. It should be noted, however, that because the fifth storey, comprising entirely cross-bedded facies, was set back from the cliff top and therefore not visible in the photomontages, the statistics do not reflect the return to cross-bedded facies at the top of the sandbody.

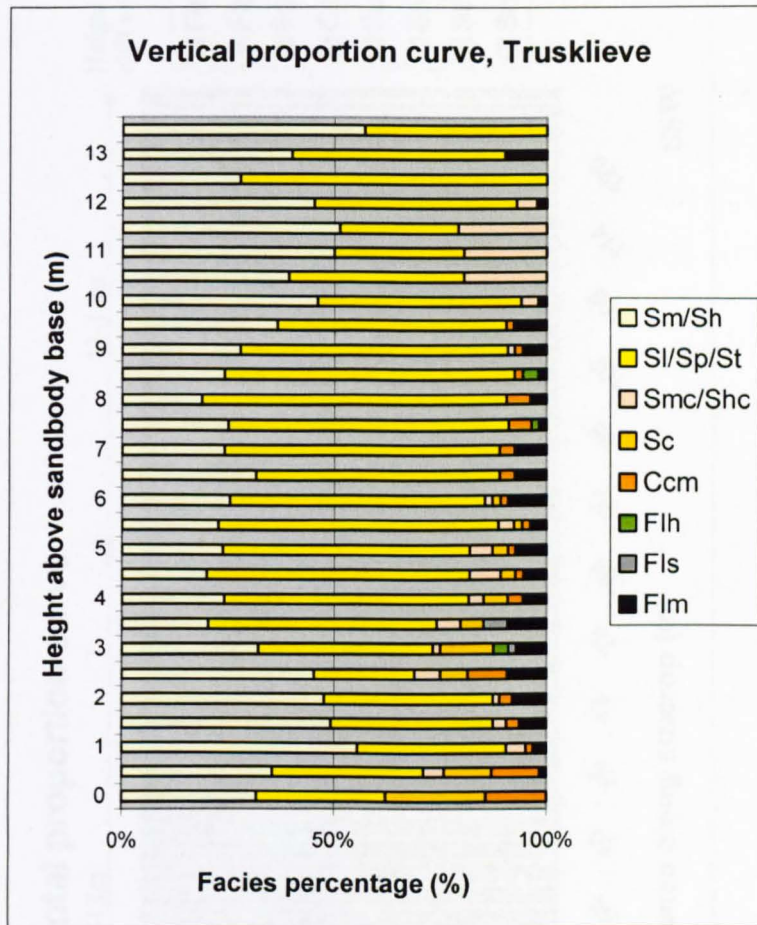
The vertical proportion curve shows clearly that finer-grained material is more abundant in the lower three-quarters of the sandbody, while conglomeratic facies are mostly confined to the lower two-thirds (Fig. 5.2). There is an overall decrease in heterogeneity upwards within the Tullig Sandstone (Fig. 5.2), which would be more pronounced if the homogeneous Storey 5 (facies Sp/St/Sl) was represented in the vertical proportion curve. The overall net to gross of the outcrop (considering facies Sm/Sh, Sl/Sp/St, Smc/Shc and Sc as pay and the other facies as non-pay) is 91.5%.

Table 5.3. Trusklieve, whole outcrop: Tullig Sandstone vertical facies proportions. See Figs 4.1 and 4.3 for relevant photomontages and interpretations. The data for the graph appears in App. C2.

Height from base of sand-body (m)	% of facies occurrence 							
		Sm/Sh	Sl/Sp/St	Smc/Shc	Sc	Ccm	Flh	Fls
13.5	57.14	42.86	0	0	0	0	0	0
13.0	40.00	50.00	0	0	0	0	0	10.00
12.5	27.78	72.22	0	0	0	0	0	0
12.0	45.24	47.62	4.76	0	0	0	0	2.38
11.5	51.16	27.91	20.93	0	0	0	0	0
11.0	50.00	30.43	19.57	0	0	0	0	0
10.5	39.13	41.30	19.57	0	0	0	0	0
10.0	46.00	48.00	4.00	0	0	0	0	2.00
9.5	36.54	53.85	0	0	1.92	0	0	7.69
9.0	27.78	62.96	1.85	0	1.85	0	0	5.56
8.5	24.08	68.52	0	0	1.85	3.70	0	1.85
8.0	18.87	71.70	0	0	5.66	0	0	3.77
7.5	25.00	66.07	0	0	5.36	1.79	0	1.78
7.0	24.07	64.82	0	0	3.70	0	0	7.41
6.5	31.48	57.41	0	0	3.70	0	0	7.41
6.0	25.45	60.00	1.82	1.82	1.82	0	0	9.09
5.5	22.64	66.04	3.77	1.89	1.89	0	0	3.77
5.0	23.64	58.18	5.45	3.64	1.82	0	0	7.27
4.5	20	61.82	7.27	3.64	1.82	0	0	5.45
4.0	24.07	57.41	3.70	5.56	3.70	0	0	5.56
3.5	20.37	53.70	5.56	5.56	0	0	5.55	9.26
3.0	32.14	41.07	1.79	12.50	0	3.57	1.79	7.14
2.5	45.31	23.44	6.25	6.25	9.38	0	0	9.37
2.0	47.62	39.68	1.59	0	3.17	0	0	7.94
1.5	49.21	38.10	3.17	0	3.17	0	0	6.35
1.0	55.56	34.92	4.76	0	1.59	0	0	3.17
0.5	35.48	35.48	4.84	11.29	11.29	0	0	1.62
0	31.75	30.16	0	23.81	14.28	0	0	0
<b>Total %</b>	<b>34.09</b>	<b>49.89</b>	<b>4.30</b>	<b>3.18</b>	<b>3.25</b>	<b>0.35</b>	<b>0.28</b>	<b>4.66</b>

The horizontal proportion curve for Trusklieve gives a visual representation of the lateral facies distribution across the outcrop (Fig. 5.3). Since the outcrop cliff-face is oriented almost parallel to the dominant flow direction (northeast), the graph represents the facies variability in a flow-parallel direction (0m being at the downstream, northeastern end of the outcrop and 124m being the upstream, southwestern, end).

Figure 5.2. A histogram of the data in Table 5.3, showing the percentage of each facies at different heights within the Tullig Sandstone at Trusklieve.



The primary feature apparent from the horizontal proportion curve is that the very fine and very coarse facies are not evenly distributed across the width of the outcrop. The fine-grained facies (Flh, Fls, Flm) are more areally abundant at the south-southwest end of the amphitheatre, and the conglomeratic facies (Ccm, Smc, Sc) are most abundant in the southern half of the outcrop. The peak in conglomeratic facies around 12m from the northeast end of the outcrop is slightly misleading, since the exposed vertical thickness for the first 16m along the outcrop is only 3m (rather than between 11 and 15 m as elsewhere along the outcrop), meaning that only one or two thin beds of Ccm and Smc were sufficient to give high percentages for these two facies.

Areal percentages of facies Sm/Sh and Sl/Sp/St are crudely inversely proportional, one increasing when the other decreases and vice versa. There is no apparent trend in

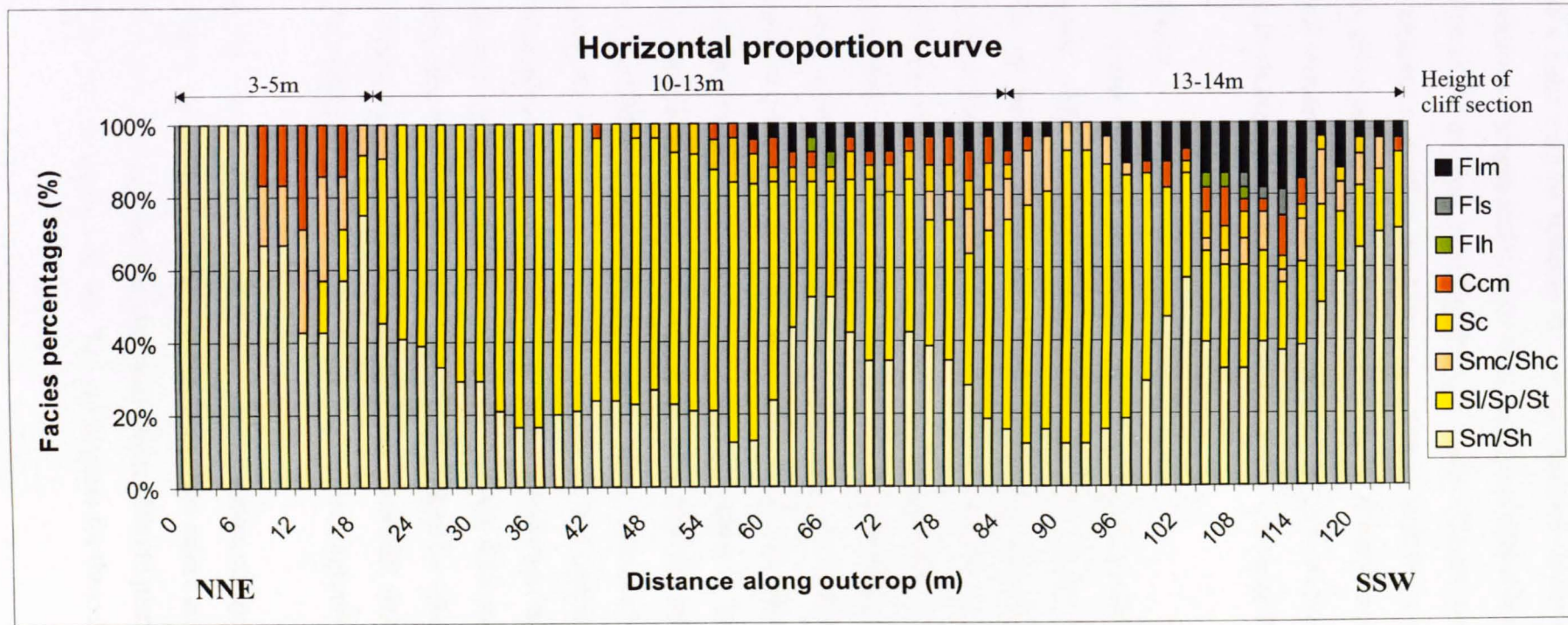


Figure 5.3. Horizontal proportion curve for the Tullig Sandstone outcrop at Trusklieve. Facies percentages were recorded every two metres along the cliff section, showing how facies changes along the length of the exposure. The outcrop is oriented close to parallel with palaeoflow, so the facies variability reflects flow-parallel changes within the channel system. Outcrop heights are noted above the graph.

the abundance of these facies from one end of the outcrop to the other. The apparent absence of a trend may be because the facies represent channel fills and bar forms, since the width and length scales of these architectural elements are close to or greater than the size of the outcrop, meaning that any facies changes associated with passing from one element to another would not be apparent within the outcrop. In addition, the superposition of one storey upon another, each of which may represent different architectural elements, means that facies trends associated with these elements will be overlain in the horizontal proportion curve and will not be separately distinguishable.

#### *5.3.1.2 Pulleen*

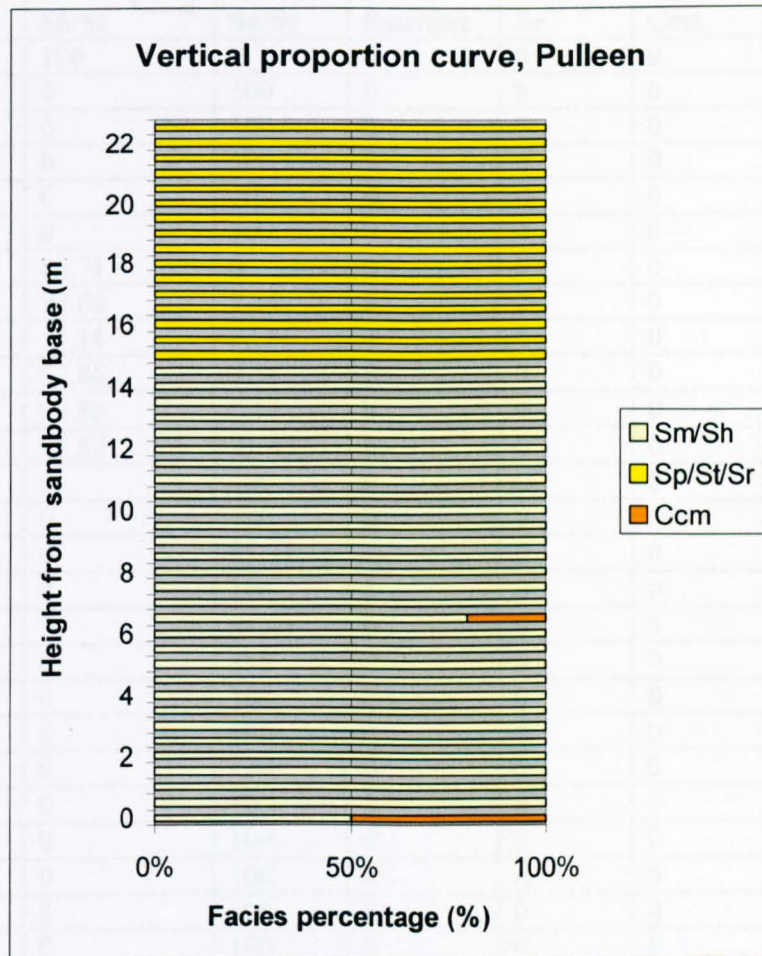
The style of the outcrop at Pulleen made detailed continuity and connectivity measurements difficult; nonetheless, estimates of these two properties and calculations of net to gross were made using the log (Fig. 4.9) and outcrop photomontages (Figs 4.10 and 4.11). Of the beds visible in the cliff section (Fig. 4.10), 36.5% are continuous across the extent of the outcrop. Continuity values could not be estimated for other beds due to the impossibility of making accurate measurements from such a long distance away from the cliff-face exposures on the headland and in the stack. A visual comparison with Trusklieve puts the continuity index at Pulleen higher, estimated at ~56 (beds extending for an estimated 20m with average thicknesses of 0.36m; see Section 4.3.2.3), meaning better lateral continuity. No low permeability facies (Flh, Fls, Flm) were encountered within the Tullig Sandstone in either the log or the cliff sections; all bed contacts were sand-on-sand giving a connectivity value of 100%. The facies distribution was calculated from the sedimentary log and photomontages shown in Figs 4.9, 4.10 and 4.11. Table 5.4 and Fig. 5.4 show the facies distribution data. To highlight the change in facies between storeys, the facies groupings have been modified; facies Sh and Sl, and facies Sp and St, have been grouped together since they are commonly associated with each other.

In summary, the outcrop at Pulleen is very homogeneous, comprising facies Sm, Sh, Sp, St and Sr to the exclusion of all other facies except minor amounts of Ccm. There is an upward change from massive sandstone (facies Sm) to planar and trough cross-bedded sandstone (facies Sp and St). The net to gross for the outcrop is 98.48%.

Table 5.4. Tullig Sandstone vertical facies proportions, Pulleen outcrop. See Figs 4.9, 4.10 and 4.11 for a log, photomontages and interpretations of this outcrop.

Height from base of sandbody (m)	% of facies occurring Sh/SI 	Sp/St 	Ccm 
22.5	0	100	0
22.0	0	100	0
21.5	0	100	0
21.0	0	100	0
20.5	0	100	0
20.0	0	100	0
19.5	0	100	0
19.0	0	100	0
18.5	0	100	0
18.0	0	100	0
17.5	0	100	0
17.0	0	100	0
16.5	0	100	0
16.0	0	100	0
15.5	0	100	0
15.0	0	100	0
14.5	100	0	0
14.0	100	0	0
13.5	100	0	0
13.0	100	0	0
12.5	100	0	0
12.0	100	0	0
11.5	100	0	0
11.0	100	0	0
10.5	100	0	0
10.0	100	0	0
9.5	100	0	0
9.0	100	0	0
8.5	100	0	0
8.0	100	0	0
7.5	100	0	0
7.0	100	0	0
6.5	80	0	20
6.0	100	0	0
5.5	100	0	0
5.0	100	0	0
4.5	100	0	0
4.0	100	0	0
3.5	100	0	0
3.0	100	0	0
2.5	100	0	0
2.0	100	0	0
1.5	100	0	0
1.0	100	0	0
0.5	100	0	0
0	50	0	50
<b>Total %</b>	<b>63.70</b>	<b>34.78</b>	<b>1.52</b>

Figure 5.4. A histogram of the data in Table 5.4, showing the percentage of each facies at different heights within the Tullig Sandstone at Pulleen. Note the good homogeneity of the outcrop, and the upward change in facies.



### 5.3.1.3 Killard

The simple, laterally continuous bed geometries and architecture of the Killard outcrop made detailed measurements of bed data unnecessary. Nearly all beds, with very few exceptions (detailed in Section 4.3.3), are continuous for the length of the outcrop (50-160m), giving a very high continuity index and indicating a higher degree of lateral continuity compared with Truskleeve. The continuity index is estimated to be ~150 (using the mean bed thickness of 0.32m from Section 4.3.3.2, and a conservative mean bed length estimate of 50m). Regarding connectivity, 90-100% of the contacts are sand on sand within each storey, again significantly different from Truskleeve.

Table 5.5. Tullig Sandstone vertical facies proportions: northern limb of syncline at Killard (see Fig. 4.13a and b). For graph see Fig. 5.5.

Height from base (m)	% of facies					
	Sh/SI 	Sp/St 	Smc/Shc 	Sc 	Ccm 	Fls/Flm 
21.5	100	0	0	0	0	0
21.0	0	100	0	0	0	0
20.5	0	100	0	0	0	0
20.0	0	100	0	0	0	0
19.5	0	100	0	0	0	0
19.0	0	100	0	0	0	0
18.5	85.71	0	0	0	0	0
18.0	92.86	7.14	0	0	0	0
17.5	57.14	42.86	0	0	0	0
17.0	92.86	7.14	0	0	0	0
16.5	92.86	7.14	0	0	0	0
16.0	78.57	21.43	0	0	0	0
15.5	0	100	0	0	0	0
15.0	0	100	0	0	0	0
14.5	0	85.71	0	0	0	0
14.0	0	100	0	0	0	0
13.5	0	71.43	0	0	0	0
13.0	0	100	0	0	0	0
12.5	0	100	0	0	0	0
12.0	0	100	0	0	0	0
11.5	0	100	0	0	0	0
11.0	0	100	0	0	0	0
10.5	0	100	0	0	0	0
10.0	0	100	0	0	0	0
9.5	0	100	0	0	0	0
9.0	0	100	0	0	0	0
8.5	0	100	0	0	0	0
8.0	0	100	0	0	0	0
7.5	0	100	0	0	0	0
7.0	0	100	0	0	0	0
6.5	0	100	0	0	0	0
6.0	14.285	85.71	0	0	0	0
5.5	7.14	71.43	0	0	0	21.43
5.0	35.71	7.14	0	0	0	57.14
4.5	92.86	0	0	0	0	7.14
4.0	100	0	0	0	0	0
3.5	92.86	0	0	0	0	7.14
3.0	100	0	0	0	0	0
2.5	100	0	0	0	0	0
2.0	85.71	0	0	0	7.14	7.14
1.5	85.71	0	14.29	0	0	0
1.0	85.71	0	14.29	0	0	0
0.5	85.71	0	0	14.29	0	0
0	85.71	0	14.29	0	0	0
<b>Total %</b>	<b>35.72</b>	<b>59.25</b>	<b>0.97</b>	<b>0.33</b>	<b>0.16</b>	<b>3.57</b>

The lack of heterogeneity in the outcrop allowed quantitative assessments to be made in the field, without requiring extensive bed measurements. Facies distributions were quantified for part of the outcrop (see Fig. 4.13), whilst the rest of the outcrop was quantified using the logs, which could be extrapolated across the outcrop due to the excellent lateral continuity. The results of the facies distribution quantification can be seen in Table 5.5 and Fig. 5.5. To highlight the change in facies between storeys, the facies groupings have been modified; facies Sh and Sl, facies Sp and St, and facies Fls and Flm have been grouped to give three facies groups rather than six separate facies.

The most apparent change within the Tullig Sandstone at Killard is the transition from horizontal and low-angle bedding in the lower third to trough and planar cross bedding in the upper two-thirds (Fig. 5.5), a change also seen in the Pulleen outcrop. Another similarity between the two localities is the concentration of coarse facies (Smc/Shc, Sc, Ccm) at the base of the sandbody. The distribution of fine-grained facies at Killard is concentrated into a few thin beds interspersed throughout the sandbody; however, there is a clear decrease in fine-grained facies from base to top. As with previous localities, the outcrop at Killard is dominated by facies Sh, Sp and St, with the addition of facies Sl and Sd, which were not abundant at Trusklieve or Pulleen, and with the almost complete loss of facies Sm.

An overall net to gross of 95.5% can be calculated by adding the percentages of sandy facies given in Table 5.5 above. This value is comparable with the 98.6% calculated for Pulleen. The high net to gross at Killard, combined with the good connectivity and lateral continuity, would indicate an excellent reservoir potential in such a sandbody. The Killard outcrop of the Tullig Sandstone is also significantly more homogeneous than the Trusklieve outcrop.

#### *5.3.1.4 Carrowmore Point*

Bed measurements at Carrowmore Point were made through the lowermost, and most heterogeneous, few metres of the outcrop on the north limb (see Table 5.6). The rest of this outcrop exhibited a simple architecture similar to Killard, with a very high degree of lateral continuity and regular bed thicknesses, and measurements of bed data were therefore not made through it.

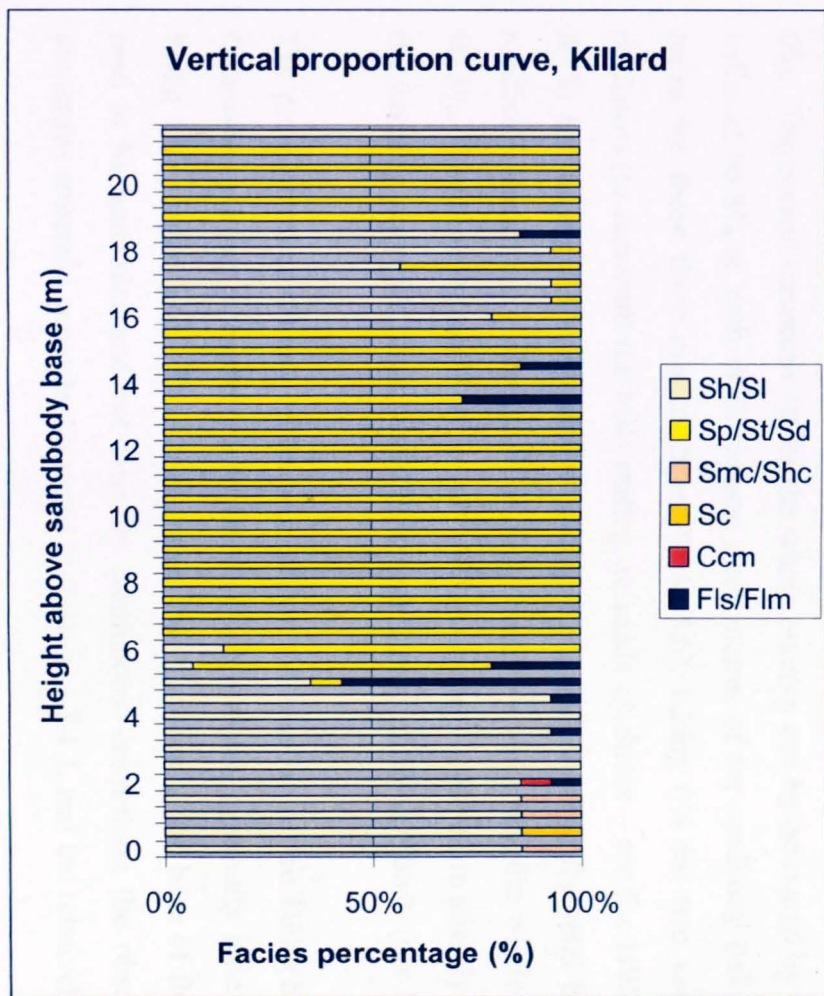


Figure 5.5. A histogram of the data in Table 5.5, showing the percentage of each facies at different heights within the Tullig Sandstone at Killard, north limb.

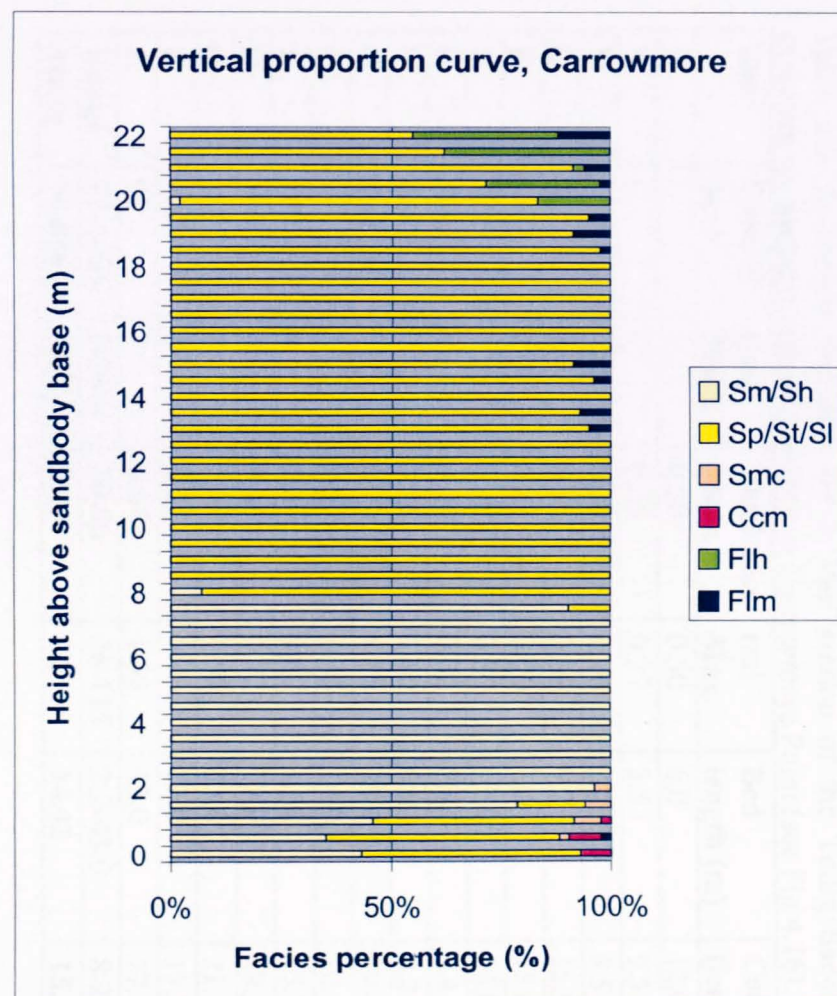


Figure 5.6. A histogram of the data in Table 5.7, showing the percentage of each facies at different heights within the Tullig Sandstone at Carrowmore Point, north limb.

Table 5.6. Sandstone bed data for a 35m section of the Tullig Sandstone: cliff exposure on northern limb of anticline at Carrowmore Point (see Fig 4.16).

Bed	Contact %/s/s	type %/s/m	Thickness (m)		Bed length (m)	Continuity (length/thick)
			Mean	Max.		
O	/	/	0.30	0.50	6.0	12.0
N	/	/	0.25	0.27	2.5	9.3
M	/	/	0.20	0.26	2.2	8.5
L	72	28	0.50	0.58	9.2	15.9
K	100	0	0.42	0.50	7.5	15.0
J	100	0	0.70	0.80	13.0	16.3
I	100	0	0.23	0.32	2.8	8.8
H	100	0	0.75	1.10	9.0	8.2
G	100	0	0.70	1.15	35.0	30.4
F	/	/	0.55	1.35	14.0	10.4
E	100	0	0.30	0.80	12.2	15.3
D	100	0	0.40	0.72	13.9	19.3
C	100	0	0.90	1.55	33.0	21.3
B	100	0	0.55	0.75	13.0	17.3
A	93	7	0.65	1.55	43.0	27.7
<b>Range</b>	<b>72-100%</b>	<b>0-28%</b>	<b>20-90</b>	<b>26-115</b>	<b>2.2-43.0</b>	<b>8.2-27.7</b>
<b>Mean</b>	<b>96.8%</b>	<b>3.2%</b>	<b>0.49</b>	<b>0.81</b>	<b>14.42</b>	<b>15.7</b>

Table 5.6 above shows that even in the most heterogeneous part of the outcrop, the connectivity is still very high, at 96.82%. Connectivity continues to be high in the upper three-quarters of the sandbody, with all but four beds having values of 100%; of those four, one has an estimated value of 90% while the other three have values of 0%. The overall connectivity for the whole outcrop can be estimated by according a value of 96.8% to each of the lowest three metres of the sandbody (taken from the mean for those three metres, from Table 5.6), taking 0% for two metres of the thickness (to represent the beds resting on muds or shales – see the NW log in Fig. 4.15) and taking 100% for the remaining 17m, and dividing the total by 22m (the sandbody thickness). The result is a connectivity value for the whole outcrop of 90.5%. The high connectivity in most of the outcrop is therefore slightly reduced by the laterally extensive fine-grained beds near the top of the sandbody (see Fig. 4.15).

The poor lateral continuity of the beds within the first 3m of the Tullig Sandstone at Carrowmore Point is expressed by the low value of the continuity index, the mean being 15.7 (Table 5.6). The value shows that the beds at the base of the sandbody tend to be lenticular and not laterally continuous, confirming the observations of numerous erosional contacts discussed in Section 4.3.4.1, and the relatively low mean

bed length (14.42m). However, the overall lateral continuity improves greatly above the first 3m, with the great majority of beds continuing across the outcrop (~80m). From the log, 48 beds are counted through the upper 19m; adding together their 80m lengths and the lengths listed in Table 5.6, the mean bed length for the whole outcrop is calculated to be 64.4m. Bed thicknesses decrease upwards from the 0.49m average calculated for the lowermost 3m; the mean bed thickness of the 48 beds over the upper 19m is 0.39m, and the mean cross bed thickness is 0.29m (Section 4.3.4.1). The continuity index for the upper 19m is calculated as 205.1 (for a representative bed 0.39m thick and 80m in length). The outcrop average for continuity index is therefore estimated to be 179.3, taking 15.7 to represent the lower 3m and 205.1 to represent the upper 19m ( $\{3 \times 15.7 + 19 \times 205.1\} / 22 = 179.3$ ). As a whole, the outcrop thus shows high lateral continuity, similar to Killard.

It was not possible to photograph the whole outcrop, therefore for facies distribution calculations, six transects were made through the part of the outcrop where the full thickness of the sandbody was exposed. This revealed that the beds in the upper two-thirds were very laterally continuous, and could be traced across the entire length of the exposure (80m+). For this reason, the log was used to extrapolate facies across the outcrop, with the transect observations added to the data where they differed from the log observations. The resulting data is shown in Table 5.7, and in the accompanying vertical proportion graph in Fig. 5.6. A horizontal proportion curve was also produced from the data, and is shown in Fig. 5.7. The data table for the horizontal proportions is shown in App. C3.

Table 5.7 and Figure 5.6 show that within the lower few metres of the sandbody at Carrowmore, there is an upward increase in homogeneity and in the areal percentage of sandy facies. The net to gross ratio for the sandbody, obtained by summing the total percentages of sandy facies given in Table 5.7, is 96%, a very high value, similar to Killard and Pulleen. The high degree of connectivity (Table 5.6), when taken together with this high net to gross ratio, would give an excellent reservoir potential. The horizontal proportion curve (Fig. 5.7) reveals no pronounced trends along the length of the outcrop. The lateral continuity discussed above means that facies are continuous across the outcrop, and the percentages of each facies remains quite consistent from one side of the exposure to the other, a distance of over 160 metres.

Table 5.7. Tullig Sandstone vertical facies proportions: northern limb of anticline at Carrowmore (see Fig. 4.16). Figure 5.6 shows a graph of this data.

Height from base (m)	% of facies					
	Sm/Sh 	Sp/St 	Shc/Smc 	Ccm 	Flh 	Fls/Flm 
22.0	0	54.76	0	0	33.33	11.91
21.5	0	61.90	0	0	38.10	0
21.0	0	91.67	0	0	2.38	5.95
20.5	0	71.43	0	0	26.19	2.38
20.0	2.38	80.95	0	0	16.67	0
19.5	0	95.24	0	0	0	4.76
19.0	0	91.67	0	0	0	8.33
18.5	0	97.62	0	0	0	2.38
18.0	0	100	0	0	0	0
17.5	0	100	0	0	0	0
17.0	0	100	0	0	0	0
16.5	0	100	0	0	0	0
16.0	0	100	0	0	0	0
15.5	0	100	0	0	0	0
15.0	0	91.67	0	0	0	8.33
14.5	0	96.43	0	0	0	3.57
14.0	0	100	0	0	0	0
13.5	0	92.86	0	0	0	7.14
13.0	0	95.24	0	0	0	4.76
12.5	0	100	0	0	0	0
12.0	0	100	0	0	0	0
11.5	0	100	0	0	0	0
11.0	0	100	0	0	0	0
10.5	0	100	0	0	0	0
10.0	0	100	0	0	0	0
9.5	0	100	0	0	0	0
9.0	0	100	0	0	0	0
8.5	0	100	0	0	0	0
8.0	7.14	92.86	0	0	0	0
7.5	90.48	9.52	0	0	0	0
7.0	100	0	0	0	0	0
6.5	100	0	0	0	0	0
6.0	100	0	0	0	0	0
5.5	100	0	0	0	0	0
5.0	100	0	0	0	0	0
4.5	100	0	0	0	0	0
4.0	100	0	0	0	0	0
3.5	100	0	0	0	0	0
3.0	100	0	0	0	0	0
2.5	100	0	0	0	0	0
2.0	96.43	0	3.57	0	0	0
1.5	78.57	15.48	5.95	0	0	0
1.0	45.24	46.43	5.95	2.38	0	0
0.5	34.52	53.57	2.38	7.14	0	2.38
0	42.86	50.00	0	7.14	0	0
<b>Total %</b>	<b>31.06</b>	<b>64.21</b>	<b>0.40</b>	<b>0.37</b>	<b>2.59</b>	<b>1.37</b>

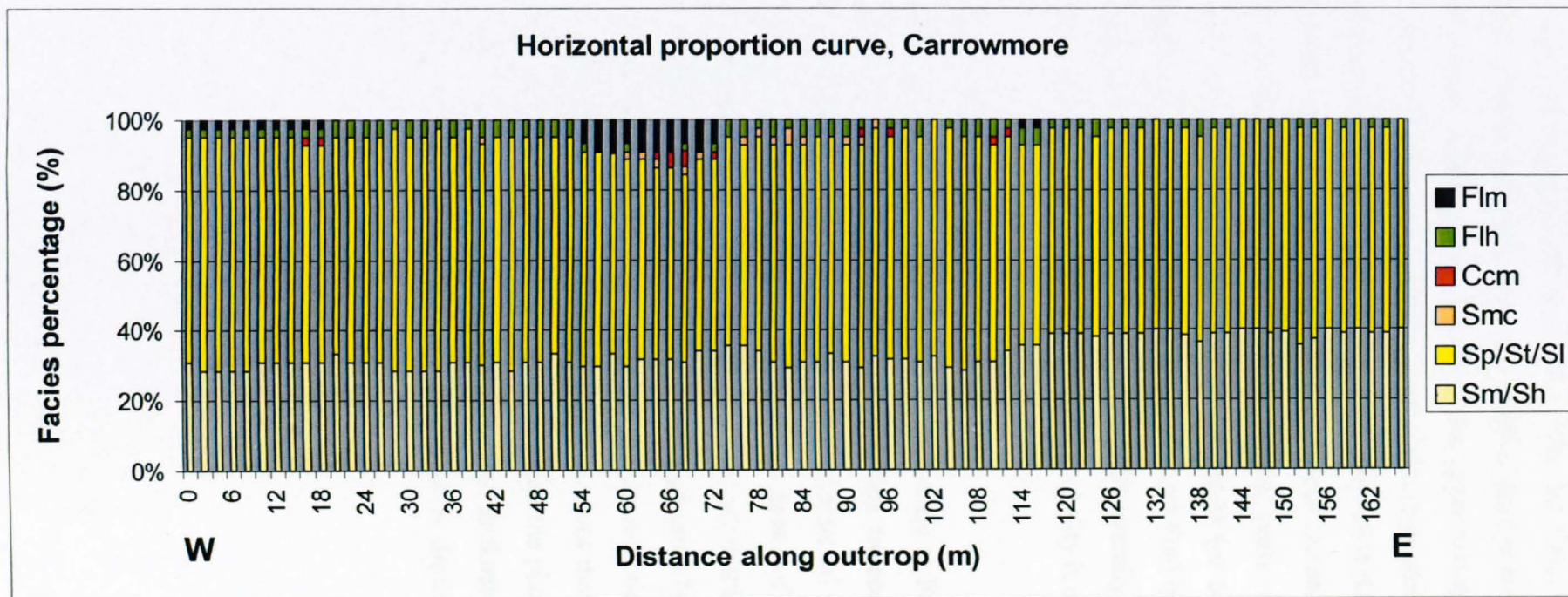


Figure 5.7. Horizontal proportion curve for the Tullig Sandstone outcrop at Carrowmore Point. Facies percentages were recorded every two metres along the cliff section, showing how facies changes along the length of the exposure. From 0 to 80 metres the whole thickness of the sandbody is exposed, and the measurements are from actual observations; from 80m to 168m the sandbody is only exposed for its lower few metres, and the log has been used to extrapolate observations into the area of no exposure. The outcrop is oriented close to perpendicular to palaeoflow, so the facies variability reflects changes across the width of the channel system.

The facies distribution at Carrowmore Point is similar to the preceding localities in two main ways: firstly, the coarse facies (Smc/Shc, Sc, Ccm) are concentrated at the base of the sandbody; secondly, there is a marked change from facies Sm/Sh in the lower third to cross-bedded facies (Sp, St) in the upper two-thirds (compare Fig. 5.6 with Figs 5.4 and 5.5, and see logs in Fig. 4.15). The most notable difference between the Tullig Sandstone at Carrowmore Point and at previously discussed localities is the occurrence of fine-grained facies near the very top of the sandbody at Carrowmore Point. At Trusklieve, Pulleen and Killard the upper parts of the Tullig Sandstone comprise only a low percentage of fine-grained facies (or none at all), whereas at Carrowmore Point up to 45% by area is facies Flh and Fls/Flm within the uppermost 4m. The fact that the fine-grained beds are frequently laterally continuous reduces the connectivity within this upper 4m, and the reservoir quality is also reduced as a result.

#### *5.3.1.5 Furreera, Liscannor Bay*

The homogeneity of the single storey Tullig Sandstone at Furreera made gathering bed measurement and detailed vertical proportion data unnecessary. It was apparent from observation that there is almost no fine-grained material within the sandbody (as discussed in Section 4.3.5.1), giving it a net to gross of close to 100%. The connectivity is therefore also 100%. Observation reveals that lateral continuity is low, because the dominant facies type at Furreera is trough cross bedding, and the outcrop orientation (east-west) is normal to palaeoflow (mean direction 347°; Section 4.3.5), so that numerous trough-shaped internal erosion surfaces that form the base of beds are displayed in the cliff. Measurements made from the photomontage in Fig. 4.23 give a mean bed length of 7.16m, and the mean bed thickness is 0.29m (see Section 4.3.5.1), giving a continuity index of 25. This value is similar to the 27.5 calculated for Trusklieve.

### 5.3.2 Tullig Cyclothem mouthbar sandbodies

#### 5.3.2.1 Tullig Point mouthbar

The mouthbar sandbody at Tullig Point is exposed in an inaccessible cliff section, as described in Section 4.3.6, but it was possible to calculate most values for the bed data using the accurately scaled interpreted photomontage, and the log taken at Tullig Point (Table 5.8). Mean bed thickness calculated from the photomontage is 0.66m, but when calculated from the log, mean bed thickness is found to be 0.18m, and the modal thickness is lower still (0.1-0.15m; see App. B3). The discrepancy is likely to be due to the difficulty of picking out individual thin beds from the cliff photomontage, the photos for which were taken from a long distance away. In some cases, thin beds of the same facies have been combined in the interpreted photomontage. This artificial amalgamation of beds for measurement purposes causes a decrease in the continuity index.

Table 5.8. Sandstone (and *fine-grained*) bed data for the mouthbar sandbody at Tullig Point (Fig. 4.24). Minimum bed thicknesses are shown because, unlike for Tullig Sandstone outcrops, the majority of beds are continuous across the whole outcrop and do not taper to zero. Continuity indices are only calculated for the sandstone beds.

Bed	Contact %/s	type %/s/m	Thickness (m)			Bed length (m)	Continuity (length/thick)
			Min.	Mean	Max.		
M	100	0	0.48	0.74	1.05	>80	>76.2
L	0	100	0.45	0.80	1.00	>80	>80.0
<i>f</i>	-	-	0.07	0.12	0.23	>80	
K	0	100	0.55	0.70	1.00	>80	>80.0
<i>e</i>	-	-	0.12	0.19	0.54	>80	
J	100	0	0.05	0.40	0.67	>80	>119.4
<i>d</i>	-	-	0.05	0.08	0.15	>80	
I	100	0	0.55	0.60	0.75	>80	>106.7
H	0	100	0.18	0.22	0.35	>80	>228.6
<i>c</i>	-	-	0.03	0.12	0.23	>80	
G	0	100	0.27	0.50	0.73	>80	>109.6
<i>b</i>	-	-	0	0.09	0.11	32	
F	100	0	0.13	0.29	0.82	>80	>97.6
E	100	0	0.28	0.40	0.53	>80	>150.9
D	100	0	0.35	0.60	0.70	>80	>114.3
C	47.4	52.6	0.41	0.50	0.68	>80	>117.6
<i>a</i>	-	-	0	0.16	0.22	40	
B	100	0	0	0.40	1.87	45	24.1
A	/	/	0	1.10	1.52	68	44.7
Range	0-100	0-100	0-0.55	0.22- 1.10	0.35- 1.87	45->80	24.1-228.6
Mean	62.3%	37.7%	0.13	0.66	0.72	76.08	>103.8

The beds in the mouthbar sandbody are very laterally continuous in comparison to those seen in the channel sandbodies, with a high mean continuity index of >103.8 (which would be higher if the bed thicknesses observed from the log, rather than from the photomontage, were used). The connectivity, at 62.3%, is much lower than for the fluvial channel sands, because the laterally continuous fine-grained beds interrupt the vertical sand connectivity. The net to gross for this outcrop, calculated by summing the percentages of sandy facies given in Table 5.9, is 91.8%, although it is likely that if millimetre-scale grainsize variations were considered this figure would be slightly lower. The lower vertical connectivity, as compared with the Tullig Sandstone, also reduces the quality of the mouthbar in terms of reservoir potential of such sandbodies.

Table 5.9. Tullig Point mouthbar sandbody vertical facies proportions (see Fig. 4.23).  
See Fig. 5.8 for corresponding vertical proportion curve.

Height from erosive base of sandbody (m)	% chance of facies occurring Sh/Sh <sub>2</sub> /Sl <sub>2</sub> 	 Sp/Sp <sub>2</sub> /St	 Flh	 Fls/Flm
10.0	100	0	0	0
9.5	100	0	0	0
9.0	100	0	0	0
8.5	93.1	6.9	0	0
8.0	67.65	17.65	14.7	0
7.5	29.41	64.71	5.88	0
7.0	31.43	31.43	37.14	0
6.5	71.43	8.57	20	0
6.0	66.67	5.55	16.67	11.11
5.5	36.11	33.33	5.56	25
5.0	22.22	66.67	0	11.11
4.5	55.56	38.89	0	5.55
4.0	83.33	16.67	0	0
3.5	59.46	32.43	0	8.11
3.0	59.46	29.73	0	10.81
2.5	86.49	13.51	0	0
2.0	91.89	8.11	0	0
1.5	100	0	0	0
1.0	100	0	0	0
0.5	100	0	0	0
0	100	0	0	0
<b>Total %</b>	<b>74.01</b>	<b>17.82</b>	<b>4.76</b>	<b>3.41</b>

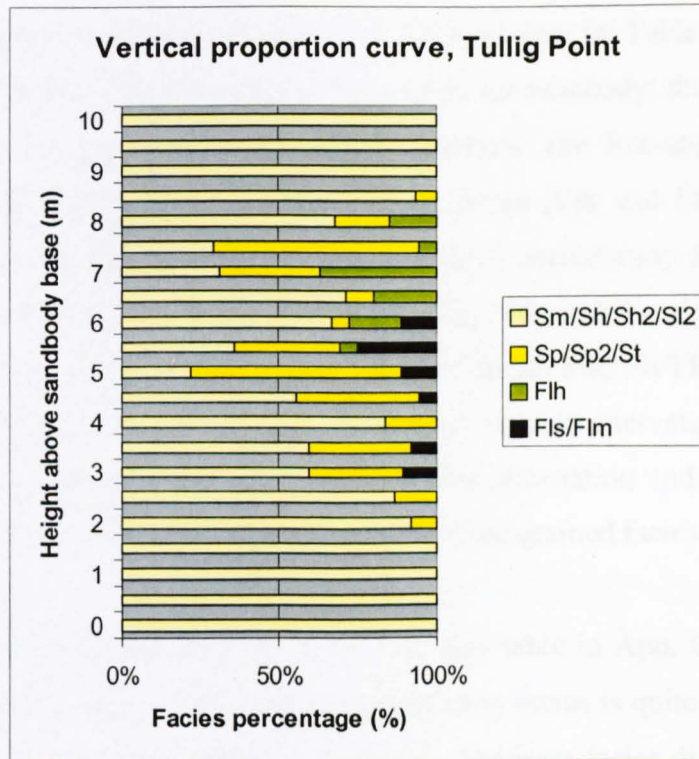


Figure 5.8. A graph of the data in Table 5.9, showing the percentage of each facies at different heights within the mouthbar sandbody at Tullig Point.

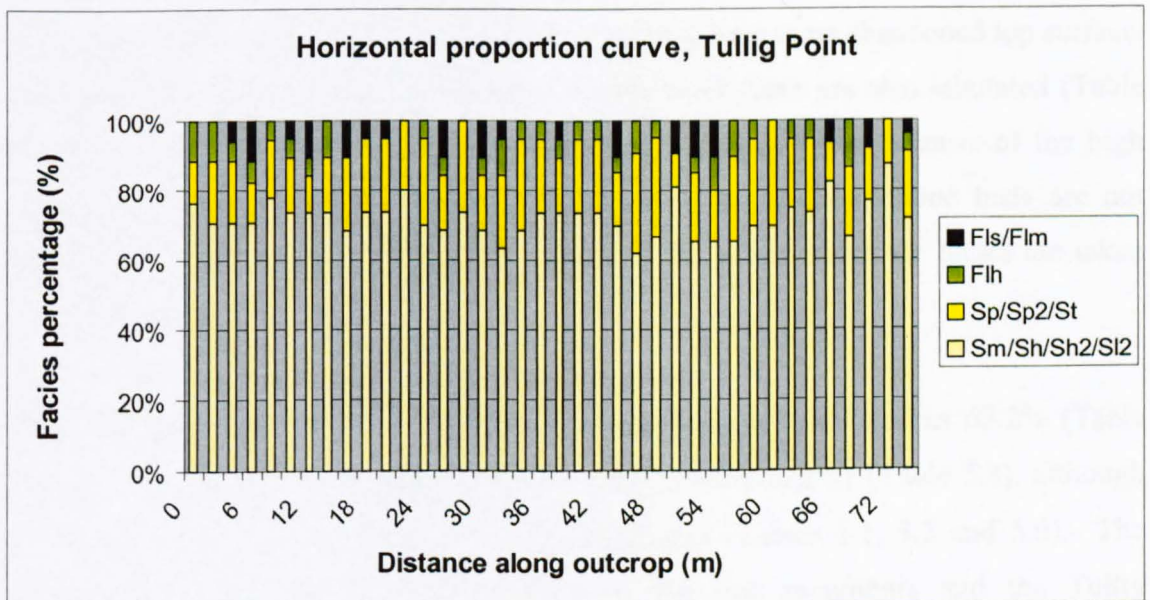


Figure 5.9. A graph of the data in App. C5, showing the percentage of each facies at every two metres along the length of the outcrop of the mouthbar sandbody at Tullig Point.

The vertical proportion curve in Fig. 5.8 (data shown in Table 5.9) shows the distribution of facies within the Tullig Point mouthbar sandbody; the dominant facies in the outcrop are horizontally laminated sandstone and low-angle cross-bedded sandstone (facies Sh/Sh<sub>2</sub>/Sl/Sl<sub>2</sub>). Fine-grained facies (Flh and Fls/Flm) are more common within the upper half of the unit, and are clustered away from the very top and base. Both the vertical proportion curve (Fig. 5.8) and the photomontage (Fig. 4.23) show the apparent pattern of distribution of facies Flh, Fls/Flm and Sp/Sp<sub>2</sub>/St, with the three facies groups occurring at roughly regular intervals, associated with each other. As discussed in Section 4.3.6.3, this association and apparent regular distribution of facies may make the occurrence of fine-grained facies easier to predict.

The horizontal distribution of facies (Fig. 5.9, data table in App. C4) is fairly even along the whole outcrop, and the percentage of each facies is quite consistent, never varying by more than 20% within each facies. The even facies distribution reflects the high lateral continuity, shown by the high continuity index (Table 5.8).

#### *5.3.2.2 Killard mouthbar*

The mouthbar at Killard is more heterogeneous than the mouthbar at Tullig. Beds were measured on the southern limb of the Killard syncline (Fig. 4.27 and Table 5.10), where the mouthbar is exposed from its sharp base to its abandoned top surface. Limited data from the smaller exposure on the north limb are also tabulated (Table 5.11). The tables include measurements of fine-grained beds, because of the high proportion of finer facies within the sandbody, but the fine-grained beds are not included in the means and ranges, so that only the sandy, reservoir facies are taken into account in the statistics.

The connectivity for the Killard mouthbar sandbody is calculated as 67.2% (Table 5.10), very similar to the figure for the Tullig Point mouthbar (Table 5.8), although not as high as the values for the Tullig Sandstone (Tables 5.1, 5.2 and 5.6). The marked difference in connectivity between the two mouthbars and the Tullig Sandstone outcrops indicates that the two types of sandbody clearly represent different styles of facies architecture and different facies percentages and, by extension, different depositional environments. Bed thicknesses within the Killard mouthbar are similar to those from the Tullig Point mouthbar, although the mean is

slightly higher at Killard, because “Bed V” was not separated out into its constituent cross beds (compare Tables 5.8 and 5.10). Bed lengths in the Killard mouthbar are similar to those in the Tullig Point mouthbar, with beds extending across the entire south limb outcrop (80m+). A discontinuous bed at the base brings the mean bed length figure down to 76.8m, again very similar to the mean bed length for beds in the Tullig Point mouthbar. The continuity indices for the beds are high (mean >100.4), very similar to Tullig Point (Table 5.8), indicating high lateral continuity and few lenticular beds, although as at Tullig Point, amalgamation of some beds for measurement purposes results in an artificial reduction in values.

Table 5.10. Sandstone (and *fine-grained*) bed data for Killard mouthbar, south limb. Ranges and means apply to sands only. \*Bed V comprises 10-20 cross beds, which were not measured separately; minimum, maximum and mean values are for to “Bed V” as a whole.

Bed	Contact %/s/s	type %/s/m	Thickness (m)			Bed length (m)	Continuity (length/thick)
			Min.	Mean	Max.		
Z	15	85	0.60	1.45	1.99	>80	40.2
Y	-	-	0.12	0.30	0.34	>80	
X	0	100	0.12	0.50	0.58	>80	137.9
W	-	-	0.09	0.30	0.40	>80	
V*	30	70	2.16	4.25	6.24	>80	12.8
U	-	-	0	0.20	0.41	~17	
T	65	35	1.48	2.00	2.42	>80	33.1
S	-	-	0.04	0.10	0.20	23	
R	100	0	0.48	1.26	1.74	>80	
Q	100	0	0.18	0.37	0.66	>80	121.2
P	100	0	0.15	0.38	0.53	>80	150.9
O	100	0	0.29	0.45	0.56	>80	142.9
N	0	100	0.21	0.52	0.59	>80	135.6
M	-	-	0.06	0.10	0.15	>80	
L	100	0	0.11	0.20	0.28	>80	285.7
K	100	0	0.14	0.20	0.26	>80	307.7
J	100	0	0.13	0.24	0.30	>80	266.7
I	0	100	0.09	0.21	0.33	>80	242.4
H	-	-	0.35	0.60	0.82	>80	
G	100	0	0.40	0.67	0.77	>80	103.9
F	100	0	0.12	0.23	0.45	>80	177.8
E	100	0	0.22	0.41	0.53	>80	150.9
D	0	100	0.16	0.26	0.49	>80	163.3
C	-	-	0.03	0.09	0.17	>80	
B	100	0	0	0.18	0.58	20	34.5
A	/	/	0.35	0.49	0.78	>80	102.6
Range	0-100	0-100	0.12-2.16	0.50-4.25	0.58-6.24	20->80	12.8-307.7
Mean	67.2%	32.8%	0.38	0.73	1.06	76.84	>100.4

The statistics from the northern limb outcrop of the Killard mouthbar are similar to those from the southern limb (compare Tables 5.10 and 5.11). The main difference is the connectivity, which is 0% for the northern outcrop. The lack of connectivity is because on the northern limb only the top 1-3m of the mouthbar are sandy (Fig. 4.29 and Section 4.3.7.3), and the sandstone beds are separated by muddy beds, so there are no sand-on-sand contacts. The mean continuity index across both limbs is 117.5.

Table 5.11. Sandstone (and *fine-grained*) bed data for Killard mouthbar, north limb of syncline. Ranges and means are calculated using sand bed data only.

Bed	Contact type		Thickness (m)			Bed length (m)	Continuity (length/thick)
	%s/s	%s/m	Min.	Mean	Max.		
M	0	100	1.34	1.44	1.54	~100	64.9
L	-	-	0.30	0.40	0.49	~100	
K	0	100	0.32	0.40	0.49	~100	204.1
J	-	-	0.30	0.37	0.52	~100	
<b>Range</b>	0	100	0.32-1.34	0.40-1.44	0.49-1.54	-	64.9-204.1
<b>Mean</b>	<b>0%</b>	<b>100%</b>	<b>0.83</b>	<b>0.92</b>	<b>1.02</b>	<b>~100</b>	<b>134.5</b>

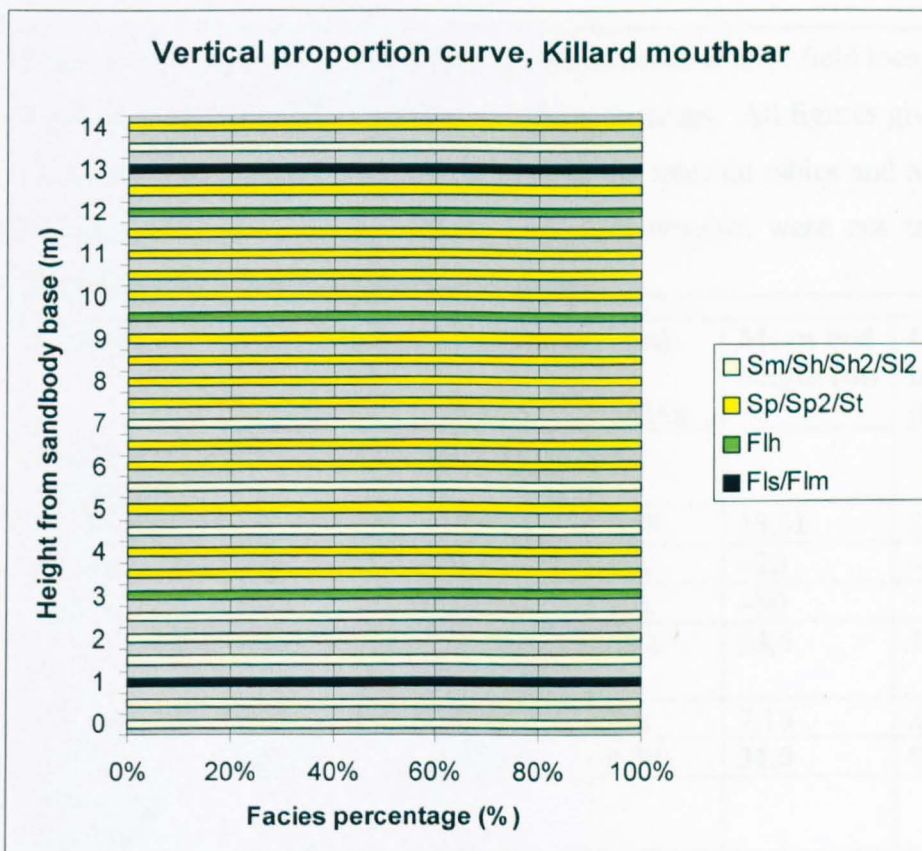


Fig. 5.10. Graph showing the facies distribution for the Killard mouthbar, based on the sedimentary log (starting from 6.5m n Fig. 4.26).

Due to the impossibility of creating a photomontage of this part of the outcrop that would allow facies distribution measurement (Fig. 4.29 is viewed from too far away), no directly measured vertical proportion data was generated. However, the continuity of the beds (see Tables 5.10 and 5.11) is high, meaning that the vertical distribution is very consistent across the outcrop. A vertical proportion curve (Fig. 5.10) based on the log (Fig. 4.26) shows:  $S_m/Sh/Sh_2/Sl_2 = 43.5\%$ ;  $Sp/Sp_2/St = 43.2\%$ ;  $Flh = 9.1\%$ ;  $Fls/Flm = 4.2\%$ . The resulting net to gross ratio is high at 86.8%, although the moderate vertical connectivity (67.2%) reduces the reservoir quality of the sandbody.

#### 5.4 Summary and discussion

The statistics calculated in this chapter complement the observations and descriptions of Chapter 4 to give a fuller understanding of the characteristics of the Tullig Sandstone and the mouthbar sandbodies. Tables 5.12, 5.13 and 5.14 summarise the bed measurements and facies distribution observations, and facilitate comparisons between the different outcrops. The trends along palaeoflow (southwest to northeast) and other major observations apparent from these comparisons are presented below.

Table 5.12. The results of bed measurements made at each field locality, for both the Tullig Sandstone outcrops and the mouthbar outcrops. All figures given are the mean values for each locality, and can be seen in the relevant tables and associated text in Sections 5.3.1 and 5.3.2. Where bed measurements were not taken, mean bed thicknesses have been calculated from logs.

Locality	Connectivity (%/s bed contacts)	Thickness (m)		Mean bed length (m)	Continuity index (length/thick)
		Mean	Max.		
<b>Tullig Sandstone:</b>					
Trusklieve	80	0.37	0.58	13.55	27.5
Pulleen	100	0.36	NA	~20	~56
Killard	95	0.32	NA	~50	~150
Carrowmore Point	90.5	0.39	0.81	64.4	179.3
Furreera	100	0.26	NA	7.16	25
<b>Mean</b>	<b>93.1</b>	<b>0.34</b>	<b>0.70</b>	<b>31.0</b>	<b>87.6</b>
<b>Mouthbar sandbodies:</b>					
Tullig Point	62.3	0.66	0.72	76.08	>103.8
Killard	67.2	0.73	1.06	76.84	>117.5
<b>Mean</b>	<b>64.75</b>	<b>0.695</b>	<b>0.89</b>	<b>~76.46</b>	<b>&gt;110.6</b>

#### 5.4.1 Internal architecture statistics

- The connectivity within the Tullig Sandstone is very high, averaging 93.1%. There is no apparent trend in connectivity along palaeoflow (i.e. from southwest to northeast along the present coastline), with values peaking at both Pulleen, midway between Trusklieve and Furreera, and at Furreera, which is the northeasternmost outcrop (Fig. 5.11).
- The mean bed thicknesses are similar at all five outcrops, varying between 0.26m and 0.39m. A possible trend of slightly decreasing bed thickness along palaeoflow is interrupted by the value for Carrowmore (Fig. 5.12).
- Mean bed lengths increase along palaeoflow from Trusklieve northeastwards, although not in a smooth trend (Fig. 5.13). Furreera is an exception to the northeasterly increase in bed length. This is because the Furreera outcrop, which trends east-west, is close to normal to palaeoflow (the mean direction at Furreera is  $347^{\circ}$ ), while the other outcrops, which trend either NE-SW or ENE-WSW and show flow to the ENE, NE and NNE, are parallel to sub-parallel to palaeoflow, and therefore show along-channel, rather than across-channel, bed dimensions. The Tullig Sandstone at Furreera is dominated by trough cross bedding, which, when viewed in cross-section, produces lenticular bed geometries, leading to a reduction in observed bed lengths compared for example with Killard, where the trough cross beds are seen at an oblique angle and thus appear longer. The overall increase in bed length may reflect a decrease in erosional scour downstream, meaning that the preservation potential of individual beds is increased. However, it is important to remember that bed length measurements are also partly dependent on the size of the outcrop (Geehan and Underwood, 1993). Caution should therefore be used when looking for trends in the data, although the outcrop scales at the localities visited were similar to each other (generally  $\sim 100\text{m}$ ), so that effects of outcrop dimensions on the bed length data should be similar as well.
- The continuity index increases from southwest to northeast, reflecting the increase in bed lengths from Trusklieve to Carrowmore Point (see Fig. 5.14). Again, the outcrop of the Tullig Sandstone at Furreera is the exception to this trend, for the same reasons as those given above.

- Within the majority of outcrops, beds show increasing lengths and increasingly simple geometries towards the top of the Tullig Sandstone, with a decrease in erosional scour and lenticularity.

There are immediate and obvious differences between the architectural statistics of the two mouthbar sandbodies and those of the Tullig Sandstone. These differences are highlighted in the points below, with corresponding data displayed in Table 5.12. The statistics presented here show that the two mouthbars are very similar.

- The mean bed length of the two mouthbars is 76.5m, higher than for the Tullig Sandstone outcrops (31.0m). The beds lengths are in excess of 80m throughout the thickness of both mouthbars, whereas the Tullig Sandstone outcrops, even when they do show beds with comparable lengths, do not show these bed lengths throughout the sandbody thickness. In addition, the orientation of the Tullig Point mouthbar is east-west, at a higher angle to palaeoflow than the Killard mouthbar, and yet both show very similar bed lengths, which implies that the beds are laterally extensive in all directions rather than just in a downstream direction.
- The lateral continuity index for the mouthbars at Tullig Point and Killard is high (>110.6) compared with the Tullig Sandstone outcrops (averaging 87.6). The mouthbars would have even higher values if all the beds had been individually identified, rather than sometimes amalgamated to make facies mapping easier.
- The mean connectivity of the mouthbars (64.8%) is lower than for the Tullig Sandstone (93.1%) by over 28%. This difference is due both to the increased percentage of fine-grained facies and the increased lateral continuity of the beds in the mouthbars compared with the fluvial Tullig Sandstone.

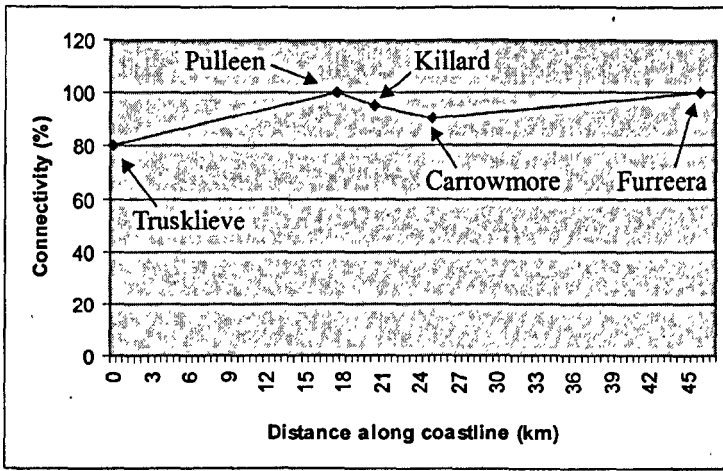


Fig. 5.11. Graph showing changing connectivity values along the coastline from Trusklieve to Furreera, parallel to palaeoflow.

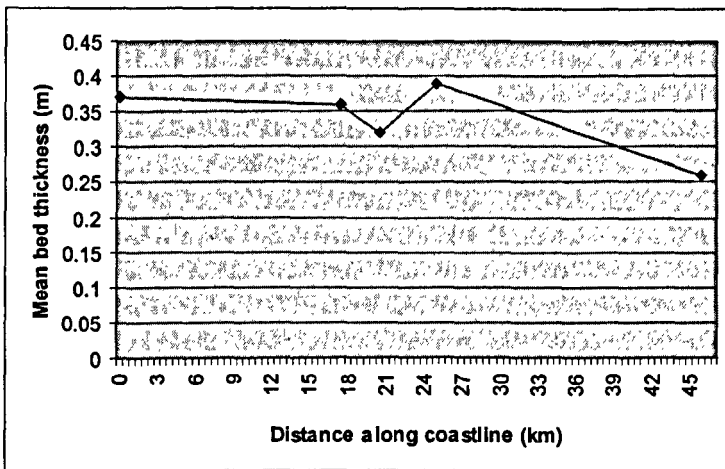


Fig. 5.12. Graph showing changing mean bed thickness values along the coastline from Trusklieve to Furreera, parallel to palaeoflow.

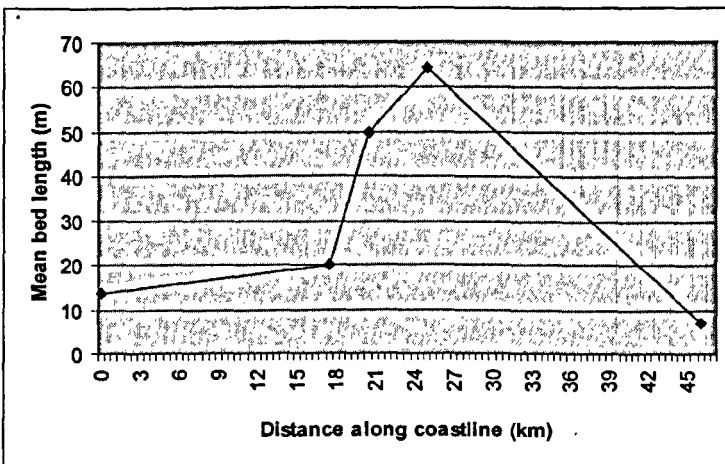


Fig. 5.13. Graph showing changing mean bed lengths along the coastline from Trusklieve to Furreera, parallel to palaeoflow.

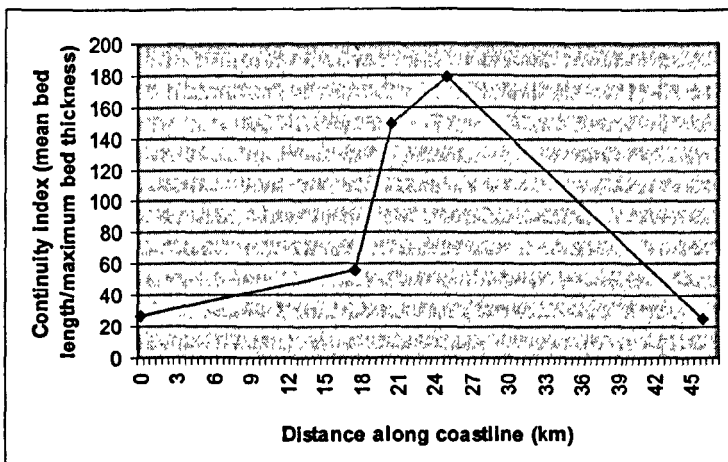


Fig. 5.14. Graph showing changing continuity indices along the coastline from Trusklieve to Furreera, parallel to palaeoflow.

#### 5.4.2 Facies distribution statistics

- The percentage of sandy facies in the Tullig Sandstone outcrops remains consistent along palaeoflow from southwest to northeast, varying by less than 9% and remaining between 91% and 100%.
- The variation in type of sandy facies creates a trend parallel to palaeoflow and to the present-day coastline, with massive sandstone and horizontally bedded sandstone percentages reducing from southwest to northeast while trough and planar cross-bedded sandstone percentages increase to compensate (see Fig. 5.15). This suggests that the processes generating facies Sm and Sh, bank collapse and high velocity subcritical flow respectively, become less important downstream, while the formation and migration of dune forms becomes more common.
- There is an overall decrease in the percentage of coarse-grained facies from southwest to northeast (Fig. 5.16). The trend is fairly smooth, decreasing sharply from Trusklieve to Pulleen and continuing to fall more gently to Furreera. This decrease in conglomeratic facies is interpreted to reflect a decrease in erosive potential of the fluvial system in a downstream direction, which agrees with the observation in Section 4.4.1 (Table 4.1) that the channels show progressively less erosional relief in a downstream direction.
- There is no overall trend in the percentage by area of fine-grained facies from southwest to northeast (Fig. 5.16). Peaks in abundance occur both at Trusklieve and Carrowmore Point.
- Within individual outcrops, there is a vertical trend of increasing facies homogeneity towards the top of the Tullig Sandstone (e.g. Figs 5.2, 5.4, 5.5). Cross-bedded facies are more prevalent towards the top, at the expense of fine and coarse-grained facies, in all outcrops except Carrowmore Point. At Carrowmore, although cross bedding becomes more dominant upwards, there is also an increase in fine-grained facies near the top of the Tullig Sandstone. The reduction in conglomeratic facies with height is probably due to the reduced availability of fine-grained material to erode as the channel storeys aggrade. Over time, succeeding channels erode and rework underlying sandy channel deposits, rather than the fine-grained delta front material at the base of the Tullig Sandstone.

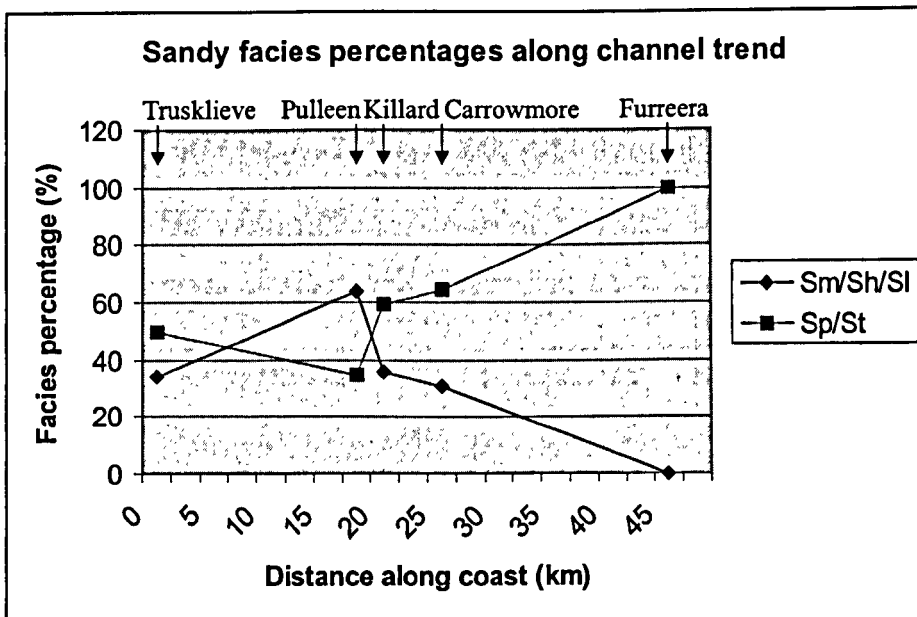


Figure 5.15. Graph showing the percentage by outcrop area of the two sandy facies categories along the Co. Clare coastline, which parallels the palaeoflow direction (southwest to northeast).

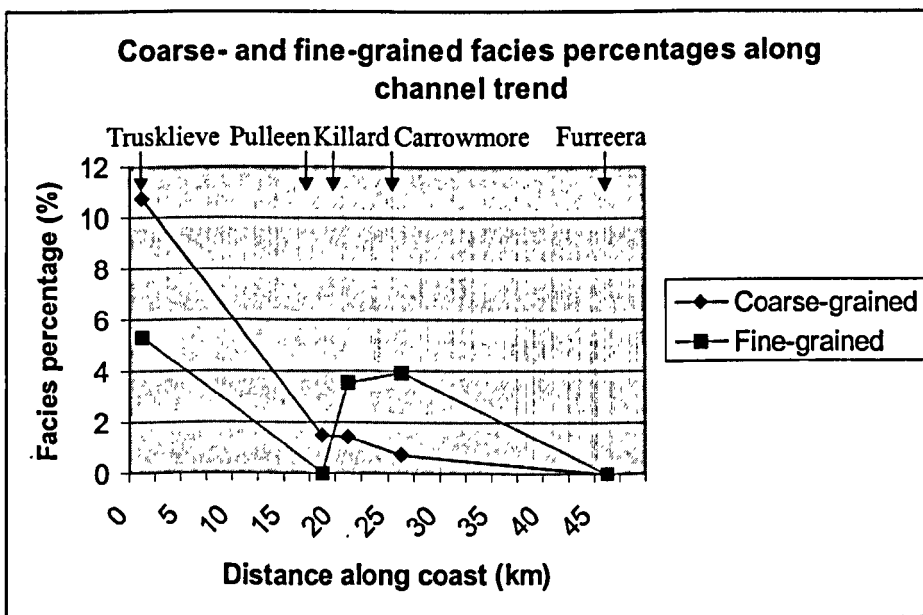


Figure 5.16. Graph showing the percentage by outcrop area of fine- and coarse-grained facies, grouped into two categories for simplicity, at the five Tullig Sandstone outcrops from Trusklieve (0km) to Furreera (46km).

Table 5.13. Summary of facies distribution statistics from all Tullig Sandstone outcrops, from southwest (Trusklieve) to northeast (Furreera).

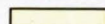
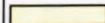
Locality	% of facies 						Net to gross	
	Sm/Sh/SI	Sp/St	Smc/Shc	Sc	Ccm	Flh	Fls/Flm	
Trusklieve	34.09	49.89	4.30	3.18	3.25	0.35	4.94	91.46
Pulleen	63.70	34.78	0	0	1.52	0	0	98.48
Killard	35.72	59.25	0.97	0.33	0.16	0	3.57	96.27
Carrowmore Point	31.06	64.21	0.40	0	0.37	2.59	1.37	96.04
Liscannor	0	100	0	0	0	0	0	100
<b>Mean</b>	<b>32.9</b>	<b>61.6</b>	<b>1.1</b>	<b>0.7</b>	<b>1.1</b>	<b>0.6</b>	<b>2.0</b>	<b>96.5</b>

Table 5.14. Summary of facies distributions statistics from the two mouthbar sandbodies at Tullig Point and Killard.

Locality	% of facies 				Net to gross
	Sm/Sh/SI	Sp/St	Flh	Fls/Flm	
Tullig Point	74.01	17.82	4.76	3.41	92.86
Killard	43.49	43.27	9.07	4.17	86.76
<b>Mean</b>	<b>58.8</b>	<b>30.5</b>	<b>6.9</b>	<b>3.8</b>	<b>89.8</b>

In terms of architecture and facies distribution, the main trends in the Tullig Sandstone apparent from the data presented in this chapter are the decrease in erosional scour and abundance of conglomeratic facies, and the increase in bed length, in both downstream and vertical directions. These observations suggest a downstream increase in deposition relative to erosion, which supports the view that the delta front is to the northeast and that the fluvial deposits have an increased preservation potential in the area closest to the delta front. Preservation potential is increased by higher subsidence rates, which are often a feature of deltas and have been postulated for the deltas of Co. Clare by several writers (e.g. Rider, 1978; Pulham, 1989). The data also suggest a decrease in erosional scour over time, leading to thicker upper storeys (e.g. at Pulleen, Killard and Carrowmore) and increased bed lengths with height within the Tullig Sandstone. This reduction in erosion with time suggests an increase in accommodation space over time, which would increase the aggradation rate of the fluvial system and simultaneously reduce the overall rate of erosion. An increase in accommodation space could be caused either by increasing subsidence

rates or rising eustatic sea-level, or by a combination of both. Either factor would result a rise in relative sea-level and the eventual drowning of the delta, if sediment supply was not sufficient to allow aggradation to keep pace with relative sea-level rise. The occurrence of the *R. stubblefieldi* marine band in the succession above the Tullig Sandstone is evidence of the drowning of the delta and the eventual introduction of marine conditions throughout the field area (e.g. Pulham, 1987), which supports the attributing of the trends discussed above to rising relative sea-level.

#### **5.4.3 Other potential uses of the data**

In addition to using the data gathered from the outcrops along the coast of Co. Clare for building reservoir models, they could be used for generating populations of shale bed lengths and distributions, and for testing both the models presented in Chapter 6 and other models of fluvio-deltaic successions. The detailed measurements and description of the Tullig Sandstone and associated Tullig Cyclothem mouthbar sandbodies provide a useful resource with which to compare other fluvio-deltaic successions, especially those influenced by similar controls such as glacio-eustasy.

## Chapter 6

### Outcrop-based reservoir modelling of fluvial facies architecture

#### 6.1 Introduction

To see how the data presented in Chapters 4 and 5 can be used to predict reservoir characteristics and the distribution of heterogeneities, it is necessary to use the software available in the petroleum exploration and production industry to create three-dimensional models from the outcrop data. In this way, the possible impact of detailed field studies on models of analogous subsurface reservoirs can be better understood. The dual aims of the modelling were: 1) to construct static models of the Tullig Sandstone geology, to assist outcrop-based interpretation; and 2) to assess the utility of the modelling program and its applicability to outcrop data. This chapter describes the design and construction of reservoir models based on the results of fieldwork (Chapters 4 and 5), presents the results of such models, and discusses their importance for reservoir evaluation.

#### 6.2 Background to reservoir modelling

##### 6.2.1 The definition and importance of geological reservoir models

Reservoir modelling, according to Seifert and Jensen (2000), “refers to the development of a numerical model of a given reservoir and provides a gridded framework that is filled with lithofacies or genetic unit values, each of which can in turn be associated with effective flow, acoustic, or other properties”. The purpose of a model is to represent realistically the available information and use this information as a basis for simulating the spatial distribution of the properties or attributes being studied, such as facies type or permeability.

In the past it has been observed that oil recovery predictions are very sensitive to the way in which the geology of a reservoir is understood and represented in a model (Hearn *et al.*, 1986). A detailed reservoir description is necessary, particularly when the reservoir is heterogeneous in terms of rock properties (porosity, permeability) and/or lithology, because a poor description leads to large errors in predictions of hydrocarbon volumes, flow pathways, well locations and extraction efficiencies. Geological models

need to incorporate the different types and scales of heterogeneity in order to quantify uncertainties in predictions, and to reduce the economic risk associated with pursuing a hydrocarbon prospect (Hatløy, 1994). Even small, bed-scale variations, although seldom modelled, must be understood so that their effects can be incorporated into large-scale models. Reservoir heterogeneities are known to have a major impact on fluid flow (Holden *et al.*, 1998), and modelling fluid flow through heterogeneous reservoirs requires the integration of reservoir architectures and geometries, rock properties and quantitative predictions of variations in the petrophysical properties (Willis and White, 2000).

Discontinuous shales have often presented problems for reservoir engineers trying to understand their effect on fluid flow (Haldorsen and Chang, 1986). The discontinuity of sandbodies in many fluvial reservoirs, for example such as the Snorre field in the North Sea, has also led to low recoveries due to poor understanding of sandbody architecture (Holden *et al.*, 1998). Changing the architectural model or correlation model used for reservoir modelling can have a dramatic impact on volumetric estimates; Ainsworth *et al.* (1999) showed that for the Sikrit oil field, Thailand, using a lithostratigraphic correlation model led to a 43% overestimate of the recovery factor relative to a chronostratigraphic model. Uncertainties relating to the spatial correlation of permeability (strongly related to facies distribution) are easily transferred into predictions of reservoir performance (Kupfersberger and Deutsch, 1999), making the economics of a hydrocarbon prospect difficult to evaluate accurately. To combat all of the above problems, the construction of an accurate, representative geological model is essential.

### **6.2.2 Use of outcrop data**

To help construct an accurate and realistic geological model, data from analogous field outcrops can be used to reduce uncertainty. The detailed information that can be gathered from a field outcrop is especially useful, considering that computer models have shown that even small-scale features, such as shale drapes and variations in permeability within a facies, have statistically significant effects on flow simulations (Willis and White, 2000). Data is available in field outcrops at this small scale, and, when used to refine 3-D reservoir models, can significantly reduce uncertainty. The excellent understanding of permeability distribution and continuity needed for a

successful, detailed, 3-D simulation (Weber and van Geuns, 1990) can often be achieved by studies of field analogues (e.g. Willis and White, 2000). Although the centimetre- and meter-scale variations seen in the field cannot practically be incorporated into models covering many cubic kilometres, the effects of those small-scale variations (for example on permeability and porosity) can be quantified and averaged and thus “scaled up” to be useful in a model. If estimates of reservoir properties were made without looking at the small-scale variations, the resulting model could be significantly different from the real situation.

Field analogues are also very useful in understanding the larger-scale architecture and geometry of a sandbody or system of linked sandbodies. With a limited number of wells, the way in which reservoir bodies are connected in the subsurface is difficult to predict. Comparing well-logs and core from a subsurface reservoir with sedimentary logs from field examples, where patterns of connectivity are described and quantified, enables better prediction of connectivity and correlation in the subsurface. Another use of field analogues is in testing models. Testing a particular modelling process on known outcrop data can help identify and correct any problems or limitations within that modelling process, as demonstrated by MacDonald and Aasen, 1994, who tested a stochastic model on two Cretaceous parasequences in the Book Cliffs, Utah. Testing a modelling process is a very important step before the process is used to model potential hydrocarbon prospects.

The types of data needed from fieldwork include vertical and horizontal facies distributions, measurements of grainsize, permeability, thicknesses of different facies types, lengths and thicknesses of fine-grained impermeable facies, connectivity, and architecture. All these properties and characteristics potentially affect the flow of fluid through a reservoir.

### **6.2.3 Different modelling methods**

Before computers were capable of handling large quantities of data, models necessarily had to be quite simple, and were often two-dimensional. One method employed within the hydrocarbon exploration and production industry was that of constructing 2-D permeability and flow models between a 3-D network of known wells. This method is particularly suited to large onshore fields where reservoirs are drained by numerous

closely spaced wells (e.g. Jackson *et al.*, 1991). Other relatively simple models focus on sand and shale body geometries, using statistical databases of measurements to populate models; Haldorsen and Chang, for example, use outcrop studies to obtain a distribution of shale lengths that are then digitised and used to populate a 2-D flow model (Haldorsen and Chang, 1986; Haldorsen *et al.*, 1987).

The majority of models constructed today, however, are three-dimensional. The advantages of 3-D modelling include the ability to easily visualise spatial relationships, the increased accuracy in modelling faults and volumes, the better representation of three-dimensional heterogeneity, and the easier integration of data from multiple locations across the study area (Roxar, 2003a). 3-D models are of two main types, deterministic and stochastic. Deterministic modelling produces a single result from a particular set of input data and, although it can be useful, this approach cannot easily take into account the uncertainty associated with the input data or simulate the potential real-world variability in the resulting model.

Stochastic modelling is a method that generates numerous realisations from a single set of input data; from these multiple, equally probable (“equiprobable”) realisations, the likelihood of best-case, worst-case and intermediate scenarios can be calculated, and the uncertainty relating to any particular result can be quantified (e.g. Sharif *et al.*, 2000). In an industry where risk is a crucial factor and must be assessed as accurately as possible, this ability to quantify uncertainty is very useful. Other advantages of stochastic modelling include the ability of the technique to produce a realistic level of heterogeneity on even small scales (Eschard *et al.*, 1998), and to incorporate a wide range of complex input data. Numerical simulation in a stochastic model also allows the spatial distribution of input data to be reproduced within the model, using variograms, which are graphs showing how values vary in space (Roxar, 2003b). Experimental variograms are calculated from data that has had any linear trends removed by transformation. Once a variogram has been calculated, a variogram model (which can be spherical, Gaussian or exponential) that fits the experimental variogram is selected and put into the reservoir model, so that the spatial distribution of data generated by the modelling process mimics the spatial distribution of the input data. Horizontal and vertical variograms can be used, to take into account the variability of the data in all three dimensions (Ravenne and Beucher, 1988). The transformations

performed on the original data are back-applied, after simulation using the variograms has been performed, to ensure that real trends in the input data are not lost.

Reservoir models can incorporate some deterministic data - for example a network of faults, the positions and geometries of which are known accurately through seismic imaging - and can still use stochastic techniques to model other properties such as facies type, permeability, porosity, and sandbody geometry. Stochastic models can be grouped into object-based and pixel-based models: object-based models will create objects, for example sandbodies, channels and shale breaks that are fitted into the modelling grid (e.g. Hjort and Omre, 1994); pixel-based models use variograms to populate the grid with values, unrelated to any facies bodies of particular dimensions (e.g. Seifert and Jensen, 2000). More advanced models allow the combination of both techniques; for example if a reservoir comprises channel bodies that show internal heterogeneities, the object method will generate the channel bodies and the pixel method will generate the internal heterogeneity of those bodies using variograms (e.g. Hatløy, 1994). The model used in this study is capable of combining the two techniques, and uses the Metropolis-Hastings simulation algorithm to fit the objects into the grid. Many other algorithms can be used (e.g. sequential indicator simulation, probability field simulation, truncated Gaussian simulation etc.). The impact of the simulation method on the final model is investigated by Journel *et al.* (1998) and Seifert and Jensen (2000), and the latter authors conclude that using a model which combines pixel-based and object-based simulation methods is the most appropriate way to model braided fluvial systems.

#### **6.2.4 Summary**

A basic understanding of the principles involved in reservoir modelling is important, because the modeller needs to be aware of how the input data is used to produce the model and how the outcomes can be affected by changes in input data and modelling method. Some techniques will be better suited to correctly modelling particular reservoirs than others; this means that a good understanding of the geology of the reservoir is also of prime importance, so that a modelling method that will be able to take account of the geological model can be chosen. In summary, reservoir modelling can greatly help reduce the uncertainties and risks associated with developing a hydrocarbon prospect, but a model is only as good as the sum of its parts. Care must be

taken to use all available data to inform the modelling process; analogue data from field studies can be vital in this regard, providing an improved understanding of reservoir geology and increasing the amount of data available for conditioning a reservoir model.

### **6.3 Methodology**

The software used for the modelling presented here is Roxar's IRAP reservoir modelling system (RMS), version 7.0. The program is a powerful 3-D modelling tool, which incorporates structural, stratigraphic and rock property modelling, and allows reservoir and flow simulation. RMS incorporates the possibility of both deterministic and stochastic modelling, the later allowing numerous equiprobable realisations to be generated from one set of input data. This stochastic approach allows the probability of any particular outcome to be calculated, which means that the uncertainty involved in prediction of reservoir properties and behaviour can be quantified. Other advantages of RMS are its ability to produce realistic heterogeneity models through stochastic techniques, and its honouring of complex data; detailed field data can thus be input to the model without requiring upscaling that would render such detail insignificant.

1) The first step in creating the models presented here was the construction of a structural framework and 3-D modelling grid. Using ready-made horizons (which are groups of myriad points, each with x, y and z values) included in the software package, three stratigraphic horizons were created for the models. This was done by flattening a ready-made horizon (making  $z = 0$  for every point) and then extrapolating it to make it correspond in size to the area from which the outcrop data to be input was gathered. The extrapolation was done by creating a polygon with its four corners at the required locations of the corners of the new horizons, and then performing a gridding operation on the flattened horizon to extrapolate it out to meet the polygon edges. The resulting, larger, horizon was then duplicated twice, and operations were performed on these two duplicates to translate one to a z value of 25m, and the other to 50m. The horizon at a depth of 0m was named TopTullig; the horizons at 25m and 50m were named BaseTullig and horizon A respectively. The maximum and minimum x, y, z coordinates and dimensions for the three horizons are listed in Table 6.1 below.

It must be noted that although the top surface of the Tullig Sandstone can be assumed to be flat, since it represents a flooding surface, the base is not flat, and is seen in the field

to have erosional relief of up to several metres. However, without data to describe the three-dimensional shape of the basal surface (which is impossible to gather from the field), any attempt to “shape” the BaseTullig horizon in the model would be very subjective and the resulting horizon would not necessarily bear any resemblance to the real shape of this surface. Therefore no attempt has been made to give topography to the BaseTullig, and it has been modelled as a flat surface.

<b>Horizon name</b>	<b>Min. x (m)</b>	<b>Max. x (m)</b>	<b>Min. y (m)</b>	<b>Max. y (m)</b>	<b>x dist. (m)</b>	<b>y dist. (m)</b>	<b>z (m)</b>
TopTullig	452500	472500	5924800	5950000	20000	25200	0
BaseTullig	“	“	“	“	“	“	25
Horizon A	“	“	“	“	“	“	50

Table 6.1. Horizon names and dimensions. In this model, x increases to the southeast, y increases to the northeast and z increases vertically upwards.

2) The second step in creating the models was to create a geological grid within which the modelling could be carried out. Most geological models created in RMS contain between 1 million and 10 million cells, compared with simulation grids (used for example for flow simulation), which are scaled up from geological grids and typically comprise around 50,000 cells. In order to keep the number of cells below 10 million, but to include the four main studied outcrops of the Tullig Sandstone, (Trusklieve, Pulleen, Killard and Carrowmore, spread over 25km from southwest to northeast), it was necessary to specify cells of certain dimensions. These cell dimensions, together with the grid dimensions and corner-point locations, are listed in Table 6.2. The Furreera outcrop could not be included in the model, since it is 20km further north than Carrowmore Point and its inclusion would increase the grid size by several million cells. To reflect the orientation of the Tullig Sandstone, the y-axis of the geological grid was oriented northeast-southwest, aligned with the dominant palaeoflow. Figure 6.1 shows how the grid corresponds to the Co. Clare coastline. The TopTullig and BaseTullig horizons were specified as defining the top and base of the grid, but also extend beyond the area covered by the grid.

A second grid, also oriented parallel to palaeoflow but covering a much smaller area, was designed to model solely the Trusklieve outcrop. Making the area of interest so

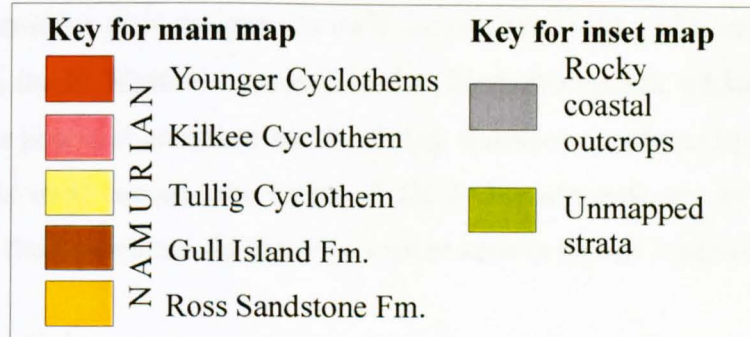
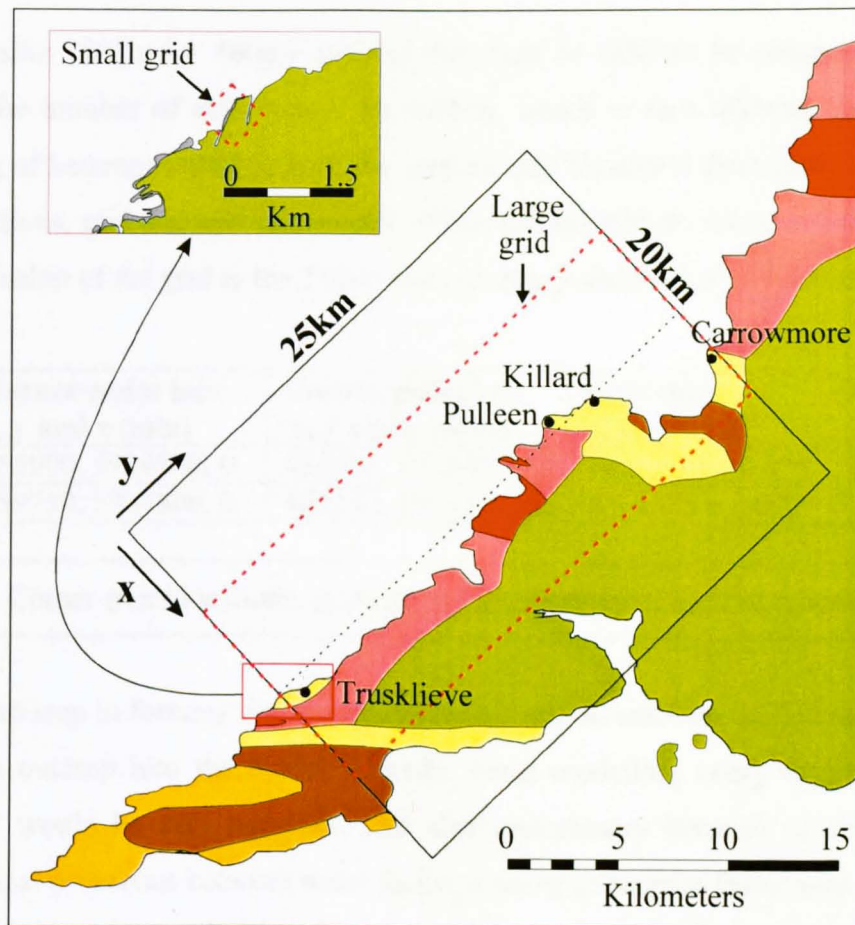


Figure 6.1. Map of County Clare (after Wignall and Best, 2000), showing the location of the horizons and modelling grids created in RMS relative to the coastline. The solid black line represents the extent of horizons TopTullig and BaseTullig, while the red dashed lines delimit the large and small modelling grids. While the large grid covers four of the main localities at which the Tullig Sandstone was logged and photographed, the small grid (shown in the enlarged inset map of Trusklieve) covers an area of 500m by 500m, encompassing the four logs from the Trusklieve outcrop.

much smaller (500m by 500m) enabled the sizes of cells to be reduced while still keeping the number of cells below 10 million, which in turn allowed more detailed modelling of heterogeneities in both the vertical and horizontal directions. The corner-point locations, grid and cell dimensions of this second grid are listed in Table 6.2, and the relationship of the grid to the Trusklieve outcrop is shown in Fig. 6.1 (inset).

<b>Grid</b>	<b>Corner-point loc. x, y and z (min)</b>	<b>Corner-point loc. x, y and z (max)</b>	<b>Grid dim.s x, y, z (km)</b>	<b>Cell dim.s x,y,z (m)</b>
Large	455900, 5924800, 0	465900, 5950000, 25	10 x 25.2 x 0.025	50, 50, 1
Small	459750, 5924800, 0	460250, 5925300, 25	0.5 x 0.5 x 0.025	5, 5, 0.1

Table 6.2. Corner-point locations, grid and cell dimensions of the two modelling grids.

3) The third step in forming the geological model was to enter the sedimentary log data from each outcrop into the model. Firstly, since modelling every facies defined in Chapter 3 would be very complex, and also unnecessary because of similarities in petrophysical properties between some facies, a set of composite facies was established. These composite facies, their codes, and the facies that comprise them are listed in Table 6.3. Porosities were assigned to each facies code (Table 6.3), using well-log and core data from the El Wastani formation in the Nile Delta system, which is described in Chapter 2 as a potential analogue for the Tullig Sandstone system (Section 2.5). Nile Delta data was used because the rocks of the Tullig outcrops are so compacted and cemented that their porosities do not reflect those seen in typical reservoir sandbodies.

The sedimentary logs taken from each locality were then converted into facies logs based on the new composite facies. The logs created are listed in Table 6.4; logs with vertical resolutions of 1m were created for Pulleen, Killard and Carrowmore. Two logs were created for each sedimentary log at Trusklieve, one with a vertical resolution of 0.1m to include all the heterogeneity of the original logs, and one with a vertical resolution of 1m to be suitable for the larger 25km by 10km grid. The specific format for well-log data that can input to RMS is shown in App. D1-13, where the logs derived from the sedimentary logs shown in App. A are displayed. The data file for each well log consists of a header giving the well location and the key to the facies in the log, and a list of depths and corresponding facies within the log. Figure 6.2 gives an example of how an original sedimentary log is converted to a facies log for the model. The set of

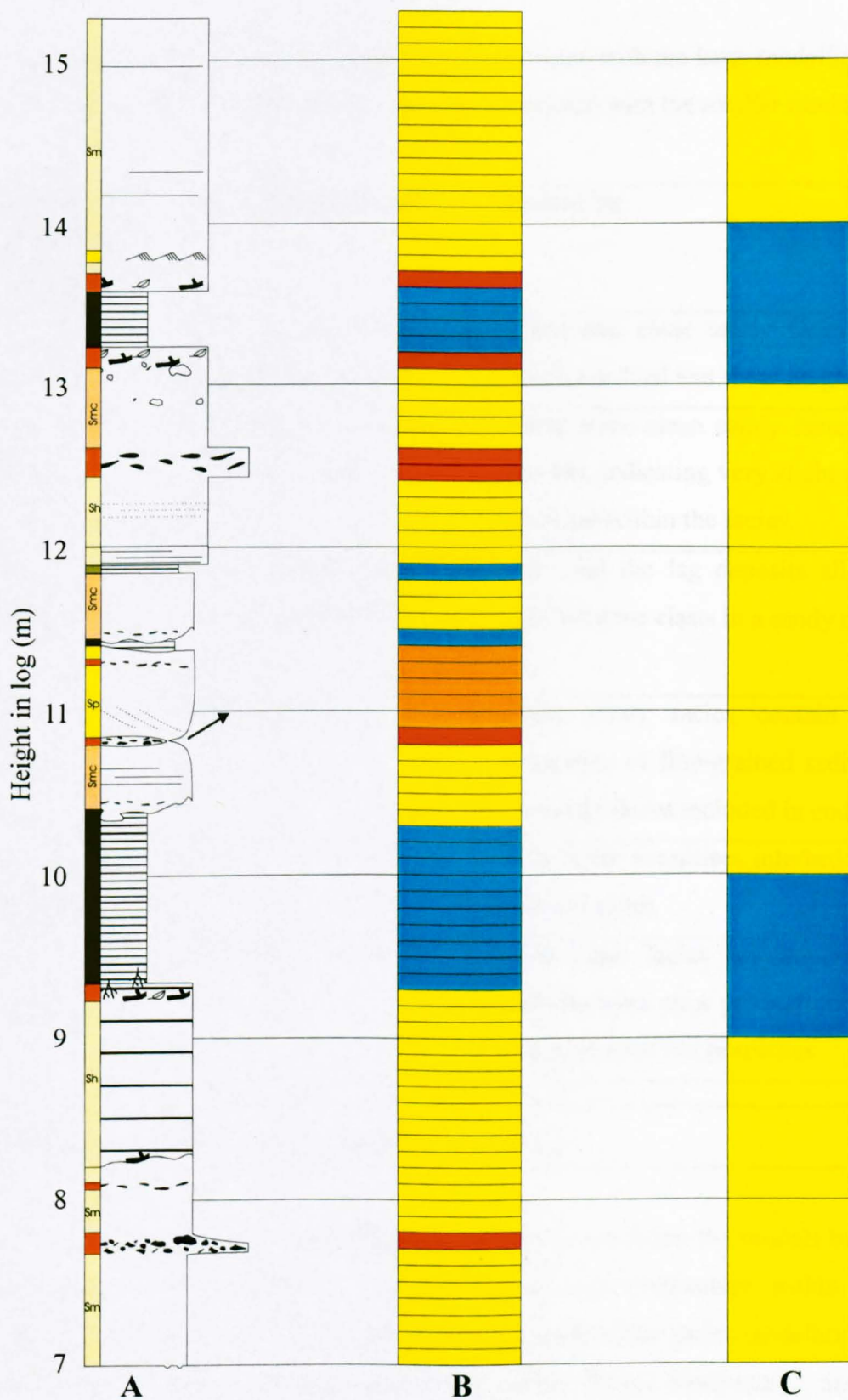


Figure 6.2. Diagram showing the conversion of an original sedimentary log (Trusklieve 4, see App. A 5) to a facies log for input to an RMS geological model. A = original log  
 B = facies log (vertical resolution 0.1m)  
 C = facies log (vertical resolution 1m).  
 Log scale: 25mm represents 1m

Colour key used in modelling	
<span style="display: inline-block; width: 20px; height: 15px; background-color: yellow; border: 1px solid black;"></span> 1 (Sm/Sh)	<span style="display: inline-block; width: 20px; height: 15px; background-color: #90EE90; border: 1px solid black;"></span> 4 (Sh <sub>2</sub> /Sp <sub>2</sub> /Sl <sub>2</sub> )
<span style="display: inline-block; width: 20px; height: 15px; background-color: orange; border: 1px solid black;"></span> 2 (Sp/St/Sl)	<span style="display: inline-block; width: 20px; height: 15px; background-color: cyan; border: 1px solid black;"></span> 5 (Flh)
<span style="display: inline-block; width: 20px; height: 15px; background-color: red; border: 1px solid black;"></span> 3 (Ccm)	<span style="display: inline-block; width: 20px; height: 15px; background-color: blue; border: 1px solid black;"></span> 6 (Fls/Flm)

For key to sedimentary log see Table 3.1

coarser-resolution logs were imported and associated with the large modelling grid, and the finer-resolution logs were imported and associated with the smaller modelling grid.

<b>Facies codes for model (and assigned porosity)</b>	<b>Incorporated facies</b>	<b>Reasoning</b>
1 (35%)	Sm, Sh, upper (non-lag) parts of Smc and Shc	These two clean sandy facies are both parallel bedded and show no grading
2 (35%)	Sp, St, Sl, upper (non-lag) parts of Sc	These three clean sandy facies all have foresets, indicating very slight changes in grainsize within the facies.
3 (18%)	Ccm, conglomeratic lags of facies Smc, Shc and Sc	Ccm and the lag deposits all comprise mud/siltstone clasts in a sandy matrix
4 (25%)	Sh <sub>2</sub> , Sp <sub>2</sub> , Sl <sub>2</sub>	These sandy facies contain a higher proportion of fine-grained sediment than the sandy facies included in codes 1 & 2
5 (10%)	Flh	This facies comprises interbedded sands, silts and muds
6 (0%)	Fls, Flm	Both these facies are impermeable to hydrocarbons on a production timescale, and have very low porosities

Table 6.3. Composite facies created for modelling.

4) The fourth step in the modelling process was to condition the models based on the quantitative data relating to facies distribution and architecture within the Tullig Sandstone. Within RMS there are two separate modules for facies modelling: Geomod, which employs a simple object-based tool called 'Facies Elementary'; and Geoplex, which contains three more advanced modelling tools, 'Facies Channels', 'Facies Composite' and 'Facies Belts'. 'Facies Elementary' and 'Facies Belts' are not used here, the former because it is insufficiently complex, the latter because it is primarily designed for modelling pro-and retro-gradational systems such as shorefaces, delta fronts and carbonate environments, in which faces belts are elongate normal to the

principal flow/slope direction. However, the tools ‘Facies Channels’ and ‘Facies Composite’ are both useful; both are object based, and deal with complex channel environments and geological objects respectively.

<b>Logs created for the Large Grid</b>	<b>Logs created for the Small Grid</b>
Trusk1LS	Trusk1SS
Trusk2LS	Trusk2SS
Trusk3LS	Trusk3SS
Trusk4LS	Trusk4SS
Pulleen	
KillardN	
KillardS	
CarrowmoreSE	
CarrowmoreNW	

Table 6.4. List of names of logs input to the two geological modelling grids.

#### **6.4 Modelling specifications**

‘Facies Channels’ was the modelling tool used to create facies distribution models within the large and small modelling grids. Appendices D14 to D20 show the different options that can be selected for the modelling process, with the options chosen highlighted with red boxes. The specifications chosen were based on the data collected in the field; for example, a maximum value of 35m was used for channel-belt thickness, and a value of 5 was used as the maximum number of channels per channel-belt (to represent the maximum of 5 channel storeys seen in the field). Each modelling grid will be discussed separately below.

##### **6.4.1 Large modelling grid: Trusklieve to Carrowmore Point**

The size of this modelling grid necessitated a large cell size and therefore a coarse (1m) vertical resolution in the blocked wells (as explained in Section 6.2). The blocked wells are shown in Figs 6.3 and 6.4, whilst the facies thickness distributions based on these blocked wells are displayed as histograms for individual facies in App. D 21 to D26; these graphs are summarised in the histogram in Fig. 6.5. The volume fraction of channel facies to be modelled, 0.936, was taken from the blocked wells (see Table 6.5),

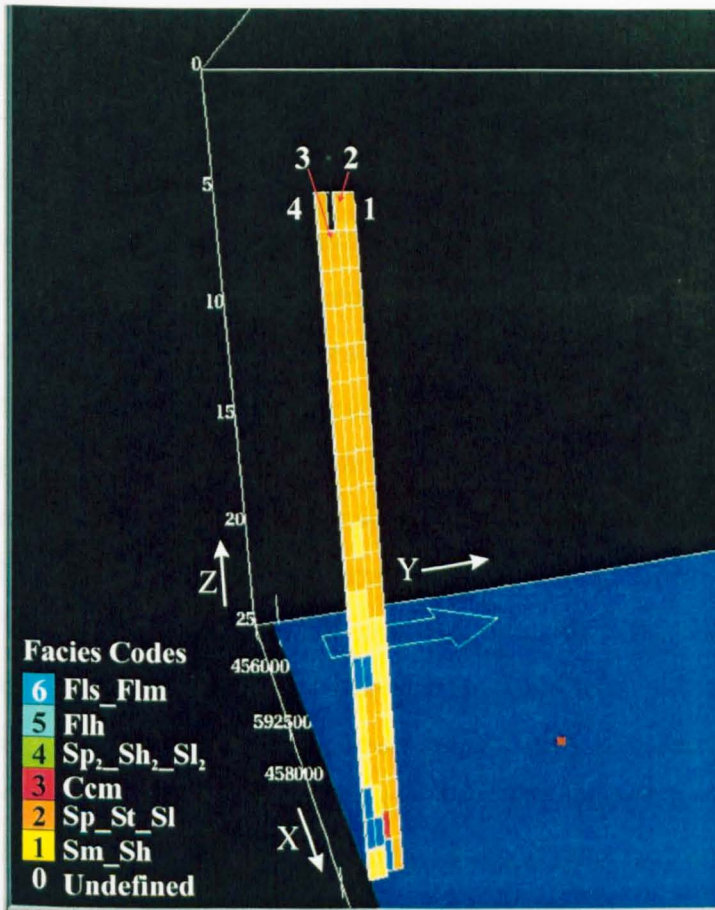


Figure 6.3. Four of the nine blocked wells created for the large modelling grid; these wells represent the four Trusklieve logs. The dimensions of grid cells are 50m x 50m x 1m (X, Y, Z). The extreme vertical exaggeration in this figure allows the individual grid cells and their facies codes to be seen. Dimensions are in metres.

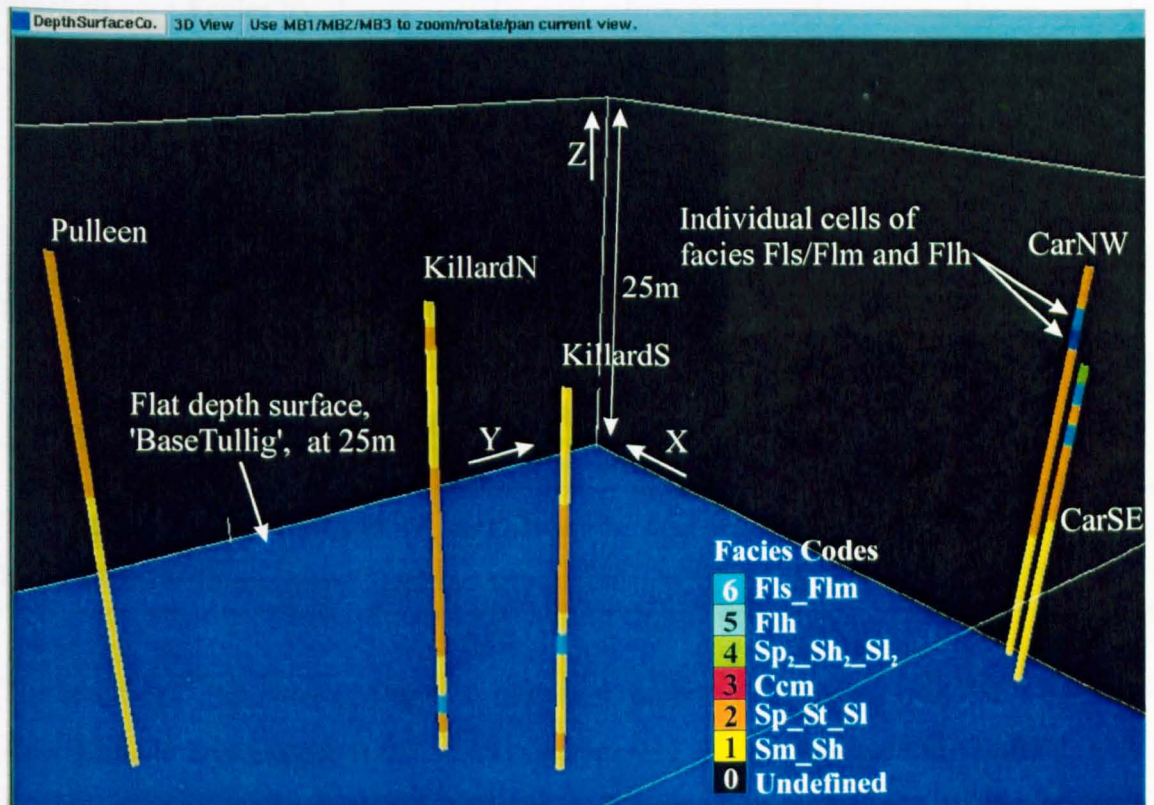


Figure 6.4. Five of the blocked wells created for the large modelling grid. Unlike Fig. 6.3, the grid lines are not displayed in this view, but individual cells can still be seen where a facies code occupies only one cell before a different code replaces it (labelled).

and is the total of facies Sm/Sh, Sp/St/SI, and Ccm. A subdivision of the channels into 'channel-fill' facies and 'barrier' facies can also be made within the model. Facies Sm/Sh was used to represent channel-fill facies, because the basal parts of individual stories in the field were usually filled with massive sandstone (see Sections 4.3 and 5.3). The 'barrier' facies elements of the model are often assigned low permeabilities and used to represent impermeable channel barriers such as fine-grained channel fill, but in this case the 'barrier' facies was specified to be the Sp/St/SI facies and assigned a porosity of 35% (see Table 6.3), to represent the bars within the channels, which (as noted in Section 4.3.1.2) primarily comprise cross-bedded facies and would not be barriers to flow in a reservoir. The volume fraction of the channels occupied by 'barrier' facies (Sp/St/SI) was set to 0.568, ( $0.532/0.936 = 0.568$ ; see Table 6.5). Crevasse facies in the model were specified to be facies Flh, the characteristics of which correspond to typical crevasse splay facies (see Section 3.4.2), and were assigned a volume fraction of 2.7 (Table 6.5). The background facies was assigned a volume fraction of 3.7 (Table 6.5), and was specified to be Fls/Flm, which is seen in the field to be the prevailing background sediment in the absence of sandbody facies.

<b>Blocked Well</b>	<b>Facies % Sm/Sh</b>	<b>Sp/St/SI</b>	<b>Ccm</b>	<b>Sh<sub>2</sub>/Sp<sub>2</sub>/SI<sub>2</sub></b>	<b>Flh</b>	<b>Fls/Flm</b>
Trusk1	19.0	76.2	4.8	0	0	0
Trusk2	9.5	76.2	9.5	0	0	4.8
Trusk3	30	60	0	0	0	10
Trusk4	33.3	52.4	0	0	0	14.3
Pulleen	54.2	41.7	4.1	0	0	0
KillardN	40.9	50.0	4.55	0	4.55	0
KillardS	63.1	31.6	5.3	0	0	0
CarSE	50	33.3	0	5.6	11.1	0
CarNW	31.8	54.5	4.5	0	4.5	4.5
<b>Totals (%)</b>	<b>36.7</b>	<b>53.2</b>	<b>3.2</b>	<b>0.5</b>	<b>2.7</b>	<b>3.7</b>

Table 6.5. The percentages of each facies in each blocked well, derived from the blocked wells for use in the large modelling grid.

The stacking pattern was specified as clustered rather than dispersed (see Table 6.6, and App. D16) to correspond to the close superposition of channels seen in the field, with limited intervening background sediment. Channel-belt width and thickness were specified to correspond to the field outcrops, which show thicknesses up to 32m

(Pulham, 1987) and suggest a channel-belt width within the range 250-15000m (see Section 4.3.1.6). A single channel-belt in the model was therefore sufficient to cover the modelling grid completely, representative of the single channel system seen in the field. Channel-belt amplitude and sinuosity were given values of 500m and 1.1 respectively, both low values, but values that correspond with the conclusions in Chapter 4, where the Tullig Sandstone is interpreted as a braided, low-sinuosity channel system. The number of channels in each belt was set as five, to match the maximum number of storeys (each a separate channel) seen at any one outcrop in the field.

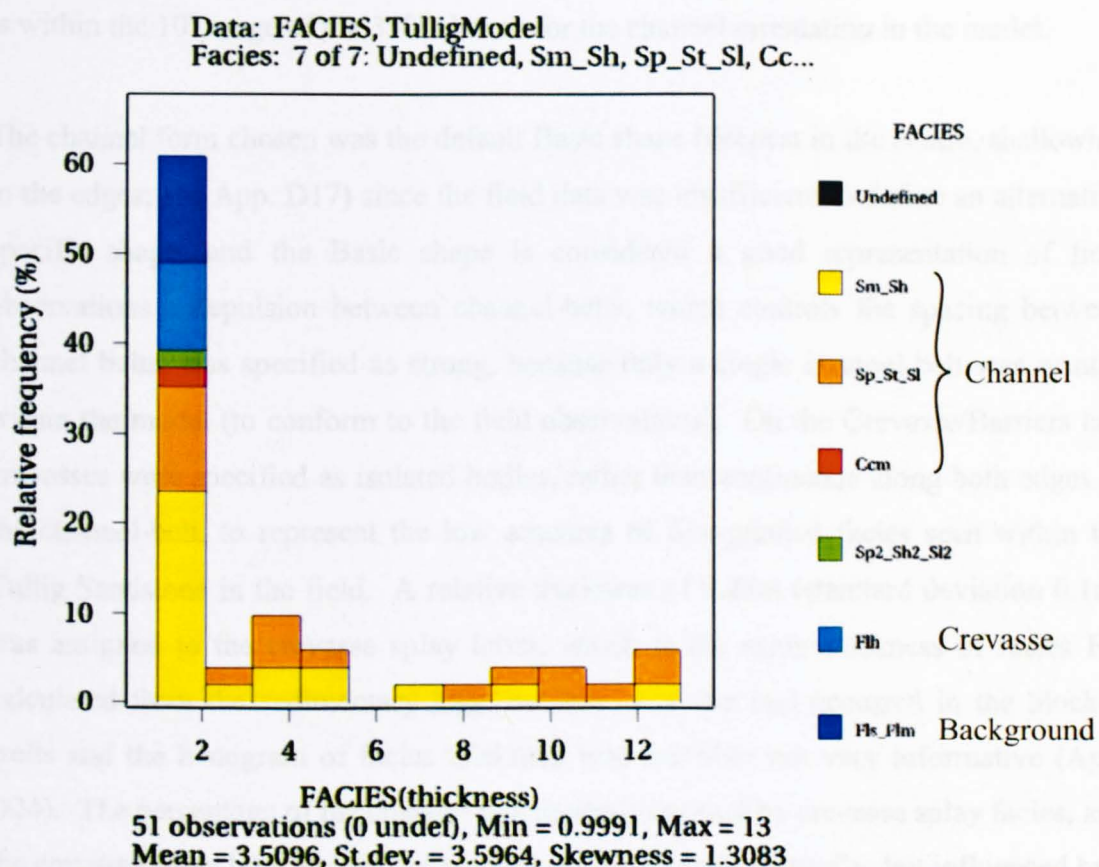


Figure 6.5. Histogram showing the distribution of facies thicknesses in metres, taken from the blocked wells of the large modelling grid and colour coded by facies. Cell thickness for this grid is 1m, making 1m the minimum possible bed thickness.

Individual channel thickness was specified to be similar to the mean storey thickness recorded in the field. Individual channel width was also based on field evidence, and because no clear channel margins were seen in any outcrop, the value given was wider than the widest outcrop to account for this. A correlation strength of 0.5 between width and thickness was chosen as an arbitrary value to express a medium amount of

correlation between the two dimensions. Amplitude and sinuosity of individual channels were assigned arbitrarily but with a low-sinuosity braided interpretation as a basis; ideally, multiple realisations could be run to see what effect changing these values would have on the final model, but this was precluded by time constraints here. The channel-belt orientation was set similar to the mean palaeocurrent direction calculated from the field data. The y-axis of the grid is oriented at  $000^{\circ} - 180^{\circ}$ , but represents a direction of  $045^{\circ}$  in the real world. The real world mean palaeocurrent direction of  $028^{\circ}$  (Section 4.4) thus translates to a direction of  $342^{\circ}$  in the model, which is within the  $10^{\circ}$  range of the  $350^{\circ}$  chosen for the channel orientation in the model.

The channel form chosen was the default Basic shape (deepest in the centre, shallowing to the edges; see App. D17) since the field data was insufficient to define an alternative specific shape, and the Basic shape is considered a good representation of field observations. Repulsion between channel-belts, which controls the spacing between channel belts, was specified as strong, because only a single channel-belt was wanted within the model (to conform to the field observations). On the Crevasse/Barriers tab, crevasses were specified as isolated bodies, rather than continuous along both edges of the channel-belt, to represent the low amounts of fine-grained facies seen within the Tullig Sandstone in the field. A relative thickness of 0.25m (standard deviation 0.1m) was assigned to the crevasse splay lobes, which is the mean thickness of facies Flh calculated from the sedimentary logs, because only one bed occurred in the blocked wells and the histogram of facies thickness was therefore not very informative (App. D24). The percentage of the channel-belt margins covered by crevasse splay facies, and the crevasse splay lobe widths and lengths, were assigned arbitrarily, but influenced by

Following page: Table 6.6. Specifications used for facies modelling using the Facies Channels tool in the large grid. The “jobs” panels, and individual tabs, where these data are specified are shown in Apps. D14 to D20. Reasons for the specifications shown here are given in the text. \*“Barrier” as used in the modelling job set-up refers to 3-D facies objects within the channels (rather than outside them, like crevasses). These in-channel objects can be barriers to hydrocarbon flow (if they are specified as non-porous, impermeable lithologies) but in this model they represent in-channel bars of facies Sp/St/S1 and are thus not barriers to flow.

<b>Preference</b>	<b>Choice</b>
<b>General</b>	
Blocked wells used for conditioning	Trusk1, Trusk2, Trusk3, Trusk4, Pulleen, KillardN, KillardS, CarSE, CarNW
Condition on well data/and raw logs	Yes, yes
Channel system	Multi-channel mode
Auxiliary facies	Crevasses, barriers*
Channel facies	Sm/Sh
Crevasse facies	Flh
Barrier* facies	Sp/St/SI
Background facies	Fls/Flm
<b>Volume fraction</b>	
Channel system volume fraction: type	Global
- value	0.9 (i.e. 90% of volume is channel system)
- tolerance	0.005
Crevasse volume fraction:	Fraction of channel system volume
- type	Global
- value	0.05 (i.e. 5% of volume is channel system)
- tolerance	0.02
Barrier* fraction of channel volume	0.57
Stacking pattern	Clustered
Belt width	5000m
Belt thickness	35m
Belt amplitude	500m
Belt sinuosity	1.1
Number of channels in a belt	5
Tolerance	1
Channel thickness	10m 2 s.d.
Channel width	700m 100 s.d.
Correlation width/thickness	0.5
Amplitude of individual channels	400m, 50 s.d.
Sinuosity	1.1
Orientation	350° 10° variation
<b>Form/repulsion</b>	
Channel form	Basic
Repulsion	Strong
<b>Crevasse/barrier</b>	
Crevasse geometry:	Isolated crevasses
- relative thickness	0.25m, 0.1 s.d.
- channel margin coverage	0.4
- relative lobe width normal to channel	1
- absolute lobe length parallel “ “	400m
Number of crevasse belts per channel	2
Vertical position	Random
Barriers: thickness	5.5m, 2 s.d.
- width	200m, 25 s.d.
- length	250m, 50 s.d.

observations of the extent of beds of facies Flh in the field. The number of crevasse belts per channel (2) and their vertical position (random) were left as the default values because no information on crevasse geometries was discovered in the field. For the 'barrier' facies within the channels, representing bar-forms comprising facies Sp/St/Sl, a thickness of 5.5m was specified, with a standard deviation of 2; both values were taken from the bed thickness histogram generated from the blocked wells (App. D 22), and the thickness corresponds well to the thickness of probable bar-forms measured in the field (e.g. Section 4.3.1.1). The width (200m, s.d. 25) and length (250m, s.d. 50) of the 'barrier' facies were chosen based on field observations of the lateral and downstream continuity of beds of facies Sp/St/Sl.

The final two tabs that could be set up to simulate field observations were the Correlation tabs (see App. D19 and D20), which can be opened from the Geometry tab (App. D16). Using the Correlation tabs, correlations between logs that were either walked out in the field or postulated based on sedimentary characteristics could be included in the model. The only drawback of the tool is that it only allows correlations between beds of the specified channel facies (in this case Sm/Sh). Nonetheless, the tool enabled correlations between the two Killard wells (App. D19) and the four Trusklieve wells (App. D20) to be specified.

#### **6.4.2 Small modelling grid: Trusklieve**

The small size of this modelling grid (500m x 500m x 25m) allowed a small cell size and therefore a fine (0.1m) vertical resolution in the blocked wells. The blocked wells are shown in Fig. 6.6, and the facies thickness distributions based on these blocked wells are displayed as histograms for individual facies in App. D 27 to D30; these graphs are summarised in Fig. 6.7. Facies percentages for the small grid are given in Table 6.7.

For facies modelling in the small grid, the Facies Channel tool was used, in the same way that has been described for the large modelling grid in Section 6.4.1. Where there are differences in input values, these differences are explained; otherwise the set-up and preferences remain the same as those already described. Table 6.8 lists the specifications used for the small grid.

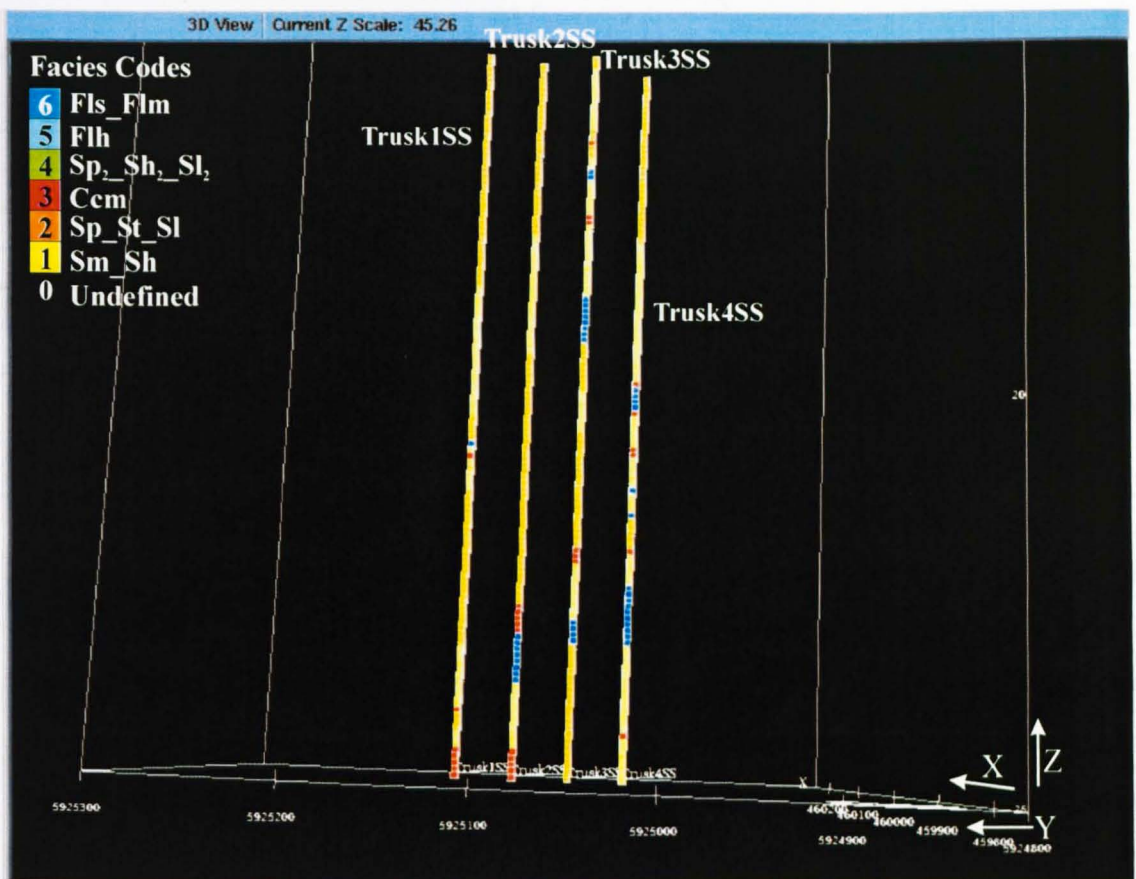


Figure 6.6. The four blocked wells created for the small modelling grid (focussed on the Trusklieve outcrop) are shown here. Each interval of a blocked well is a single grid cell. The dimensions of the grid cells in the Trusklieve grid are 5m x 5m x 0.1m (X, Y, Z). There is strong vertical exaggeration in this figure to allow individual cells to be seen.

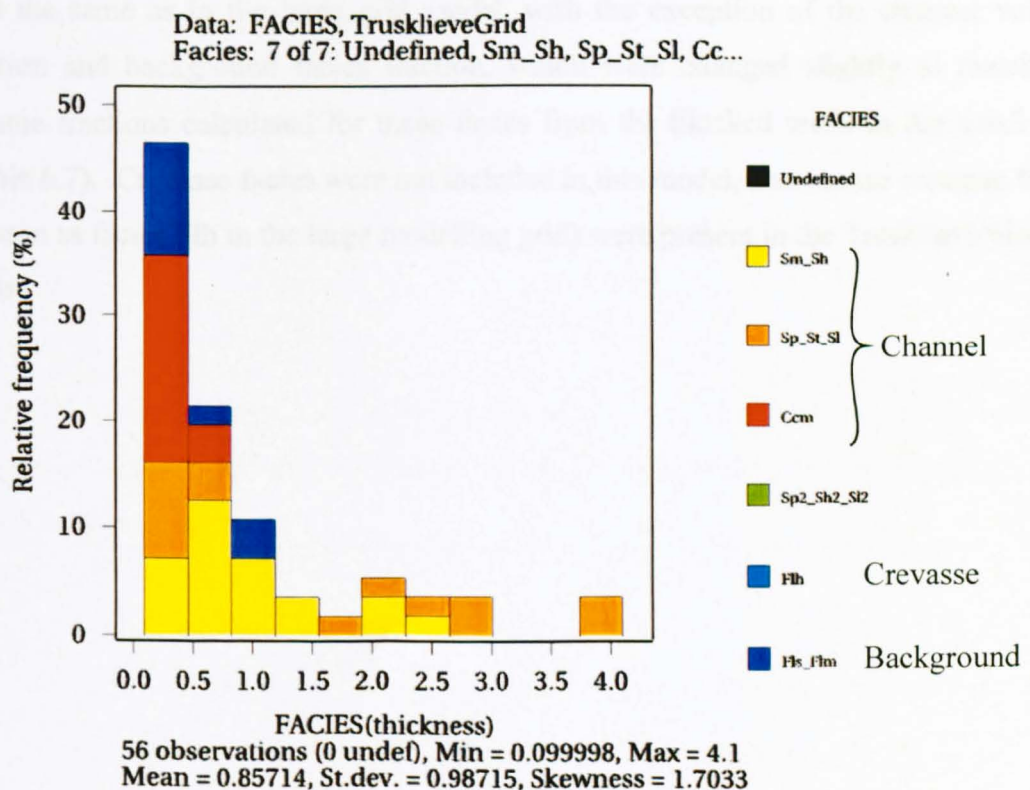


Figure 6.7. Histogram showing the distribution of facies thicknesses, taken from the blocked wells of the small modelling grid and colour coded by facies. Cell thickness for this grid is 0.1m, making 0.1m the minimum possible bed thickness.

<b>Blocked Well</b>	<b>Facies % Sm/Sh</b>	<b>Sp/St/SI</b>	<b>Ccm</b>	<b>Sh<sub>2</sub>/Sp<sub>2</sub>/Sl<sub>2</sub></b>	<b>Flh</b>	<b>Fls/Flm</b>
Trusk1SS	33.1	59.5	6.6	0	0	0.8
Trusk2SS	25.0	59.2	8.3	0	0	7.5
Trusk3SS	38.2	45.5	4.9	0	0	11.4
Trusk4SS	52.5	29.2	5.0	0	0	13.3
<b>Totals (%)</b>	<b>37.2</b>	<b>48.3</b>	<b>6.2</b>	<b>0</b>	<b>0</b>	<b>8.3</b>

Table 6.7. The percentages of each facies in each blocked well, derived from the blocked wells for use in the small modelling grid.

The main difference between the specifications for the small and large grids is the channel geometry. The channel-belt width and thickness were changed to correspond to the smaller size of the small grid, because values much greater than the grid size caused errors. As long as a single belt could cover the grid, the difference in belt width would not impact the number of belts in the small grid. The thicknesses of individual channels and barrier facies had to be changed as well, to correspond to the facies thicknesses observed in the blocked wells (see histograms in App. D27-30). The facies thicknesses were thinner than for the large grid, because the resolution of the blocked wells in the small grid was finer, thus allowing thinner beds to be modelled. The other values were kept the same as in the large grid model, with the exception of the channel volume fraction and background facies fraction, which were changed slightly to match the volume fractions calculated for these facies from the blocked wells in the small grid (Table 6.7). Crevasse facies were not included in this model, because no crevasse facies (chosen as facies Flh in the large modelling grid) were present in the Trusklieve blocked wells.

<b>Preference</b>	<b>Choice</b>
<b>General</b>	
Blocked wells used for conditioning	Trusk1SS, Trusk2SS, Trusk3SS, Trusk4SS
Condition on well data/and raw logs	Yes, yes
Channel system	Multi-channel mode
Auxiliary facies	Barriers*
Channel facies	Sm/Sh
Barrier* facies	Sp/St/SI
Background facies	Fls/Flm
<b>Volume fraction</b>	
Channel system volume fraction: type - value	Global 0.895 (i.e. 89.5% of volume is channel system)
- tolerance	0.03
Barrier* fraction of channel volume	0.537
Stacking pattern	Clustered
Belt width	500m
Belt thickness	25m
Belt amplitude	500m
Belt sinuosity	1.1
Number of channels in a belt	5
Tolerance	1
Channel thickness	1m 0.7 s.d.
Channel width	200m 20 s.d.
Correlation width/thickness	0.5
Amplitude of individual channels	400m, 50 s.d.
Sinuosity	1.1
Orientation	350° 10° variation
<b>Form/repulsion</b>	
Channel form	Basic
Repulsion	Strong
<b>Crevasse/barrier</b>	
Barriers: thickness	1.66m, 1.467 s.d.
- width	120m, 25 s.d.
- length	250m, 50 s.d.

Table 6.8. The specifications listed in this table are those used for facies modelling using the Facies Channels tool in the small grid. Reasons for the specifications shown here are given in the text.

## 6.5 Modelling results

### 6.5.1 Results from the large modelling grid

Once all the specifications had been set up as described in Section 6.4.1 above, the modelling job for the large grid was executed. The facies model took about 36 hours to be completed, during which time channel objects were repeatedly generated, put into the grid, and either accepted or rejected depending on whether they fitted the blocked wells; this process was monitored by the modelling tool, and examples of the graphs created can be seen in App. D31-35 (which are for the small grid). By the end of the modelling, the grid was populated by channels and other facies objects. Figure 6.8 shows the finished model, and Fig. 6.9 shows a cross-section that goes through the northernmost well locations to show how the model matches the blocked wells.

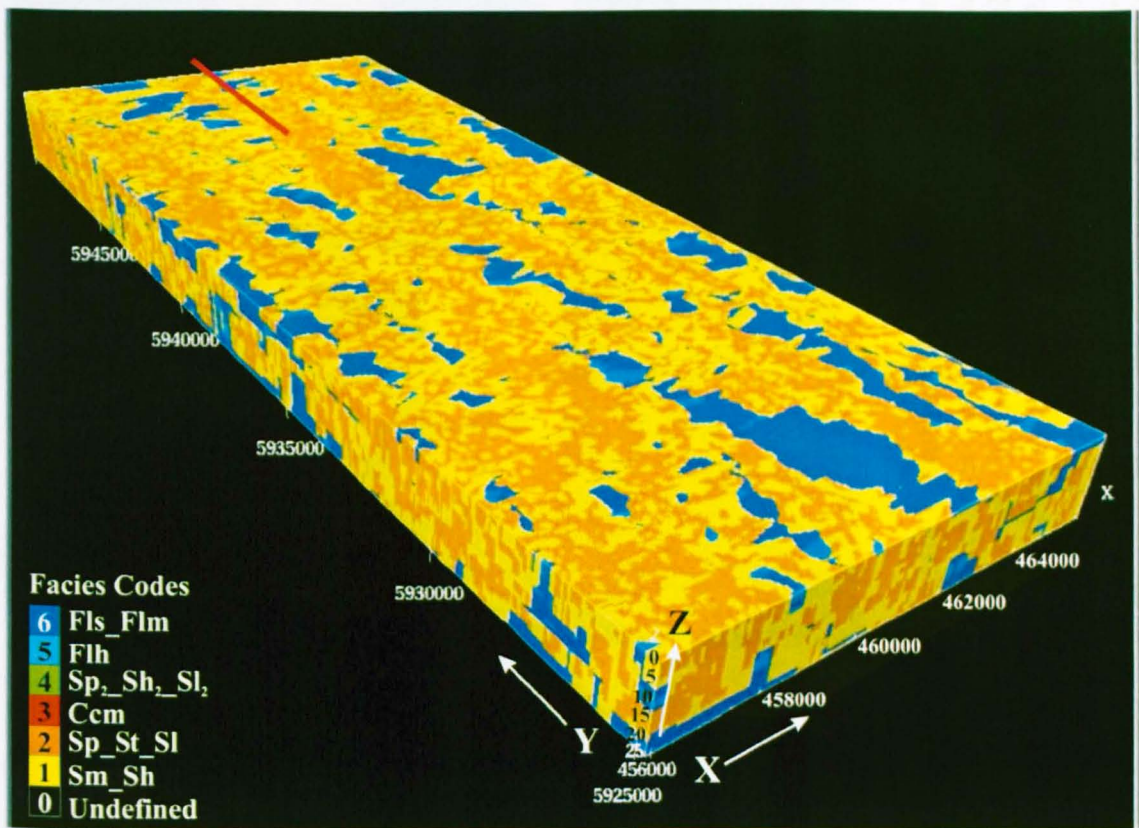


Figure 6.8. An image of the facies model created for the large modelling grid, viewed from the west. Note the northeast-southwest orientation of the channels (facies 1 and 2) and the intervening areas of fine-grained sediment (facies 5 and 6). Scales are in metres. The red line shows the approximate position of the cross-section in Fig. 6.9

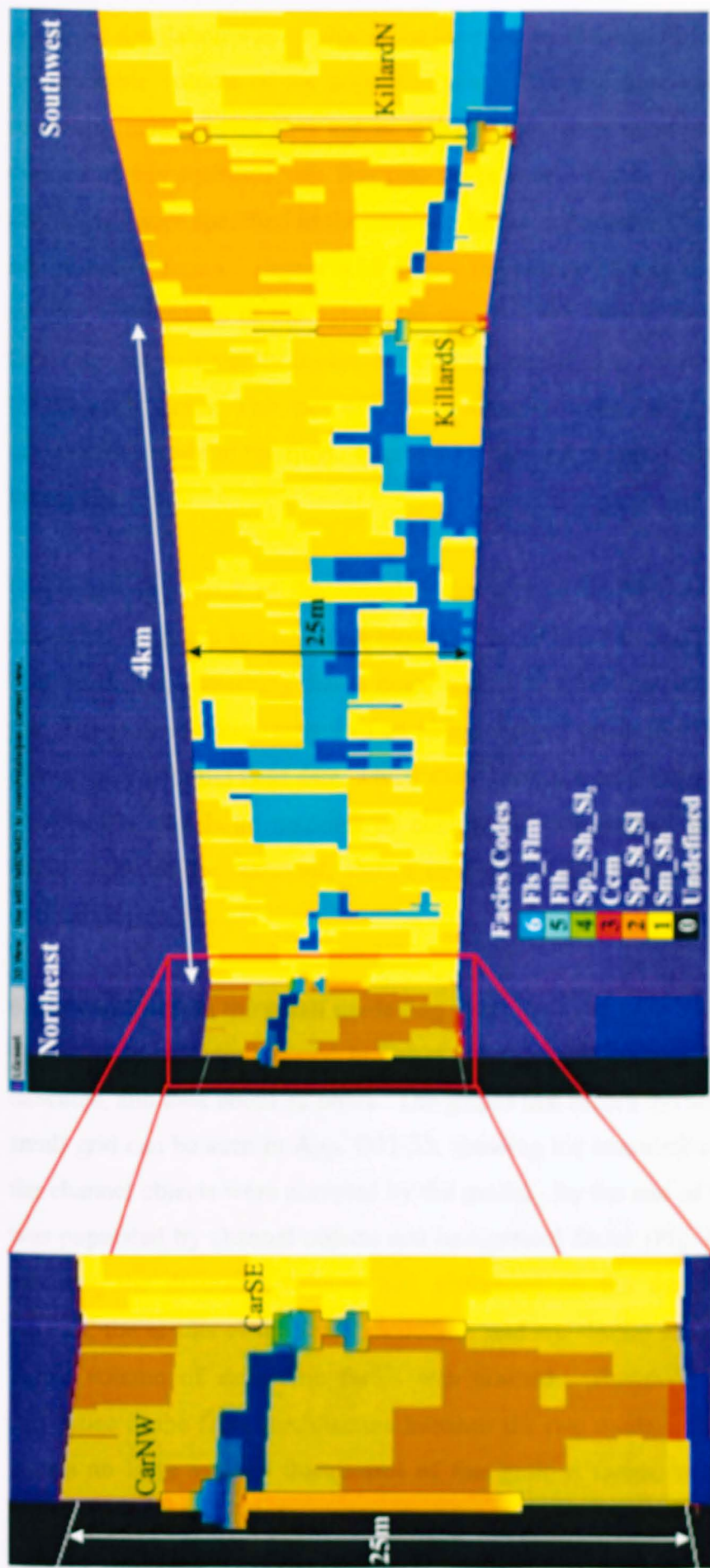


Figure 6.9. A close-up view of the northern end of the "coastline" cross-section through the large modelling grid. The cross-section intersects each of the wells (which are constructed from sedimentary logs taken at the field outcrops). The cylinder logs for each locality are shown, and two Carrowmore Point logs included in the model can be seen in the enlargement, where the match between the logs and the facies in the cross-section is apparent. The colours and widths of the cylinder logs follow the Facies Codes key (although the colours are slightly blurred and shifted up relative to the width-changes, a quirk of the software). For example, facies 6, Fls/Flm, has a relative width of 6 and is coloured dark blue, while facies Sm/Sh has a width of 1 and is coloured dark blue. The cross-section shows that the distribution of fine-grained facies (in blue tones) in the model is dissimilar to that observed in the field, with thicknesses of up to 20m occurring, far greater than the maximum thicknesses of ~2m seen in outcrop.

A second simulation was conducted on the completed facies model, in order to calculate the drainable volume of the populated grid. The drainable volume is the volume of reservoir-quality facies that are in contact with each other and could in theory be drained of any hydrocarbons that may be present. Facies Sm/Sh, Sp/St/Sl, Ccm and Sh<sub>2</sub>/Sp<sub>2</sub>/Sl<sub>2</sub> were specified as the reservoir facies, with facies Flh and Fls/Flm as sealing, non-reservoir facies. Figure 6.10 shows the results of this simulation; the drainable volume corresponds to the volume of the reservoir facies, indicating that the sealing facies are not sufficiently continuous or interconnected to prevent complete drainage of the reservoir facies. This lack of lateral continuity in the fine-grained facies mirrors the observations made in the field. Figure 6.11 shows a cross-section that goes through the nine wells.

One surprising result of the model is the vertical thicknesses of fine-grained facies generated. Figs 6.8 and 6.9 show blocks of facies Fls, Flm and Flh that extend for up to 20m vertically, something that is never seen in the field outcrops. Fig. 6.8 also shows that fine-grained facies extend in an along-channel orientation for up to 5km, another discrepancy with the field data, which show limited lateral extents of fine-grained beds. Nonetheless, the large volumes of continuous fine-grained facies do not affect the connectivity of the reservoir, shown by the fact that the entire sandstone volume is drained (Fig. 6.10).

### **6.5.2 Results from the small modelling grid**

Once the specifications listed in Table 6.8 had been entered, the modelling job was executed, and took about 32 hours. The graphs that record the modelling process for the small grid can be seen in App. D31-35, showing the cumulative frequency with which the channel objects were accepted by the model. By the end of the modelling, the grid was populated by channel objects and background facies (Fig. 6.12). A simulation to calculate the drainable volume was performed on the finished model (Fig. 6.13). Overall, the results of the small modelling grid are similar to the large grid in that the entire volume of sandstone facies was drained. However, there is an important difference in the facies architecture between the two models; the small modelling grid shows no large vertical thicknesses of fine-grained facies, with most occurrences of facies Flm, Fls and Flh being less than 2m thick (Fig. 6.12). Lateral extents of fine-grained facies also appear reduced compared with the large grid, with many fine-

grained intervals extending for less than half the grid length (<250m). The differences in architecture between the two models are partly due to the fact that in the smaller model, the vertical resolution of the blocked wells is finer.

## **6.6 Discussion**

### **6.6.1 Similarity of models to field observations**

A visual inspection of the large and small grid models (Figs 6.8, 6.9, 6.12) reveals that the large model produces sandstone facies architectures closer to those observed in the field. The large grid model displays thick “units” of facies Sm/Sh and Sp/St/Sl, replicating the thick (11-22m) upper storeys seen at Killard, Carrowmore and Pulleen, which comprise predominantly one or other of these two facies. The reason the large grid models these sandy storeys so well is because the coarse 1m vertical resolution of the blocked wells in the large model allowed the channel body thickness to be specified as a value close to the thickness of the individual stories seen in the field. Therefore individual channels put into the model closely resembled the storeys measured in the field.

In contrast, the fine (0.1m) resolution of the blocked wells in the small grid meant that the bed thickness statistics from those wells showed reduced channel facies thicknesses (Sm/Sh) compared with the large grid (compare Figs 6.9 and 6.12). The channel-belt thickness specified in the simulation set-up had to be very close to the mean thickness of the designated channel facies calculated from the blocked wells in order for the model to be populated successfully with channel sandbodies. As a result, the model produced had unrealistically thin channels that did not resemble the channel stories seen in the field. Effectively, individual beds were being modelled rather than individual storeys/channels. A visual comparison of the large and small grid models shows that while the large grid exhibits storey-scale architectural similarity to the actual outcrops, the small grid displays a close resemblance to the small-scale facies/bedding “maps” of the field outcrops presented in Chapter 4 (e.g. Figs 4.1, 4.3 and 4.16).

The field observations regarding the architecture of the fine-grained facies is simulated well only in the small model. At outcrop, laterally persistent, thick, fine-grained facies are not encountered within the Tullig Sandstone, and even where fine-grained beds can be traced for tens of metres along strike, they cannot be positively identified in nearby

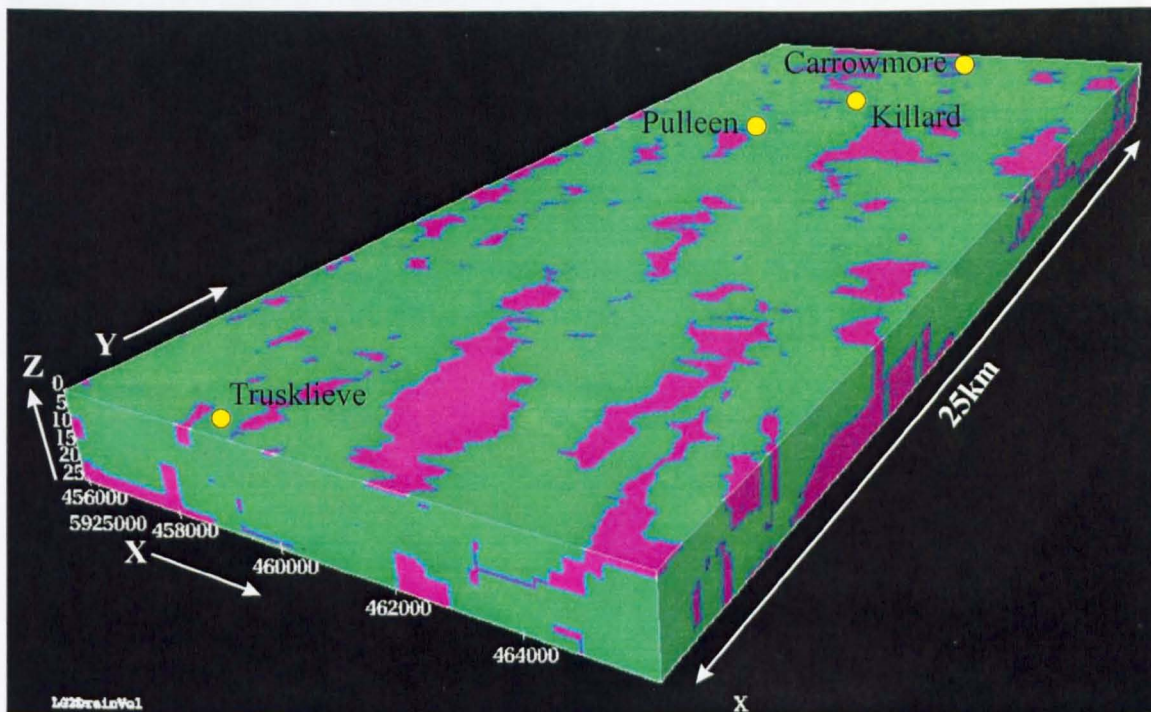


Figure 6.10. The facies model for the large grid, displayed in terms of drainable volume. The green areas are interconnected (and therefore drainable) reservoir facies (Sm/Sh, Sp/St/Sl, Ccm, Sh<sub>2</sub>/Sp<sub>2</sub>/Sl<sub>2</sub>); the pinky-purple areas are impermeable facies (Flh, Fls/Flm). The grid is viewed from the south.

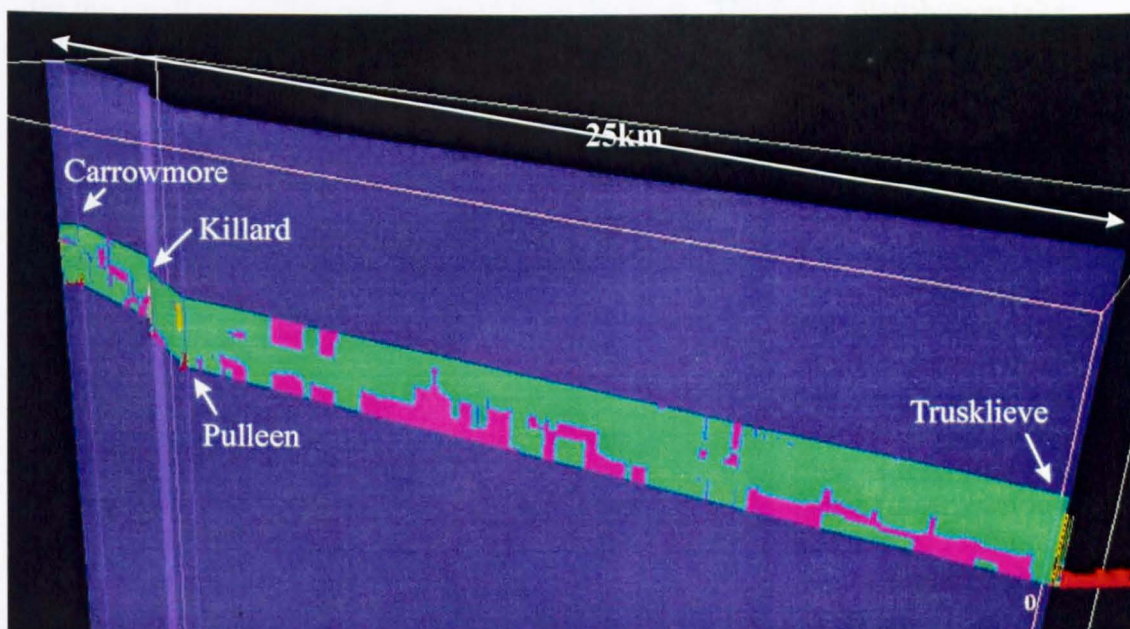


Figure 6.11. A cross-section through the drainable volume for the large grid. The section line goes from one blocked well to the next and is effectively a slice along the real-world coastline. The colour scheme is as in Fig. 6.10 above. The section is viewed from the west-northwest.

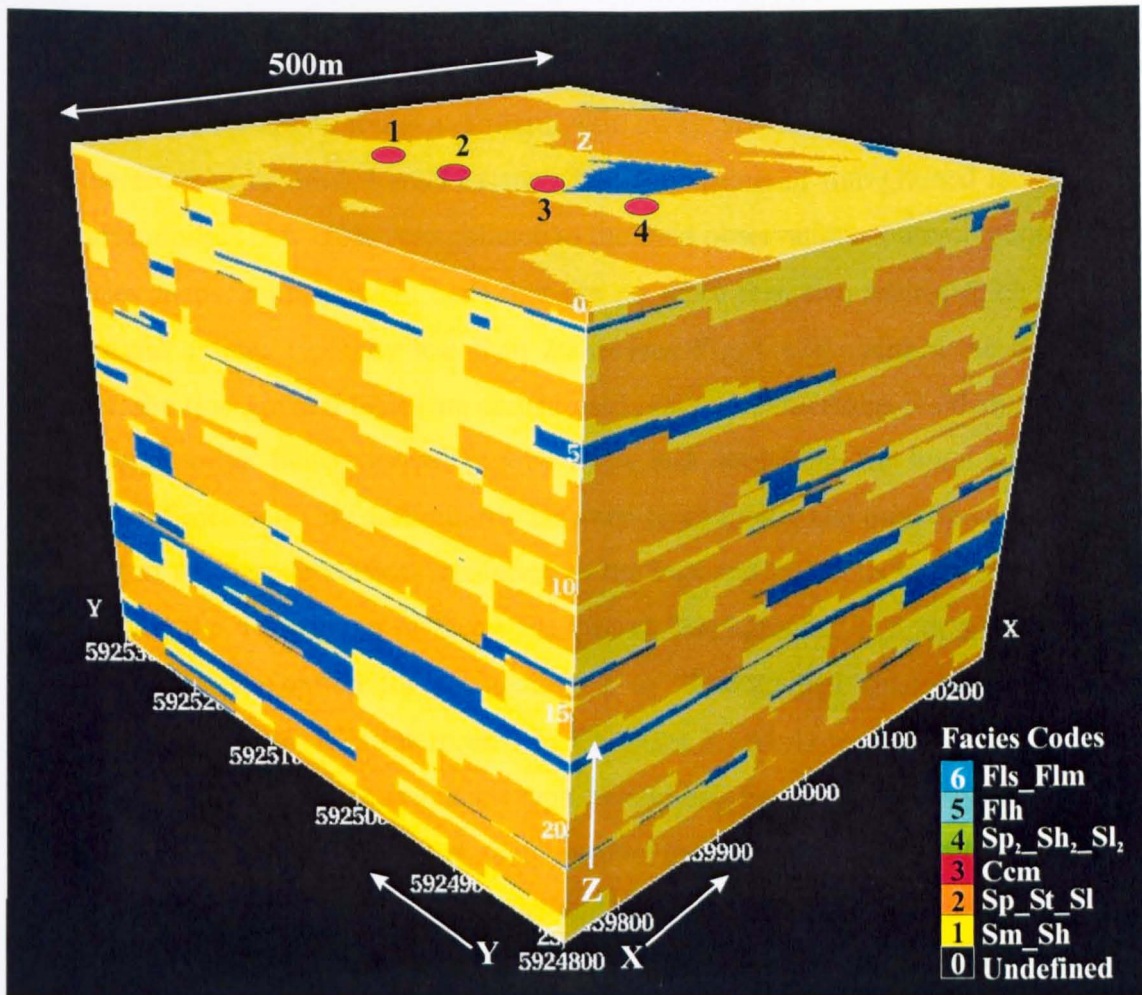


Figure 6.12. Image showing the volume generated by the Facies Channels simulation for the small modelling grid, viewed from the west. The facies distribution takes account of the blocked wells and fits the volume fractions specified in the job set-up. Well locations are shown in red.

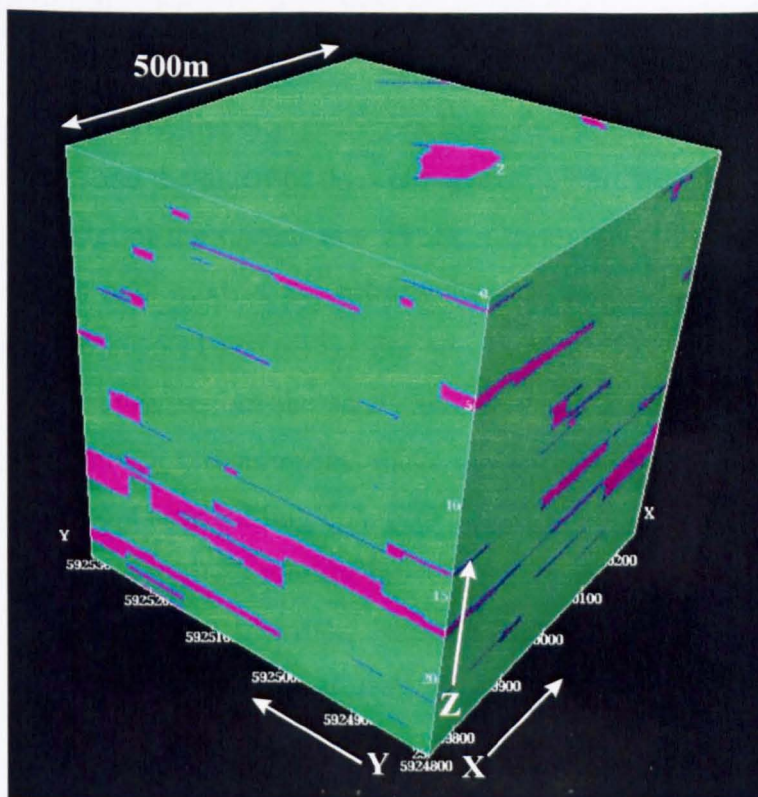


Figure 6.13. An image of the small grid, viewed from the WNW, showing the drainable volume (i.e. the volume of the facies model that is both interconnected and of reservoir quality). In this model, facies 1 (Sm/Sh) and 2 (Sp/St/SI) were specified as reservoir-quality facies (green) while facies 5 and 6 (Flh, Fls/Flm - purple) are the impermeable, sealing facies.

outcrops (for example the fine-grained facies within the upper few metres of the outcrop at Carrowmore cannot be found at Killard, 4km away; see Sections 4.3.3 and 4.3.4) and must therefore be of limited areal extent. The dimensions of fine-grained facies in the small grid model show close resemblance to the field observations, outcrop photographs and facies maps, with mud/silt beds that are no more than two metres thick and that show lateral extents typically less than 200m (see Fig. 6.12). Within the large grid, however, the fine-grained facies are considerably more areally extensive than those seen in the field, often being several metres thick and stretching for hundreds or even thousands of metres. This dissimilarity between large model and outcrop is likely to be the result of the coarser vertical resolution of the logs and grid cells in the large grid. It is likely that the designation of facies Fls/Flm as “background” (i.e. floodplain) in the model (there is no option for designating it as “fine-grained channel abandonment facies”, which is how it is interpreted in Chapters 3 and 4) means that the facies is modelled as an areally extensive facies type, accounting for the disparity between model and outcrop. It should be noted that, despite the mismatch in fine-grained facies architecture between the large grid model and the outcrops, the total percentage of fine-grained facies was the same in the model as in the field, having been specified in the modelling set-up. This means that the large model is grouping the fine-grained fraction into volumetrically large “patches”, and is therefore not reproducing the thinner but laterally extensive silts and mudstones seen at outcrop, which would result in reduced tortuosity of flow paths within the model compared with the outcrop.

Interestingly, the discrepancy in fine-grained facies architecture between the large grid model and the outcrops does not appear to adversely affect the connectivity or reservoir potential of the system as a whole. Comparing the large and small grid models shows that in both models, the entire volume of sandy facies is interconnected and drainable (Figs 6.10, 6.11 and 6.13). The way in which both models predict a very high degree of connectivity within the sandy facies of the Tullig Sandstone system agrees with the connectivity measurements made in the field and confirms that the models agree with the field data regarding connectivity. It is therefore concluded that differences in scale of vertical resolution of the models, and the architectural dissimilarity between the large model and the outcrops, are not necessarily significant in terms of volumetric hydrocarbon recovery, as long as net to gross ratios are high. However, the ease of extraction, particularly for oil, is expected to vary significantly depending on how

realistically the fine-grained facies are modelled, with a more realistic (i.e. finer-resolution) model resulting in increased difficulty of extraction. It is expected that an analysis of fluid flow through the large and small modelling grids would reveal dissimilarities in flow pathways, demonstrating an increased tortuosity of flow paths and therefore an increased difficulty of oil extraction in the smaller, finer-resolution model. The far lower viscosity of gas would mean that gas extraction would not be affected as significantly as oil extraction, so for the El Wastani gas-filled sands either model would represent a reasonable simulation of the reservoirs, since the connectivity is high in both, and the recoverable volume is not affected by the differences between the models.

### **6.6.2 Limitations of models**

The problem of accurately modelling numerous facies using the Facies Channels tool is demonstrated by the differences between the large and small models, and by the differences between the models and the outcrops. For example, within the confines of the model it is not possible to have more than one facies designated as “channel” facies, meaning that the main channel-fill facies seen in the field (Sm, Sh, Sp, St, Sl, Smc and Shc) had to be combined and modelled as “channel” and “intra-channel barrier” facies. The result is that the architecture of the channel storeys seen in the field is not accurately reproduced within either the small or the large modelling grid. The large grid has the correct channel geometries, but the channels comprise only one facies; the small grid shows the correct distribution and interbedding of facies, but cannot reproduce the storey architecture.

If the modelling tool allowed several facies to be grouped into the “channel” facies, the architectures of individual beds and individual storeys could be simulated within a single model, whereas only one or the other can be modelled at a time using the existing modelling tool. The problem is not so acute when considering fluid flow and drainability, because in this study the porosities of the main channel-fill facies are very similar, so considering them all as a single facies will not affect reservoir properties. However, if trends were seen within channels in an outcrop, for example fining-up, the facies changes seen in the vertical profile (e.g. Ccm to Sm to Sp to Sr to Flh to Flm) could be accounted for by specifying a vertical trend in porosity and/or permeability within a single channel body prior to the modelling of fluid flow.

Another way to tackle the problem of modelling multiple facies would be to combine facies codes 1, 2 and 3 (facies Sm/Sh, Sp/St/SI and Ccm) and designate the resulting single facies as “channel” facies in the blocked wells and in the modelling set-up. However, combining these three facies would reduce the amount of detailed facies distribution information in the models and would lessen the ability of the model to realistically simulate the field observations. The visual appearance of the model and the distribution of sandy channel-fill facies are of less significance in terms of hydrocarbon considerations than the distribution and geometry of the impermeable facies. The finer resolution of the small grid allows more precise simulation of the areal extents, thicknesses and distributions of the fine-grained facies than the large grid, and therefore will provide a more detailed, and conceivably more accurate, picture of fluid flow pathways and drainable volumes than the large grid model.

A final problem encountered while using RMS concerned the mouthbar sandbodies seen in the field (at Tullig Point and Killard). Mouthbar sandbodies are frequently good reservoirs for oil and gas and the heterogeneities within them are of immediate concern to those companies with hydrocarbon prospects in deltaic environments. It is not possible to model mouthbars (or any discrete non-channel sandbody) using the Facies Channel tool, although this might be useful, considering the fact that, in the real world, fluvial channels often cut into mouthbar deposits (as seen at Pulleen – see Section 4.3.2). Facies Composite would be a more appropriate modelling tool for mouthbar simulation. While Facies Channels allows a number of different architectural elements within a channel system to be modelled, Facies Composite uses simple objects that can be specified to resemble channels (elongate, with convex-down bases) or spheroidal shapes that could represent mouthbars. Each object type is associated with a particular facies. However, using the Facies Composite modelling tool, the internal complexity of the mouthbar sandbodies studied in the field can not be modelled; all that would be possible is the addition of a petrophysical trend to the mouthbar objects, for example a coarsening-up signature of increasing porosity and permeability with height. The detailed internal architecture and facies distribution would be lost in the modelling process.

## Chapter 7

### Conclusions and recommendations for further work

#### 7.1 Conclusions

The fieldwork conducted on the Namurian fluvial and deltaic sediments that crop out along the coast of the County Clare allowed the description, quantification and interpretation of the internal architectures and facies distributions of the Tullig Sandstone, and of two smaller sandbodies stratigraphically lower in the Tullig Cyclothem. An interpretation of the palaeoenvironment in which the Tullig Cyclothem sediments were deposited was made, and compared with existing models of the Western Irish Namurian Basin.

The interpretation of facies seen in the field area was consistent with previous work (e.g. Pulham, 1987) and allowed the identification of three main facies associations: a coarsening-up mouthbar facies association, a shallow-water interdistributary bay facies association, and a fluvial facies association. The studies of the Tullig Sandstone allowed identification of channel-fill and bar-form architectural elements. Channel-fill deposits were variable in terms of facies and architecture, exhibiting: 1) internal scour surfaces and associated lags of intraformational conglomerate; 2) massive sandstones interpreted as bank-collapse deposits; 3) organic-rich massive sandstones interpreted as flood-related deposits; 4) fine-grained intervals interpreted as abandoned channel fills showing *in situ* plant material and internal deformation; and 5) thick successions of dune-scale cross bedding interpreted to represent the migration of dune fields along the channels. All such channel-fills were characterised by an absence of dipping accretion surfaces. One particular element in the Truskleeve outcrop (Storey 2, sub-storey III) was interpreted as a cross-bar channel based on its geometry, orientation and facies. Bars (macroforms) were identified in the Truskleeve outcrop, and both downstream and lateral accretion geometries were recognised. Downstream macroform accretion was also interpreted for the lower few metres of the Carrowmore Point outcrop. The macroforms seen in outcrop were interpreted as mid-channel bar forms (also known in the literature as braid bars), and displayed a range of facies but were dominated by cross-bedded sandstones.

The geometries, facies and architectures seen in the Tullig Sandstone led to its interpretation as a low sinuosity braided fluvial system, based on the high percentage of channel-fill compared with macroform deposits, the occurrence of downstream accretion and limited lateral accretion, the similar mean grainsize of the bar deposits and channel-fill deposits, consistently north- to northeast-directed palaeocurrents, and the absence of a fining-up signature that characterises meandering fluvial systems. Palaeocurrent data from throughout the Tullig Sandstone indicated overall flow to the north-northeast, with a range of flow directions from north-northwest to east-southeast. Flow depths were calculated to be within the range 3-8m, with depths of erosion at storey bases up to 8.5m but decreasing downstream, and thicknesses of individual stories up to 22m. The lower stories of the Tullig Sandstone were found to be thinner than the upper stories. Sandbody thickness decreases sharply at the northernmost locality (Furreera), which is considered to represent a location in the lower delta plain where channels are no longer stacked in a multistorey pattern but have diverged and are single-storey distributaries.

Facies distribution data showed downstream and vertical trends of 1) decreasing percentages of conglomeratic facies 2) decreasing percentages of massive sandstones 3) increasing facies homogeneity. Together with the decrease in depth of erosion downstream, and the increase in storey thickness towards the top of the Tullig Sandstone, these facts are interpreted to represent an increasing rate of generation of accommodation space over time, and in a downstream (NNE) direction. The overall percentage of fine-grained facies in the Tullig Sandstone is low, at 3.5%, and the connectivity between sandstone facies within the sandbody is high, calculated to be 93%.

The upper parts of the coarsening-up mouthbar facies associations at Tullig Point and Killard show sharp-based sandy successions between 8 and 15m thick, dominated by argillaceous planar laminated and cross-bedded sandstones, and showing evidence of wave and storm reworking and bioturbation by fauna typical of shallow, brackish water delta front environments. The mouthbar at Killard is calculated to be about 2km wide normal to palaeoflow. The mouthbar sandbodies have a higher percentage of fine-grained facies than the Tullig Sandstone, at 10%, and show a lower connectivity of sandy facies (65%).

The field observations support the basin model advocated by Wignall and Best (2000), which considers the Tullig Cyclothem to represent a fluvio-deltaic system prograding to the NNE into a northward-deepening basin. The controls on the erosion and deposition of the Tullig Sandstone are not able to be resolved unequivocally, with effects of autocyclic incision induced by fluvial scour, and allocyclic incision induced by relative sea-level fall (as proposed by Hampson *et al.*, 1997), both considered to have had an effect.

A study of available data, from both published literature and unpublished reports, revealed a distinct similarity between the deltaic cyclothem of the Namurian of County Clare and the Plio-Pleistocene El Wastani Formation of the Nile Delta. Controls on the Nile Delta depositional system are interpreted to have been similar to controls on the Co. Clare delta, both systems being fluvially dominated and wave influenced and displaying sedimentary cyclicities controlled by glacio-eustatic sea-level fluctuations, linked to ~100ka periodicity Milankovitch orbital eccentricity cycles. The comparison of facies between the Co. Clare outcrops and the FMI logs from the Rosetta 3 well show that the sedimentary characteristics of the two depositional systems are also similar. For all these reasons the analogy between the two systems is considered to be good.

Using the detailed field data from the Tullig Sandstone outcrops to condition the modelling process resulted in models that reproduced some aspects of the outcrops, but failed to simulate others. Using smaller grid cells made modelling facies thicknesses more accurate and gave a distribution of fine-grained facies that realistically corresponded to the outcrops. However, larger-scale architectures were not reproduced successfully in the high-resolution model. The lower-resolution model, while unable to accurately simulate the distribution of fine-grained facies, was more successful in reproducing the channel storeys and stacking patterns, but could not repeat the downstream decrease in number of storeys. Despite these discrepancies between the outcrops and the models, the high net to gross ratio of the Tullig Sandstone meant that the connectivity within both models was high, regardless of the different distributions of fine-grained facies within each model. This means that the recoverable hydrocarbon volume would theoretically remain unaffected, although the ease of extraction, particularly of oil, would be reduced in the high-resolution model.

## ***7.2 Recommendations for further work***

The exhaustive quantitative study of the Tullig Sandstone and mouthbar sandbody outcrops proved helpful in confirming theories of palaeoenvironment and basin orientation. Similar studies may be possible for the sandbodies of the succeeding Kilkee and Doonlicky cyclothems, and would help to improve understanding of the changes in palaeoenvironment of the WINB over time. Using the same quantitative approach would aid interpretation of any ancient fluvial system, particularly if sections through different parts of the system in a downstream direction were visible in outcrop.

To complement the modelling results presented in this thesis, it would be interesting to model flow through the facies models created from the outcrop data. An additional function of the RMS package is the ability to model fluid flow, and simulating flow through the models would improve understanding of how important the architectural discrepancies between the models and the outcrop data really were. For example, although the connectivity remained unaffected by the differences in architecture and facies distributions between the two models, fluid pathways could be significantly impacted. Data about the behaviour of fluid within sandstone reservoirs is vital in the positioning of wells and for reservoir management during the producing life of a field. A fluid flow/streamlines simulation would show how the distribution of fine-grained impermeable facies would affect the streamlines (flow pathways) of hydrocarbons being drained from a reservoir with the characteristics of the Tullig Sandstone.

The models produced were the first results of a complex stochastic modelling process. One of the primary reasons for using computer models of geological data is to enable numerous simulations, based on the same input data, to be created. Due to time constraints this was not possible within the scope of this thesis, but repeat runs of the modelling process would be the logical next step in both the testing of the model's capability of reproducing outcrop characteristics, and in analysing the range of outcomes possible from the data. It would also be interesting and valuable to change the input parameters away from the outcrop values, to test the effects of increasing percentages of fine-grained facies and increasing facies thicknesses on connectivity and drainability. Such methods could be used to discover an upper percentage limit

of fine-grained facies beyond which the connectivity of a fluvial sandbody would become significantly reduced. At present the results show that a net-to-gross of around 90% does not adversely affect connectivity, but an investigation of the affect of net-to-gross on connectivity would be a valuable extension of the modelling experiments presented here.

Another possible piece of work is the testing of the models on outcrop data not included in the original model construction. For example, at Trusklieve there is a second exposure of the Tullig Sandstone, in a steep-sided and inaccessible coastal inlet perpendicular to the main studied outcrop. This second outcrop could be evaluated using photomontage techniques and by correlation with the documented accessible outcrop, and could then be compared with a corresponding section through the models, to see if the models had accurately predicted the facies architecture and distribution for that outcrop. Such a process would provide a useful test, giving an indication, beyond the general observances made in Chapter 6, of the ability of the models to reproduce reality.

The Co. Clare data could also be used to inform construction of reservoir models for the sandbodies of the El Wastani Formation, or indeed, for any subsurface reservoir model where the depositional environment and characteristics were considered to be similar to those of the Tullig Cyclothem. The field data presented here would be useful in constraining models for fluvial and deltaic sandbodies that were not well-understood in terms of their architectures and facies distributions.



## References

- ABU OLLO, S. AND EL-KHOLY, H. 1992. West Abu Qir discovery, its exploration significance and case history as part of the Nile Delta exploration tasks. *Proceedings of the 11<sup>th</sup> Egyptian General Petroleum Company (EGPC) Petroleum Conference, Cairo, Egypt 2 (exploration)*, 514-543.
- AINSWORTH, R.B., SANLUNG, M. AND DUIVENVOORDEN, S.T.C. 1999. Correlation techniques, perforation strategies, and recovery factors: an integrated 3-D reservoir modelling study, Sirikit field, Thailand. *American Association of Petroleum Geologists Bulletin* 83, 1535-1551.
- ALFY, M., POLO, F. AND SHASH, M. 1992. The geology of Abu Madi gas field. *Proceedings of the 11<sup>th</sup> EGPC Petroleum Conference, Cairo, Egypt 2 (exploration)*, 485-513.
- ALLEN, J.R.L. 1963. The classification of cross-stratified units with notes on their origins. *Sedimentology* 2, 93-114.
- ALLEN, J.R.L. 1964. Primary current lineation in the Lower Old Red Sandstone (Devonian), Anglo-Welsh Basin. *Sedimentology* 3, 89-108.
- ALLEN, J.R.L. 1968. *Current ripples*. North Holland, Amsterdam.
- ALLEN, J.R.L. 1970a. A quantitative model of climbing ripples and their cross-laminated deposits. *Sedimentology* 14, 5-26.
- ALLEN, J.R.L. 1970b. Studies in fluvial sedimentation: a comparison of fining-upward cyclothems, with special reference to coarse-member composition and interpretation. *Journal of Sedimentary Petrology* 40, 298-323.
- ALLEN, J.R.L. 1972. A theoretical and experimental study of climbing-ripple cross-lamination, with a field application to the Uppsala esker. *Geog. Annlr.* 53A, 157-187.
- ALLEN, J.R.L. 1983a. Studies in fluvial sedimentation: bars, bar-complexes and sandstone sheets (low sinuosity braided streams) in the Brownstones (L. Devonian), Welsh Borders. *Sedimentary Geology* 33, 237-293.
- ALLEN, J.R.L. 1983b. Gravel overpassing on humpback bars supplied with mixed sediment: examples from the Lower Old Red Sandstone, southern Britain. *Sedimentology* 30, 285-294.
- ALLEN, J.R.L. AND BANKS, N.L. 1972. An interpretation and analysis of recumbent folded deformed cross-bedding. *Sedimentology* 19, 257-283.
- ASHLEY, G. M. 1990. Classification of large-scale subaqueous bedforms; a new look at an old problem. *Journal of Sedimentary Petrology* 60, 161-172.

- ASHWORTH, P. J., BEST, J.L., RODEN, J.E., BRISTOW, C.S. AND KLAASSENS, G.J. 2000. Morphological evolution and dynamics of a large, sand braid-bar, Jamuna River, Bangladesh. *Sedimentology* 47, 533-555.
- AUTIN, W. J., BURNS, S.F., MILLER, R.T., SAUCIER, R.T. AND SNEAD, J.I. 1991. Quaternary geology of the lower Mississippi valley. In: Morrison, R.B. (ed.), *Quaternary nonglacial geology: Conterminous US. The geology of North America. Geological Society of America K-2*, 547-582.
- BAINES, J.G. 1977. *The stratigraphy and sedimentology of the Skipton Moor Grits (Namurian E<sub>1c</sub>) and their lateral equivalents*. PhD. Thesis, University of Keele, England.
- BANDEL, K. 1967. Trace fossils from two upper Pennsylvanian sandstones in Kansas. *Paleontological Contributions – University of Kansas Paper* 18, 1-13.
- BARSOUM, K., AIOLFI, C., DALLA, S. AND KAMAL, M. (IEOC). 1998. Evolution and hydrocarbon occurrence in the Plio-Pleistocene succession of the Egyptian Mediterranean margin: examples from the Nile Delta basin. *Proceedings of the 14<sup>th</sup> EGPC Petroleum Conference, Cairo, Egypt 1 (exploration)*, 386-401.
- BATES, C.C. 1953. Rational theory of delta formation. *American Association of Petroleum Geologists Bulletin* 37, 2119-2162.
- BELLAICHE, G. AND MART, Y. 1995. Morphostructure, growth patterns, and tectonic control of the Rhone and Nile deep-sea fans: a comparison. *American Association of Petroleum Geologists Bulletin* 79, 259-284.
- BENTHAM, P.A., TALLING, P.J. AND BURBANK, D.W. 1993. Braided stream and flood-plain deposition in a rapidly aggrading basin: the Escanilla formation, Spanish Pyrenees. In: Best, J.L. and Bristow, C.S. (eds), *Braided Rivers*. Geological Society Special Publication 75, 177-194.
- BENNINGTON, J.B. Updated 1999. Course notes "Geol 135 Sedimentation", [http://people.hofstra.edu/faculty/J\\_B\\_Bennington/135notes/diagenesis.html](http://people.hofstra.edu/faculty/J_B_Bennington/135notes/diagenesis.html)
- BERNER, R. 1981. Authigenic mineral formation resulting from organic matter decomposition in modern sediments. *Fortschritte der Mineralogie* 59, 117-135.
- BEST, J.L. AND ASHWORTH, P.J. 1997. Scour in large braided rivers and the recognition of sequence stratigraphic boundaries. *Nature* 387, 275-277.
- BEST, J.L. AND BRIDGE, J.S. 1992. The morphology and dynamics of low amplitude bedwaves upon upper stage plane beds and the preservation of planar laminae. *Sedimentology* 39, 737-752.
- BG TCM internal report. 1995. Unpublished.
- BG TCM internal report. 1996. Unpublished.

BG internal report (Dr. R.J.B. Trythall, Z&S Geology Ltd.). 1997. *Well Rosetta-3 (Ji 57-1): Volume 1 Structural and sedimentological interpretation of FMI data*. Unpublished.

BG internal report. 1998. Unpublished.

BHATTACHARYA, J. AND WALKER, R.G. 1991. River- and wave-dominated depositional systems of the Upper Cretaceous Dunvegan Formation, northwestern Alberta. *Bulletin of Canadian Petroleum Geology* 30, 165-191.

BRIDGE, J.S. 1985. Palaeochannel patterns inferred from alluvial deposits: a critical evaluation. *Journal of Sedimentary Petrology* 55, 579-589.

BRIDGE, J.S. 1993. The interaction between channel geometry, water flow, sediment transport and deposition in braided rivers. In: Best, J.L. and Bristow, C.S. (eds), *Braided Rivers*. Geological Society Special Publication 75, 13-71.

BRIDGE, J.S. 2003. *Rivers and floodplains*. Blackwell Science, Oxford.

BRIDGE, J.S. AND BEST, J.L. 1988. Flow, sediment transport and bedform dynamics over the transition from upper-stage plane beds: implications for the formation of planar laminae. *Sedimentology* 35, 753-763.

BRIDGE, J.S. AND MACKEY, S.D. 1993. A theoretical study of fluvial sandstone body dimensions. In: Flint, S. and Bryant, I.D. (eds) *The geological modelling of hydrocarbon reservoirs and outcrop analogues*. International Association of Sedimentologists Special Publication 15, 213-236.

BRIDGE, J.S. AND TYE, R.S. 1993. Interpreting the dimensions of ancient fluvial channel bars, channels, and channel belts from wireline-logs and cores. *American Association of Petroleum Geologists Bulletin* 84, 1205-1228.

BRISTOW, C.S. 1987. *Sedimentology of large braided rivers ancient and modern*. Unpublished PhD thesis, University of Leeds, 274 pp.

BRISTOW, C.S. 1987. Brahmaputra River: channel migration and deposition. In: Etheridge, F.G., Flores, R.M. and Harvey, M.D. (eds) *Recent developments in fluvial sedimentology*. Society of Economic Palaeontologists and Mineralogists Special Publications 39, 63-74.

BRISTOW, C.S. 1988. Controls on sedimentation in the Rough Rock Group. In: Besly, B. and Kelling, G. (eds) *Sedimentation in a synorogenic basin complex: the Upper Carboniferous of northwest Europe*. Blackie, Glasgow.

BRISTOW, C.S. 1993. Sedimentary structures exposed in bar tops in the Brahmaputra River, Bangladesh. In: Best, J.L. and Bristow, C.S. (eds), *Braided Rivers*. Geological Society Special Publication 75, 277-289.

- BRISTOW, C.S. AND BEST, J.L. 1993. Braided Rivers: perspectives and problems. In: Best, J.L. and Bristow, C.S. (eds), *Braided Rivers*. Geological Society Special Publication 75, 1-11.
- BRISTOW, C.S. AND MYERS, K.J. 1989. Detailed sedimentology and gamma-ray characteristics of a Namurian deltaic succession I: Sedimentology and facies analysis. In: Whateley, M.K.G. and Pickering, K.T. (eds) *Deltas - sites and traps for fossil fuels*. Geological Society Special Publication 41, 75-80.
- CAMPBELL, C.V. 1976. Reservoir geometry of a fluvial sheet sandstone. *American Association of Petroleum Geologists Bulletin* 60, 1009-1020.
- CANT, D.J. 1982. Fluvial facies models and their application. In: Scholle, P.A. and Spearing, D. (eds) *Sandstone depositional environments*. AAPG, Tulsa, Oklahoma.
- CANT, D.J. AND WALKER, R.G. 1978. Fluvial processes and facies sequences in the sandy braided South Saskatchewan River, Canada. *Sedimentology* 25, 625-648.
- CAPUTO, M.V. AND CROWELL, J.C. 1985. Migration of glacial centres across Gondwana during the Palaeozoic era. *Geological Society of America Bulletin* 96, 1020-1036.
- CARTER, R.M., ABBOTT, S.T., FULTHORPE, C.S., HAYWICK, D.W. AND HENDERSON, R.A. 1991. Application of global sea-level and sequence-stratigraphic models in Southern Hemisphere Neogene strata from New Zealand. *International Association of Sedimentologists Special Publication* 12, 41-65.
- CHAKRABORTY, C. AND BOSE, P.K. 1992. Ripple/dune to upper stage plane bed transition: some observations from the ancient record. *Geological Journal* 27, 349-359.
- CHAPIN, M., DAVIES, P., GIBSON, J.L. AND PETTINGHILL, H.S. 1994. Reservoir architecture of turbidite sheet sandstones in laterally extensive outcrops, Ross Formation, western Ireland. In: *Submarine fans and turbidite systems*. GCSSEPM Foundation 15<sup>th</sup> Annual Research Conference. 53-68.
- CHUMAKOV, I.S. 1967. Pliocene and Pleistocene deposits of the Nile Valley in Nubia and Upper Egypt. *Transactions of the Geological Institute of the Academy of Science (USSR)* 170, 1-110.
- COLEMAN, J.M. 1981. *Deltas: processes and models of deposition for exploration*. 124pp. Burgess Publishing Company, CEPCO Division, Minneapolis.
- COLEMAN, J.M., GAGLIANO, S.M. AND WEBB, J.E. 1964. Minor sedimentary structures in a prograding distributary. *Marine Geology* 1, 240-258.
- COLEMAN, J.M., ROBERTS, H.H., MURRAY, S.P. AND SALAMA, M. 1981. Morphology and dynamic sedimentology of the eastern Nile Delta shelf. *Marine Geology* 42, 301-326.

- COLEMAN, J.M., SUHAYDA, J.N., WHELAN, T. AND WRIGHT, L.D. 1974. Mass movement of the Mississippi river delta sediments. *Transactions of the Gulf Coast Association Geological Society* 24, 49-68.
- COLEMAN, J.M. AND WRIGHT, L.D. 1975. Modern river deltas: variability of processes and sandbodies. In: Broussard, M.L. (ed.) *Deltas, models for exploration*. Houston Geological Society, Houston.
- COLLIER, R.E.LL., LEEDER, M.R. AND MAYNARD, J.R. 1990. Transgressions and regressions: a model for the influence of tectonic subsidence, deposition and eustasy, with application to Quaternary and Carboniferous examples. *Geological Magazine* 127, 117-128.
- COLLINSON, J.D. 1970. Deep channels, massive beds and turbidity current genesis in the Central Pennine Basin. *Proceedings of the Yorkshire Geological Society* 37, 495-519.
- COLLINSON, J.D. 1986. Alluvial Sediments. In: Reading, H.G. (ed.) *Sedimentary environments and facies (second edition)*. Blackwell Scientific Publications, Oxford.
- COLLINSON, J.D. AND ELLIOTT, T. (compilers). 1991. *Turbidite, slope and deltaic depositional systems in the Namurian basin of western Ireland*. Sedimentary Research Associates.
- COLLINSON, J.D., ELLIOTT, T. AND MARTINSEN, O. (compilers). 1989. *Field guide to the Western Irish Namurian Basin*. Sedimentary Research Associates.
- COLLINSON, J.D., HOLDSWORTH, B.K., JONES, C.M. AND MARTINSEN, O.J. 1992. Discussion of: "The Millstone Grit (Namurian) of the southern Pennines viewed in the light of eustatically controlled sequence stratigraphy" by W.A. Read. *Geological Journal* 27, 173-174.
- COLLINSON, J.D., MARTINSEN, O., BAKKEN, B. AND KLOSTER, A. 1991. Early fill of the Western Irish Namurian Basin: a complex relationship between turbidites and deltas. *Basin Research* 3, 223-242.
- COLLINSON, J.D. AND THOMPSON, D. B. 1982. *Sedimentary structures*. George Allen and Unwin, London, United Kingdom (GBR).
- CORBEANU, R.M., SOEGAARD, K., SZERBIAK, R.B. THURMOND, J.B., MCMECHAN, G.A., WANG, D., SNELGROVE, S., FORSTER, C.B. AND MENITOVE, A. 2001. Detailed internal architecture of a fluvial channel sandstone determined from outcrop, cores, and 3-D ground-penetrating radar: example from the middle Cretaceous Ferron Sandstone, east-central Utah. *American Association of Petroleum Geologists Bulletin* 85, 1583-1608.
- COUTELLIER, V. AND STANLEY, D.J. 1987. Late Quaternary stratigraphy and palaeogeography of the eastern Nile Delta, Egypt. *Marine Geology* 77, 257-275.
- COWAN, G., SWALLOW, J., MADDOX, S., LYNCH, S., DEARLOVE, M., SOBHANI, K., NASHAAT, M., LOUDEN, E., CHARALAMBIDES, P., COOLEN, P. AND HOUSTON, R.

1998. The Rosetta field: a fast track development case study, Nile Delta, Egypt. *Proceedings of the 14<sup>th</sup> EGPC Petroleum Conference, Cairo, Egypt 2 (exploration)*, 222-234.

CROKER, P.F. 1995. The Clare Basin: a geological and geophysical outline. In: Croker, P.F. and Shannon, P.M. (eds) *The petroleum geology of Ireland's offshore basins*. Geological Society Special Publication 93, 327-339.

CURTIS, C.D. 1986. Microorganisms, concretions and diagenetic cements. In: *Sediments down-under: 12th international sedimentological congress; abstracts*. Bureau of Mineral Resources, Geology and Geophysics, Canberra, Australia. 72pp.

DAVIES, S.J. AND ELLIOTT, T. 1996. Spectral gamma ray characterisation of high resolution sequence stratigraphy: examples from the Upper Carboniferous fluvio-deltaic systems, County Clare, Ireland. In: Howell, J.A. and Aitken, J.F. (eds) *High resolution sequence stratigraphy: innovations and applications*. Geological Society Special Publication 104, 25-35.

DEIBIS, S., FUTYAN, A., INCE, D.M., MORLEY, R.J., SEYMOUR, W.P. AND THOMPSON, S. 1986. The stratigraphic framework of the Nile Delta and its implications with respect to the region's hydrocarbon potential. *Proceedings of the 8<sup>th</sup> EGPC Petroleum Conference, Cairo, Egypt 2 (exploration)*, 164-174.

DOHERTY, M., JAMIESON, G., KILENYI, T. AND TRAYNER, P. (GECO). 1988. The geology and seismic stratigraphy of the offshore Nile Delta. *Proceedings of the 9<sup>th</sup> EGPC Petroleum Conference, Cairo, Egypt 2 (exploration)*, 408-426.

DOTT, R.H. AND BORGEOIS, J. 1982. Hummocky stratification: significance of its variable bedding sequences. *Geological Society of America Bulletin* 93, 663-680.

DREYER, T. 1990. Sandbody dimensions and infill sequences of stable humid climate delta plain channels. In: Buller, A.T. (ed.) *North Sea oil and gas reservoirs 2*. London, Graham and Trotman, 337-351.

DREYER, T., FÄLT, L.-M., HØY, T., KNARUD, R., STEEL, R. AND CUEVAS, J.-L. 1990. Sedimentary architecture of field analogues for reservoir information (SAFARI): a case study of the fluvial Escanilla Formation, Spanish Pyrenees. In: Flint, S. and Bryant, I.D. (eds) *The geological modelling of hydrocarbon reservoirs and outcrop analogues*. International Association of Sedimentologists Special Publication 15, 57-80.

DREYER, T., SCHIE, A. AND WALDERHAUG, O. 1990. Mini-permeameter-based study of permeability trends in channel sand bodies. *American Association of Petroleum Geologists Bulletin* 74, 359-374.

EAGER, R.M.C. 1977. Some new Namurian bivalve faunas and their significance in the origin of *Carbonicola* and in the colonisation of Carboniferous deltaic environments. *Phil. Trans. Royal Soc. London, Series B*, 280, 535-570.

EAGER, R.M.C., BAINES, J.G., COLLINSON, J.D., HARDY, P.G., OKOLO, S.A. AND POLLARD, J.E. 1985. Trace fossil assemblages and their occurrence in Silesian (mid-

Carboniferous) deltaic sediments of the Central Pennine Basin, England. In: Curran, H.A (ed.) *Biogenic structures; their use in interpreting depositional environments*. SEPM Special Publication 35, 99-149.

EL-HEINY, I. AND MORSY, S. 1992. Stratigraphic correlation of Neogene sediments in the eastern Nile Delta and Gulf of Suez, Egypt. *Proceedings of the 11<sup>th</sup> EGPC Petroleum Conference, Cairo, Egypt 1 (exploration)*, 166-193.

ELLIOTT, T. 1974. Interdistributary bay sequences and their genesis. *Sedimentology* 21, 611-622.

ELLIOTT, T. 1978. Deltas. In: Reading, H.G. (ed.) *Sedimentary Environments and Facies*. Blackwell Scientific Publications, Oxford.

ELLIOTT, T. 1986. Deltas. In: Reading, H.G. (ed.) *Sedimentary Environments and Facies*. Blackwell Scientific Publications, Oxford.

ELLIOTT, T. AND DAVIES, S.J. 1994. *High resolution sequence stratigraphy of an Upper Carboniferous basin-fill succession, County Clare, western Ireland*. County Clare field guide.

ESCHARD, R., LEMOUZY, P., BACCHIANA, C., DESAUBLIAUX, G., PARPANT, J. AND SMART, B. 1998. Combining sequence stratigraphy, geostatistical simulations, and production data for modelling a fluvial reservoir in the Chaunoy field (Triassic, France). *American Association of Petroleum Geologists Bulletin* 82, 545-568.

FISK, H.N., MCFARLAN, E.JR., KOLB, C.R. AND WILBERT, L.J. 1954. Sedimentary framework of the modern Mississippi delta. *Journal of Sedimentary Petrology* 24, 76-99.

FITZSIMMONS, R. 1994. Field-based testing of high resolution sequence stratigraphic concepts; the Campanian Eagle Formation, Mesaverde Group, Bighorn basin, northwestern Wyoming, USA. PhD thesis, University of Liverpool, Liverpool, UK. 396pp.

FLORES, R.M., HOHMANN, J.J. AND ETHRIDGE, F.G. 1991. Heterogeneity of Upper Cretaceous Gallup Sandstone regressive facies, Gallup sag, New Mexico. In: Nations, J.D. and Eaton, J.G. (eds) *Stratigraphy, depositional environments and sedimentary tectonics of the western margin, Cretaceous Western Interior seaway*. Geological Society of America Special Paper 260, 189-209.

FREY, R.W. AND SEILACHER, A. 1980. Uniformity in marine invertebrate ichnology. *Lethaia* 13, 183-207.

FRIEND P.F. 1983. Towards the field classification of alluvial architecture or sequence. In: Collinson, J.D. and Lewis, J. (eds) *Modern and ancient fluvial systems*. International Association of Sedimentologists Special Publications 6, 345-354.

FRIEND P.F., SLATER, M.J. AND WILLIAMS, R.C. 1979. Vertical and lateral buildings of river sandstone bodies, Ebro Basin, Spain. *Journal of the Geological Society of London* 136, 39-46.

GALLOWAY, W.E. AND HOBDAY, D.K. 1996. *Terrigenous clastic depositional systems (second edition)*. Springer-Verlag, New York.

GARFUNKEL, Z. AND DERIN, B. 1984. Permian-early Mesozoic tectonism and continental margin formation in Israel and its implications for the history of the eastern Mediterranean. In: Dixon, J.E. and Robertson, A.H.F. (eds) *The Geological Evolution of the Eastern Mediterranean*. Geological Society Special Publication 17, 187-201.

GAWTHORPE, R.L., COLLIER, R.E.L., ALEXANDER, J., BRIDGE, J.S. AND LEEDER, M.R. 1993. Ground penetrating radar: application to sandbody geometry and heterogeneity studies. In: North, C.P. and Prosser, D.J. (eds) *Characterisation of fluvial and aeolian reservoirs*. Geological Society Special Publication 73, 421-432.

GEEHAN, G. AND UNDERWOOD, J. 1993. The use of length distributions in geological modelling. In: Flint, S. and Bryant, I.D. (eds) *The geological modelling of hydrocarbon reservoirs and outcrop analogues*. International Association of Sedimentologists Special Publication 15, 205-212.

GEZEIRY, M.M. AND SHANDAWILY, A.R. 1994. West Abu Qir field, an interactive geoscientific model, Nile Delta, Egypt. *Proceedings of the 12<sup>th</sup> EGPC Petroleum Conference, Cairo, Egypt 1 (exploration)*, 224-239.

GILL, W.D. 1979. Syndepositional sliding and slumping in the West Clare Namurian Basin, Ireland. *Geological Survey of Ireland, Special Paper 4*, 31 pp.

GVIRTZMAN, G., MARTINOTTI, G.M. AND MOSHKOVITZ, S. 1997. Stratigraphy of the Plio-Pleistocene sequence of the Mediterranean coastal belt of Israel and its implications for the evolution of the Nile Cone. In: Van Couvering, J.A. (ed.) *The Pleistocene boundary and the beginning of the Quaternary: World and regional geology* 9, 156-168. Cambridge University Press.

HALDORSEN, H.H. AND CHANG, D.M. 1986. Notes on stochastic shales; from outcrop to simulation model. In: Lake, L.W. and Carroll, H.B. Jr. *Reservoir characterization* 445-485. Academic Press, Orlando, FL, United States.

HALDORSEN, H.H., CHANG, D.M. AND BEGG. 1987. Discontinuous vertical permeability barriers: a challenge to engineers and geologists. In: Kleppe, J., Berg, E.W., Buller, A.T., Hjelmeland, O. and Torsaeter, O. (eds) *Proceedings of the North Sea oil and gas reservoirs seminar* 127-151. Graham and Trotman, London, UK.

HALFAR, J., RIEGEL, W. AND WALTHER, H. 1998. Facies architecture and sedimentology of a meandering fluvial system: a Palaeogene example from the Weissenster Basin, Germany. *Sedimentology* 45, 1-17.

HALIM, A.A., FOUAD, O., WORKU, T., KHALED, A.A. AND FAWZY, H.E. 1996. Aspects of reservoir potential of the Miocene-Pliocene sequences in north Alexandria

and surrounding areas offshore Nile Delta, Egypt. *Proceedings of the 13<sup>th</sup> EGPC Petroleum Conference, Cairo, Egypt 1 (exploration)*, 224-241.

HAMPSON, G.J., ELLIOTT, T. AND DAVIES, S.J. 1997. The application of sequence stratigraphy to Upper Carboniferous fluvio-deltaic strata of the onshore UK and Ireland: implications for the southern North Sea. *Journal of the Geological Society of London* 154, 719-733.

HAMPTON, M.A., LEE, H.J. AND LOCAT, J. 1996. Submarine landslides. *Reviews of Geophysics* 34, 33-59.

HAQ, B.U., HARDENBOL, J. AND VAIL, P.R. 1987. Chronology of fluctuating sea-levels since the Triassic. *Science* 235, 1156-1166.

HARMS, J.C., SOUTHARD, J. B., SPEARING, D. R., AND WALKER, R. G. 1975. Depositional environments as interpreted from primary sedimentary structures and stratification sequences. *SEPM Short Course, no.2*.

HARWOOD, C., AYYAD, M. AND HODGSON, N. 1998. The application of sequence stratigraphy in the exploration for Plio-Pleistocene hydrocarbons in the Nile Delta. *Proceedings of the 14<sup>th</sup> EGPC Petroleum Conference, Cairo, Egypt 2 (exploration)*, 1-13.

HATLØY, A.S. 1994. Numerical facies modelling combining deterministic and stochastic methods. In: Yarus, J.M. and Chambers, R.L. (eds) *Stochastic modeling and geostatistics; principles, methods, and case studies*. AAPG Computer Applications in Geology 3, 109.

HEARN, C.L., HOBSON, J.P. AND FOWLER, M.L. 1986. Reservoir characterization for simulation, Hartzog Draw Field, Wyoming. In: Lake, L.W. and Carroll, H.B. Jr. *Reservoir characterization* 341-372. Academic Press, Orlando, FL, United States.

HELMY, M. AND FOUAD, O. 1994. Prospectivity and play assessment of Abu Qir Bay area, Nile Delta, Egypt. *Proceedings of the 12<sup>th</sup> EGPC Petroleum Conference, Cairo, Egypt 1 (exploration)*, 277-292.

HJELLBAKK, A. 1997. Facies and fluvial architecture of a high-energy braided river: the Upper Proterozoic Seglommen Member, Varanger Peninsula, northern Norway. *Sedimentary Geology* 114, 131-161.

HJORT, N.L., AND OMRE, H. 1994. Topics in spatial statistics. *Scandinavian Journal of Statistics* 21, 289-357.

HODSON, F. 1954. The beds above the Carboniferous limestone in north-west county Clare, Eire. *Journal of the Geological Society of London* 109, 259-283.

HODSON, F. AND LEWARNE, G.C. 1961. A mid-Carboniferous (Namurian) basin in parts of the counties of Limerick and Clare, Ireland. *Journal of the Geological Society of London* 117, 307-333.

HOLDEN, L., HAUGE, R., SKARE, Ø. AND SKORSTAD, A. 1998. Modelling of fluvial reservoirs with object models. *Mathematical Geology* 30, 473-496.

HOLDSWORTH, B.K. AND COLLINSON, J.D. 1988. Millstone Grit cyclicity revisited. In: Besly, B.M. and Kelling, G. (eds) *Sedimentation in a synorogenic basin complex: the Upper Carboniferous of northwest Europe*. Blackie, Glasgow.

HORNE, J.C., FERM, J.C., CARUCCIO, F.T. AND BAGANZ, B.P. 1978. Depositional models in coal exploration and mine planning in the Appalachian region. *American Association of Petroleum Geologists Bulletin* 62, 2379-2411.

HURST, E.H. 1931-1966. *The Nile Basin*. Vols. 1-9. Physical and Nile Control Department, Ministry of Public Works, Cairo.

IEOC internal report, 1968. Unpublished.

IEOC internal report, 1985. Unpublished.

JACKSON, R.G. 1975. Hierarchical attributes and a unifying model of bed forms composed of cohesionless material and produced by shearing flow. *Geological Society of America Bulletin* 86, 1523-1533.

JACKSON, R.G. 1976. Large scale ripples of the lower Wabash River. *Sedimentology* 23, 593-632.

JACKSON, S.R., TOMUTSA, L., SZPAKIEWICZ, M., CHANG, M.M., HONARPOUR, M.M. AND SCHATZINGER, R.A. 1991. Construction of a reservoir model by integrating geological and engineering information; Bell Creek Field, a barrier/strandplain reservoir. In: Lake, L.W., Carroll, H.B. Jr., Wesson, T.C. (eds) *Reservoir characterization II*, 524-556. Academic Press, London.

JO, H.R. AND CHOUGH, S.K. 2001. Architectural analysis of fluvial sequences in the northwestern part of Kyongsang Basin (Early Cretaceous), SE Korea. *Sedimentary Geology* 144, 307-334.

JONES, B.G. AND RUST, B.R. 1983. Massive sandstone facies in the Hawkesbury Sandstone, a Triassic fluvial deposit near Sydney, Australia. *Journal of Sedimentary Petrology* 53, 1249-1259.

KAMEL, H., EITA, T. AND SARHAN, M. 1998. Nile Delta hydrocarbon potentiality. *Proceedings of the 14<sup>th</sup> EGPC Petroleum Conference, Cairo, Egypt 2 (exploration)*, 485-503.

KUPFERSBERGER, H. AND DEUTSCH, C.V. 1999. Methodology for integrating analog geologic data in 3-d variogram modelling. *American Association of Petroleum Geologists Bulletin* 83, 1262-1278.

LECLAIR, S.F. AND BRIDGE, J.S. 2001. Quantitative interpretation of sedimentary structures formed by river dunes. *Journal of Sedimentary Research* 71, no.5, 713-716.

- LEEDER, M.R. 1973. Fluvial fining-upwards cycles and the magnitude of palaeochannels. *Geological Magazine* **110**, 265-276.
- LEEDER, M.R. 1982. *Sedimentology: process and product (sixth impression)*. Chapman and Hall, London.
- LEEDER, M.R. 1999. *Sedimentology and sedimentary basins: from turbulence to tectonics*. Blackwell Science, Oxford.
- LEEDER, M.R. AND MCMAHON, S.F. 1987. Upper Carboniferous (Silesian) basin subsidence in northern Britain. In: Besly, B.M. and Kelling, G. (eds) *Sedimentation in a synorogenic basin complex: the Upper Carboniferous of northwest Europe*. Blackie, Glasgow.
- LEVEY, R.A. 1978. Bed-form distribution and internal stratification of coarse-grained point bars, Upper Congaree River, SC. In: Miall, A.D. (ed.) *Fluvial Sedimentology*. Canadian Society of Petroleum Geology Memoirs **5**, 105-127.
- LORENZ, J.C., HEINZE, D.M., CLARK, J.A. AND SEARLS, C.A. 1985. Determination of widths of meander-belt sandstone reservoirs from vertical downhole data, Mesa Verde Group, Piceance Creek Basin, Colorado. *American Association of Petroleum Geologists Bulletin* **69**, 710-721.
- LORT, J.M. 1973. Summary of seismic studies in the eastern Mediterranean. In: *Selection of papers on the eastern Mediterranean region (23<sup>rd</sup> Congress of the CIESM, Athens 1972)*. *Geological Society of Greece Bulletin* **10**, 99-108.
- LOWE, D.R. 1982. Sediment gravity flows, II. Depositional models with special reference to the deposits of high density turbidity currents. *Journal of Sedimentary Petrology* **52**, 279-297.
- LOWE, D.R. 1988. Suspended-load fallout rate as an independent variable in the analysis of current structures. *Sedimentology* **35**, 765-776.
- LOWRY, P. AND RAHEIM, A. 1991. Characterization of delta front sandstones from a fluvial-dominated delta system. In: Lake, L.W., Carroll, H.B. Jr., Wesson, T.C. (eds) *Reservoir characterization II*, 665-676. Academic Press, London.
- MACDONALD, A.C. AND AASEN, J.O. 1994. A prototype procedure for stochastic modelling of facies tract distribution in shoreface reservoirs. In: Yarus, J.M. and Chambers, R.L. (eds) *Stochastic modeling and geostatistics; principles, methods, and case studies*. AAPG Computer Applications in Geology **3**, 109.
- MADDOX, S.J., HODGSON, N., SWALLOW, J.L., LOUDON, E.M.M. AND SOBHANI, K. 1998. Plio-Pleistocene clastic reservoirs of the offshore Nile Delta, Arab Republic of Egypt. *Proceedings of Geo '98, 3<sup>rd</sup> Middle East Geoscience Conference, Bahrain*.
- MALDONADO, A. AND STANLEY, D.J. 1976. The Nile Cone: submarine fan development by cyclic sedimentation. *Marine Geology* **20**, 27-40.

- MALOVITSKIY, Y.P., EMELYANOV, E.M., KAZAKOV, O.V., MOSKALENKO, V.N., OSIPOV, G.V., SHIMKUS, K.M. AND CHUMAKOV, I.S. 1975. Geological structure of the Mediterranean sea floor (based on geological-geophysical data). *Marine Geology* 18, 231-261.
- MARZO, M., NIJMAN, W. AND PUIGDEFABREGAS, C. 1988. Architecture of the Castissent fluvial sheet sandstones, Eocene, South Pyrenees, Spain. *Sedimentology* 35, 719-738.
- MAYNARD, J.R. 1992a. Discussion of: "The Millstone Grit (Namurian) of the southern Pennines viewed in the light of eustatically controlled sequence stratigraphy" by W.A. Read. *Geological Journal* 27, 295-297.
- MAYNARD, J.R. 1992b. Sequence stratigraphy of the Upper Yeadonian of northern England. *Marine and Petroleum Geology* 9, 197-206.
- MAYNARD, J.R., HOFMANN, W., DUNAY, R.E., BENTHAM, P.N., DEAN, K.P. AND WATSON, I. 1997. The Carboniferous of Western Europe: the development of a petroleum system. *Petroleum Geoscience* 3, 97-115.
- MCCABE, P.J. 1977. Deep distributary channels and giant bedforms in the Upper Carboniferous of the Central Pennines, northern England. *Sedimentology* 24, 271-290.
- MCKEE, E.D. AND WEIR, G.W. 1953. Terminology for stratification and cross-stratification in sedimentary rocks. *Geological Society of America Bulletin* 64, 381-389.
- MIALL, A.D. 1977. A review of the braided river depositional environment. *Earth Science Reviews* 13, 1-62.
- MIALL, A.D. 1978. Lithofacies types and vertical profile models in braided river deposits: a summary. In: Miall, A.D. (ed.) *Fluvial Sedimentology*. Memoirs of the Canadian Society of Petroleum Geologists 5, 597-604.
- MIALL, A.D. 1985. Architectural-element analysis: a new method of facies analysis applied to fluvial deposits. *Earth Science Reviews* 22, 261-308.
- MIALL, A.D. 1996. *The geology of fluvial deposits: sedimentary facies, basin analysis and petroleum geology*. Springer.
- MILLER, M.C., MCCAVE, I.N. AND KOMAR, P.D. 1977. Threshold of sediment motion under unidirectional currents. *Sedimentology* 24, 507-528.
- MORRIS, P. AND MAX, M.D. 1995. Magnetic crustal character in central Ireland. *Geological Journal* 30, 49-67.
- MOSCONI, A., REBORA, A., VENTURINO, G., BOCC, P. AND KHALIL, M.H. 1996. Egypt – Nile Delta and North Sinai Cenozoic tectonic evolutionary model: a proposal. *Proceedings of the 13<sup>th</sup> EGPC Petroleum Conference, Cairo, Egypt 1 (exploration)*, 203-223.

- OKOLO, S.A. 1983. Fluvial distributary channels in the Fletcher Bank Grit (Namurian R2b), at Ramsbottom, Lancashire, England. In: Collinson, J. D. and Lewin, J. (eds) *Modern and ancient fluvial systems*. Special Publication of the International Association of Sedimentologists 6, 421-433.
- OLSEN, T. 1993. Large fluvial systems: the Atane Formation, a fluvio-deltaic example from the Upper Cretaceous of central Greenland. *Sedimentary Geology* 85, 457-473.
- OMRAN, M.A. AND FATHY, H.M. 1997. Seismic stratigraphy of the Nile Cone sediments. *Journal of the King Abdulaziz University: Earth Science* 9, 87-112.
- PRYOR, W.A. 1973. Permeability-porosity patterns and variations in some Holocene sand bodies. *American Association of Petroleum Geologists Bulletin* 57, 162-189.
- PULHAM, A.J. 1987. *Depositional and syn-sedimentary deformation processes in Namurian deltaic sequences of West County Clare, Ireland*. Unpublished PhD thesis, University of Wales, Swansea.
- PULHAM, A.J. 1989. Controls on internal structure and architecture of sandstone bodies within Upper Carboniferous fluvial-dominated deltas, County Clare, Western Ireland. In: Whateley, M.K.G. and Pickering, K.T. (eds) *Deltas - sites and traps for fossil fuels*. Geological Society Special Publication 41, 167-177.
- PYE, K. (ed.). 1994. *Sediment transport and depositional processes*. Blackwell Scientific Publications.
- QUELLENEC, R.E. AND KRUK, C.B. 1976. Nile suspended load and its importance for Nile Delta morphology. *Proceedings of the Seminar on Nile Delta Sedimentology* 130-145. UNESCO/ASRT/UNDP, Alexandria.
- RAVENNE, C. AND BEUCHER, H. 1988. Recent development in description of sedimentary bodies in a fluvio deltaic reservoir and their 3D conditional simulations. SPE 18310: paper prepared for presentation at the 63<sup>rd</sup> Annual Technical Conference and Exhibition of the Society of Petroleum Engineers, Houston, Texas, USA, October 1988. 14pp.
- READING, H.G. (ed.). 1986. *Sedimentary environments and facies*. Blackwell Scientific Publications.
- REYNOLDS, A.D. 1999. Dimensions of paralic sandstone bodies. *Bulletin of the American Association of Petroleum Geologists Bulletin* 83, 211-229.
- RIDER, M.H. 1969. *Sedimentological studies in the West Clare Namurian, Ireland and the Mississippi River delta*. Unpublished PhD thesis, Imperial College, London.
- RIDER, M.H. 1974. The Namurian of West County Clare. *Proceedings of the Royal Irish Academy* 74B, 125-142.
- RIDER, M.H. 1978. Growth faults in Carboniferous of Western Ireland. *Bulletin of the American Association of Petroleum Geologists* 62, 2191-2213.

- RIDER, M.H. 1996. *The Geological Interpretation of Well Logs (second edition)*. Whittles Publishing, Caithness, Scotland.
- RIZZINI, A., VEZZANI, F., COCOCETTA, V. AND MILAD, G. 1978. Stratigraphy and sedimentation of a Neogene-Quaternary section in the Nile Delta area. *Marine Geology* **27**, 327-348.
- ROSS, D.A. AND UCHUPI, E. 1977. Structure and sedimentary history of southeastern Mediterranean Sea – Nile Cone area. *American Association of Petroleum Geologists Bulletin* **61**, 872-902.
- ROXAR INC. 2003a. *RMS Version 7.0.2.1: Introduction to 3D geological modelling*. Roxar Inc., Wimbledon, London, UK.
- ROXAR INC. 2003b. *IRAP RMS Version 7.0: Heterogeneity modelling for reservoir characterisation*. Roxar Inc., Wimbledon, London, UK.
- RUSSELL, R.J. 1936. Physiography of the lower Mississippi River Delta. In: Trask, P.D. (ed.) *Recent Marine Sediments*. American Association of Petroleum Geologists, Tulsa, Oklahoma.
- RYER, T.A. 1981. Deltaic coals of Ferron Sandstone Member of the Mancos Shale: predictive model for Cretaceous coal-bearing strata of the Western Interior. *American Association of Petroleum Geologists Bulletin* **65**, 2323-2340.
- RILEY, N.J., CLAOUE-LONG, J.C., HIGGINS, A.C., OWENS, B., SPEARS, A., TAYLOR, L. AND VARKER, W.J. 1994. Geochronometry and geochemistry of the European mid-Carboniferous boundary global stratotype proposal, Stonehead Beck, North Yorkshire, UK. *Annales de la Société Géologique de Belgique* **116**, 275-289.
- SAID, R. 1981. *The Geological Evolution of the River Nile*. Springer-Verlag, New York.
- SAID, R. 1993a. The evolution of the Nile Delta. In: Thornweihle and Schandelmeier (eds) *Research in Northeast Africa* 615-619. Balkema, Rotterdam.
- SAID, R. 1993b. *The River Nile. Geology, Hydrology and Utilisation*. Pergamon Press, New York.
- SALEM, R. 1976. Evolution of Eocene-Miocene sedimentation patterns in northern Egypt. *American Association of Petroleum Geologists Bulletin* **60**, 34-64.
- SARHAN, M., TALAAT, M., BARSOUM, K., BERTELLO, F. AND NOBILI, M. 1996. The Pliocene play in the Mediterranean offshore: structural setting and growth faults controlled hydrocarbon accumulations in the Nile Delta basin, a comparison with the Niger Delta basin. *Proceedings of the 13<sup>th</sup> EGPC Petroleum Conference, Cairo, Egypt 1 (exploration)*, 121-139.
- SAUCIER, R.T. 1994. *Geomorphology and Quaternary History of the Lower Mississippi Valley*. Mississippi River Commission, Vicksburg, Mississippi.

SAUNDERSON, H.C. AND LOCKETT, F.P.J. 1983. Flume experiments on bedforms and structures at the dune plane bed transition. In: Collinson, J. D. and Lewin, J. (eds) *Modern and ancient fluvial systems*. Special Publication of the International Association of Sedimentologists 6, 49-59.

SEIFERT, D. AND JENSEN, J.L. 2000. Object and pixel-based reservoir modelling of a braided fluvial reservoir. *Mathematical Geology* 32, 581-603.

SESTINI, G. 1984. Tectonics and sedimentary history of the NE African margin (Egypt – Libya). In: Dixon, J.E. and Robertson, A.H.F. (eds) *The Geological Evolution of the Eastern Mediterranean*. Geological Society Special Publication 17, 161-175.

SESTINI, G. 1989. Nile Delta: a review of depositional and geological history. In: Whateley, M.K.G. and Pickering, K.T. (eds) *Deltas: sites and traps for fossil fuels*. Geological Society Special Publication 41, 99-127.

SEVASTOPULO, G.D. 1981b. Upper Carboniferous. In: Holland, C.H. (ed.) *A geology of Ireland* 173-188. Scottish Academic Press, Edinburgh.

SHANNON, P. 1991. Tectonic framework and petroleum potential of the Celtic Sea, Ireland. In: Spencer, A.M. (ed.) *Multidisciplinary petroleum geoscience: generation, accumulation and production of Europe's hydrocarbons*. Oxford University Press.

SHANNON, P. AND BRAITHWAITE, K. (compilers). 1997. *BG E&P County Clare field guide*. BG plc. Research and Technology.

SHANLEY, K W. AND MCCABE, P.J. 1993. Alluvial architecture in a sequence stratigraphic framework: a case history from the Upper Cretaceous of southern Utah, USA. In: Flint, S. and Bryant, I.D. (eds) *The geological modelling of hydrocarbon reservoirs and outcrop analogues*. International Association of Sedimentologists Special Publication 15, 21-55.

SHARIF, A., MACDONALD, A.C., KJØRHOLT, O. AND GULBRANDSEN, S. 2000. Integrated reservoir characterisation and uncertainty analysis using stochastic methods and streamline simulations. SPE 65178: paper prepared for presentation at the *Society of Petroleum Engineers European Petroleum Conference, Paris, France, October 2000*. 14pp.

SINGH, A. AND BHARDWAJ, B.D. 1991. Fluvial facies model of the Ganga River sediments, India. *Sedimentary Geology* 72, 135-146.

SMITH, G.A. 1986. Coarse-grained non-marine volcanoclastic sediment: terminology and depositional process. *Geological Society of America Bulletin* 97, 1-10.

SMITH, N.D., CROSS, T.A., DUFFICY, J.P. AND CLOUGH, S.R. 1989. Anatomy of an avulsion. *Sedimentology* 36, 1-23.

SNEH, A., WEISSBROD, T., EHRLICH, A., HOROWITZ, A., MOSHKOVITZ, S. AND ROSENFELD, A. 1986. Holocene evolution of the northeastern corner of the Nile Delta. *Quaternary Research* 26, 194-206.

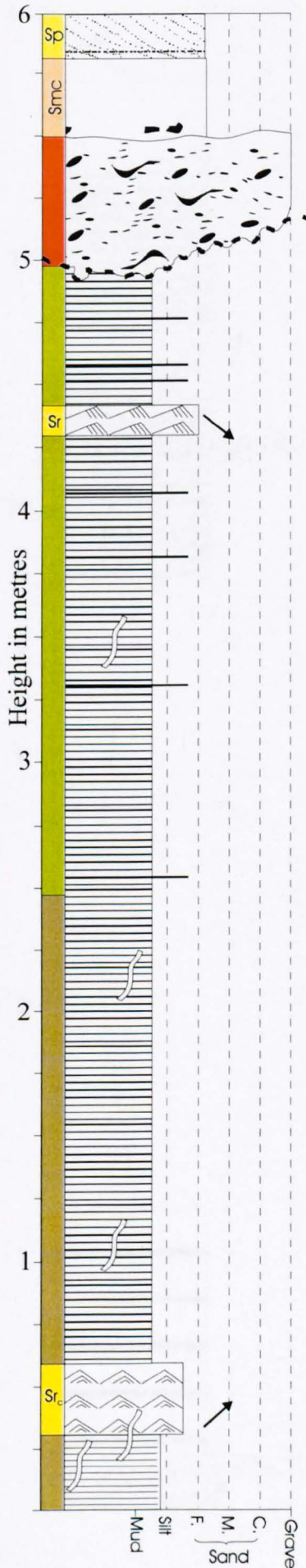
- STANLEY, D.J. AND WARNE, A.G. 1994. Worldwide initiation of Holocene marine deltas by deceleration of sea-level rise. *Science* **265**, 228-231.
- STRACHAN, L.J. 2002. Slump-initiated and controlled syndepositional sandstone remobilisation: an example from the Namurian of County Clare, Ireland. *Sedimentology* **49**, 25-41.
- SUMMERHAYES, C.P., SESTINI, G., MISDORP, R. AND MARKS, N. 1978. Nile Delta: nature and evolution of continental shelf sediments. *Marine Geology* **27**, 43-65.
- THOMAS, B. 1981. *The evolution of plants and flowers*. Peter Lowe.
- TROWBRIDGE, A.C. 1930. Building of the Mississippi delta. *American Association of Petroleum Geologists Bulletin* **14**, 867-901.
- TUCKER, M.E. 1996. *Sedimentary rocks in the field (second edition)*. John Wiley & Sons, Chichester.
- TURNER, B.R. AND MONRO, M. 1987. Channel formation and migration by mass-flow processes in the Lower Carboniferous fluvialite Fell Sandstone Group, northeast England. *Sedimentology* **34**, 1107-1122.
- WALKER, R.G. AND CANT, D.J. 1984. Sandy fluvial systems. In: Walker, R.G. (ed.) *Facies Models (second edition)*. Geoscience Canada Reprint Series **1**, 71-90.
- WEBER, K.J. AND VAN GEUNS, L.C. 1990. Framework for constructing clastic reservoir simulation models. *Journal of Petroleum Technology* **42**, 1248-1253.
- WEISE, B.R. 1979. Sedimentological aspects of oil fields of the Niger delta. *Geologie en Mijnbouw* **50** 559-576.
- WELLS, J.T. AND COLEMAN, J.M. 1984. Deltaic morphology and sedimentology, with special reference to the Indus River delta. In: Haq, B.U. and Milliman, J.D. (eds) *Marine geology and oceanography of Arabian Sea and coastal Pakistan* 85-100. Van Nostrand Reinhold Co. New York, NY, United States.
- WIGGER, S., SIMPSON, M., NADA, H., LARSEN, M. AND HAGGAG, M. 1996. Ha'py field: the result of Pliocene exploration in the Ras El Barr concession, Nile Delta. *Proceedings of the 13<sup>th</sup> EGPC Petroleum Conference, Cairo, Egypt 1 (exploration)*, 181-192.
- WIGNALL, P.B. AND BEST, J.L. 2000. The Western Irish Namurian Basin Reassessed. *Basin Research* **12**, 1-22.
- WIGNALL, P.B. AND BEST, J.L. In press. Sedimentology and kinematics of a large, retrogressive growth-fault system in Upper Carboniferous deltaic sediments, Western Ireland.
- WILLIAMS, G.P. 1986. River meanders and channel size. *Journal of Hydrology* **88**, 147-164.

- WILLIAMS, H.- AND SOEK, H.F. 1993. Predicting reservoir sandbody orientation from dipmeter data: the use of sedimentary dip profiles from outcrop studies. In: Flint, S. and Bryant, I.D. (eds) *The geological modelling of hydrocarbon reservoirs and outcrop analogues*. International Association of Sedimentologists Special Publication 15, 143-156.
- WILLIAMS, P.F. AND RUST, B.R. 1969. The sedimentology of a braided river. *Journal of Sedimentary Petrology* 39, 649-679.
- WILLIS, B.J. AND WHITE, C.D. 2000. Quantitative outcrop data for flow simulation. *Journal of Sedimentary Research* 70, 788-802.
- WINDLEY, B.F. 1995. *The Evolving Continents (third edition)*. John Wiley & Sons, Chichester.
- WORNHART, W.JR. AND VAIL, P.R. 1991. An integrated approach to exploration in the 90's: well log – seismic sequence stratigraphic analysis. *Transactions of the Gulf Coast Association of Geological Societies*.
- WRIGHT, L.D. 1977. Sediment transport and deposition at river mouths: a synthesis. *Geological Society of America Bulletin* 88, 857-868.
- WRIGHT, L.D. 1985. River deltas. In: Davis, R.A. (ed.) *Coastal sedimentary environments*. Springer, New York.
- WRIGHT, L.D. AND COLEMAN, J.M. 1971. Effluent expansion and interfacial mixing in the presence of a salt wedge, Mississippi River Delta. *Journal of Geophysical Research* 76, 8649-8661.
- WRIGHT, L.D. AND COLEMAN, J.M. 1973. Variations in morphology of major river deltas as functions of ocean wave and river discharge regimes. *American Association of Petroleum Geologists Bulletin* 57, 370-398.
- WRIGHT, L.D. and COLEMAN, J.M. 1974. Mississippi River mouth processes: effluent dynamics and morphologic development. *Journal of Geology* 82, 751-778.
- YALIN, M. S. 1972. *Mechanics of sediment transport*. Pergamon Press, Oxford.
- YALIN, M. S. AND FINLAYSON, G. D. 1972. On the velocity distribution of the flow carrying sediment in suspension. *Sedimentation*. (Privately published.)
- ZAGHLOUL, Z.M., TAHA, A.A., HEGAB, O. AND EL-FAWAL, F. 1977. The Neogene-Quaternary sedimentary basins of the Nile Delta. *Egyptian Journal of Geology* 21, 1-19.

## Appendices A-D

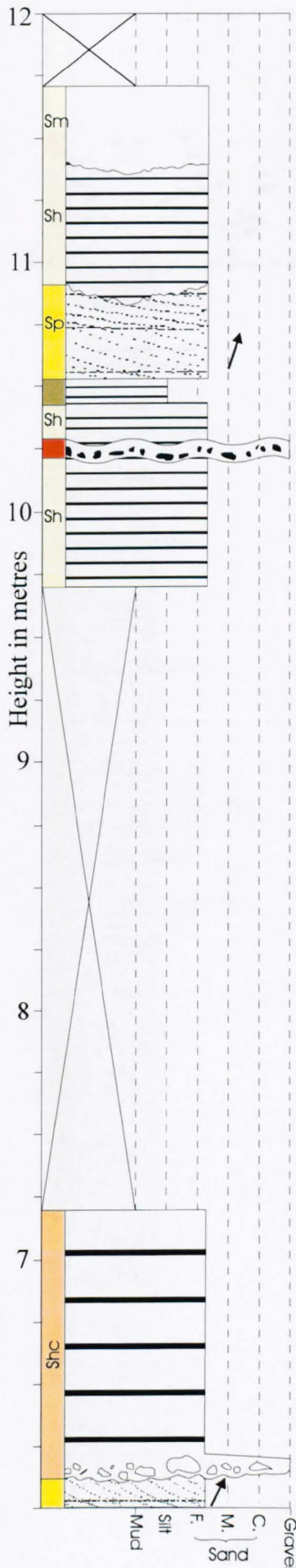
Appendix A1. Key to sedimentological, trace fossil, and other miscellaneous symbols used in the logs throughout this thesis.

Sedimentary structures Symbol	Meaning	Sedimentary structures Symbol	Meaning
	Unidirectional current ripples		Massive, structureless
	Asymmetric ripples, no internal structure visible		Convolute lamination
	Bidirectional wave ripples		Deformed bedding (more pervasive than convolute lamination)
	Symmetric ripples, no internal structure visible		Beds deformed by load and flame structures
	Single set of climbing ripples		Internal loading/pillow structures
	Multiples sets of climbing ripples		Siderite nodules
	Climbing ripples, no stoss sides preserved		Fractured but <i>in situ</i> rock
	Unidirectional lenticular bedding		Conglomeratic clasts, mostly fine lithologies
	Bidirectional lenticular bedding		Conglomeratic clasts, mostly sand lithologies
	Wavy lamination		Deformed clasts
or 			Flow aligned clasts
	Parallel lamination	<b>Trace fossils</b>	
or 			<i>Arenicolites</i>
	Horizontal bedding (large scale)		<i>Monocraterion</i> , <i>Skolithos</i>
	Planar cross bedding (and faint planar cross bedding)		<i>Curvolithus</i> , <i>Asterichnus</i> or <i>Pelecypodichnus</i>
or 			Unclassified vertical burrows
	Trough cross bedding (and faint trough cross bedding)	<b>Miscellaneous features</b>	
or 			Small plant fragments (often broken up)
	Hummocky cross stratification		Larger plant fragments (for example, trunks or limbs of large plants)
			<i>In situ</i> rootlets/plants



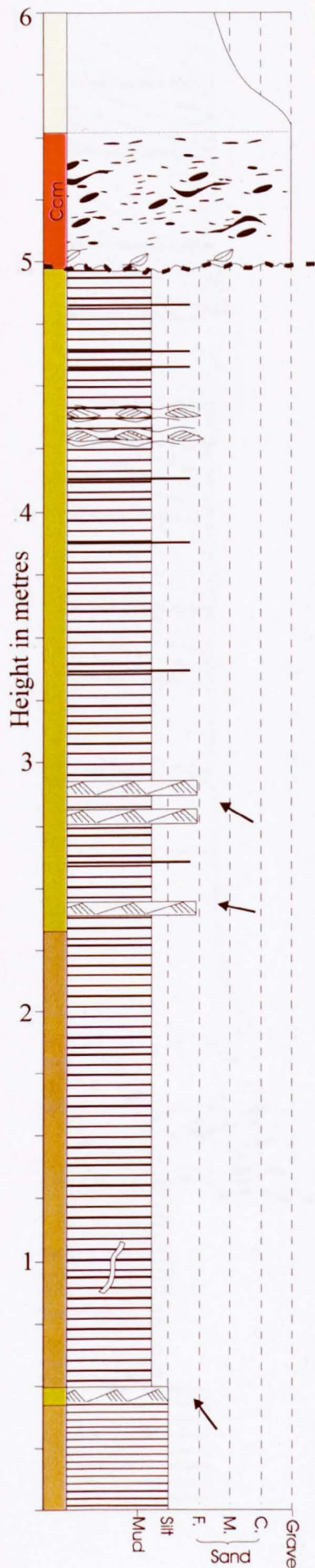
Lithology	Interpretation
Dune-scale cross-bedded sandstone.	Fluvial channel fill, dune bedforms.
Massive sandstone with basal lag.	Rapid deposition in channel.
Erosively based fine sandstone with deformed mudstone clasts.	Base of Storey 1 channel eroding into unlithified delta front muds and silts.
Current-rippled sandstone, preserved foresets.	
Interlaminated muds, silts and fine sands with infrequent bioturbation.	
Interlaminated muds and silts, infrequent bioturbation.	Delta front quiet water deposition, some wave and current influence. Fast enough deposition to discourage bioturbation.
Aggradational current ripples; fast deposition.	
Laminated grey silts, some bioturbation.	

A2. Log 1, taken at northern end of Trusklieve outcrop.



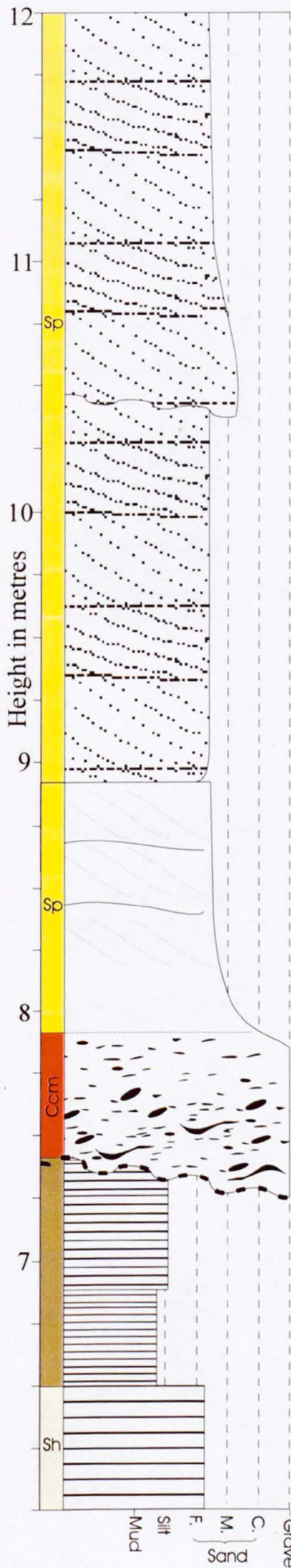
Lithology	Interpretation
Erosively based massive sandstone.	Rapid deposition from bank collapse slurry flow.
Erosively based parallel bedded sandstone.	Upper stage plane beds indicate rapid flow.
Fine sandstone with planar cross-bedding and sharp base.	Migration of straight crested dunes within channel.
Thin silt layer.	Deposition from suspension during slow flow.
Parallel bedded sandstone.	
Where visible, appears to be planar cross-bedded sandstone.	Migration of straight crested dunes within channel.
Erosively based parallel bedded sandstone with conglomeratic lag.	Minor internal erosion surface probably formed during flood stage flow.

A2. Log 1, taken at northern end of Trusklieve outcrop.



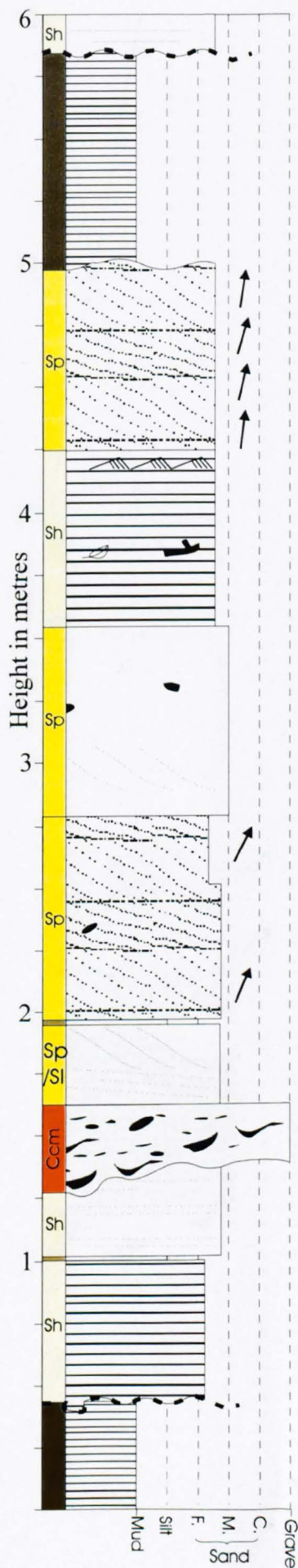
Lithology	Interpretation
Erosively based conglomerate with deformed mud rip-up clasts and organic material. Succeeded by fining-up massive sandstone.	Base of Storey 1: fluvial channel eroding into mouthbar deposits.
Lenticular bedding with opposing cross-lamination directions.	Mouthbar front, wave influence causing bi-directional cross-lamination.
Interlaminated muds and silts with thin (1-3mm) sand layers and rare thin (<50mm) current-rippled fine sandstones.	Deposition of coarser sediments from currents during period of higher flow.
Interlaminated muds and silts with sparse bioturbated horizons.	Relatively fast rate of deposition from suspension discourages bioturbation.
Mid-grey/cream laminated silts; layer of sinuous asymmetric current ripples.	Delta front/distal mouth bar; quiet water deposition.

A3. Log 2, taken at centre-north of Trusklieve outcrop.



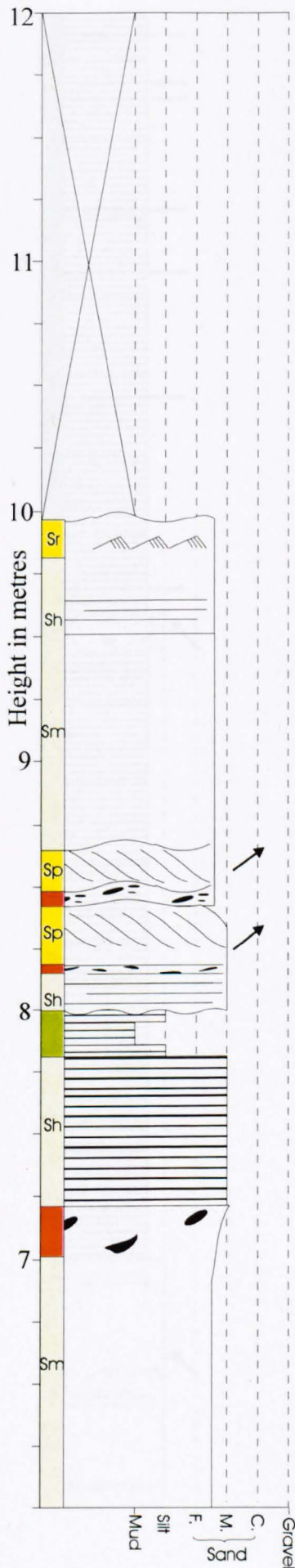
Lithology	Interpretation
Erosional base to thick planar cross-bedded unit.	Channel fill comprising successive straight-crested dunes.
Rip-up clast conglomerate with erosional base. Succeeded by planar cross-bedded unit.	Base of Storey 3: flood stage flow erodes new channel storey and deposits coarse clastics before flow velocity wanes to allow straight-crested dune formation.
Planar laminated silt, sharp but non-erosive base.	Fine-grained channel plug forms during abandonment.
Planar bedded sandstone.	

A3. Log 2, taken at centre-north of Trusklieve outcrop.



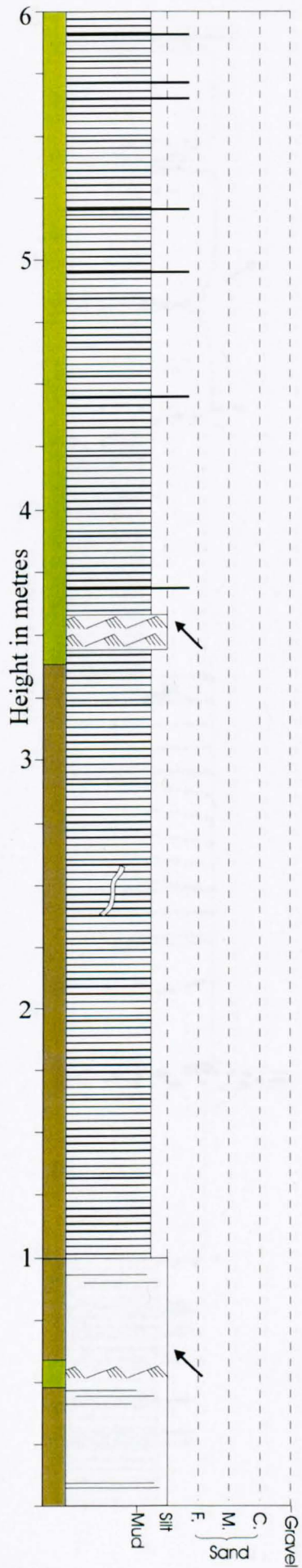
Lithology	Interpretation
Erosively based sandstone with faint lamination.	Base of Storey 4 channel element.
Laminated mudstone.	Abandonment of channel, filled with fine-grained sediment.
Horizontally bedded and planar laminated sandstone with planar cross sets at top. Merges laterally with organic-rich sandstone bed seen at same level (13m) in log 4.	Flood flows deposit organic debris and form upper-stage plane beds before flow velocity decreases, allowing straight-crested dunes to form and migrate within channel.
Medium-fine sandstone with planar cross-bedding, fining up. Grades into massive sand with faint cross-bedding and rare clasts.	Straight-crested dunes form and migrate within channel, and bank collapse causes massive sandstone beds to form from slurry flows..
Erosively based channel with 0.3m channel relief. Coarse lag of deformed mud/silt clasts. Capped by thin silt.	Internal erosion surface and conglomeratic lag within third channel storey, probably caused by flood stage flow.
Medium sandstone with faint lamination. Shows lateral thickness changes.	Very strong flow causing upper stage plane bed formation.
Erosive and loaded base to sandstone, parallel laminated. Capped by thin silt/fine sand.	Base of Storey 3, eroding into still soft abandonment deposits. Filled by upper stage plane beds, causing loading of still-soft muds below.
Laminated muds, no bioturbation.	Abandonment of channel, filled with fine-grained sediment.

A4. Log 3, taken at centre-south of Trusklieve outcrop.



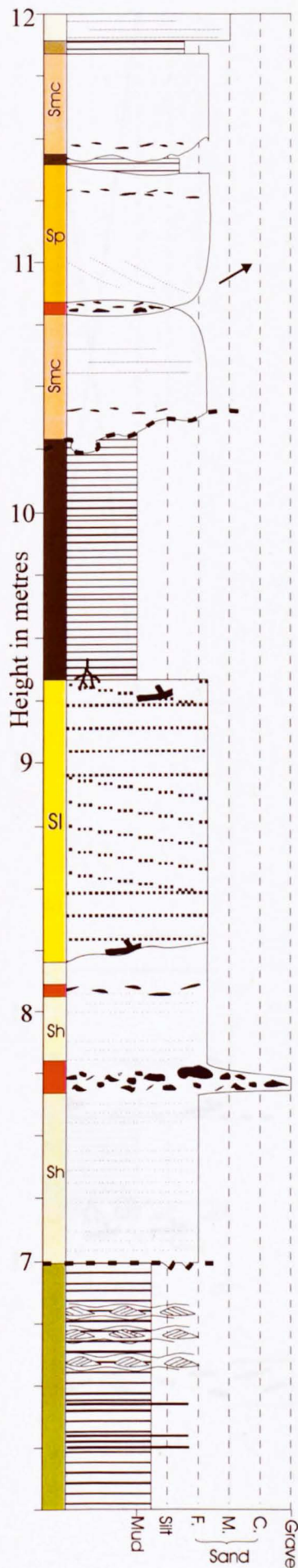
Lithology	Interpretation
Inaccessible for logging purposes.	
Laminated base to sandstone with localised cross-lamination.	
Undulating contact with massive sandstone with clast lag and foresets at base which follow undulation.	Migration of straight-crested dunes within channel, followed by deposition of massive sands from bank collapse slurry flows.
Erosively based parallel laminated sandstone with clast horizon; fines at top, also planar cross-bedding.	
Parallel laminated sandstone with silt/mudstone cap.	Upper stage plane beds followed by waning flow and minor fine-grained deposition.
Massive sandstone coarsens up, with mud clasts at top.	Fourth channel storey fill, rapid deposition from slurry flows probably due to bank collapse.

A4. Log 3, taken at centre-south of Trusklieve outcrop.



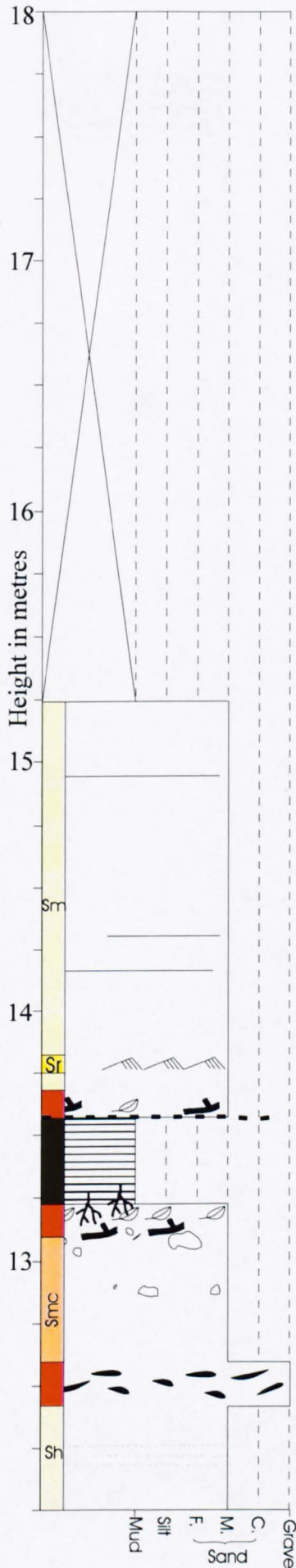
Lithology	Interpretation
<p>Laminated muds/silts with very rare bioturbated horizons grading very gradually upwards into laminated muds, silts and sands with some current ripples.</p>	<p>Delta front quiet water deposition, occasional current influence; relatively fast deposition discourages bioturbation.</p>
<p>Grey silt, some lamination, one layer with current ripples.</p>	<p>Delta front/distal mouth bar, some current influence.</p>

A5. Log 4, taken at south end of Trusklieve outcrop.



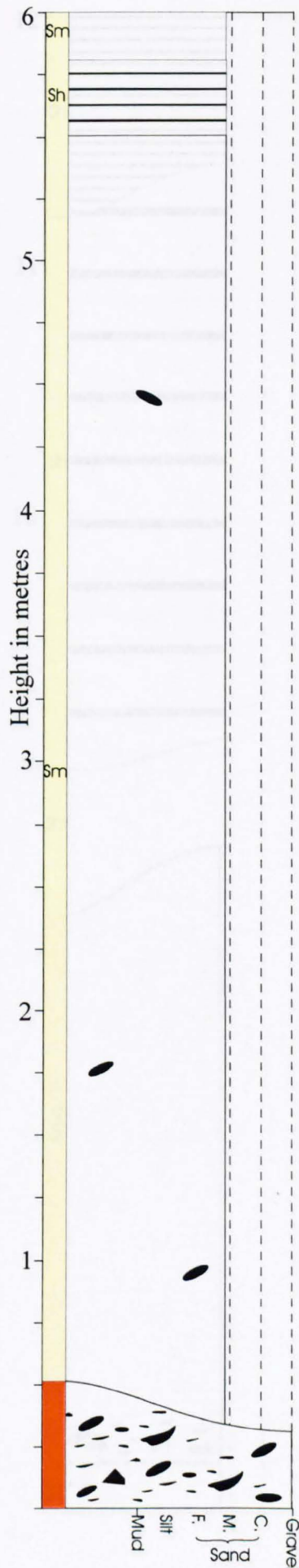
Lithology	Interpretation
Erosively based massive sandstone with clast lag, capped by silty sand.	Rapid deposition of bank collapse material followed by slower flow allowing fine-grained deposition.
Thin silty sand lens.	
Faint foresets and conglomeratic layers within sandstone.	
Silt lens with mud clasts.	
Erosively based, loaded sandstone with faint parallel bedding and flow-aligned clast lag.	Third storey of channel body with dune bedforms and fluctuating flow strength.
Laminated mudstone with <i>in situ</i> <i>Stigmaria</i> rootlets at base. Shows internal deformation in places.	Channel abandonment and fine-grained fill, with some vegetation growth.
Low-relief scour surfaces with bedding running parallel; occasional large wood and plant fragments at base and near top.	Low-angle bedding shows fast flow within channel; organic matter from flood deposition.
Scour marks at base of coarsening-up sandstone; faint parallel lamination and thin conglomeratic layer (mudstone and siltstone clasts, <20mm and flow-aligned).	Upper-stage plane beds formed in fast flow conditions within second storey of fluvial channel (erodes out first storey).
Increased sand content towards top; bi-directional lenticular cross-lamination.	Shallowing, with increased wave influence.

A5. Log 4, taken at south end of Trusklieve outcrop.



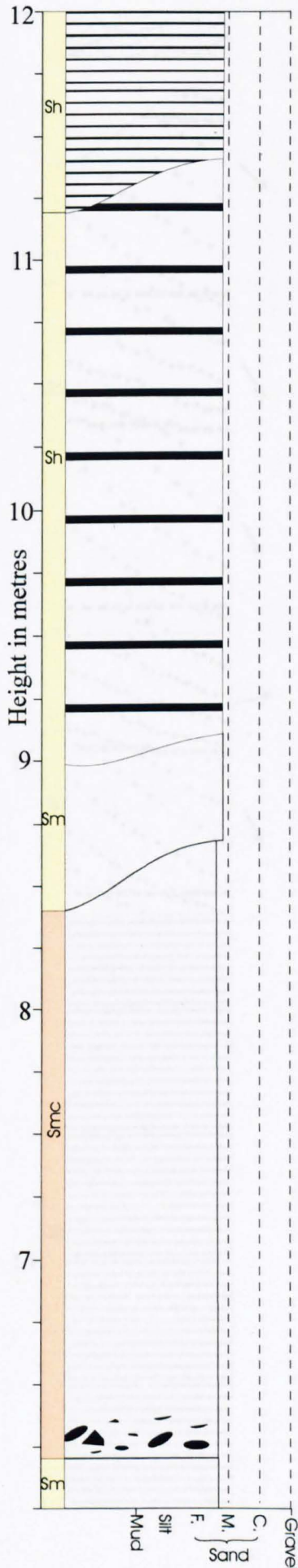
Lithology	Interpretation
	Inaccessible part of section
Sharp based sandstone with wood fragments at base; faint bedding with some ripple lamination.	Reoccupation of channel, forming fourth storey.
Laminated muds, <i>in situ Stigmaria</i> roots, no bioturbation.	Abandonment of channel, filled with fine-grained sediment and colonised by plants.
Massive sandstone with randomly oriented clasts; organic material at top.	Channel fill with variable flow and flood deposition prior to abandonment.
Faint lamination; conglomeratic layer with flow-aligned clasts up to 0.25m long.	

A5. Log 4, taken at south end of Trusklieve outcrop.



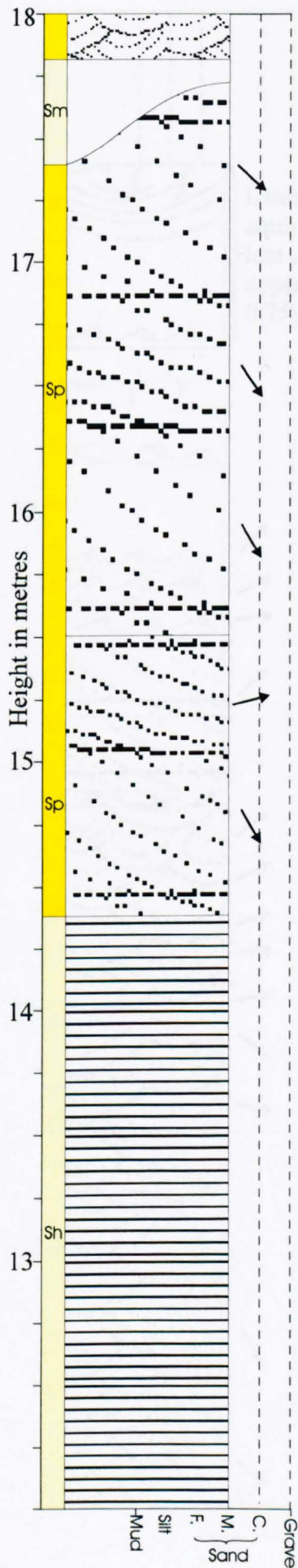
Lithology	Interpretation
Planar laminated sandstone.	Fast flow creates upper stage plane beds.
Massive sandstone with rare scattered rounded siltstone clasts up to 50mm in diameter.	Very rapid deposition from high density slurry flows, probably due to bank collapse.
Mud-clast conglomerate, showing lenticular bedding in places.	High flow stage deposits, clasts eroded from underlying unconsolidated muds and silts.

A6. Log taken through the Tullig Sandstone at Pulleen.



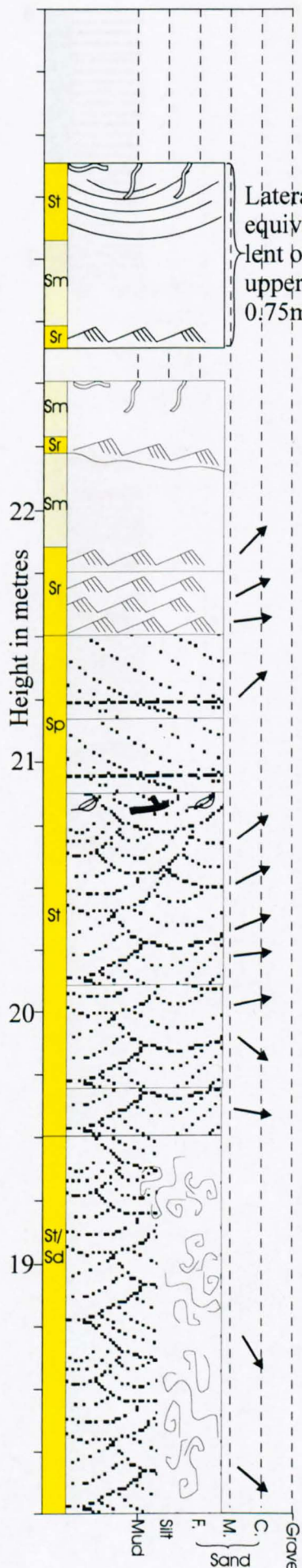
Lithology	Interpretation
Parallel laminated sandstone above 1.5m deep scour surface. Laminae parallel to scour base.	Upper stage plane beds deposited after erosion by flood-stage flow.
Massive sandstone, well-bedded with beds averaging 0.3m thick.	Repeated cycles of very rapid deposition from high density flows.
Massive sandstone above scour surface.	Erosion followed by very rapid deposition from high density slurry flows.
Massive sandstone with rare scattered rounded siltstone clasts up to 50mm in diameter.	Very rapid deposition from high density slurry flows, probably due to bank collapse.

A6. Log taken through the Tullig Sandstone at Pulleen.



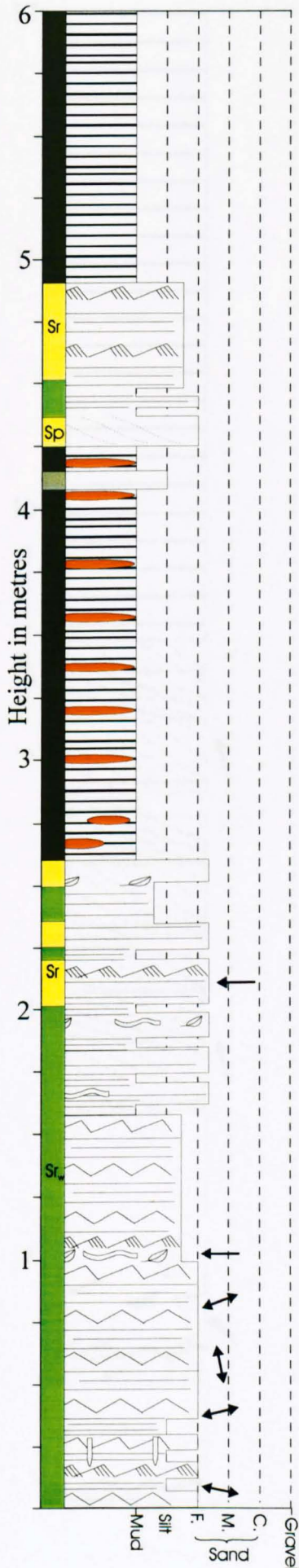
Lithology	Interpretation
Massive sandstone filling scour, passing up into trough cross-beds showing intense dewatering in places.	Erosion by flood flow, followed by rapid deposition of 3-D dunes, deformed soon after deposition.
Large tabular cross-sets with bedding surfaces continuous over tens of metres.	Large dunes formed under high flow stage conditions.
Two sets of planar cross-bedded sandstone.	2-D dunes deposited during high flow stage.
Parallel laminated, well-bedded sandstone. Beds ~ 0.2m thick.	Plane beds deposited during upper stage flow.

A6. Log taken through the Tullig Sandstone at Pulleen.



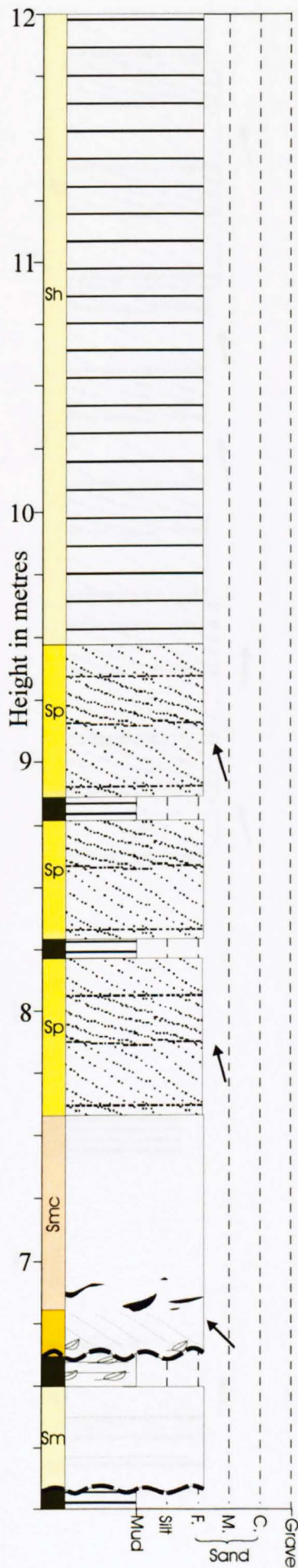
Lithology	Interpretation
Massive sandstone with ripples at base drapes surface of massive sandstone below. Lateral to this, trough cross-set scours into bed below instead. Top surface shows rare <i>Thalassanoides</i> traces and numerous vertical burrows/rootlets.	Bank-collapse sands drape bed below, and some discrete scour and fill shows presence of erosional currents. Final abandonment and bioturbation.
Ripples at base of massive sandstone sheet, local doming on top surface.	Low stage flow produces ripples; a pulse of rapid deposition gives a massive sand bed, deformed by subsequent dewatering.
Cross-laminated sandstone sheet.	Lower stage flow produces ripples as flood wanes.
Sheets of planar cross-bedding.	2-D dunes, formed by high stage flow, possibly waning after flood.
Plant material (leaves, logs) at top of final cross-bed set.	Flood debris deposited at top of cross-bedded flood stage deposits.
Well-developed trough cross-beds.	3-D dunes, formed by high stage flow.
Trough cross-beds showing intense dewatering in places.	Rapid deposition of 3-D dunes, deformed by fluidization soon after deposition.

A6. Log taken through the Tullig Sandstone at Pulleen.



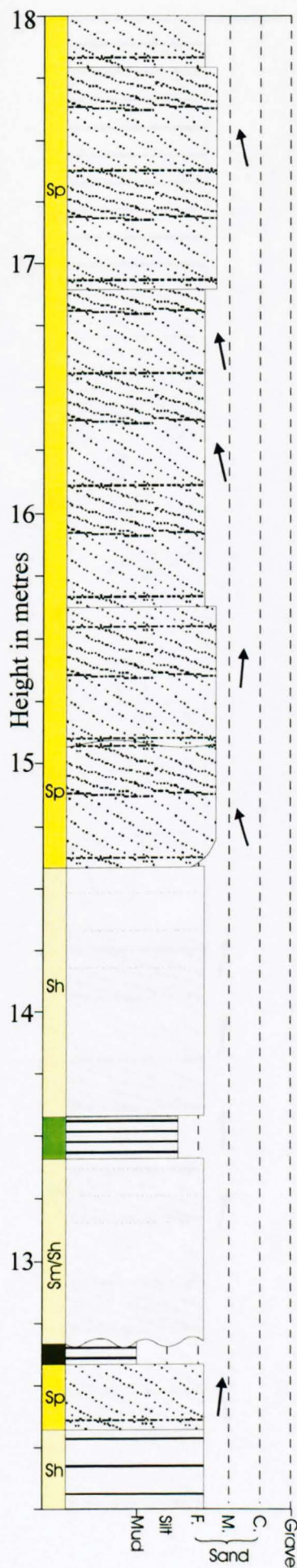
Lithology	Interpretation
Laminated mudstone.	Deposition in quiet water environment (interdistributary bay?) due to abandonment.
Laminated mudstone with concretion layers, coarsening up to silts and fine sand with parallel laminations and current ripples.	Mouthbar abandonment followed by a pulse of flood-related coarser deposition.
Interbedded mud/siltstone and fine sand, coarsening up, with organic matter and trace fossils ( <i>Skolithos</i> , <i>Asterichnus</i> ) in some horizons.	Pulses of flood-related deposition in minor mouthbar or interdistributary bay, with intervening quiescent periods allowing bioturbation.
Interbedded silt and fine sand with wave and current ripples in silty sand layers and planar lamination throughout the rest; limited bioturbation ( <i>Monocraterion</i> and <i>Asterichnus</i> ) in some horizons.	Minor mouthbar progradation, with occasional wave and current influence.

A7. Log taken on southern limb of Killard outcrop.  
 N.B. Top surface of Killard mouthbar (A16) is below this log.



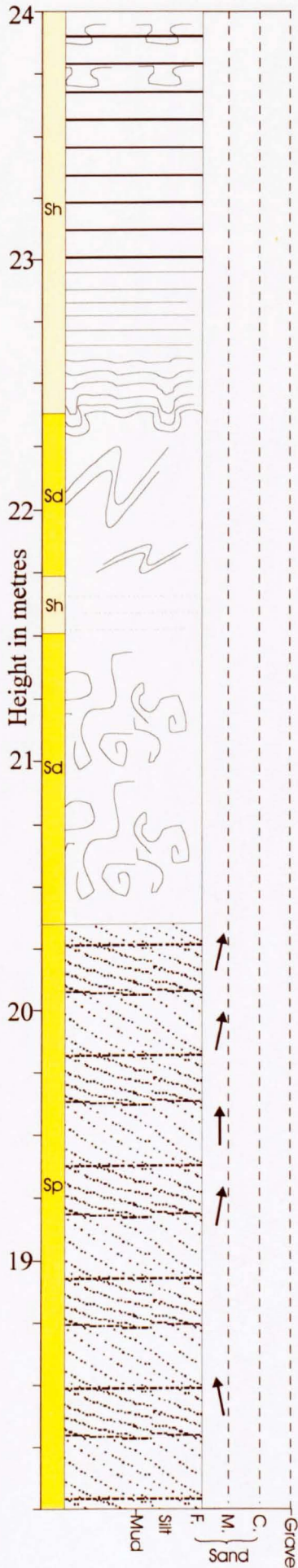
Lithology	Interpretation
Planar bedded sandstone.	Deposition in fast-flowing channel giving upper stage plane beds.
Fine sandstone with planar cross-bedding, with thin mudstone interbeds of limited lateral extent .	Channel fill with straight-crested bedforms and brief periods of abandonment and fine fill.
Erosive channel with organic lag and faint cross-bedding; deformed mudstone rip-up clasts. Massive sandstone for most of thickness.	Second channel storey erodes into abandonment deposits. Rapid deposition gives massive structure.
Thin organic-rich mud.	Temporary abandonment and fine-grained deposition .
Erosively based massive sandstone with some faint planar bedding.	First storey of fluvial channel.

A7. Log taken on southern limb of Killard outcrop.



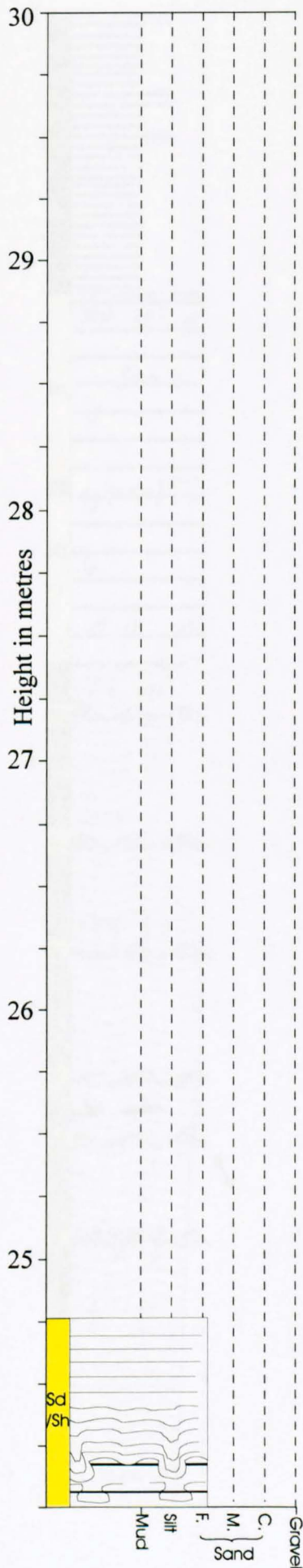
Lithology	Interpretation
<p>Planar cross-bedded sandstone, finer at base, with undulating top surface overlain by similar sands.</p>	<p>Channel-fill sediments, with straight-crested dune bedforms and occasional periods of abandonment and fine-grained deposition.</p>
<p>Sandstone with faint planar bedding.</p>	
<p>Thin laminated silty sandstone.</p>	
<p>Erosively based massive sandstone with planar bedding at top.</p>	

A7. Log taken on southern limb of Killard outcrop.



Lithology	Interpretation
Loaded base to laminated sandstone, grading into planar bedded sandstone with loaded layers nearer top.	
Liquified sandstone with deformed and loaded appearance. Some undeformed faint planar bedding.	Fast deposition leading to instability and liquefaction of channel sands, possibly initiated by seismic activity.
Planar cross-bedded sandstone.	Channel-fill sediments, with straight crested dune bedforms.

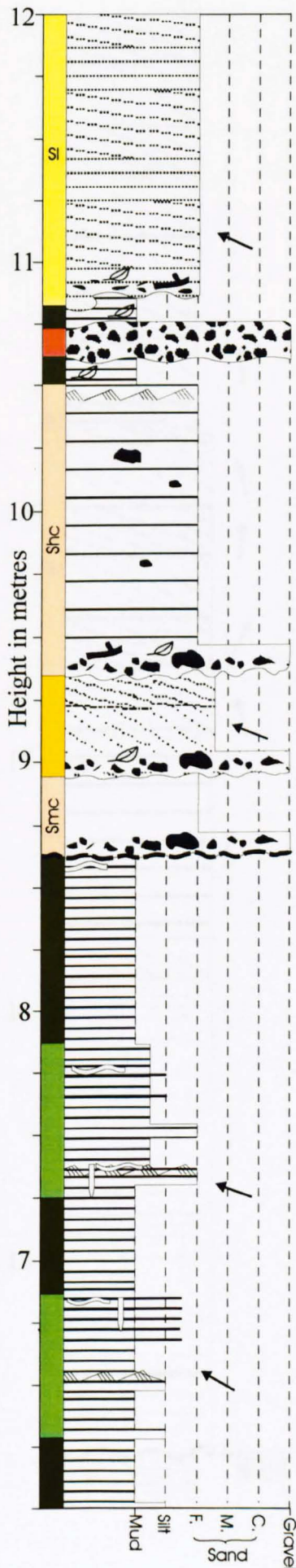
A7. Log taken on southern limb of Killard outcrop.



Lithology	Interpretation
<p>Loaded layers within horizontally laminated sandstone, grading into planar bedded sandstone at top.</p>	<p>Fast deposition leading to instability and liquefaction of channel sands, possibly initiated by seismic activity.</p>

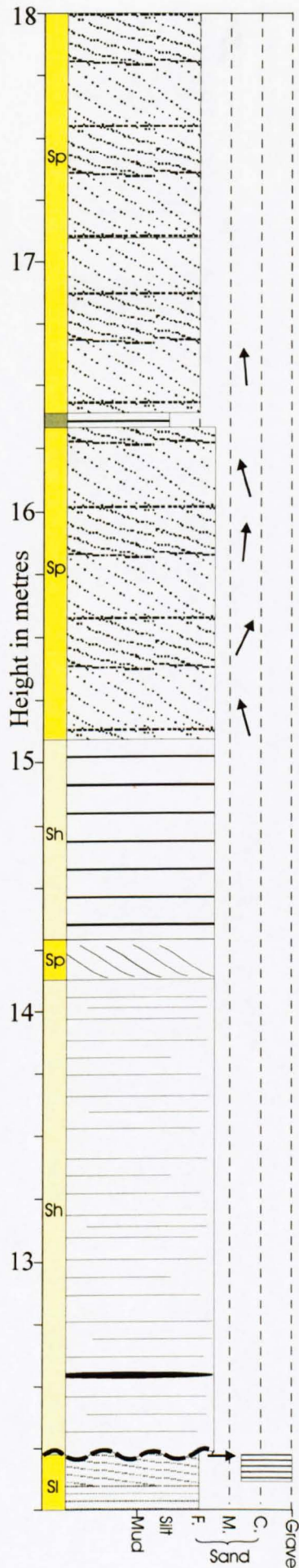
A7. Log taken on southern limb of Killard outcrop.





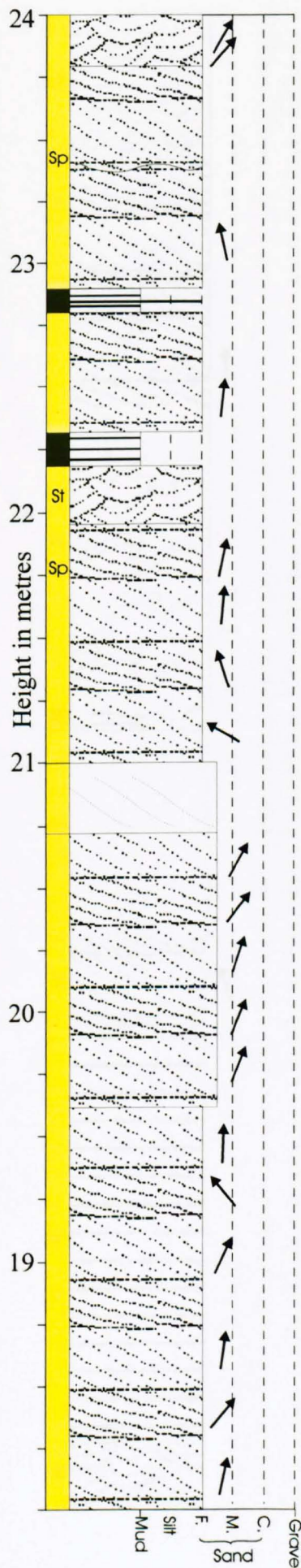
Lithology	Interpretation
Erosive and loaded base to low angle cross-bedded sandstone with thin flow aligned clast lag and organic debris.	Flood deposits eroding into unconsolidated muds, fining-up to swept-out dune-style channel fill,
Laminated mudstone cut by erosively based conglomerate containing deformed rip-up clasts of laminated mudstone.	Brief channel abandonment and fine fill, interrupted by flood deposits before further mudstone deposition.
Erosively based planar bedded sandstone with conglomeratic lag, organic debris and occasional "floating" clasts. Ripple cross-lamination at top.	Deposits from waning flood flow, filling scour.
Erosively based sandstone with conglomeratic lag and planar cross bedding.	Straight-crested dunes filling second channel scour.
Erosively based massive sandstone with conglomeratic lag (rip-up clasts of mud/silt, up to 10cm).	Strongly erosive fluvial channel, with very rapid deposition.
Laminated mudstone with silt and fine sand intercalations, getting coarser and more frequent towards the top until mudstone dominates again. Current ripples are seen in silty sand layers. Limited bioturbation ( <i>Skolithos</i> , <i>Asterichnus</i> ).	Distal mouthbar sedimentation with occasional thin sands from flood events and bioturbation during periods of slower, fine-grained deposition. Lack of wave ripples indicates depth below storm wave base.

A8. Log taken on northern limb of Killard outcrop.



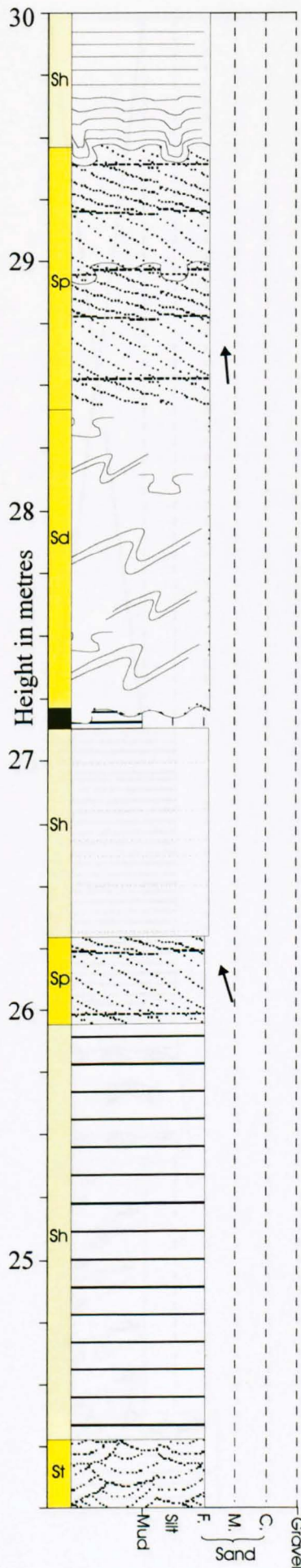
Lithology	Interpretation
<p data-bbox="605 698 973 943">Fine to medium sandstone with planar cross-bedding, some planar bedding and occasional trough cross bedding, especially nearer top. Occasional internal erosion/scour surfaces and thin mud/siltstone beds, more towards top.</p>	<p data-bbox="1006 698 1380 824">Channel fill, straight crested dune bedforms. Occasional brief abandonment and subsequent reoccupation of channel.</p>
<p data-bbox="605 1758 973 2002">Erosively based horizontally bedded sandstone with thin silt lens and occasional primary current lineation. Lateral to this, base of Sh sandstone is in erosive contact with a laminated silty mudstone (0-0.8m thick, and laterally continuous over 100m).</p>	<p data-bbox="1006 1328 1380 1386">Flow slows slightly to allow dune formation and migration.</p> <p data-bbox="1006 1758 1380 1966">Channel scour, strong currents form upper stage plane beds with a brief lull for silt deposition. Laminated mudstone indicates period of abandonment before second storey of fluvial sandbody partially erodes it.</p>

A8. Log taken on northern limb of Killard outcrop.



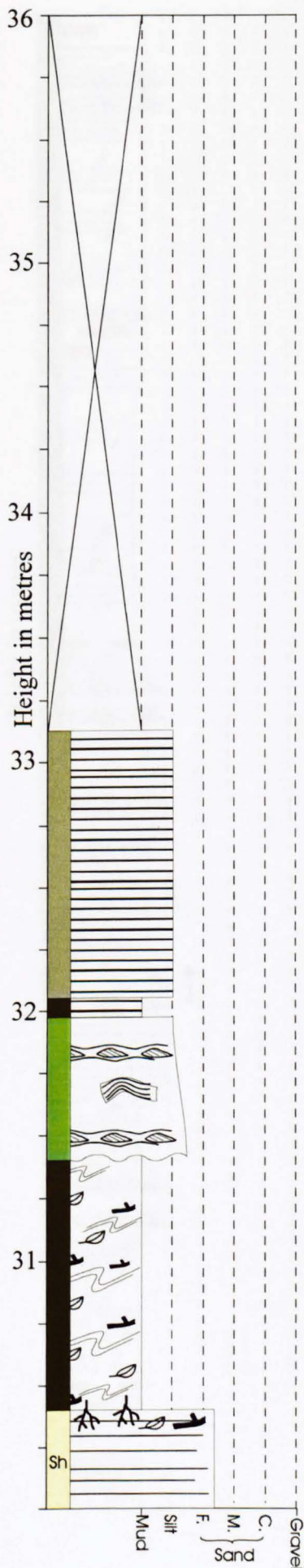
Lithology	Interpretation
<p>Fine to medium sandstone with excellent planar cross-bedding and occasional trough cross-bedding, especially nearer top. Occasional internal erosion/scour surfaces and thin mud/siltstone beds, more towards top.</p>	<p>Channel fill, with straight and sinuous crested dunes; occasional brief abandonment and subsequent reoccupation of channel.</p>

A8. Log taken on northern limb of Killard outcrop.



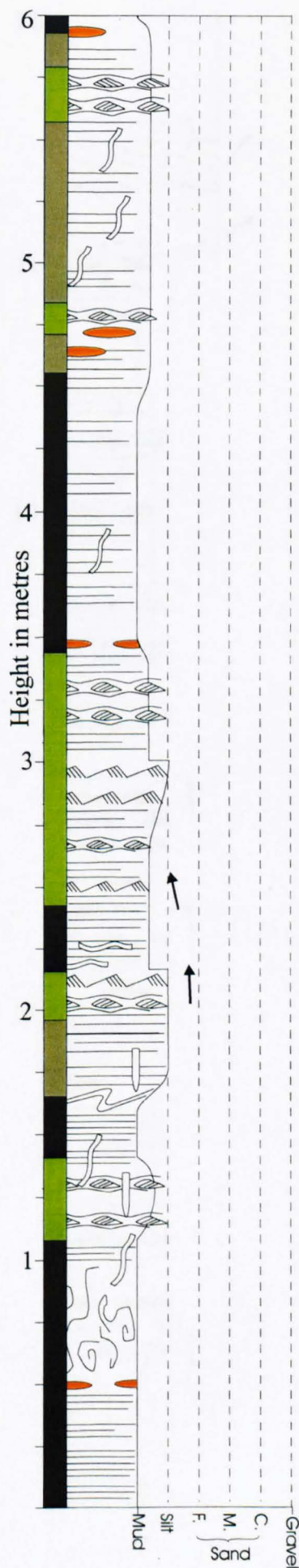
Lithology	Interpretation
Loaded and erosive base to parallel laminated sandstone, only deformed near base.	Fast pulses of deposition lead to loading.
Loaded base to otherwise undeformed planar cross-bedded sandstone.	Reduced rate of deposition allows bedding to remain intact and dunes to form.
Deformed and convoluted bedding with load features. Changes to planar cross-bedded sandstone nearer top.	Rapid deposition causing instability and deformation within channel.
[Faded text]	[Faded text]
[Faded text]	Increase in flow velocity creates upper stage plane beds.

A8. Log taken on northern limb of Killard outcrop.



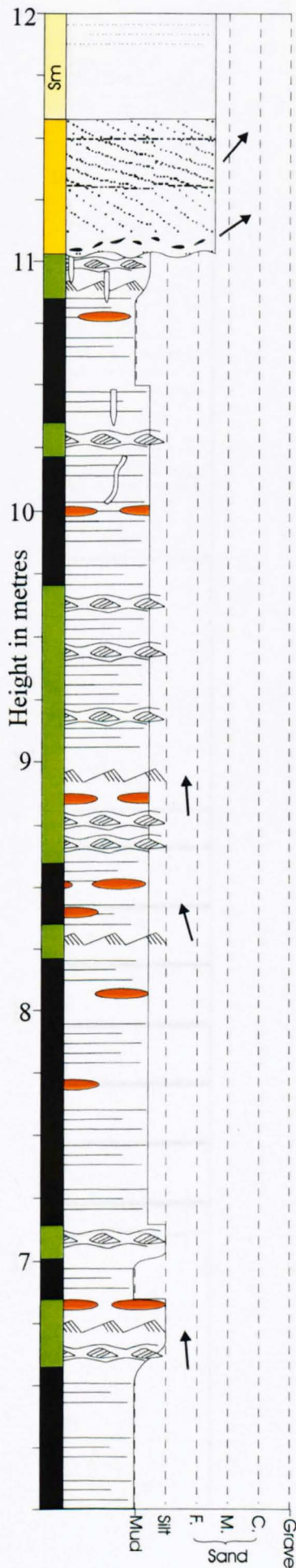
Lithology	Interpretation
<p>Parallel laminated silt, no bioturbation.</p>	
<p>Erosively based sandstone fining-up to silt, with lenticular bedding and occasional deformed clasts.</p>	<p>Small channel or crevasse splay-type sedimentation.</p>
<p>Highly organic-rich shaley bed with convoluted bedding. No apparent bioturbation.</p>	<p>Channel abandonment and lake-type sedimentation with lots of organic material.</p>
<p>Planar laminated sandstone with abundant plant debris and <i>in situ</i> <i>Stigmara</i> roots.</p>	<p>End of channel fill sedimentation, abandonment and colonisation by plants.</p>

A8. Log taken on northern limb of Killard outcrop.



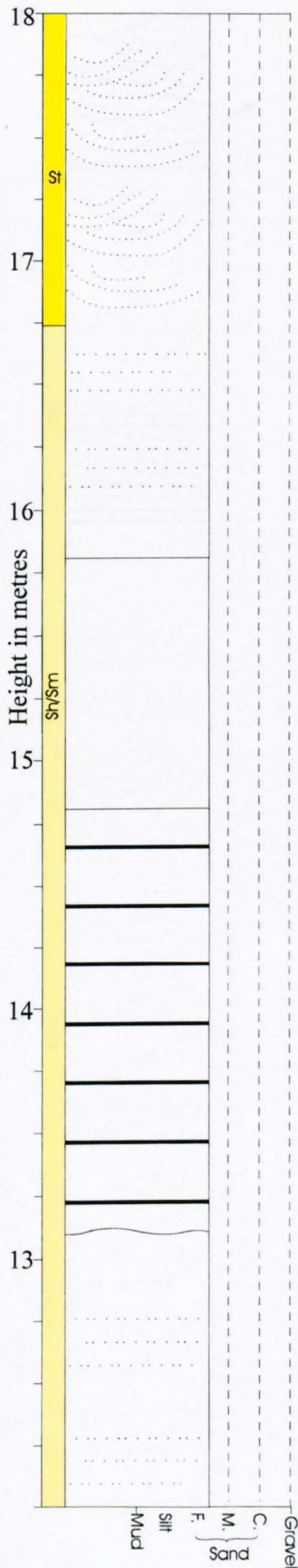
Lithology	Interpretation
<p>Generally coarsening-up cycles (mud to silt) with heterolithic bedding. Current ripples and lenticular bedding in the silt/ silty sands. Intense bioturbation in some horizons (<i>Skolithos</i>, <i>Asterichnus</i>, <i>Monocraterion</i>) and some siderite nodules. No apparent overall trend.</p>	<p>Distal mouthbar sequence with pulses of current influence; some periods of slower deposition allow bioturbation.</p>
<p>Mudstone with convoluted laminations.</p> <p>Laminated mudstone with siderite nodules.</p>	<p>Rapidly deposited sediment liquefies and deforms.</p> <p>Delta front deposition, below storm wave base.</p>

A9. Log from south-east end of Carrowmore outcrop.



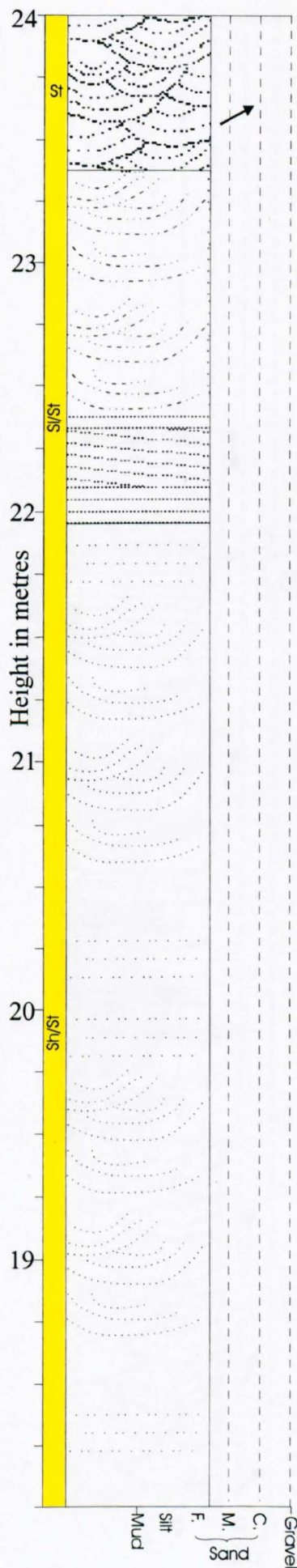
Lithology	Interpretation
Faint planar bedding in fine to medium massive sandstone.	Fast deposition within same active channel.
Erosively based sandstone with thin clast lag (clasts 40-50mm, aligned) with planar cross bedding above.	Fluvial channel with straight-crested dune bedforms.
Generally coarsening-up cycles (mud to silt) with current ripples and lenticular bedding in the silts. Lots of bioturbation and siderite. No apparent overall trend.	Distal mouthbar sequence; some periods of slower deposition allow bioturbation.

A9. Log from south-east end of Carrowmore outcrop.



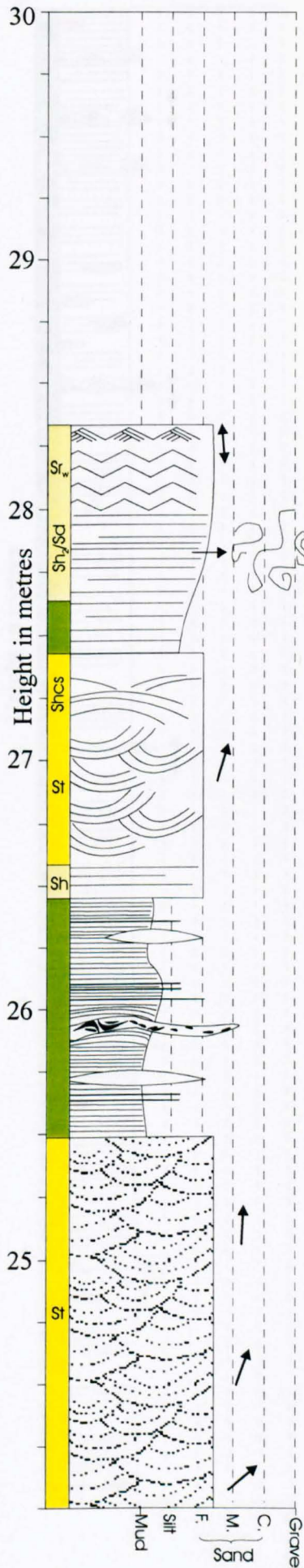
Lithology	Interpretation
<p>Faint planar and trough cross bedding.</p>	<p>Post-depositional dewatering makes bedding indistinct.</p>
<p>Faint planar bedding grades into clearly planar bedded unit, then massive sandstone.</p>	<p>Fast deposition within same active channel.</p>

A9. Log from south-east end of Carrowmore outcrop.



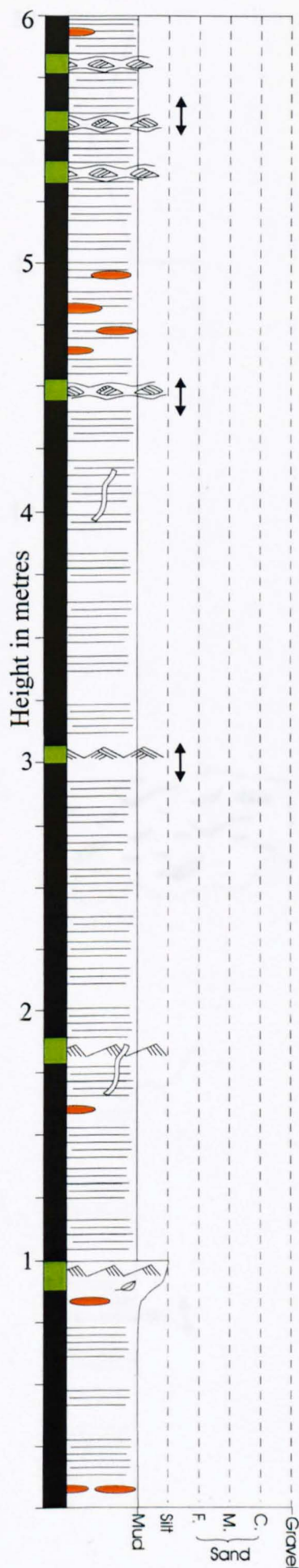
Lithology	Interpretation
<p>Sharp base to very well-bedded unit showing well-developed trough cross bedding.</p>	<p>Sinuuous crested dunes dominate channel deposition.</p>
<p>Sharp base to low angle cross-bedded unit which changes to trough cross bedding upwards.</p>	<p>Strong current influence leads to sweeping out of bedforms before waning to give troughs. Still faint bedding, indicating dewatering?</p>
<p>Faint planar beds and trough cross bedding.</p>	<p>Post-depositional dewatering makes bedding indistinct.</p>

A9. Log from south-east end of Carrowmore outcrop.



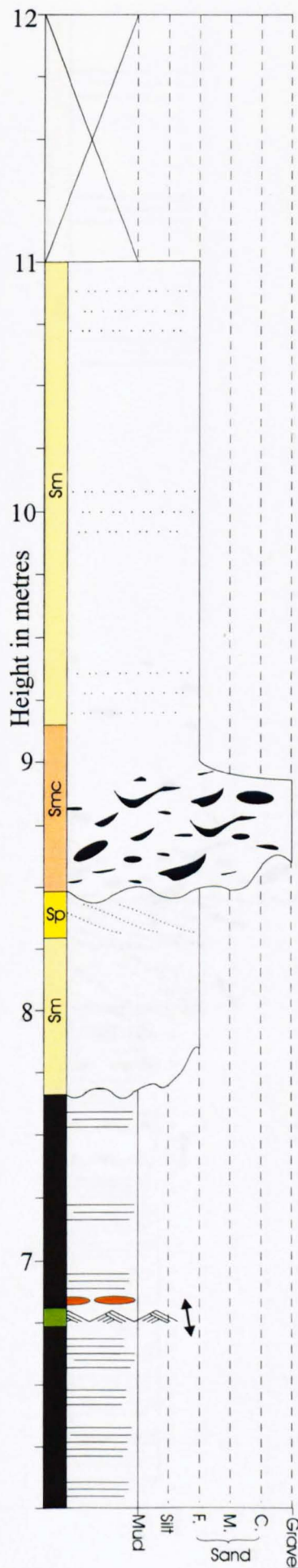
Lithology	Interpretation
<p>Aggradational ripples with upper surface showing bidirectional ripples. Deformation and convoluted laminations seen lateral to this log.</p>	<p>Waning currents allow deposition from suspension prior to channel abandonment and later wave reworking of upper surface.</p>
<p>Interlaminated sand and silt; coarsens up to parallel laminated sandstone.</p>	<p>Deposition from suspension as current influence wanes.</p>
<p>Interval of well-developed trough cross bedding, appearing hummocky in places.</p>	<p>Stronger currents causing dune formation, with wave reworking causing hummocky cross stratification. Flooding of fluvial channel by basinal water?</p>
<p>Interlaminated muds and silts with a few thin (&lt;3mm) silty sand layers, infilling topography of bed below. Sand lenses thicken (up to 0.2m) laterally, but pinch out.</p>	<p>Channel abandonment and fine-grained fill with pulses of faster flow delivering coarser sediment.</p>
<p>Very well-bedded unit showing excellent trough cross bedding. Upper surface shows preserved depositional topography.</p>	<p>Sinuous crested dunes dominate channel-fill.</p>

A9. Log from south-east end of Carrowmore outcrop.



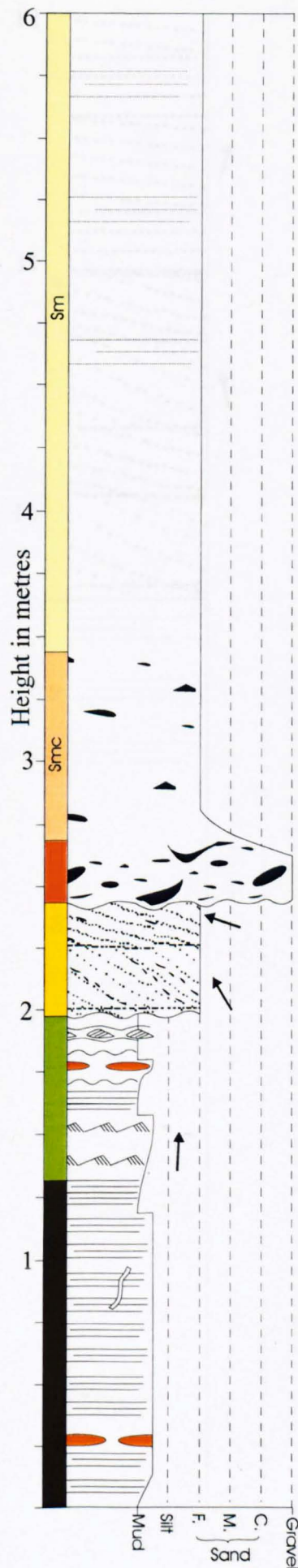
Lithology	Interpretation
<p>Parallel laminated mudstone with occasional silt ripples; increasingly silty towards top, including lenticular bedding with bi-directional cross-lamination. Several concretion layers.</p>	<p>Delta front/distal mouth bar, with occasional current deposition. Evidence of wave influence.</p>

A10. Log from south-west end of Carrowmore outcrop.



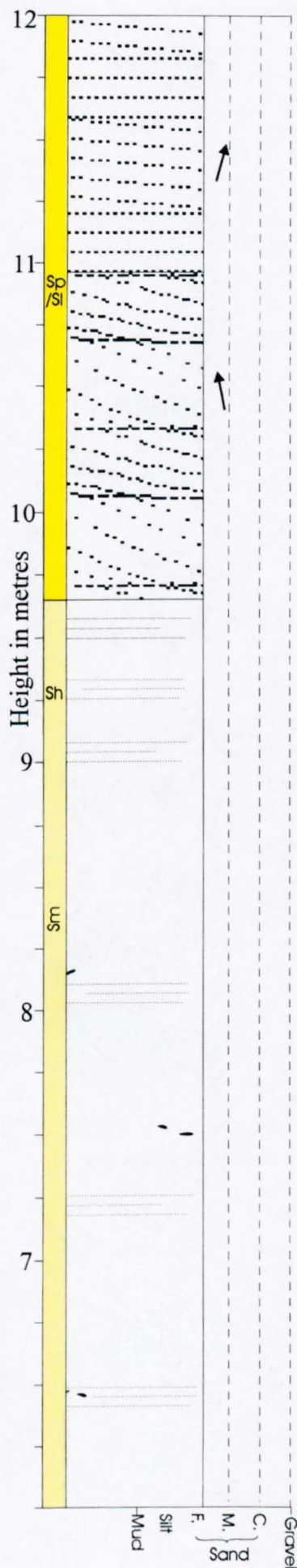
Lithology	Interpretation
<p>Erosively based sandstone with conglomeratic lag of deformed mudstone clasts (up to 10cm). Faint parallel bedding.</p>	<p>Second channel cut, very rapid deposition slowing upwards.</p>
<p>Erosively based massive sandstone (1m relief) with faint planar cross-bedding near top.</p>	<p>Fluvial channel eroding delta front; very rapid deposition slowing to give dune migration.</p>
<p>Parallel laminated mudstone with occasional silt ripples; several concretion layers.</p>	<p>Delta front/distal mouth bar, with occasional current deposition. Evidence of wave influence.</p>

A10. Log from south-west end of Carrowmore outcrop.



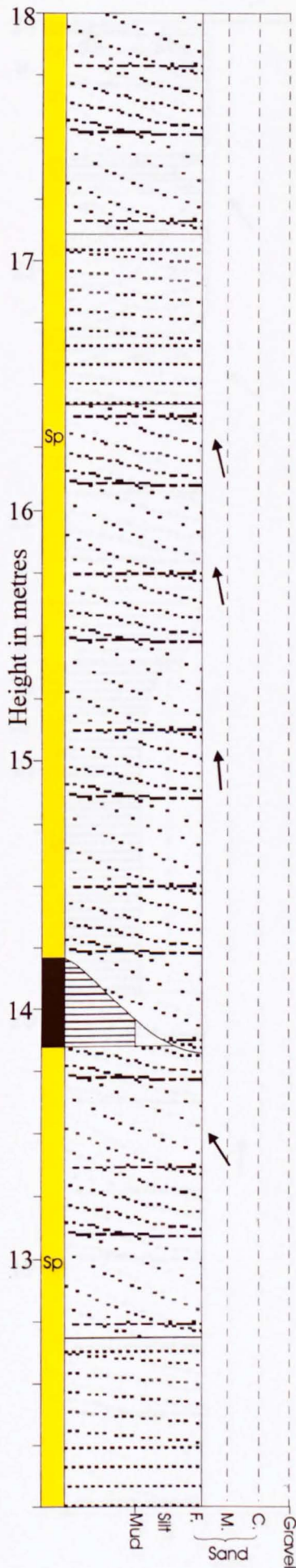
Lithology	Interpretation
<p>Erosively based sandstone with conglomeratic lag of deformed mudstone rip-up clasts up to 0.15m long. Fines up, with occasional flow-aligned clasts and massive structure with occasional faint lamination</p>	<p>Strong erosion and rapid deposition within channel, probably coupled with some dewatering (giving rise to the more massive structure)</p>
<p>Erosively based sandstone (2m relief) with rip-up clasts aligned along foresets of the planar cross-bedding</p>	<p>Fluvial channel eroding delta front; shows dune bedforms</p>
<p>Two coarsening-up cycles (overall fining up) with current ripples, siderite nodules and lenticular bedding.</p>	<p>More current influence, but decrease in silt.</p>
<p>Laminated mud/siltstone with occasional nodular layers.</p>	<p>Delta front quiet water deposition, below storm wave base.</p>

A11. Log from north-west end of Carrowmore outcrop.



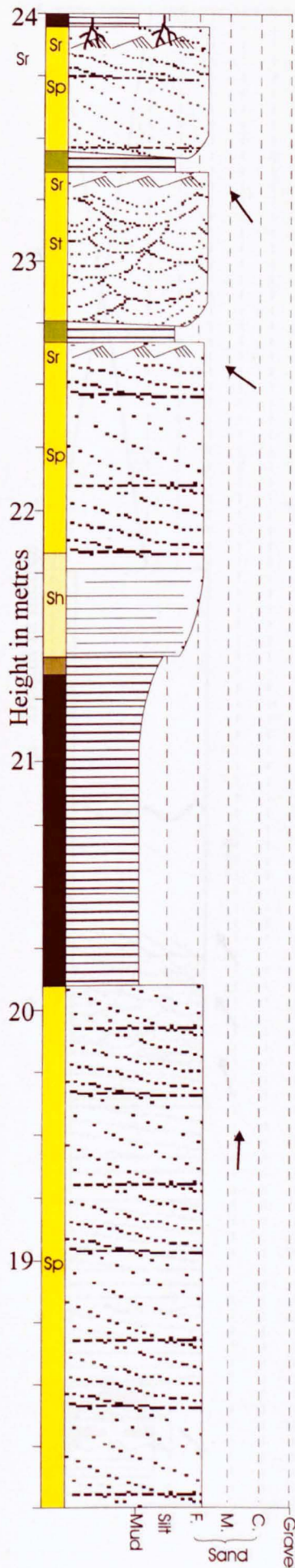
Lithology	Interpretation
<p>Very well-developed planar to low angle cross-bedding</p>	<p>Fluvial channel with straight-crested dune bedforms and a flow regime close to the transition from dunes to upper-stage plane beds..</p>
<p>Planar lamination appears within the top half metre of the bed.</p>	
<p>Massive appearance with some faint planar laminations and occasional floating clasts.</p>	<p>Rapid deposition and possible dewatering. Some slight current influence.</p>

A11. Log from north-west end of Carrowmore outcrop.



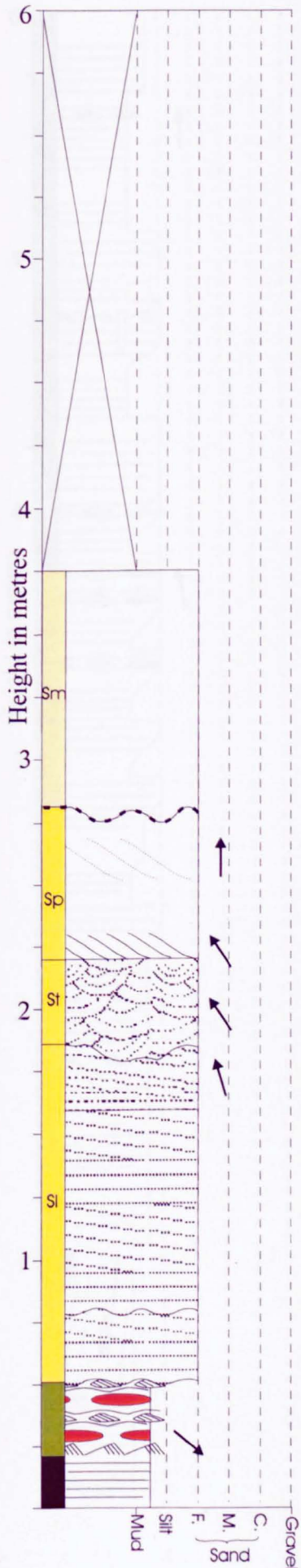
Lithology	Interpretation
Very well-developed planar to low angle cross bedding	Fluvial channel with straight-crested dune bedforms and constant flow regime.
Laterally impersistent laminated mudstone, cut out by erosive base of next cross-bedded unit.	Brief abandonment and silting-up of part of channel prior to re-commencement of straight-crested dune formation.

A11. Log from north-west end of Carrowmore outcrop.



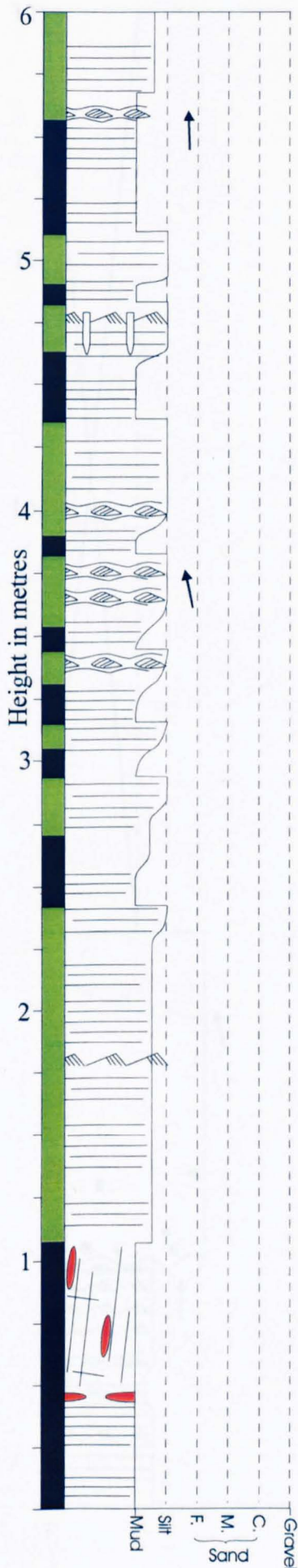
Lithology	Interpretation
<p>Rootlets occur on top surface.</p>	<p>Final abandonment of channel, and formation of swamp-type environment.</p>
<p>Storey becomes increasingly rippled towards the top, with thin silty intercalations. Occasional trough cross-beds also occur.</p>	<p>Finer-grained deposition and ripple lamination from waning flows.</p>
<p>Laterally persistent laminated mudstone, succeeded by coarsening-up cross-bedded unit.</p>	<p>Temporary abandonment of channel prior to recommencement of straight-crested dune formation and later, final, abandonment.</p>

A11. Log from north-west end of Carrowmore outcrop.



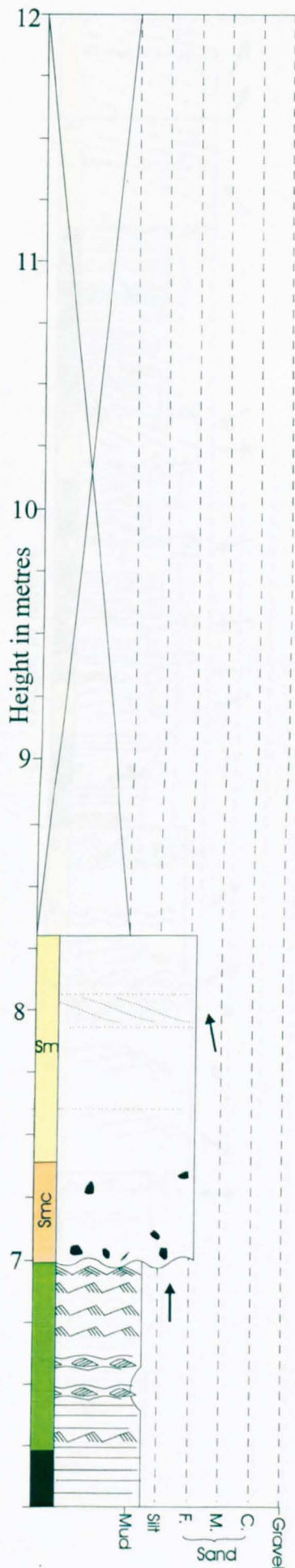
Lithology	Interpretation
<p>Base of massive sandstone is strongly erosive.</p>	<p>Second storey cuts down into first; rapid deposition gives massive sandstone.</p>
<p>Erosive base with 1m relief to trough cross-bedded unit. Grades to more massive sandstone with occasional planar cross-bedding.</p>	<p>Migration of straight and sinuous crested dune bedforms.</p>
<p>Erosively based sandstone with low-angle cross bedding.</p>	<p>Fluvial channel with numerous internal erosion surfaces; base cuts into delta front sediments.</p>
<p>Erosively based sandstone with large scale planar bedding.</p>	
<p>Erosively based planar bedded sandstone.</p>	
<p>Laminated mud/siltstone with occasional current ripple cross-lamination. Lenticular bedding and siderite nodules nearer top.</p>	<p>Delta front/distal mouth bar with occasional current deposition.</p>

A12. Log from north-centre of Carrowmore outcrop.



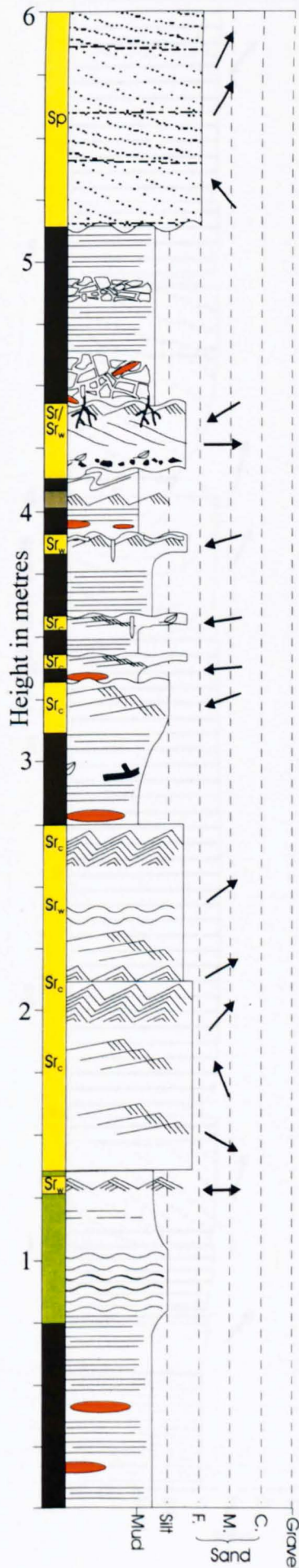
Lithology	Interpretation
<p>Sparse bioturbation in some strata (<i>Scolithos</i>). Occasional rippled beds within silty layers.</p>	<p>Slow overall rate of sedimentation with occasional current and/or wave influence.</p>
<p>Parallel laminated mud/siltstone in a series of coarsening-up cycles, with silty layers showing lenticular bedding or current ripples. Overall heterolithic appearance.</p>	<p>Distal mouth bar-type sequence, with current influence.</p>
<p>Highly fractured laminated mudstone, with nodules developed along cracks.</p>	<p>Pro-delta deposition from suspension. Fractures form soon after deposition, as nodules develop shortly after sedimentation. Related to liquefaction?</p>

A13. Log from north-east end of Carrowmore outcrop.



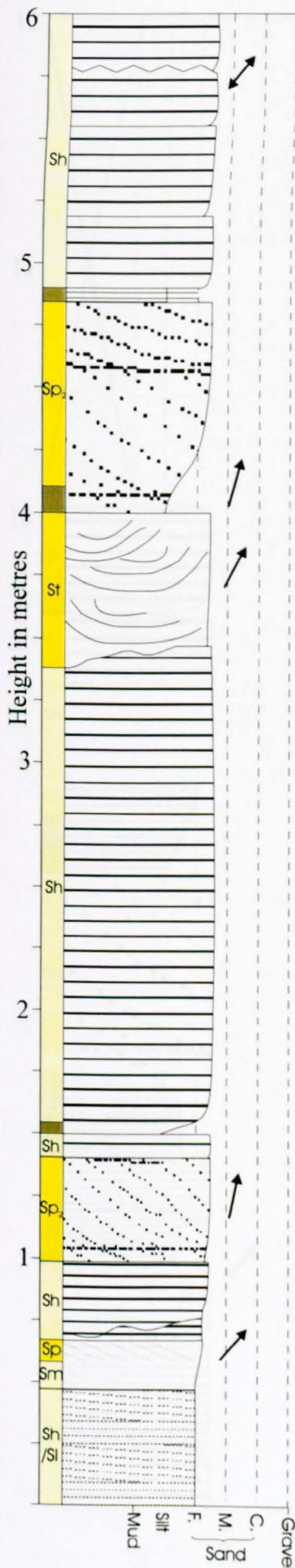
Lithology	Interpretation
Erosively based massive sandstone with lag of mud clasts and faint planar cross-bedding nearer top.	Fluvial channel, strong erosion and initially rapid deposition, waning slightly toward top.
Finely interbedded mud and siltstone with current ripples in silty intervals and occasional lenticular bedding (very fine sand/silt). Wave ripple cross-lamination at top.	Increased current and wave influence, probably shallower.

A13. Log from north-east end of Carrowmore outcrop.



Lithology	Interpretation
Erosively based medium-coarse sandstone with dune-scale planar cross-bedding and occasional ripple lamination at intervals.	Fluvial channel cutting through delta front deposits.
Laminated mud/siltstone with horizons brecciated/collapsed <i>in situ</i> . Siderite nodules formed before brecciation.	Quiet water deposition in inter-distributary bay. Collapse a more recent feature.
Erosive and loaded base to fine cross-bedded sand with current ripples at top. Fine clast lag with organic material. <i>Stigmara</i> rootlets	Deposit from waning overbank flow, with subsequent exposure allowing plant colonisation.
Convolute lamination in mud.	
Coarsening-up cycles, parallel laminated with silty sand tops showing climbing ripples or current ripples. Some bioturbation ( <i>Skolithos</i> , ? <i>Curvolithus</i> ) and organic material.	Interdistributary bay with crevasse splay sands. Overall fining-up trend indicates relative increase in distance from feeder channel.
Slightly finer grainsize with climbing ripples and aggradational ripples.	Rapid deposition from sand-laden currents - interdistributary bay invaded by crevasse splay.
Fine sandstone with ripple cross-lamination and climbing ripples, whole form preserved.	Rapid deposition from sand-laden currents - interdistributary bay invaded by crevasse splay.
Parallel laminated mud/siltstone with sideritic nodules. Coarsens up to silt with wavy laminations. Finer top shows wave ripples.	Interdistributary bay quiet water environment with some wave re-working. Organic-rich, iron-rich waters cause siderite precipitation.

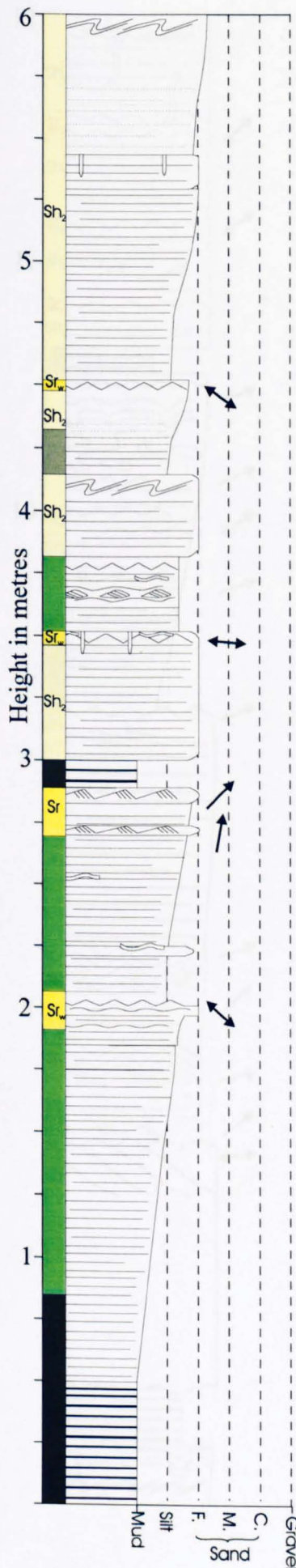
A14. Log from east end of Furreera outcrop, Liscannor Bay.



Lithology	Interpretation
Horizontally bedded units, one with wave reworked top.	Increase in flow strength causes upper stage plane beds. Reworking by basinal waves.
Silt with two very thin sand layers.	Decrease in flow strength causes silt deposition from suspension from effluent plume.
Planar cross-bedded with silt at base, draping lower parts of foresets.	Continued fluvial influence and tractional currents give dune bedforms.
Trough cross-bedded unit, erosional base.	
Blocky, parallel bedded unit.	Deposition in axial mouthbar crest setting, strong tractional currents.
First laterally continuous planar cross-bedded set.	Frictional, fluvial influence shown by migration of dune bedforms.
Horizontally bedded unit with erosive base, cuts out bed below.	Frictional, fluvial influence shown by erosive contact and upper stage plane beds.
Massive, becoming faintly cross-bedded towards top.	Rapid deposition from suspension in the presence of tractional currents in an axial mouthbar crest setting.
Low angle cross-bedding to parallel bedding, with sharp straight erosive base.	

A15. Log from Tullig Point outcrop (below Tullig Sst).

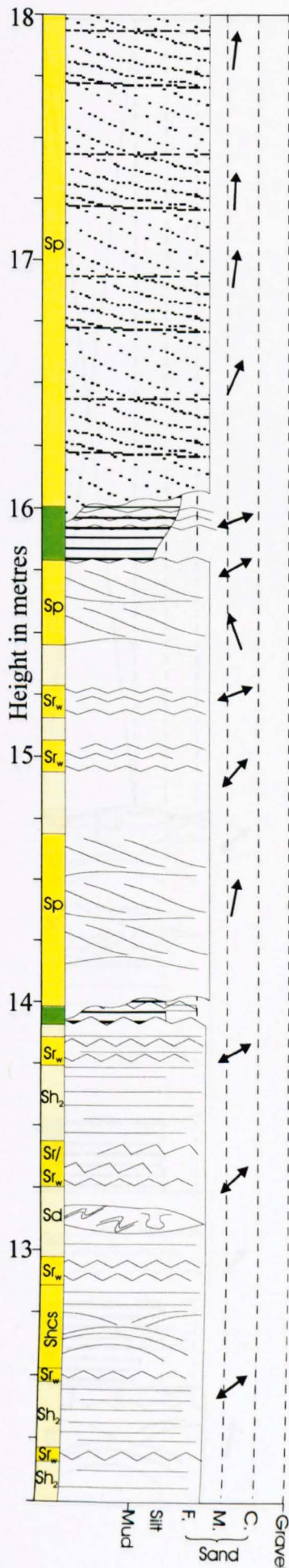




Lithology	Interpretation
Vertical burrows ( <i>Monocraterion</i> ) in laminated fine sand.	
Parallel laminated silty sand, sand layers becoming more frequent and thicker upwards.	
Coarsening-up bed becomes structureless upwards. Top is wave reworked.	
Convolute lamination at top of fine sand bed.	Minor dewatering of rapidly deposited, very wet sediment.
Lenticular bedding, symmetric wave ripples at top.	
Bioturbation ( <i>Skolithos</i> , ? <i>Pelecypodichnus</i> ) and wave reworking of top surface of bed suggests brief pause in sedimentation.	
Coarsening-up sequence of muds and silts, interlaminated on mm scale, with occasional thin (5-35 mm) layers of fine sand. Some wave ripples; current ripples in sands. Parallel to irregular lamination. Few trace fossils (? <i>Planolites</i> ).	Prograding mouthbar facies, bar back area within storm wave base. Material deposited from suspension.

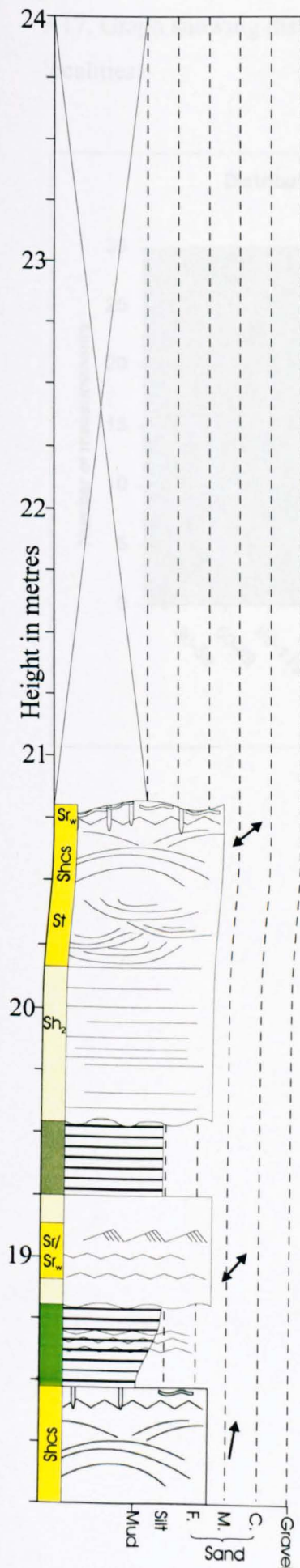
A16. Log through Killard mouthbar (south limb). Killard location: N 52°45.073' W 09°32.920'. Accuracy 5m.





Lithology	Interpretation
Planar cross-bedded medium to fine sandstone.	Cross bedding indicates stronger flow as depositional environment approaches channel mouth.
Interbedded fine silt and sand, sandy layers show wave ripples. Cut out laterally by bed above.	
Fine to medium erosively based sandstone, cuts out silt below. Planar cross bedded, strongly wave rippled in places.	Progradation of axial mouthbar facies, with significant wave reworking. Strong traction currents give erosional surfaces and cross bedding, indicating friction-dominated deposition.
Interlaminated muddy silt and fine sand, with wave ripples. 23m lateral extent.	
Some current ripples, northeast directed current.	
Deformed and loaded unit, max. 1.8m thick, dies out laterally (15m lateral extent).	

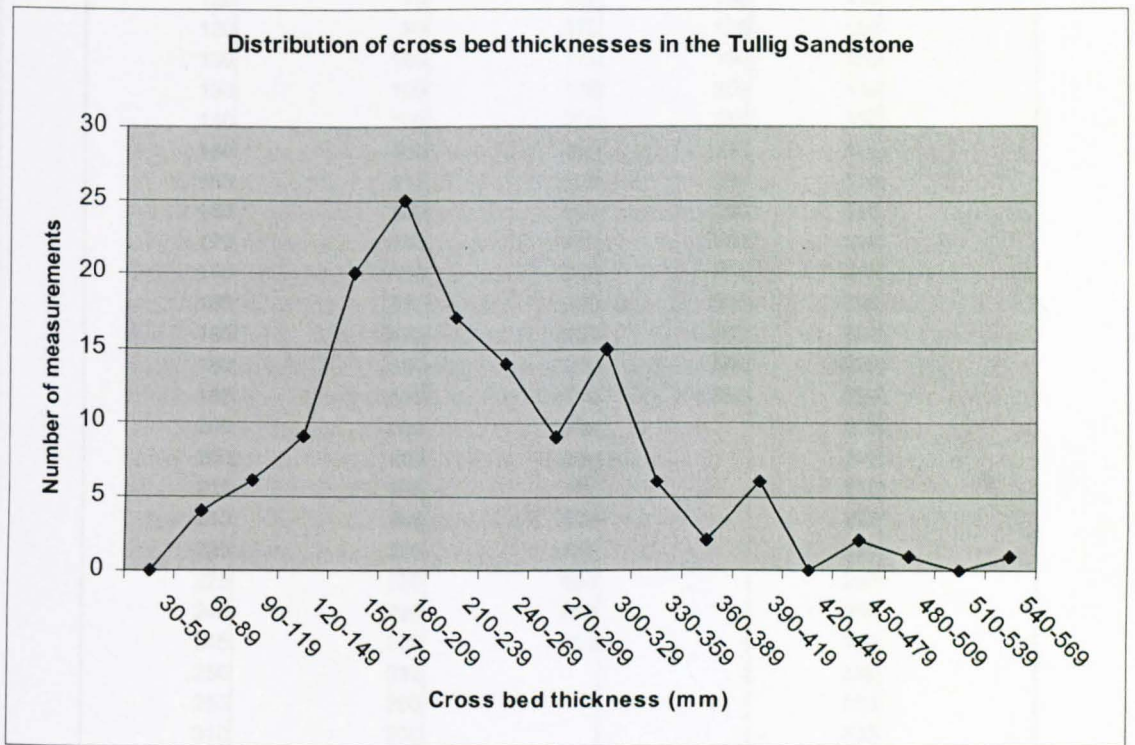
A16. Log through Killard mouthbar (south limb).



Lithology	Interpretation
<p>Erosively based parallel bedded sandstone with trough cross-bedding in upper third, and hummocky cross-stratification in the upper 0.5m. Wave ripples near top surface, which is intensely bioturbated showing abandonment (<i>Asterichnus</i>, <i>Skolithos</i>).</p>	<p>Strong flow causes sinuous dune formation and migration, before the mouthbar is abandoned, storm and wave reworked, and bioturbated.</p>
<p>Fine silt, parallel laminated.</p>	<p>Brief quiescent periods, possibly caused by temporary channel avulsion.</p>
<p>Erosively based sandstone with wave and current ripples.</p>	
<p>Muddy siltstone with sandy, wave rippled interbeds.</p>	
<p>Hummocky cross stratification, with top surface rippled and bioturbated, (<i>Monocraterion</i>, <i>Asterichnus</i>)</p>	<p>Pause in deposition, allowing storm and wave reworking and bioturbation.</p>

A16. Log through Killard mouthbar (south limb).

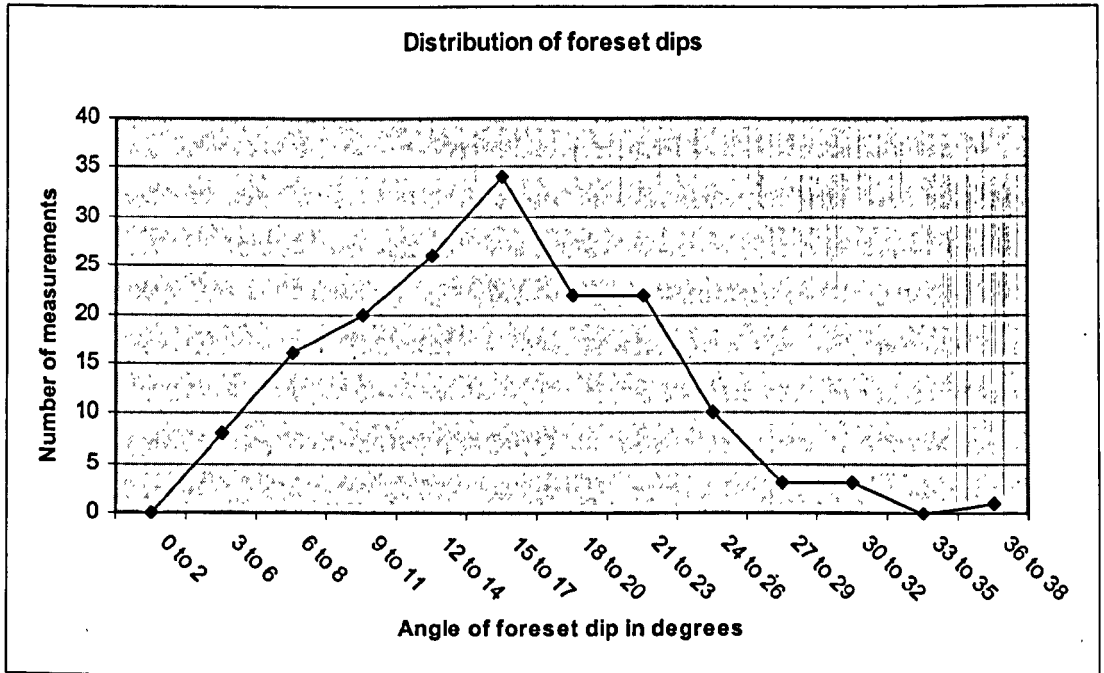
A17. Graph showing distribution of cross bed thicknesses in the Tullig Sandstone for all localities.



A17 cont. Table of data relating to graph

	Cross bed thickness (mm)					
	Truskleeve	Killard (north)	Killard (south)	Carrowmore	Liscannor	All localities
	80	60	100	130	140	
	120	70	160	150	150	
	120	70	170	170	150	
	130	100	175	190	150	
	130	100	180	200	150	
	140	100	200	210	150	
	150	100	200	220	170	
	150	110	220	250	170	
	150	130	240	250	180	
	170	130	240	300	190	
	175	150	250	310	195	
	180	150	250	380	200	
	180	170	260	400	200	
	180	180	270	500	200	
	185	190	270	850	200	
	200	200	290		205	
	200	200	300		210	
	210	205	310		210	
	215	205	350		220	
	220	210	450		220	
	225	220	630		230	
	240	220	800		250	
	245	225	950		300	
	250	230			330	
	250	250			330	
	310	260			335	
	540	270			340	
		270			340	
		280			450	
		290			600	
		290			650	
		290				
		300				
		300				
		300				
		305				
		305				
		310				
		310				
		310				
		320				
		380				
		390				
		400				
		400				
		405				
		410				
<b>Total</b>	<b>5345</b>	<b>11070</b>	<b>7265</b>	<b>4510</b>	<b>7815</b>	<b>36005</b>
<b>Mean</b>	<b>197.962963</b>	<b>235.5319149</b>	<b>315.8695652</b>	<b>300.66667</b>	<b>244.2188</b>	<b>250.034722</b>

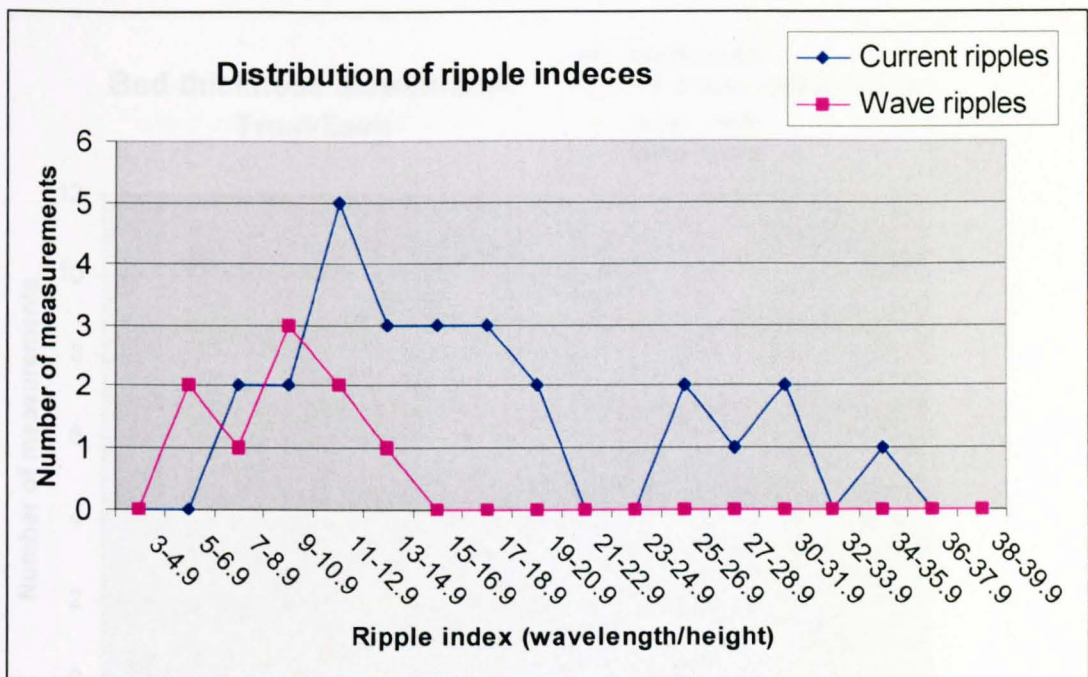
A18. Graph showing distribution of foreset dip angles for cross beds at all localities.



A18 cont. Table of data relating to graph

Angles of foreset dips in degrees at each locality (corrected for regional dip)						
	Truskieve	Carrowmore	Killard (north)	Killard (south)	Liscannor	All localities
	3	5	5	3	14	
	6	6	5	4	14	
	7	7	5	6	14	
	7	12	5	8	15	
	7	12	6	9	15	
	8	13	7	9	15	
	8	14	8	10	16	
	8	16	8	10	16	
	8	17	9	11	17	
	9	19	9	11	17	
	9	19	9	12	19	
	9	20	10	12	20	
	9	20	10	12	21	
	10	21	10	12	22	
	10	23	12	12	22	
	11	23	12	13	32	
	11	24	13	14		
	12	26	14	14		
	12	26	14	15		
	12	29	15	16		
	12	30	15	16		
	14		15	16		
	14		16	16		
	15		16	16		
	16		16	16		
	16		16	17		
	19		16	17		
	19		17	17		
	20		17	17		
	20		17	18		
	21		18	18		
	21		19	19		
	21		20	20		
	21		20	20		
	23		20	21		
	25		20	21		
			20	25		
			21			
			21			
			22			
			22			
			22			
			22			
			23			
			23			
			23			
			24			
			24			
			25			
			25			
			26			
			28			
			29			
			30			
			36			
Total	473	382	930	523	289	2597
Mean	13.13888889	18.19047619	16.90909091	14.13513514	18.0625	15.73939394

A19. Graph of ripple index distributions, from all localities



A19 cont. Data table to accompany graph.

Locality	Current ripples			Ripple index
	Wavelength (mm)	Height (mm)		
Truskieve	70	6	11.66666667	
	75	10	7.5	
	55	4	13.75	
	50	6	8.333333333	
	100	10	10	
	60	3	20	
	60	4	15	
Carrowmore	75	4	18.75	
	110	4	27.5	
	80	4	20	
	75	4	18.75	
	100	8	12.5	
	80	6	13.33333333	
	100	10	10	
	60	4	15	
	62	2	31	
60	2	30		
Liscannor	50	2	25	
	75	3	25	
	150	8	18.75	
	120	8	15	
	120	10	12	
	140	4	35	
Liscannor	85	6	14.16666667	
	70	6	11.66666667	
Killard mouthbar	Wave ripples			
	70	6	11.66666667	
	55	4	13.75	
	55	6	9.166666667	
	60	6	10	
	60	10	6	
	60	8	7.5	
	60	6	10	
Liscannor	200	16	12.5	
	200	30	6.666666667	

B1. Bed thickness data (excluding cross beds) from Trusklieve.

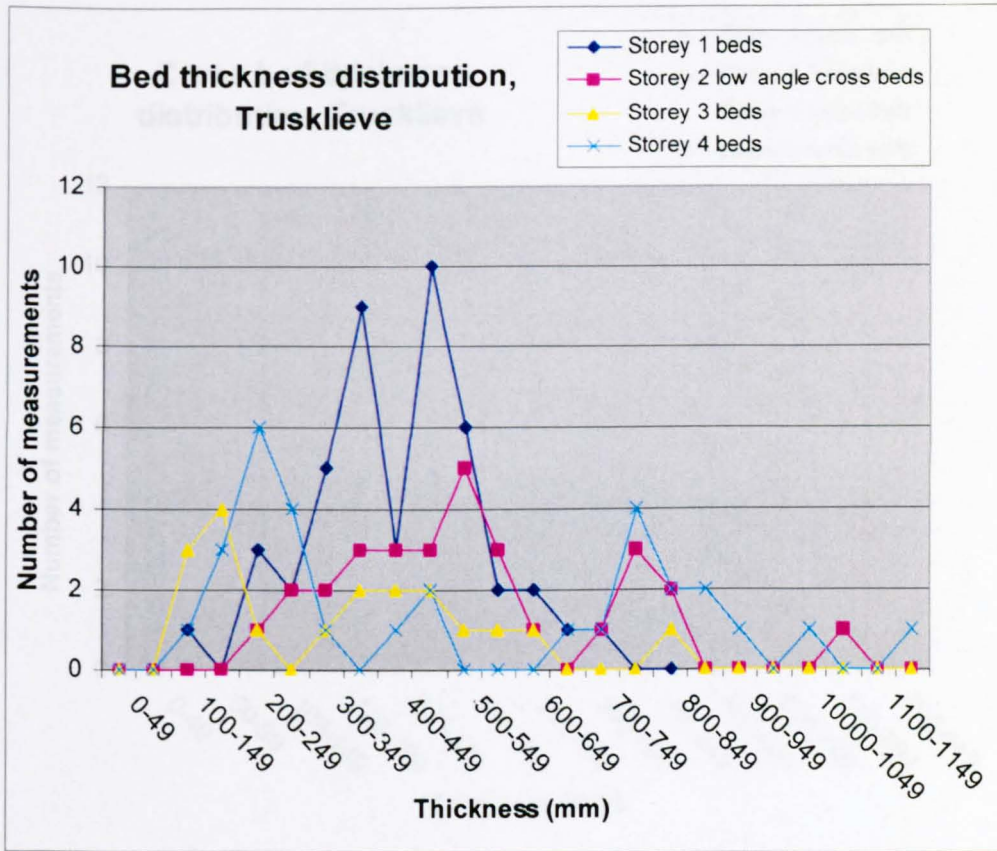
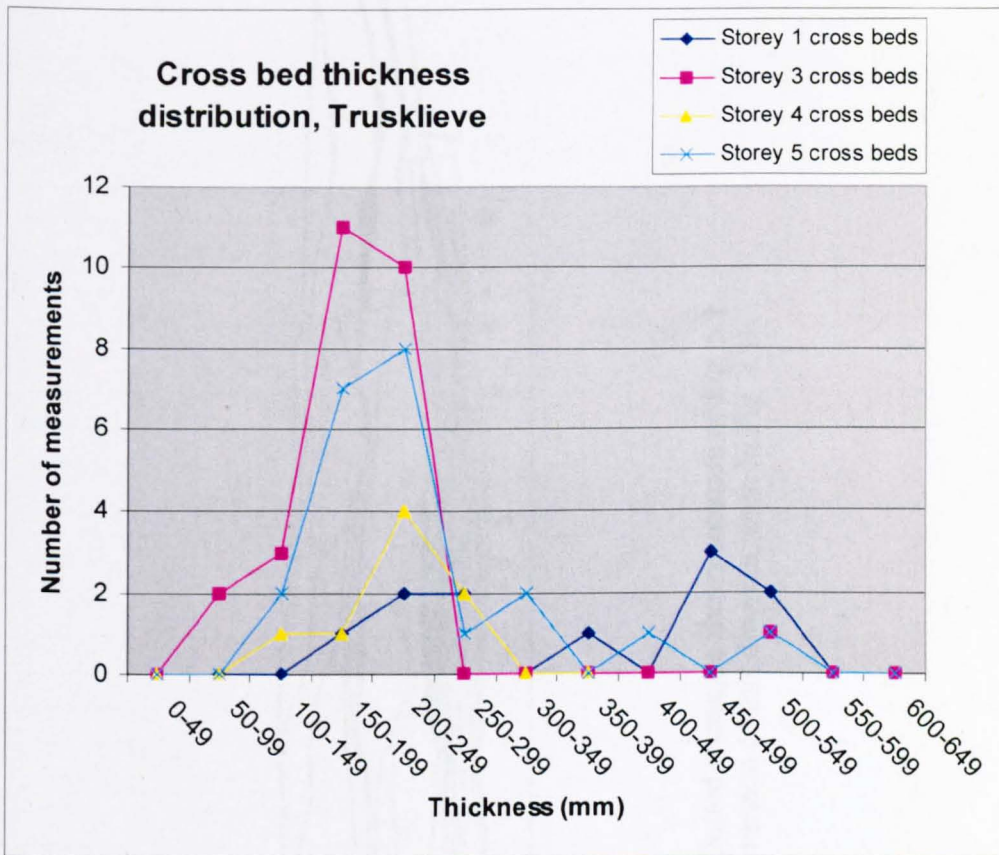


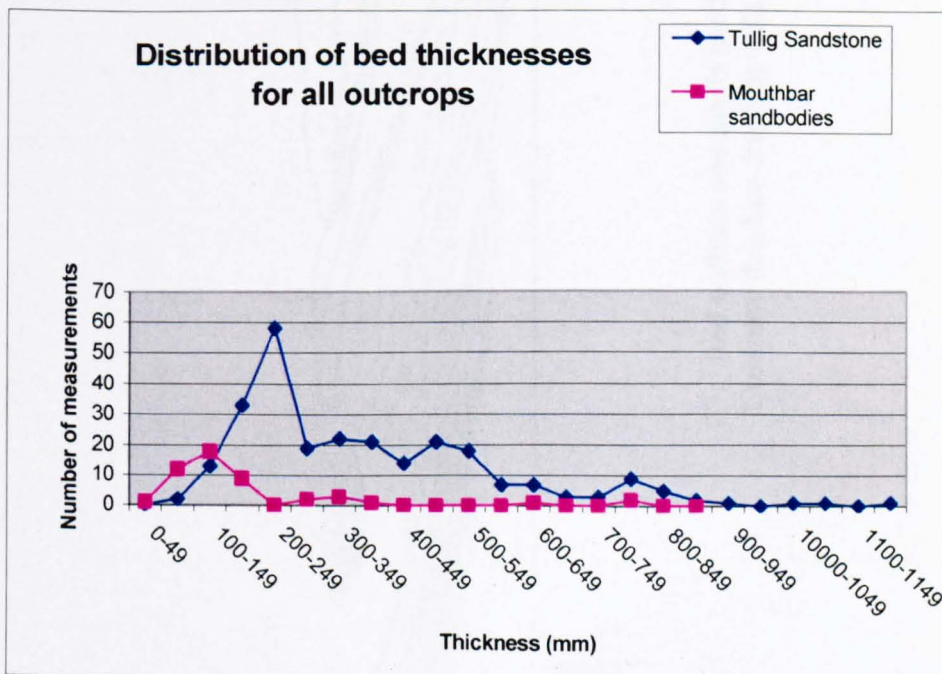
Table to accompany graphs in B1 and B2.

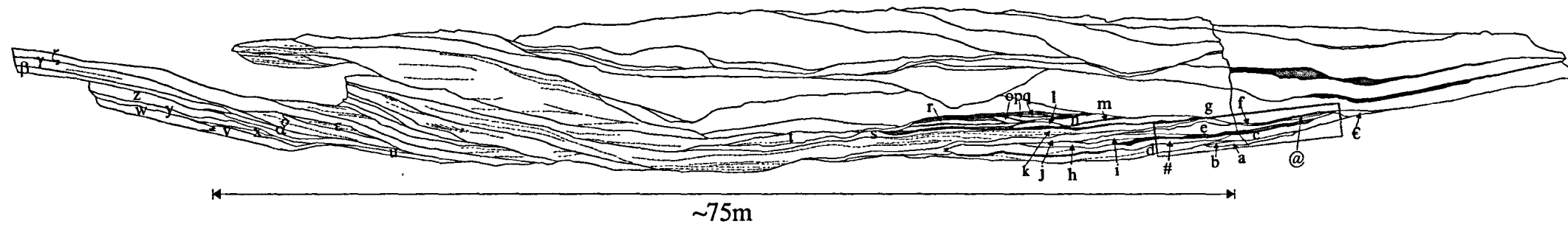
Thickness (mm)	Storey1		Storey2	Storey3		Storey4		Storey5
	# of beds	x-beds	SI x-beds	beds	x-beds	beds	x-beds	x-beds
0-49	0	0	0	0	0	0	0	0
50-99	0	0	0	0	0	2	0	0
100-149	1	0	0	3	3	1	1	2
150-199	0	1	0	4	11	3	1	7
200-249	3	2	1	1	10	6	4	8
250-299	2	2	2	0	0	4	2	1
300-349	5	0	2	1	0	1	0	2
350-399	9	1	3	2	0	0	0	0
400-449	3	0	3	2	0	1	0	1
450-499	10	3	3	2	0	2	0	0
500-549	6	2	5	1	1	0	0	1
550-599	2	0	3	1	0	0	0	0
600-649	2	0	1	1	0	0	0	0
650-699	1	0	0	0	0	1	0	0
700-749	1	0	1	0	0	1	0	0
750-799	0	0	3	0	0	4	0	0
800-849	0	0	2	1	0	2	0	0
850-899	0	0	0	0	0	2	0	0
900-949	0	0	0	0	0	1	0	0
950-999	0	0	0	0	0	0	0	0
1000-1049	0	0	0	0	0	1	0	0
1050-1099	0	0	1	0	0	0	0	0
1100-1149	0	0	0	0	0	0	0	0
1150-1199	0	0	0	0	0	1	0	0

B2. Cross bed thickness data from Trusklieve.



B3 Bed thickness data from all outcrops





C1. Bed outlines and labels used in Table 5.1. Dotted rectangle shows location of Fig. 5.1. Compare this line drawing with the full colour version of this diagram, seen in Fig. 4.1b.

C2. Horizontal proportion facies distribution data, Tullig Sandstone, Trusklieve outcrop.

Distance along outcrop (m)	% Sm/Sh	% Sp/St	% Smc	% Sc	% Ccm	% Flh	% Fls	% Flm
0	100	0	0	0	0	0	0	0
2	100	0	0	0	0	0	0	0
4	100	0	0	0	0	0	0	0
6	100	0	0	0	0	0	0	0
8	66.66	0	16.67	0	16.67	0	0	0
10	66.66	0	16.67	0	16.67	0	0	0
12	42.86	0	28.57	0	28.57	0	0	0
14	42.86	14.29	28.57	0	14.28	0	0	0
16	57.14	14.29	14.29	0	14.28	0	0	0
18	75	16.67	8.33	0	0	0	0	0
20	45.45	45.46	9.09	0	0	0	0	0
22	40.91	59.09	0	0	0	0	0	0
24	39.13	60.87	0	0	0	0	0	0
26	33.33	66.67	0	0	0	0	0	0
28	29.17	70.83	0	0	0	0	0	0
30	29.17	70.83	0	0	0	0	0	0
32	20.83	79.17	0	0	0	0	0	0
34	16.67	83.33	0	0	0	0	0	0
36	16.67	83.33	0	0	0	0	0	0
38	20	80	0	0	0	0	0	0
40	20.83	79.17	0	0	0	0	0	0
42	24	72	0	0	4	0	0	0
44	24	76	0	0	0	0	0	0
46	23.08	73.08	0	3.84	0	0	0	0
48	26.92	69.23	0	3.85	0	0	0	0
50	23.08	69.23	0	7.69	0	0	0	0
52	20.83	70.84	0	8.33	0	0	0	0
54	20.83	66.67	0	8.33	4.17	0	0	0
56	12	72	0	12	4	0	0	0
58	12.5	70.83	0	8.33	4.17	0	0	4.17
60	24	60	0	4	8	0	0	4
62	44	40	0	4	4	0	0	8
64	52	32	0	4	4	4	0	4
66	52	32	0	4	0	4	0	8
68	42.31	42.31	0	7.69	3.85	0	0	3.84
70	34.62	50	0	3.84	3.85	0	0	7.69
72	34.62	46.15	0	7.69	3.85	0	0	7.69
74	42.31	42.31	0	7.69	3.84	0	0	3.85
76	38.46	34.62	7.69	7.69	7.69	0	0	3.85
78	34.62	38.46	7.69	7.69	7.69	0	0	3.85
80	28	36	12	8	8	0	0	8
82	18.52	51.85	11.11	7.41	7.41	0	0	3.7
84	15.38	57.69	11.54	3.85	3.85	0	0	7.69
86	11.54	65.38	15.38	0	3.85	0	0	3.85
88	15.38	65.38	15.39	0	0	0	0	3.85
90	11.54	80.77	7.69	0	0	0	0	0
92	11.54	80.77	7.69	0	0	0	0	0
94	15.38	73.08	7.69	0	0	0	0	3.85

C2 cont.

96	18.52	66.67	3.7	0	0	0	0	11.11
98	28.57	57.14	0	0	3.57	0	0	10.72
100	46.43	35.71	0	0	7.14	0	0	10.72
102	57.14	28.57	0	3.57	3.57	0	0	7.15
104	39.29	25	3.57	7.14	7.14	3.57	0	14.29
106	32.14	28.57	3.57	7.14	10.72	3.57	0	14.29
108	32.14	28.57	7.14	7.14	3.58	3.57	3.57	14.29
110	39.29	25	10.71	0	3.57	0	3.57	17.86
112	37.04	18.52	3.7	3.7	11.11	0	7.41	18.52
114	38.46	23.08	11.54	3.85	7.69	0	0	15.38
116	50	26.92	15.38	3.85	0	0	0	3.85
118	58.33	16.67	8.33	4.17	0	0	0	12.5
120	65.22	17.39	8.69	4.35	0	0	0	4.35
122	69.57	17.39	8.69	0	0	0	0	4.35
124	70.83	20.83	0	0	4.17	0	0	4.17
<b>Totals (%)</b>	<b>34.16</b>	<b>49.93</b>	<b>4.17</b>	<b>3.18</b>	<b>3.18</b>	<b>0.36</b>	<b>0.28</b>	<b>4.74</b>

C3. Horizontal proportion facies distribution data, Tullig Sandstone, Carrowmore Point outcrop.

Distance along outcrop (m)	% Sm/Sh/SI	% Sp/St	% Smc	% Ccm	% Flh	% Fls/Flm
0	30.95	64.29	0	0	2.38	2.38
2	28.57	66.67	0	0	2.38	2.38
4	28.57	66.67	0	0	2.38	2.38
6	28.57	66.67	0	0	2.38	2.38
8	28.57	66.67	0	0	2.38	2.38
10	30.95	64.29	0	0	2.38	2.38
12	30.95	64.29	0	0	2.38	2.38
14	30.95	64.29	0	0	2.38	2.38
16	30.95	61.91	0	2.38	2.38	2.38
18	30.95	61.91	0	2.38	2.38	2.38
20	33.33	61.91	0	0	4.76	0
22	30.95	64.29	0	0	4.76	0
24	30.95	64.29	0	0	4.76	0
26	30.95	64.29	0	0	4.76	0
28	28.57	69.05	0	0	2.38	0
30	28.57	66.67	0	0	4.76	0
32	28.57	66.67	0	0	4.76	0
34	28.57	69.05	0	0	2.38	0
36	30.95	64.29	0	0	4.76	0
38	30.95	66.67	0	0	2.38	0
40	30.23	62.79	2.33	0	4.65	0
42	30.95	64.29	0	0	4.76	0
44	28.57	66.67	0	0	4.76	0
46	30.95	64.29	0	0	4.76	0
48	30.95	64.29	0	0	4.76	0
50	33.33	61.91	0	0	4.76	0

## C3 cont.

52	30.95	64.29	0	0	4.76	0
54	29.55	61.36	0	0	2.27	6.82
56	29.55	61.36	0	0	0	9.09
58	33.33	57.14	0	0	0	9.53
60	29.55	59.09	2.27	0	2.27	6.82
62	31.82	56.82	2.27	0	0	9.09
64	31.82	54.55	2.27	2.27	0	9.09
66	31.82	54.54	0	4.55	0	9.09
68	31.11	53.33	2.22	4.45	2.22	6.67
70	34.09	54.55	2.27	0	0	9.09
72	34.09	54.55	0	2.27	2.27	6.82
74	35.72	59.52	0	0	4.76	0
76	35.72	57.14	2.38	0	4.76	0
78	34.15	60.97	2.44	0	2.44	0
80	30.95	61.91	2.38	0	4.76	0
82	29.27	63.41	4.88	0	2.44	0
84	30.95	61.91	2.38	0	4.76	0
86	30.95	64.29	0	0	4.76	0
88	33.33	61.91	0	0	4.76	0
90	30.95	61.91	2.38	0	4.76	0
92	29.27	63.41	2.44	2.44	2.44	0
94	32.5	65	2.5	0	0	0
96	31.71	63.41	0	2.44	2.44	0
98	31.71	65.85	0	0	2.44	0
100	30.95	64.29	0	0	4.76	0
102	32.5	67.5	0	0	0	0
104	29.27	68.29	0	0	2.44	0
106	28.57	66.67	0	0	4.76	0
108	30.95	64.29	0	0	4.76	0
110	30.95	61.91	0	2.38	4.76	0
112	34.15	60.97	0	2.44	2.44	0
114	35.72	57.14	0	0	4.76	2.38
116	35.72	57.14	0	0	4.76	2.38
118	39.02	58.54	0	0	2.44	0
120	39.02	58.54	0	0	2.44	0
122	39.02	58.54	0	0	2.44	0
124	38.1	57.14	0	0	4.76	0
126	39.02	58.54	0	0	2.44	0
128	39.02	58.54	0	0	2.44	0
130	39.02	58.54	0	0	2.44	0
132	40	60	0	0	0	0
134	40	57.5	0	0	2.5	0
136	38.46	58.98	0	0	2.56	0
138	36.58	58.54	0	0	4.88	0
140	39.02	58.54	0	0	2.44	0
142	39.02	58.54	0	0	2.44	0
144	40	60	0	0	0	0
146	40	60	0	0	0	0
148	39.02	58.54	0	0	2.44	0
150	39.47	60.53	0	0	0	0
152	35.9	61.54	0	0	2.56	0
154	37.5	60	0	0	2.5	0

## C3 cont.

156	40	60	0	0	0	0
158	39.02	58.54	0	0	2.44	0
160	40	60	0	0	0	0
162	39.02	58.54	0	0	2.44	0
164	39.02	58.54	0	0	2.44	0
166	40	60	0	0	0	0
<b>Totals (%)</b>	<b>33.45</b>	<b>61.61</b>	<b>0.43</b>	<b>0.34</b>	<b>2.8</b>	<b>1.37</b>

## C4. Horizontal proportion facies distribution data, mouthbar sandbody, Tullig Point.

Distance along outcrop (m)	% Sm/Sh/ Sl	% Sp/St	% Flh	% Fls/Flm
0	76.47	11.76	11.77	0
2	70.59	17.65	11.76	0
4	70.59	17.65	5.88	5.88
6	70.59	11.77	5.88	11.76
8	77.78	16.67	5.55	0
10	73.69	15.79	5.26	5.26
12	73.68	10.53	5.26	10.53
14	73.68	15.79	10.53	0
16	68.42	21.05	0	10.53
18	73.69	21.05	0	5.26
20	73.69	21.05	0	5.26
22	80	20	0	0
24	70	25	5	0
26	68.42	15.79	5.26	10.53
28	73.68	26.32	0	0
30	68.42	15.79	5.26	10.53
32	63.16	21.05	10.53	5.26
34	68.42	26.32	5.26	0
36	73.69	21.05	5.26	0
38	73.69	15.79	5.26	5.26
40	73.69	21.05	5.26	0
42	73.69	21.05	5.26	0
44	70	15	5	10
46	61.91	28.57	9.52	0
48	66.67	28.57	4.76	0
50	80.95	9.52	0	9.53
52	65	20	5	10
54	65	15	10	10
56	65	25	10	0
58	70	25	5	0
60	70	30	0	0
62	75	20	5	0
64	73.69	21.05	5.26	0
66	82.35	11.77	0	5.88
68	66.67	20	13.33	0
70	76.92	15.39	0	7.69
72	87.5	12.5	0	0
<b>Totals (%)</b>	<b>71.72</b>	<b>19.39</b>	<b>5.1</b>	<b>3.79</b>

D1. Log Trusklieve 1, formatted for importing into RMS, for the large modelling grid.

1.0

Vertical

Trusk1LS 460000 5925120

1

FACIES DISC 0 Undefined 1 Sm\_Sh 2 Sp\_St\_Sl 3 Ccm 4 Sp2\_Sh2\_Sl2 5 Flh 6  
Fls\_Flm

460000	5925120	5	2
460000	5925120	6	2
460000	5925120	7	2
460000	5925120	8	2
460000	5925120	9	2
460000	5925120	10	2
460000	5925120	11	2
460000	5925120	12	2
460000	5925120	13	2
460000	5925120	14	2
460000	5925120	15	2
460000	5925120	16	2
460000	5925120	17	1
460000	5925120	18	1
460000	5925120	19	1
460000	5925120	20	1
460000	5925120	21	2
460000	5925120	22	2
460000	5925120	23	2
460000	5925120	24	2
460000	5925120	25	3

D2. Log Trusklieve 2, formatted for importing into RMS, for the large modelling grid.

1.0

Vertical

Trusk2LS 460000 5925080

1

FACIES DISC 0 Undefined 1 Sm\_Sh 2 Sp\_St\_Sl 3 Ccm 4 Sp2\_Sh2\_Sl2 5 Flh 6  
Fls\_Flm

460000	5925080	5	2
460000	5925080	6	2
460000	5925080	7	2
460000	5925080	8	2
460000	5925080	9	2
460000	5925080	10	2
460000	5925080	11	2
460000	5925080	12	2
460000	5925080	13	2
460000	5925080	14	2
460000	5925080	15	2
460000	5925080	16	2
460000	5925080	17	1
460000	5925080	18	1
460000	5925080	19	2
460000	5925080	20	2
460000	5925080	21	2
460000	5925080	22	2
460000	5925080	23	3
460000	5925080	24	6
460000	5925080	25	3

D3. Log Trusklieve 3, formatted for importing into RMS, for the large modelling grid.

1.0

Vertical

Trusk3LS 460010 5925040

1

FACIES DISC 0 Undefined 1 Sm\_Sh 2 Sp\_St\_Sl 3 Ccm 4 Sp2\_Sh2\_Sl2 5 Flh 6  
Fls\_Flm

460010	5925040	6	2
460010	5925040	7	2
460010	5925040	8	2
460010	5925040	9	2
460010	5925040	10	2
460010	5925040	11	2
460010	5925040	12	2
460010	5925040	13	2
460010	5925040	14	1
460010	5925040	15	2
460010	5925040	16	1
460010	5925040	17	1
460010	5925040	18	6
460010	5925040	19	2
460010	5925040	20	2
460010	5925040	21	2
460010	5925040	22	1
460010	5925040	23	6
460010	5925040	24	1
460010	5925040	25	1

D4. Log Trusklieve 4, formatted for importing into RMS, for the large modelling grid.

1.0

Vertical

Trusk4LS 460010 5925000

1

FACIES DISC 0 Undefined 1 Sm\_Sh 2 Sp\_St\_Sl 3 Ccm 4 Sp2\_Sh2\_Sl2 5 Flh 6  
Fls\_Flm

460010	5925000	5	2
460010	5925000	6	2
460010	5925000	7	2
460010	5925000	8	2
460010	5925000	9	2
460010	5925000	10	2
460010	5925000	11	2
460010	5925000	12	2
460010	5925000	13	2
460010	5925000	14	2
460010	5925000	15	2
460010	5925000	16	1
460010	5925000	17	1
460010	5925000	18	6
460010	5925000	19	1
460010	5925000	20	1
460010	5925000	21	1
460010	5925000	22	6
460010	5925000	23	6
460010	5925000	24	1
460010	5925000	25	1

D5. Pulleen log, formatted for importing into RMS, for the large modelling grid.

1.0

Vertical

Pulleen 459240 5942864

1

FACIES	DISC	0	Undefined	1	Sm_Sh	2	Sp_St_Sl	3	Ccm	4	Sp2_Sh2_Sl2	5	Flh	6
Fls_Flm														
459240					5942864								2	2
459240					5942864								3	2
459240					5942864								4	2
459240					5942864								5	2
459240					5942864								6	2
459240					5942864								7	2
459240					5942864								8	2
459240					5942864								9	2
459240					5942864								10	2
459240					5942864								11	2
459240					5942864								12	1
459240					5942864								13	1
459240					5942864								14	1
459240					5942864								15	1
459240					5942864								16	1
459240					5942864								17	1
459240					5942864								18	1
459240					5942864								19	1
459240					5942864								20	1
459240					5942864								21	1
459240					5942864								22	1
459240					5942864								23	1
459240					5942864								24	1
459240					5942864								25	3

D6. Killard N log, formatted for importing into RMS, for the large modelling grid.

1.0

Vertical

KillardN 460440 5944943

1

FACIES	DISC	0	Undefined	1	Sm_Sh	2	Sp_St_Sl	3	Ccm	4	Sp2_Sh2_Sl2	5	Flh	6
Fls_Flm														
460440					5944943								4	1
460440					5944943								5	2
460440					5944943								6	1
460440					5944943								7	1
460440					5944943								8	1
460440					5944943								9	1
460440					5944943								10	1
460440					5944943								11	2
460440					5944943								12	2
460440					5944943								13	2
460440					5944943								14	2
460440					5944943								15	2
460440					5944943								16	2
460440					5944943								17	2
460440					5944943								18	2
460440					5944943								19	2
460440					5944943								20	1
460440					5944943								21	1
460440					5944943								22	5

460440	5944943	23	2
460440	5944943	24	1
460440	5944943	25	3

D7. Killard S log, formatted for importing into RMS, for the large modelling grid.

1.0

Vertical

KillardS 461200 5945544

1

FACIES DISC 0 Undefined 1 Sm\_Sh 2 Sp\_St\_Sl 3 Ccm 4 Sp2\_Sh2\_Sl2 5 Flh 6  
Fls\_Flm

461200	5945544	7	1
461200	5945544	8	1
461200	5945544	9	1
461200	5945544	10	1
461200	5945544	11	1
461200	5945544	12	2
461200	5945544	13	2
461200	5945544	14	2
461200	5945544	15	2
461200	5945544	16	2
461200	5945544	17	1
461200	5945544	18	5
461200	5945544	19	1
461200	5945544	20	1
461200	5945544	21	1
461200	5945544	22	1
461200	5945544	23	2
461200	5945544	24	1
461200	5945544	25	1

D8. Carrowmore SE log, formatted for importing into RMS, for the large modelling grid.

1.0

Vertical

CarSE 462540 5949552

1

FACIES DISC 0 Undefined 1 Sm\_Sh 2 Sp\_St\_Sl 3 Ccm 4 Sp2\_Sh2\_Sl2 5 Flh 6  
Fls\_Flm

462540	5949552	8	4
462540	5949552	9	5
462540	5949552	10	2
462540	5949552	11	5
462540	5949552	12	2
462540	5949552	13	2
462540	5949552	14	2
462540	5949552	15	2
462540	5949552	16	1
462540	5949552	17	1
462540	5949552	18	1
462540	5949552	19	1
462540	5949552	20	1
462540	5949552	21	1
462540	5949552	22	1
462540	5949552	23	1
462540	5949552	24	1
462540	5949552	25	2

D9. Carrowmore NW log, formatted for importing into RMS, for the large modelling grid.

1.0

Vertical

CarNW 462240 5949853

1

FACIES DISC 0 Undefined 1 Sm\_Sh 2 Sp\_St\_Sl 3 Ccm 4 Sp2\_Sh2\_Sl2 5 Flh 6  
Fls\_Flm

462240	5949853	4	2
462240	5949853	5	2
462240	5949853	6	5
462240	5949853	7	6
462240	5949853	8	2
462240	5949853	9	2
462240	5949853	10	2
462240	5949853	11	2
462240	5949853	12	2
462240	5949853	13	2
462240	5949853	14	2
462240	5949853	15	2
462240	5949853	16	2
462240	5949853	17	2
462240	5949853	18	1
462240	5949853	19	1
462240	5949853	20	1
462240	5949853	21	1
462240	5949853	22	1
462240	5949853	23	1
462240	5949853	24	1
462240	5949853	25	3

D10. Log Truskieve 1, formatted for importing into RMS, for the small modelling grid.

1.0

Vertical

Trusk1SS 460000 5925120

1

FACIES DISC 0 Undefined 1 Sm\_Sh 2 Sp\_St\_Sl 3 Ccm 4 Sp2\_Sh2\_Sl2 5 Flh 6  
Fls\_Flm

460000	5925120	13	2
460000	5925120	13.1	2
460000	5925120	13.2	2
460000	5925120	13.3	2
460000	5925120	13.4	2
460000	5925120	13.5	2
460000	5925120	13.6	2
460000	5925120	13.7	2
460000	5925120	13.8	2
460000	5925120	13.9	2
460000	5925120	14	2
460000	5925120	14.1	2
460000	5925120	14.2	2
460000	5925120	14.3	2
460000	5925120	14.4	2
460000	5925120	14.5	2
460000	5925120	14.6	2
460000	5925120	14.7	2
460000	5925120	14.8	2
460000	5925120	14.9	2
460000	5925120	15	2
460000	5925120	15.1	2

460000	5925120	15.2	2
460000	5925120	15.3	2
460000	5925120	15.4	2
460000	5925120	15.5	2
460000	5925120	15.6	2
460000	5925120	15.7	2
460000	5925120	15.8	2
460000	5925120	15.9	2
460000	5925120	16	2
460000	5925120	16.1	2
460000	5925120	16.2	2
460000	5925120	16.3	2
460000	5925120	16.4	2
460000	5925120	16.5	2
460000	5925120	16.6	2
460000	5925120	16.7	2
460000	5925120	16.8	2
460000	5925120	16.9	2
460000	5925120	17	1
460000	5925120	17.1	1
460000	5925120	17.2	1
460000	5925120	17.3	1
460000	5925120	17.4	1
460000	5925120	17.5	1
460000	5925120	17.6	1
460000	5925120	17.7	1
460000	5925120	17.8	1
460000	5925120	17.9	1
460000	5925120	18	1
460000	5925120	18.1	1
460000	5925120	18.2	1
460000	5925120	18.3	1
460000	5925120	18.4	1
460000	5925120	18.5	1
460000	5925120	18.6	1
460000	5925120	18.7	1
460000	5925120	18.8	1
460000	5925120	18.9	1
460000	5925120	19	1
460000	5925120	19.1	1
460000	5925120	19.2	2
460000	5925120	19.3	2
460000	5925120	19.4	2
460000	5925120	19.5	2
460000	5925120	19.6	6
460000	5925120	19.7	1
460000	5925120	19.8	3
460000	5925120	19.9	1
460000	5925120	20	1
460000	5925120	20.1	1
460000	5925120	20.2	1
460000	5925120	20.3	1
460000	5925120	20.4	2
460000	5925120	20.5	2
460000	5925120	20.6	2
460000	5925120	20.7	2
460000	5925120	20.8	2
460000	5925120	20.9	2
460000	5925120	21	2
460000	5925120	21.1	2
460000	5925120	21.2	2

460000	5925120	21.3	2
460000	5925120	21.4	2
460000	5925120	21.5	2
460000	5925120	21.6	2
460000	5925120	21.7	2
460000	5925120	21.8	2
460000	5925120	21.9	2
460000	5925120	22	2
460000	5925120	22.1	2
460000	5925120	22.2	2
460000	5925120	22.3	2
460000	5925120	22.4	2
460000	5925120	22.5	2
460000	5925120	22.6	2
460000	5925120	22.7	2
460000	5925120	22.8	2
460000	5925120	22.9	1
460000	5925120	23	1
460000	5925120	23.1	1
460000	5925120	23.2	1
460000	5925120	23.3	1
460000	5925120	23.4	1
460000	5925120	23.5	1
460000	5925120	23.6	1
460000	5925120	23.7	1
460000	5925120	23.8	1
460000	5925120	23.9	3
460000	5925120	24	2
460000	5925120	24.1	2
460000	5925120	24.2	2
460000	5925120	24.3	1
460000	5925120	24.4	1
460000	5925120	24.5	3
460000	5925120	24.6	3
460000	5925120	24.7	3
460000	5925120	24.8	3
460000	5925120	24.9	3
460000	5925120	25	3

D11. Log Trusklieve 2, formatted for importing into RMS, for the small modelling grid.

1.0

Vertical

Trusk2SS 460000 5925080

1

FACIES DISC 0 Undefined 1 Sm\_Sh 2 Sp\_St\_Sl 3 Ccm 4 Sp2\_Sh2\_Sl2 5 Flh 6  
Fls\_Flm

460000	5925080	13.1	2
460000	5925080	13.2	2
460000	5925080	13.3	2
460000	5925080	13.4	2
460000	5925080	13.5	2
460000	5925080	13.6	2
460000	5925080	13.7	2
460000	5925080	13.8	2
460000	5925080	13.9	2
460000	5925080	14	2
460000	5925080	14.1	2
460000	5925080	14.2	2
460000	5925080	14.3	2
460000	5925080	14.4	2

460000	5925080	14.5	2
460000	5925080	14.6	2
460000	5925080	14.7	2
460000	5925080	14.8	2
460000	5925080	14.9	2
460000	5925080	15	2
460000	5925080	15.1	2
460000	5925080	15.2	2
460000	5925080	15.3	2
460000	5925080	15.4	2
460000	5925080	15.5	2
460000	5925080	15.6	2
460000	5925080	15.7	2
460000	5925080	15.8	2
460000	5925080	15.9	2
460000	5925080	16	2
460000	5925080	16.1	1
460000	5925080	16.2	1
460000	5925080	16.3	1
460000	5925080	16.4	1
460000	5925080	16.5	1
460000	5925080	16.6	1
460000	5925080	16.7	1
460000	5925080	16.8	1
460000	5925080	16.9	1
460000	5925080	17	1
460000	5925080	17.1	1
460000	5925080	17.2	1
460000	5925080	17.3	1
460000	5925080	17.4	1
460000	5925080	17.5	1
460000	5925080	17.6	1
460000	5925080	17.7	1
460000	5925080	17.8	1
460000	5925080	17.9	1
460000	5925080	18	1
460000	5925080	18.1	2
460000	5925080	18.2	2
460000	5925080	18.3	2
460000	5925080	18.4	2
460000	5925080	18.5	2
460000	5925080	18.6	2
460000	5925080	18.7	2
460000	5925080	18.8	2
460000	5925080	18.9	2
460000	5925080	19	2
460000	5925080	19.1	2
460000	5925080	19.2	2
460000	5925080	19.3	2
460000	5925080	19.4	2
460000	5925080	19.5	2
460000	5925080	19.6	2
460000	5925080	19.7	2
460000	5925080	19.8	2
460000	5925080	19.9	2
460000	5925080	20	2
460000	5925080	20.1	2
460000	5925080	20.2	2
460000	5925080	20.3	2
460000	5925080	20.4	2
460000	5925080	20.5	2

460000	5925080	20.6	2
460000	5925080	20.7	2
460000	5925080	20.8	2
460000	5925080	20.9	2
460000	5925080	21	2
460000	5925080	21.1	2
460000	5925080	21.2	2
460000	5925080	21.3	2
460000	5925080	21.4	2
460000	5925080	21.5	2
460000	5925080	21.6	2
460000	5925080	21.7	2
460000	5925080	21.8	2
460000	5925080	21.9	2
460000	5925080	22	2
460000	5925080	22.1	2
460000	5925080	22.2	3
460000	5925080	22.3	3
460000	5925080	22.4	3
460000	5925080	22.5	3
460000	5925080	22.6	3
460000	5925080	22.7	6
460000	5925080	22.8	6
460000	5925080	22.9	6
460000	5925080	23	6
460000	5925080	23.1	6
460000	5925080	23.2	6
460000	5925080	23.3	6
460000	5925080	23.4	6
460000	5925080	23.5	6
460000	5925080	23.6	1
460000	5925080	23.7	1
460000	5925080	23.8	1
460000	5925080	23.9	1
460000	5925080	24	1
460000	5925080	24.1	1
460000	5925080	24.2	1
460000	5925080	24.3	1
460000	5925080	24.4	1
460000	5925080	24.5	1
460000	5925080	24.6	3
460000	5925080	24.7	3
460000	5925080	24.8	3
460000	5925080	24.9	3
460000	5925080	25	3

D12. Log Trusklieve 3, formatted for importing into RMS, for the small modelling grid.

```

1.0
Vertical
Trusk3SS 460010 5925040
1
FACIES DISC 0 Undefined 1 Sm_Sh 2 Sp_St_Sl 3 Ccm 4 Sp2_Sh2_Sl2 5 Flh 6
Fls_Flm
460010      5925040      12.8  2
460010      5925040      12.9  2
460010      5925040      13     1
460010      5925040      13.1  1
460010      5925040      13.2  1
460010      5925040      13.3  1
460010      5925040      13.4  1

```

460010	5925040	13.5	1
460010	5925040	13.6	1
460010	5925040	13.7	1
460010	5925040	13.8	1
460010	5925040	13.9	1
460010	5925040	14	1
460010	5925040	14.1	2
460010	5925040	14.2	2
460010	5925040	14.3	3
460010	5925040	14.4	2
460010	5925040	14.5	2
460010	5925040	14.6	1
460010	5925040	14.7	1
460010	5925040	14.8	6
460010	5925040	14.9	6
460010	5925040	15	1
460010	5925040	15.1	1
460010	5925040	15.2	1
460010	5925040	15.3	1
460010	5925040	15.4	1
460010	5925040	15.5	1
460010	5925040	15.6	3
460010	5925040	15.7	3
460010	5925040	15.8	1
460010	5925040	15.9	1
460010	5925040	16	1
460010	5925040	16.1	1
460010	5925040	16.2	1
460010	5925040	16.3	1
460010	5925040	16.4	1
460010	5925040	16.5	1
460010	5925040	16.6	1
460010	5925040	16.7	1
460010	5925040	16.8	1
460010	5925040	16.9	1
460010	5925040	17	6
460010	5925040	17.1	6
460010	5925040	17.2	6
460010	5925040	17.3	6
460010	5925040	17.4	6
460010	5925040	17.5	6
460010	5925040	17.6	6
460010	5925040	17.7	6
460010	5925040	17.8	2
460010	5925040	17.9	2
460010	5925040	18	2
460010	5925040	18.1	2
460010	5925040	18.2	2
460010	5925040	18.3	2
460010	5925040	18.4	2
460010	5925040	18.5	2
460010	5925040	18.6	1
460010	5925040	18.7	1
460010	5925040	18.8	1
460010	5925040	18.9	1
460010	5925040	19	1
460010	5925040	19.1	1
460010	5925040	19.2	1
460010	5925040	19.3	2
460010	5925040	19.4	2
460010	5925040	19.5	2

460010	5925040	19.6	2
460010	5925040	19.7	2
460010	5925040	19.8	2
460010	5925040	19.9	2
460010	5925040	20	2
460010	5925040	20.1	2
460010	5925040	20.2	2
460010	5925040	20.3	2
460010	5925040	20.4	2
460010	5925040	20.5	2
460010	5925040	20.6	2
460010	5925040	20.7	2
460010	5925040	20.8	2
460010	5925040	20.9	2
460010	5925040	21	2
460010	5925040	21.1	2
460010	5925040	21.2	3
460010	5925040	21.3	3
460010	5925040	21.4	3
460010	5925040	21.5	1
460010	5925040	21.6	1
460010	5925040	21.7	1
460010	5925040	21.8	1
460010	5925040	21.9	1
460010	5925040	22	1
460010	5925040	22.1	1
460010	5925040	22.2	1
460010	5925040	22.3	1
460010	5925040	22.4	6
460010	5925040	22.5	6
460010	5925040	22.6	6
460010	5925040	22.7	6
460010	5925040	22.8	2
460010	5925040	22.9	2
460010	5925040	23	2
460010	5925040	23.1	2
460010	5925040	23.2	2
460010	5925040	23.3	2
460010	5925040	23.4	2
460010	5925040	23.5	2
460010	5925040	23.6	2
460010	5925040	23.7	2
460010	5925040	23.8	2
460010	5925040	23.9	2
460010	5925040	24	2
460010	5925040	24.1	2
460010	5925040	24.2	2
460010	5925040	24.3	2
460010	5925040	24.4	2
460010	5925040	24.5	2
460010	5925040	24.6	2
460010	5925040	24.7	2
460010	5925040	24.8	2
460010	5925040	24.9	2
460010	5925040	25	2

D13. Log Trusklieve 4, formatted for importing into RMS, for the small modelling grid.

1.0

Vertical

Trusk4SS 460010 5925000

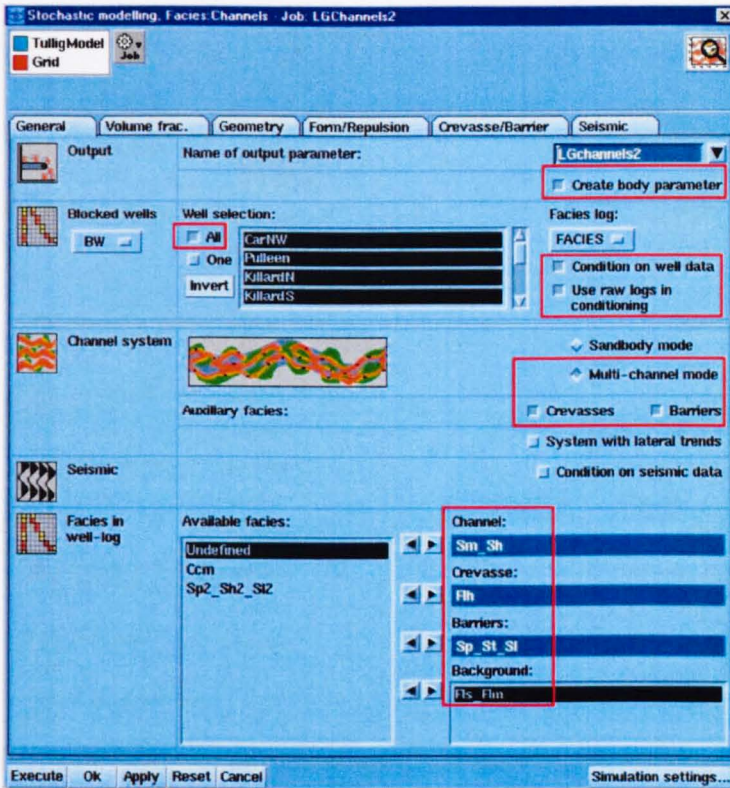
1

FACIES DISC 0 Undefined 1 Sm\_Sh 2 Sp\_St\_Sl 3 Ccm 4 Sp2\_Sh2\_Sl2 5 Flh 6  
Fls\_Flm

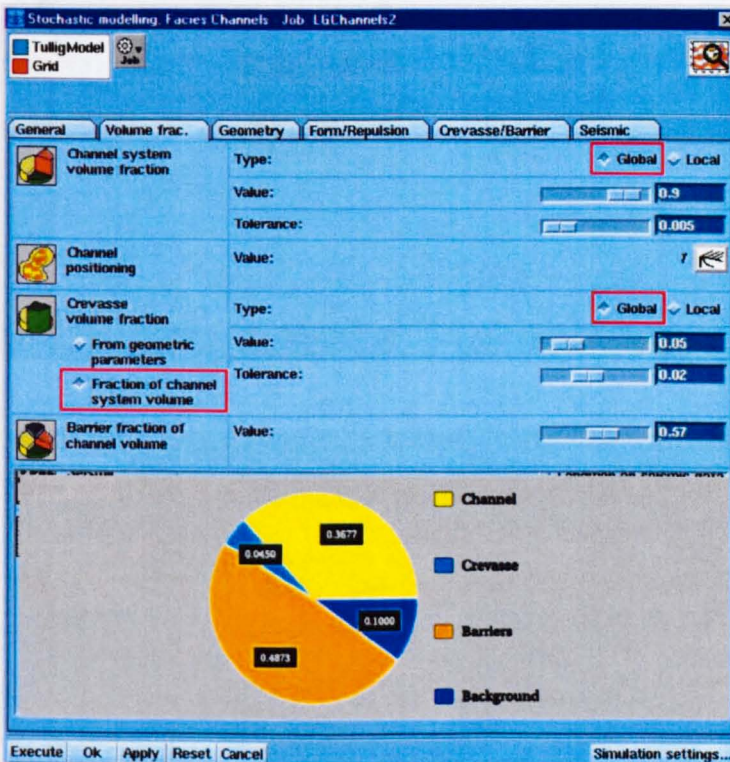
460010	5925000	13.1	2
460010	5925000	13.2	2
460010	5925000	13.3	2
460010	5925000	13.4	2
460010	5925000	13.5	2
460010	5925000	13.6	2
460010	5925000	13.7	2
460010	5925000	13.8	2
460010	5925000	13.9	2
460010	5925000	14	2
460010	5925000	14.1	2
460010	5925000	14.2	2
460010	5925000	14.3	2
460010	5925000	14.4	2
460010	5925000	14.5	2
460010	5925000	14.6	2
460010	5925000	14.7	2
460010	5925000	14.8	2
460010	5925000	14.9	2
460010	5925000	15	2
460010	5925000	15.1	2
460010	5925000	15.2	2
460010	5925000	15.3	2
460010	5925000	15.4	2
460010	5925000	15.5	2
460010	5925000	15.6	2
460010	5925000	15.7	2
460010	5925000	15.8	2
460010	5925000	15.9	2
460010	5925000	16	2
460010	5925000	16.1	1
460010	5925000	16.2	1
460010	5925000	16.3	1
460010	5925000	16.4	1
460010	5925000	16.5	1
460010	5925000	16.6	1
460010	5925000	16.7	1
460010	5925000	16.8	1
460010	5925000	16.9	1
460010	5925000	17	1
460010	5925000	17.1	1
460010	5925000	17.2	1
460010	5925000	17.3	1
460010	5925000	17.4	1
460010	5925000	17.5	1
460010	5925000	17.6	1
460010	5925000	17.7	1
460010	5925000	17.8	1
460010	5925000	17.9	1
460010	5925000	18	1
460010	5925000	18.1	1
460010	5925000	18.2	1
460010	5925000	18.3	1

460010	5925000	18.4	3
460010	5925000	18.5	6
460010	5925000	18.6	6
460010	5925000	18.7	6
460010	5925000	18.8	6
460010	5925000	18.9	3
460010	5925000	19	1
460010	5925000	19.1	1
460010	5925000	19.2	1
460010	5925000	19.3	1
460010	5925000	19.4	1
460010	5925000	19.5	3
460010	5925000	19.6	3
460010	5925000	19.7	1
460010	5925000	19.8	1
460010	5925000	19.9	1
460010	5925000	20	1
460010	5925000	20.1	1
460010	5925000	20.2	6
460010	5925000	20.3	1
460010	5925000	20.4	1
460010	5925000	20.5	1
460010	5925000	20.6	6
460010	5925000	20.7	2
460010	5925000	20.8	2
460010	5925000	20.9	2
460010	5925000	21	2
460010	5925000	21.1	2
460010	5925000	21.2	3
460010	5925000	21.3	1
460010	5925000	21.4	1
460010	5925000	21.5	1
460010	5925000	21.6	1
460010	5925000	21.7	1
460010	5925000	21.8	6
460010	5925000	21.9	6
460010	5925000	22	6
460010	5925000	22.1	6
460010	5925000	22.2	6
460010	5925000	22.3	6
460010	5925000	22.4	6
460010	5925000	22.5	6
460010	5925000	22.6	6
460010	5925000	22.7	6
460010	5925000	22.8	1
460010	5925000	22.9	1
460010	5925000	23	1
460010	5925000	23.1	1
460010	5925000	23.2	1
460010	5925000	23.3	1
460010	5925000	23.4	1
460010	5925000	23.5	1
460010	5925000	23.6	1
460010	5925000	23.7	1
460010	5925000	23.8	1
460010	5925000	23.9	1
460010	5925000	24	1
460010	5925000	24.1	1
460010	5925000	24.2	1
460010	5925000	24.3	3
460010	5925000	24.4	1

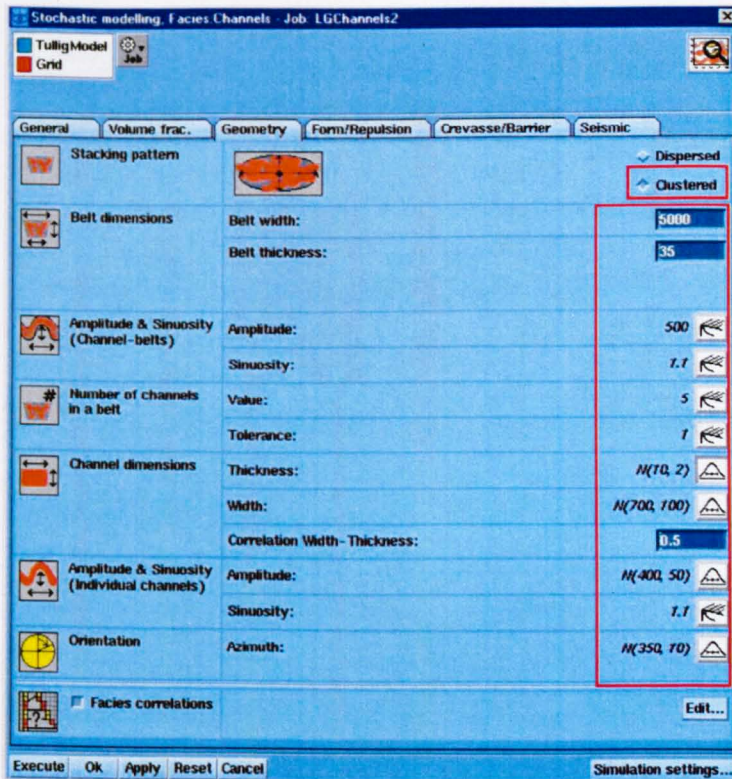
460010	5925000	24.5	1
460010	5925000	24.6	1
460010	5925000	24.7	1
460010	5925000	24.8	1
460010	5925000	24.9	1
460010	5925000	25	1



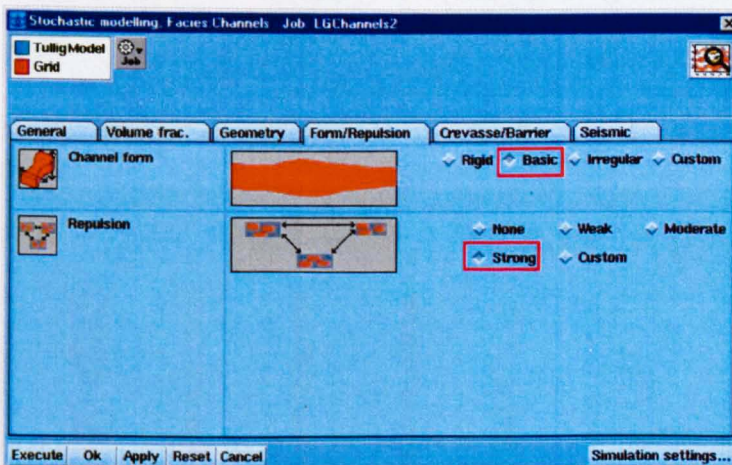
D14. "General" preferences tab for Facies Channels modelling job, large grid. Chosen options are shown by red boxes.



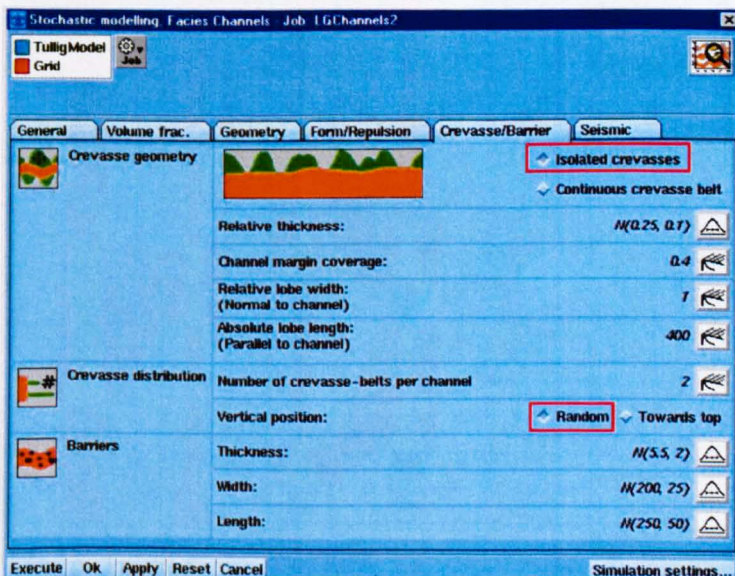
D15. "Volume fraction" tab for Facies Channels modelling job, large grid. Chosen options are shown by red boxes.



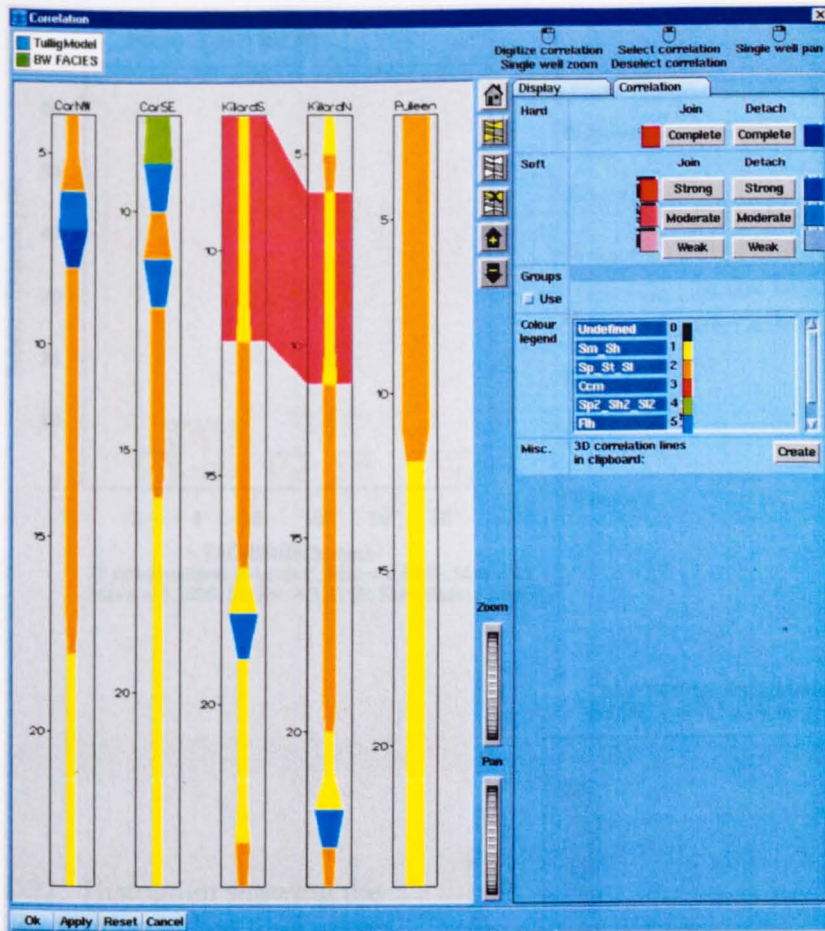
D16. "Geometry" tab for Facies Channels modelling job, large grid. Chosen options are shown by red boxes.



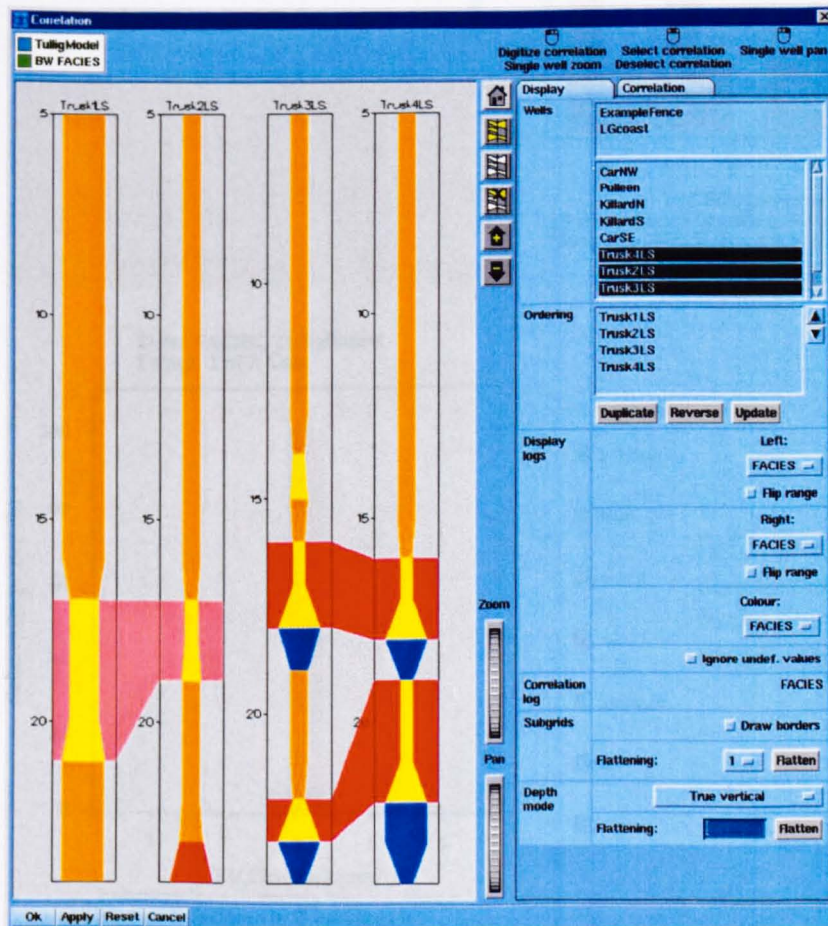
D17. "Form/repulsion" tab for Facies Channels modelling job, large grid. Chosen options are shown by red boxes.



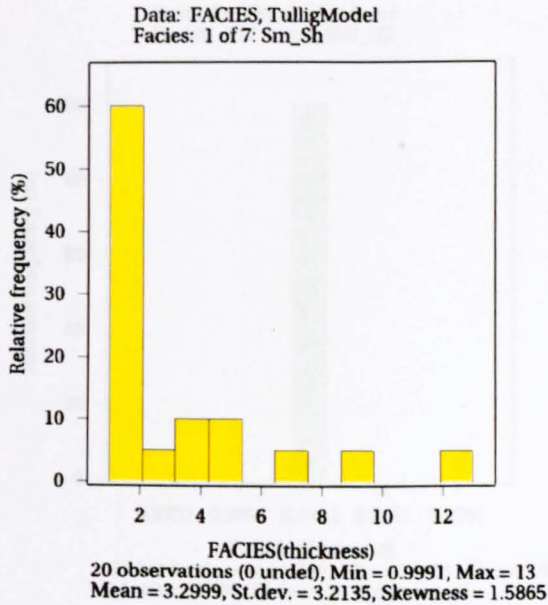
D18. "Crevasse/barrier" tab for Facies Channels modelling job, large grid. Chosen options are shown by red boxes.



D19. "Correlation" tab for Facies Channels modelling job, large grid. Those beds and storeys seen to correlate in the field are linked here. The link in this case is a hard link, completely joined, between beds of Sm/Sh facies in the two logs from Killard.

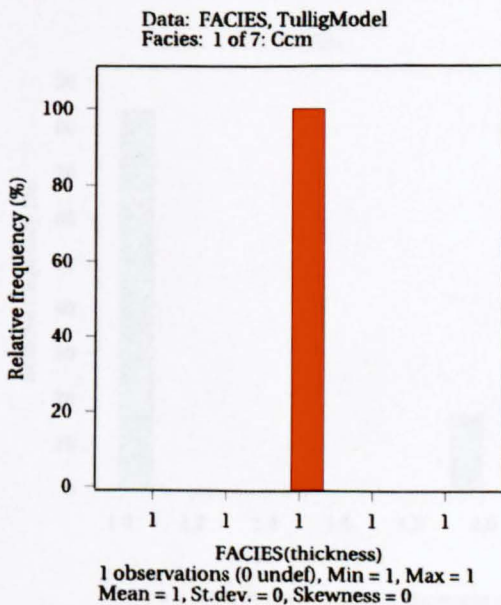
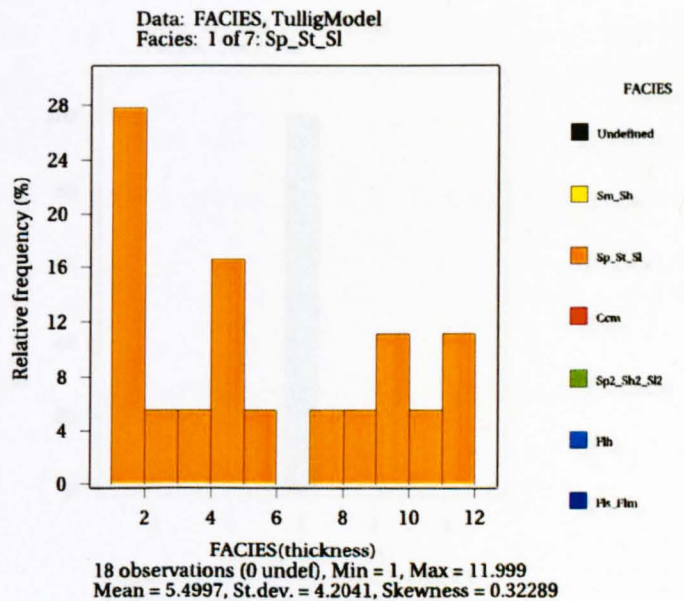


D20. "Correlation Display" tab for Facies Channels modelling job, large grid. Those beds and storeys seen to correlate in the field are linked here. Two of the links in this case are hard links, between wells 3 and 4 at Trusk-lieve, while a third link between wells 1 and 2 is a soft link, moderately joined.

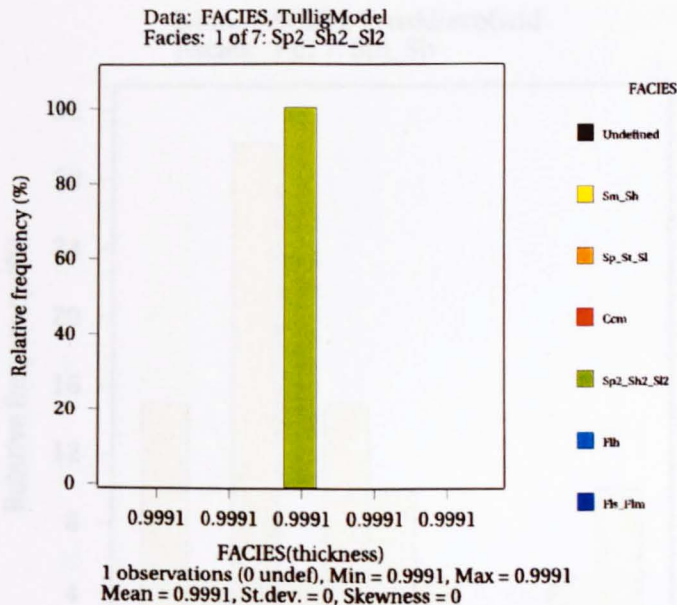


D21. Histogram showing the distribution of bed thicknesses in the blocked wells of the large modelling grid, for facies Sm/Sh.

D22. Histogram showing the distribution of bed thicknesses in the blocked wells of the large modelling grid, for facies Sp/St/Sl.

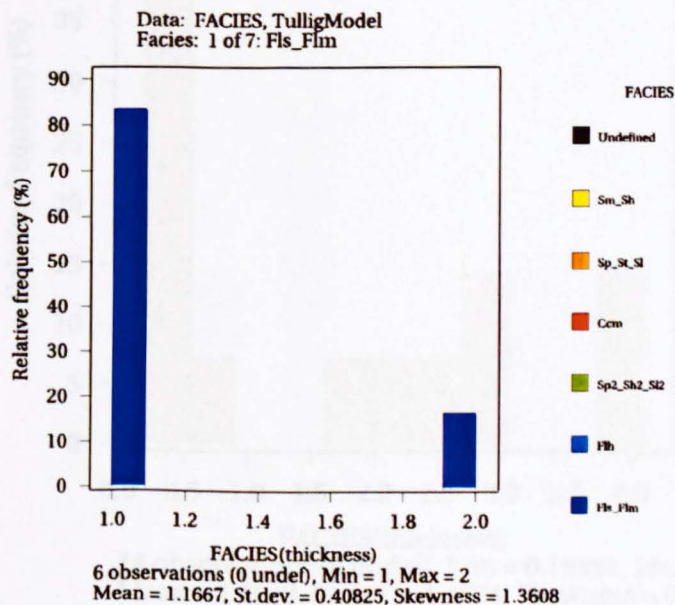
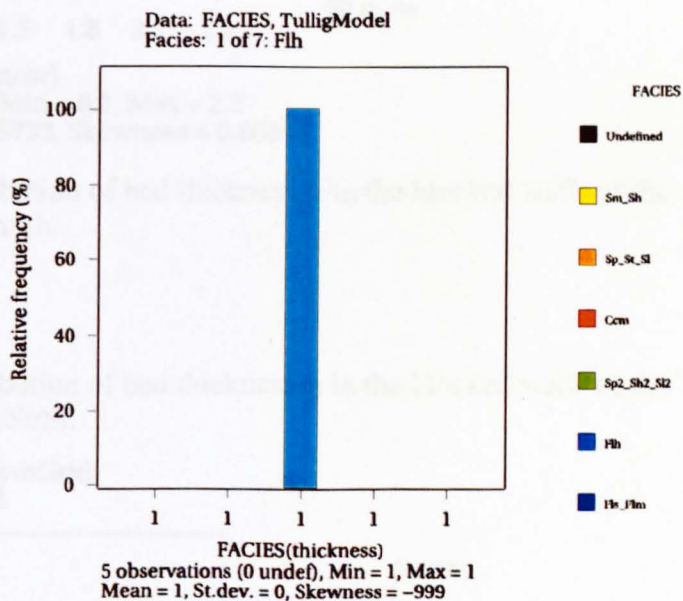


D23. Histogram showing the distribution of bed thicknesses in the blocked wells of the large modelling grid, for facies Sm/Sh.



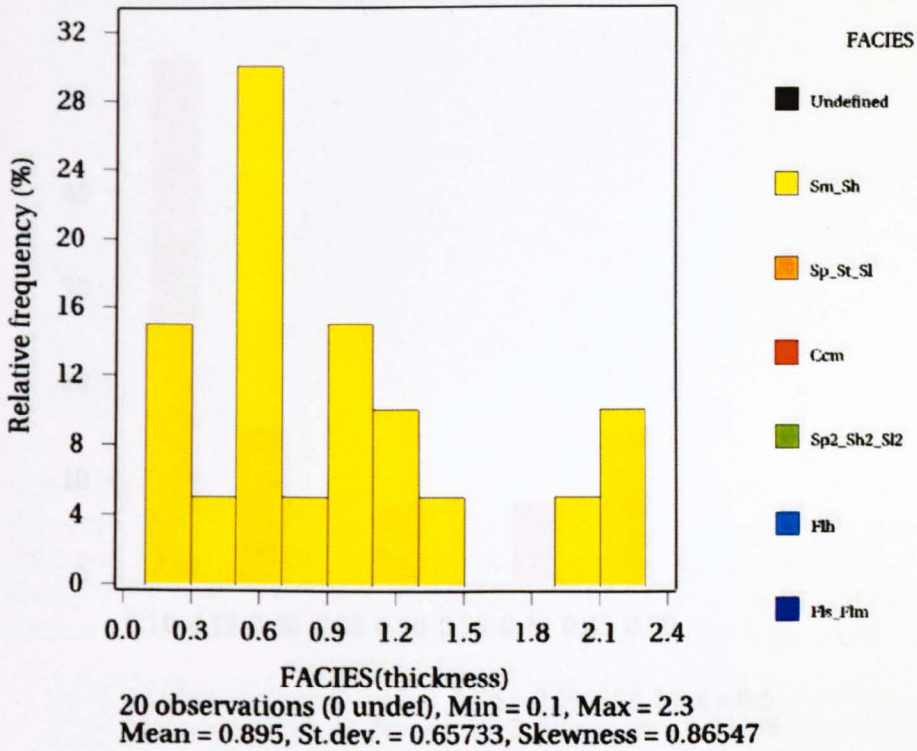
D24. Histogram showing the distribution of bed thicknesses in the blocked wells of the large modelling grid, facies Sh<sub>2</sub>/Sp<sub>2</sub>/Sl<sub>2</sub>.

D25. Histogram showing the distribution of bed thicknesses in the blocked wells of the large modelling grid, for facies Flh.



D26. Histogram showing the distribution of bed thicknesses in the blocked wells of the large modelling grid, for facies Fls/Flm.

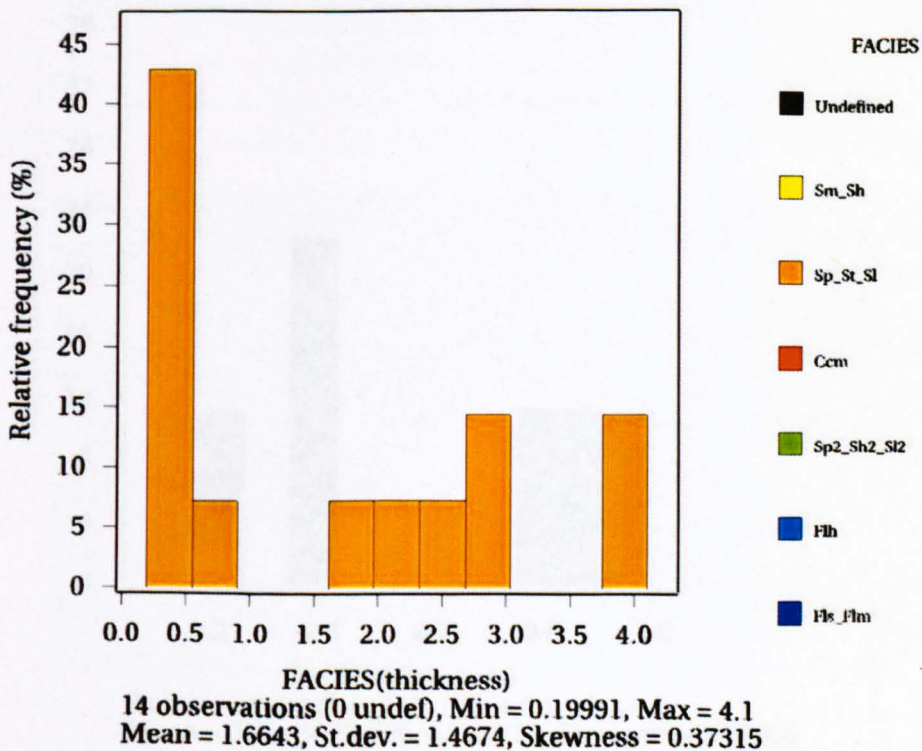
Data: FACIES, TrusklieveGrid  
 Facies: 1 of 7: Sm\_Sh

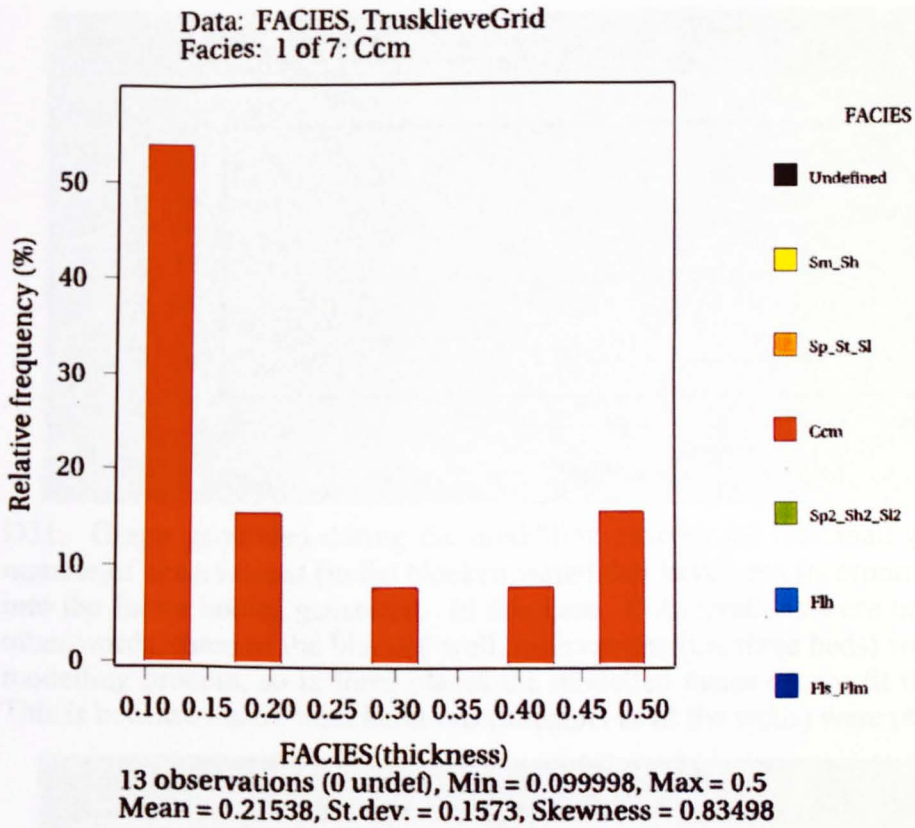


D27. Histogram showing the distribution of bed thicknesses in the blocked wells of the small modelling grid, for facies Sm/Sh.

D28. Histogram showing the distribution of bed thicknesses in the blocked wells of the small modelling grid, for facies Sp/St/Sl.

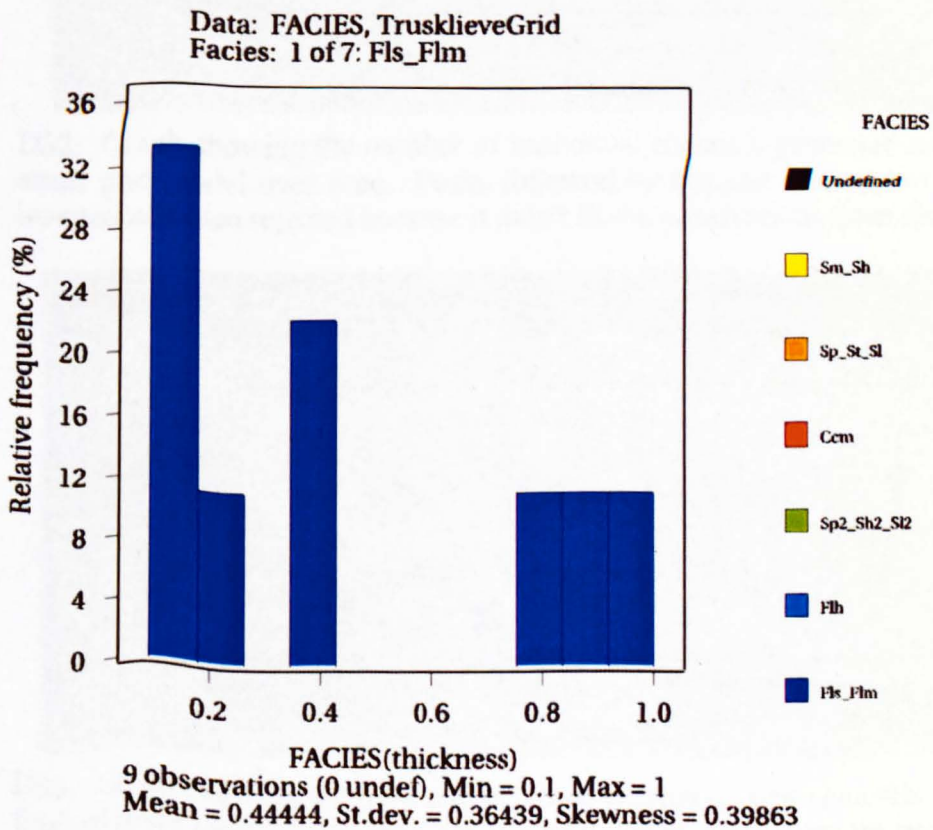
Data: FACIES, TrusklieveGrid  
 Facies: 1 of 7: Sp\_St\_Sl

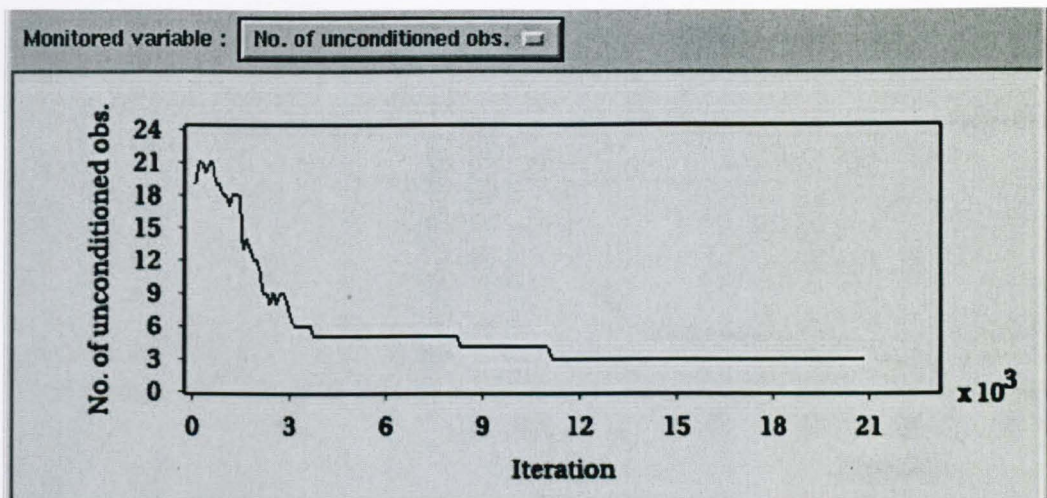




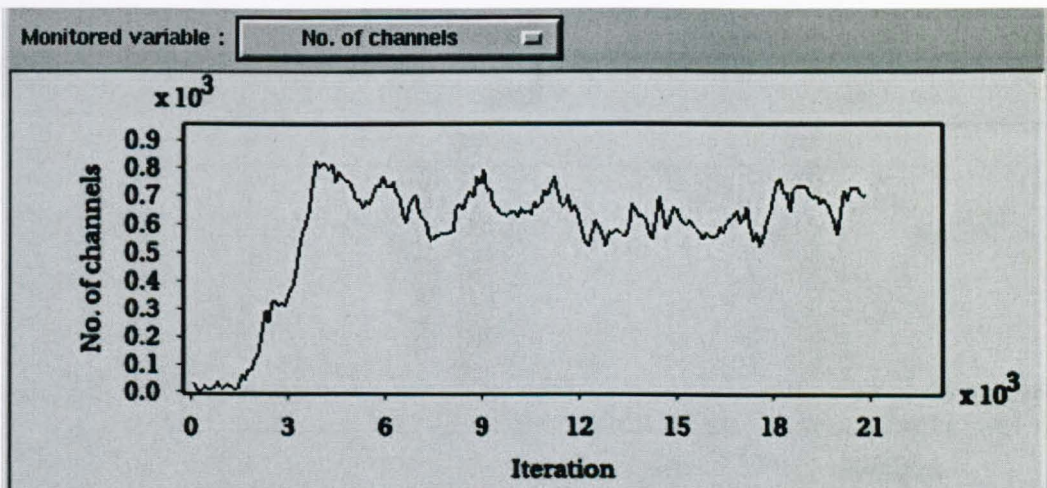
D29. Histogram showing the distribution of bed thicknesses in the blocked wells of the small modelling grid, for facies Ccm.

D30. Histogram showing the distribution of bed thicknesses in the blocked wells of the small modelling grid, for facies Fls/Flm.

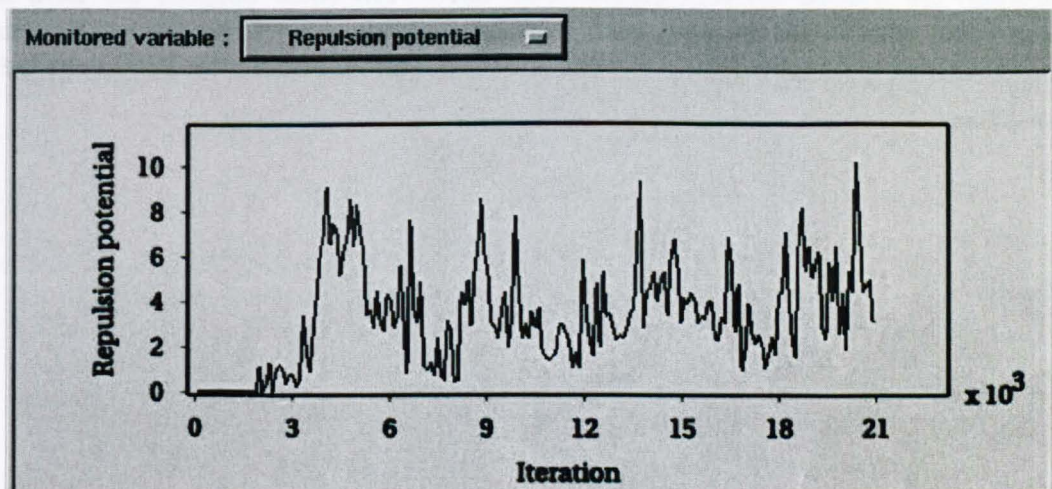




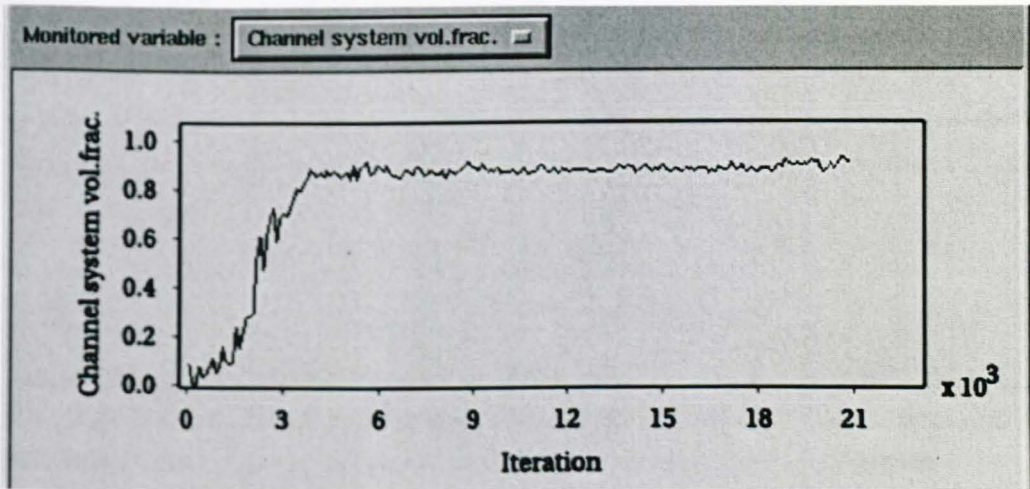
D31. Graph generated during the modelling process for the small grid, showing the number of observations (in the blocked wells) that have been incorporated (conditioned) into the facies bodies generated. In this case, 3 observations were not conditioned; in other words, three of the blocked well observations (i.e. three beds) were ignored in the modelling process, so in three places the modelled facies do not fit the blocked wells. This is because insufficient iterations (attempts to fit the wells) were performed.



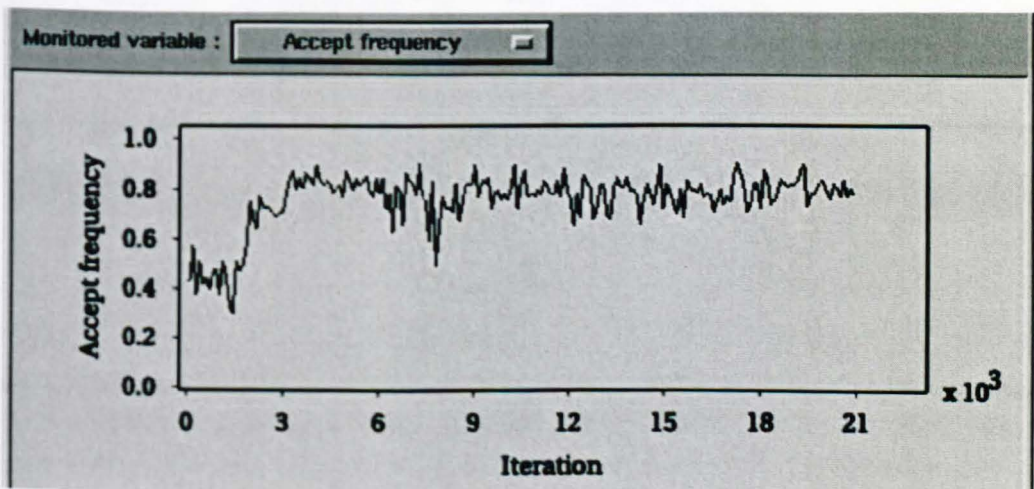
D32. Graph showing the number of individual channels generated and fitted into the small grid model over time. Peaks followed by troughs show where a channel was inserted and then rejected because it didn't fit the observations from the blocked wells.



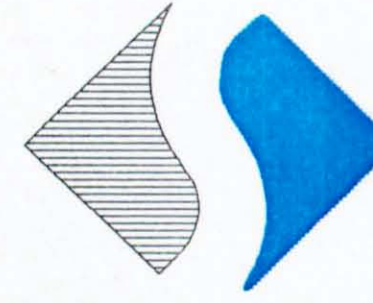
D33. Graph showing the repulsion potential exerted on new channels. It increases over time as more channels are fitted into the grid, leaving less room for new channels.



D34. Graph generated during the modelling process for the small grid, showing the volume fraction of the model filled with channel system facies. This volume increases over time as more channels are added to the model, until the volume fraction specified in the job set-up has been reached. At that point the model is completed and finishes.



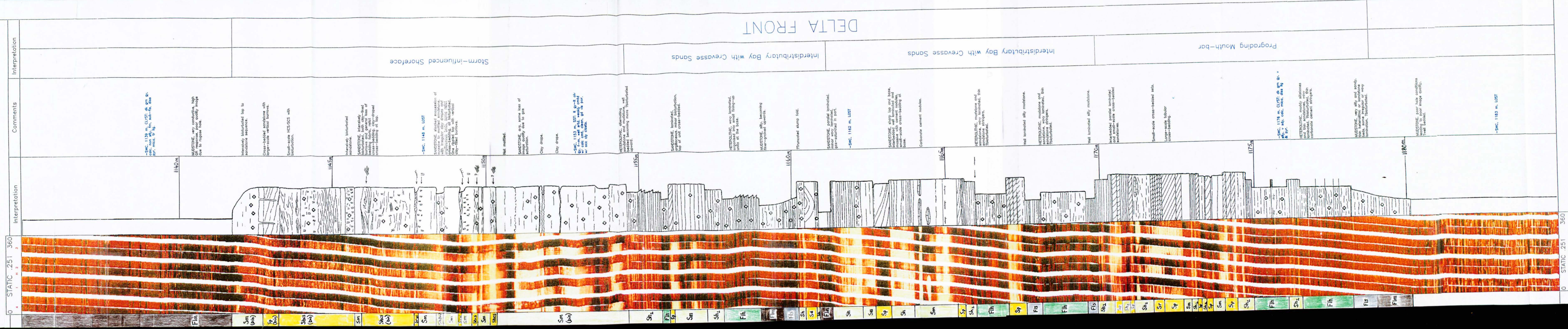
D35. Graph generated during the modelling process for the small grid, showing the frequency with which new channels are accepted in the grid. Initially this figure is low but after the blocked wells have been incorporated into the model, the remaining channels are not constrained by observational data, only by the volume fraction and other specifications entered in the job set-up, and the accept frequency increases.



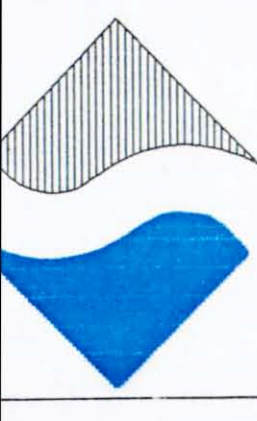
British Gas E & P  
ROSETTA  
ROSETTA - 3 (J1 57-1)  
Enclosure 1

FMI Sedimentological Interpretation

B Sand  
1142 - 1179 m



0 STATIC .251 360  
1  
2  
3  
4



**British Gas E & P**  
**ROSETTA**  
**ROSETTA - 3 (Ji 57-1)**

Enclosure 2

FMI Sedimentological Interpretation

C Sand  
1322 - 1369 m

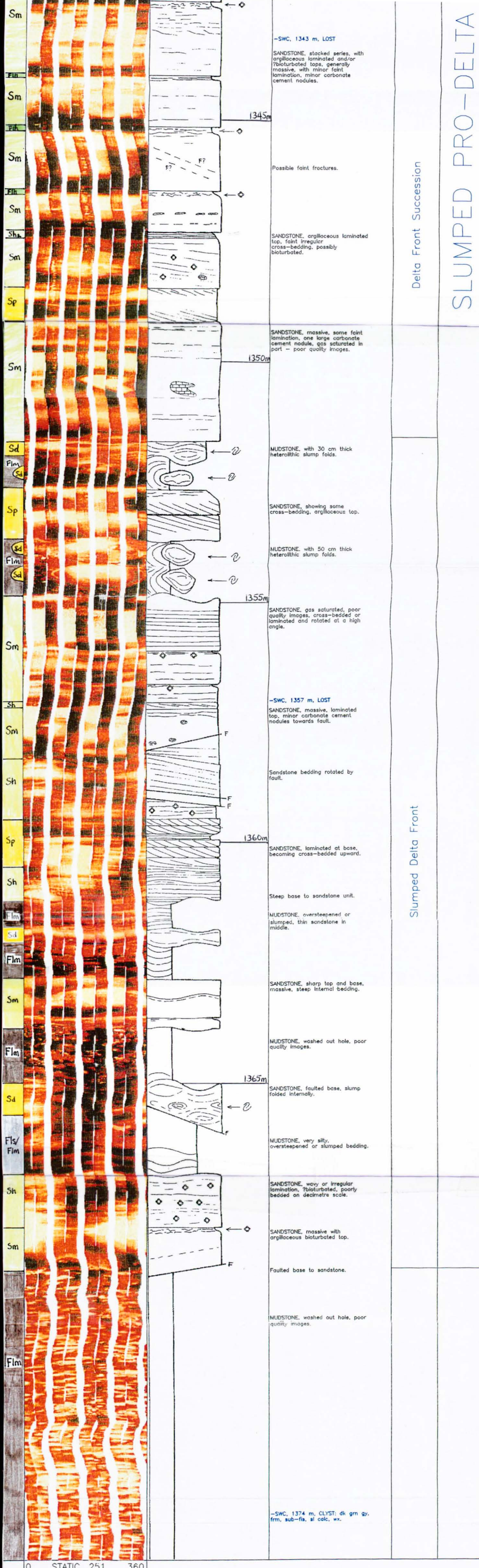
STATIC .251 360 2 3 4 1	Interpretation	Comments	Interpretation	
		-SWC, 1315 m, CLYST: dk gm gy, frm, sub-fis, sl calc, wx.		
		1320m		
		MUDSTONE, poor quality images due to rugose hole conditions, drape over cement nodule at base.		
		MUDSTONE, very silty, massive to mottled, ?bioturbated, irregular cemented top.		
		ARGILLACEOUS SANDSTONE, irregular cemented top, little internal structure, one carbonate cement nodule.		
		1325m		
		MUDSTONE, very silty, becoming less structured and more ?bioturbated upwards.		
		-SWC, 1326 m, LOST		
		Patchy carbonate cement nodules.		
		Possible small-scale slump fold.		
		SANDSTONE, massive, sharp base, laminated at base, irregular ?bioturbated top.		
		1330m		
		HETEROLITHIC, mudstone and thin sandstone, wavy or irregular lamination, ?bioturbated, fault shows minor offset.		
		SANDSTONE, massive, minor faint lamination, sharp top and base.		
		HETEROLITHIC, mudstone and thin sandstone, wavy or irregular lamination, ?bioturbated, fault shows minor offset.		
	1335m			
	SANDSTONE, gas saturated, poor quality images.			
	HETEROLITHIC, small-scale coarsening-up sequence.			
	SANDSTONE, sharp top and base, gas saturated, poor quality images.			
	-SWC, 1337 m, SST: lt gy-ll olv gy, f-m, well srt'd, weakly cmt'd w/ calc cmt, cln, gd via por.			
	Probable ophiomorpha burrow.			
	SANDSTONE, massive, cross-bedded ?reworked top, minor carbonate cement nodule.			
	1340m			
	HETEROLITHIC, mudstone and sandstone, wavy laminated, ?bioturbated.			
	-SWC, 1343 m, LOST			
	SANDSTONE, stacked series, with argillaceous laminated and/or ?bioturbated tops, generally massive, with minor faint lamination, minor carbonate cement nodules.			
	1345m			
	Possible faint fractures.			
	SANDSTONE, argillaceous laminated top, faint irregular cross-bedding, possibly bioturbated.			
	1350m			
	SANDSTONE, massive, some faint lamination, one large carbonate cement nodule, gas saturated in part - poor quality images.			

Flooded Delta Front

Delta Front Succession

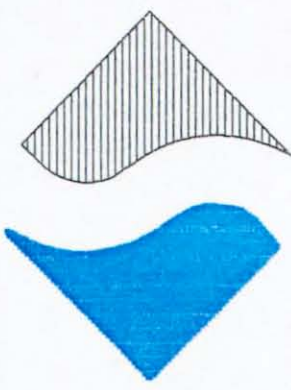
SLUMPED PRO-DELTA

# SLUMPED PRO-DELTA



Delta Front Succession

Slumped Delta Front

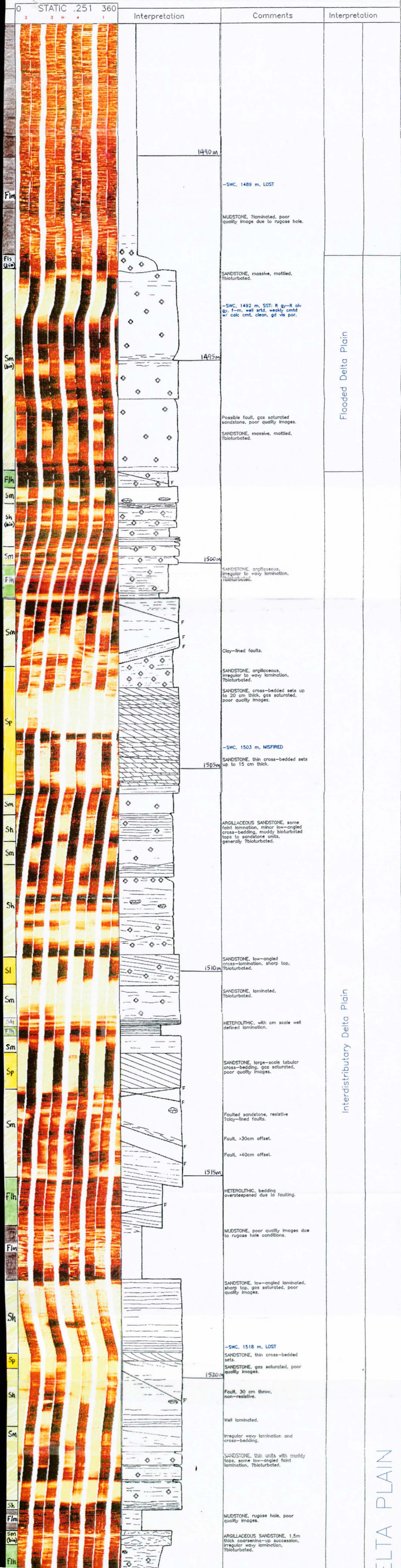


British Gas E & P  
ROSETTA  
ROSETTA - 3 (Ji 57-1)

Enclosure 3

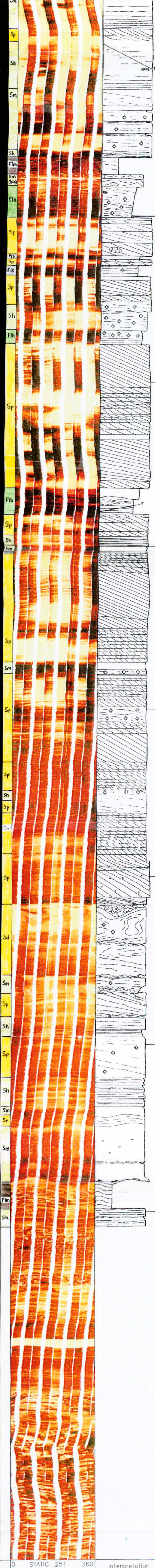
FMI Sedimentological Interpretation

D Sand  
1491 - 1553 m



DELTA PLAIN

Major Fluvial Distributary Channel



-SWC, 1518 m, LOST  
 SANDSTONE, thin cross-bedded sets.  
 SANDSTONE, gas saturated, poor quality images.

1520m  
 Fault, 30 cm throw, non-resistive.

Well laminated.

Irregular wavy lamination and cross-bedding.

SANDSTONE, thin units with muddy tops, some low-angled faint lamination, ?bioturbated.

MUDSTONE, rugose hole, poor quality images.

ARGILLACEOUS SANDSTONE, 1.5m thick coarsening-up succession, irregular wavy lamination, ?bioturbated.

1525m  
 SANDSTONE, cross-bedded, gas saturated, poor quality images.

Carbonate cement nodule c. 10cm diameter.

ARGILLACEOUS SANDSTONE, very fine irregular lamination, ?bioturbated.

SANDSTONE, large-scale tabular cross-bedding.

1530m  
 -SWC, 1529 m, SST: lt gy-ft olv gy, f-m, well artd, weakly cmtd w/ calc cmt, clin, gd vis por.  
 SANDSTONE, small-scale cross-bedding, sets 5-20 cm thick.

SANDSTONE, large-scale tabular cross-bedding, gas saturated, poor quality images.

Laminated heterolithic draped over ?debris flow.

Fault, 10cm offset.

1535m  
 -SWC, 1534 m, MISFRED

SANDSTONE, large-scale tabular cross-bedding, with reactivation surfaces, smaller cross-bedded sets at top.

SANDSTONE, small-scale cross bedding, with sets 5-20cm thick.

Clay drape.

-SWC, 1538 m, LOST  
 SANDSTONE, small-scale cross-bedding, with sets 5-20cm thick, two sets show tabular cross-bedding.

1540m  
 GWC at 1540 m.

Tabular cross-bedding.

SANDSTONE, small-scale cross bedding, with sets 5-20cm thick.

Bioturbated top to sandstone.

SANDSTONE, small-scale cross bedding, with sets 5-20cm thick.

1545m  
 SANDSTONE, pebbly, large-scale cross-bedding, erosive top.

SANDSTONE, slumped, loded irregular top.

SANDSTONE, slumped, some vague cross-bedding.

-SWC, 1547 m, SST: lt gy-ft olv gy, f-m, well artd, weakly cmtd w/ calc cmt, clin, gd vis por.

Erosion surface at top of cross-bedded sandstone.

1550m  
 SANDSTONE, faint cross-bedding, ?bioturbated, sharp base, heterolithic well laminated top.

-SWC, 1551 m, MISFRED

SANDSTONE, pebbly, massive, irregularly laminated base, cross-bedded top.

SANDSTONE, massive, mud clasts at base, steep base, ?erosional.

MUDSTONE, oversteepened bedding, rugose hole, poor quality images.

1555m  
 Parallel laminated sandstone.

-SWC, 1556 m, LOST

0 STATIC .251 360  
 4 1 H 2 3

Interpretation